

UNCLASSIFIED

AD NUMBER

AD466392

NEW LIMITATION CHANGE

TO

**Approved for public release, distribution
unlimited**

FROM

**Distribution authorized to U.S. Gov't.
agencies and their contractors;
Administrative/Operational Use; May 1965.
Other requests shall be referred to
Director, Air Force Aero Propulsion
Laboratory, Attn: RTD, Wright-Patterson
AFB, OH 45433.**

AUTHORITY

AFAPL ltr, 21 Jul 1971

THIS PAGE IS UNCLASSIFIED

I
I
E
466392

AFAPL-TR-65-45

Part III

20
JPC

ROTOR-BEARING DYNAMICS DESIGN TECHNOLOGY

Part III: Design Handbook for Fluid Film Type Bearings

REF FILE COPY
REF FILE COPY

Mechanical Technology Incorporated

TECHNICAL REPORT AFAPL-TR-65-45, PART III

May 1965

Air Force Aero Propulsion Laboratory
Research and Technology Division
Air Force Systems Command
Wright-Patterson Air Force Base, Ohio

DDC
JUL 21 1965

REF FILE COPY
REF FILE COPY
JISIA E

Best Available Copy

NOTICES

When U.S. Government drawings, specifications, or other data are used for any purpose other than a definitely related Government procurement operation, the Government thereby incurs no responsibility nor any obligation whatsoever, and the fact that the government may have formulated, furnished, or in any way supplied the said drawings, specifications, or other data, is not to be regarded by implication or otherwise, or in any manner licensing the holder or any other person or corporation, or conveying any rights or permission to manufacture, use, or sell any patent invention that may in any way be related thereto.

Qualified users may obtain copies of this report from the Defense Documentation Center.

Defense Documentation Center release to the Clearinghouse for Federal Scientific and Technical Information (formerly OTS) is not authorized. Foreign announcement and dissemination by the Defense Documentation Center is not authorized. Release to foreign nationals is not authorized.

DDC release to OTS is not authorized in order to prevent foreign announcement and distribution of this report. The distribution of this report is limited because it contains technology identifiable with items on the strategic embargo lists excluded from export or re-exports under U. S. Export Control Act of 1949 (63 Stat. 7), as amended (50 U.S.C. App. 2020, 2031), as implemented by AFR 400-10.

Copies of this report should not be returned to the Research and Technology Division unless return is required by security considerations, contractual obligations or notice on a specific document.

NOTICE: When government or other drawings, specifications or other data are used for any purpose other than in connection with a definitely related government procurement operation, the U. S. Government thereby incurs no responsibility, nor any obligation whatsoever; and the fact that the government may have formulated, furnished, or in any way supplied the said drawings, specifications, or other data is not to be regarded by implication or otherwise as in any manner licensing the holder or any other person or corporation, or conveying any rights or permission to manufacture, use or sell any patented invention that may in any way be related thereto.

(18) (19)
APL - TR-65-45 - Pt. 3

Part III

(b)

ROTOR-BEARING DYNAMICS DESIGN TECHNOLOGY

Part III: Design Handbook for Fluid Film Type Bearings.

(Upper Case)

(5)

Mechanical Technology, Incorporated, Latham,
N.Y.

TECHNICAL REPORT AFAPL-TR-65-45, PART III

(11) May 1965

(9) Final rept. 1 Apr 64 - 1 Apr 65,

Air Force Aero Propulsion Laboratory
Research and Technology Division
Air Force Systems Command
Wright-Patterson Air Force Base, Ohio

(10) by Jorgen W. Lund, Elie B. Arwas, H. S. Cheng
C. W. Ng and Coda H. T. Pan.

FOREWORD

This report was prepared by Mechanical Technology Incorporated, 968 Albany-Shaker Road, Latham, New York 12110 under USAF Contract No. AF 33(615)-1895. ^{See: AD446 290} The contract was initiated under Project No. 3145, "Dynamic Energy Conversion Technology," Task No. 314511, "Nuclear Mechanical Power Units." The work was administered under the direction of the Air Force Aero Propulsion Laboratory, Research and Technology Division, with Mr. John L. Morris (AFPL) acting as project engineer.

This report covers work conducted from 1 April 1964 to 1 April 1965.

This report was submitted by the authors for review on 7 April 1965. It is Part III of final documentation issued in multiple parts. This report also is identified by the contractor's designation MTI-65TR14.

The editor of this report, assisted by Mr. J. L. Morris, is Mr. J. W. Lund. Contributors to this report are Messrs. E. B. Arwas, H. S. Cheng, J. W. Lund, C. W. Ng, C. H. T. Pan, and B. Sternlicht.

This technical report has been reviewed and is approved.

Arthur V. Churchill
ARTHUR V. CHURCHILL, Chief
Fuels and Lubricants Branch
Technical Support Division
Air Force Aero Propulsion Laboratory

ABSTRACT

This design handbook presents data and methods for use in analyzing the dynamical performance of a rotor supported in fluid film type bearings. The data are given in form of design charts covering:

1. The dynamic bearing coefficients
2. The onset of hydrodynamic instability
3. The critical speeds and the unbalance response of a simple rotor-bearing system

The design charts are in dimensionless form and cover a wide range of bearing geometries and operating conditions.

Several different types of fluid film bearings are considered together with various forms of lubrication:

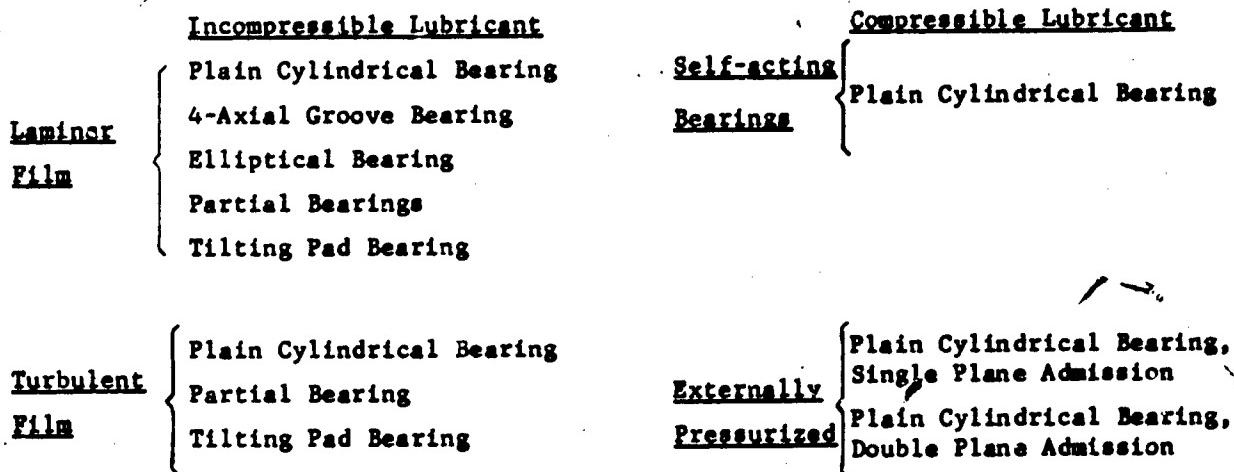


TABLE OF CONTENTS

	Page
ABSTRACT -----	iii
ILLUSTRATIONS -----	v
SYMBOLS -----	xii
A { I. INTRODUCTION -----	1
II. PRIMARY ASPECTS OF THE DYNAMICS OF A ROTOR-BEARING SYSTEM -----	4
III. OUTLINE OF THE DESIGN PROCEDURE FOR A ROTOR-BEARING SYSTEM -----	17
IV. THE SELECTION OF BEARING TYPE AND BEARING DIMENSIONS -----	21
Description of Bearing Types -----	21
Selection of Bearing Type -----	23
Selection of Bearing Dimensions -----	26
Figures 1 to 13 -----	30
Figures A-1 to A-14 -----	44
B { V. SPRING AND DAMPING COEFFICIENTS FOR FLUID FILM JOURNAL BEARINGS ..	58
Use of the Design Charts:	
a. Liquid Lubricant, Laminar Film -----	64
b. Liquid Lubricant, Turbulent Film.....	68
c. Gas Lubricant, Hydrodynamic Bearing ..	68
d. Gas Lubricant, Hydrostatic Bearing	69
Figures B-1 to B-124 -----	74
C { VI. THE STABILITY OF A ROTOR-BEARING SYSTEM -----	201
Discussion -----	201
Use of The Design Charts:	
a. Liquid Lubricant, Laminar Film	202
b. Liquid Lubricant, Turbulent Film	204
c. Gas Lubricant, Hydrodynamic Bearing ..	205
d. Gas Lubricant, Hydrostatic Bearing.....	207
Figures C-1 to C-17 -----	211
D { VII. THE CRITICAL SPEEDS AND RESPONSE OF A ROTOR-BEARING SYSTEM	230
Discussion -----	230
Use of the Design Charts	231
Figures D-1 to D-40 -----	239
E { VIII. NUMERICAL EXAMPLES -----	280
IX. REFERENCES -----	298

ILLUSTRATIONS

<u>FIGURE</u>		<u>Page</u>
1.	Measured Synchronous Whirl with Hydrostatic Gas Bearings	30
2.	Measured Synchronous Whirl with Hydrostatic Gas Bearings	31
3.	Measured and Calculated Whirl Orbits	32
4.	Measured and Calculated Whirl Orbits	33
5.	Measured Onset of Hydrodynamic Instability	34
6.	Summary of Bearing Types treated in the Report	35
7.	Geometry of the Plain Cylindrical and the 4-Axial Groove Bearing ...	36
8.	Geometry of the Elliptical and the Partial Bearing	37
9.	Geometry of the Tilting Pad Bearing	38
10.	Geometry of the Hydrostatic Bearing	39
11.	Dimensionless Design Parameters	40
12.	Dynamical Model of Rotor-Bearing System	41
13.	Dynamical Model of the Bearing Fluid Film	42

Load Carrying Capacity of Fluid Film Bearings

A-1	The Plain Cylindrical and the 4-Axial Groove Bearing	44
A-2	The Elliptical Bearing	45
A-3	The 50 Degree Partial Bearing	46
A-4	The 60 Degree Partial Bearing	47
A-5	The 80 Degree Partial Bearing	48
A-6	The 6 Shoe Tilting Pad Bearing	49
A-7	The 6 Shoe Tilting Pad Bearing	50
A-8	The 5 Shoe Tilting Pad Bearing	51
A-9	The 5 Shoe Tilting Pad Bearing	52
A-10	The 4 Shoe Tilting Pad Bearing	53
A-11	The 4 Shoe Tilting Pad Bearing	54
A-12	The Plain Cylindrical Gas Bearing, L/D = 0.5	55
A-13	The Plain Cylindrical Gas Bearing, L/D = 1	56
A-14	The Plain Cylindrical Gas Bearing, L/D = 2	57

Illustrations (Continued)

Page

Figure	<u>Spring and Damping Coefficients</u>	
	a. Liquid Lubricant, Laminar Film	
B-1	The Plain Cylindrical Bearing, L/D = 0.5 -----	74
B-2	The Plain Cylindrical Bearing, L/D = 0.5 -----	75
B-3	The Plain Cylindrical Bearing, L/D = 1 -----	76
B-4	The Plain Cylindrical Bearing, L/D = 1 -----	77
B-5	The 4-Axial Groove Bearing, L/D = 0.5 -----	78
B-6	The 4-Axial Groove Bearing, L/D = 0.5 -----	79
B-7	The 4-Axial Groove Bearing, L/D = 1 -----	80
B-8	The 4-Axial Groove Bearing, L/D = 1 -----	81
B-9	The Elliptical Bearing, L/D = 0.5, m = 0.25 -----	82
B-10	The Elliptical Bearing, L/D = 0.5, m = 0.25 -----	83
B-11	The Elliptical Bearing, L/D = 0.5, m = 0.5 -----	84
B-12	The Elliptical Bearing, L/D = 0.5, m = 0.5 -----	85
B-13	The Elliptical Bearing, L/D = 1, m = 0.25 -----	86
B-14	The Elliptical Bearing, L/D = 1, m = 0.25 -----	87
B-15	The Elliptical Bearing, L/D = 1, m = 0.5 -----	88
B-16	The Elliptical Bearing, L/D = 1, m = 0.5 -----	89
B-17	The 50 Degree Partial Bearing, L/D = 0.25 -----	90
B-18	The 50 Degree Partial Bearing, L/D = 0.25 -----	91
B-19	The 50 Degree Partial Bearing, L/D = 0.5 -----	92
B-20	The 50 Degree Partial Bearing, L/D = 0.5 -----	93
B-21	The 50 Degree Partial Bearing, L/D = 0.75 -----	94
B-22	The 50 Degree Partial Bearing, L/D = 0.75 -----	95
B-23	The 60 Degree Partial Bearing, L/D = 0.25 -----	96
B-24	The 60 Degree Partial Bearing, L/D = 0.25 -----	97
B-25	The 60 Degree Partial Bearing, L/D = 0.5 -----	98
B-26	The 60 Degree Partial Bearing, L/D = 0.5 -----	99
B-27	The 60 Degree Partial Bearing, L/D = 0.75 -----	100
B-28	The 60 Degree Partial Bearing, L/D = 0.75 -----	101
B-29	The 80 Degree Partial Bearing, L/D = 0.5 -----	102
B-30	The 80 Degree Partial Bearing, L/D = 0.5 -----	103
B-31	The 80 Degree Partial Bearing, L/D = 0.75 -----	104
B-32	The 80 Degree Partial Bearing, L/D = 0.75 -----	105

Illustrations (Continued)

<u>Figure</u>		<u>Page</u>
B-33	The 80 Degree Partial Bearing, L/D = 1	106
B-34	The 80 Degree Partial Bearing, L/D = 1	107
B-35	The 100 Degree Partial Bearing, L/D = 1	108
B-36	The 100 Degree Partial Bearing, L/D = 1	109
B-37	The 6 Shoe Tilting Pad Bearing, L/D = 0.25	110
B-38	The 6 Shoe Tilting Pad Bearing, L/D = 0.5	111
B-39	The 6 Shoe Tilting Pad Bearing, L/D = 0.75	112
B-40	The 5 Shoe Tilting Pad Bearing, L/D = 0.25	113
B-41	The 5 Shoe Tilting Pad Bearing, L/D = 0.5	114
B-42	The 5 Shoe Tilting Pad Bearing, L/D = 0.75	115
B-43	The 4 Shoe Tilting Pad Bearing, L/D = 0.5	116
B-44	The 4 Shoe Tilting Pad Bearing, L/D = 0.75	117
B-45	The 4 Shoe Tilting Pad Bearing, L/D = 1	118
B-46	The 6 Shoe Tilting Pad Bearing, Load on Pad, L/D = 0.5	119
B-47	The 5 Shoe Tilting Pad Bearing, Load on Pad, L/D = 0.5	120
B-48	The 4 Shoe Tilting Pad Bearing, Load on Pad, L/D = 0.75	121
B-49	The 4 Shoe Tilting Pad Bearing, Effect of Pad Inertia	122
B-50	The 4 Shoe Tilting Pad Bearing, Effect of Pad Inertia	123
B-51	The 4 Shoe Tilting Pad Bearing, Effect of Pad Inertia	124
B-52	The 4 Shoe Tilting Pad Bearing, Effect of Pad Inertia	125
B-53	The 12 Shoe Tilting Pad Bearing, Vertical Rotor	126
B-54	The 6 Shoe Tilting Pad Bearing, Vertical Rotor	127
B-55	The 4 Shoe Tilting Pad Bearing, Vertical Rotor	128

b. Liquid Lubricant, Turbulent Film

B-56	The Plain Cylindrical Bearing, Re = 1663	130
B-57	The Plain Cylindrical Bearing, Re = 1663	131
B-58	The Plain Cylindrical Bearing, Re = 2378	132
B-59	The Plain Cylindrical Bearing, Re = 2378	133
B-60	The Plain Cylindrical Bearing, Re = 3326	134
B-61	The Plain Cylindrical Bearing, Re = 3326	135
B-62	The Plain Cylindrical Bearing, Re = 5820	136
B-63	The Plain Cylindrical Bearing, Re = 5820	137

Illustrations (Continued)

<u>Figure</u>		<u>Page</u>
B-64	The Plain Cylindrical Bearing, Re = 8314 -----	138
B-65	The Plain Cylindrical Bearing, Re = 8314 -----	138
B-66	The Plain Cylindrical Bearing, Re = 13,304 -----	141
B-67	The Plain Cylindrical Bearing, Re = 13,304 -----	141
B-68	The 100 Degree Partial Bearing, Re = 1663 -----	141
B-69	The 100 Degree Partial Bearing, Re = 1663 -----	141
B-70	The 100 Degree Partial Bearing, Re = 2378 -----	141
B-71	The 100 Degree Partial Bearing, Re = 2378 -----	141
B-72	The 100 Degree Partial Bearing, Re = 3326 -----	141
B-73	The 100 Degree Partial Bearing, Re = 3326 -----	141
B-74	The 100 Degree Partial Bearing, Re = 5820 -----	141
B-75	The 100 Degree Partial Bearing, Re = 5820 -----	141
B-76	The 100 Degree Partial Bearing, Re = 8315 -----	151
B-77	The 100 Degree Partial Bearing, Re = 8315 -----	151
B-78	The 100 Degree Partial Bearing, Re = 13,304 -----	151
B-79	The 100 Degree Partial Bearing, Re = 13,304 -----	151
B-80	The 4 Shoe Tilting Pad Bearing, Re = 0 -----	151
B-81	The 4 Shoe Tilting Pad Bearing, Re = 1663 -----	151
B-82	The 4 Shoe Tilting Pad Bearing, Re = 2378 -----	151
B-83	The 4 Shoe Tilting Pad Bearing, Re = 3326 -----	151
B-84	The 4 Shoe Tilting Pad Bearing, Re = 5820 -----	151
B-85	The 4 Shoe Tilting Pad Bearing, Re = 8314 -----	151
B-86	The 4 Shoe Tilting Pad Bearing, Re = 13,304 -----	161
B-87	The 3 Shoe Tilting Pad Bearing, Re = 0 -----	161
B-88	The 3 Shoe Tilting Pad Bearing, Re = 1663 -----	161
B-89	The 3 Shoe Tilting Pad Bearing, Re = 2378 -----	161
B-90	The 3 Shoe Tilting Pad Bearing, Re = 3326 -----	161
B-91	The 3 Shoe Tilting Pad Bearing, Re = 5820 -----	161
B-92	The 3 Shoe Tilting Pad Bearing, Re = 8314 -----	161
B-93	The 3 Shoe Tilting Pad Bearing, Re = 13,304 -----	161

Illustrations (Continued)

Figure

s. Gas Lubricant, Hydrodynamic Bearing

- B-94 The Plain Cylindrical Gas Bearing, K_{xx} , L/D = 0.5 -----
- B-95 The Plain Cylindrical Gas Bearing, K_{xy} , L/D = 0.5 -----
- B-96 The Plain Cylindrical Gas Bearing, K_{yx} , L/D = 0.5 -----
- B-97 The Plain Cylindrical Gas Bearing, K_{yy} , L/D = 0.5 -----
- B-98 The Plain Cylindrical Gas Bearing, ωC_{xx} , L/D = 0.5 -----
- B-99 The Plain Cylindrical Gas Bearing, ωC_{xy} , L/D = 0.5 -----
- B-100 The Plain Cylindrical Gas Bearing, ωC_{yx} , L/D = 0.5 -----
- B-101 The Plain Cylindrical Gas Bearing, ωC_{yy} , L/D = 0.5 -----
- B-102 The Plain Cylindrical Gas Bearing, K_{xx} , L/D = 1 -----
- B-103 The Plain Cylindrical Gas Bearing, K_{xy} , L/D = 1 -----
- B-104 The Plain Cylindrical Gas Bearing, K_{yx} , L/D = 1 -----
- B-105 The Plain Cylindrical Gas Bearing, K_{yy} , L/D = 1 -----
- B-106 The Plain Cylindrical Gas Bearing, ωC_{xx} , L/D = 1 -----
- B-107 The Plain Cylindrical Gas Bearing, ωC_{xy} , L/D = 1 -----
- B-108 The Plain Cylindrical Gas Bearing, ωC_{yx} , L/D = 1 -----
- B-109 The Plain Cylindrical Gas Bearing, ωC_{yy} , L/D = 1 -----

d. Gas Lubricant, Hydrostatic Bearing

- B-110 The Hydrostatic Gas Bearing, Single Plane Admission, L/D = 0.5. Stiffness
- B-111 The Hydrostatic Gas Bearing, Single Plane Admission, L/D = 0.5. Damping
- B-112 The Hydrostatic Gas Bearing, Single Plane Admission, L/D = 0.5 Damping
- B-113 The Hydrostatic Gas Bearing, Single Plane Admission, L/D = 1. Stiffness
- B-114 The Hydrostatic Gas Bearing, Single Plane Admission, L/D = 1. Damping
- B-115 The Hydrostatic Gas Bearing, Single Plane Admission, L/D = 1. Damping
- B-116 The Hydrostatic Gas Bearing, Single Plane Admission, L/D = 2. Stiffness
- B-117 The Hydrostatic Gas Bearing, Single Plane Admission, L/D = 2. Damping
- B-118 The Hydrostatic Gas Bearing, Single Plane Admission, L/D = 2. Damping
- B-119 The Hydrostatic Gas Bearing, Double Plane Admission, L/D = 1. Stiffness
- B-120 The Hydrostatic Gas Bearing, Double Plane Admission, L/D = 1. Damping
- B-121 The Hydrostatic Gas Bearing, Double Plane Admission, L/D = 1. Damping
- B-122 The Hydrostatic Gas Bearing, Double Plane Admission, L/D = 2. Stiffness
- B-123 The Hydrostatic Gas Bearing, Double Plane Admission, L/D = 2. Damping
- B-124 The Hydrostatic Gas Bearing, Double Plane Admission, L/D = 2. Damping

Illustrations (Continued)

Figures

Hydrodynamic Instability

a. Liquid Lubricant. Laminar Film

- C-1 The Plain Cylindrical Bearing -----
C-2 The 4-Axial Groove Bearing -----
C-3 The Elliptical Bearing -----
C-4 The 50 Degree Partial Bearing -----
C-5 The 60 Degree Partial Bearing -----
C-6 The 80 Degree Partial Bearing -----
C-7 The 100 Degree Partial Bearing -----

b. Liquid Lubricant. Turbulent Film

- C-8 The Plain Cylindrical and the 100 Degree Partial Bearing, $Re = 0$ ---
C-9 The Plain Cylindrical and the 100 Degree Partial Bearing, $Re = 1663$ -
C-10 The Plain Cylindrical and the 100 Degree Partial Bearing, $Re = 2378$ -
C-11 The Plain Cylindrical and the 100 Degree Partial Bearing, $Re = 3326$ -
C-12 The Plain Cylindrical and the 100 Degree Partial Bearing, $Re = 5820$ -
C-13 The Plain Cylindrical and the 100 Degree Partial Bearing, $Re = 8315$ -
C-14 The Plain Cylindrical and the 100 Degree Partial Bearing, $Re = 13,304$ -

c. Gas Lubricant. Hydrodynamic Bearing

- C-15 The Plain Cylindrical Gas Bearing, $L/D = 0.5$ -----
C-16 The Plain Cylindrical Gas Bearing, $L/D = 1$ -----
C-17 The Plain Cylindrical Gas Bearing, $L/D = 2$ -----

Critical Speeds and Unbalance Response

a. Critical Speeds

- D-1 Plain Cylindrical Bearings, $L/D = 0.5$, Laminar Film -----
D-2 Plain Cylindrical Bearings, $L/D = 1$, Laminar Film -----
D-3 4-Axial Groove Bearings, $L/D = 0.5$, Laminar Film -----
D-4 4-Axial Groove Bearings, $L/D = 1$, Laminar Film -----
D-5 Elliptical Bearings, $L/D = 0.5$, $m = 0.25$, Laminar Film -----
D-6 Elliptical Bearings, $L/D = 0.5$, $m = 0.5$, Laminar Film -----
D-7 Elliptical Bearings, $L/D = 1$, $m = 0.25$, Laminar Film -----
D-8 Elliptical Bearings, $L/D = 1$, $m = 0.5$, Laminar Film -----

Illustrations (Continued)

Figure

- D-9 6 Shoe Tilting Pad Bearings, Load between Pads, Laminar Film
- D-10 5 Shoe Tilting Pad Bearings, Load between Pads, Laminar Film
- D-11 4 Shoe Tilting Pad Bearings, Load between Pads, Laminar Film
- D-12 6 Shoe Tilting Pad Bearings, Load on Pad, Laminar Film
- D-13 5 Shoe Tilting Pad Bearings, Load on Pad, Laminar Film
- D-14 4 Shoe Tilting Pad Bearings, Load on Pad, Laminar Film
- D-15 100 Degree Partial Bearings, Laminar Film, $Re = 1663$
- D-16 100 Degree Partial Bearings, Turbulent Film, $Re = 5820$
- D-17 100 Degree Partial Bearings, Turbulent Film, $Re = 13,304$
- D-18 Plain Cylindrical Bearings, Turbulent Film, $Re = 1663$
- D-19 Plain Cylindrical Bearings, Turbulent Film, $Re = 5820$
- D-20 Plain Cylindrical Bearings, Turbulent Film, $Re = 13,304$

b. Amplitude at the Critical Speeds due to Unbalance

- D-21 Plain Cylindrical Bearings, $L/D = 0.5$, Laminar Film
- D-22 Plain Cylindrical Bearings, $L/D = 1$, Laminar Film
- D-23 4-Axial Groove Bearings, $L/D = 0.5$, Laminar Film
- D-24 4-Axial Groove Bearings, $L/D = 1$, Laminar Film
- D-25 Elliptical Bearings, $L/D = 0.5$, $m = 0.25$, Laminar Film
- D-26 Elliptical Bearings, $L/D = 0.5$, $m = 0.5$, Laminar Film
- D-27 Elliptical Bearings, $L/D = 1$, $m = 0.25$, Laminar Film
- D-28 Elliptical Bearings, $L/D = 1$, $m = 0.5$, Laminar Film
- D-29 6 Shoe Tilting Pad Bearings, Load between Pads, Laminar Film
- D-30 5 Shoe Tilting Pad Bearings, Load between Pads, Laminar Film
- D-31 4 Shoe Tilting Pad Bearings, Load between Pads, Laminar Film
- D-32 6 Shoe Tilting Pad Bearings, Load on Pad, Laminar Film
- D-33 5 Shoe Tilting Pad Bearings, Load on Pad, Laminar Film
- D-34 4 Shoe Tilting Pad Bearings, Load on Pad, Laminar Film
- D-35 100 Degree Partial Bearings, Turbulent Film, $Re = 1663$
- D-36 100 Degree Partial Bearings, Turbulent Film, $Re = 5820$
- D-37 100 Degree Partial Bearings, Turbulent Film, $Re = 13,304$
- D-38 Plain Cylindrical Bearings, Turbulent Film, $Re = 1663$
- D-39 Plain Cylindrical Bearings, Turbulent Film, $Re = 5820$
- D-40 Plain Cylindrical Bearings, Turbulent Film, $Re = 13,304$

SYMBOLS

a	Orifice radius, inch
B	Damping coefficient for hydrostatic bearing, lbs.sec./in
C	Radial bearing clearance, i.e. the difference between the radius of curvature of the bearing surface and the journal radius, inch
C'	Clearance of pivot circle in the tilting pad bearing, see Page 65, inch
$C_{xx}, C_{xy}, C_{yx}, C_{yy}$	Bearing damping coefficients, lbs.sec/in
D	Journal diameter, inch
d	Feeder hole diameter, inch
e	Eccentricity of journal center with respect to bearing center,in
I	Mass moment of inertia of pivoted shoe around longitudinal axis, lbs.in.sec ²
I	Transverse mass moment of inertia of rotor around CG, lbs.in.sec
I_p	Polar mass moment of inertia of rotor, lbs.in.sec ² .
K	Bearing stiffness, lbs/in
K_r	Rotor stiffness, lbs/in
K_s	Bearing support stiffness, lbs/in
$K_{xx}, K_{xy}, K_{yx}, K_{yy}$	Bearing spring coefficients, lbs/in
L	Bearing length, inch
L_1	Distance between admission planes in a hydrostatic bearing, inch
L_2	= L-L ₁ , combined length of hydrostatic bearing outside admission planes, inch
s	Rotor span between bearings, inch
M	Rotor mass per bearing, see Page 202, lbs sec ² /in
M, M_{crit}	= I/R ² , Equivalent mass of pivoted shoe, lbs.sec ² /in
m	Ellipticity of elliptical bearing, see Fig. 8.

N	Rotor speed, RPM
\bar{N}	Total number of feeder holes in hydrostatic bearing (on the charts \bar{N} is used instead of N)
P_a	Ambient pressure, psia
P_s	Supply pressure for hydrostatic bearing, psia
R	= $\frac{1}{2}D$, journal radius, inch
Re	= $x_0 N D C / \mu$, Reynolds number
R	Gas constant, in ² /sec ² .°R
s	= $\frac{\pi N D L}{W} \left(\frac{R}{C} \right)^2$, Sommerfeld number
T	Total temperature, °R
V_c	Volume of feeder hole below orifice, in ³
W	Bearing load, lbs.
x	Rotor amplitude, see Fig. on Page 231, inch
x, y	Journal center coordinates, inch
\dot{x}, \dot{y}	Components of journal center velocity, in/sec
a	$= \alpha_{11} + \alpha_{12}$, for first critical speed and static unbalance $= \alpha_{11} - \alpha_{12}$, for second critical speed and dynamic unbalance
α_{11}, α_{12}	Influence coefficients for the rotor, see Page 231, in/lbs
δ	Eccentricity of unbalanced mass, see Figure on Page 231, in.
δ	= a^2/dC , Inherent compensation factor for hydrostatic bearing
e	= e/C , Eccentricity ratio
Λ	= $\frac{12 \pi \mu N}{P_a} \left(\frac{R}{C} \right)^2$, Compressibility number
Λ_s	= $\frac{6 \bar{N} a^2 \sqrt{RT}}{P_s C^3 \sqrt{1+\delta^2}}$, Restrictor coefficient
μ	Lubricant viscosity, lbs.sec/in ²
v	Whirl frequency, radians/sec
ξ	$= 1$, for first critical speed and static unbalance $= (\text{distance between rotor masses})/\lambda$, see Figure on Page 231.

- ξ = $\frac{L_2}{D}$ for hydrostatic bearing
 ρ = $\frac{M}{\xi^2 C}$, Rotor flexibility parameter
♦ Bearing attitude angle
 ω = $2\pi N$, Angular speed of rotor, radians/sec
 ω_n First or second critical speed, radians/sec

INTRODUCTION

The trend towards high-speed turbomachinery has accentuated the fact that fluid film bearings possess stiffness and damping properties which have an appreciable effect on the dynamic behavior of the rotor-bearing system. Thus, it has become recognized that the static properties (i.e. load carrying capacity, flow, power loss, temperature rise, etc) are only some considerations in bearing design. In fact, the dynamic characteristics will often govern the particular bearing selection. It has been shown that the dynamic properties will affect the threshold of instability, critical speeds, unbalance response, noise attenuation, etc. Each bearing type (e.g. cylindrical, axial groove, elliptical, pivoted shoe, etc), lubrication system (e.g. self-acting, hybrid), fluid property (e.g. compressible, incompressible, and two-phase), and regime of operation (e.g. laminar, transition, and turbulent) will influence the dynamic performance of the system to a differing degree. Therefore, in choosing the bearing type for a specific operating condition and environment, one must consider both the dynamic and the static aspects.

The calculation of the dynamic properties of bearings has been extremely difficult and laborious and only the advent of high-speed, high storage computers has made it practical. These solutions, however have lagged considerably behind steady-state analyses. While at present there are several books and numerous reports and papers available that treat the steady-state performance and design of bearings, only a few papers are available on dynamic properties. This handbook partially* fills this gap. The text is presented in such a form that as solutions for other bearing types are made available, they can be readily added to this handbook. The complexity of the analysis and the numerous parameters also introduce the problem of generalization of the results so as to make them broadly applicable. In this text the generalization has been accomplished through the use of dimensionless parameters. Decoupling of the bearings from the rotor system has also been important in order to make the results applicable to a variety of rotor configurations.

* The scope of this program permitted only a limited coverage of bearing types, dimensions (L/D , m , arc length, etc) and ranges of operating parameters (Re , Λ , P_s/P_a , etc).

While the trend to high speed machinery has required the establishment of the dynamic properties of bearings, the presence of more severe environmental requirements (.e.g extreme temperatures and pressures, radiation, etc), has also focused on this need. High speed aircraft, space power systems (Brayton and Rankine dynamic conversion machinery), cryogenic refrigeration machinery, guidance and control equipment, centrifuges, etc. are just a few examples of new machinery requirements. Many of these use process fluid lubrication such as liquid metal, gas or vapor. The use of these fluids in high speed machinery is relatively recent; therefore, experience is limited, and in many cases unfavorable. Many of the troubles can be attributed to poor design or trial and error procedure. At the same time it should be recognized that the analysis with these process fluids is considerably more complex because of the introduction of nonlinearity and at least one additional parameter (Reynolds number, compressibility number, quality) has to be considered. To ensure satisfactory operation and to prevent failures of the machinery it is essential, as part of the actual design procedure, to perform an investigation of the dynamics of the rotor-bearing system. Such an investigation must include the calculation of the system critical speeds, a calculated prediction of the maximum vibratory amplitude and a check on the stability of the rotor. Through the calculations it can be determined if the rotor has adequate stiffness for its weight and if the chosen bearing types and the selected bearing dimensions are adequate for the operational requirements. It is the purpose of this handbook to set forth the required design methods and to give as much design data as is currently available in easy to use form.

The data are given in form of design charts which employ dimensionless parameters. Thereby, the charts become generally valid and apply to a wide range of operating conditions and design configurations. The charts cover three types of data:

1. Dynamic coefficients for several bearing types and bearing geometries (spring and damping coefficients). The data can be used directly together with existing computer programs to calculate the unbalance response and the stability of a general rotor-bearing system.
2. The regions of stable and unstable operation of a rotor bearing system.
3. The effect of fluid film bearings on the critical speeds and the unbalance response of a rotor-bearing system.

The first chapter in the handbook contains a brief review of the most important aspects of rotor-bearing dynamics from a design point of view. This is followed by a chapter in which the usual procedure for arriving at a design of a rotor-bearing system is outlined. The various steps in the design procedure are then treated separately in the subsequent chapters which at the same time give a detailed explanation for using the accompanying design charts.

That part of the design procedure which deals with the steady-state performance of the system, or the strength and mechanical integrity of the rotor and its support structure, has only been included to the extent that it makes the use of the presented data more efficient. A more complete coverage of the associated design problems can be found in standard reference books and numerous reports.

Most of the given design data have been computed specifically for the present handbook. This includes many of the charts for the dynamic bearing coefficients, almost all of the stability data and all of the charts for the critical speeds and the unbalance response. The balance of the data for the dynamic bearing coefficients has been compiled from several sources given in the reference list.

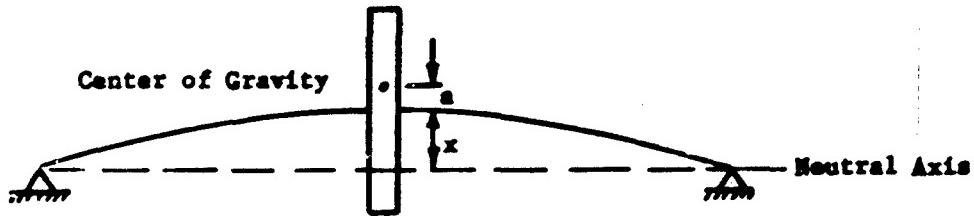
The handbook treats those bearing types which are classified as fluid film bearings. Design data for ball bearings are given in an accompanying report.

PRIMARY ASPECTS OF THE DYNAMICS OF A MOTOR-BEARING SYSTEM

The principal part in any piece of rotating machinery is the rotor itself. Its function is to generate or transmit power. It consists of a shaft on which may be mounted such components as turbine wheels, compressor wheels, gears, the rotor of an electric motor or generator, etc. The shaft is frequently made of an integral piece of material, although the diameter may vary along the length of the shaft, and the components are either integral with, shrunk on or mechanically fastened to the shaft. The shaft is supported in bearings with separate the rotating surface of the shaft from the stationary supports. The bearings may be either fluid film bearings, using oil, other liquids, gas, or even two phase fluids as a lubricant, or they may be rolling element bearings like ball bearings.

The rotor is never completely rigid and in many applications it is actually quite flexible. Hence, the rotor vibrates if it is subjected to excitational forces. These forces may be aerodynamic, magnetic, mechanical, etc. By far the most common of such excitations are the unbalance forces present in the rotor. They generally derive from the manufacturing processes where it is not possible to ensure that the center of gravity of the rotor masses coincide exactly with the geometric symmetry axis of the rotor. The unbalance may be distributed throughout the rotor and varies in both magnitude and angular position along the length of the rotor. As the rotor is brought up in speed the centrifugal forces due to the unbalance cause the rotor to deflect and the bent rotor whirs around its neutral axis synchronous with the speed of rotation. This phenomenon is known as synchronous whirl. It should be noted that synchronous whirl is actually not a vibration of the rotor in the normal sense of the word. The deflected shape of the rotor itself remains unchanged during the motion and it is only when the whirl amplitude is measured in any fixed direction (for instance, by a probe) that the motion appears as a vibration. However, from the point of view of describing synchronous whirl the analogy to a vibratory motion is very strong. This analogy becomes evident when considering the phenomenon of the critical speed of the rotor. For the purpose of illustration assume the rotor to consist of a single heavy disc mounted on a flexible shaft whose weight is very small compared to that of the disc. Let the mass of the disc be $M \frac{\text{lbs.}}{\text{sec.}^2}$ in and let the stiffness of the rotor be $K_r \frac{\text{lbs.}}{\text{in.}}$ (i. e. K_r is

determined as the force which causes a one inch deflection at the center of the shaft). Furthermore, let the mass center of gravity of the disc be eccentric by a distance a inch with respect to the axis of the shaft and let the angular speed of the rotor be ω radians/sec. The shaft center at the disc will be whirling in an orbit with radius x inch, such that the center of gravity of the disc will be whirling with a radius of $(x+a)$. Hence, the shaft pulls the disc inwards with a force of: $K_x \cdot x$ lbs. and the centrifugal force pulls outwards with a force of: $M\omega^2(x+a)$ lbs. For equilibrium the two forces must be equal:



$$K_x x = M\omega^2(x+a)$$

i.e.

$$x = \frac{Ma}{K_x - M\omega^2}$$

from which the whirl radius of the shaft center at the disc can be computed. It is immediately seen that when the rotor speed is such that:

$$\omega = \omega_c \sqrt{\frac{K_x}{M}}$$

then the denominator becomes zero and x becomes infinitely large. The corresponding speed ω_c is called the critical speed of the rotor. It may further be noted that for $\omega < \omega_c$ the radius x is positive, i.e., x and a are in the same direction, such that the center of gravity of the disc is outside the orbit of the center of the shaft. For speeds above the critical speed x becomes negative and the center of gravity is inside the shaft center orbit. Hence, in going through the critical speed there is an inversion of the center of gravity or, in the terminology of vibrations the phase angle between the amplitude and the exciting force (i.e. the unbalance) changes from zero to 180 degrees. As the rotor speed becomes very large, then $x = -a$ and the center of gravity of the disc coincides with the center of the shaft orbit and is therefore stationary.

The theoretically infinitely large amplitude at the critical speed does not occur in practice since there is always some damping present in the system.

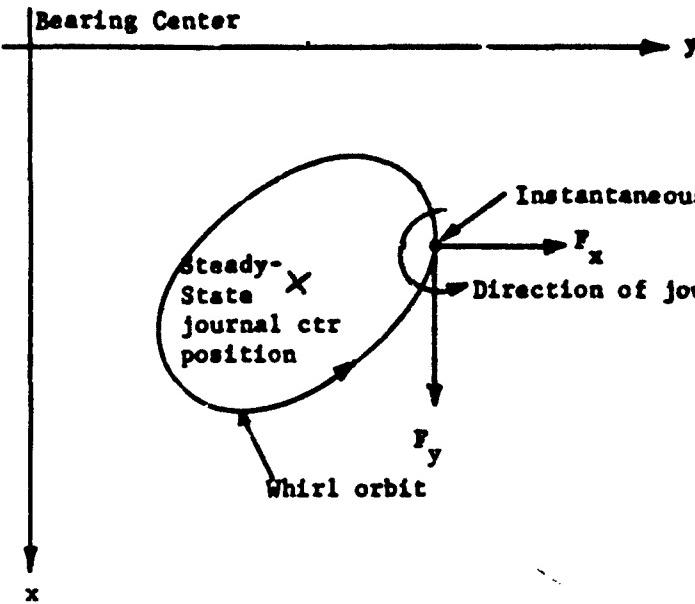
However, any inherent material damping in the shaft itself does not contribute to limit the amplitude since the shape of the deflected rotor does not change during the whirl motion. Instead, the major source of damping is in most cases the journal bearings and without this or a similar source it would be very difficult to pass through the critical speed. It is, therefore, evident that the bearings play a major role in the dynamics of the rotor.

The most common journal bearing type is the fluid film bearing in which the rotor journal and the bearing sleeve are separated by a thin film of lubricant. The lubricant may be oil, water, liquid metal, or a two phase fluid gas. In the case of self-acting bearings the geometry is such that the rotation of the journal causes the bearing to act as a viscous pump whereby pressures are generated in the lubricant film forcing separation of the journal and the sleeve. Under steady-state conditions the total pressure force equals the static load on the bearing. However, if the center of the rotating journal is in motion, as for instance, during synchronous whirl, additional pressures are set up in the lubricant film which act as dynamic forces on the journal in addition to the static force. The dynamic force depends on both the amplitude and the velocity of the journal center motion but in contrast to conventional mechanical forces the dynamic force does not have the same direction as the imposed amplitude. Resolving the dynamic force into two components, F_x and F_y , along fixed coordinate axes in the bearing, say an x-axis and a y-axis, and likewise resolving the journal center motion into x and y displacements, the dynamic force components may be expressed by:

$$F_x = -K_{xx}x - C_{xx}\dot{x} - K_{xy}y - C_{xy}\dot{y}$$

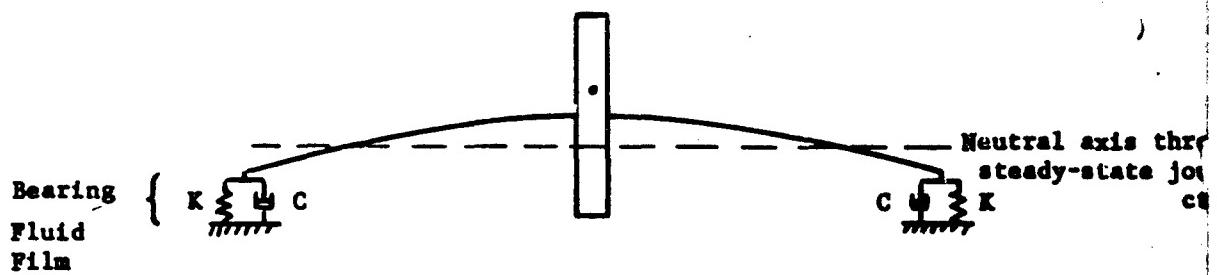
$$F_y = -K_{yx}x - C_{yx}\dot{x} - K_{yy}y - C_{yy}\dot{y}$$

where $\dot{x} = \frac{dx}{dt}$ (x-velocity) and $\dot{y} = \frac{dy}{dt}$ (y-velocity). To illustrate:



Strictly speaking the given equations are only exact for infinitesimal small amplitudes but in practice they prove to be valid even for amplitudes as large as a third of the bearing clearance. The 8 coefficients: K_{xx} , C_{xx} C_{yy} are called spring and damping coefficients such that, for instance, K_{xy} is the spring coefficient yielding a restraining force in the x-direction due to a displacement in the y-direction. These coefficients are calculated from lubrication theory and are properties of the particular bearing. They depend on the bearing configuration, the lubricant properties and, more important, they bind to a given steady-state journal center position. Consequently, they change with the speed of the rotor.

To illustrate the effect of the bearing on the dynamics of the rotor assume for simplicity that the bearing may be represented by a single spring coefficient K and a single damping coefficient C instead of the actual 8 coefficients. Returning to the single-disc rotor discussed above the modified model now becomes:



The critical speed is approximately determined by:

$$\omega_c = \sqrt{\frac{K_x r / (K_x + K_y)}{M}} = \sqrt{\frac{K_x}{M}} \cdot \sqrt{\frac{r}{K_x + K_y}}$$

which is less than the critical speed previously calculated with rigid bearings where: $\omega_c = \sqrt{\frac{K_x}{M}}$. Hence, the flexibility of the fluid film lowers the critical speed. It is not uncommon for the reduction to amount to 30 to 40 percent and cases can be cited where the reduction is even greater, e.g. with soft gas bearings. Although ignored in the above equation the damping may cause the reduction to be less than stated. This is readily seen when considering a bearing with so much damping that the bearing acts like it was rigid in which case the critical speed becomes equal to $\sqrt{\frac{K_x}{M}}$. This effect is frequently of importance in oil lubricated bearings. On the other hand, in gas bearing applications the rotor is very stiff compared to the gas film in which case the damping causes a slight reduction in the critical speed.

When the flexibility of the bearing film is taken into account it is found that for whole rotor partakes in the synchronous whirl motions although the size of the whirl orbit changes along the length of the rotor. Furthermore, the presence of damping in the bearing film limits the amplitude in passing through the critical speed. The damping is frequently sufficiently large that the critical speed may hardly be noticed and even with instrumentation it may be difficult to identify and measure the critical speed with better accuracy than ± 10 percent in rotor speed. This, however, is also due to the fact that there are 8 bearing coefficients instead of just two. With two coefficients as assumed above the stiffness in the vertical and the horizontal direction are the same and likewise for the damping coefficients. Hence, due to the symmetry of the system the whirl orbit is circular. When there are 8 bearing coefficients the system is unsymmetrical and the whirl orbit becomes elliptical. In essence, this implies that the stiffness and damping coefficients in two mutually perpendicular directions are dissimilar. Therefore, there will be one critical speed based on the smallest stiffness and another critical speed based on the largest stiffness. Theoretically then, there are two resonant amplitude peaks but due to damping the peaks overlap sufficiently that in practice they appear as one broad peak. Consequently, it is difficult to define by measurements the exact rotor speed at which the critical

speed is encountered. Neither is it possible to define the critical speed by means of a change in the phase angle between unbalance and amplitude. The observed phase angle value depends on the direction in which the amplitude is measured.

Figures 1 to 4 show typical examples of synchronous whirl orbits and rotor amplitudes. The amplitudes are measured by capacitance probes which are mounted inside or just adjacent to the bearing. The probes are 90 degrees apart and give the rotor amplitudes as sine-waves as shown by the bottom picture in Fig. 1. By simultaneously displaying the signals from the two probes on an oscilloscope a picture of the whirl orbit is obtained on the screen as shown by the top picture in Fig. 1. Hence, the probes can be thought of as coordinate axis for measuring the rotor motion and they may be labeled x-probe and y-probe in analogy to x-axis and y-axis. To illustrate assume that the x-signal and the y-signal are 90 degrees out of phase so that they may be written:

$$x = a \cos \omega t \quad y = b \cos(\omega t - 90^\circ) = b \sin \omega t$$

(a = peak x-amplitude, b = peak y-amplitude, ω = frequency, Radians, sec)

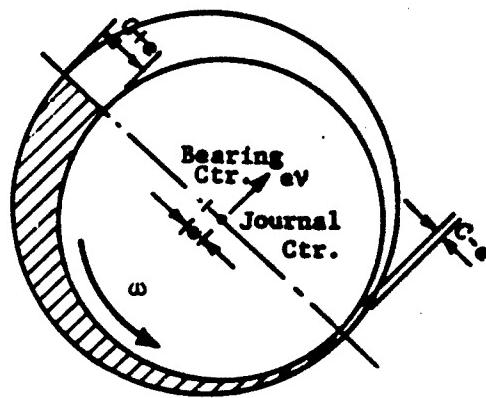
Combining the signals yields:

$$\frac{x^2}{a^2} + \frac{y^2}{b^2} = 1$$

i.e. an ellipse with major axis: a (along the x-axis) and minor axis: b (along the y-axis). If the signals are either in phase or 180 degrees out of phase the whirl orbit becomes a straight line. For phase angle values between 0 and 180 degrees the orbit is an ellipse whose orientation with respect to the axes depend on the particular value of the phase angle and on the magnitude of the peak amplitudes. This is clearly illustrated by Figs. 2,3 and 4. Figure 2 (and also Fig. 1) is obtained with a rotor supported in hybrid gas bearings externally pressurized with rotation) and shows the synchronous whirl orbit, due to unbalance, as a function of rotor speed. The amplitude reaches a peak at approximately 18,000 RPM which is either the first or the second critical speed (the two critical speeds are the two rigid body modes and they are too close together to separate). The increase in amplitude beyond 25,000 RPM is caused by a pedestal resonance. Apart from the change in size it may also be noted that the orientation of the elliptical orbit changes with speed. Figures 3 & 4 present measured synchronous whirl orbits obtained with a 100 degree, Silicone oil lubricated, partial bearing and with a fully

turbulent lubricant film (Reynolds number = 5820 and 8314, respectively) The measurements are compared to theoretical results which are calculated on the basis of theoretically derived spring and damping coefficients representing the bearing film. The overall agreement is very good. Each orbit is shown in the x-y-coordinate system corresponding to the two probes and is obtained for a particular value of the Sommerfeld Number $\frac{\mu N}{P} \left(\frac{R}{C}\right)^2$ where: μ is the lubricant viscosity, N is the rotor speed in rps, R is the journal radius, C is the radial clearance and P is the bearing loading per unit projected bearing area. Hence, the Sommerfeld number gives a direct indication of the rotor speed.

Whereas Figs. 1 to 4 show synchronous whirl with elliptical orbits Fig. 3 shows the onset of hydrodynamic instability in a gas lubricated journal bearing. The orbit has two lobes and is generated by a simple superposition of synchronous whirl and half-frequency whirl. The small lobe "corresponds" to the synchronous whirl and disappears as the amplitude builds up. If the speed is increased further the orbit increases rapidly in size and eventually the bearing will fail due to contact between the journal and the bearing. With gas bearings an instability failure can be very serious and may cause extensive damage to both the rotor and the bearings and even with liquid or oil lubricated bearings it is very difficult to operate a rotor beyond the onset of instability. The hydrodynamic instability is known as either fractional frequency whirl ("half-frequency whirl") or resonant whip ("oil whip"). The instability is inherent in the very principle by which lubrication works. To illustrate, consider for simplicity a vertical rotor supported in plain journal bearing with length L , radius R , radial clearance C and an angular rotor speed of $\omega \frac{\text{radian}}{\text{sec.}}$.



Let the journal ride eccentric in the bearing clearance with an eccentricity e . Consider a flow balance for one half of the lubricant film (shaded in the figure) and assume that no pressure is present in the film:

$$\text{flow in} = \frac{1}{2} L R \omega (C+e) \frac{\text{in}^3}{\text{sec}}$$

$$\text{flow out} = \frac{1}{2} L R \omega (C-e) \frac{\text{in}^3}{\text{sec}}$$

Since the flow into the film volume is greater than the flow going out the film will normally develop a pressure such that the inflow is reduced and the outflow is increased with side leakage taking place. It is by this mechanism that a hydrodynamic bearing is able to generate its load carrying capacity. However, assume that the journal center is not stationary but whirls with an instantaneous angular speed of $v \frac{\text{radians}}{\text{sec}}$ around the bearing center. The journal center velocity is then: $ev \frac{\text{in}}{\text{sec}}$ and the considered film volume increases with time at the rate of: $2L\dot{v} \frac{\text{in}^3}{\text{sec}}$. In this case the flow balance can be written:

$$(\text{flow in}) = (\text{flow out}) + (\text{rate of change of volume})$$

or

$$\frac{1}{2} L R \omega (C+e) = \frac{1}{2} L R \omega (C-e) + 2L\dot{v}$$

which is satisfied if:

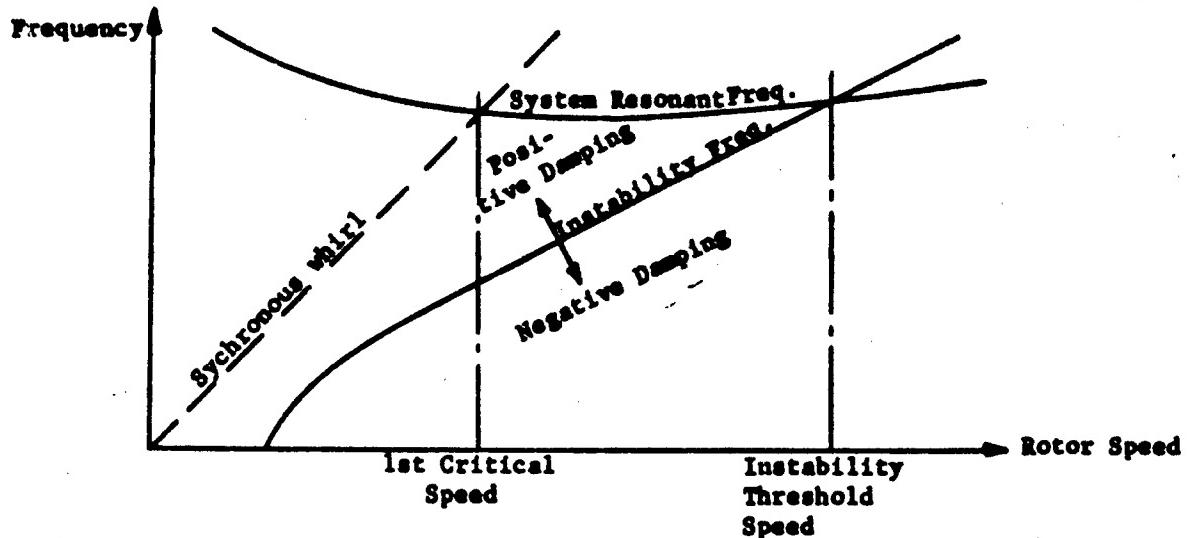
$$v = \frac{1}{2} \omega$$

When the above flow balance is satisfied no pressure is developed in the bearing film. Hence, when the whirl frequency equals half of the rotational speed the bearing loses its load carrying capacity and it becomes unstable.

The purpose of the above illustration is to show that whirl may cause instability and that the instability whirl frequency has an inherent tendency to equal a half of the rotor speed. However, as already mentioned the illustration is only valid for a vertical rotor or a lightly loaded bearing where the motor whirls around the bearing center and the whirl orbit is a circle. In general the bearing is under static load. Consequently the center of the whirl orbit is dis-

placed from the bearing center and the orbit becomes elliptical. This has the effect of reducing the instability whirl frequency although the reduction is only noticeable when the static load and eccentricity is high (for a sufficiently high eccentricity, the instability may actually be eliminated in the oil lubricated bearing). Furthermore, the simple concept of instability as being caused by a complete loss of load carrying capacity is no longer valid for a loaded bearing. Rather, the onset of instability can be viewed as being caused by the bearing losing its damping ability. A brief explanation of this phenomenon will be given in the following.

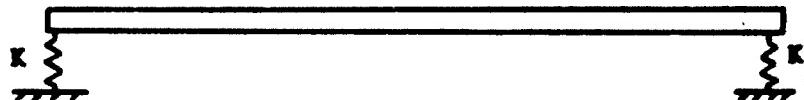
It can be shown that, for the purpose of describing the onset of instability, a journal bearing can be represented by a single effective spring coefficient and a single, effective damping coefficient. These coefficients can be calculated from the 8 dynamic bearing coefficients as shown in Ref. 16. However, the two coefficients derived in this manner depend on the whirl frequency such that the effective damping coefficient is negative for small frequencies and becomes positive for higher frequencies. The frequency at which the damping becomes zero shall be called the instability frequency. The ratio between the instability frequency and the rotor speed equals approximately 0.5 in most cases except at high eccentricity ratios (e.g. at low speeds) where the ratio is usually smaller. Therefore, the instability frequency can be found as a function of speed as shown by the corresponding curve in the figure below. For frequencies less than the instability frequency (i.e. in the region below the curve) the effective damping is negative, and for frequencies greater than the instability frequency the damping is positive. The effective spring coefficient of the bearing together with the flexibility of the rotor determines the resonant frequencies of the rotor-bearing system. Since the bearing stiffness is a function of speed the resonant frequencies become speed dependent. The lowest of these resonant frequencies is shown by the curve labeled: "System Resonant Frequency" in the figure below. This curve intersects the curve for the instability frequency at a speed denoted as: "Instability Threshold Speed":



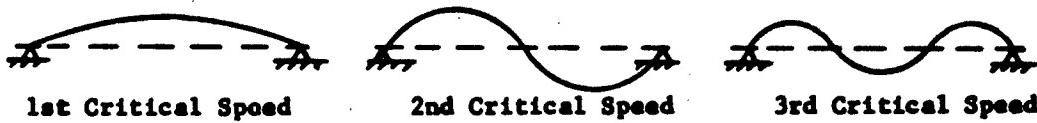
Assume that the rotor is subjected to a small disturbance. It will then tend to vibrate at its lowest resonant frequency. However, if the rotor is running below the instability threshold speed the bearings provide positive damping and the vibration dies out. As the speed is increased the damping available for the vibration diminishes until it becomes equal to zero at the instability threshold speed. Attempting to increase the speed beyond the threshold speed causes the damping to become negative such that any imposed disturbance is amplified and the system is unstable.

From the figure it is seen that if the rotor mass is increased or the shaft is made more flexible the system's natural frequency is lowered, whereby the intersection between the two frequency curves shifts to the left and the threshold speed is reduced. Conversely, if external damping is present in the system (for instance, in the supports) the curve of the film instability frequency is lowered thereby raising the threshold speed. The latter characteristic suggests means by which an otherwise unstable system may be stabilized and also explains why some machinery, notably rotary pumps, may operate stable well above the theoretical threshold speed. The damping capacity of the liquid passing through the impeller acts as external damping to the system and stabilizes the rotor.

Turning again to the phenomenon of critical speeds the preceding discussion has only mentioned the lowest critical speed (the first critical speed). Since the rotor is an elastic body there are, of course, infinitely many critical speeds but only the lowest two or three critical speeds are of importance in practice. Each critical speed has associated with it a mode shape which is simply the shape of the deflected rotor at the critical speed. To illustrate the interaction between the rotor and its bearings at the critical speeds consider a simple model consisting of a uniform shaft supported in bearings with equal stiffness, denoted as K :



If the bearings are rigid ($K = \infty$) the shaft behaves like a simply supported beam with mode shapes:



Rigid Bearings, Flexible Rotor

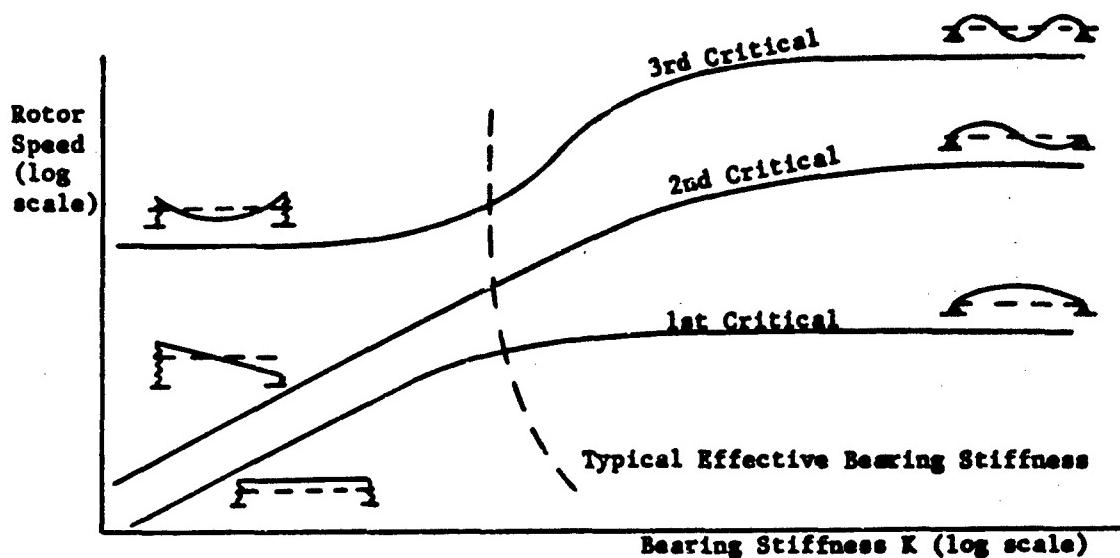
Next, assume the bearings to be very flexible in comparison with the rotor. Then the critical speeds will be lowered and the rotor will behave like a rigid body at the first and the second critical speed with mode shapes*):



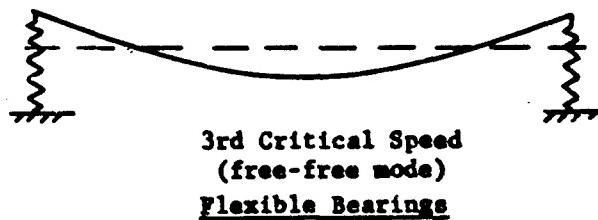
Flexible Bearings, Rigid Rotor (Rigid Body Critical Speeds)

* Strictly speaking, it is only true that the 1st critical speed is the translatory whirl mode and the second critical speed is the conical whirl mode when the transverse radius of gyration is less than 70 percent of the rotor span between bearings. In practice this condition is usually satisfied.

It should be remembered that the rotor does not vibrate but whirls. At the first rigid body critical speed the whirling rotor describes a cylindrical surface in space and the mode is called: translatory whirl. At the second rigid body critical speed the described surface is a cone with its apex between the bearings and the mode is called: conical whirl. Both of the two rigid body critical speeds are proportional to \sqrt{K} . Hence, if the critical speeds were plotted as a function of bearing stiffness on a log-log graph the rigid body critical speeds will appear as straight lines with a slope of 0.5 and the flexible rotor modes will appear as horizontal lines:



There are only two rigid body modes. Even if the bearings are very flexible the third critical speed, therefore, involves bending of the rotor itself and it is the free-free mode:



For a rotor supported in gas bearings the bearing stiffness is generally sufficiently small that the two lowest critical speeds are the rigid body modes. Actually, at this time it is recommended to require this condition since gas bearings do not possess enough damping to effectively control the resonant

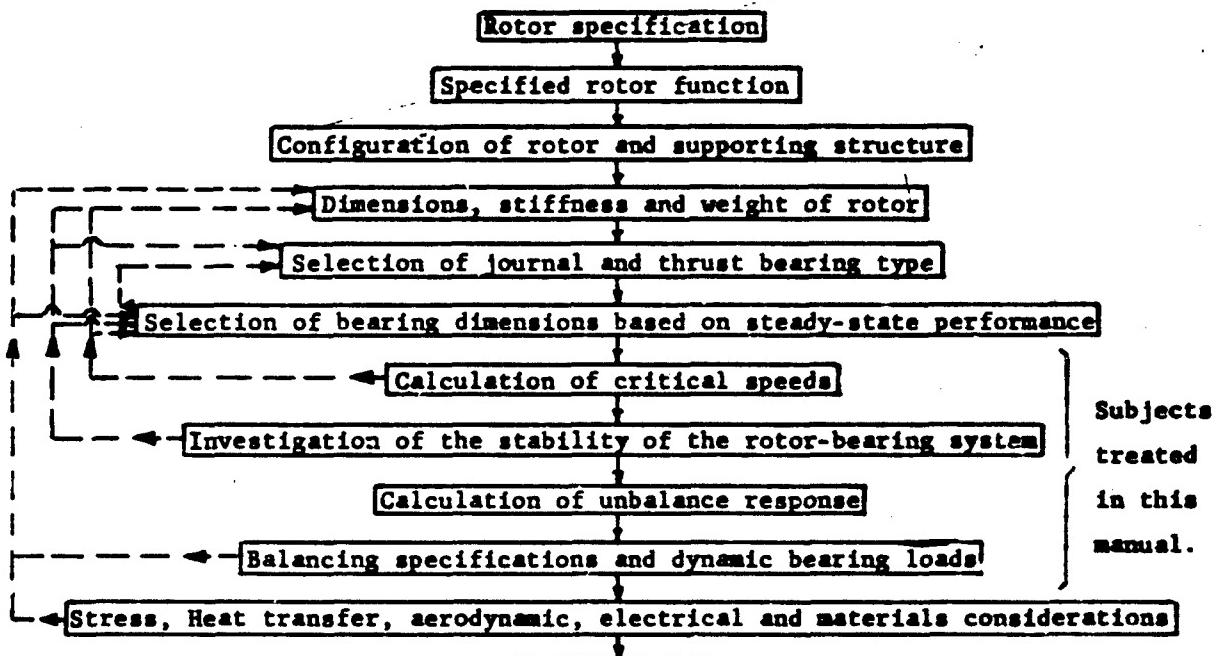
amplitude of a flexible rotor. Hence, in current design practice a gas bearing supported rotor is quite rigid and the third critical speed is normally outside the operating speed range.

The above discussion summarizes the basic elements of rotor dynamics from the point of view of design application. The three major subjects are: a) unbalance response and synchronous whirl, b) critical speeds and, c) hydrodynamic instability. To this may be added rotor balancing which, however, will be discussed in another report (Ref.1). Other considerations are in most cases of secondary importance although they may of course be very significant in certain special pieces of machinery (shock loading, non-synchronous excitation, random vibration, noise transmission, etc.). The most frequently encountered of the additional considerations are treated in Ref. 1 to the extent information is available.

OUTLINE OF THE DESIGN PROCEDURE FOR A ROTOR-BEARING SYSTEM

A successful rotor design for high performance rotating machinery applications requires the integration of many technical considerations, one of which is rotor-bearing dynamics. Compromises must be made to balance the often conflicting requirements of materials properties, stress, heat transfer, aerodynamics, and electrical design in addition to rotor-bearing dynamics. Careful attention must also be given to the supporting structures in which the bearings are mounted. These structures must maintain the alignment of the bearings with the shaft and with each other and maintain clearances around rotating members. At the same time they must provide proper structural stiffness for the support of the rotor and its dynamic loads. The design should be such that these functions are accomplished with minimum change during load and temperature transients.

The remainder of this section is devoted to the rotor-bearing dynamics aspect of rotor design. It should be remembered, however, that this is only one of many considerations that must come into play during the evolution of the rotor design. At an early stage of the design it is necessary to take into account the critical speeds and stability of the rotor-bearing system, and the methods for balancing the rotor and minimizing rotor amplitude. The following chart illustrates the relationship of rotor-bearing dynamics to other design considerations in the design procedure.



The "boxes" give the sequential steps of the design procedure while the broken lines indicate "feed-back" paths depending the outcome of the various calculations.

The particular machinery application dictates the function of the rotor. Typical examples are: turbo-generator, turbo-compressor (gas turbines in general), turbo-compressor alternator, turbo-alternator pump, motor-compressor or motor-pump. There are also multi-rotor systems where two or more rotors are coupled together as in conventional turbine-generator sets, connected with a flexible or a splined coupling, or gear shafting where the gears themselves provide the connection between the individual shafts. The required output of the machinery determines the optimum number of turbine or compressor stages and wheels and their size, or the size of the rotor and stator for an electrical motor or generator. On this basis a preliminary lay-out of the rotor can be made incorporating such other considerations as the strength of the rotor, thermal insulation, heat shielding, space for seals, space for inlet and exhaust ducts, and assembly sequence. The approximate weight of the rotor and the corresponding bearing reactions can be computed from the preliminary layout. In addition, the rotor span, the journal diameters and the space available for the bearings can be determined.

Early in the design process, attention must be given to the stiffness and the mass distribution of the rotor. Stiffness is of particular concern if the rotor is built-up of several shrink-fitted sleeves, collars and disks compressed together by means of either a nut on the shaft or a long tie bolt. Ideally, the built-up rotor is as stiff as an integral rotor if all the parts have exact dimensions and the compression between parts induced by the pre-loading is sufficiently high that it will never be exceeded by any tensile stresses caused by bending of the rotor. However, this is never achieved in practice and a reduction in stiffness is always encountered. It can only be minimized by having as few separate components as possible, by requiring tight tolerances and by specifying a high pre-load. An additional disadvantage of the built-up rotor is the possibility of encountering instability induced by dry friction and sliding between the rotor components. Such an instability sets in just above the first critical speed.

The mass distribution of the rotor is important because of its strong influence on critical speed. For example, the rotor frequently extends beyond the bearings to carry a turbine wheel, a compressor wheel or a similar relatively heavy mass. This is normally referred to as a rotor with overhung mass. Such an arrangement causes several problems. The primary reason is that the shaft sections near and through the bearings are usually the most flexible part of the rotor. This is especially the case in high speed applications where the size of the journal diameter is kept to a minimum in order to reduce the friction power loss in the bearings. Hence, the overhung masses are supported on relatively flexible "cantilevers" thereby causing a significant lowering of the critical speeds. The flexible shaft sections at the ends also make it more difficult to balance the rotor. Normally the only accessible balancing planes are at the end of the rotor and if heavy correction weights are required, the rotor will bend and make it virtually impossible to obtain a satisfactory balance.

Another effect of overhung mass is to shift the shaft nodes towards the bearings. The resulting decrease in whirl amplitude at the bearings reduces the capacity of the bearing to provide damping. Consequently, the whirl amplitude of the rotor between the bearings will get very large. This problem is especially severe at the third critical speed.

The shape of the overhung mass is also important in the way it influences the so-called gyroscopic effect. The dynamic forces on relatively thin disks like a turbine wheel tend to exert a stiffening effect on the rotor at high speed and raise the critical speed. Relatively long cylindrical masses like an alternator rotor have an opposite effect and lower the critical speed. As will be shown in subsequent chapters, the factor which determines which type of behavior will occur is the relative magnitude of the polar and transverse moments of inertia of the mass.

To arrive at a final rotor design requires detailed calculations and the incorporation of the bearing characteristics. The choice of bearing type and dimensions is largely governed by the properties of the available lubricant, the operating environments, the speed of the rotor, the load imposed on the bearings and the dynamic performance of the bearings, including stability. A more detailed discussion is given in the next chapter which also describes the various bearing types for which data are available in this manual.

Once the preliminary lay-out of the rotor and its bearings is established, the spring and damping coefficients for the bearings can be determined from the design charts, (see Figs. B-1 to B-12A), and a calculation of the critical speeds can be performed, usually by means of a computer program. If the operating speed is too close to any of the critical speeds, the rotor or the bearing design must be modified. To assist in this evaluation, the design charts, Figs. D-1 to D-20 can be used to determine the effect of bearing type and bearing dimensions on the critical speeds.

Knowing the dynamic bearing coefficients also makes it possible to check the stability of the rotor-bearing system. For this purpose a computer program may be employed or the design charts, Figs. C-1 to C-17, can be used. This is discussed in detail in a later chapter.

Finally, the magnitude of the rotor whirl amplitude and the corresponding dynamic bearing loads due to a rotor unbalance should be estimated. Thereby the sensitivity of the rotor to the location of the unbalance can be evaluated and the required balance level can be established. The calculations are normally performed by a computer program but an overall estimate can be obtained from Figs. D-21 to D-40 in which the effect of both static and dynamic unbalance is presented.

The subsequent chapters are devoted to a detailed discussion of each of the steps in the outlined design procedure and to a description of the presented design charts.

THE SELECTION OF BEARING TYPE AND BEARING DIMENSIONSDescription of Bearing Types

The wide variety of machinery applications has produced numerous bearing types to suit the different requirements. A representative selection of such bearing types are treated in the present report as summarized in Fig. 6. A brief description of each type is given below:

a. The Plain Cylindrical Bearing (See Fig. 7) is the simplest of all journal bearing types. Its performance characteristics are well established and extensive design information is available. Hence, the cylindrical bearing plays an important role in the study and analysis of rotor-bearing systems. Its practical application, on the other hand, is generally limited to the gas lubricated bearing. To make the plain cylindrical bearing practical for oil lubrication or other liquid lubricants it is necessary to provide the bearing with grooves or holes through which to supply the lubricant. Sometimes a single, circumferential groove in the middle of the bearing is used, and in other cases one or several axial grooves are provided.

b. The 4-Axial Groove Bearing (See Fig. 7) is one of the commonly used oil lubricated bearing types. It is a cylindrical bearing provided with four oil supply grooves. The oil is supplied at a nominal gage pressure which ensures an adequate oil flow and thereby some cooling of the bearing. Occasionally the grooved bearing has been used in gas bearing applications in order to improve the bearings stability but this case is not considered here.

c. The Elliptical Bearing (See Fig. 8) is another typical example of an oil lubricated bearing. It is especially used in gear and turbine applications. As a bearing type it is classified as a lobed bearing in contrast to a grooved bearing. Whereas the grooved bearing consists of a number of partial arcs with a common center the lobed bearing is made up of partial arcs whose centers do not coincide. Thus, the elliptical bearing consists of two partial arcs where the bottom arc has its center a distance $m \cdot C$ above the bearing center and vice versa for the top arc (see Fig. 8). Here C is the bearing clearance and m is called the ellipticity. The value of m is between 0 and 1. By this arrangement the bearing is preloaded which means that the journal center eccentricity

with respect to the loaded arc is increased and never becomes zero. Thereby the bearing is stiffened and its stability is somewhat improved.

d. The Partial Bearing (See Fig. 8) is in general not a practical bearing in itself. However, having available partial bearing data allows combining the partial arcs into a variety of grooved and lobed bearing configurations. The present report treats 4 partial bearing configurations: 50, 60, 80 and 100 degree arc, (the centrally loaded partial bearing). The lubricant is in all cases a liquid and the bearing film is laminar except for the 100 degree arc where turbulent flow is also considered.

e. The Tilting Pad Bearing (See Fig. 9) is widely used in high speed applications where hydrodynamic instability and misalignment are problems. The tilting pad bearing consists of a number of shoes, each shoe actually being a partial bearing, which are mounted on pivots. Hence, the shoes are free to adjust and to follow the motions of the journal. In this way the tilting pad bearing ensures inherent stability as long as the mass inertias of the shoes do not interfere with the adjustment ability of the bearing. In the present report the 3, 4, 5 and 6-shoe tilting pad bearing are considered. The load direction may either pass between the two bottom shoes ("load between pads") or it may pass through the pivot of the bottom shoe ("load on pad"), (see Fig. 9). The lubricant is incompressible (liquid) and the lubricant film is laminar. For the 3 and 4-shoe bearing, turbulent flow is also considered.

f. The Hydrostatic Bearing (see Fig. 10) finds application where the bearing load is very high, when a very stiff bearing is required or where the rotor speed is too low to allow the bearing to operate hydrodynamically. The lubricant is pressure fed to the bearing through flow restricted feeding holes and, thus, the bearing requires equipment to furnish the flow such as a pump, a compressor or an accumulator. In the present case the gas lubricated hydrostatic bearing is considered.

g. The Ball Bearing offers the advantage of compactness, simple lubrication requirements and relatively high speed capability. However, its operational life is limited. Since the ball bearing as a bearing type is entirely different from

the fluid film bearing types the design data and performance data for the ball bearing are given in a separate report.

Selection of Bearing Type

At a very early stage of the design it is necessary to choose the bearing type. Unfortunately, the choice is governed by many factors and it is dangerous to give any general rules on which to base the selection. Most frequently the bearing type is chosen on the basis of steady state performance; load carrying capacity, lubricant flow requirements, friction power loss, etc. but in many applications it is also necessary to consider the dynamical performance; dynamic load, stiffness, damping and stability. Since the present report is concerned with rotor-bearing dynamics it is not possible within this scope to also treat the rather large subject of bearing performance and design for steady state operation. Reference shall instead be given to the published literature among which References 3 & 4 may serve as representative examples. However, a brief summary will be given of the major considerations affecting the selection of the bearing type:

1. The Lubricant

Examples of lubricants are: oils, gases, liquid metals, water, vapour, etc. The choice of lubricant is dictated by what can be made available, the required auxiliary equipment, and the operating conditions as discussed later. The lubricant must be chemically stable in the operating temperature range, and if the environment is radioactive conventional lubricants are affected. From a purely lubrication point of view the most important lubricant characteristic is its viscosity and its boundary lubrication ability. For oils and most liquids the viscosity is strongly dependent on temperature and it decreases with increasing temperature. For gases the viscosity increases with temperature but the effect is not nearly as pronounced. The density-to-viscosity ratio is sometimes of importance especially with low kinematic viscosity fluids such as liquid metals, and the higher the ratio the more is the bearing likely to operate in the turbulent regime.

2. Rotor Speed

From a functional point of view there are three most commonly used bearing

types: the hydrodynamic (self-acting) bearing, the hybrid (externally pressurised with rotation) bearing, and rolling element bearings. The first two types are fluid film bearings where the rotor surface is separated from the bearing surface by a thin film of lubricant. The hydrodynamic bearing works as a viscous pump and its load carrying capacity is, therefore, proportional to the lubricant viscosity and the rotor speed. The hydrostatic bearing, on the other hand, carries its load by means of the pressure at which the lubricant is supplied. Thus, for very low speeds or where the load is very high the hydrostatic bearing should be used (alternatively a rolling element bearing). For moderately high speeds the liquid lubricated hydrodynamic bearing can be used, the latter bearing having the advantage at higher speeds due to its lower friction. For very high speeds the gas lubricated bearing should be applied.

3. Bearing Load

The bearing's load carrying capacity should be considered simultaneously with the rotor speed as discussed above. In fluid film bearings the maximum load carrying capacity is determined by specifying the minimum allowable film thickness taking into consideration the type of machinery application, possible dynamic loads and the size of possible dirt particles. With gas bearings and lubricants with low boundary lubrication ability there are certain limits imposed on the bearing load because of the dry friction and wear taking place during starting and stopping before the self-acting film has formed. If the load is too light, on the other hand, the bearing may be susceptible to hydrodynamic instability.

4. Friction Power Loss

The magnitude of the power loss in the bearing is frequently a major factor in deciding which bearing type to use. For fluid film bearings operating in the laminar regime the power loss is approximately given by:

$$\text{friction power loss} = \frac{\pi^3 \mu D^3 L N^2}{6600 \cdot C \cdot \sqrt{1-\epsilon^2}} \quad \text{HP}$$

where:
μ lubricant viscosity, lbs.sec/in²
N rotor speed, KPS
D journal diameter, inch
L bearing length, inch
C radial clearance, inch
ε eccentricity ratio = (journal center eccentricity)/(radial clearance)

For eccentricity ratios above .5 to .6 the actual power loss becomes a little higher. It is seen that the power loss increases with the square of the speed and the cube of the diameter. Thus, for high speed applications the use of an oil as the lubricant would necessitate a very small journal diameter. Thereby the rotor may become too flexible and instead it is necessary to choose a low viscosity lubricant like gas or, in some cases, liquid metal. In the latter case the bearing film frequently becomes turbulent with a corresponding increase in the power loss.

5. Operating Temperature

If the bearing operates at an elevated temperature a conventional hydrocarbon oil bearing is no longer feasible and instead a special oil or a gas bearing (in special cases a liquid metal bearing) must be used. For very low temperatures oils again are not available and the gas bearing may be applied. Apart from affecting the choice of lubricant the operating temperature also affects the selection of the bearing and shaft materials and configuration. Thus, elevated temperatures are in general accompanied by appreciable thermal gradients with corresponding distortions of the bearing geometry. It is, therefore, important to select a bearing type which is not too sensitive to thermal distortions or which can be provided with means to ensure a uniform temperature distribution.

6. Dynamic Load

In addition to the static load a bearing is also subjected to some dynamic load, for instance, unbalance forces or shock forces. Actually, the magnitude of the dynamic forces cannot be established prior to the design of the rotor-bearing system since they depend on the rotor mass, the rotor flexibility and the dynamic properties of the bearing. Even so, they should be estimated and taken into account in selecting the bearing for the application.

7. Bearing Stiffness and Damping

The bearing stiffness greatly influences the critical speeds of the rotor-bearing system. The critical speeds, in turn, are of major importance in determining the operating speed range of the rotor. As a general rule: the higher the number of critical speeds in the speed range, the more difficult becomes the operation

of the rotor and the more difficult it is to balance the rotor. Furthermore, if the unit is not a variable speed machine the design speed should be removed from the closest critical speed by at least 10 to 20 per cent. Knowing the critical speeds, however, is only sufficient in establishing those speeds at which a relatively high rotor whirl amplitude can be expected. To evaluate the amplitude it is also necessary to consider the bearing damping. To assist in comparing various bearing types on the basis of their influence on the critical speeds and the corresponding whirl amplitudes, several design charts have been prepared as discussed later.

8. Rotor-Bearing Stability

The necessity of avoiding hydrodynamic instability is frequently a determining factor in selecting the bearing type. Thus, in most high speed gas bearing applications the tilting pad bearing will be preferred over other bearing types because of its very high threshold speed. Design charts for determining the onset of instability for several bearing types are included in the present report and will be discussed later.

In any given application the considerations listed above enter into selecting the bearing type. The final choice must be based on a numerical evaluation of each of the factors. The present report gives data and methods for evaluating the factors connected with the dynamical performance and the stability of the rotor-bearing system. Data for the steady-state performance is available elsewhere, for instance Refs. 3 & 4.

Selection of Bearing Dimensions

In most cases it is difficult to separate the selection of the bearing type from the selection of the bearing dimensions. In dimensioning and designing the bearing the same factors must be considered as previously discussed for selecting the bearing type. Among the factors the dynamical performance will be treated in subsequent sections and in the following a brief discussion will be given of design data for calculating the bearings load carrying capacity. The discussion is concerned with fluid film bearings; ball bearings are treated in a separate report.

The design data for load carrying capacity are given in Figs.A-1 - to A-14. They are in dimensionless form such that they cover a wide variation in design conditions. The governing dimensionless parameters are summarized in Fig. 11 and will be further defined below.

For liquid lubricants (incompressible lubricants) there are 4 dimensionless parameters:

Length-to-diameter ratio:	L/D	Laminar
Sommerfeld Number:	$S = \frac{WNDL}{\mu} \left(\frac{L}{C}\right)^2$	
Eccentricity ratio:	$e = e/C$	
Reynolds Number:	$Re = \frac{\rho NDC}{\mu}$	Turbulent

where:

L - Bearing length, inch

D - Journal diameter, inch

R = $\frac{1}{2} D$, Journal radius, inch

C - Radial clearance, inch

e - Journal eccentricity, inch

N - Rotor speed, RPS

W - Bearing load, lbs.

μ - Lubricant viscosity, lbs.sec/in^2

ρ - Lubricant mass density, $\text{lbs.sec}^2/\text{in}^4$

The radial clearance C is always the difference between the radius of curvature of the bearing surface and the journal radius R. The journal eccentricity e is the distance between the journal center and the bearing center.

For the elliptical bearing an additional parameter enters, namely the ellipticity m. It is defined as the distance between the lobe center and the bearing center divided by the radial clearance C, see Fig. 8. Similarly, in a tilting pad bearing the center of curvature for the shoes may not coincide with the bearing center in which case a similar parameter is required as for the elliptical bearing. For the tilting pad bearing this parameter is known as the preload factor: $(1-C'/C)$. This factor is zero in all the design data for load carrying capacity.

Figs. A-1 to A-11 give the eccentricity ratio or the minimum filmthickness as a function of the Sommerfeld number for various bearing types and geometries, all with liquid lubricants. Under specified operating conditions and with known bearing dimensions the Sommerfeld number can be computed and the corresponding eccentricity ratio (or minimum filmthickness) can be found from the charts. In the cases where the eccentricity ratio is given, the minimum filmthickness can be found from:

$$\text{minimum film thickness} = C \cdot (1-\epsilon)$$

For each of the three tilting pad bearings there are 2 charts. The first chart (Figs. A-6, A-8 and A-10) gives the relationship between eccentricity ratio and Sommerfeld number. The eccentricity ratio is denoted as ϵ_B to emphasize that it applies to the complete bearing, not to the individual pads. The second chart (Figs. A-7, A-9 and A-11) gives the filmthickness over the pivot for the bottom pads as a function of ϵ_B .

The charts for partial bearings (Figs. A-3 to A-5) may occasionally be useful in estimating the eccentricity ratio and minimum filmthickness for multi-groove or multi-lobe bearings. For multi-groove bearings a close estimate is obtained by assuming that the loads is carried solely by the bottom segment of the grooved bearing. To illustrate, it is seen from Fig. 7 that the bottom segment of the present 4-axial groove bearing configuration is 90 degrees. Hence, the eccentricity ratio for the 4-axial groove bearing, already covered by Fig. A-1, can also be obtained with good accuracy from Fig. A-5 which is valid for an 80 degree partial bearing. A similar procedure can be employed for a multi-lobe bearing but only at relatively high eccentricity ratios.

It should be emphasized, however, that the outlined method must be used with great caution and judgement since all the partial bearing data in the present handbook assume a centrally loaded pad. Furthermore, extensive data for eccentricity ratio and minimum filmthickness are already available elsewhere for several multi-groove and multi-lobe bearing configurations (see Ref. 3). Thus, the chief purpose of the presented partial bearing data is not so much to define the steady-state performance of the bearing but, rather, to make it possible to determine the eccentricity ratio at which the dynamic bearing coefficients are evaluated. This will be discussed later.

For the self-acting gas bearing the dimensionless design parameters are:

Length-to-diameter ratio: L/D

$$\text{Compressibility number: } \Lambda = \frac{12\pi \mu L}{P_a} \left(\frac{L}{C}\right)^2$$

Eccentricity ratio: $\epsilon = e/C$

Bearing load parameter: $W/P_a LD$

where:

P_a - Ambient Pressure, psia

and the other symbols have been defined above.

Figs. A-12 to A-14 allow determining the eccentricity ratio for the plain cylindrical gas bearing when the values of the compressibility number Λ and the load parameter are known.

For the hydrostatic gas bearing the operating eccentricity ratio can be calculated with good approximation from:

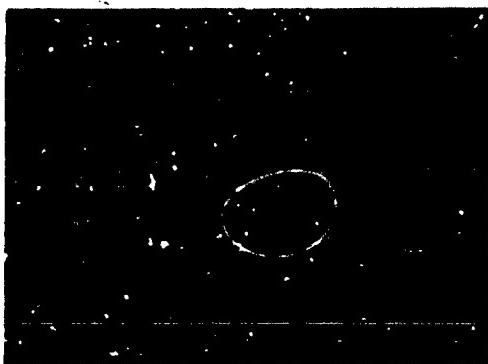
$$\epsilon = \frac{W}{CK} \quad (\epsilon < .5)$$

where K is the stiffness in lbs/in as determined from Figs. B-110 to B-122.

The calculation of K will be discussed later. The eccentricity ratio computed in this way should not exceed .4 to .5 in order to avoid lock-up.

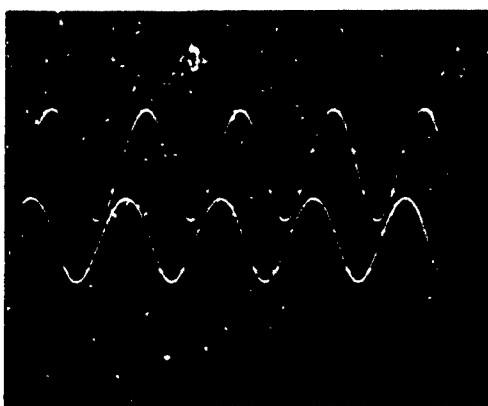
In general it is difficult to give specific rules for the smallest allowable value of the minimum film thickness. The choice is based on experience and is governed by such considerations as the size of possible dirt particles, the desired amount of cooling of the bearing and the maximum tolerable bearing surface temperature. As a rule, high speed ratios (e.g. centrifuges, high speed gears, superchargers, etc) will operate with a low eccentricity ratio ($\epsilon < .4$) while low speed gears, turbines, etc. will operate with a relatively high eccentricity ratio ($\epsilon = .4$ to .8). For further comments, consult Refs. 3 and 4.

On this basis the given design charts together with the formulae for the friction power loss can be used at least to arrive at a preliminary set of bearing dimensions.



Shaft Orbit

Scale: Vertical Axis - 24μ in./major div.
Horizontal Axis - 206μ in./major div.

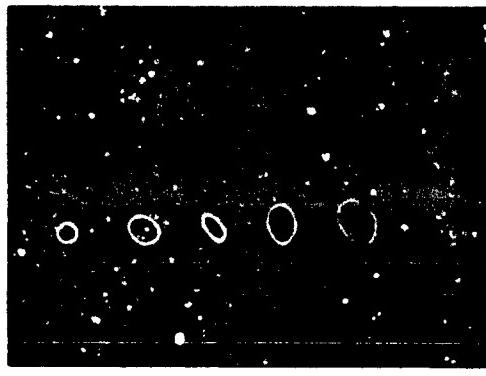


Top: Horizontal Amplitude (x-probe)
Bottom: Vertical Amplitude (y-probe)

Bearing No. 2, Probes:
Supply Pressure = 200 psig
Speed = 30,000 RPM

Bearing-to-Shaft, 50 μ m/cm
Ambient Pressure = 14.7 psia

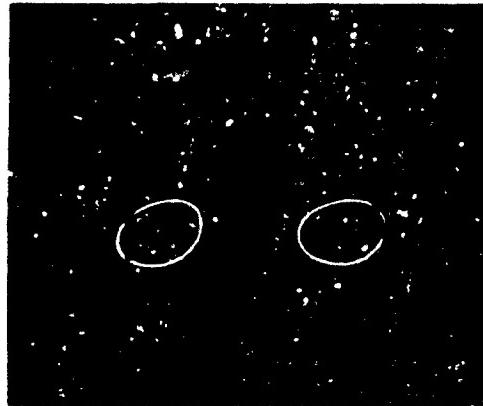
**Fig. 1 Synchronous Whirl due to Mechanical Unbalance
Hydrostatic Gas Bearing
Whirl Orbit and Corresponding Amplitude Components**



12,000 13,000 13,000 14,000 15,000 RPM

16,000 17,000 18,000 19,000 20,000 RPM

Scales: Vertical Axis - 24μ in./major div.
Horizontal Axis - 206μ in./major div.



Bearing No. 2, Probes:
Supply Pressure = 200 psig

Bearing-to-Shaft, 50 mv/cm
Ambient Pressure = 14.7 psia

Fig. 2 Synchronous Whirl due to Mechanical Unbalance
Hydrostatic Gas Bearing
Whirl Orbit as a Function of Rotor Speed

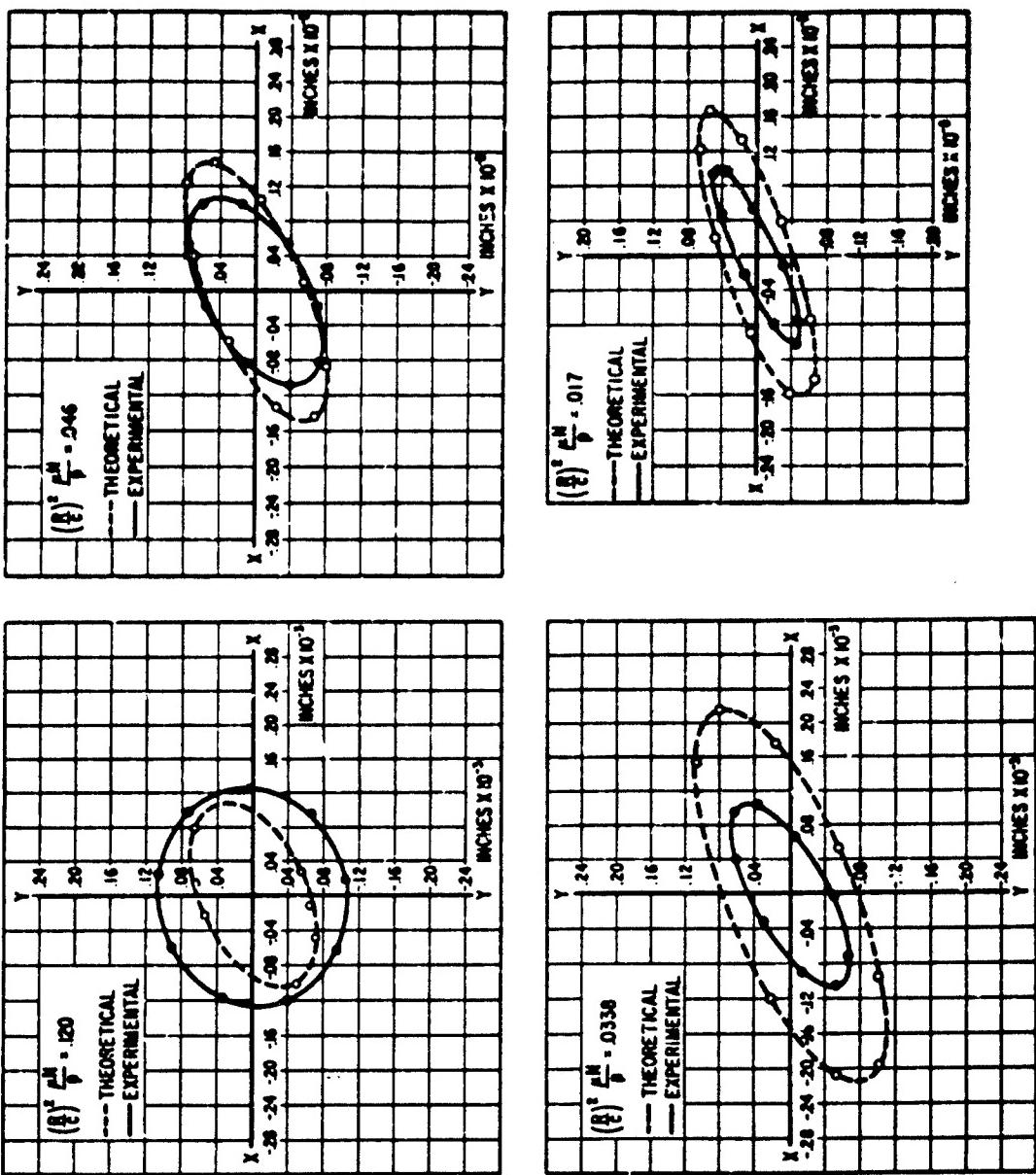


FIG. 3 Synchronous Whirl due to Mechanical Unbalance
100 Degree Partial Bearing, Turbulent Film, Reynolds No.=5420
Measured and Calculated Whirl Orbits

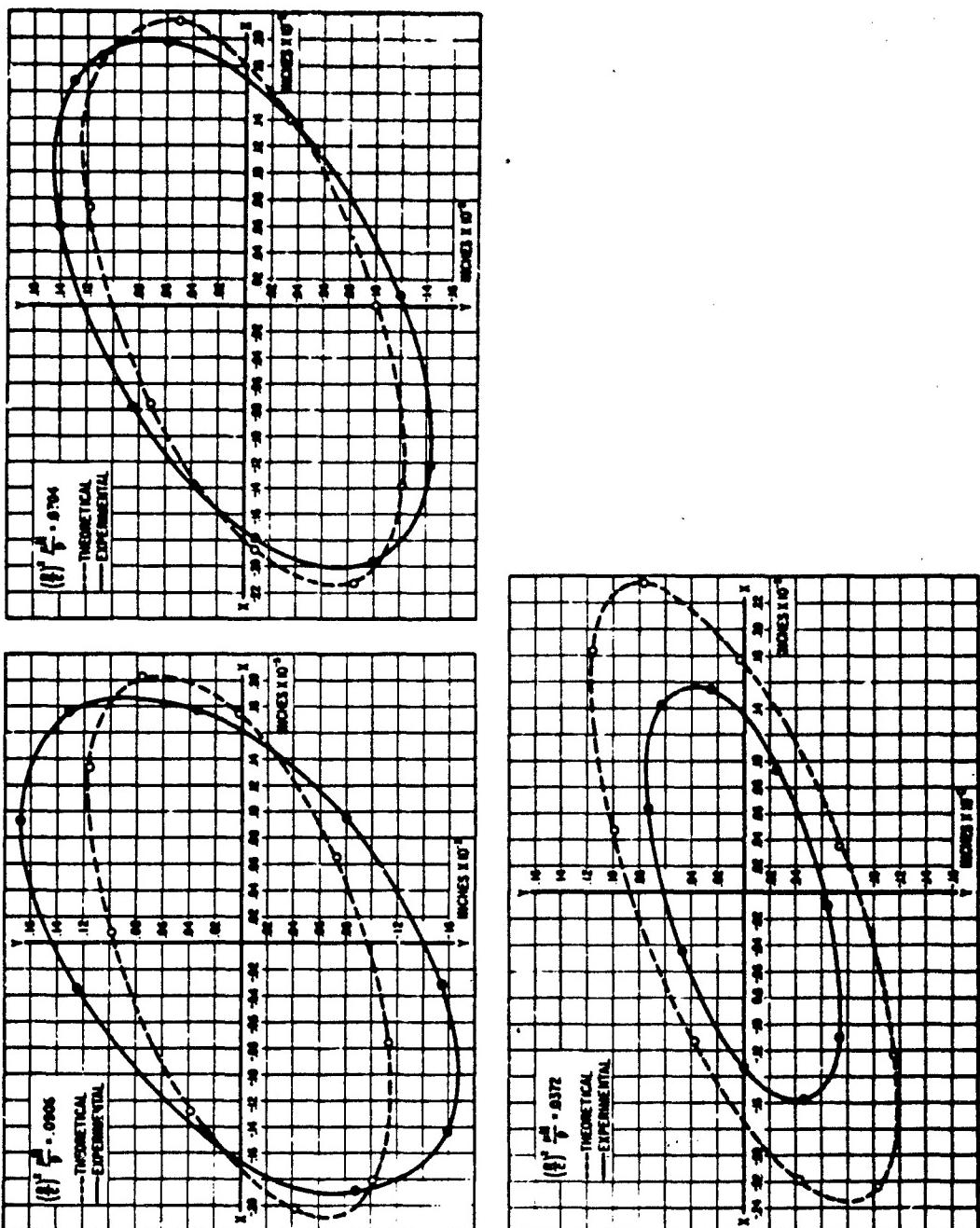
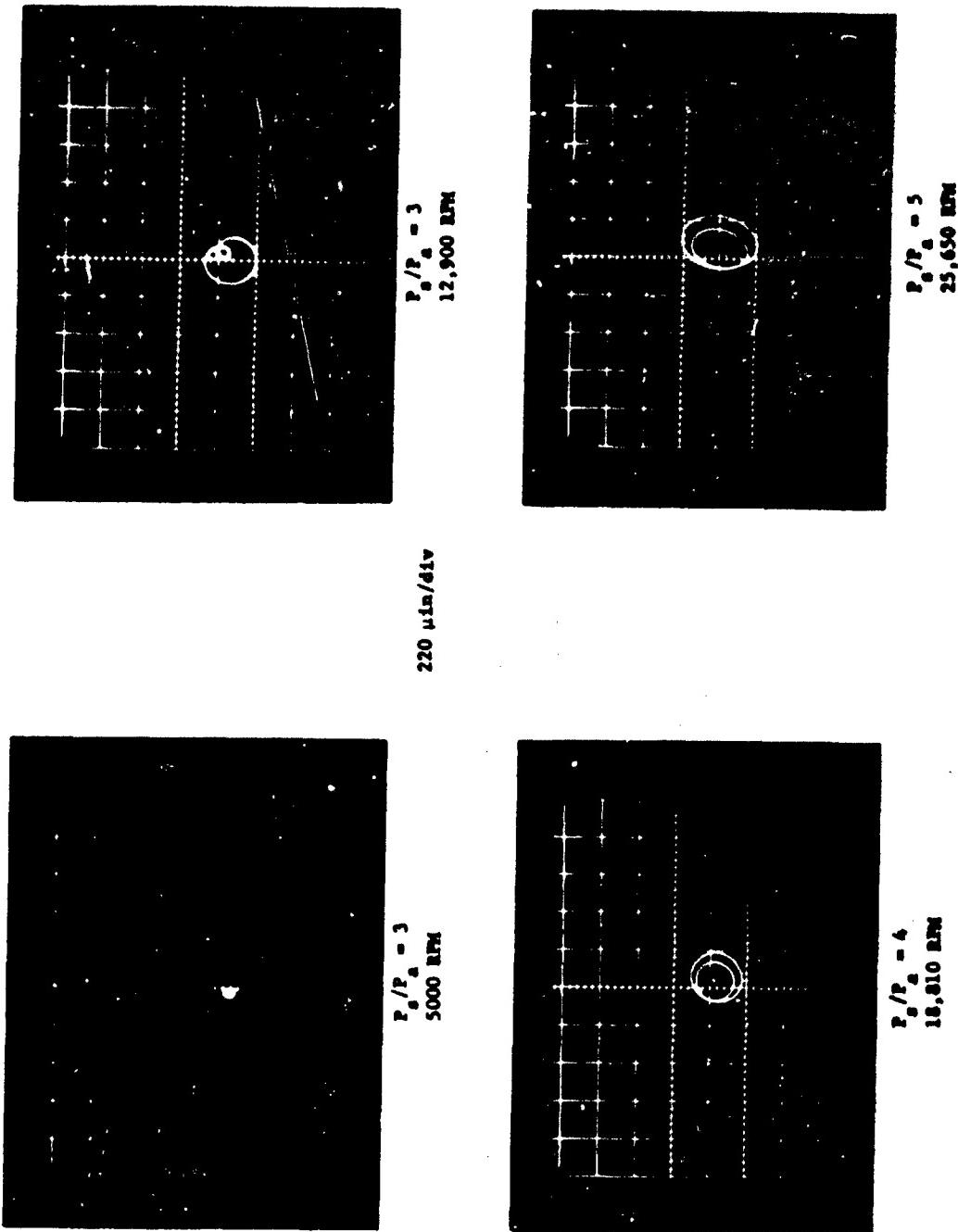


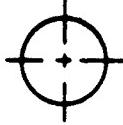
FIG. 4 Synchronous Whirl due to Mechanical Unbalance
100 Degree Partial Bearing, Turbulent Film, Reynolds No. = 314
Measured and Calculated Whirl Orbits

Fig. 5 "Onset of Hydrodynamic Instability (Fractional Frequency Whirl)
Hydrostatic Gas Bearing
Whirl Orbits

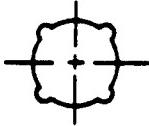


TYPES OF BEARINGS CONSIDERED

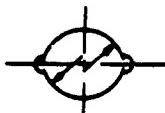
a. PLAIN CYLINDRICAL BEARING: LIQUID LUBRICATED - LAMINAR AND TURBULENT FILM
GAS LUBRICATED



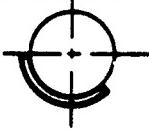
b. 4-AXIAL GROOVE BEARING LIQUID LUBRICATED - LAMINAR FILM



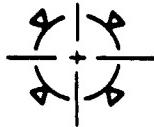
c. ELLIPTICAL BEARING LIQUID LUBRICATED - LAMINAR FILM



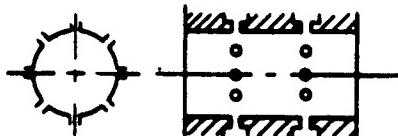
d. PARTIAL BEARING LIQUID LUBRICATED - LAMINAR AND TURBULENT FILM



e. TILTING PAD BEARING LIQUID LUBRICATED - LAMINAR AND TURBULENT FILM



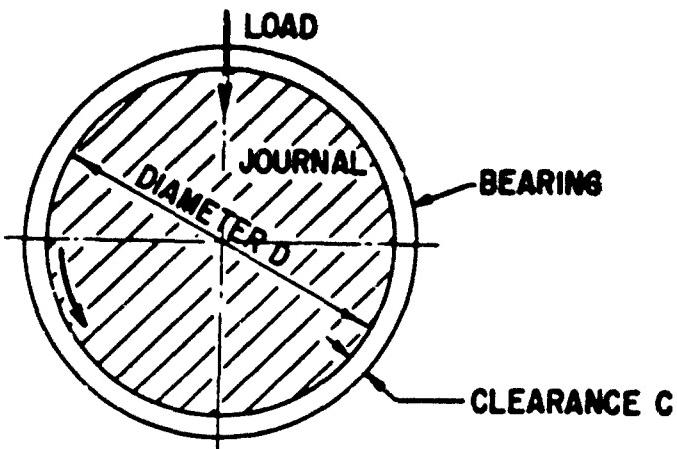
f. HYDROSTATIC BEARING GAS LUBRICATED



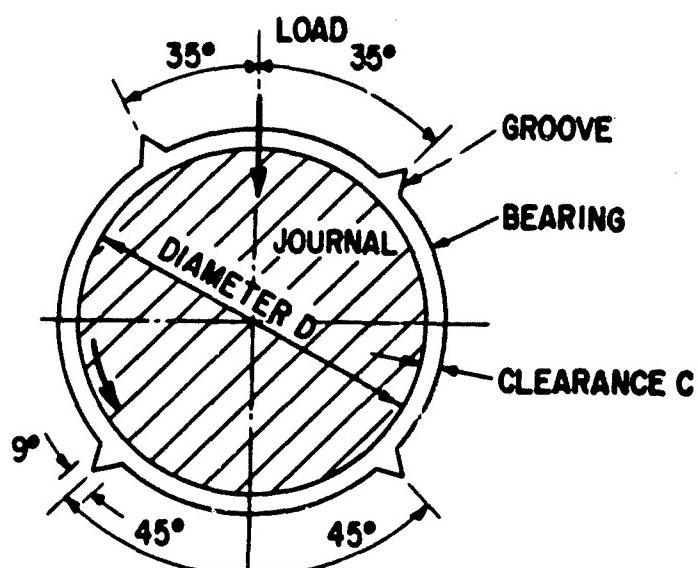
g. BALL BEARING



Fig. 6 A Schematic Summary of the Bearing Types
for which Data are given in the Report



PLAIN CYLINDRICAL BEARING



4-AXIAL GROOVE BEARING

Fig. 7 Geometry of the Plain Cylindrical Bearing
and the 4-Axial Groove Bearing

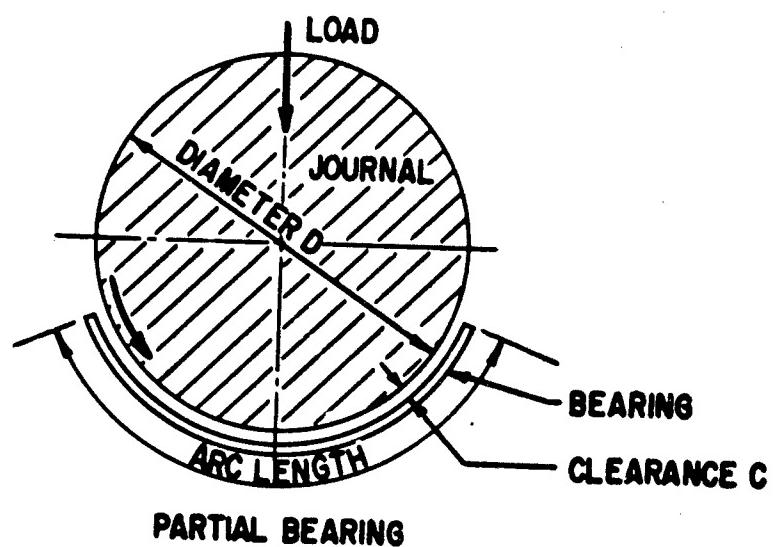
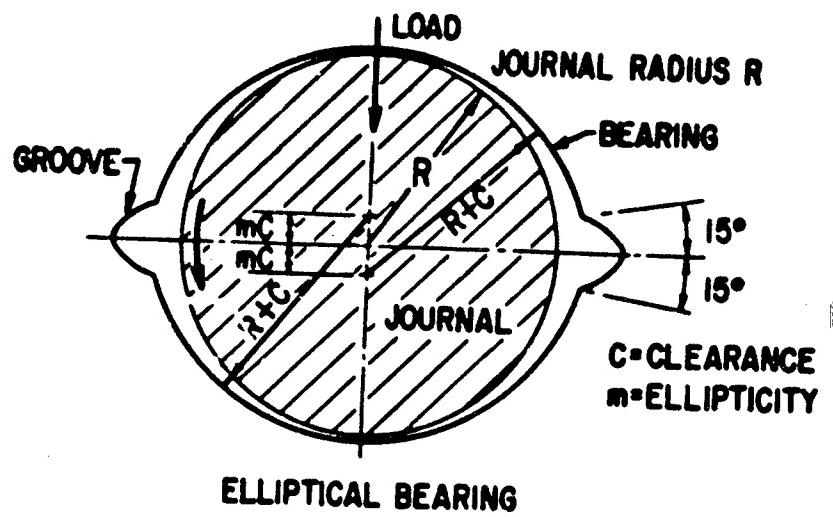


Fig. 8 Geometry of the Elliptical Bearing
and the Partial Bearing

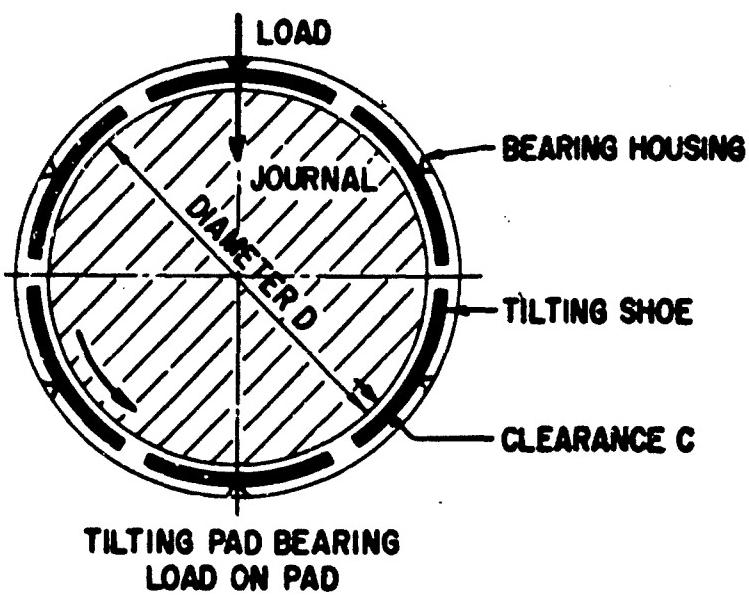
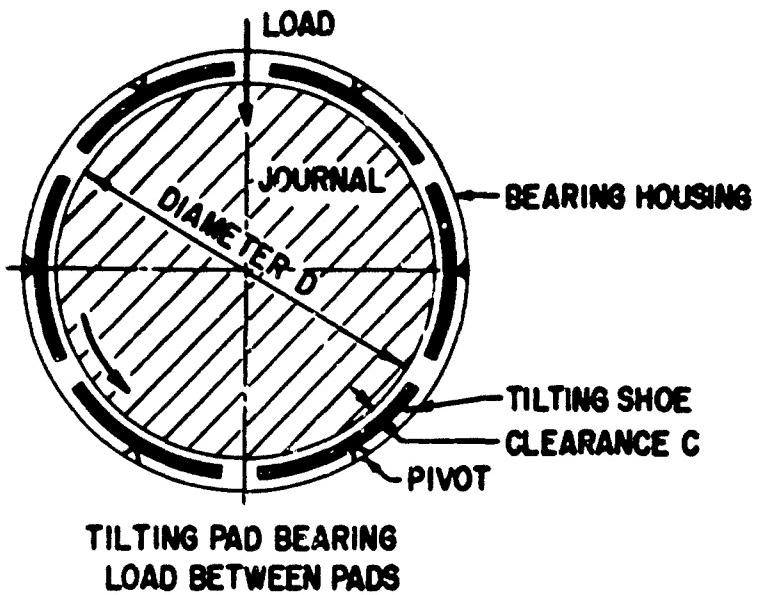


Fig. 9 Geometry of the Tilting Pad Bearing

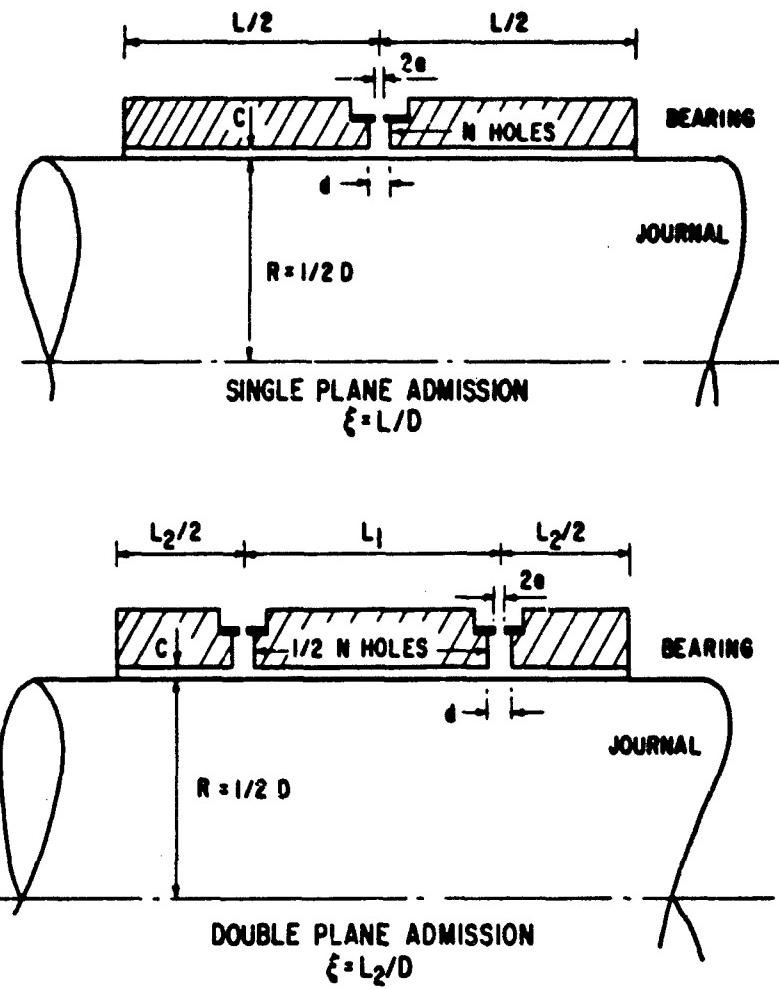


Fig. 10 Geometry of the Hydrostatic Bearing

GOVERNING, DIMENSIONLESS PARAMETERS

a. LIQUID LUBRICANT (INCOMPRESSIBLE)

INPUT PARAMETERS

$$\begin{cases} \text{LENGTH-TO-DIAMETER RATIO: } \frac{L}{D} \\ \text{SOMMERFELD NUMBER: } S = \frac{\mu N D L}{W} \left(\frac{R}{C} \right)^2 \\ \text{REYNOLDS NUMBER: } Re = \frac{\pi P D C}{\mu} \end{cases}$$

OUTPUT PARAMETERS

$$\begin{aligned} \text{SPRING COEFFICIENTS: } & \frac{c_{K_{11}}}{W}, \frac{c_{K_{12}}}{W}, \frac{c_{K_{21}}}{W}, \frac{c_{K_{22}}}{W} \\ \text{DAMPING COEFFICIENTS: } & \frac{c_{eC_{11}}}{W}, \frac{c_{eC_{12}}}{W}, \frac{c_{eC_{21}}}{W}, \frac{c_{eC_{22}}}{W} \\ \text{INSTABILITY PARAMETER: } & \frac{\sqrt{C_{WW}}}{\mu \alpha \left(\frac{R}{C} \right)^2} \end{aligned}$$

b. GAS LUBRICANT (COMPRESSIBLE)

INPUT PARAMETERS

$$\begin{cases} \text{LENGTH-TO-DIAMETER RATIO: } \frac{L}{D} \\ \text{BEARING NUMBER: } A = \frac{12 \pi L N}{F_d} \left(\frac{R}{C} \right)^2 \\ \text{LOAD: } \frac{W}{P_0 L D} \end{cases}$$

OUTPUT PARAMETERS

$$\begin{aligned} \text{SPRING COEFFICIENTS: } & \frac{c_{K_{11}}}{P_0 L D}, \frac{c_{K_{12}}}{P_0 L D}, \frac{c_{K_{21}}}{P_0 L D}, \frac{c_{K_{22}}}{P_0 L D} \\ \text{DAMPING COEFFICIENTS: } & \frac{c_{eC_{11}}}{P_0 L D}, \frac{c_{eC_{12}}}{P_0 L D}, \frac{c_{eC_{21}}}{P_0 L D}, \frac{c_{eC_{22}}}{P_0 L D} \\ \text{ECCENTRICITY RATIO: } & e \end{aligned}$$

$$\begin{aligned} \text{FEEDING PARAMETER: } & A_1 = \frac{6 \mu \bar{R}^2 \sqrt{RT}}{\rho_1 C^3} \\ \text{SUPPLY PRESSURE RATIO: } & \frac{P_1}{P_0} \end{aligned}$$

$$\text{INSTABILITY PARAMETER: } \frac{W_0}{\mu^2 L \left(\frac{R}{C} \right)^3}$$

Fig. 11 Table of Dimensionless Design Parameters

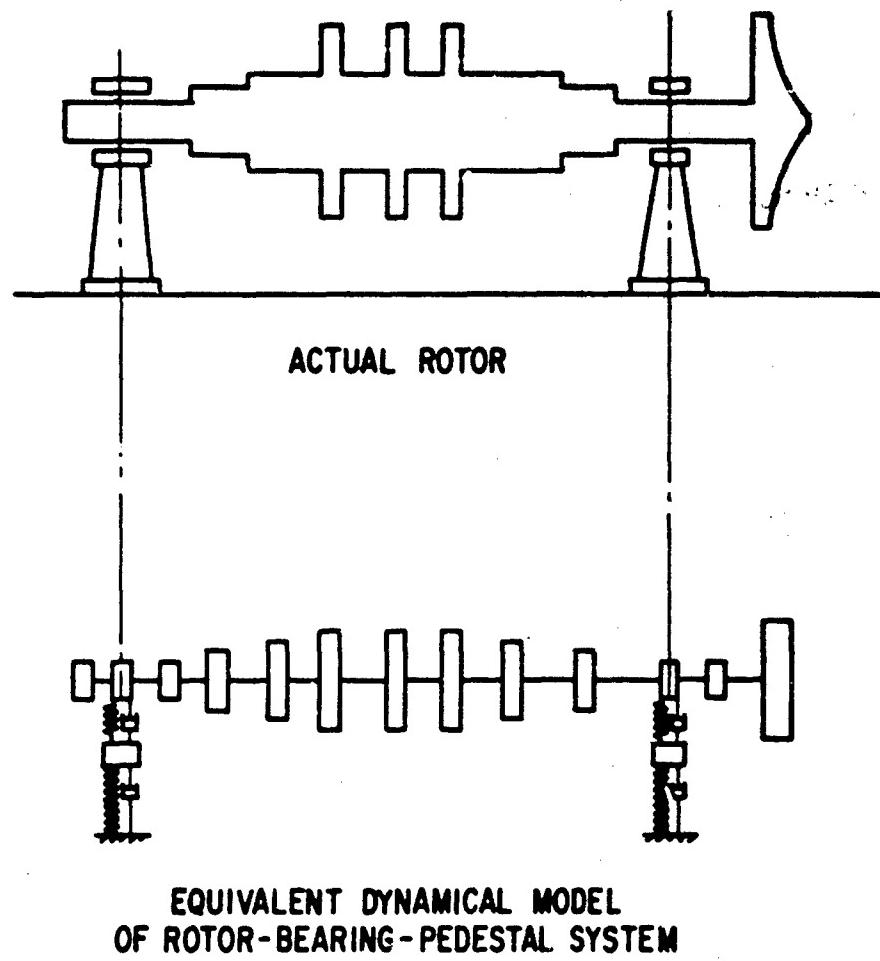
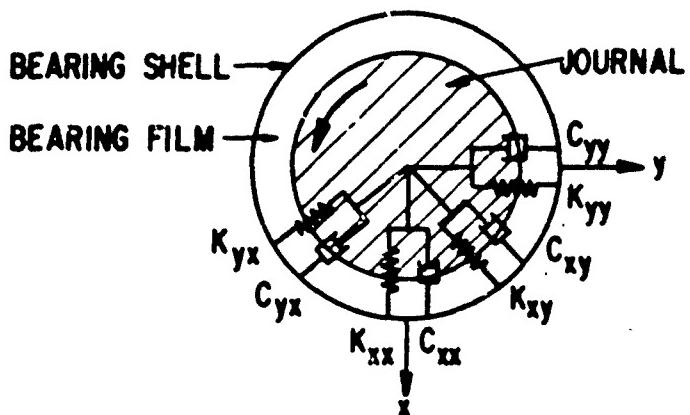
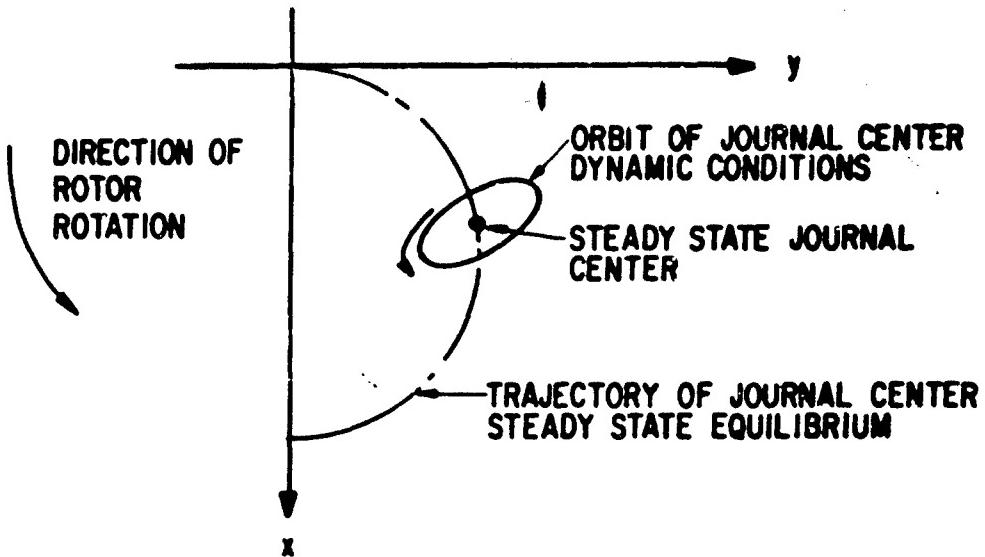


Fig. 12 Dynamical Model of Rotor-Bearing System

REPRESENTATION OF THE BEARING FILM UNDER DYNAMIC CONDITIONS



BEARING SPRING AND DAMPING COEFFICIENTS



DYNAMICAL-MOTION OF JOURNAL CENTER

Fig. 13 Dynamical Model of the Bearing Fluid Film

DESIGN CHARTS FOR
LOAD CARRYING CAPACITY OF FLUID FILM BEARINGS

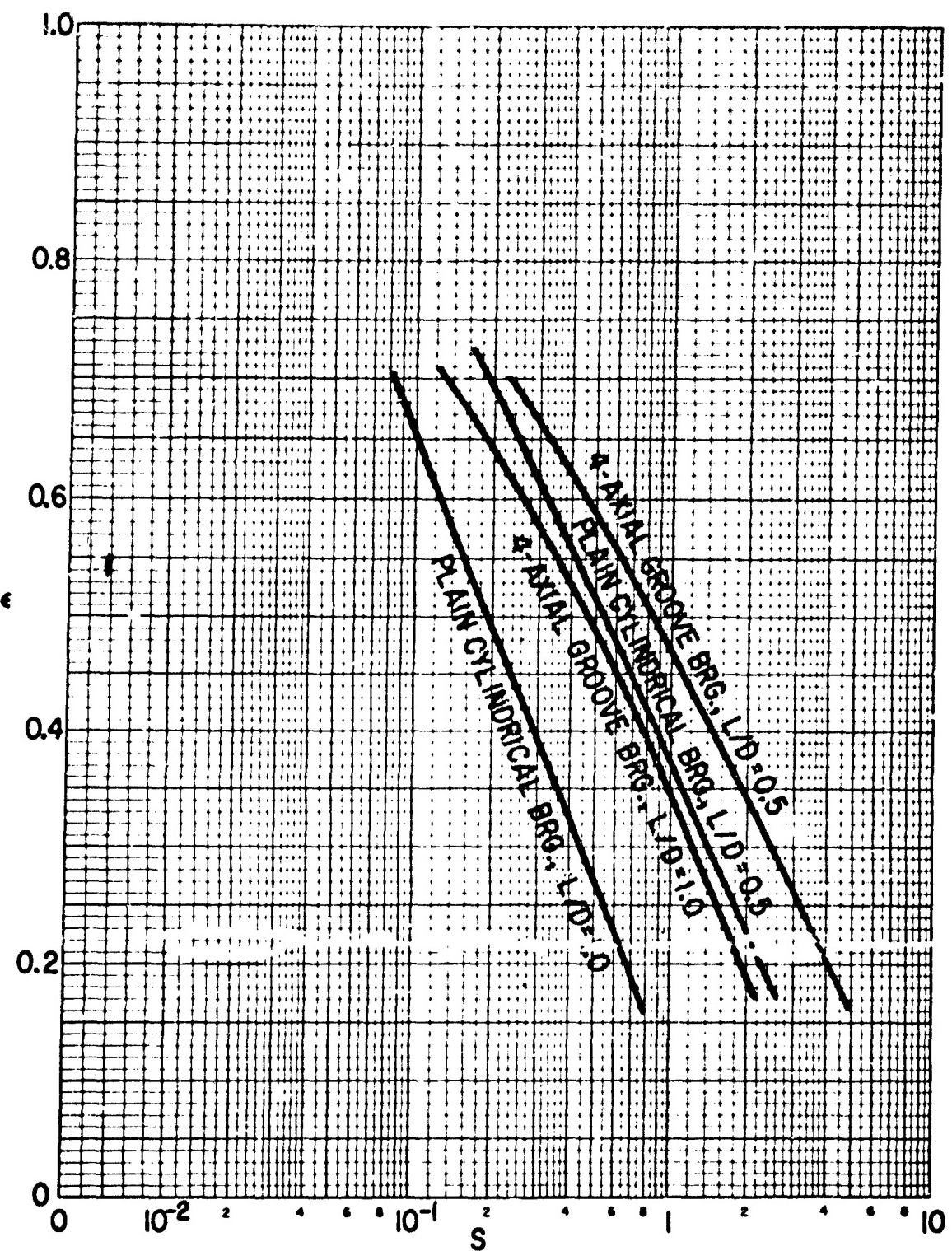


Figure A-1 The Plain Cylindrical and the 4-Axial Groove Bearing
Laminar Film
Eccentricity Ratio vs. Sommerfeld Number

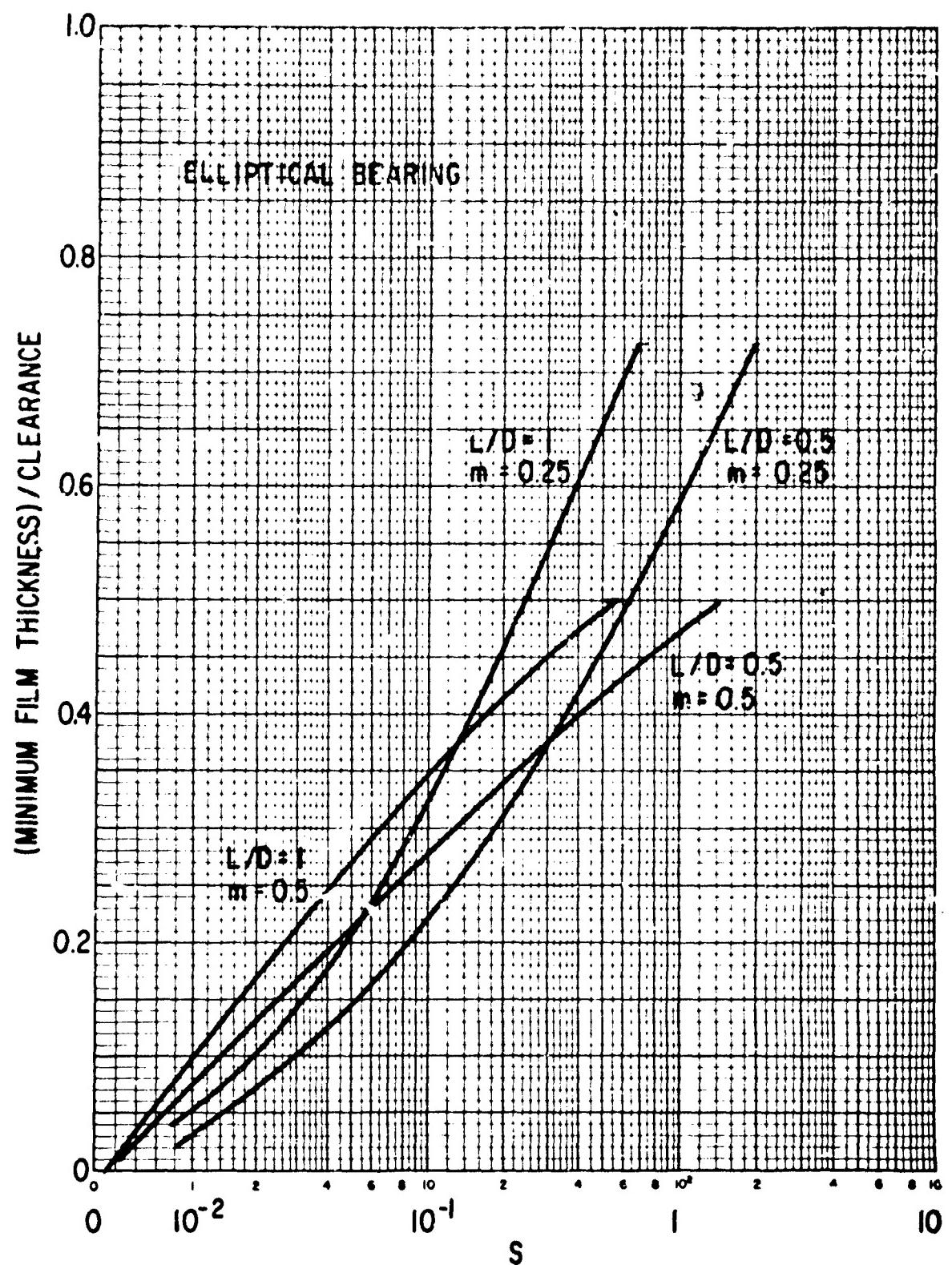


Figure A-2 The Elliptical Bearing
Laminar Film
Eccentricity Ratio vs. Sommerfeld Number

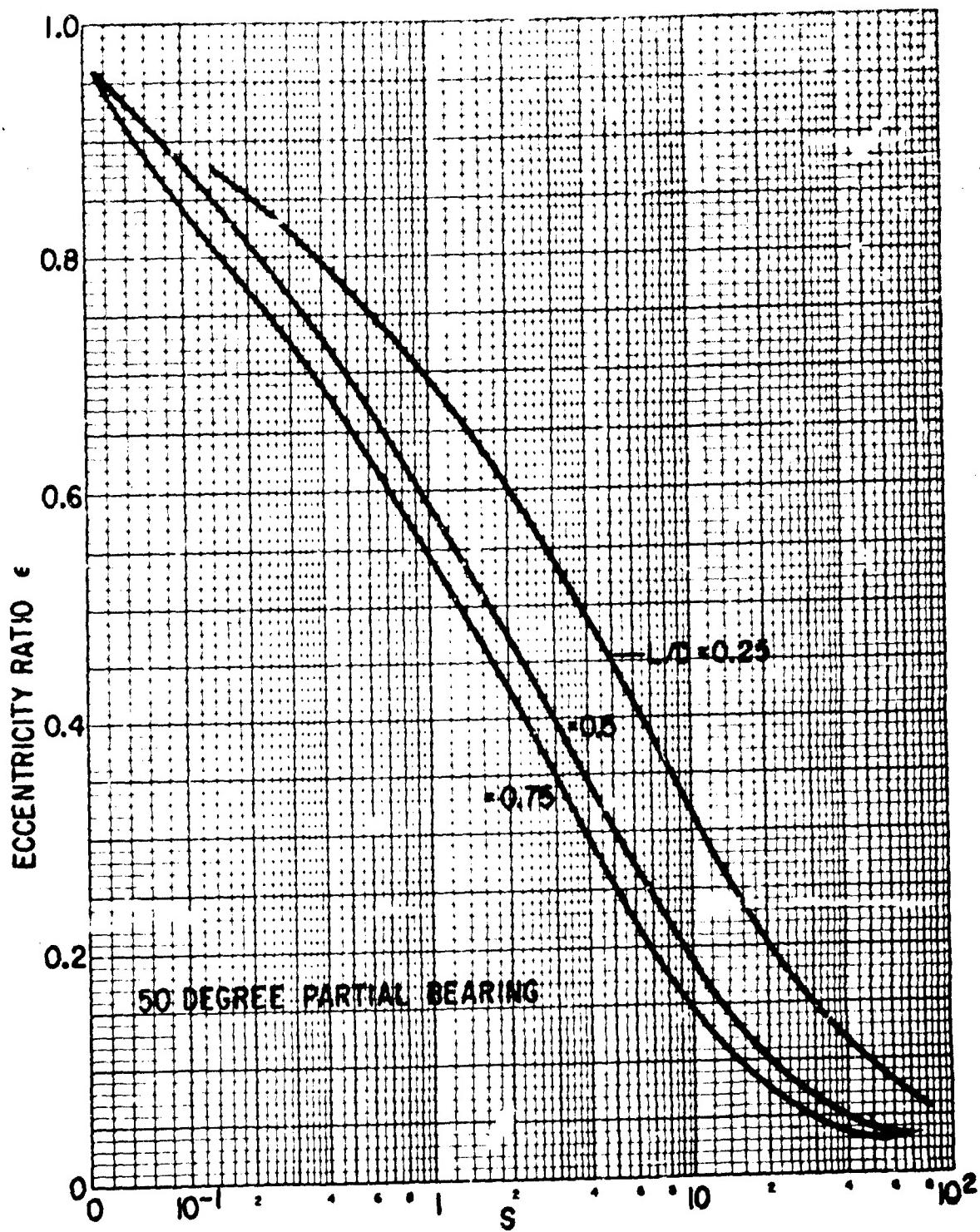
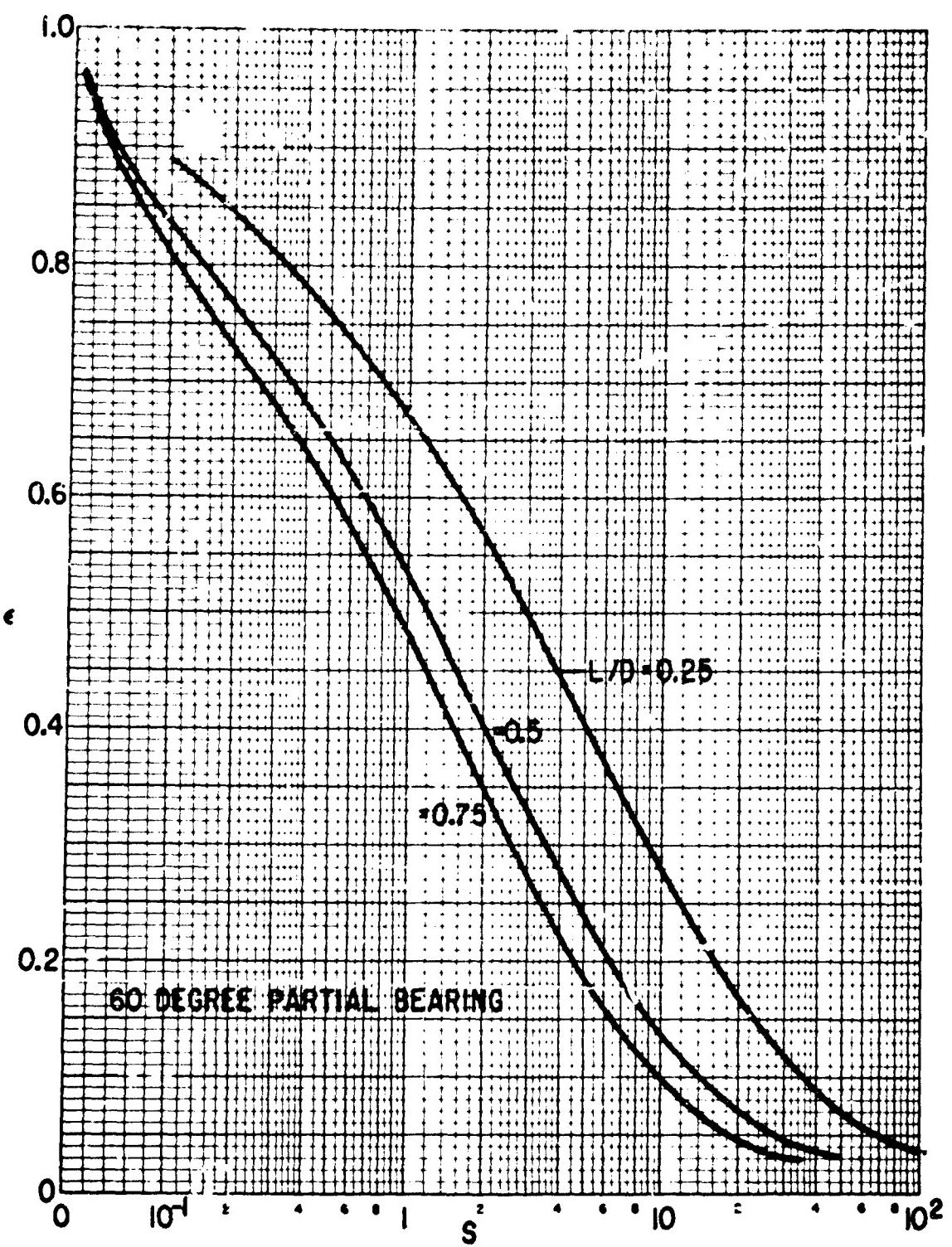


Figure A-3 The 50 Degree Partial Bearing, Centrally Loaded
Laminar Film
Eccentricity Ratio vs. Sommerfeld Number



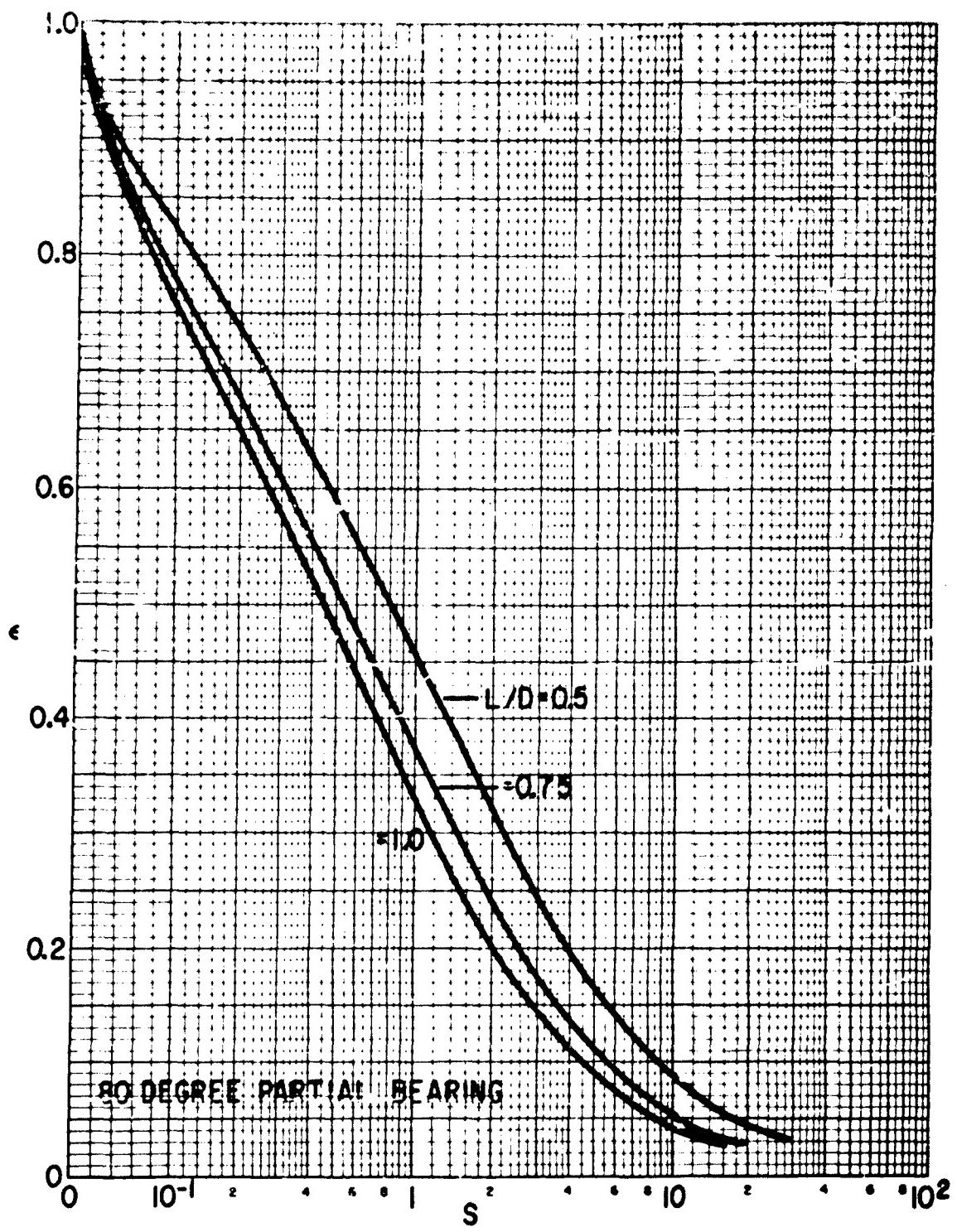


Figure A-5 The 80 Degree Partial Bearing, Centrally Loaded
Laminar Film
Eccentricity Ratio vs. Sommerfeld Number

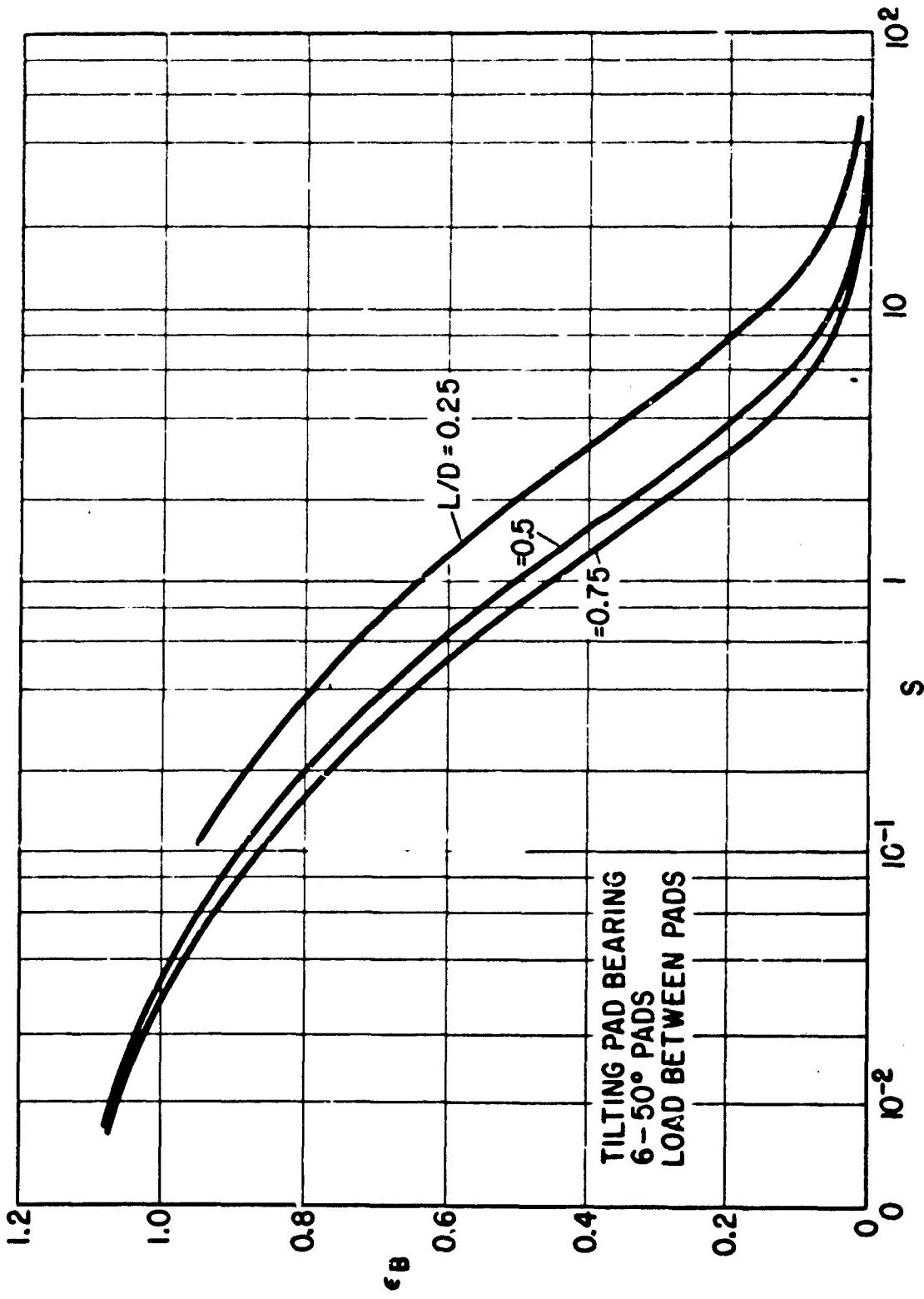


Figure A-6 The 6 Shoe Tilting Pad Bearing, Load between Pads
Lamellar Film
Eccentricity Ratio vs. Sommerfeld Number

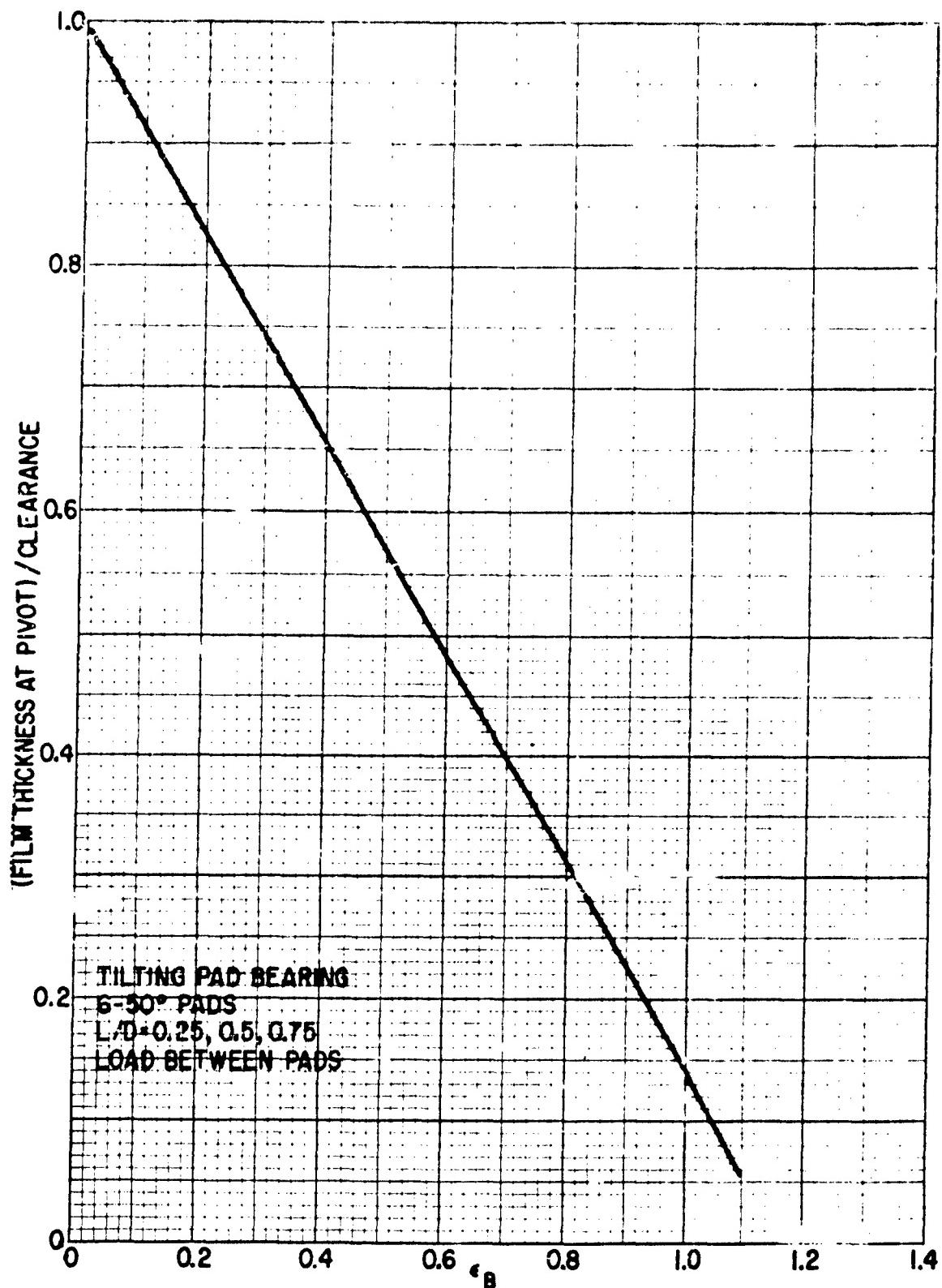


Figure A-7 The 6 Shoe Tilting Pad Bearing, Load between Pads
 Laminar Film
 Film thickness at Pivot vs. Eccentricity Ratio

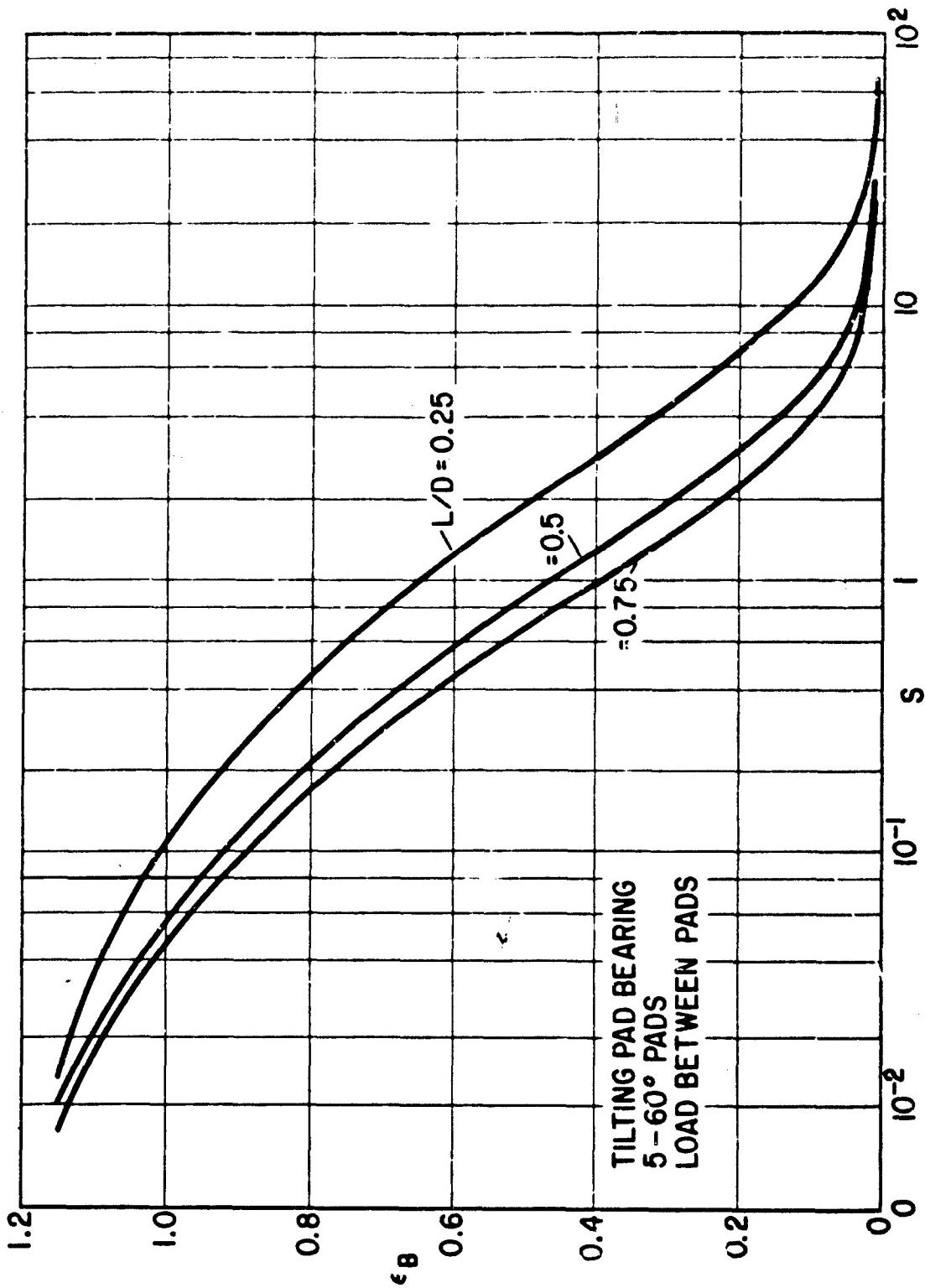


Figure A-8 The 5 Shoe Tilting Pad Bearing, Load between Pads
 Laminar Film
 Eccentricity Ratio vs. Sommerfeld Number

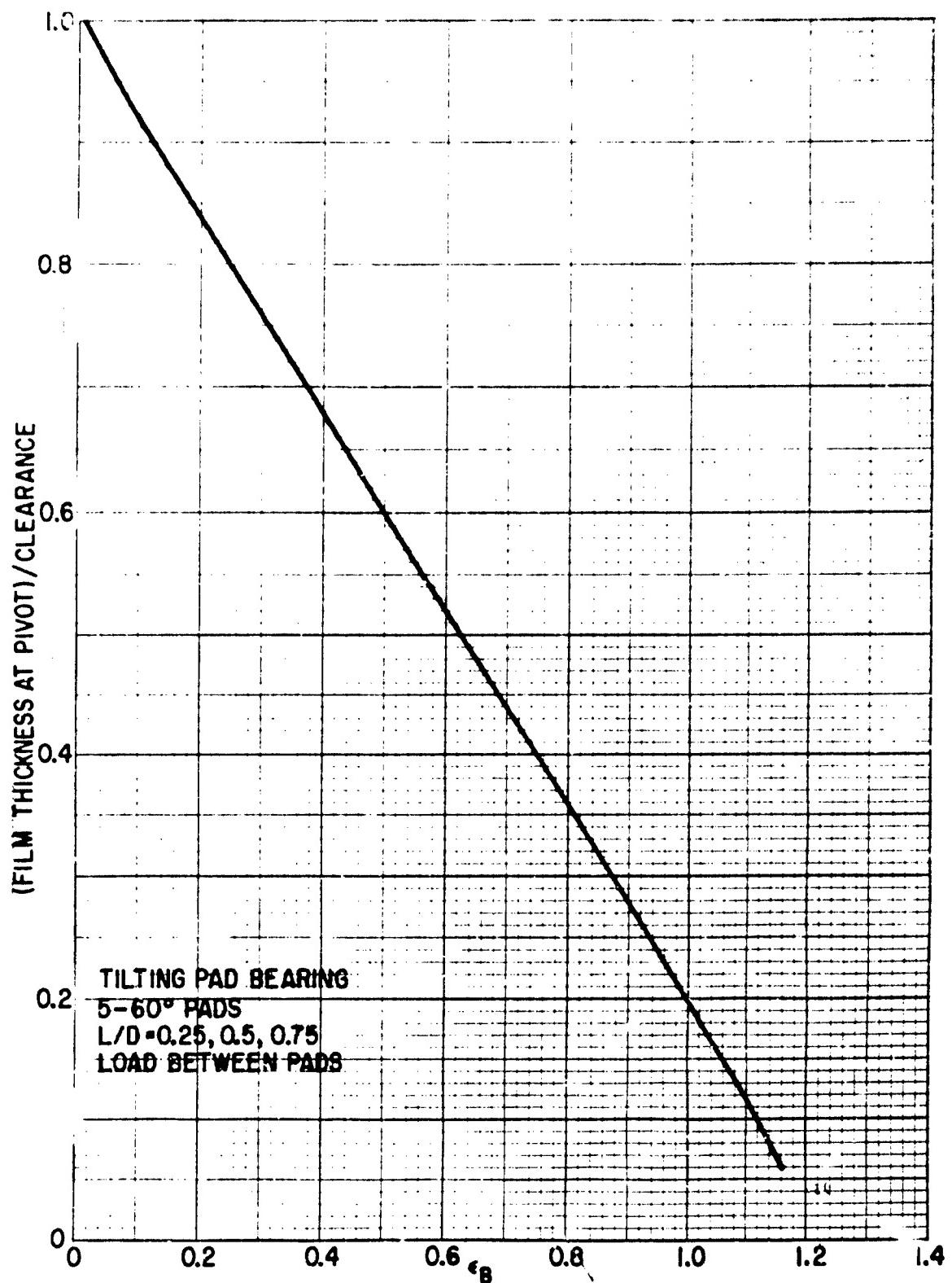
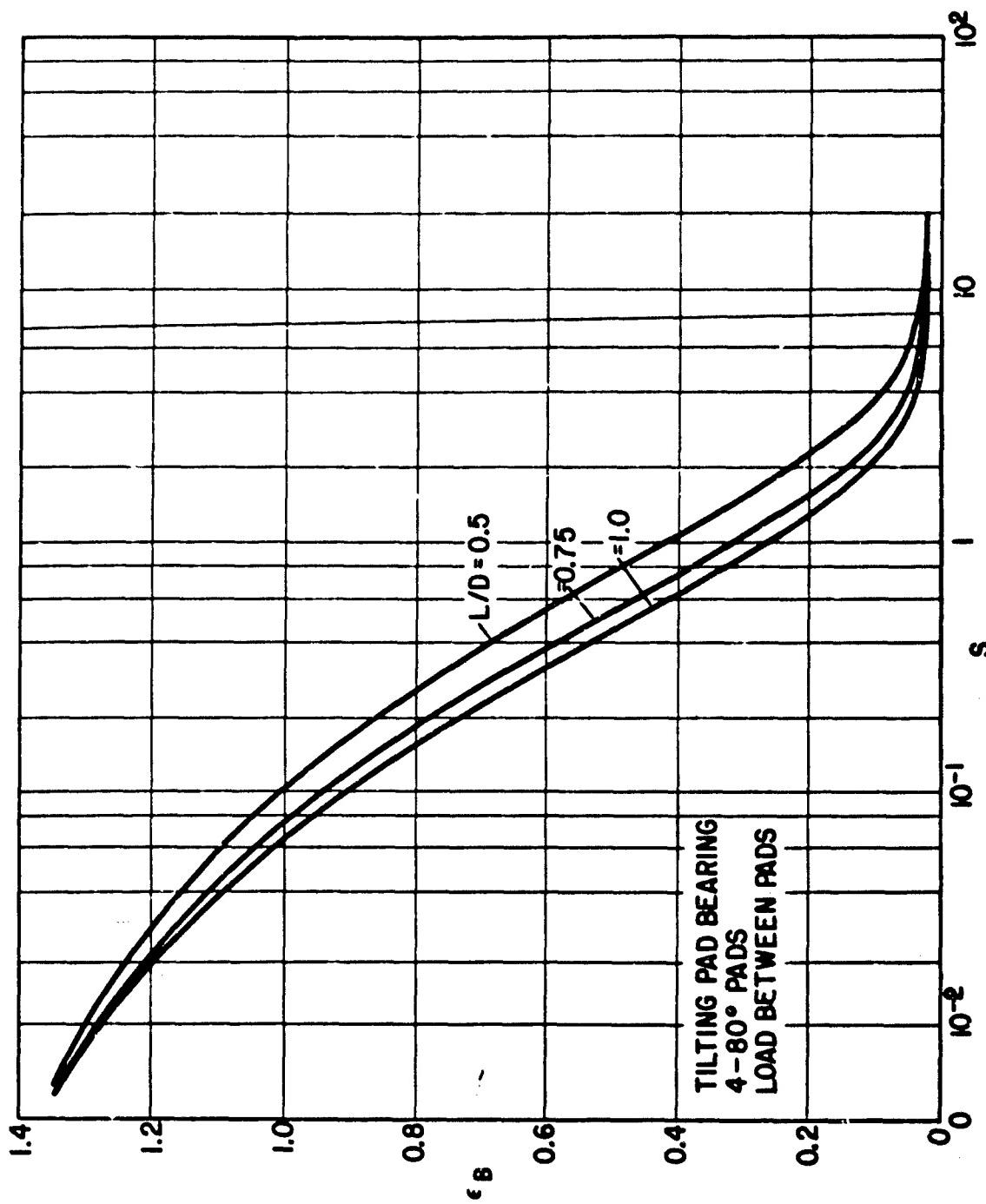


Figure A-9 The 5 Shoe Tilting Pad Bearing, Load between Pads
Laminar Film
Film thickness at Pivot vs. Eccentricity Ratio



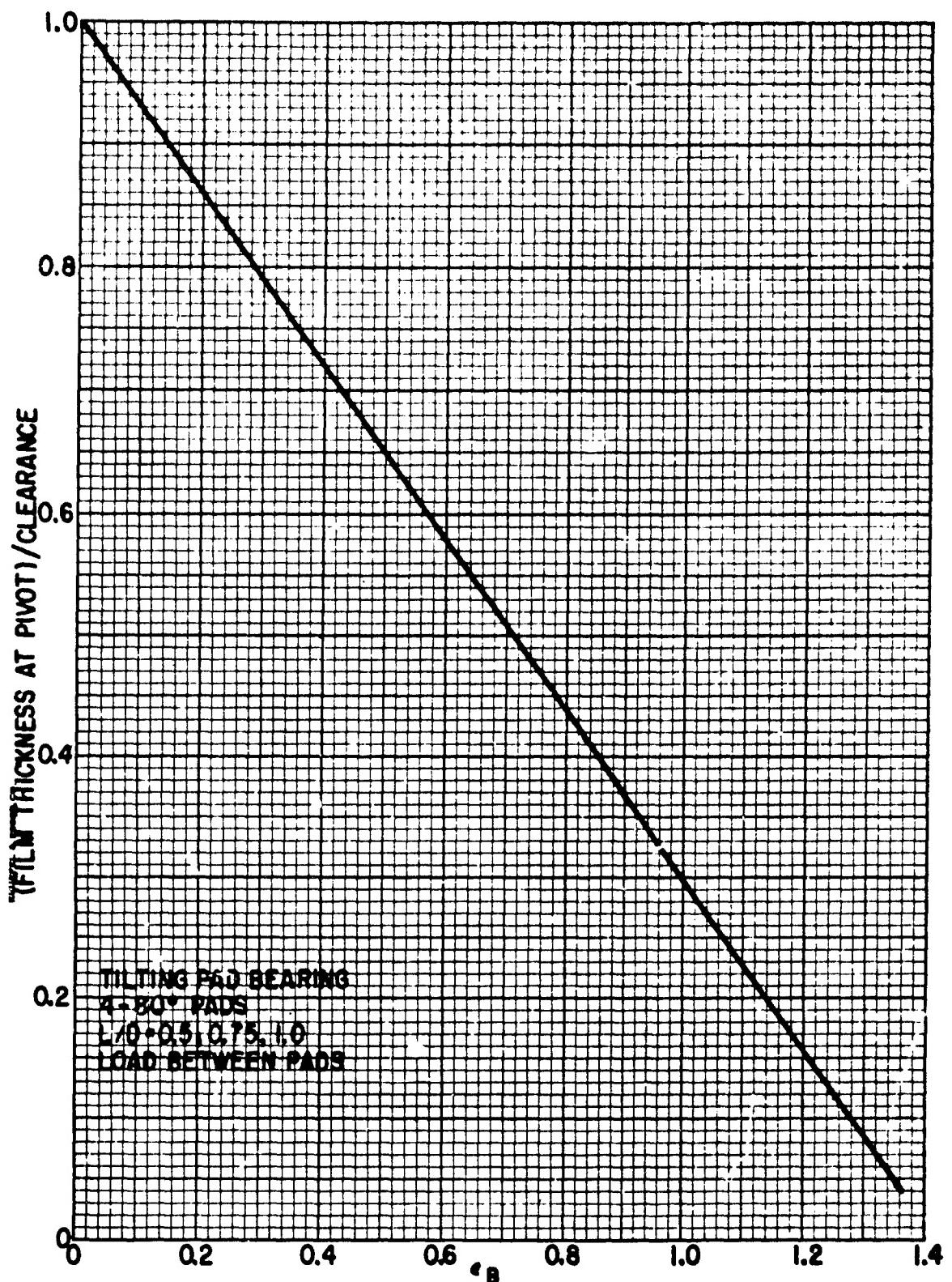


Figure A-11 The 4 Shoe Tilting Pad Bearing, Load between Pads
Laminar Film
Filmthickness at Pivot vs. Eccentricity Ratio

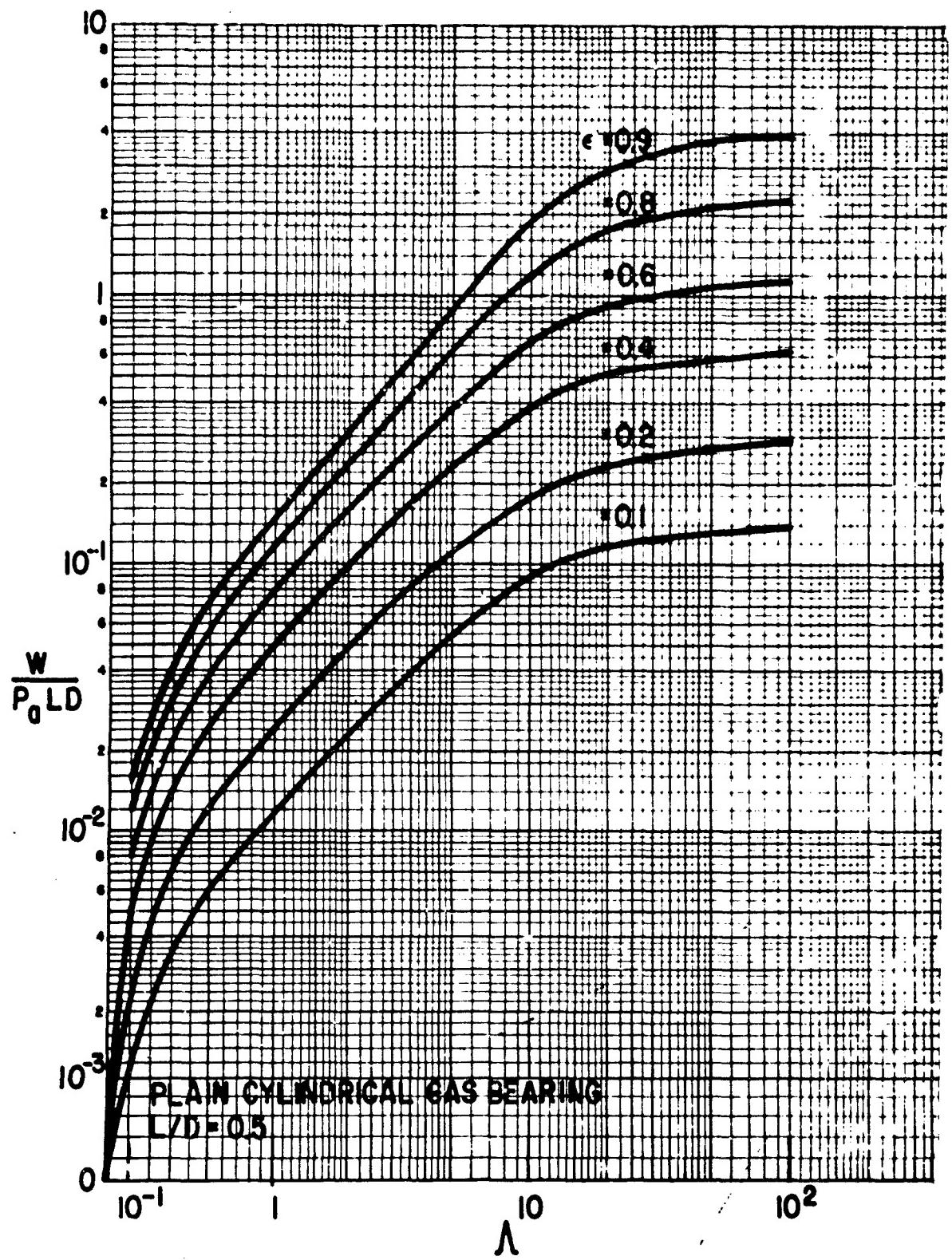


Figure A-12 The Plain Cylindrical Gas Bearing
Load vs. Compressibility Number and Eccentricity Ratio

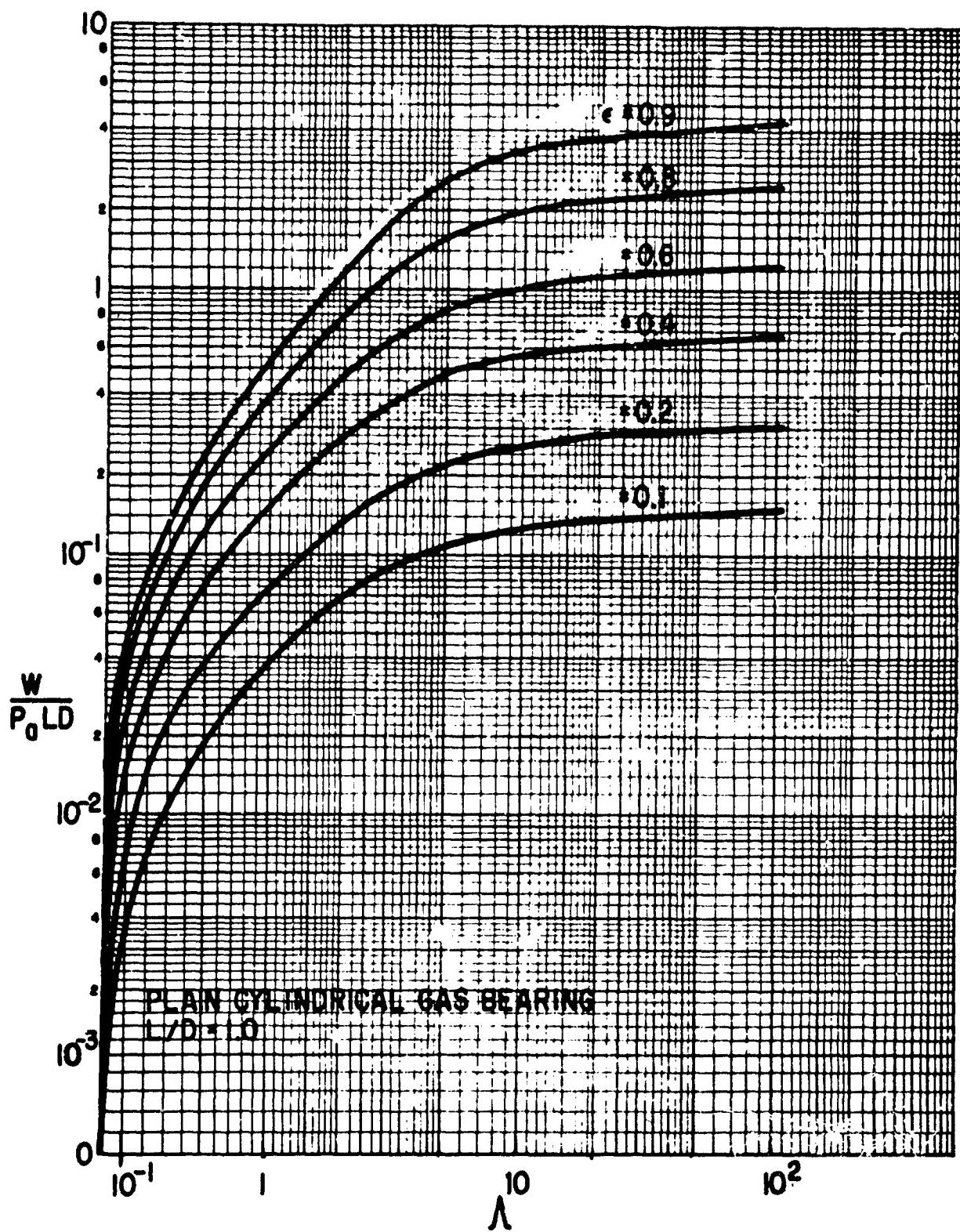


Figure A-13 The Plain Cylindrical Gas Bearing
 Load vs. Compressibility Number and Eccentricity Ratio

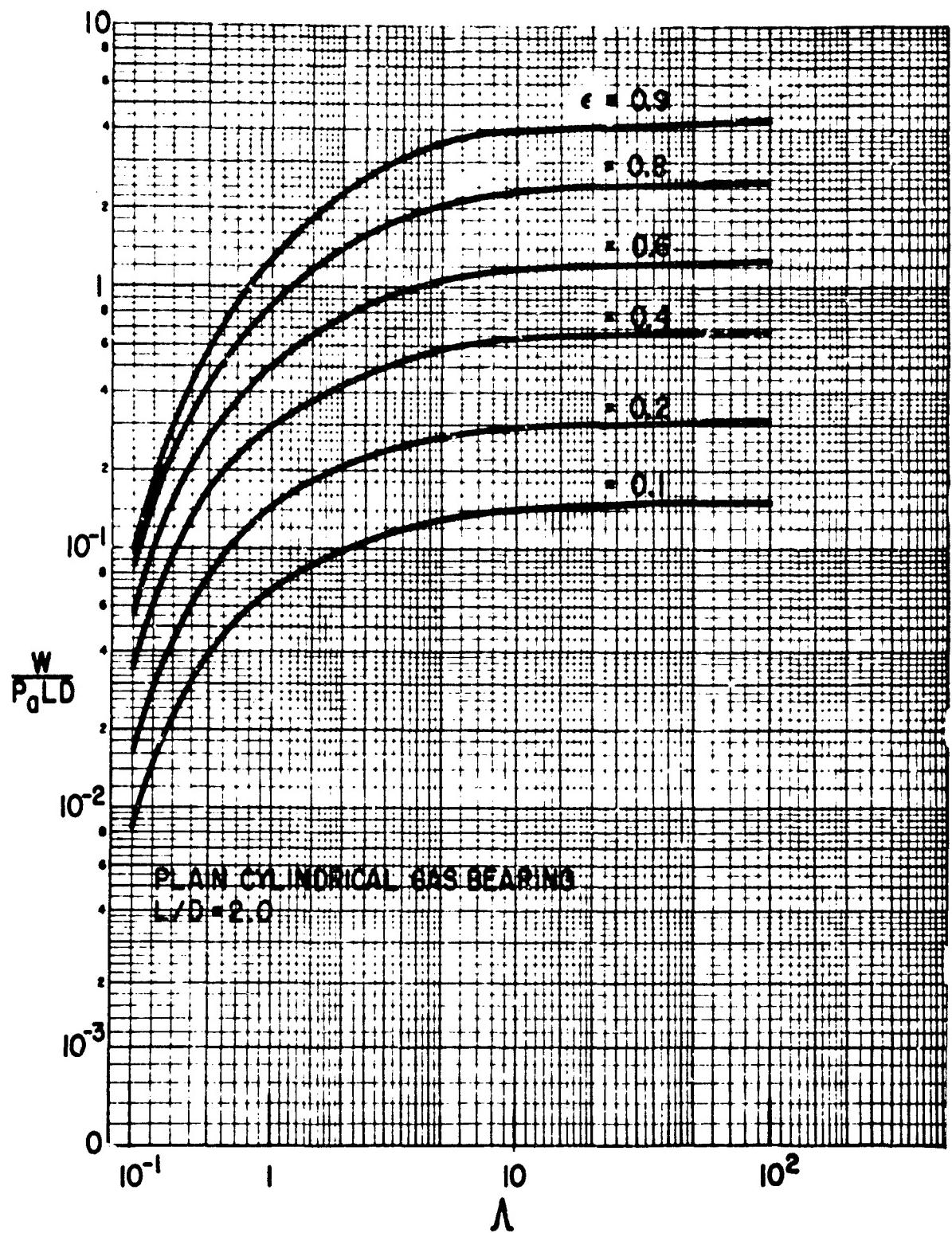


Figure A-14 The Plain Cylindrical Gas Bearing
Load vs. Compressibility Number and Eccentricity Ratio

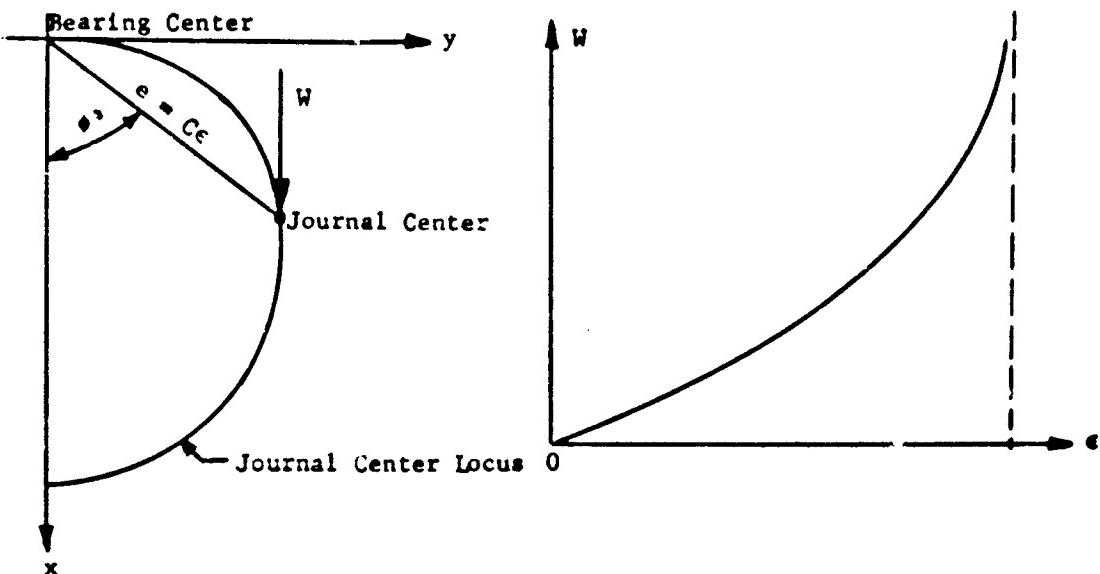
SPRING AND DAMPING COEFFICIENTS FOR FLUID FILM JOURNAL BEARINGS

The journal bearings supporting a rotor may be either of two general types: rolling element bearings or fluid film bearings. In both cases the bearings possess flexibility and damping and these properties influence the dynamic characteristics of the rotor. Thus, in order to perform a design analysis of the rotor-bearing system it is necessary to know the values of the bearing stiffness and damping. For this purpose the present report gives design data for a large number of fluid film bearing types. The data are in form of graphs, as Fig. B-1 to B-124 which will be discussed in detail below. Rolling element bearings (ball bearings) are treated in a separate report (Ref. 2).

General Concept of Spring and Damping Coefficients

In all fluid film bearings the journal is separated from the bearing surface by a thin film of lubricant. The lubricant may be an oil, another liquid or a gas, and the film may operate in the laminar or the turbulent flow regime. In hydrodynamic (self-acting)bearings the load carrying capacity is due to pressures generated in the fluid film and this in turn requires the journal to operate eccentric within the bearing or, in other words, the larger the eccentricity the higher the load carrying capacity, everything else kept the same (including the speed). This may be illustrated by considering one of the simplest bearing types namely the plain cylindrical bearing. It consists of a cylindrical sleeve with radius R and with length L . The difference between the bearing radius and the journal radius is the radial clearance C . Thus, the distance between the bearing center and the journal center, denoted as the eccentricity e , can vary between zero and C . For convenience the eccentricity is normalized with respect to the clearance, the ratio being known as the eccentricity ratio $\epsilon = e/C$. Hence, ϵ varies between 0 and 1. Assume the rotor to be running with a speed of N rps and apply a load W to the bearing, starting from zero and increasing steadily. Then the journal center will describe a locus:

B. DYNAMIC BEARING COEFFICIENTS

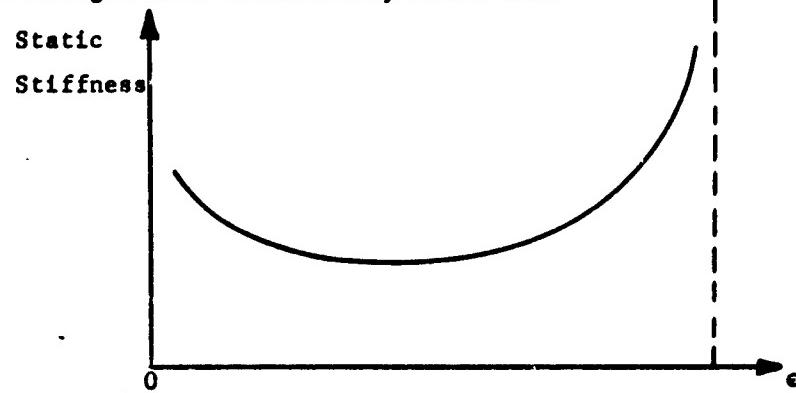


The position of the journal center with respect to the bearing center is given by the eccentricity ratio e and the attitude angle ϕ (see figure above) such that ϕ goes from approximately 90° to 0° as e goes from 0 to 1. The vertical displacement in the same direction as the load becomes $e \cos \phi$.

Introduce an x-y-coordinate system with the x-axis vertically downwards whereby $x = e \cos \phi = C e \cos \phi$ and $y = e \sin \phi = C e \sin \phi$. Hence, the static stiffness is given by:

$$\text{Static stiffness} = \frac{dw}{dx} = \frac{dw}{Cd(e \cos \phi)}$$

i.e., it is the slope of the load curve plotted as a function of the vertical displacement. Since the load curve is not linear with displacement the stiffness changes with eccentricity ratio too:



It is evident that the static stiffness alone is not sufficient to describe the total stiffness characteristics of the bearing. From the above journal center locus it is seen that even under static load the journal displacement is not in the same direction as the applied load. The displacement has both a vertical component x and a horizontal component y . This is in contrast to conventional mechanical systems where the elastic deformation usually is in the same direction as the force. Hence, it is necessary to split up the static stiffness in two parts, one part related to the x -displacement and one part related to the y -displacement. Assume the rotor to be operating at a given speed under a static load W and with journal center coordinates x and y . Increase the load by an infinitesimal small amount ΔW whereby the journal center coordinates are changed by Δx and Δy , respectively. However, to separate the effects of Δx and Δy , the change should be performed in two steps: first increase x by Δx such that W is increased by ΔW_1 and next, increase y by Δy whereby W is further increased by ΔW_2 . In total:

$$\Delta W = \Delta W_1 + \Delta W_2$$

or

$$\Delta W = \frac{\Delta W_1}{\Delta x} \cdot \Delta x + \frac{\Delta W_2}{\Delta y} \cdot \Delta y$$

For very small changes the ratios become derivatives. Since the derivatives are taken with respect to one coordinate at a time, they are partial derivatives:

$$\frac{\Delta W_1}{\Delta x} \approx \frac{\partial W}{\partial x} \quad \frac{\Delta W_2}{\Delta y} \approx \frac{\partial W}{\partial y}$$

Therefore:

$$\Delta W = \frac{\partial W}{\partial x} \cdot \Delta x + \frac{\partial W}{\partial y} \cdot \Delta y$$

This may be shown to be a separation into components of the previously discussed static stiffness as follows:

$$\frac{dW}{dx} \approx \frac{\Delta W}{\Delta x} = \frac{\partial W}{\partial x} + \frac{\partial W}{\partial y} \cdot \frac{dy}{dx}$$

For convenience the partial derivatives are designated by symbols:

$$K_{xx} = \frac{\partial W}{\partial x} \quad K_{xy} = \frac{\partial W}{\partial y}$$

They are called spring coefficients. There are, however, more than two coefficients as will be discussed.

Under static conditions the static bearing load W is opposed by an equal and opposite force W_x representing the integrated pressures in the fluid film. W_x is taken to be positive in the same direction as x such that:

$$(W_x)_{\text{static}} = -W$$

If, however, the journal center is outside the earlier shown journal center locus the fluid film pressures generate an additional horizontal force component W_y which under static conditions forces the journal back to its equilibrium position where $W_y = 0$. This means that the bearing has stiffness not only in the vertical direction (x -direction) but also in the horizontal direction (y -direction). Hence, in calculating the partial derivatives above where x is first increased by Δx , not only is W increased by ΔW_1 (more accurately it is W_x which is increased by ΔW_1) but W_y is changed by ΔW_3 . Similarly is W_y changed by ΔW_4 in increasing y by Δy . Therefore, in total:

$$(\Delta W_x)_{\text{static}} = -\Delta W = -\frac{\Delta W_1}{\Delta x} \cdot \Delta x - \frac{\Delta W_2}{\Delta y} \cdot \Delta y \approx \frac{\partial W}{\partial x} \cdot \Delta x + \frac{\partial W}{\partial y} \cdot \Delta y$$

$$(\Delta W_y)_{\text{static}} = -\frac{\Delta W_3}{\Delta x} \cdot \Delta x - \frac{\Delta W_4}{\Delta y} \cdot \Delta y \approx \frac{\partial W}{\partial x} \cdot \Delta x + \frac{\partial W}{\partial y} \cdot \Delta y$$

The minus signs are due to the convention of W_x and W_y being positive in the same direction as x and y , respectively. It is convenient to write these equations as:

$$(\Delta W_x)_{\text{static}} = -K_{xx} \cdot \Delta x - K_{xy} \cdot \Delta y$$

$$(\Delta W_y)_{\text{static}} = -K_{yx} \cdot \Delta x - K_{yy} \cdot \Delta y$$

where:

$$K_{xx} = -\frac{\partial w_x}{\partial x} \quad K_{xy} = -\frac{\partial w_x}{\partial y}$$

$$K_{yx} = -\frac{\partial w_y}{\partial x} \quad K_{yy} = -\frac{\partial w_y}{\partial y}$$

These four coefficients are the spring coefficients of the bearing. The first index gives the direction of the force, the second index gives the direction of the displacement. It is seen that a displacement in, say the x-direction, gives rise to a force not only in the x-direction, but also in the y-direction.

Under dynamic conditions the journal center no longer occupies a fixed position. It has a velocity with components \dot{x} and \dot{y} ($\dot{x} = \frac{dx}{dt}$ and $\dot{y} = \frac{dy}{dt}$ where t is time). Such a velocity induces additional pressures in the fluid film resulting in an increase of the fluid film force components w_x and w_y . This effect is called the squeeze film effect because the forces are generated by the lubricants resistance to being "squeezed" out of the bearing film. In complete analogy to the four spring coefficients the squeeze film forces can be represented by four damping coefficients: C_{xx} , C_{xy} , C_{yx} and C_{yy} . In total, the changes in the fluid film force components due to a motion of the journal center are given by:

$$\Delta w_x = -K_{xx} \cdot \Delta x - C_{xx} \dot{x} - K_{xy} \Delta y - C_{xy} \cdot \dot{y}$$

$$\Delta w_y = -K_{yx} \cdot \Delta x - C_{yx} \dot{x} - K_{yy} \cdot \Delta y - C_{yy} \cdot \dot{y}$$

The coefficients where the indices are the same (i.e. K_{xx} , C_{xx} , K_{yy} and C_{yy}) are called the direct-coupling terms (force and displacement are in the same direction) whereas the coefficients where the indices are different (i.e. K_{xy} , C_{xy} , K_{yx} and C_{yx}) are called the cross-coupling terms. Since the cross-coupling terms do not possess the necessary symmetry it is not possible by a simple rotation of the x-y-coordinate system to eliminate the cross-coupling terms.

Furthermore, the cross-coupling terms are not "pure" coefficients, i.e. a cross-coupling spring coefficient is not a pure stiffness, it also contains damping properties. This may be illustrated by considering the energy dissipated during the journal center motion. Assume the journal center to whirl in an orbit with angular frequency ω such that:

$$\Delta x = a \cos(\omega t + \phi_x) \quad \text{i.e. } \dot{x} = -\omega a \sin(\omega t + \phi_x)$$

$$\Delta y = b \sin(\omega t + \phi_y) \quad \dot{y} = \omega b \cos(\omega t + \phi_y)$$

The energy dissipated during one orbit of revolution is:

$$\begin{aligned} \text{Energy dissipated} &= \int_0^{2\pi} \left[[K_{xx} \cdot \Delta x + C_{xx} \dot{x} + K_{xy} y + C_{xy} \dot{y}] \dot{x} + [K_{yx} x + C_{yx} \dot{x} + K_{yy} y + C_{yy} \dot{y}] \dot{y} \right] dt \\ &= \pi \left\{ a^2 \omega C_{xx} + b^2 \omega C_{yy} - a \cdot b \cdot \sin(\phi_x - \phi_y) (\omega C_{xy} + \omega C_{yx}) - a \cdot b \cdot \cos(\phi_x - \phi_y) (K_{xy} - K_{yx}) \right\} \end{aligned}$$

Hence, the cross-coupling spring coefficients may contribute to the energy dissipation which is usually considered a property of a damping coefficient.

The 8 dynamic coefficients are calculated from lubrication theory. They are computed as the previously indicated partial derivatives of the components of the fluid film force. They depend not only on the bearing type and the bearing geometry but also on the steady state journal center position. Thus, to each operating point on the journal center locus (see the figure, page 59) corresponds different values of the 8 coefficients. Therefore, when the eccentricity ratio is known the dynamic coefficients are also defined. The eccentricity ratio in turn is a function of several dimensionless parameters:

for liquid lubricated, hydrodynamic bearings:

Length-to-diameter ratio : L/D

Sommerfeld Number: $S = \frac{\mu N D L}{W} \left(\frac{R}{C} \right)^2$

Reynolds Number : $Re = \pi R N D C / \mu$

(for laminar film: $Re = 0$)

laminar

turbulent

for gas lubricated, hydrodynamic bearings:

Length to-diameter ratio: L/D

Compressibility Number : $\Lambda = \frac{12 \pi \mu N}{P_a} \left(\frac{R}{C} \right)^2$

Bearing load parameter: $W/P_a L D$

for gas lubricated, hydrostatic bearings:

Length to-diameter ratio: L/D

Restrictor coefficient: $\Lambda_s = \frac{6\mu Na^2}{P_s C^3} \sqrt{\frac{RT}{1+8}}$

Supply Pressure Ratio: P_s / P_a

The symbols are defined on Page 27 and in the nomenclature list.

Use of the Design Charts

The design data for spring and damping coefficients are given in Figs. B-1 to B-124 for a wide selection of bearing types. The bearing types considered are listed in Fig. 6.

a. Liquid Lubricant, Laminar Film

The design data for the bearing types with an incompressible lubricant and a laminar film are given in Figs. B-1 to B-55. The charts give the dynamic coefficients as a function of the Sommerfeld number S. The coefficients are in dimensionless form:

$$\begin{array}{cccc} \frac{CK_{xx}}{W} & \frac{CK_{xy}}{W} & \frac{CK_{yx}}{W} & \frac{CK_{yy}}{W} \\ \frac{C\omega C_{xx}}{W} & \frac{C\omega C_{xy}}{W} & \frac{C\omega C_{yx}}{W} & \frac{C\omega C_{yy}}{W} \end{array}$$

where:

C - Radial clearance, inch

W - Bearing load, lbs.

ω - $2\pi N$. Angular speed, radians/sec

N - Rotor speed, RPS

$K_{xx}, K_{xy}, K_{yx}, K_{yy}$ - Spring coefficients, lbs/in

$C_{xx}, C_{xy}, C_{yx}, C_{yy}$ - Damping coefficients, lbs.sec/in

When the bearing dimensions, the load and the viscosity of the lubricant are known the Sommerfeld number can be computed for several values of the speed over the operating range. Entering the charts with these calculated values the correspond-

ing values of the coefficients can be computed. Thereby the coefficients become determined over the speed range and can be used in an unbalance response calculation, a stability analysis or a critical speed calculation.

For the plain cylindrical, the 4-axial groove and the partial bearing the only other parameter besides the Sommerfeld number is the $L/D =$ ratio. For the elliptical bearing an additional parameter is the ellipticity m which gives the distance between the lobe center and the bearing center normalized with respect to the radial clearance. Thus, $m = 0$ corresponds to a plain cylindrical bearing whereas $m = 1$ would mean solid contact between the journal and the bearing. In the present design charts (Figs. B-9 to B-16) two values of the ellipticity are considered: $m = 0.25$ and $m = 0.5$.

In analogy with the elliptical bearing the tilting pad bearing may not have the center of curvature of the pads coincide with the center of the bearing. If the journal radius is R and the radial clearance is C then the radius of curvature of the pads is $(R+C)$. Let the circle with center in the bearing center and touching the surface of the pads at the pivots have the radius $(R+C')$. If $C' = C$ the pad centers coincide with the bearing center and if $C' = 0$ the journal is always in solid contact with the pads. The parameter $(1 - C'/C)$ is called the preload factor and it may vary from 0 to 1 like the ellipticity m .

In Figs. B-37 to B-52 the preload factor is zero. Furthermore, Figs. B-37 to B-48 assume that the mass inertia of the shoes is very small and can be ignored. Under this assumption the 4 cross-coupling terms of the dynamic coefficients vanish and only K_{xx} , K_{yy} , C_{xx} and C_{yy} remain. In addition, for the 4 shoe bearing with the load direction passing between the two bottom pads $K_{xx} = K_{yy}$ and $C_{xx} = C_{yy}$ because of symmetry. The effect of pad mass inertia and the corresponding values of the cross-coupling terms are presented in Figs. B-49 to B-52 for the 4-shoe tilting pad bearing. The mass inertia is expressed in terms of a dimensionless parameter:

$$\frac{CWM}{\mu DL \left(\frac{R}{C} \right)^2}$$

where:

$$M = I/R^2$$

I = mass moment of inertia of a pad around a longitudinal axis passing through the pivot, lbs.in.sec²

The other symbols are defined on Page 27.

In addition to the dynamic coefficients the design charts for the tilting pad bearing also show a curve labeled "critical mass". For each Sommerfeld number this curve gives the value of the above dimensionless mass inertia parameter at which the phase angle between the journal motion and the pad motion becomes 90 degrees. If the actual pad inertia is more than approximately half the critical value the cross-coupling terms become significant. The critical mass parameter also gives some measure of the bearings stability characteristics as discussed later.

The three last charts, Figs. B-53 to B-55, apply to a vertical rotor and show the effect of the preload factor. Since the load W is equal to zero for a vertical rotor it is necessary to redefine the dimensionless form of the dynamic coefficients. The revised form is defined on the charts.

The values of the dynamic coefficients for other multi-groove bearings than the 4-axial groove bearing and for other multi-lobe bearings than the elliptical bearing can be estimated approximately from the partial bearing coefficients given in Figs. B-17 to B-36. This is best illustrated by first giving the exact and general method for calculating the dynamic coefficients of a bearing made up of several segments, say n segments (i.e. for the 4-axial groove bearing: n = 4, and for the elliptical bearing: n = 2). Consider the i'th segment, which is actually a partial bearing in itself, and let this segment be located an angle ψ_i with respect to the vertical load line for the complete bearing. ψ_i is measured in the direction of the shaft rotation from the top of the bearing to the radial line bisecting the segment. Next, it is necessary to know the steady-state loci of the journal center within the complete bearing for the given load direction. This information can be obtained from Refs. 3 or 4. Once the journal center location is available the eccentricity ratio and attitude angle for each segment can be established from simple geometrical relationships which depend on the particula

bearing configuration under investigation. Knowing the eccentricity ratio and the attitude angle for the i 'th segment allows computing the 8 dynamic coefficients for the segment: $(K_{xx})_i$, $(K_{xy})_i$, ..., $(\omega C_{yy})_i$ from the analysis described previously. Combining the n segments results in the 8 dynamic coefficients for the complete bearing as follows:

$$K_{xx} = \sum_{i=1}^n [K_{xx} \cos^2 \psi_i + K_{yy} \sin^2 \psi_i - (K_{xy} + K_{yx}) \cos \psi_i \sin \psi_i]_i$$

$$K_{xy} = \sum_{i=1}^n [K_{xy} \cos^2 \psi_i - K_{yx} \sin^2 \psi_i + (K_{xx} - K_{yy}) \cos \psi_i \sin \psi_i]_i$$

$$K_{yx} = \sum_{i=1}^n [K_{yx} \cos^2 \psi_i - K_{xy} \sin^2 \psi_i + (K_{xx} - K_{yy}) \cos \psi_i \sin \psi_i]_i$$

$$K_{yy} = \sum_{i=1}^n [K_{yy} \cos^2 \psi_i + K_{xx} \sin^2 \psi_i + (K_{xy} + K_{yx}) \cos \psi_i \sin \psi_i]_i$$

The equations for ωC_{xx} , ωC_{xy} , ωC_{yx} and ωC_{yy} are the same by simply replacing K with ωC in the four equations above.

It is evident that the segments in general are not centrally loaded. Hence, if the partial bearing data given in this handbook are to be used for calculating the dynamic coefficients of a multi-groove or multi-lobe bearing certain assumptions are required. First, for the particular steady-state operating condition the eccentricity ratio and the attitude angle for each segment must be known (e.g. from Refs. 3 or 4). Thereby the load line for each segment is also known and the angle ψ_i should be measured to this line instead of the bisecting line as used before. Next, the load line divides the segment into two arcs which normally are unequal. Multiply the smallest arc by two and use this arc length as the effective partial bearing arc for the segment. If the load line is outside the segment disregard the segment. With the obtained values of eccentricity ratio and effective arc length enter the appropriate chart from Fig. A-3 to A-10, read off the Sommerfeld number and use the corresponding chart from Figs. B-17 to B-34 to determine the 8 dynamic coefficients for the segment. Repeat this procedure for each segment and, finally, compute the overall dynamic coefficients for the complete bearing from the equations given above.

b. Liquid Lubricant, Turbulent Film

The condition of the flow in the bearing film, whether laminar or turbulent, is determined by the Reynolds number:

$$Re = \frac{\pi D C N}{\mu}$$

where:

D - journal diameter, inch

C - radial clearance, inch

N - rotor speed, RPS

μ - lubricant viscosity, lbs.sec/in²

ρ - mass density of lubricant, lbs.sec²/in⁴

When $Re < 1000$ the film is laminar. For higher Reynolds number the film becomes turbulent.

The dynamic bearing coefficients are given for three different bearing types operating in the turbulent flow regime: the plain cylindrical bearing, the 100 degree partial bearing, the 4-shoe tilting pad bearing and the 3-shoe tilting pad bearing. The data are summarized in design charts, see Figs. B-56 to B-93. Apart from the Reynolds number the dimensionless parameter are the same as for the laminar film data.

c. Gas Lubricant, Hydrodynamic Bearing

When the lubricant is compressible the Sommerfeld number is no longer adequate as the governing design parameter. Instead, the compressibility number Λ is used:

$$\Lambda = \frac{12\pi\mu N}{P_a} \left(\frac{R}{C}\right)^2$$

where:

P_a - Ambient pressure, psia

and the other symbols are defined on Page 27. In addition, one more parameter is necessary. It can either be the eccentricity ratio ϵ or the dimensionless bearing load $W/P_a LD$ (note: Sommerfeld number $S = \Lambda/(12\pi \cdot W/P_a LD)$). In the present design charts for the dynamic bearing coefficients the chosen parameters are Λ and ϵ . The relationship between Λ , ϵ and $W/P_a LD$ is shown in Figs. A-12 to A-14.

The dynamic coefficients are given in dimensionless form:

$$\begin{array}{cccc}\frac{C_K_{xx}}{P_a LD} & \frac{C_K_{xy}}{P_a LD} & \frac{C_K_{yx}}{P_a LD} & \frac{C_K_{yy}}{P_a LD} \\ \frac{C_{wC}_{xx}}{P_a LD} & \frac{C_{wC}_{xy}}{P_a LD} & \frac{C_{wC}_{yx}}{P_a LD} & \frac{C_{wC}_{yy}}{P_a LD}\end{array}$$

Hence, when the bearing dimensions, the load, the rotor speed and the gas viscosity are known the compressibility number, Λ , and the dimensionless load can be computed. Entering Figs. A-12 to A-14 the corresponding value of the eccentricity ratio can be found. With this value and the value of Λ the dynamic coefficients can be determined from Figs. B-94 to B-109. Repeating the calculations for several speeds allows determining the coefficients over the complete speed range. They can then be used in calculating the unbalance response and the critical speeds of the rotating bearing system.

When the lubricant is a gas the dynamic coefficients are actually a function of the whirl frequency in addition to depending on Λ and e . In the present case the whirl frequency is set equal to the rotational speed of the journal. This means that the design charts are only valid for calculations involving synchronous whirl, i.e. unbalance response and critical speeds.

d. Gas Lubricant. Hydrostatic Bearing

Whereas all the previously considered bearing types are self-acting and rely on the viscous pump effect (hydrodynamic effect) for generating their load capacity the hydrostatic gas bearing is pressurized from an external source (a compressor or a bottle). Therefore, the presentation of design data for the hydrostatic bearing requires a new set of design parameters. These parameters are:

$$\text{Length-to-diameter: } \xi = \begin{cases} \frac{L}{D} & \text{for single plane admission} \\ \frac{L_2}{D} & \text{for double plane admission} \end{cases}$$

$$\text{Restrictor coefficient: } \Lambda_s = \frac{6uN_a \sqrt{RT}}{P_s C^3 \sqrt{1+e^2}}$$

$$\text{Supply pressure ratio: } P_s/P_a$$

$$\text{Feeder hole volume ratio: } \frac{NV_c}{\pi DLC}$$

where:

- D - Journal diameter, inch
- R - $\frac{1}{2} D$, Journal radius, inch
- L - Bearing length, inch
- C - Radial clearance, inch
- L_1 - Distance between admission planes, inch
- L_2 - $L-L_1$, Combined length outside admission planes, inch
- P_a - Ambient pressure, psia
- P_s - Supply pressure, psia
- a - Orifice radius, inch
- d - Feeder hole diameter, inch
- N - Total number of feeder holes (in the design charts N is used in the place of \bar{N})
- V_c - Volume of feeder hole below orifice, in³
- \mathcal{R} - Gas constant, in²/sec². °R
- T - Total temperature, °R
- μ - Gas viscosity, lbe.sec/in²
- δ - a^2/dC , Inherent compensation factor

(for details, see Fig. 10)

Instead of 8 coefficients as for a hydrodynamic bearing the hydrostatic bearing has only two coefficients: a spring coefficient K and a damping coefficient B. They are given in dimensionless form:

$$\text{Dimensionless stiffness: } \frac{1+8^2}{1+\frac{2}{3}\delta^2} \cdot \frac{CK}{(P_s - P_a)DL}$$

$$\text{Dimensionless damping: } \frac{B}{\mu L \left(\frac{R}{C}\right)^3}$$

where:

- K - Spring coefficient, lbs/in
- B - Damping coefficient, lbs.sec/in

The hydrostatic gas journal bearing is a plain cylindrical bearing provided with feeder holes for admission of the pressurized gas. The feeder holes may be arranged in one or two planes, denoted as single plane or double plane admission.

The feeder holes are flow restricted by means of an orifice and some restriction may also take place in the "curtain area" between the rim of the feeder hole and the journal surface. The latter area is equal to πdC whereas the area of the orifice is πa^2 . The ratio between the two areas is: $\delta = a^2/dC$ which, therefore, gives an indication of where the major part of the flow restriction takes place.

The restrictor coefficient Λ_s gives the ratio between the flow resistance of the bearing film and the flow resistance of the feeder holes. If the film resistance is very small ($\Lambda_s \approx 0$) the pressure in the gas film becomes equal to ambient and the bearing has no stiffness or load carrying capacity. On the other hand, if the film resistance becomes very high or the feeder hole resistance is very small ($\Lambda_s \rightarrow \infty$) the pressure downstream of all the feeder holes will equal the supply pressure and again the bearing has no stiffness. There is, therefore, an optimum value of the restrictor ratio, approximately given by:

$$\Lambda_s \xi \approx .5 \text{ to } .7$$

Under this condition the stiffness is a maximum.

The restrictor coefficient together with the supply pressure ratio are the controlling design parameters for a hydrostatic bearing. However, in considering the bearing damping a third one enters namely, the feeder hole volume ratio. This parameter gives the ratio between the volume contained in all the feeder holes and the volume of the gas film. It affects the time lag between the flow and pressure when the journal performs dynamic motions. The value of the parameter should in general be less than .05 to .1 to minimize the bearings susceptibility to pneumatic hammer instability.

For given bearing dimensions and lubricant properties the controlling design parameters may be computed and Figs. B-110 to B- can be entered to determine the stiffness and damping of the hydrostatic bearing. The values given for the damping coefficient assume that the vibratory frequency is not too large.

In an actual application the journal rotation superimposes hydrodynamic pressure on the hydrostatic pressure. This effect, usually denoted as the hybrid bearing effect, has been ignored in the present design charts. The effect is normally small.

Previous page was blank, therefore not filmed.

DESIGN CHARTS FOR
SPRING AND DAMPING COEFFICIENTS

a. Liquid Lubricant, Laminar Film

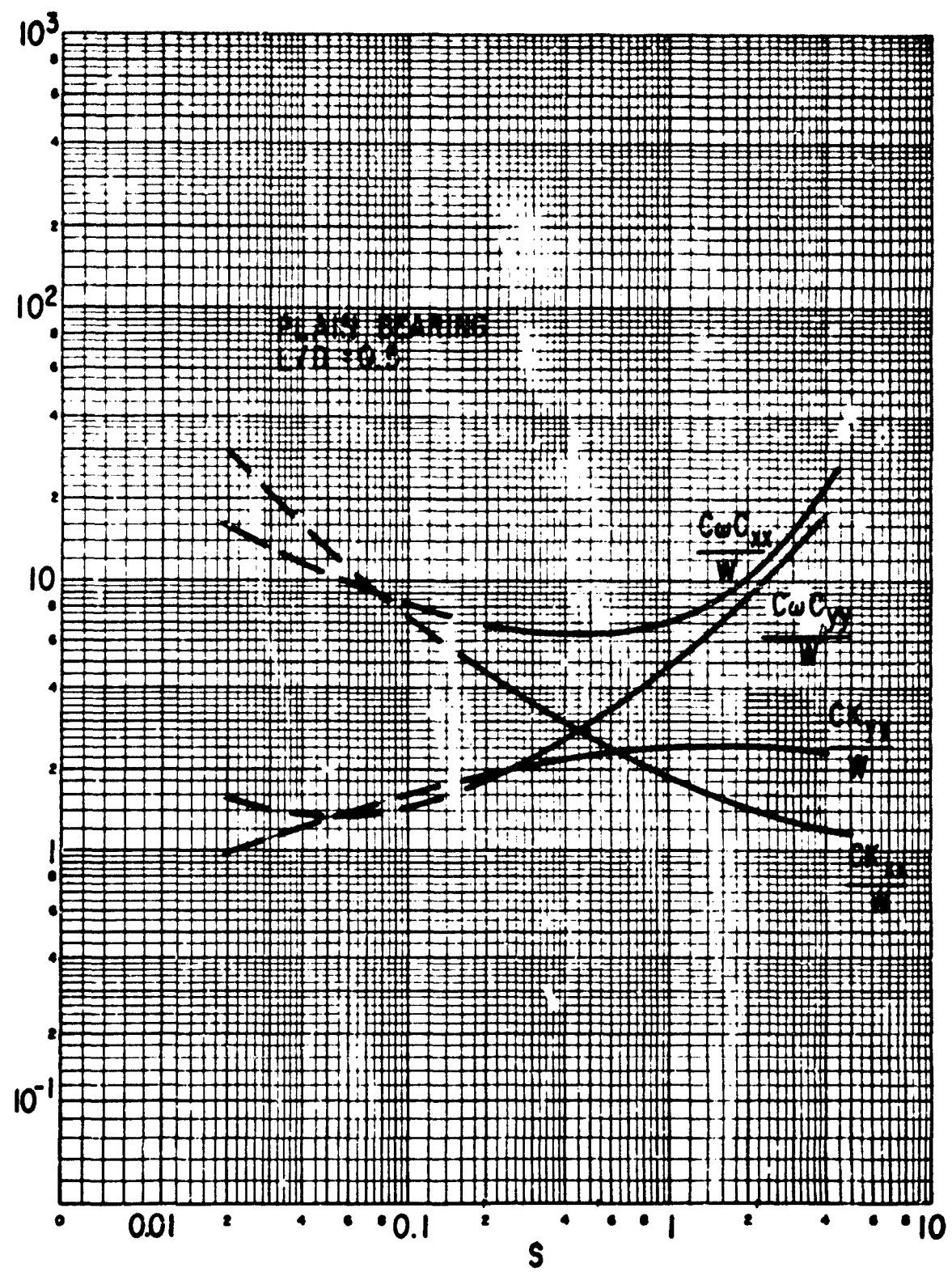


Figure B-1 The Plain Cylindrical Bearing, Laminar Film Dimensionless Dynamic Coefficients

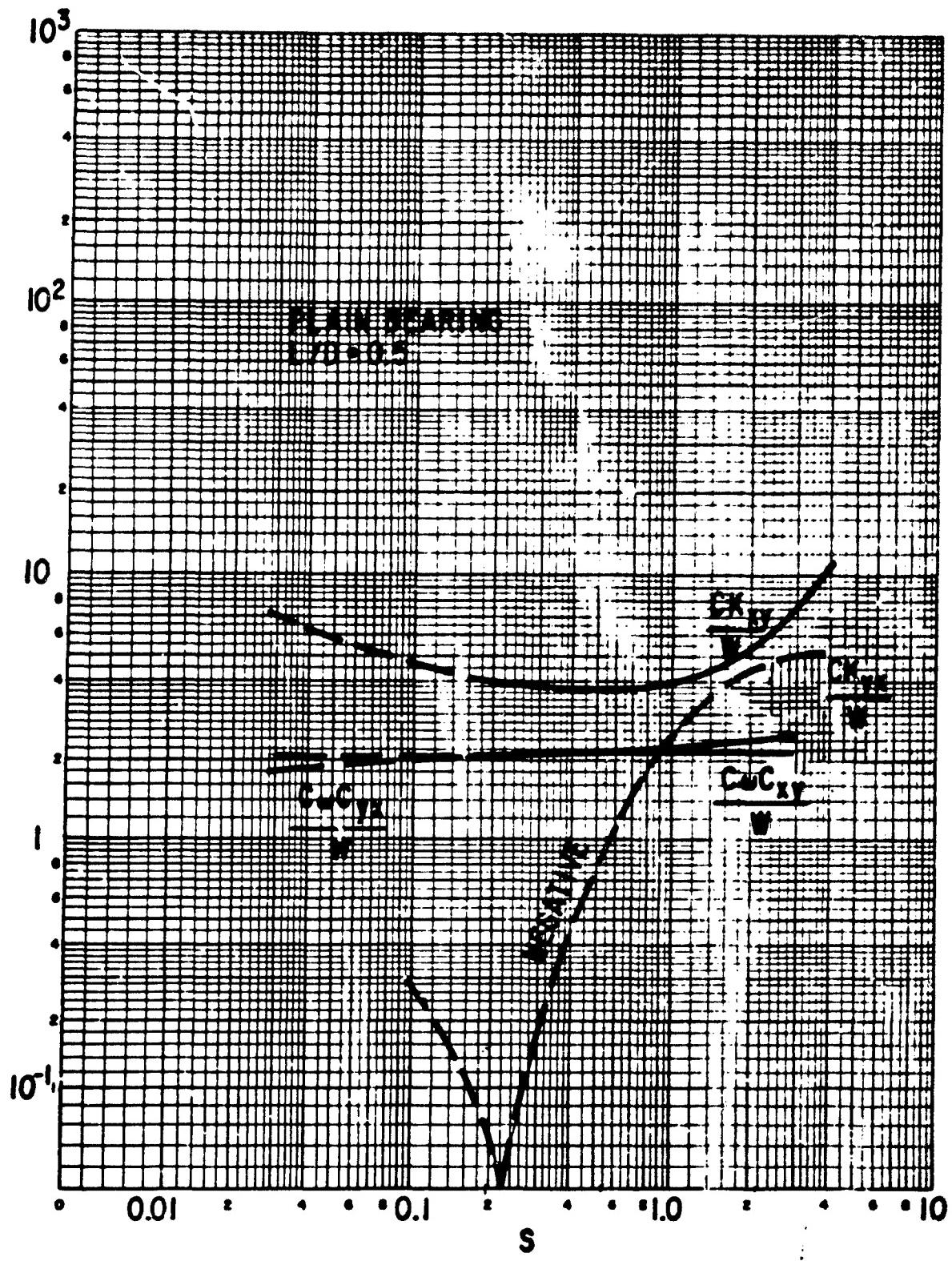


Figure B-2 The Plain Cylindrical Bearing, Laminar Film Dimensionless Dynamic Coefficients

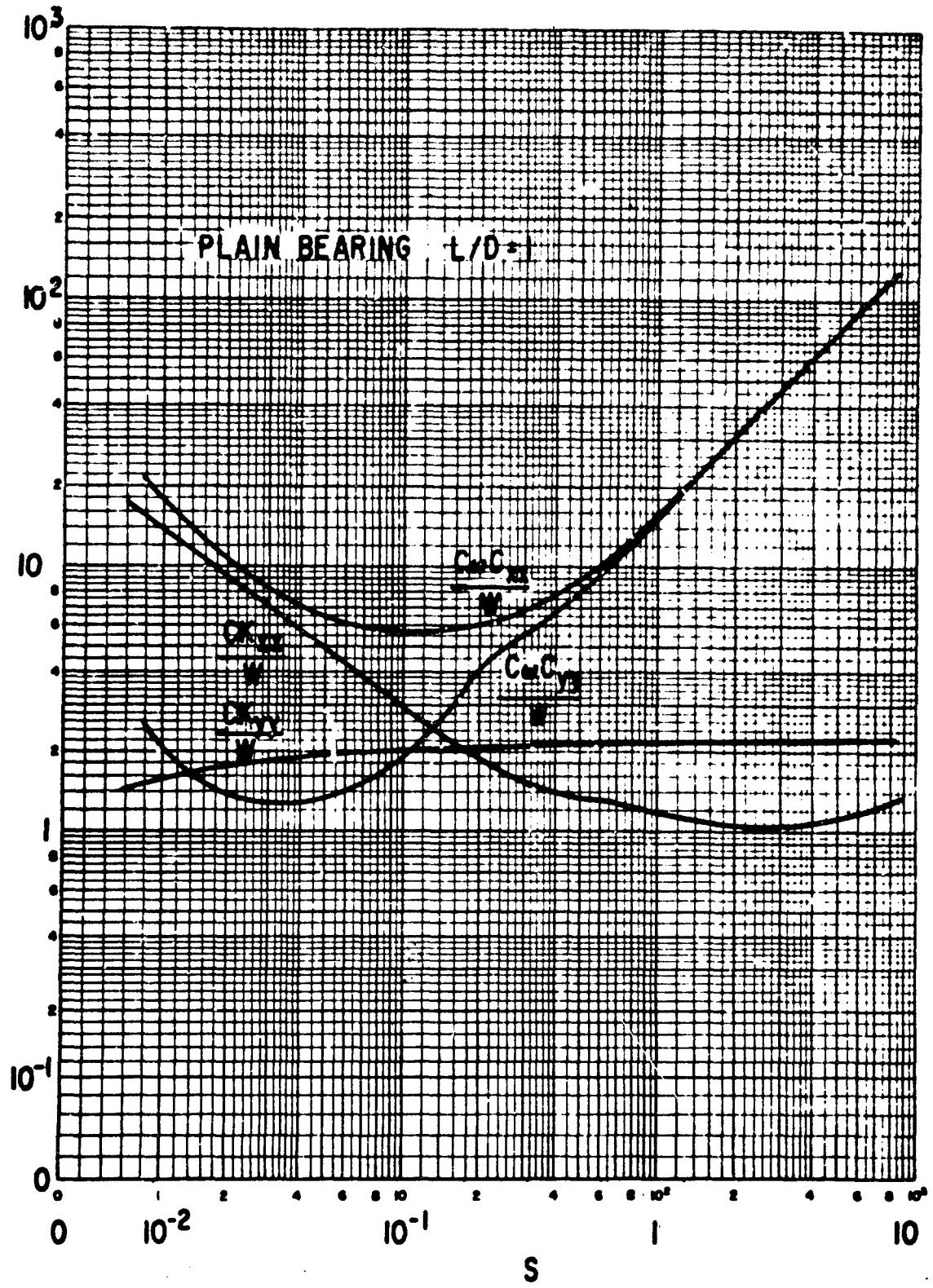


Figure B-3 The Plain Cylindrical Bearing, Laminar Film Dimensionless Dynamic Coefficients

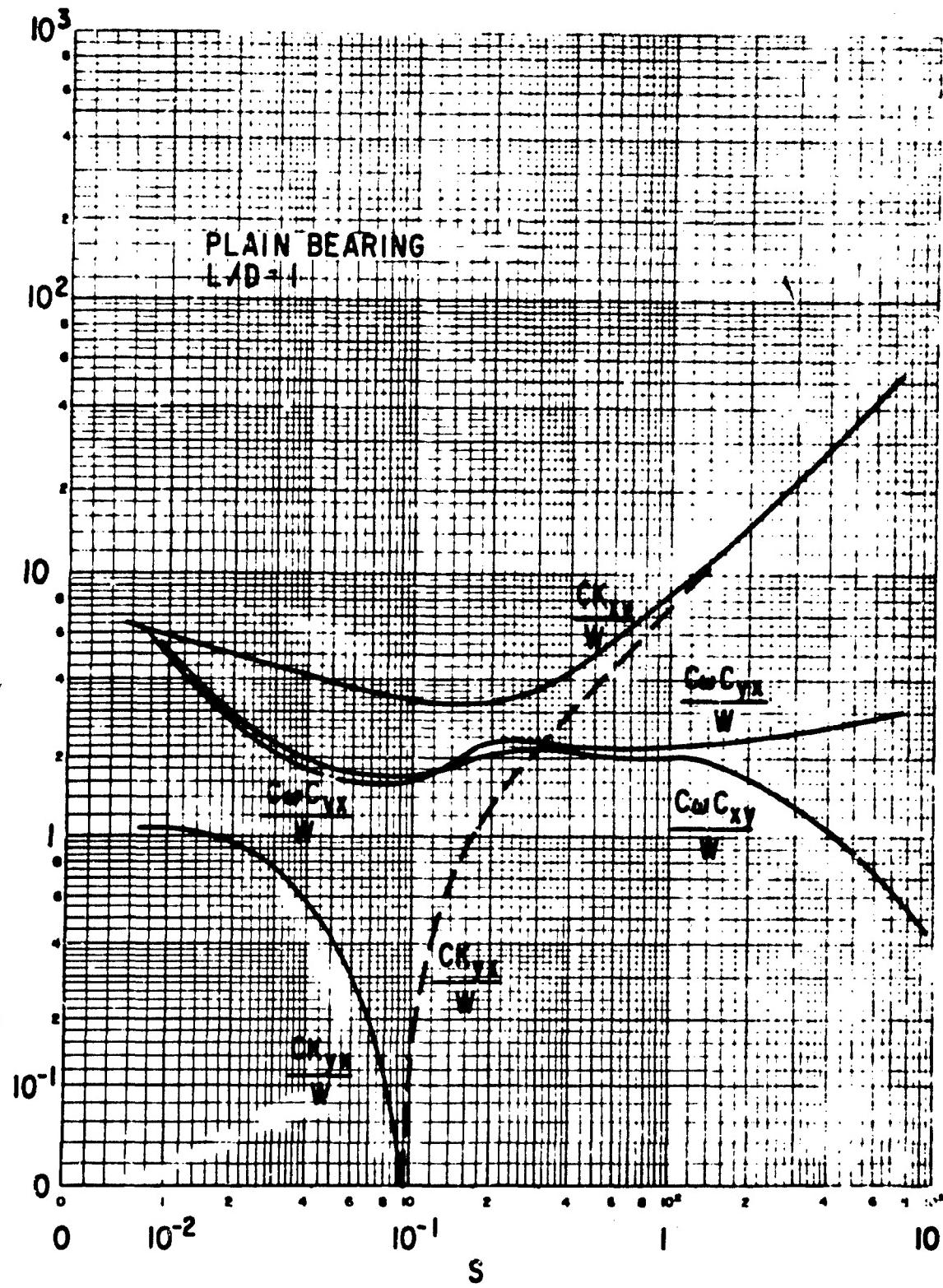


Figure B-4 The Plain Cylindrical Bearing, Laminar Film Dimensionless Dynamic Coefficients

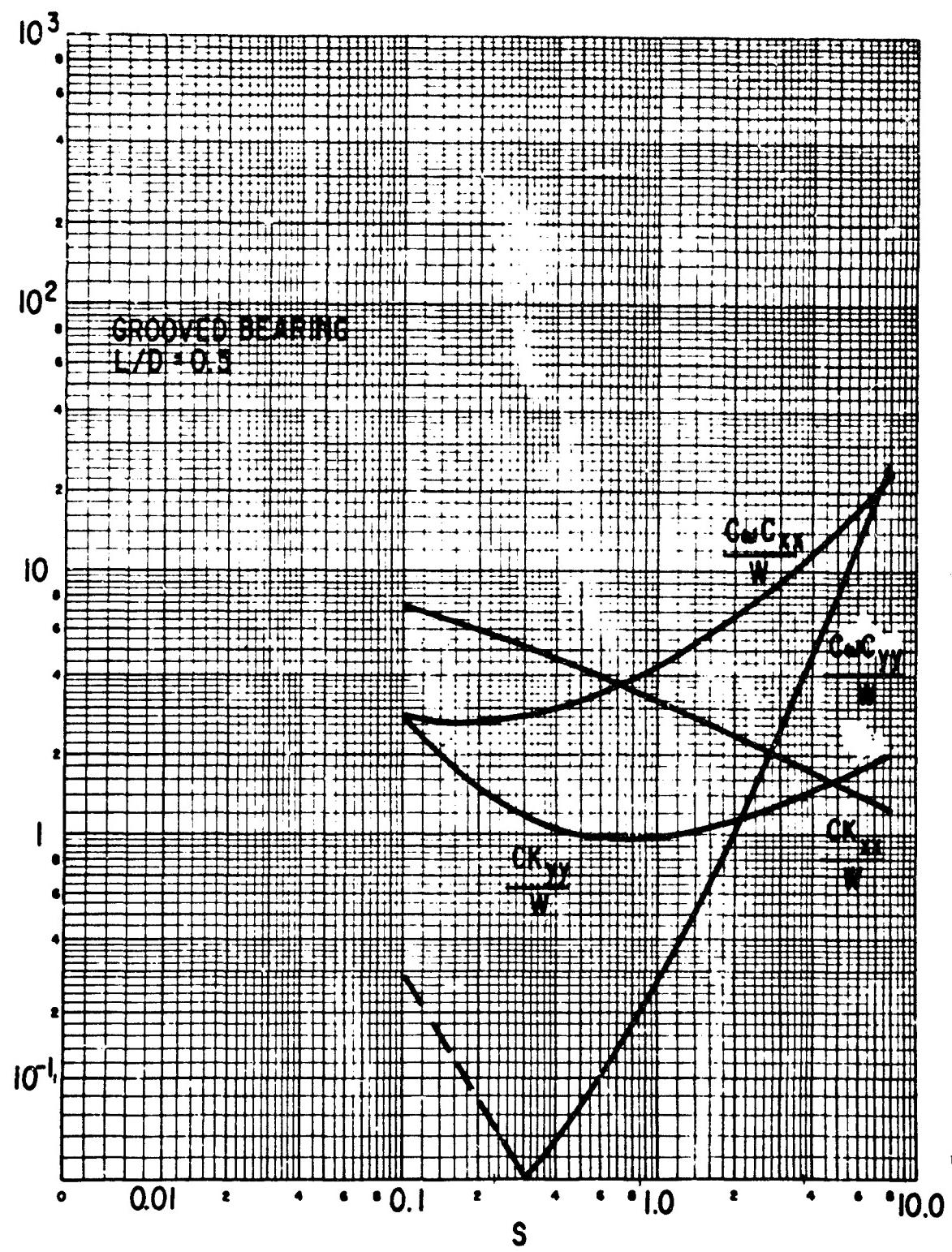


Figure B-5 The 4-Axial Groove Bearing, Laminar Film Dimensionless Dynamic Coefficients

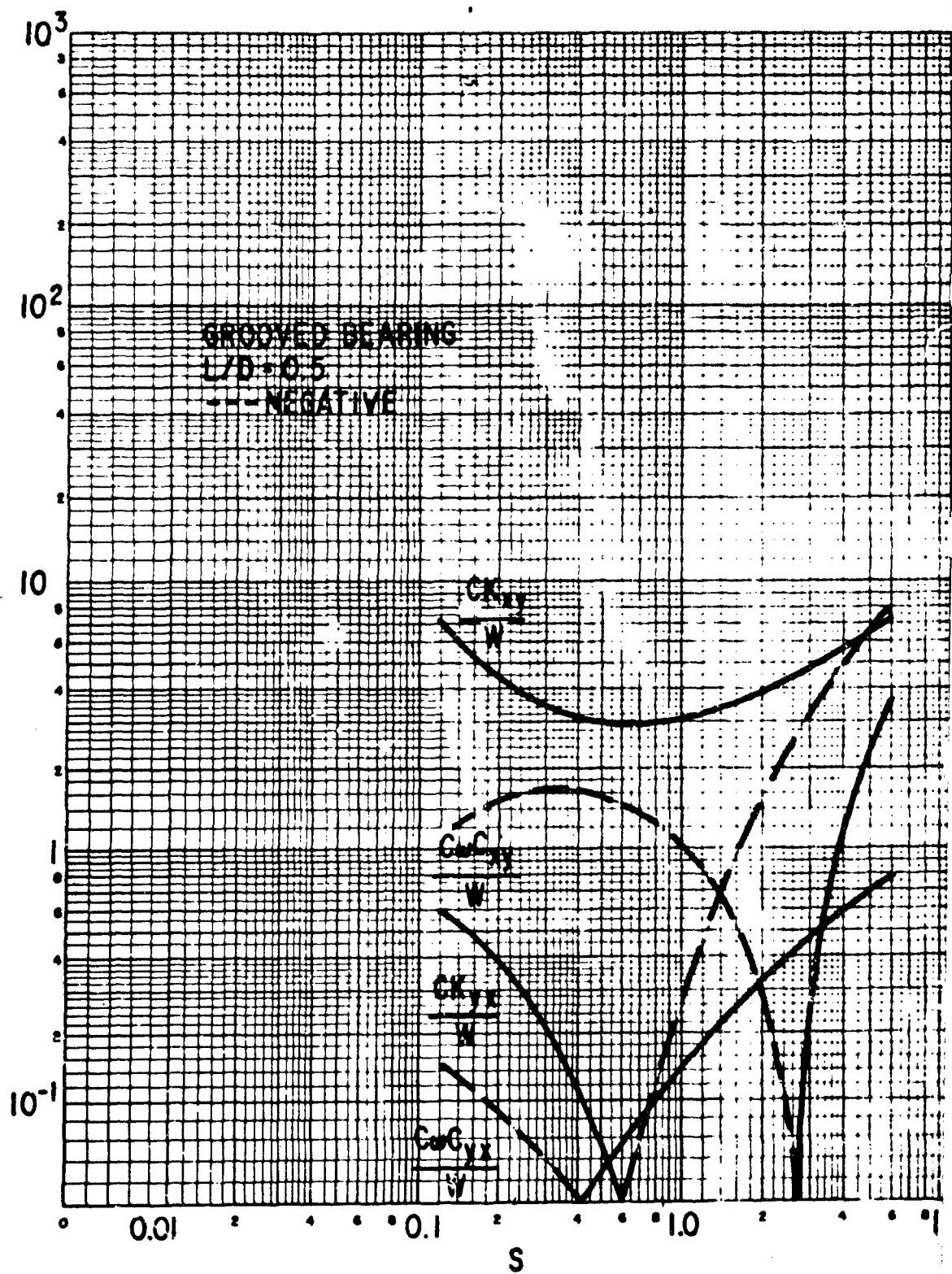


Figure B-6 The 4-Axial Groove Bearing, Laminar Film Dimensionless Dynamic Coefficients

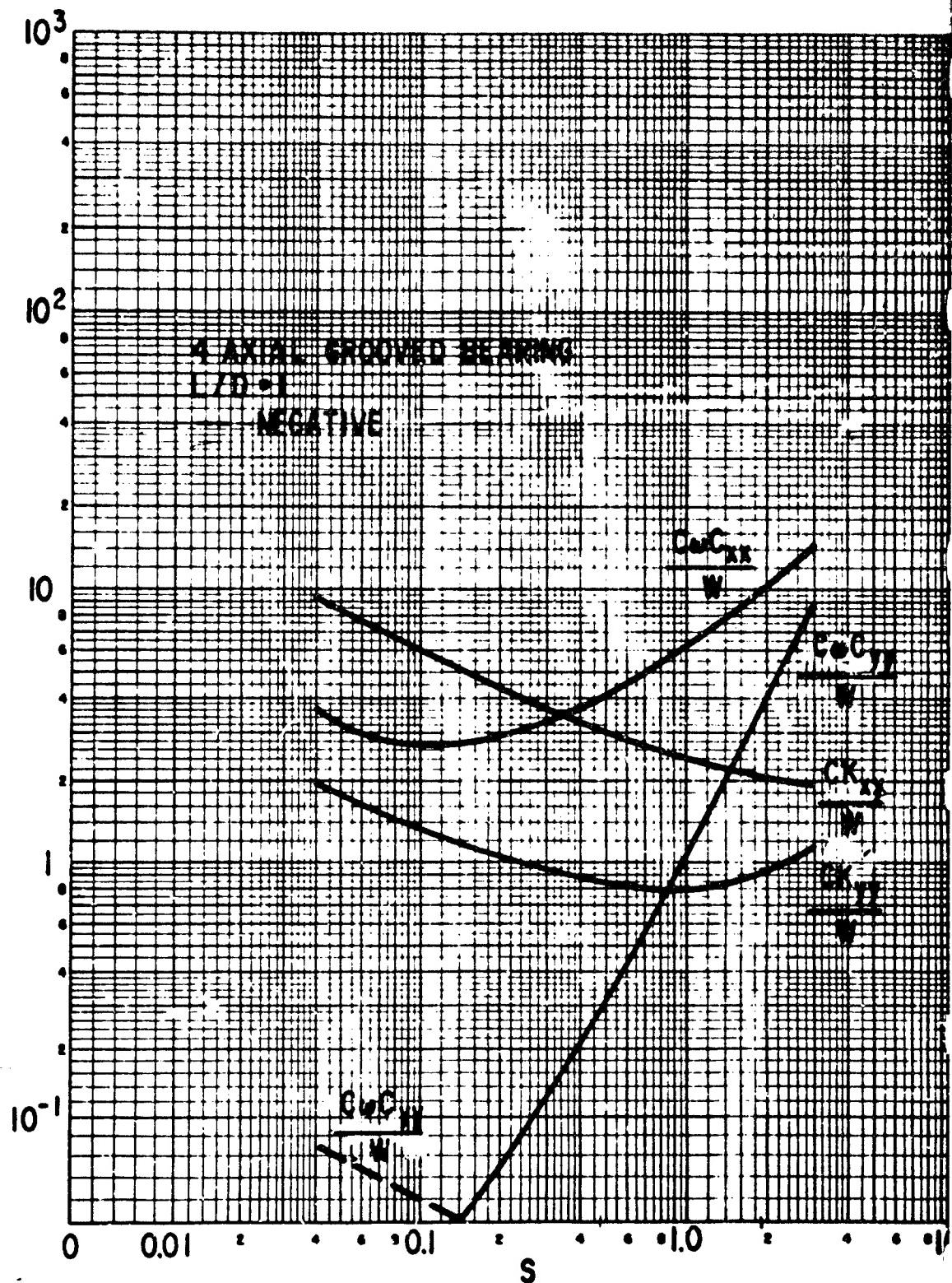


Figure B-7 The 4-Axial Groove Bearing, Laminar Film Dimensionless Dynamic Coefficients

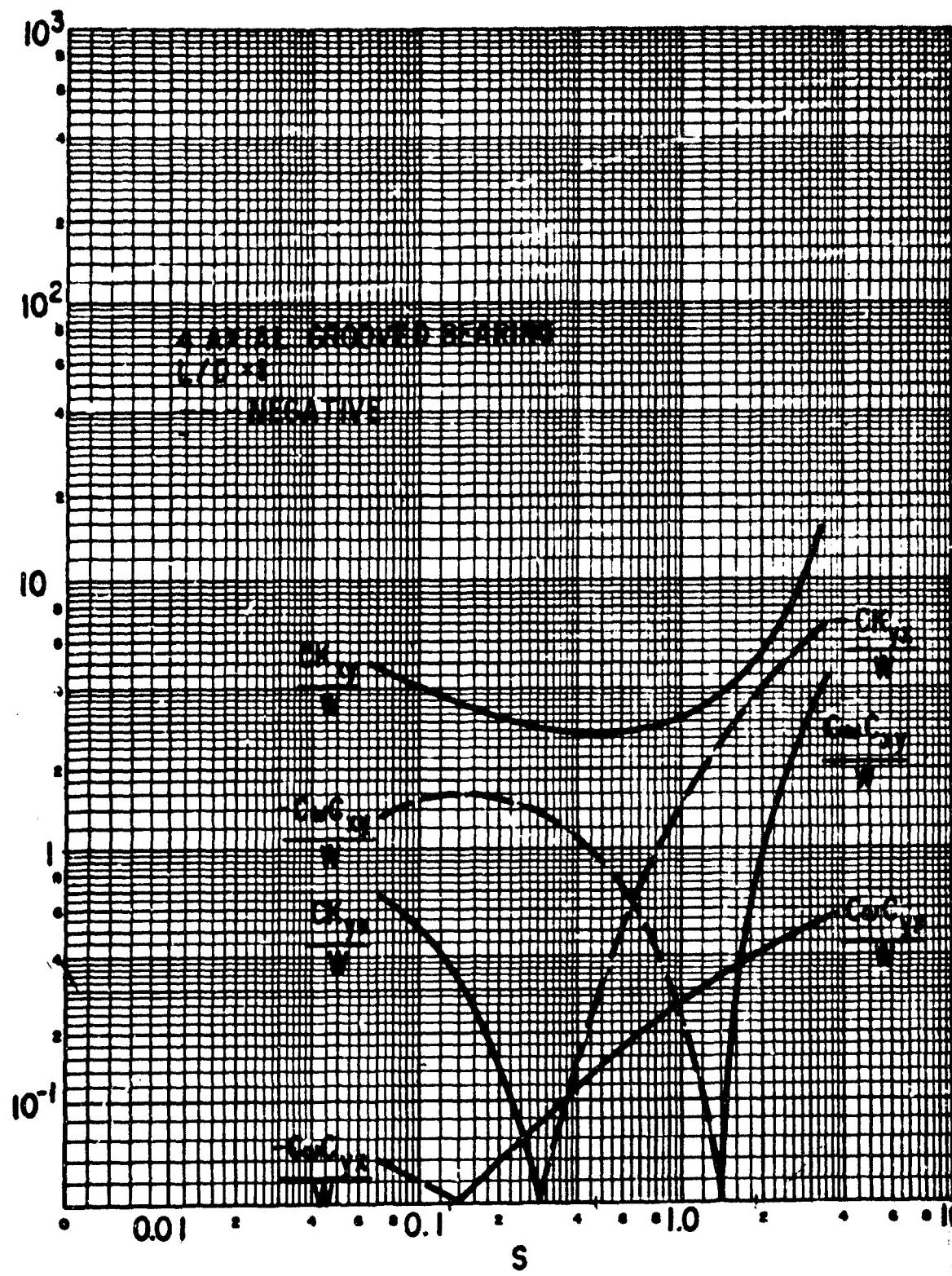


Figure B-8 The 4-Axial Groove Bearing, Laminar Film Dimensionless Dynamic Coefficients

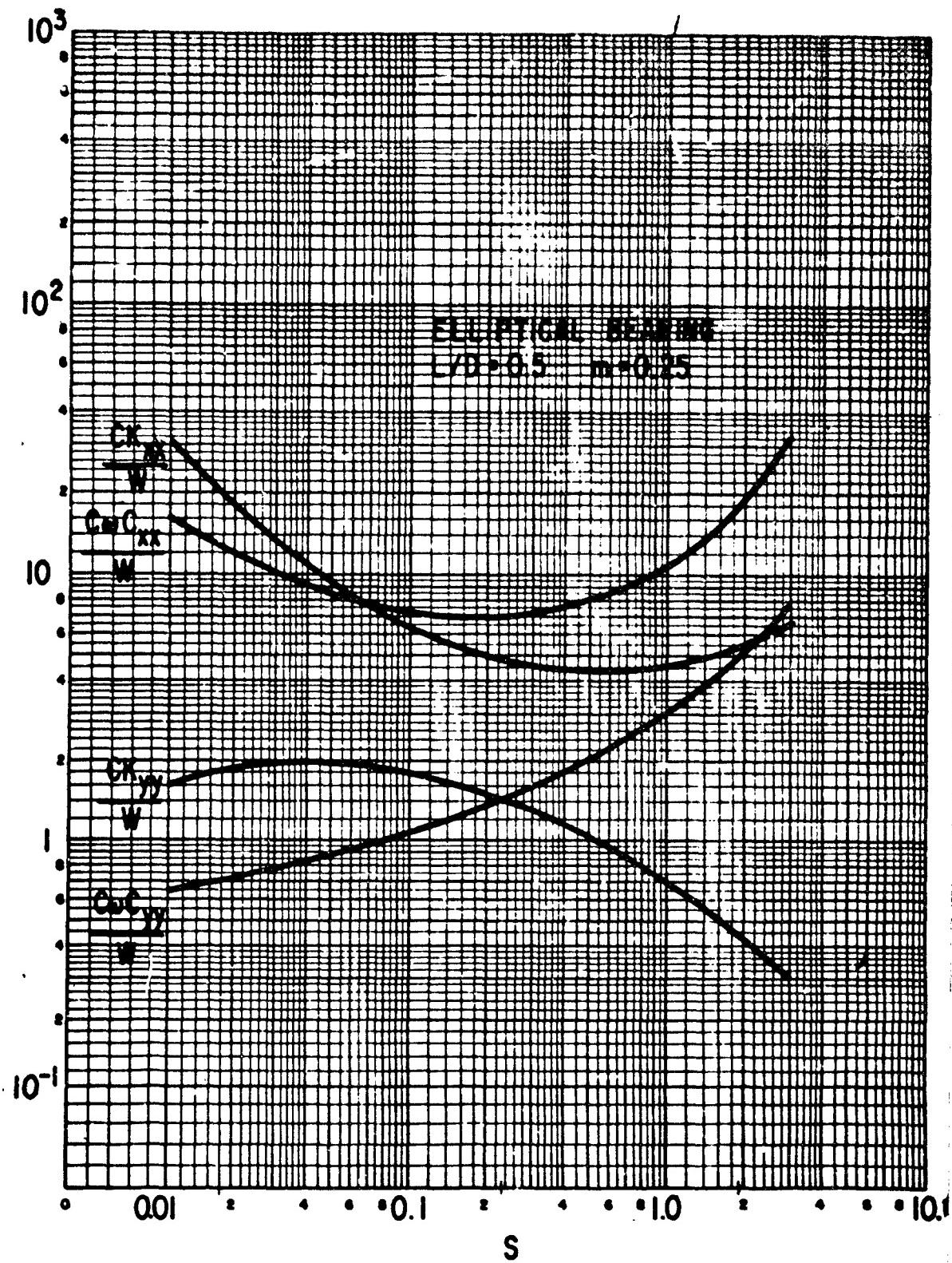


Figure B-9 The Elliptical Bearing, Laminar Film Dimensionless Dynamic Coefficients

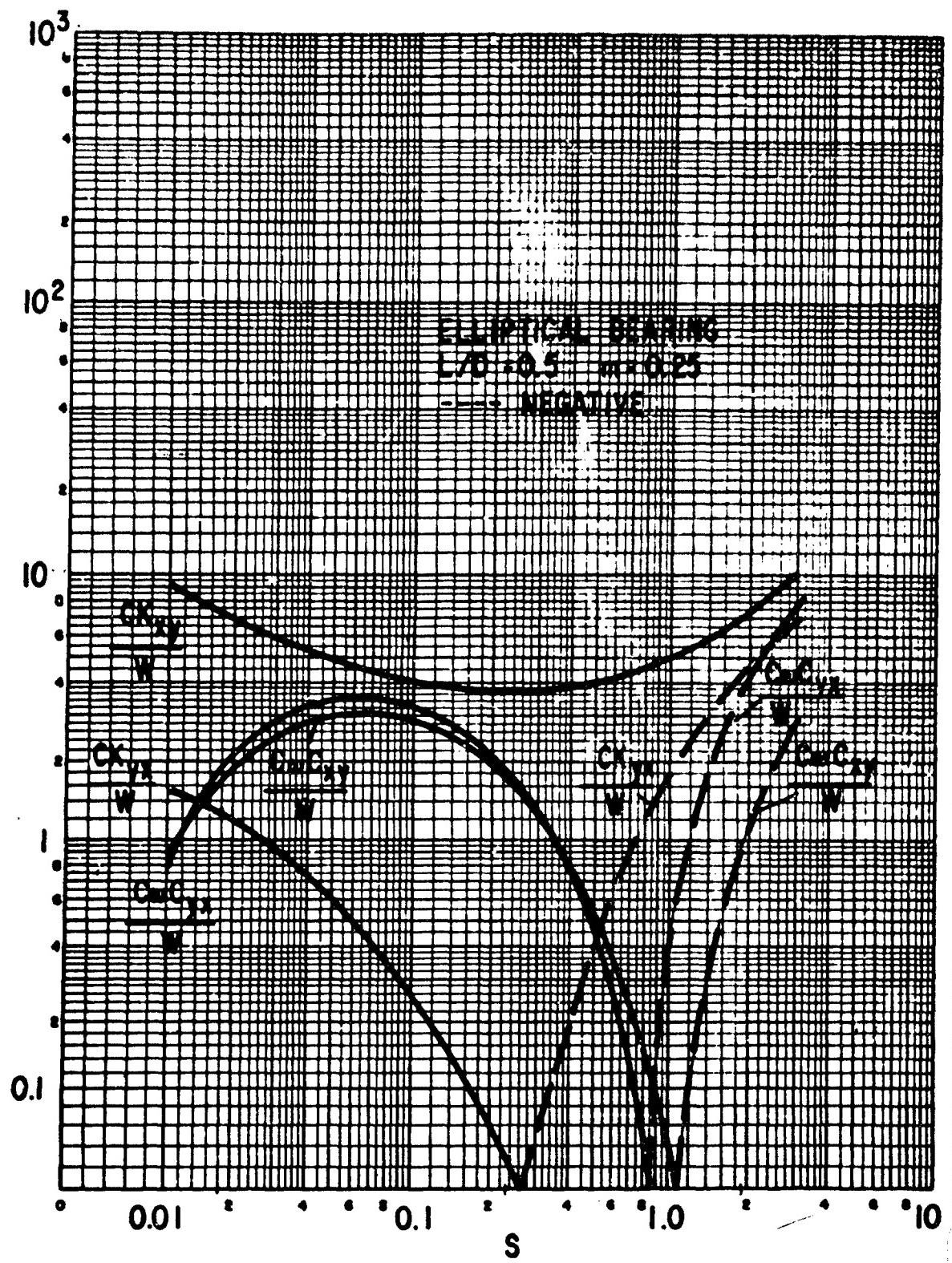


Figure B-10 The Elliptical Bearing, Laminar Film Dimensionless Dynamic Coefficients

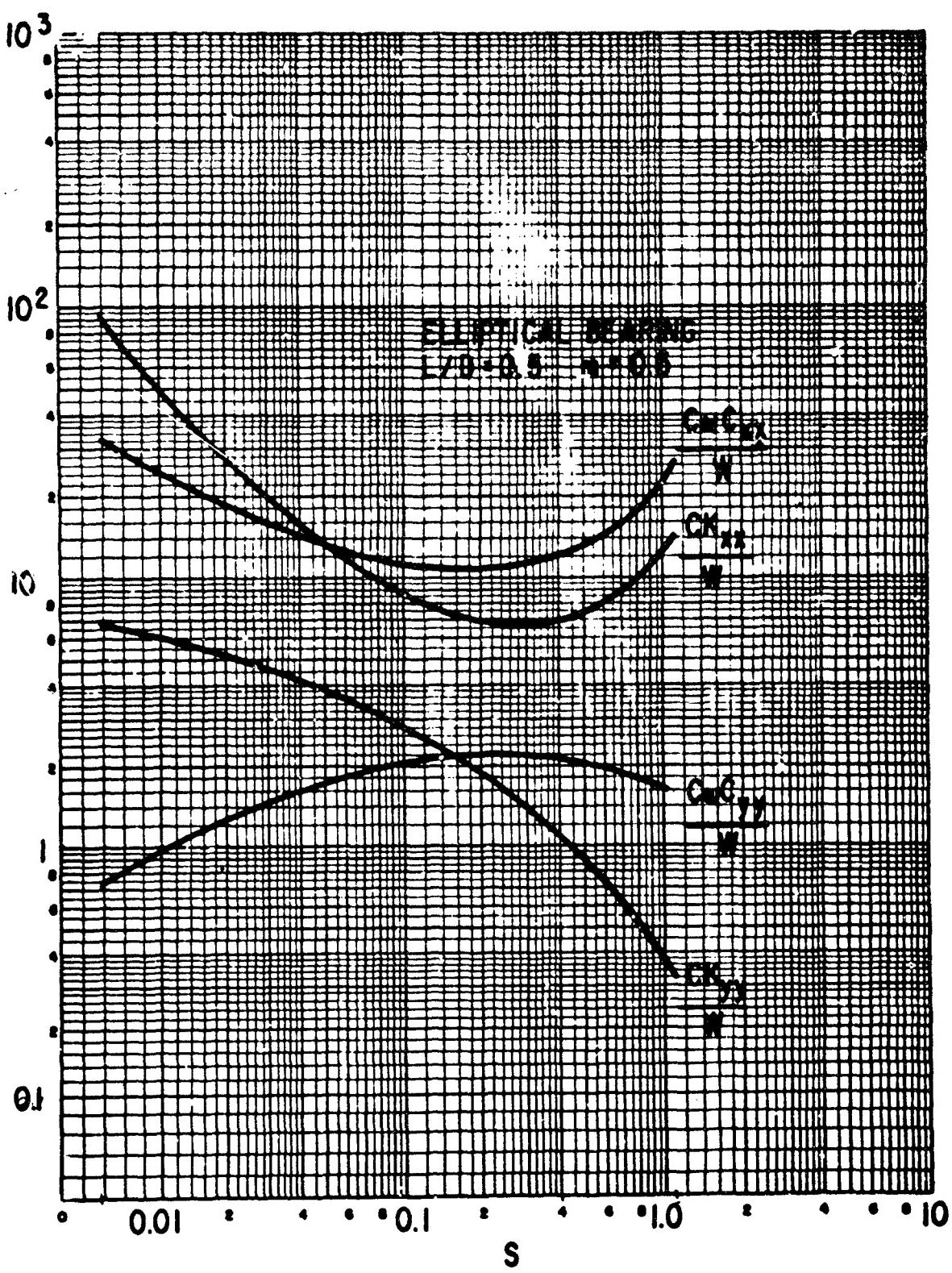


Figure B-11 The Elliptical Bearing, Laminar Film Dimensionless Dynamic Coefficients

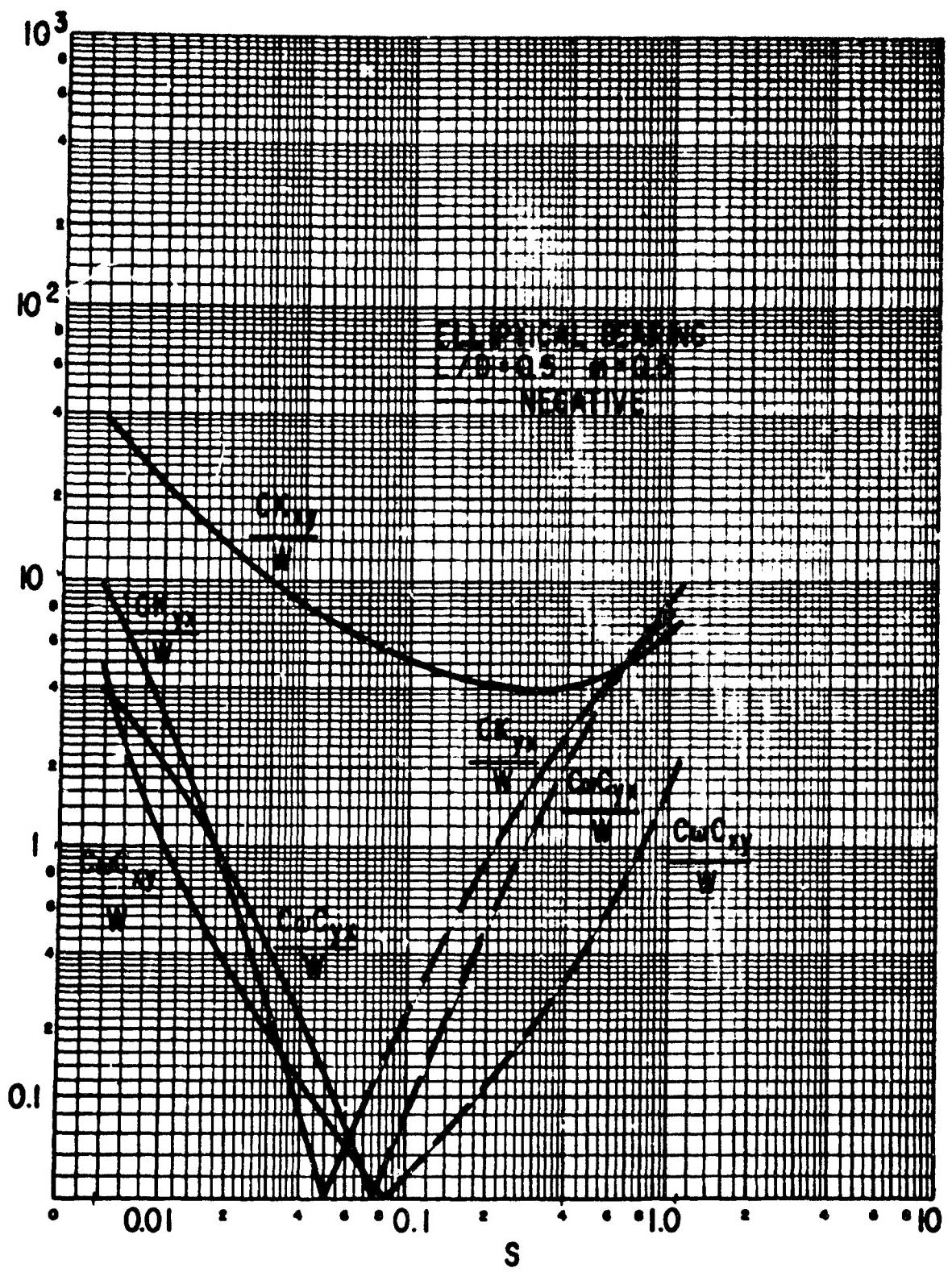


Figure B-12 The Elliptical Bearing, Laminar Film Dimensionless Dynamic Coefficients

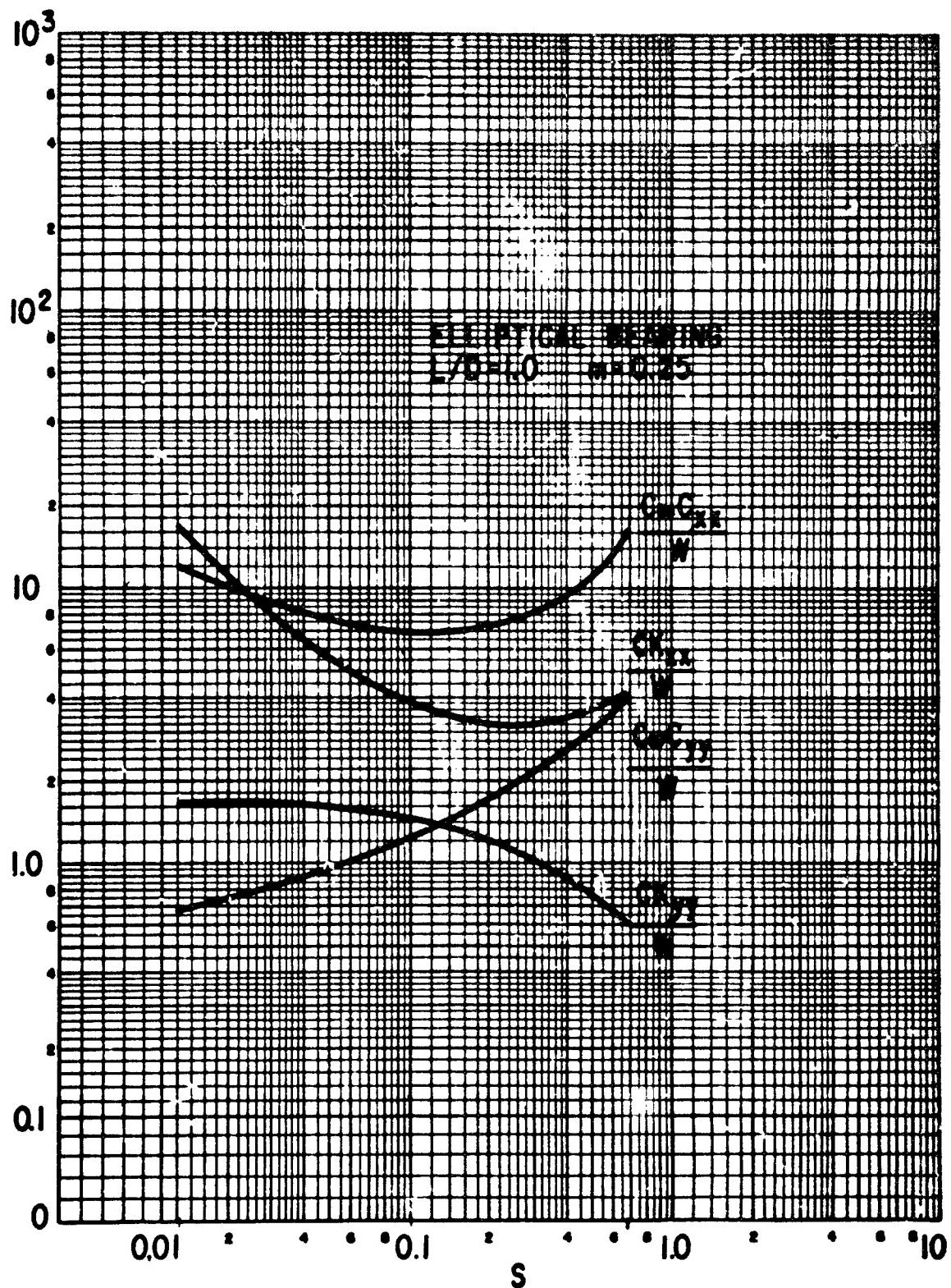


Figure B-13 The Elliptical Bearing, Laminar Film Dimensionless Dynamic Coefficients

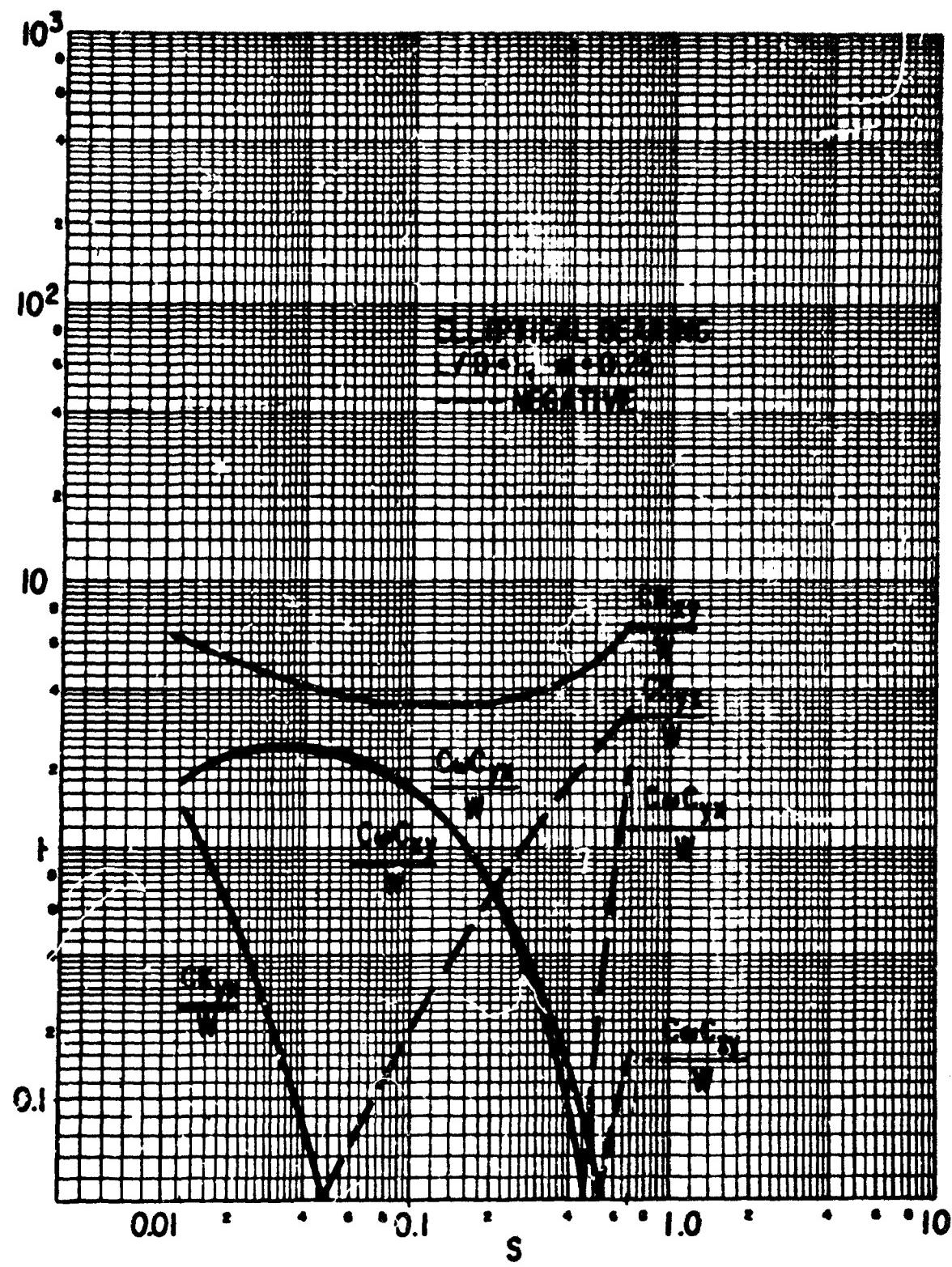


Figure B-14 The Elliptical Bearing, Laminar Film Dimensionless Dynamic Coefficients

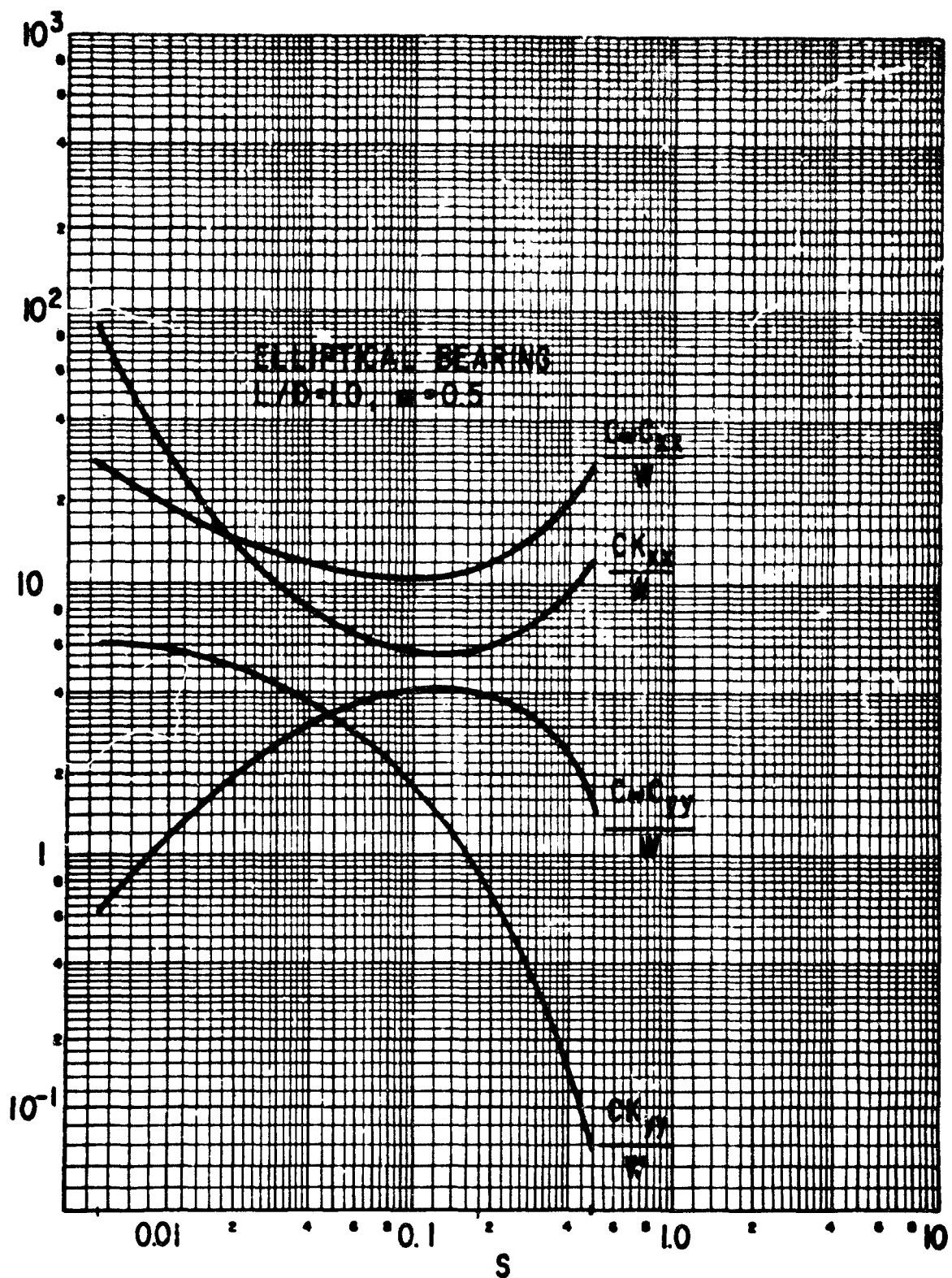


Figure B-15 The Elliptical Bearing, Laminar Film Dimensionless Dynamic Coefficients

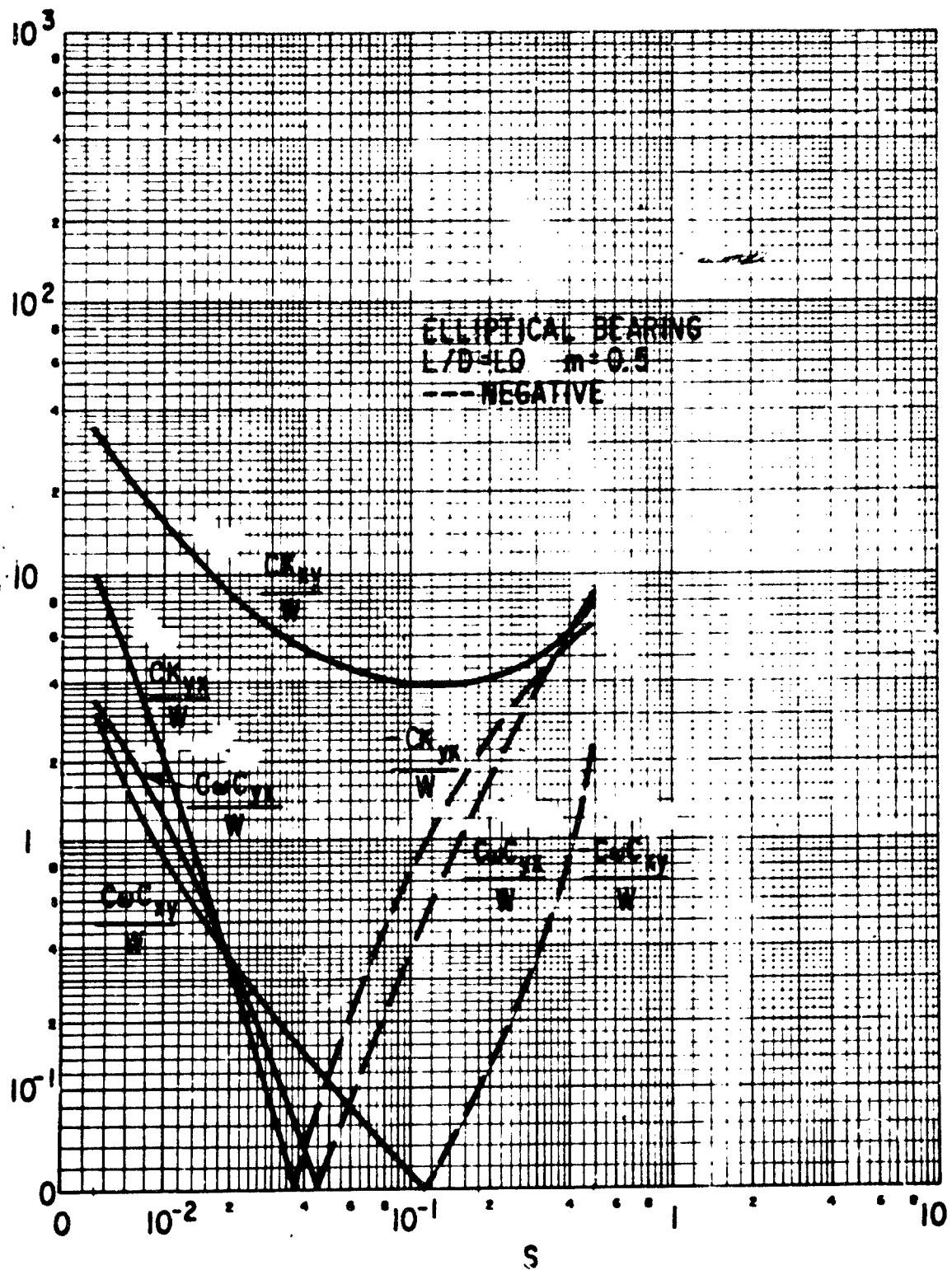


Figure B-16 The Elliptical Bearing, Laminar Film Dimensionless Dynamic Coefficients

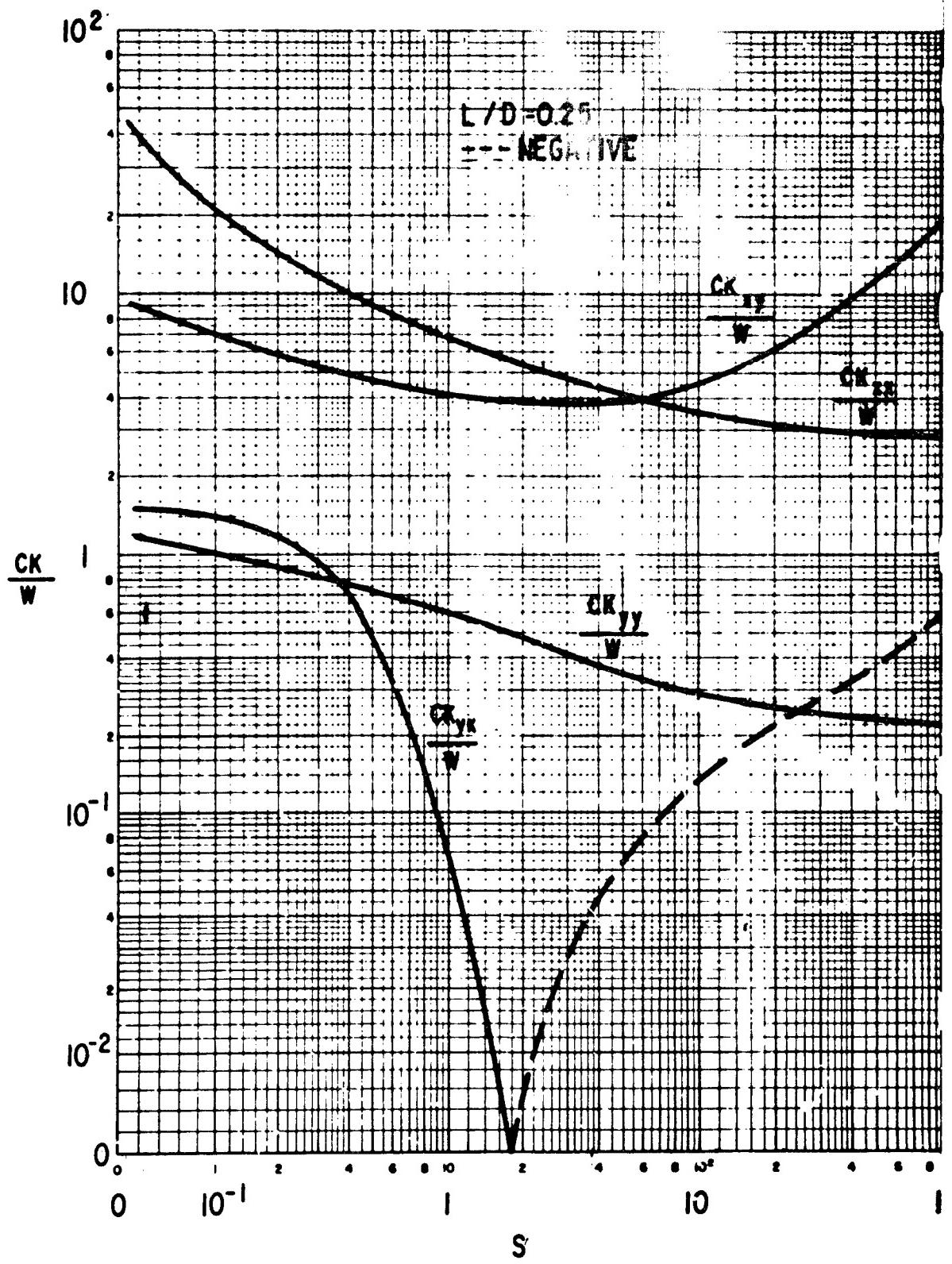


Figure B-17 The 50 Degree Partial Bearing, Centrally Loaded, Laminar Film Dimensionless Dynamic Coefficients

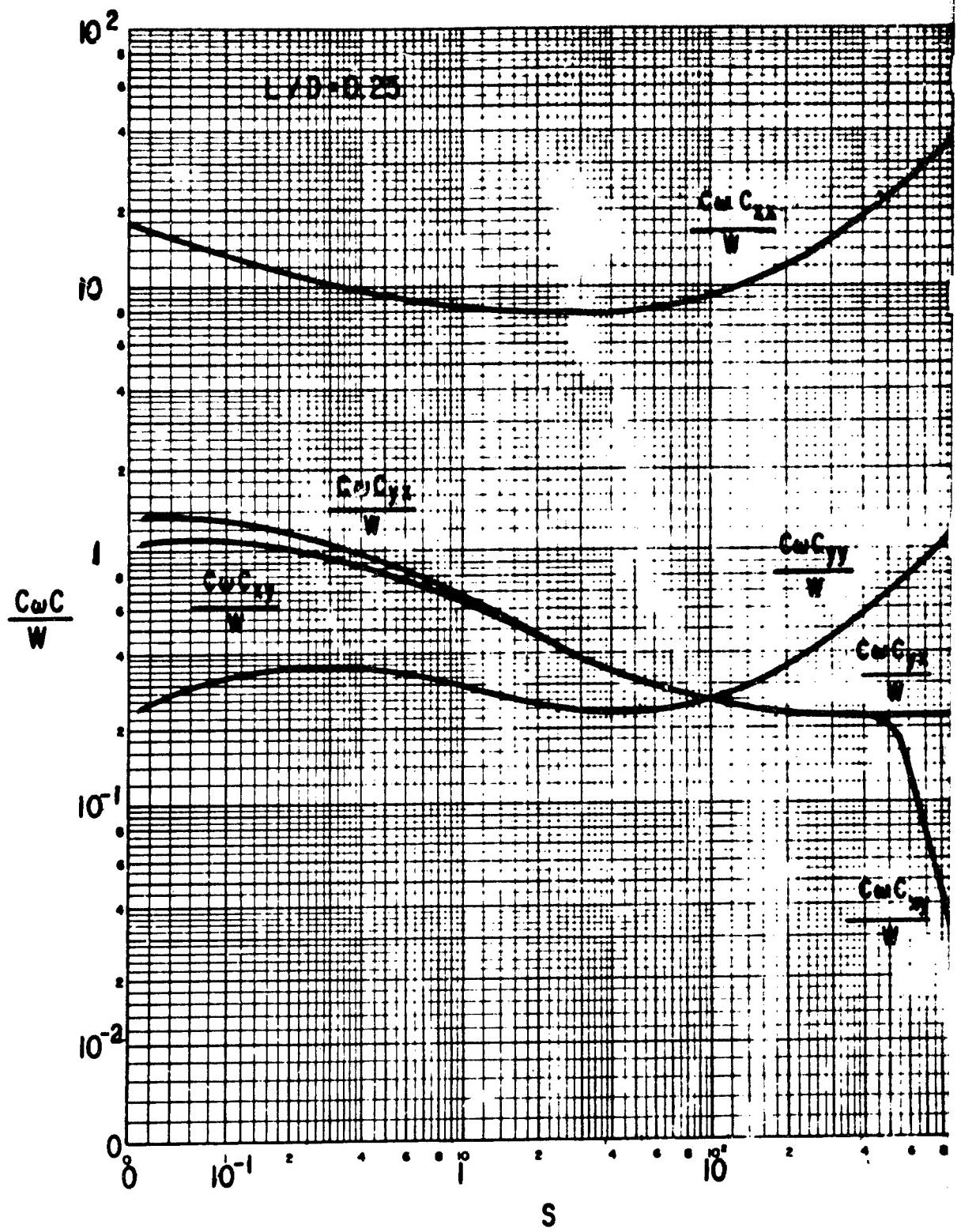


Figure B-18 The 50 Degree Partial Bearing, Centrally Loaded, Laminar Film Dimensionless Dynamic Coefficients

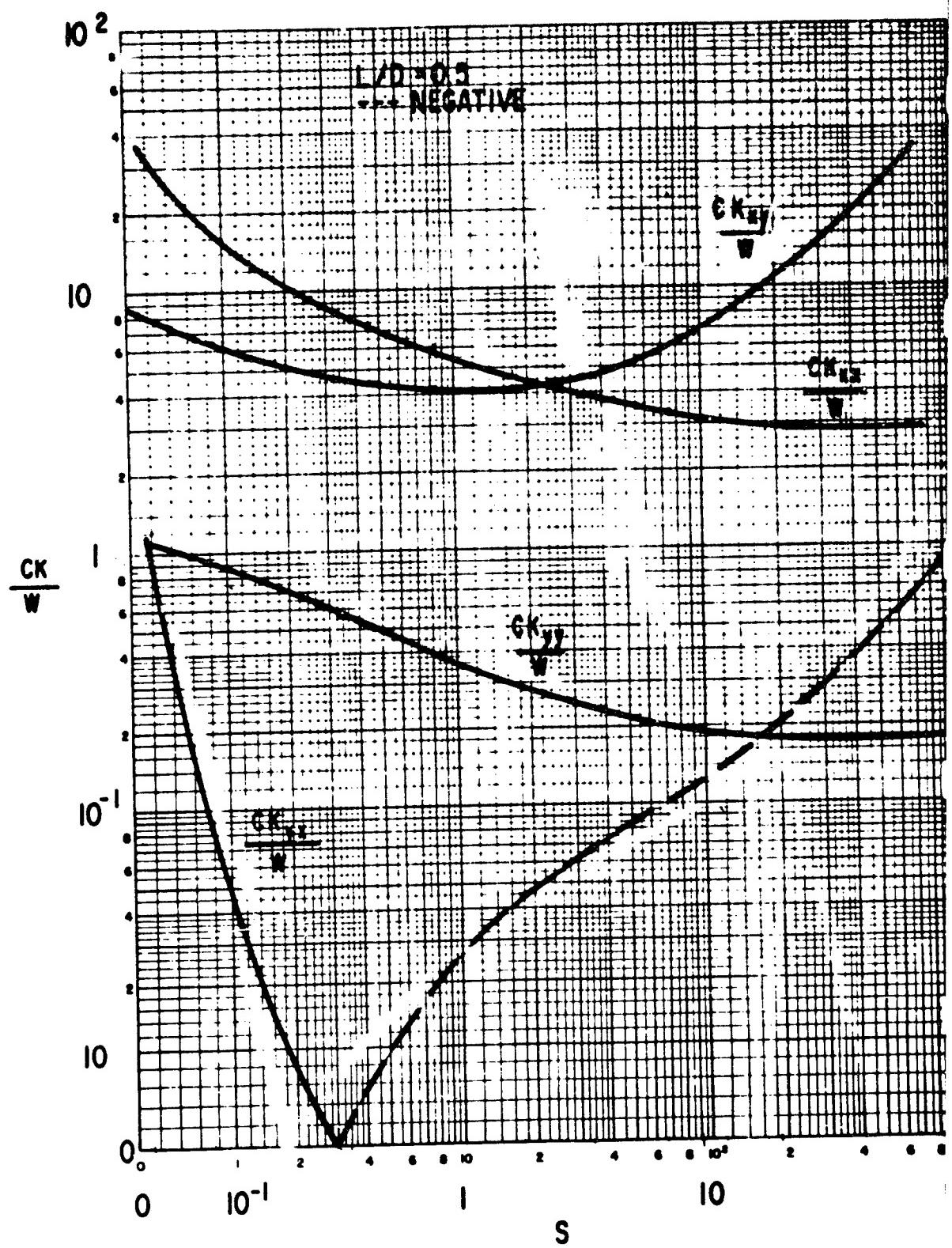


Figure B-19 The 50 Degree Partial Bearing, Centrally Loaded, Laminar Flow Dimensionless Dynamic Coefficients

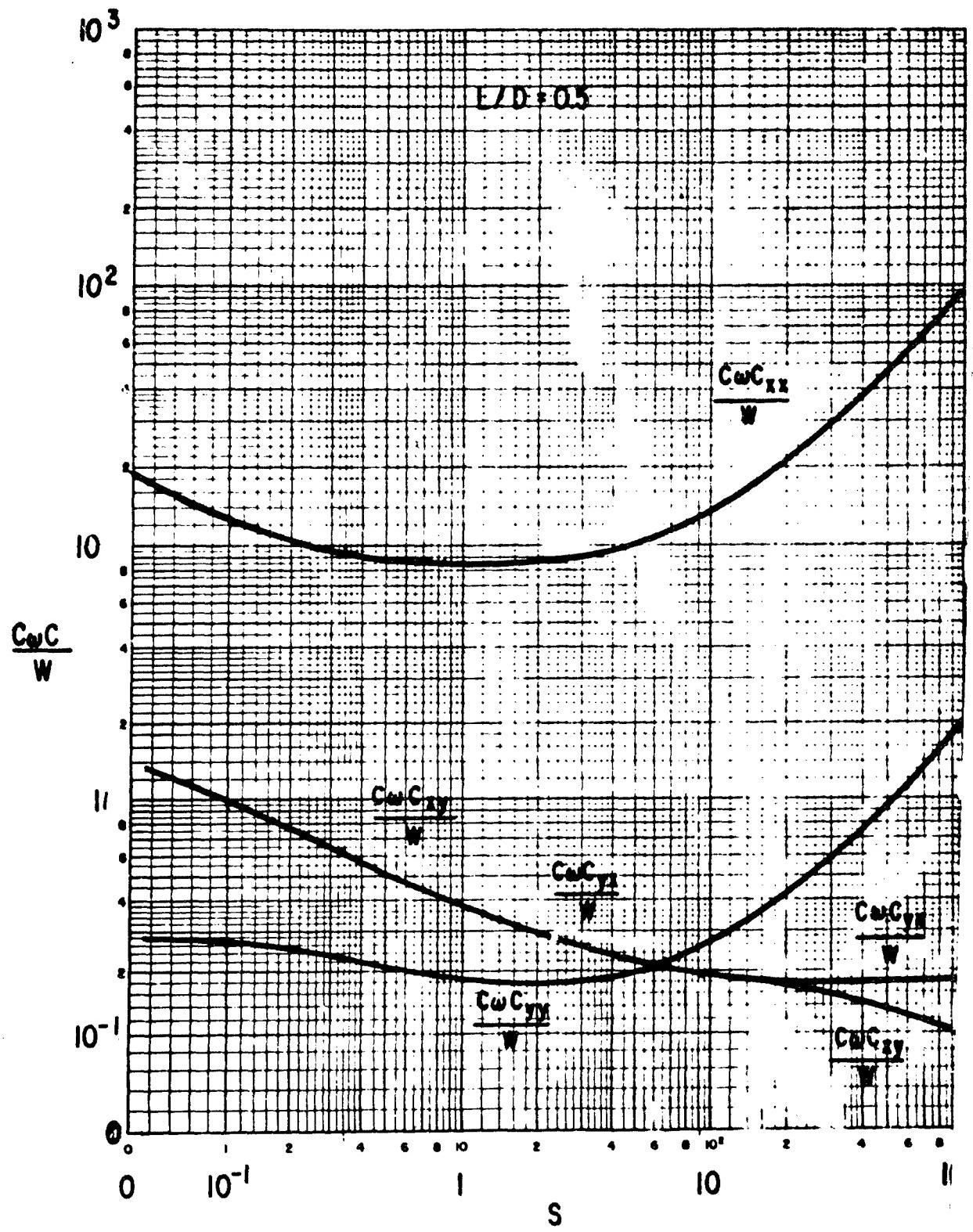


Figure B-20 The 50 Degree Partial Bearing, Centrally Loaded, Laminar Film Dimensionless Dynamic Coefficients

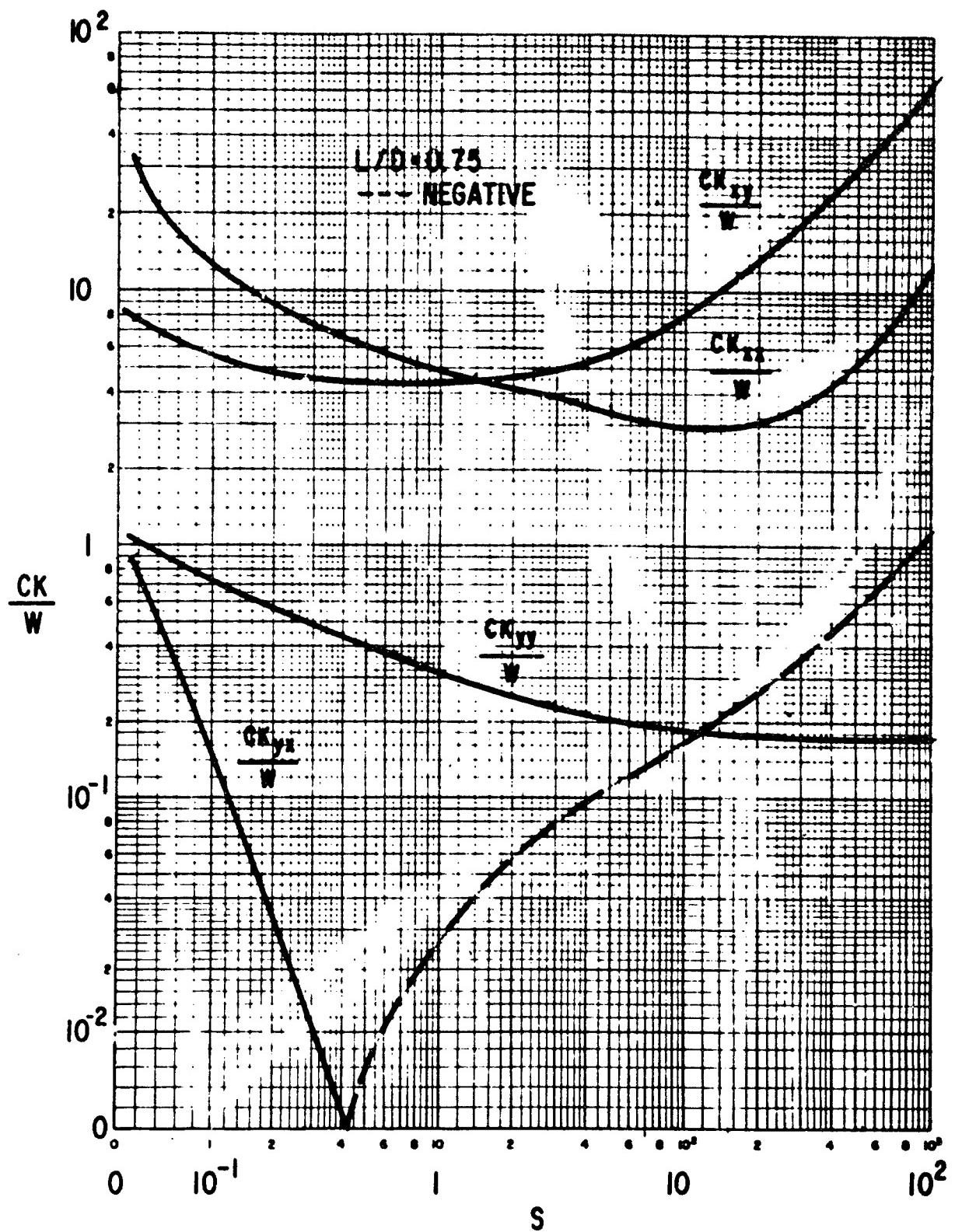


Figure B-21 The 50 Degree Partial Bearing, Centrally Loaded, Laminar Film Dimensionless Dynamic Coefficients

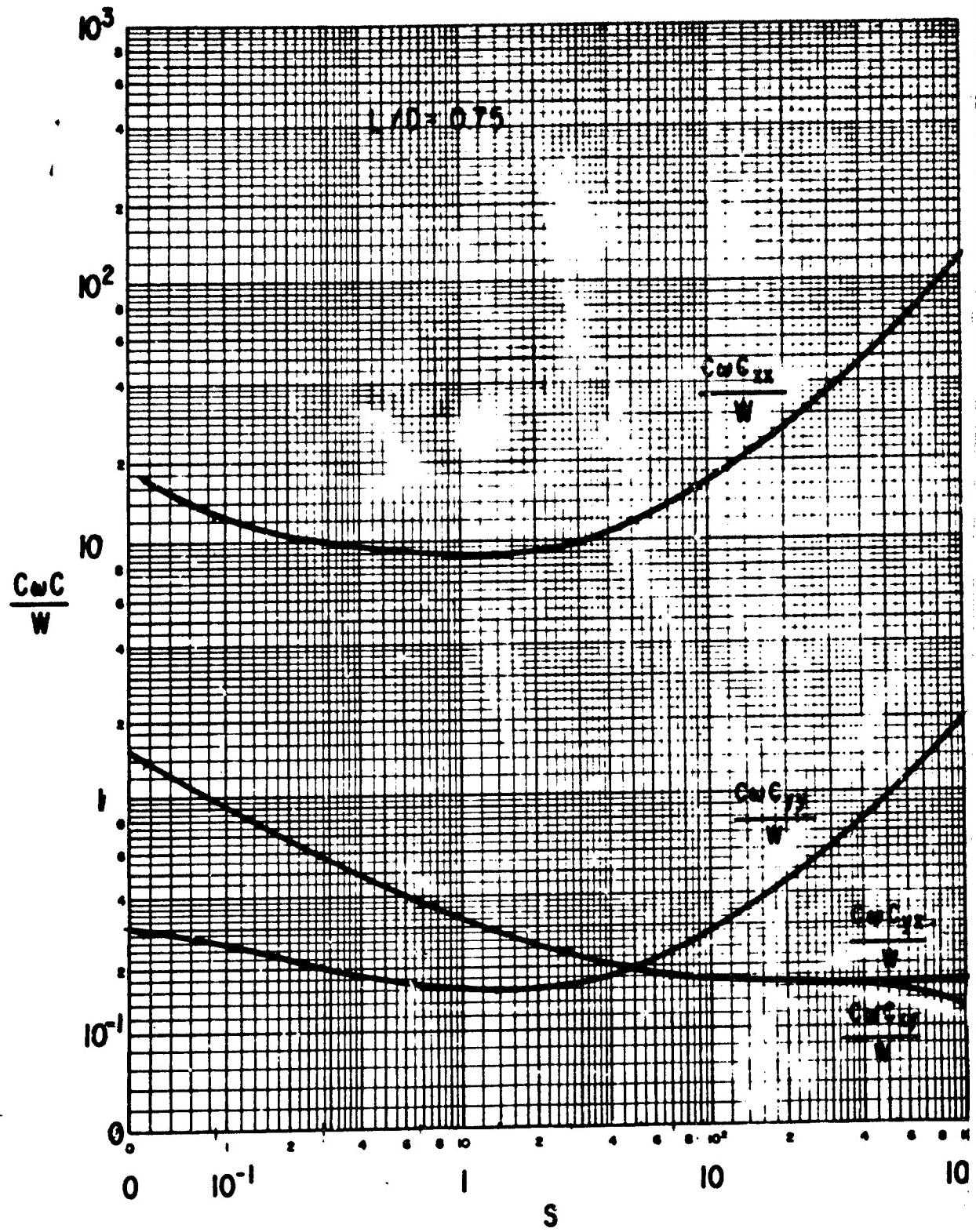


Figure B-22 The 50 Degree Partial Bearing, Centrally Loaded, Laminar Film Dimensionless Dynamic Coefficients

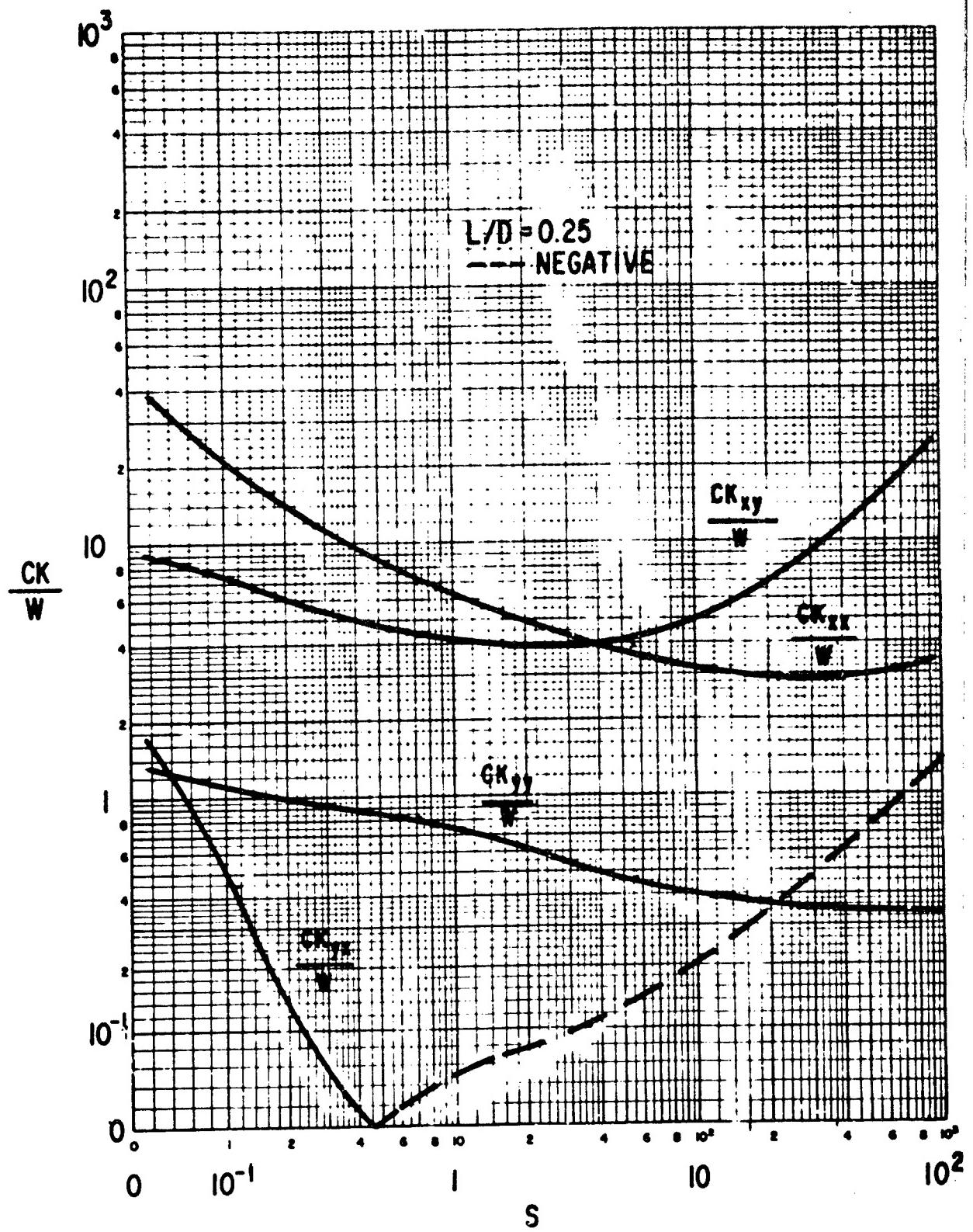


Figure B-23 The 60 Degree Partial Bearing, Centrally Loaded, Laminar Film Dimensionless Dynamic Coefficients

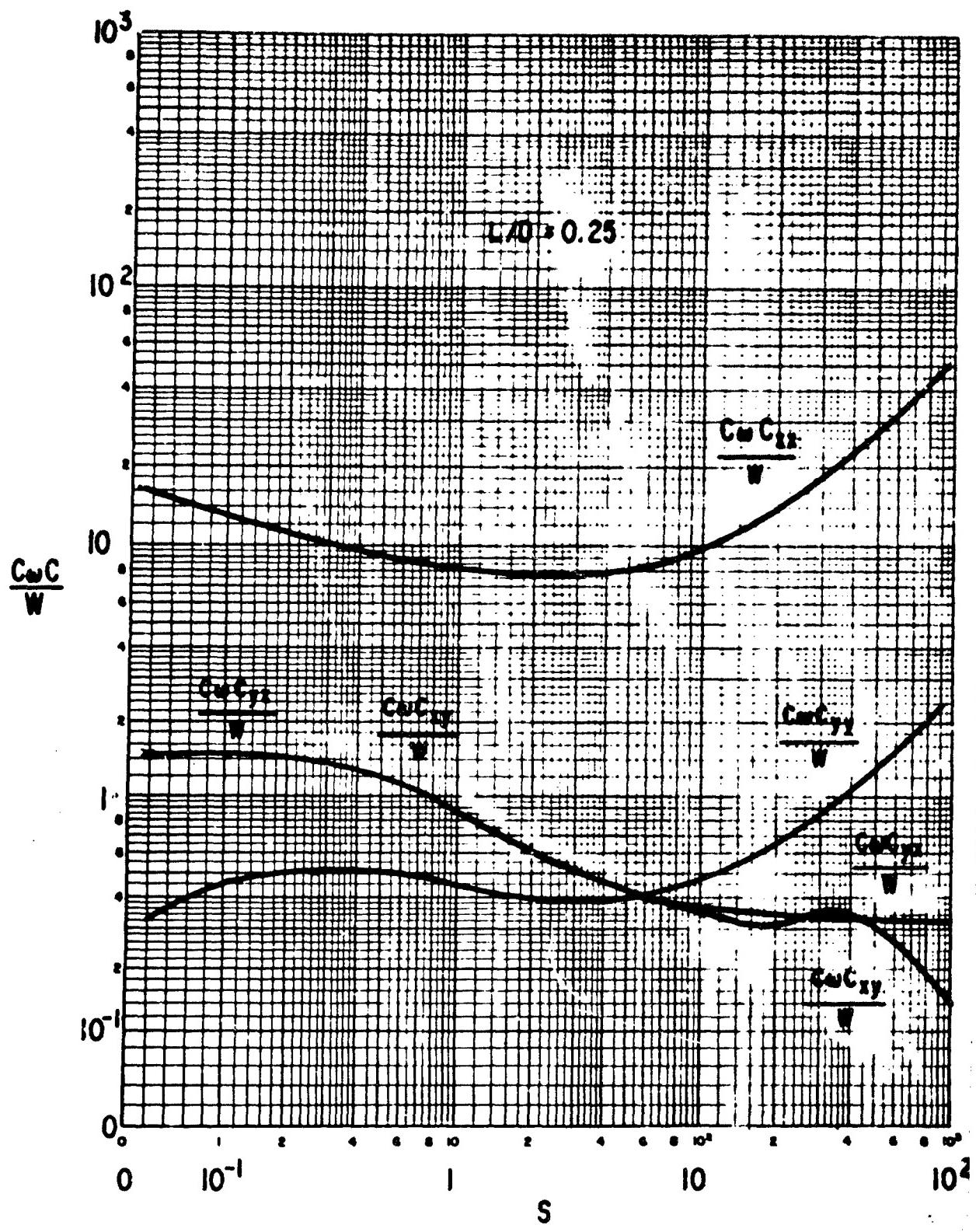


Figure B-24 The 60 Degree Partial Bearing, Centrally Loaded, Laminar Film Dimensionless Dynamic Coefficients

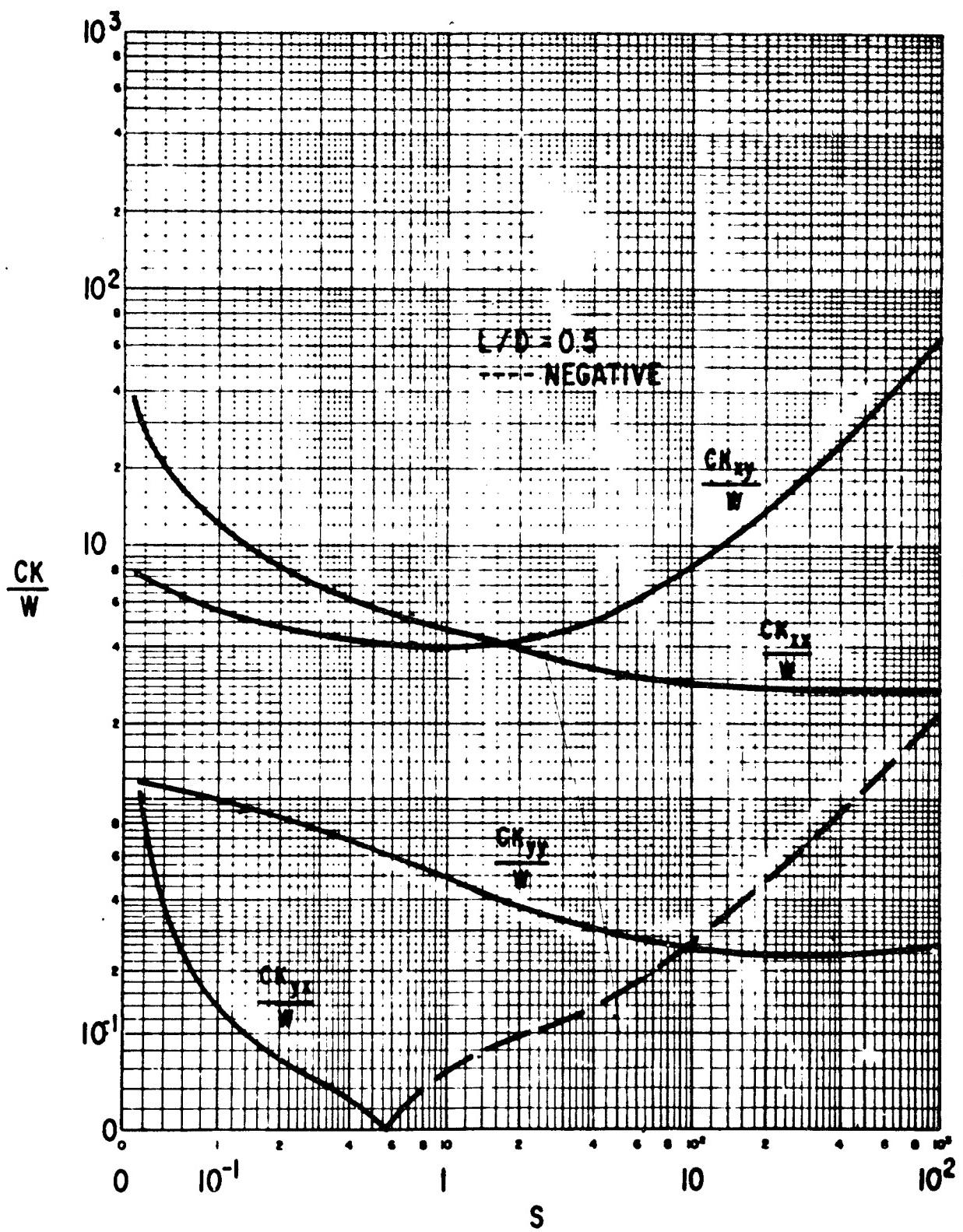


Figure B-25 The 60 Degree Partial Bearing, Centrally Loaded, Laminar Film Dimensionless Dynamic Coefficients

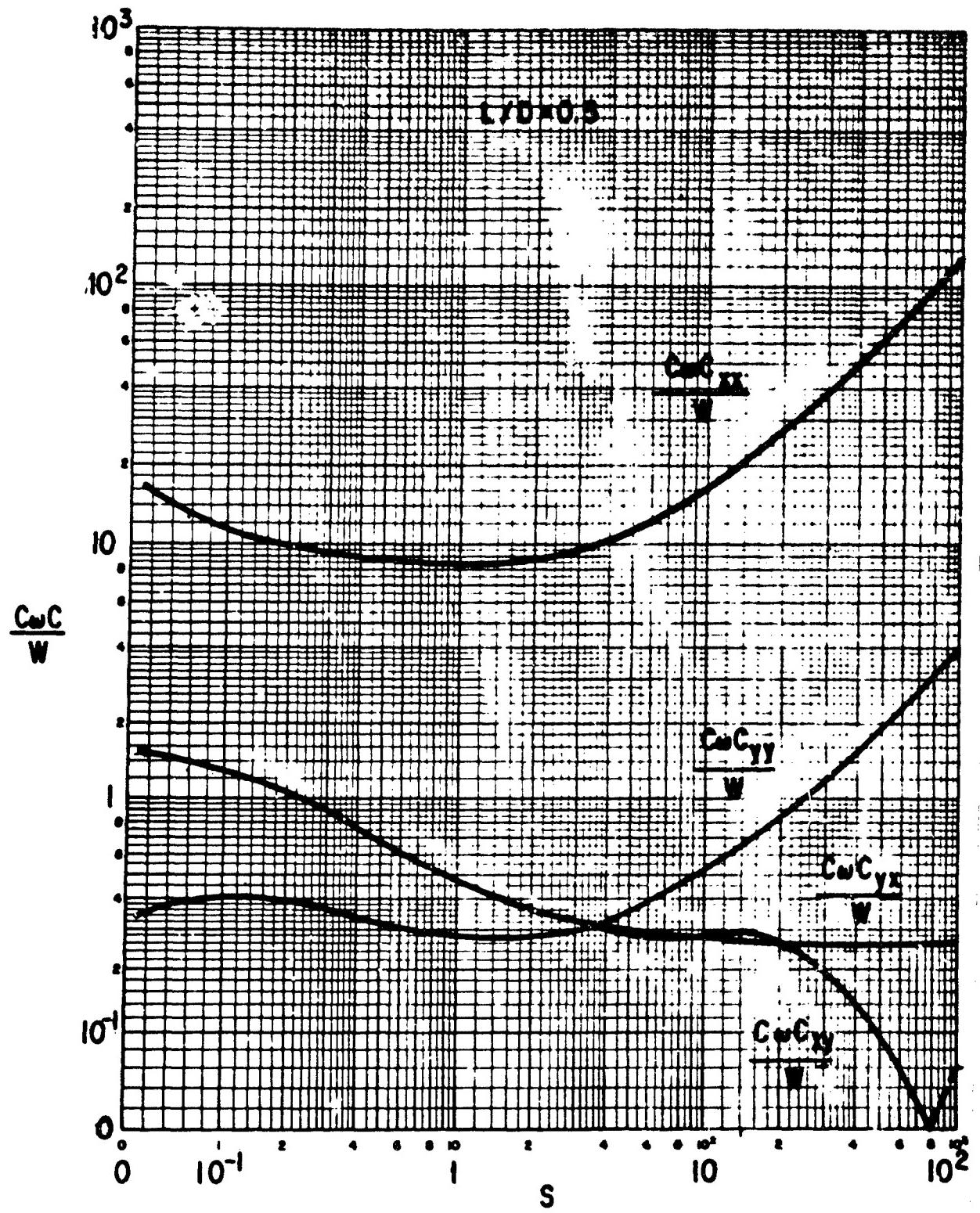


Figure B-26 The 60 Degree Partial Bearing, Centrally Loaded, Laminar Film Dimensionless Dynamic Coefficients

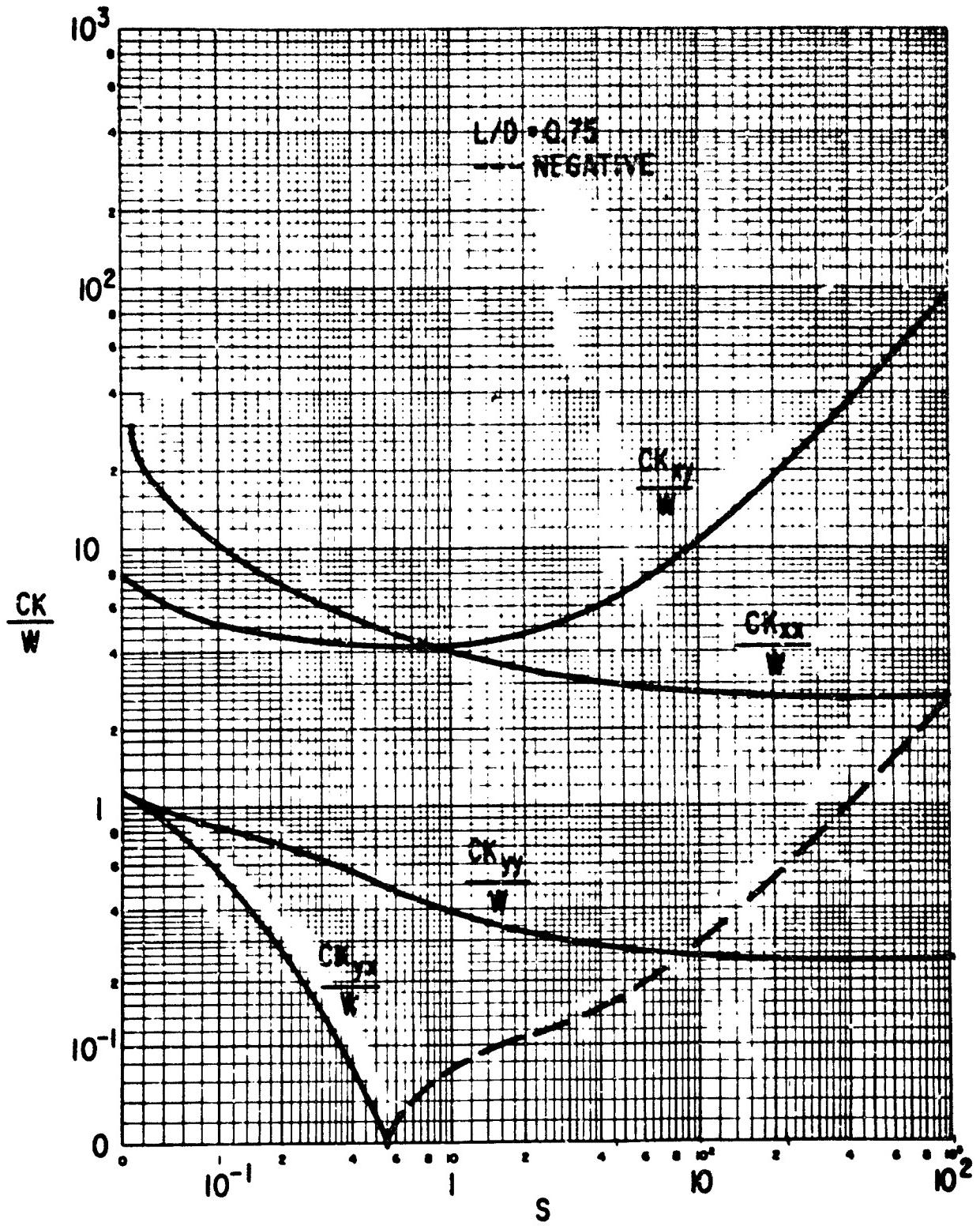


Figure B-27 The 60 Degree Partial Bearing, Centrally Loaded, Laminar Film Dimensionless Dynamic Coefficients

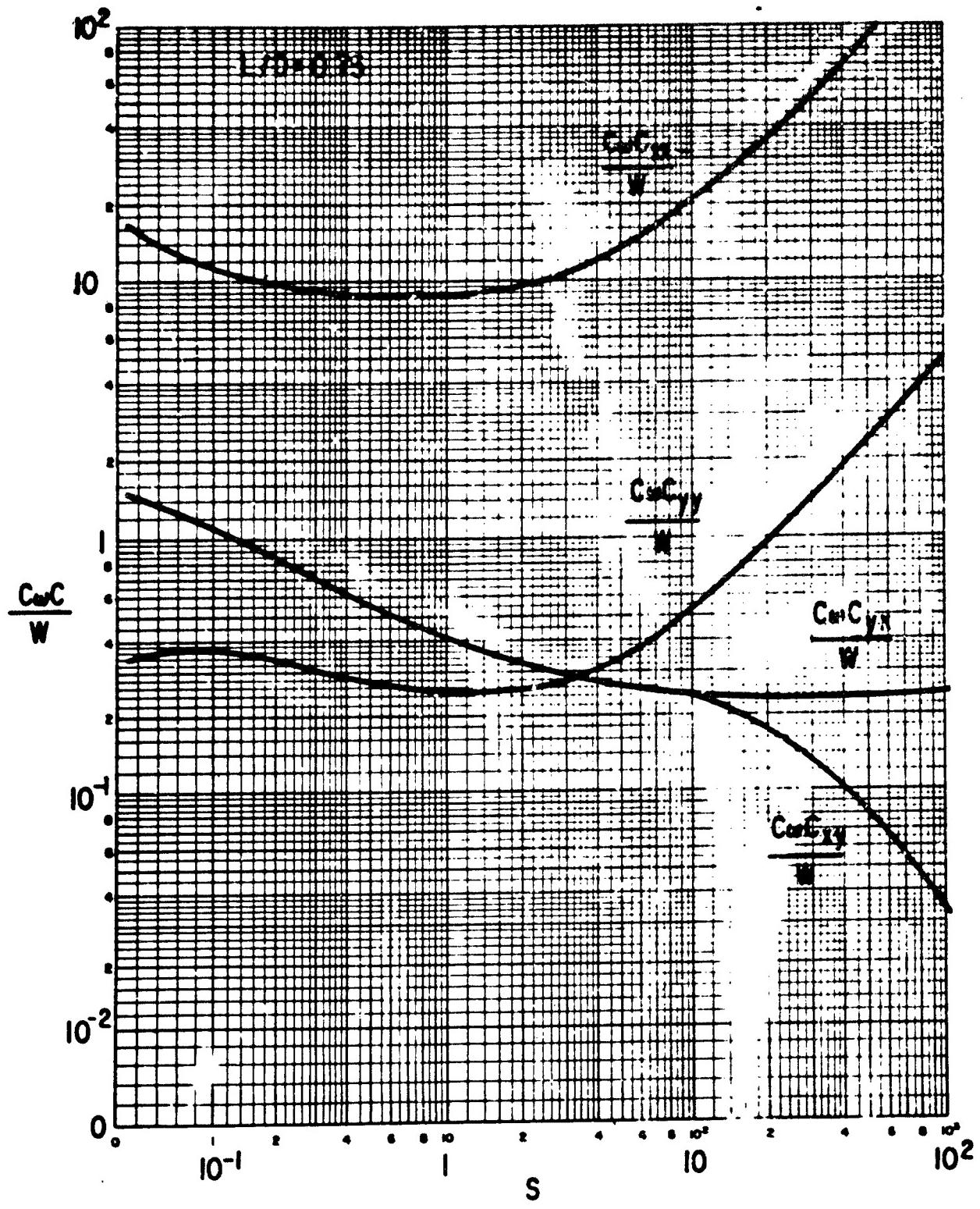


Figure B-28 The 60 Degree Partial Bearing, Centrally Loaded, Laminar Film Dimensionless Dynamic Coefficients

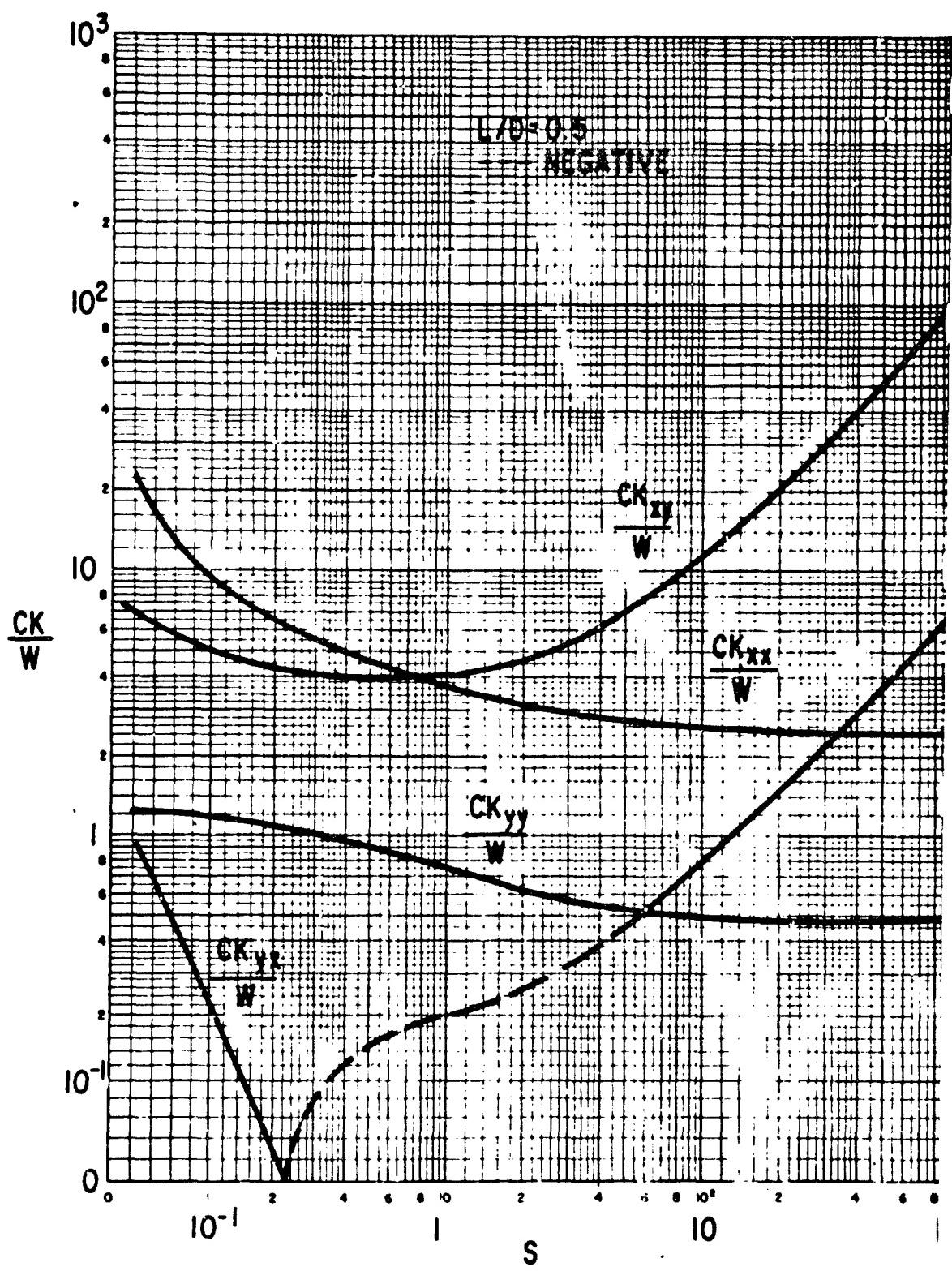


Figure B-29 The 80 Degree Partial Bearing, Centrally Loaded, Laminar Film Flow Dimensionless Dynamic Coefficients

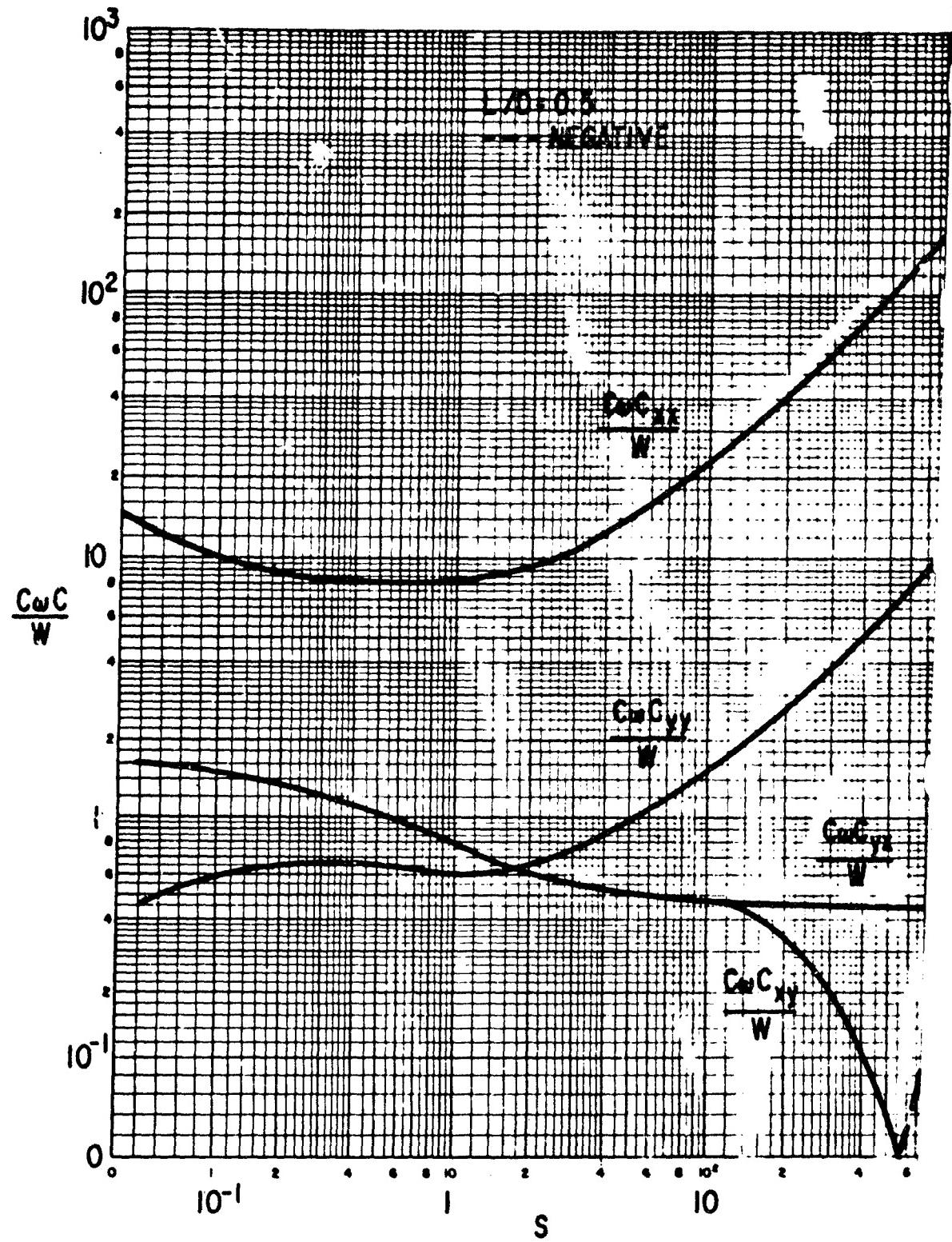


Figure B-30 The 80 Degree Partial Bearing, Centrally Loaded, Laminar Dimensionless Dynamic Coefficients

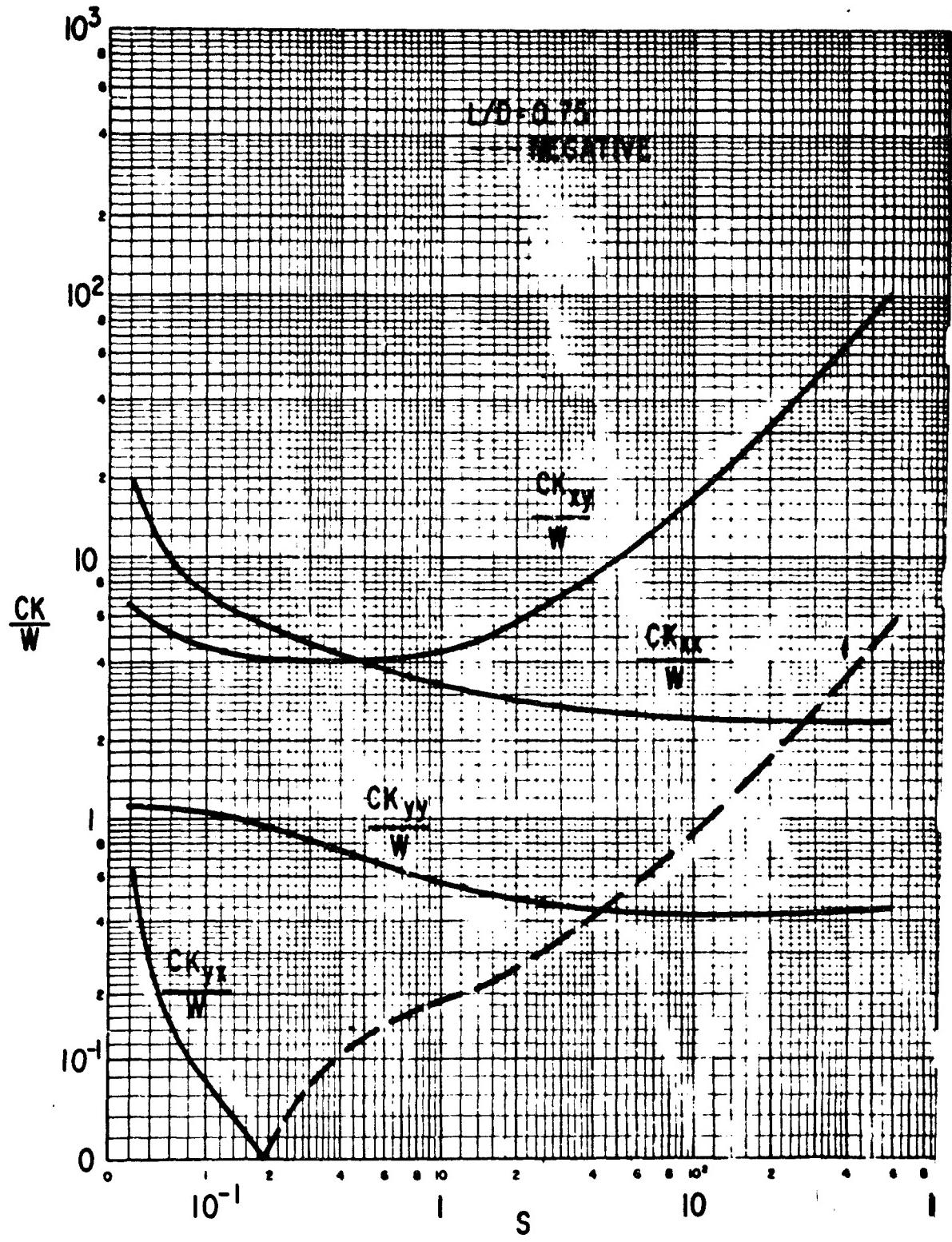


Figure B-31 The 80 Degree Partial Bearing, Centrally Loaded, Laminar Film Dimensionless Dynamic Coefficients

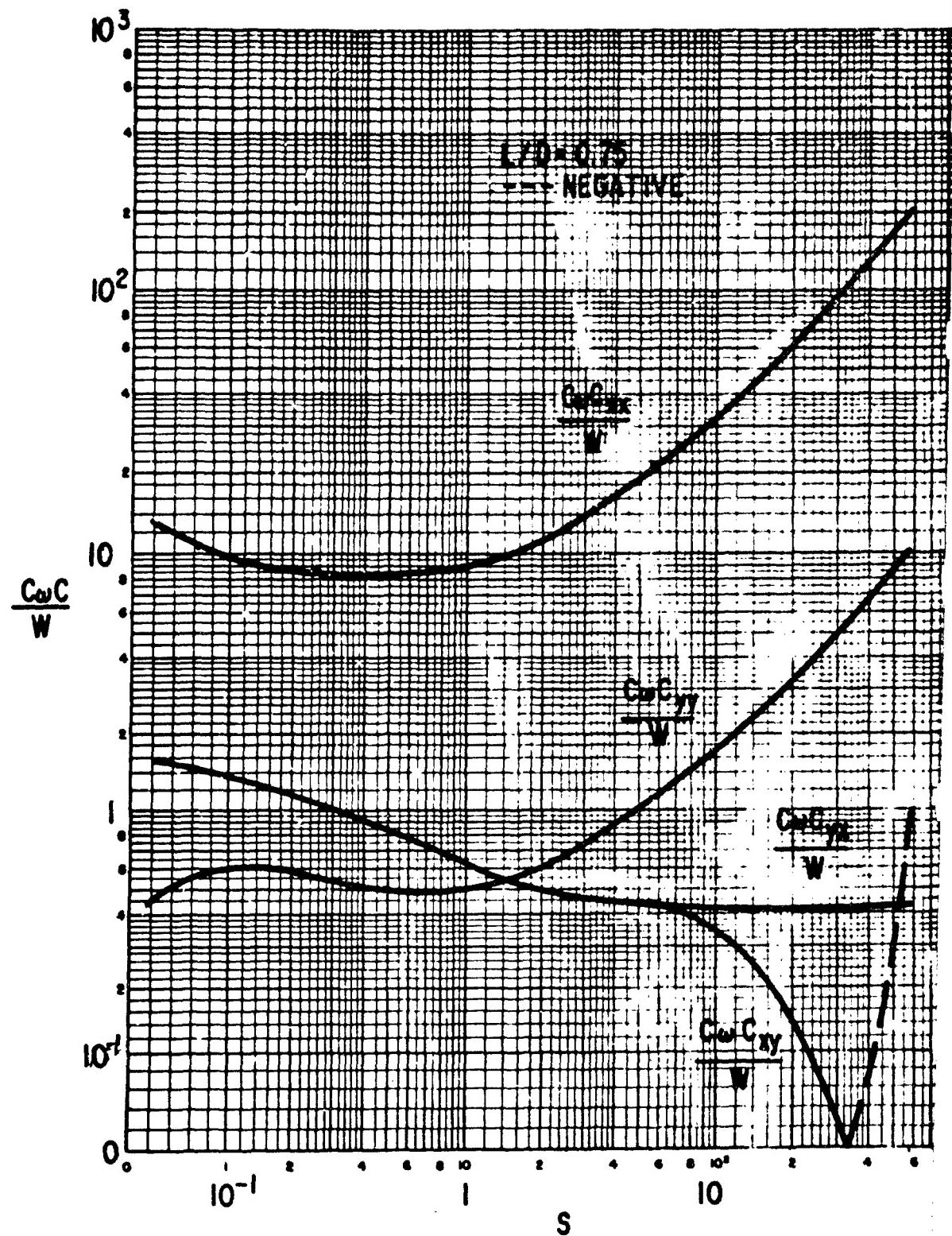


Figure B-32 The 80 Degree Partial Bearing, Centrally Loaded, Laminar Film Dimensionless Dynamic Coefficients

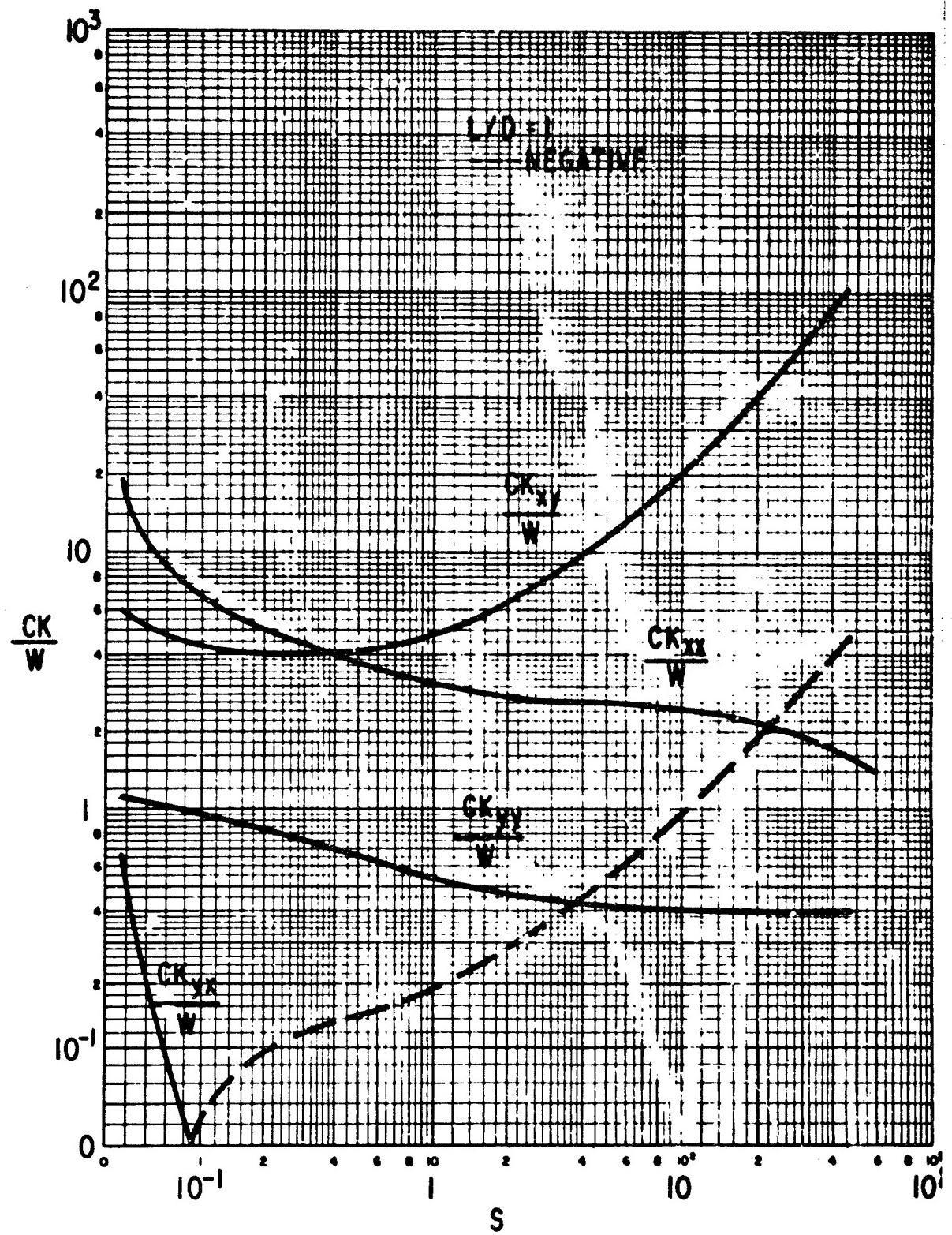


Figure B-33 The 80 Degree Partial Bearing, Centrally Loaded, Laminar Film Dimensionless Dynamic Coefficients

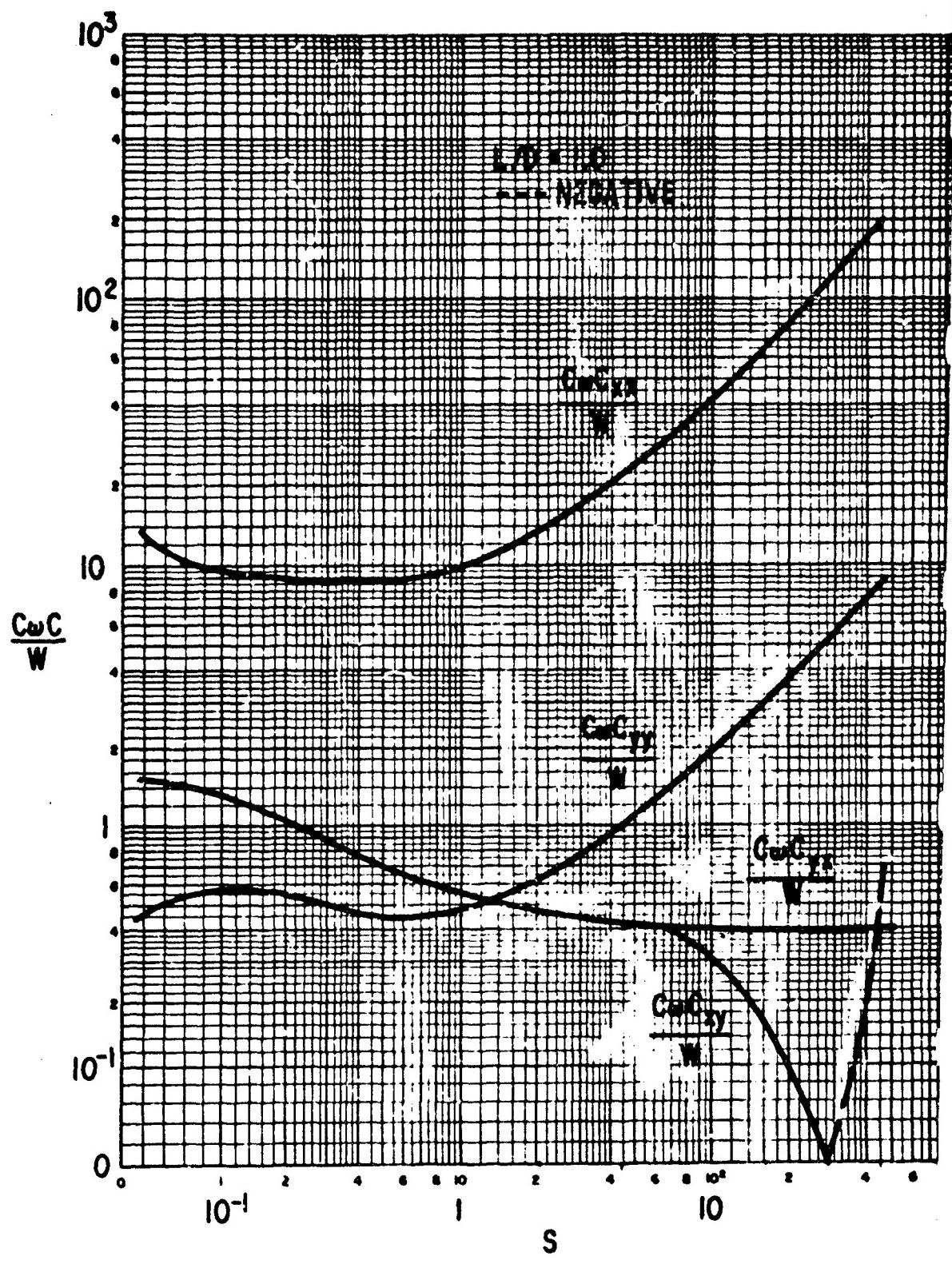


Figure B-34 The 80 Degree Partial Bearing, Centrally Loaded, Laminar Flow Dimensionless Dynamic Coefficients

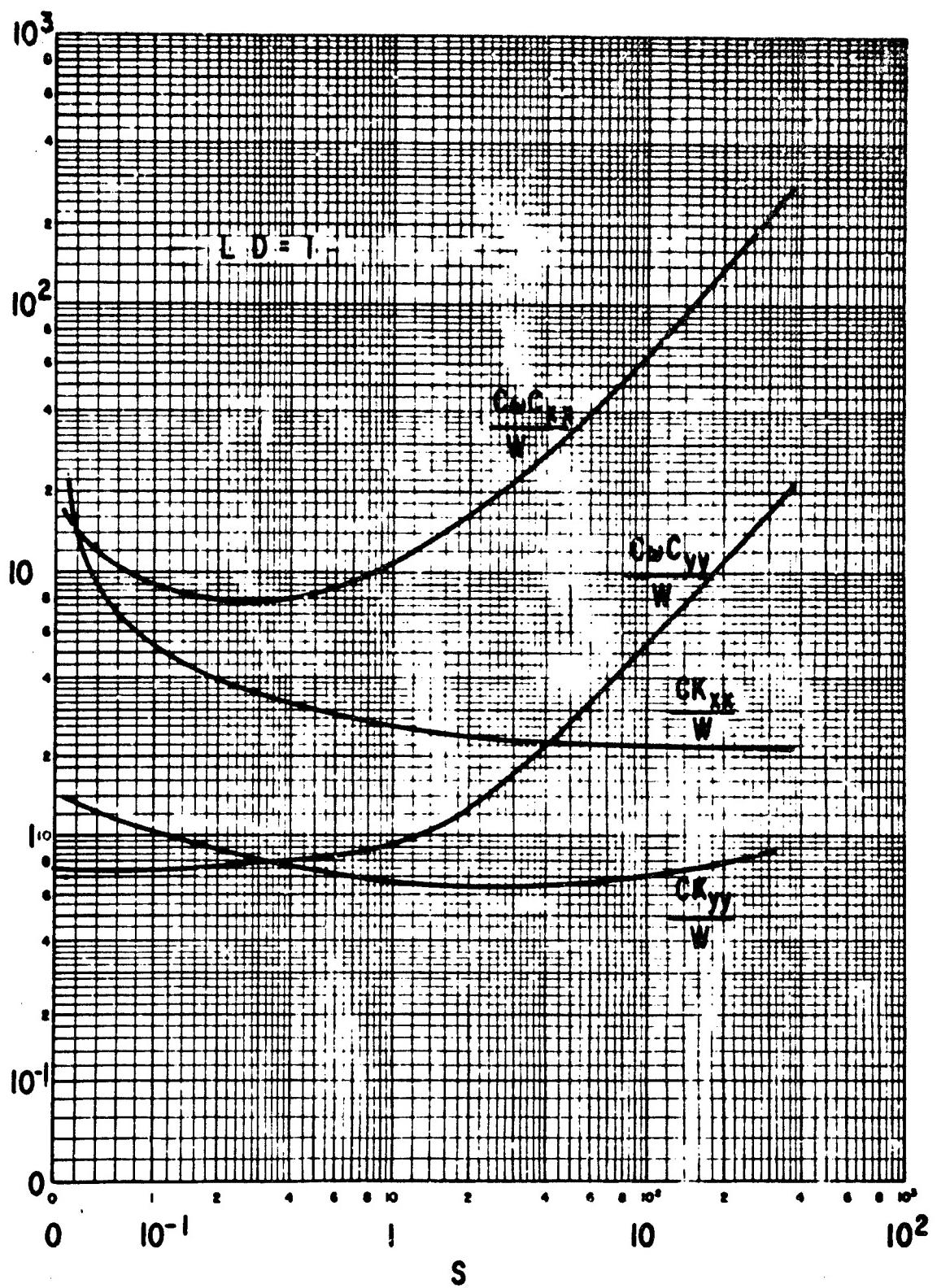


Figure B-35 The 100 Degree Partial Bearing, Centrally Loaded, Laminar Film Dimensionless Dynamic Coefficients

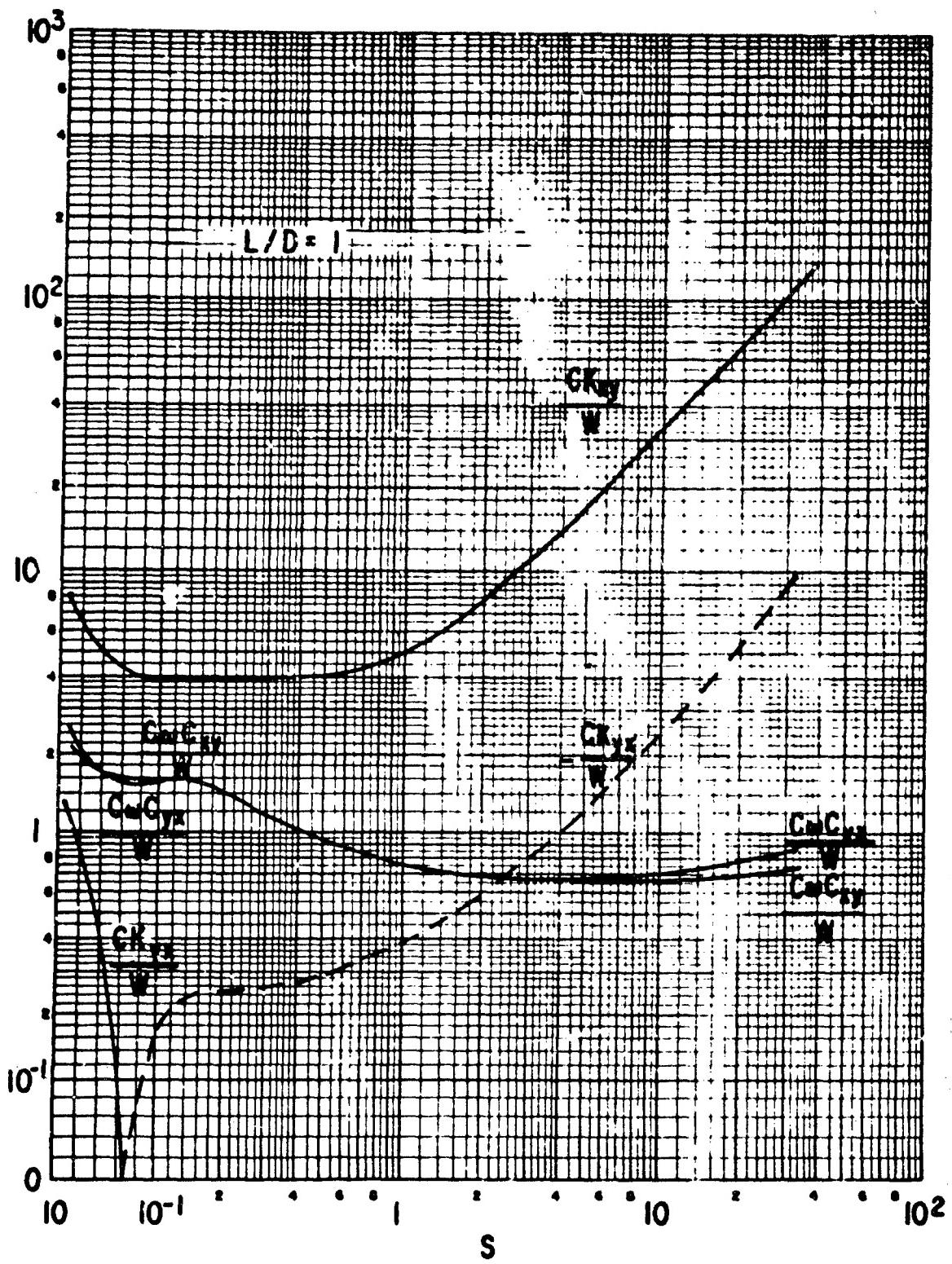


Figure B-36 The 100 Degree Partial Bearing, Centrally Loaded, Laminar Film Dimensionless Dynamic Coefficients

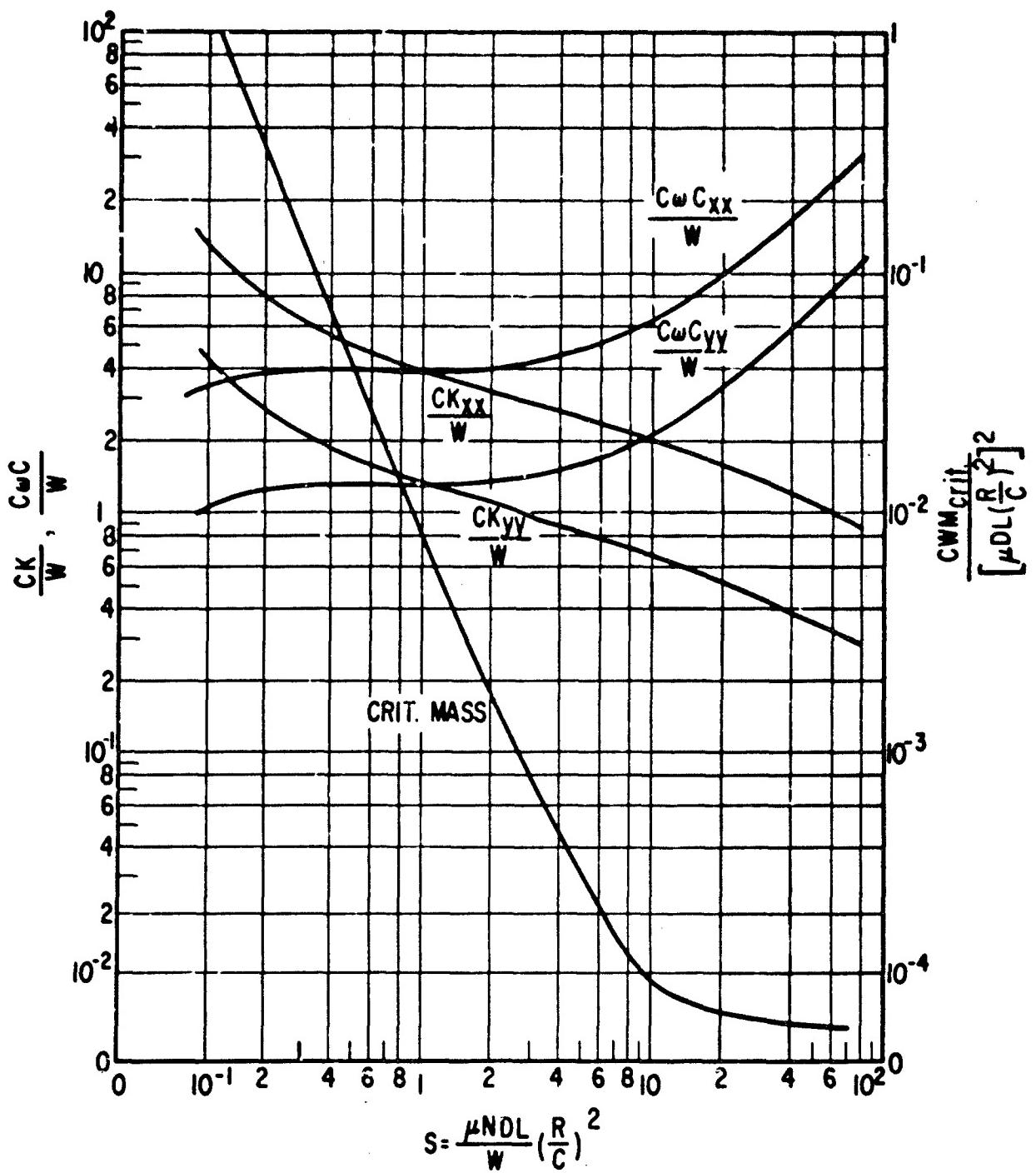


Figure B-37 The 6 Shoe Tilting Pad Bearing, L/D = .25, Laminar Film Load between Pads
 $C'/C = 1$, No Pad Inertia

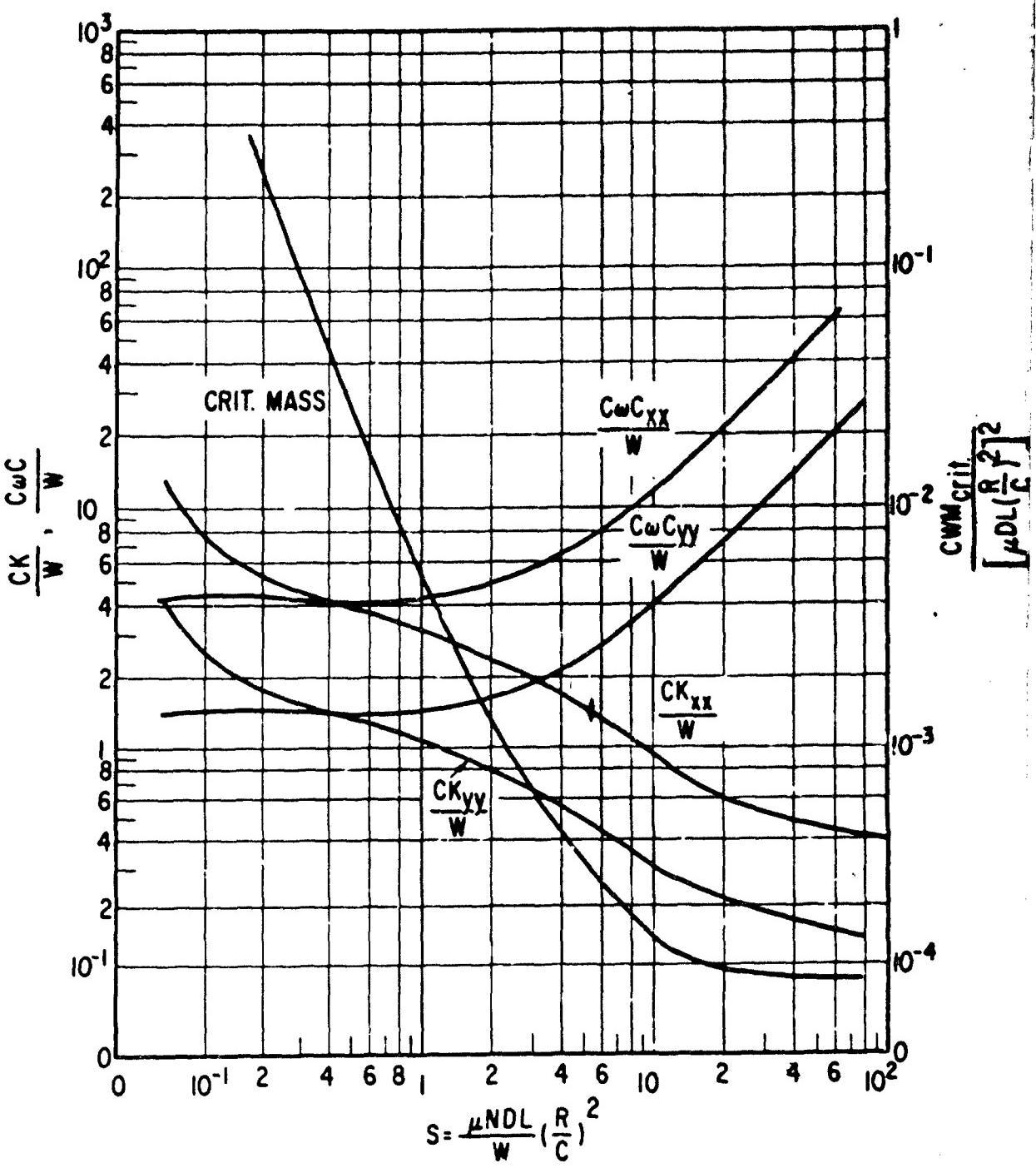


Figure B-38 The 6 Shoe Tilting Pad Bearing, $L/D = .5$, Laminar Film
Load between Pads
 $C'/C = 1$, No Pad Inertia

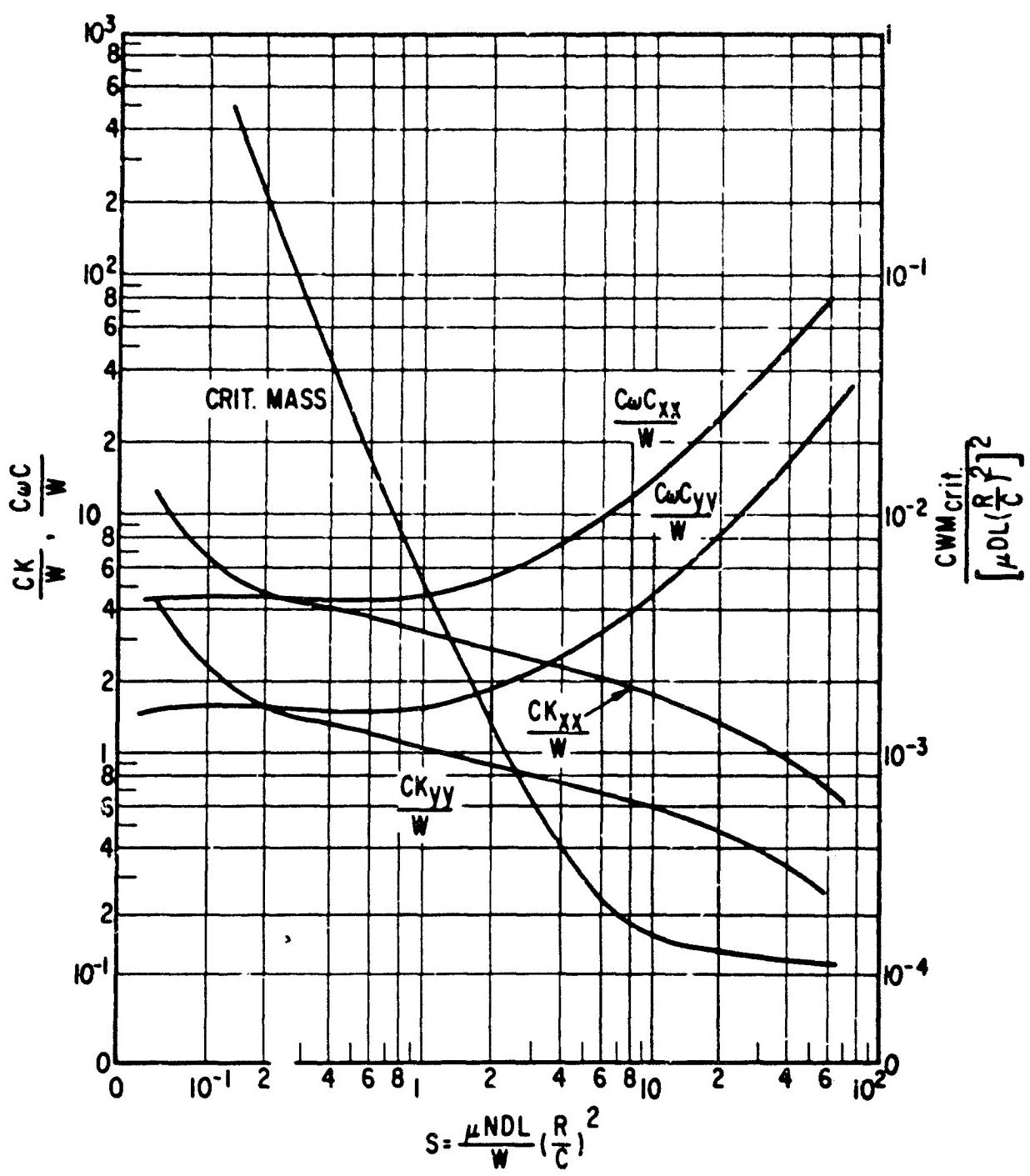


Figure B-39 The 6 Shoe Tilting Pad Bearing, L/D = .75, Laminar Film Load between Pads
 $C'/C = 1$, No Pad Inertia

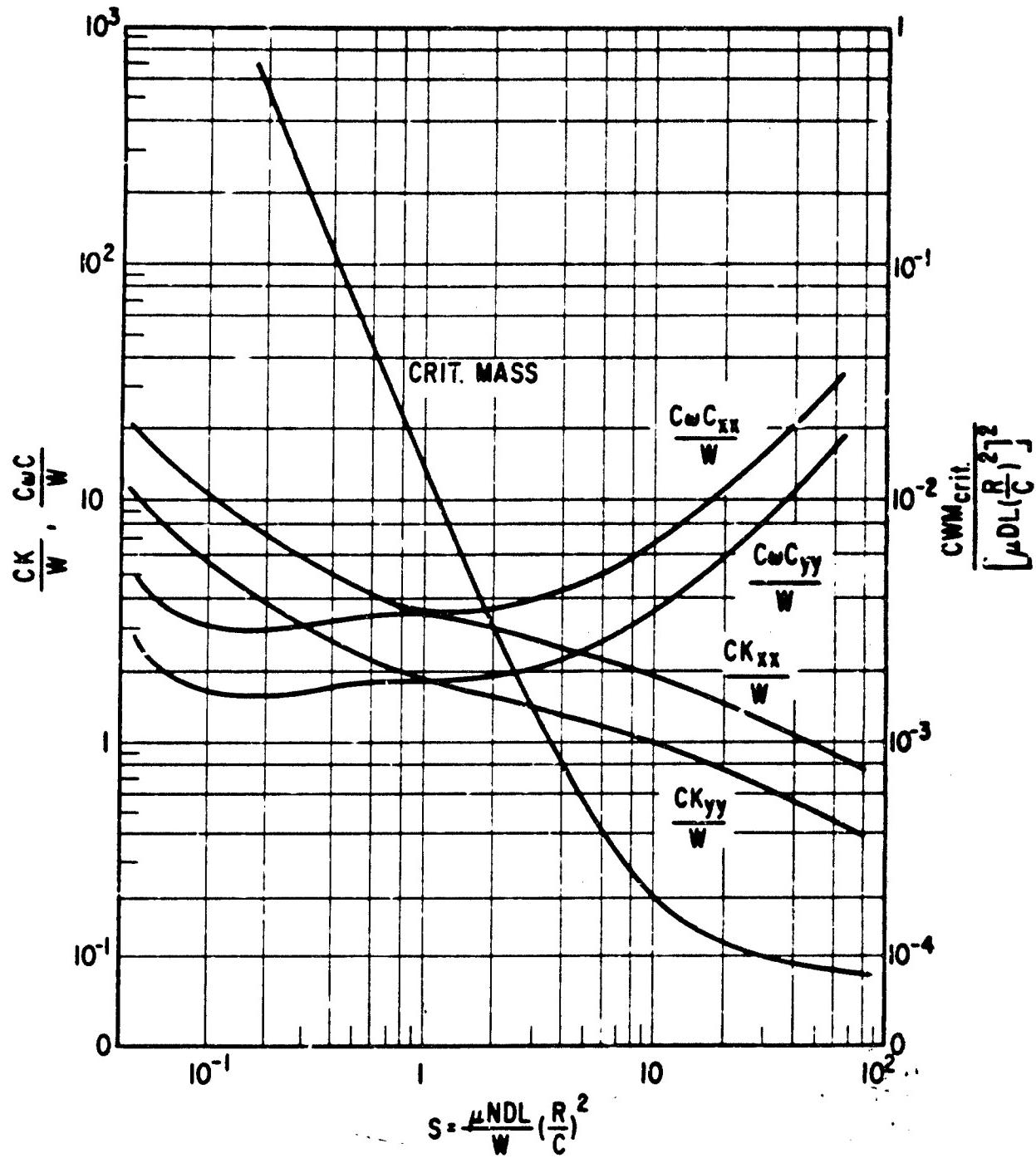


Figure B-40 The 5 Shoe Tilting Pad Bearing, $L/D = .25$, Laminar Film Load between Pads
 $C'/C = 1$, No Pad Inertia

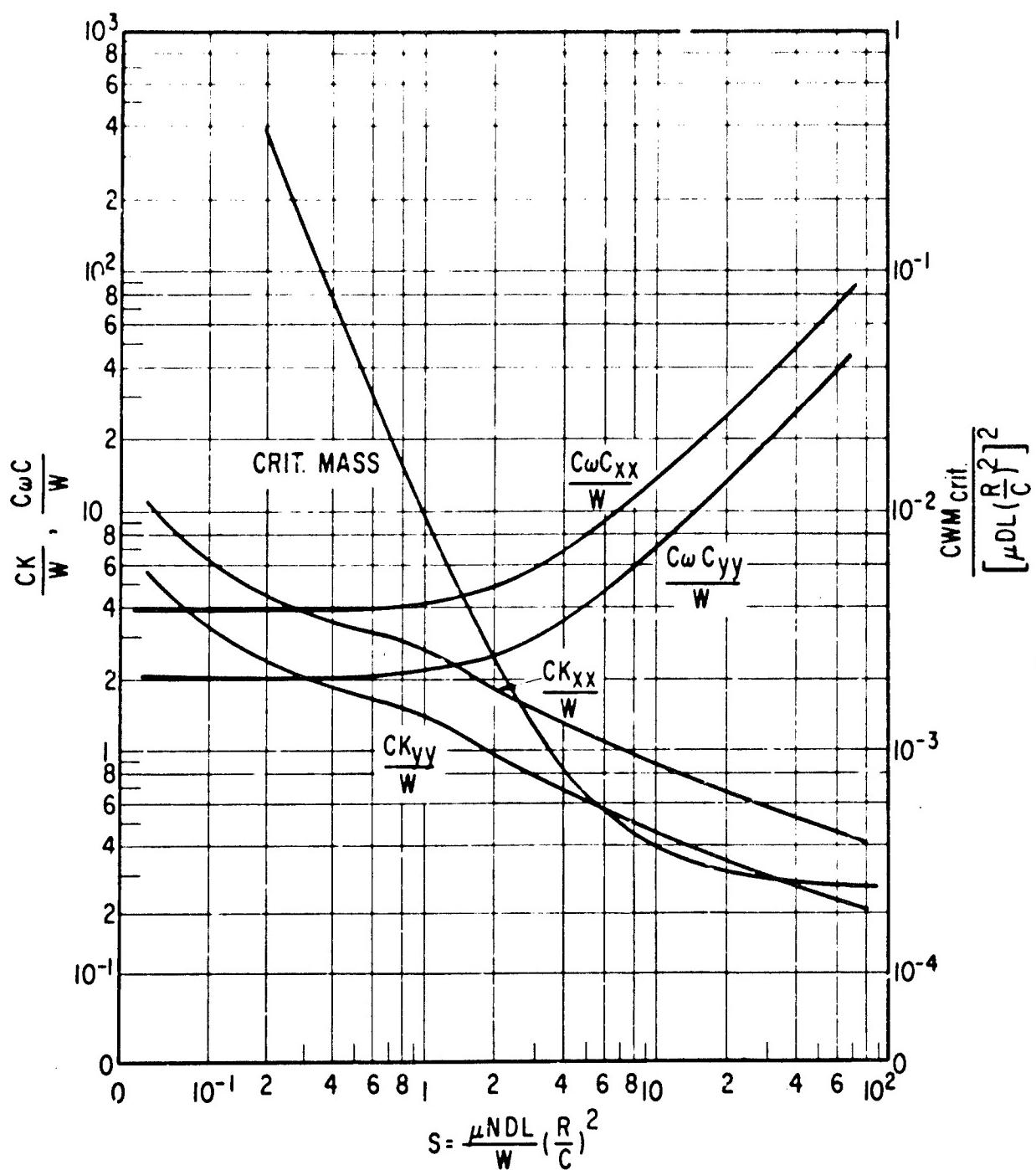


Figure B-41 The 5 Shoe Tilting Pad Bearing, $L/D = .5$, Laminar Film
Load between Pads
 $C'/C = 1$, No Pad Inertia

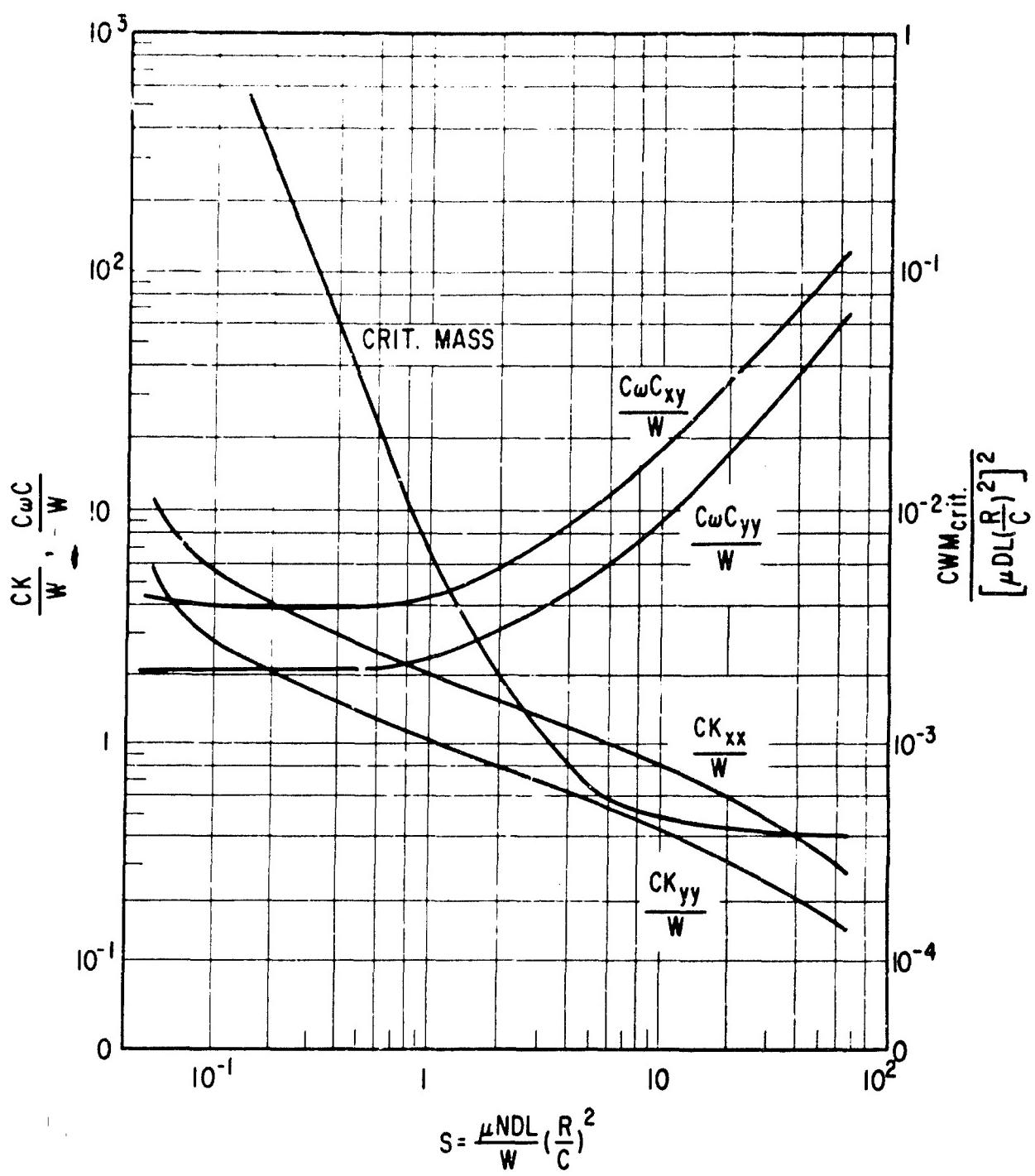


Figure B-42 The 5 Shoe Tilting Pad Bearing, L/D = .75, Laminar Film Load between Pads
 $C'/C = 1$, No Pad Inertia

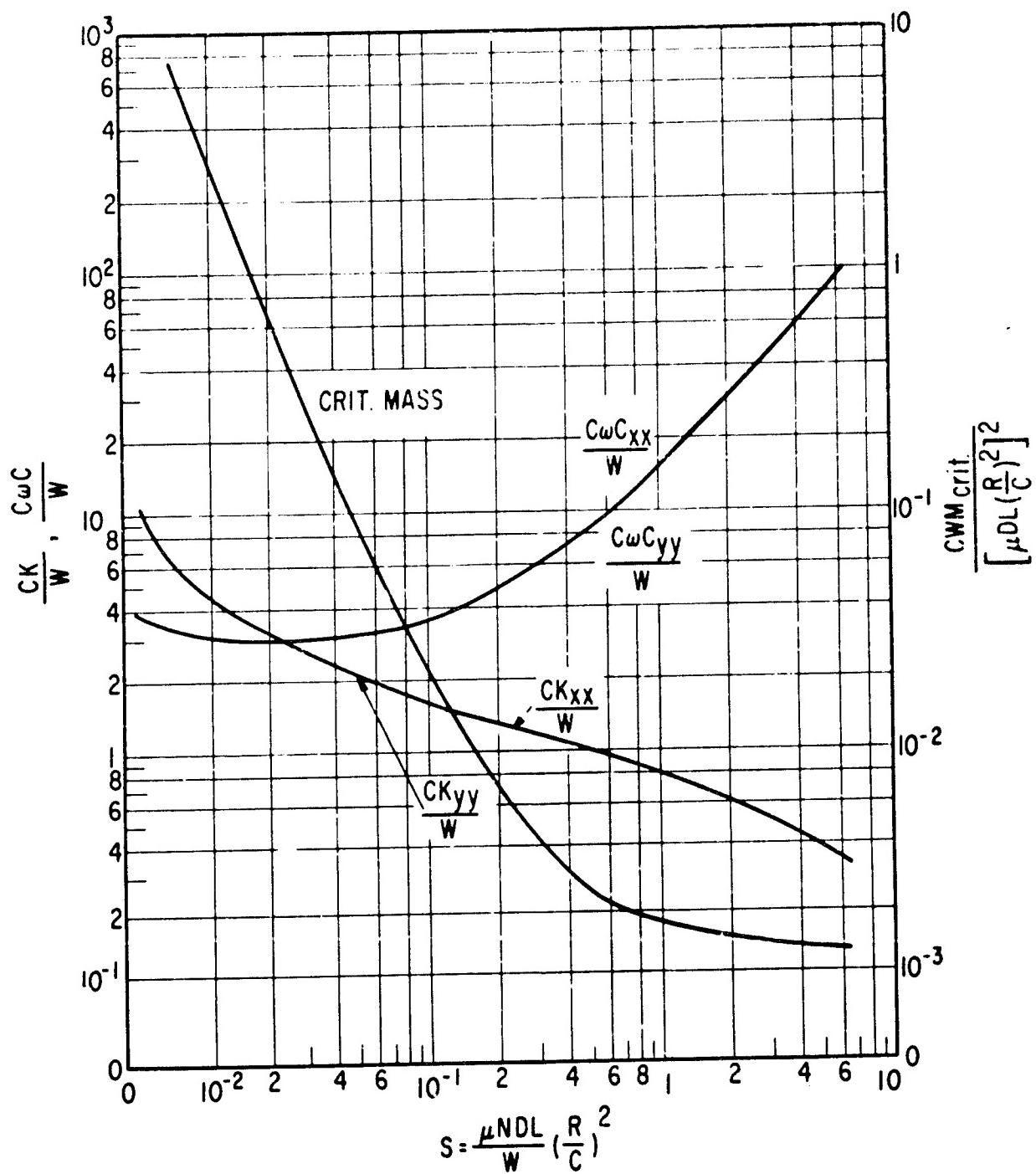


Figure B-43 The 4 Shoe Tilting Pad Bearing, $L/D = .5$, Laminar Film Load between Pads
 $C'/C = 1$, No Pad Inertia

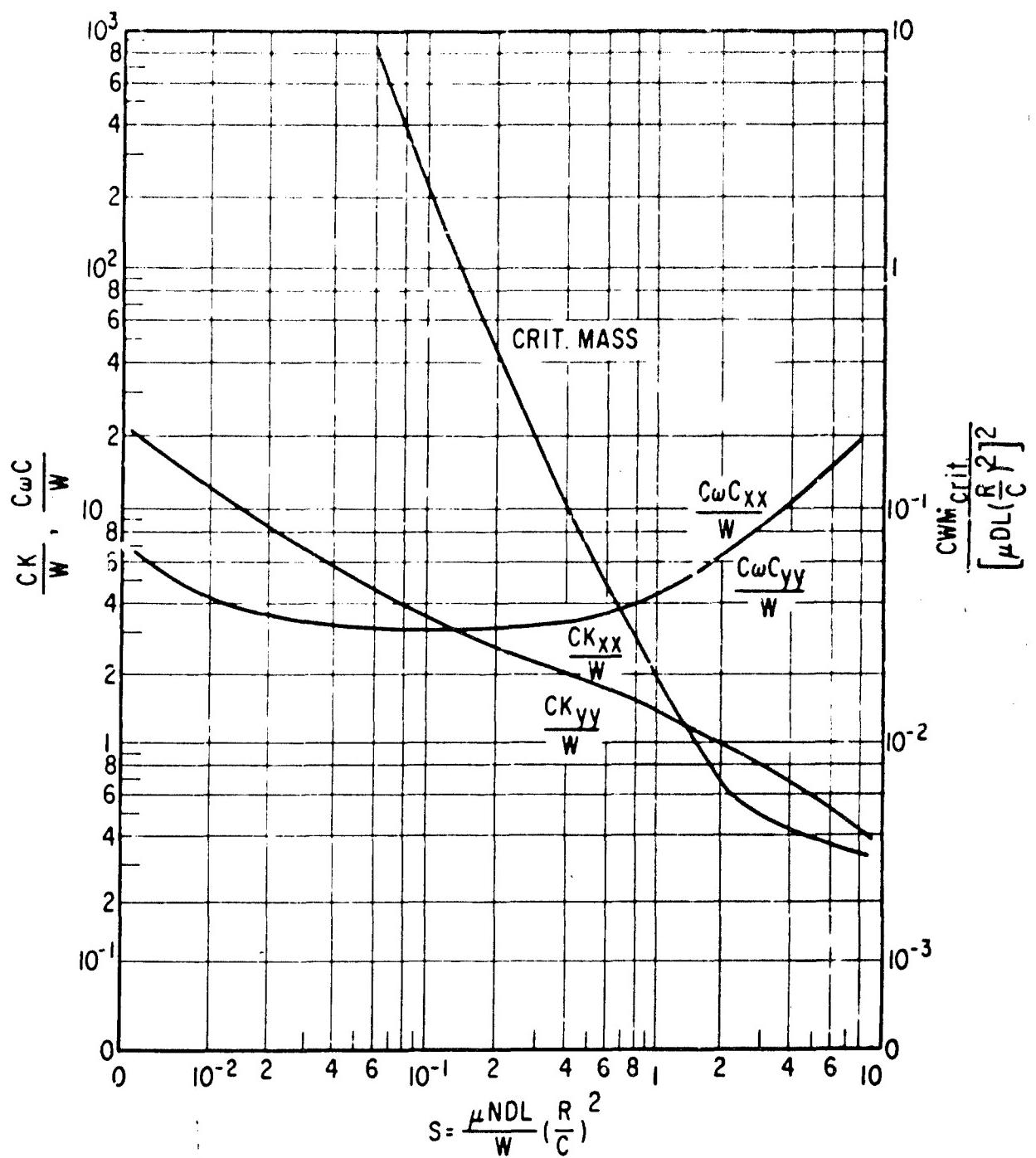


Figure B-44 The 4 Shoe Tilting Pad Bearing, L/D = .75, Laminar Film
Load between Pads
 $C'/C = 1$, No Pad Inertia

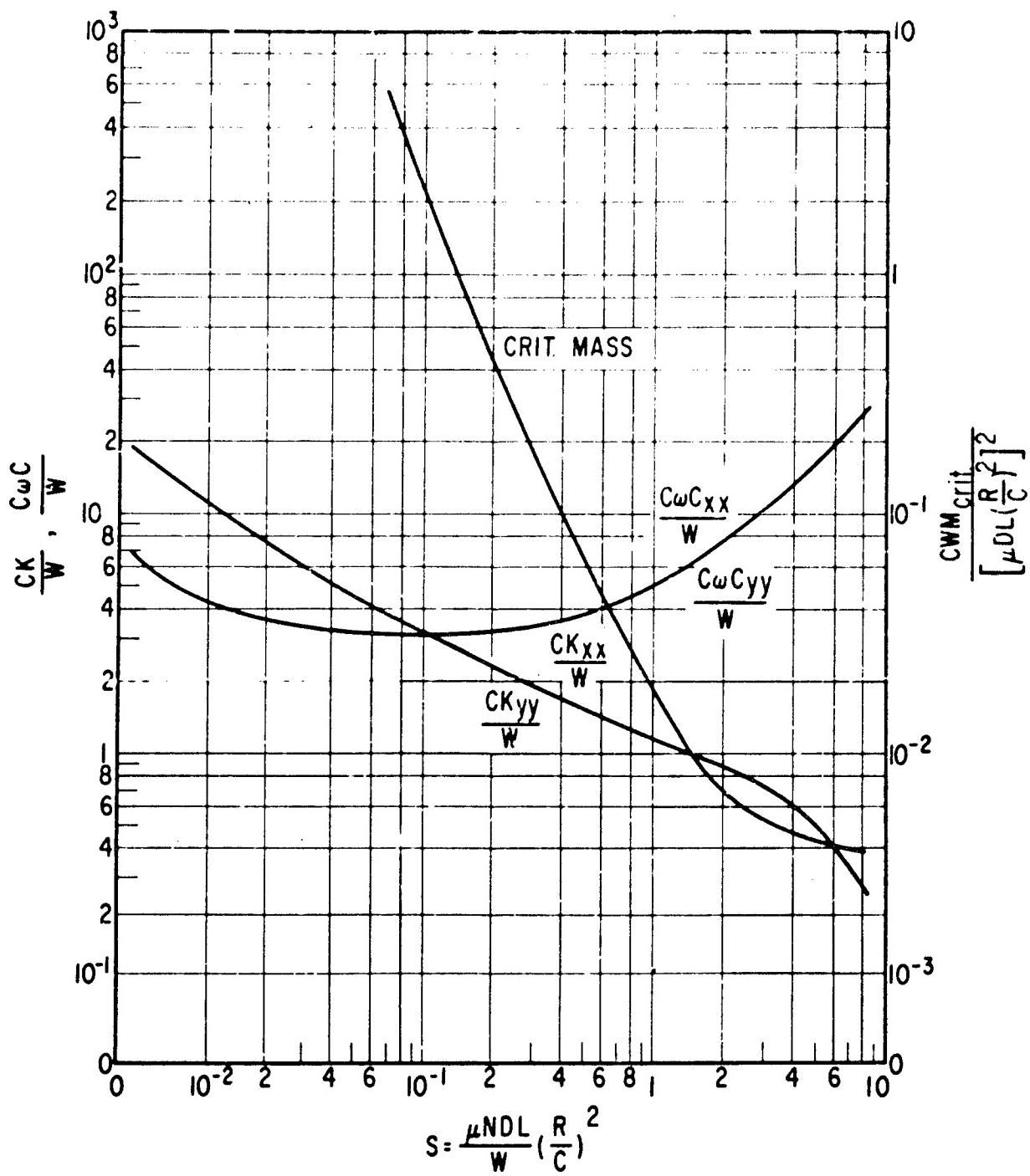


Figure B-45 The 4 Shoe Tilting Pad Bearing, $L/D = 1$, Laminar Film Load between Pads
 $C'/C = 1$, No Pad Inertia

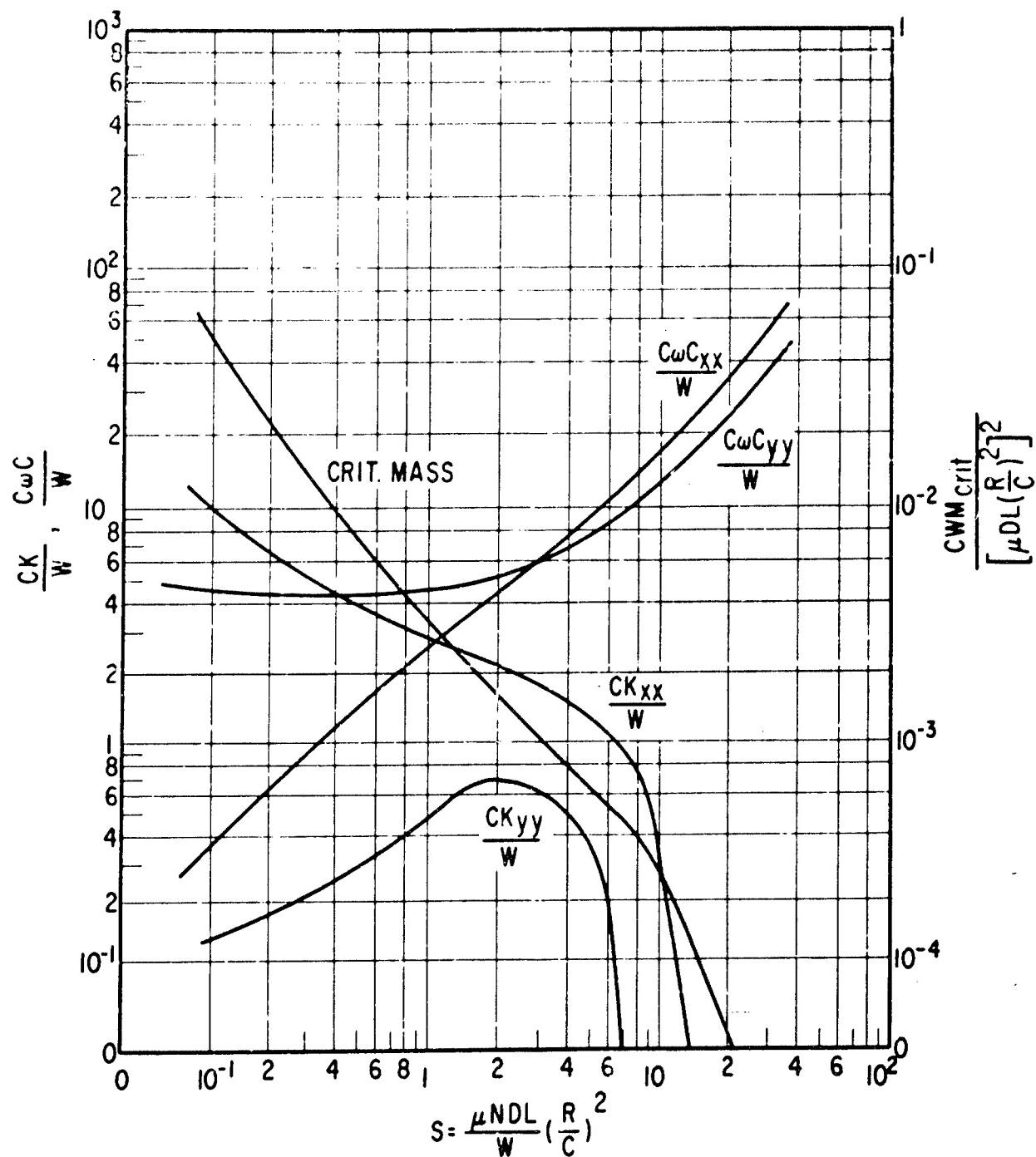


Figure B-47 The 5 Shoe Tilting Pad Bearing, $L/D = .5$, Laminar Film
Load on Pad
 $C'/C = 1$, No Pad Inertia

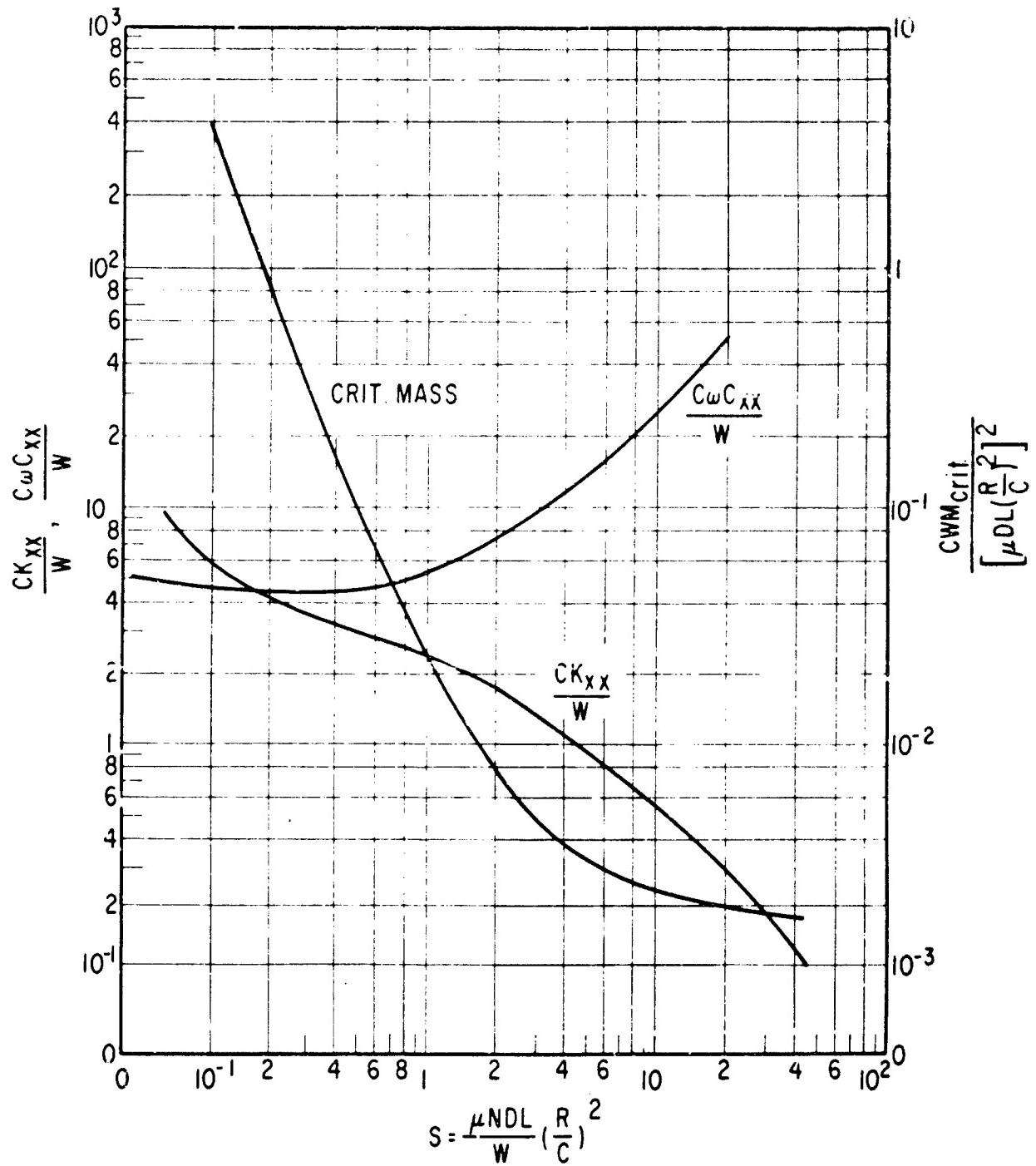


Figure B-48 The 4 Shoe Tilting Pad Bearing, L/D = .75, Laminar Film Load on Pad
 $C'/C = 1$, No Pad Inertia

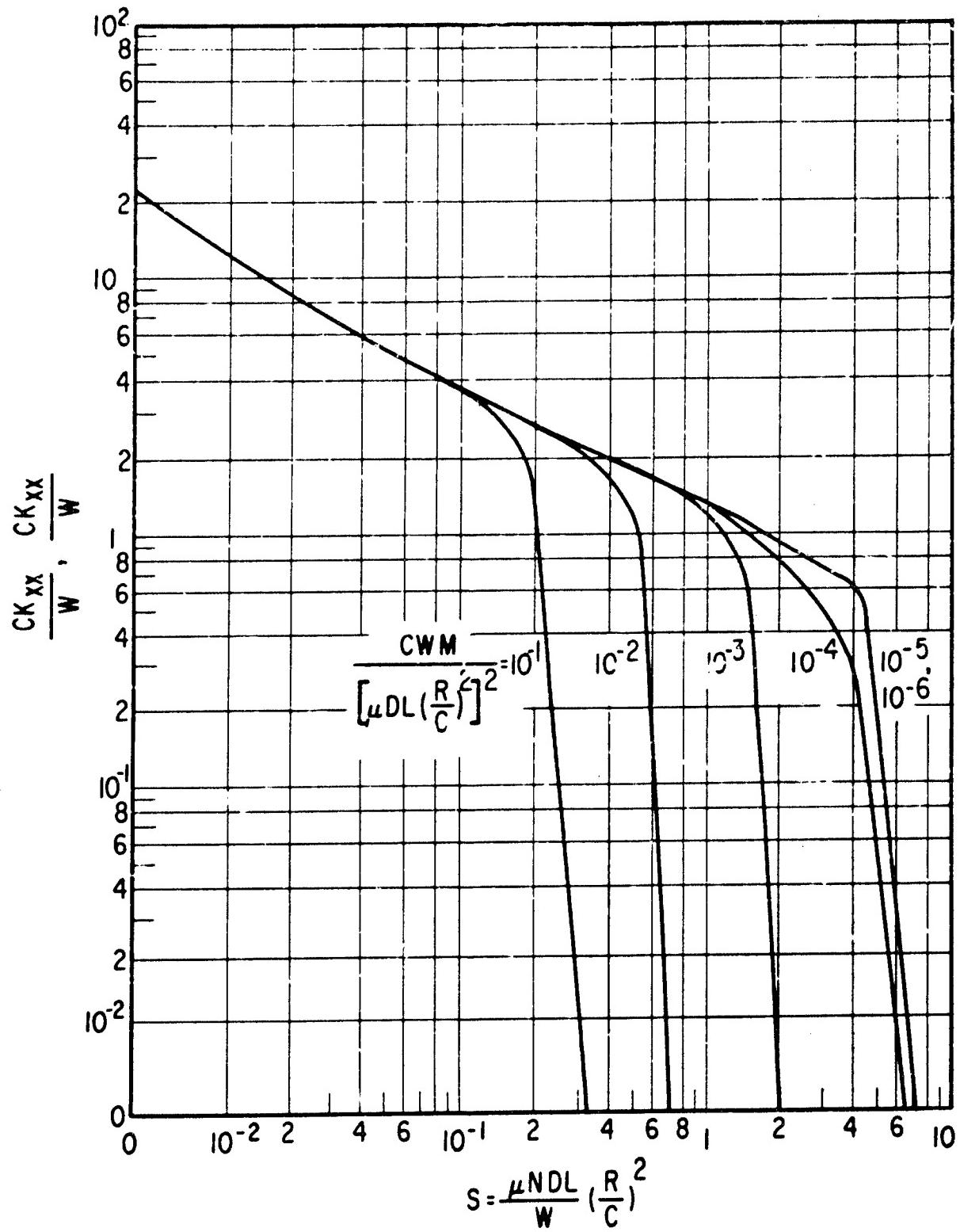


Figure B-49 The 4 Shoe Tilting Pad Bearing, L/D = .75, Laminar Film
 Load between Pads
 $C'/C = 1$, Effect of Pad Inertia

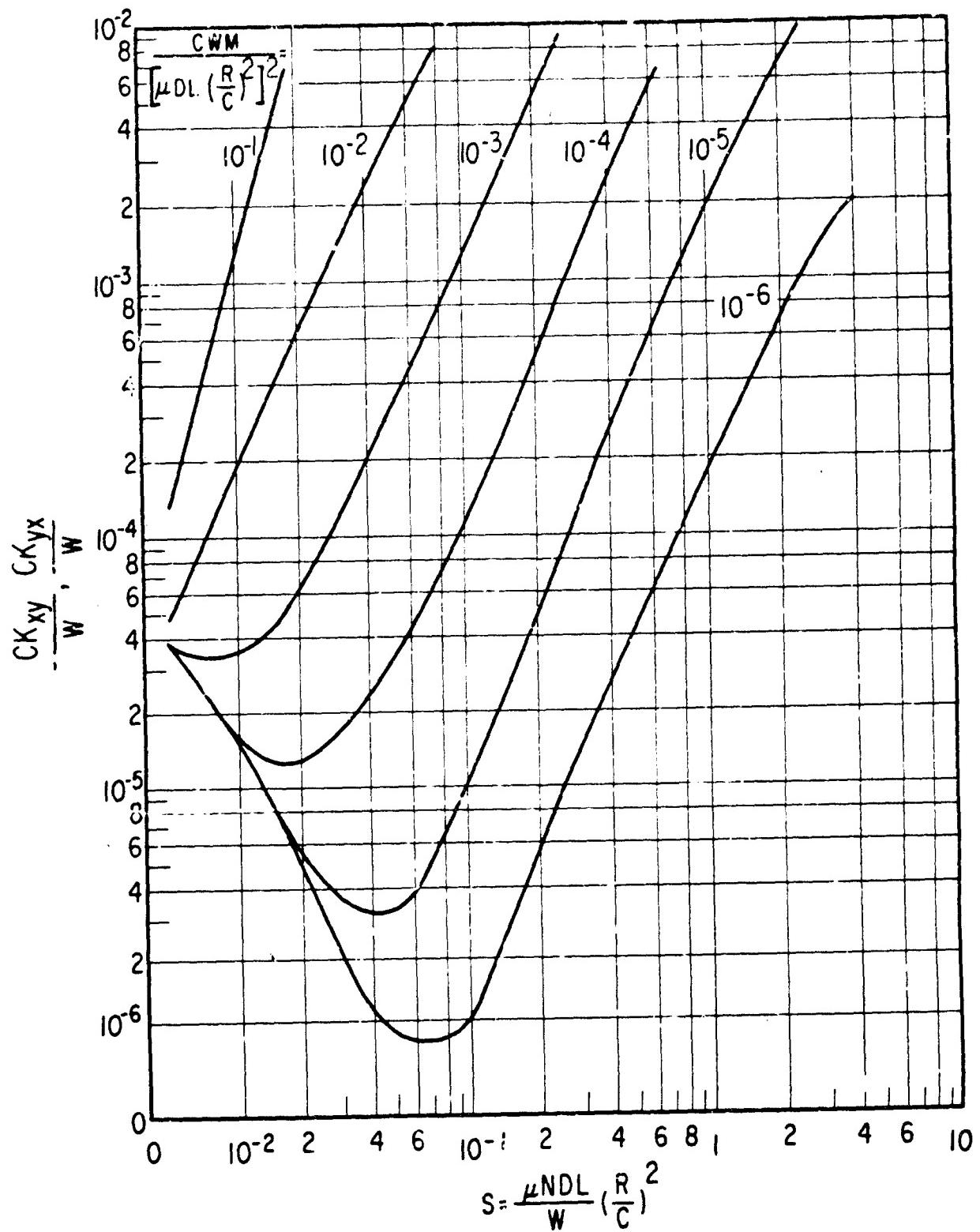


Figure B-50 The 4 Shoe Tilting Pad Bearing, $L/D = .75$, Laminar Film
 Load between Pads
 $C'/C = 1$, Effect of Pad Inertia

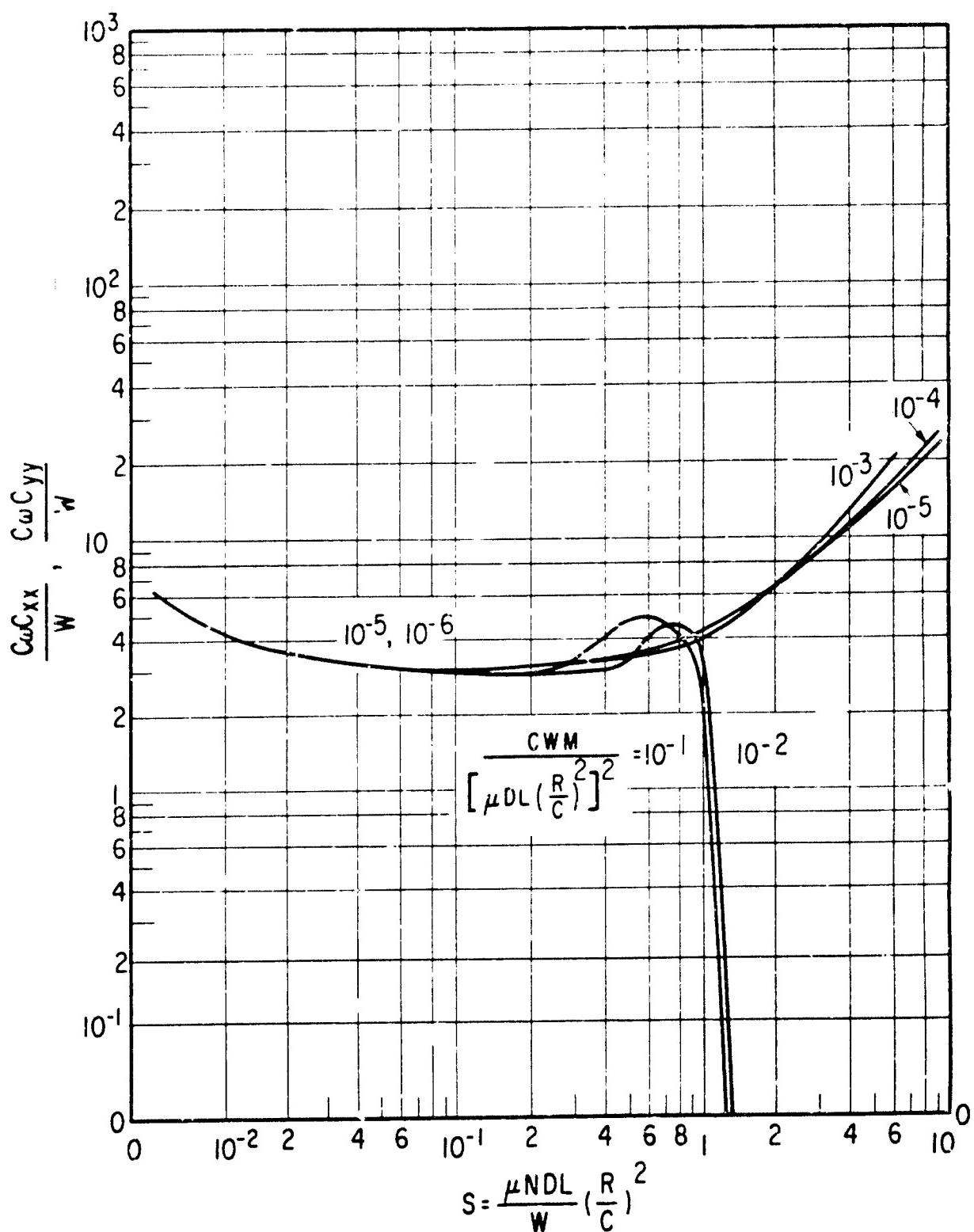


Figure B-51 The 4 Shoe Tilting Pad Bearing, $L/D = .75$, Laminar Film
 Load between Pads
 $C'/C = 1$, Effect of Pad Inertia

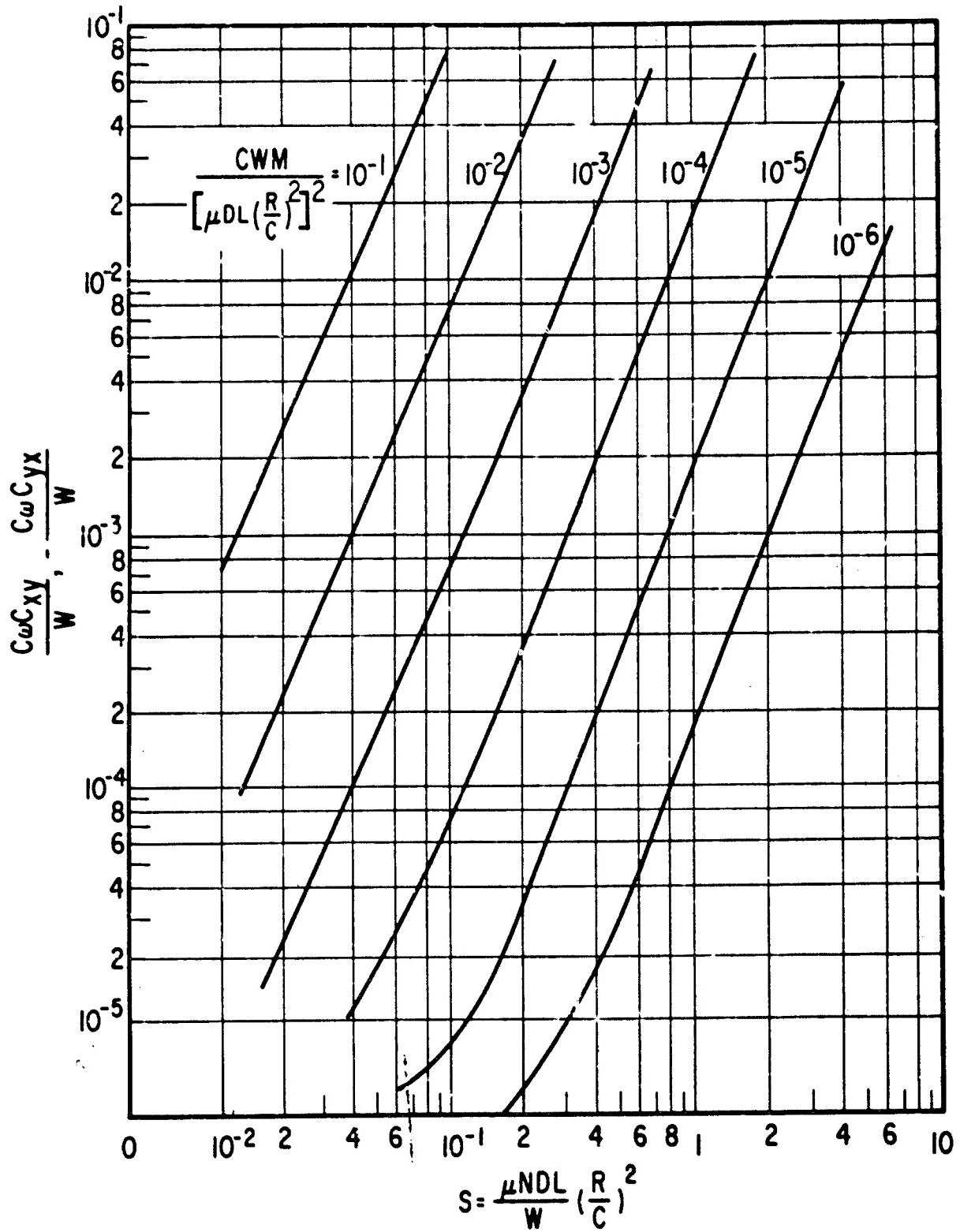


Figure B-52 The 4 Shoe Tilting Pad Bearing, $L/D = .75$, Laminar Film Load between Pads
 $C'/C = 1$, Effect of Pad Inertia

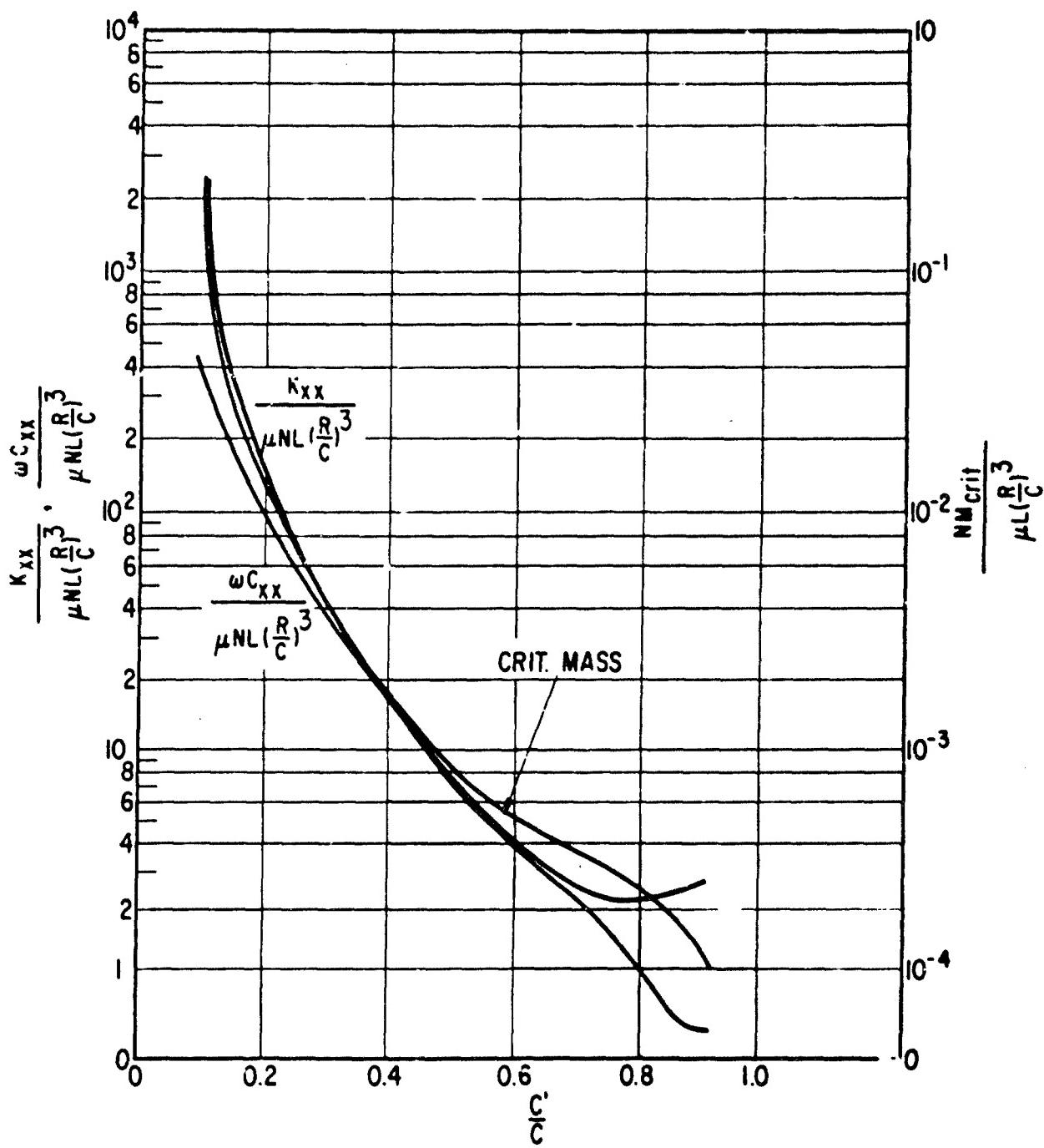


Figure B-53 The 12 Shoe Tilting Pad Bearing, $L/D = .25$, Laminar Film Vertical Rotor, Effect of Preload

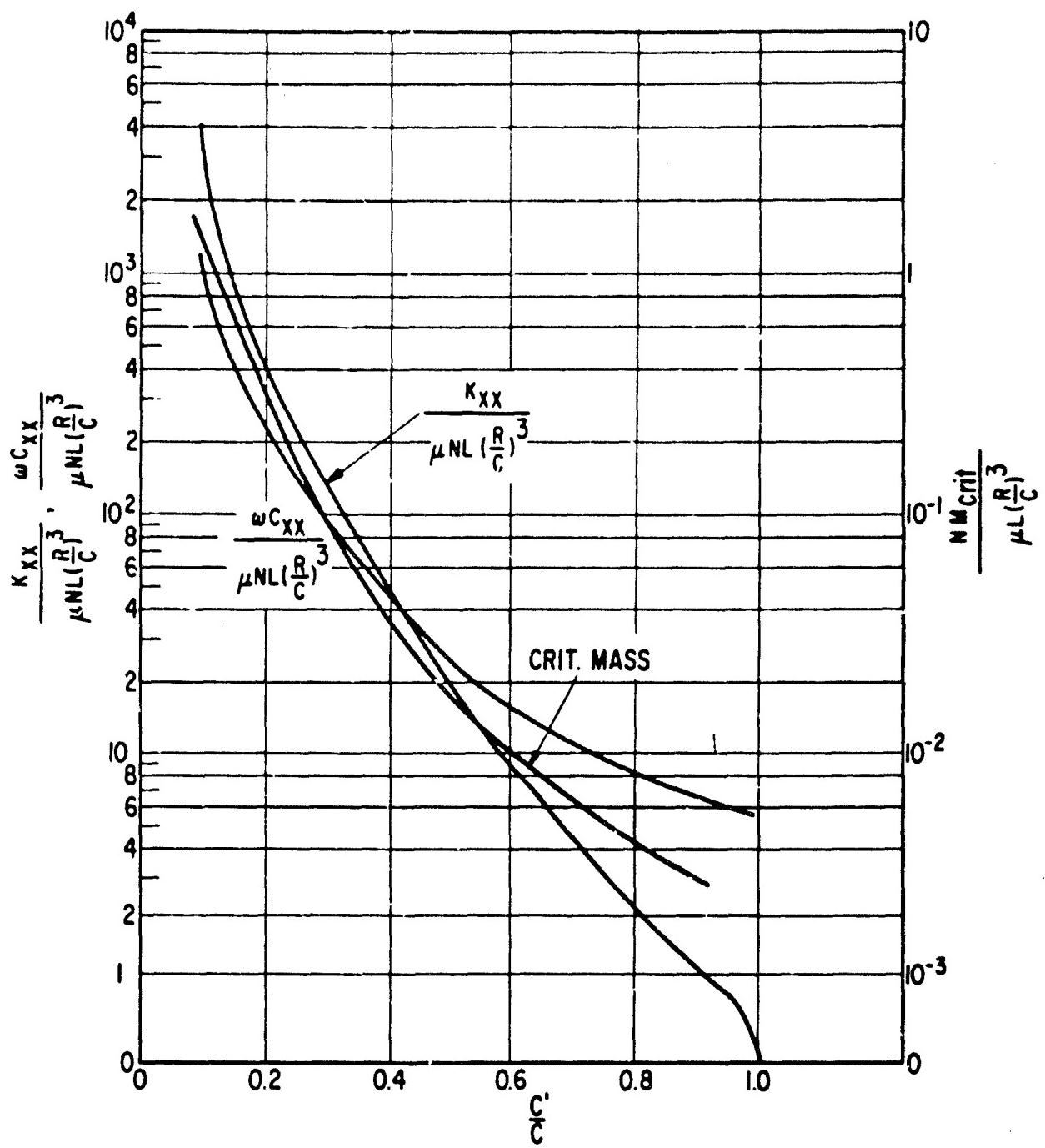


Figure B-54 The 6 Shoe Tilting Pad Bearing, L/D = .5, Laminar Film Vertical Rotor, Effect of Preload

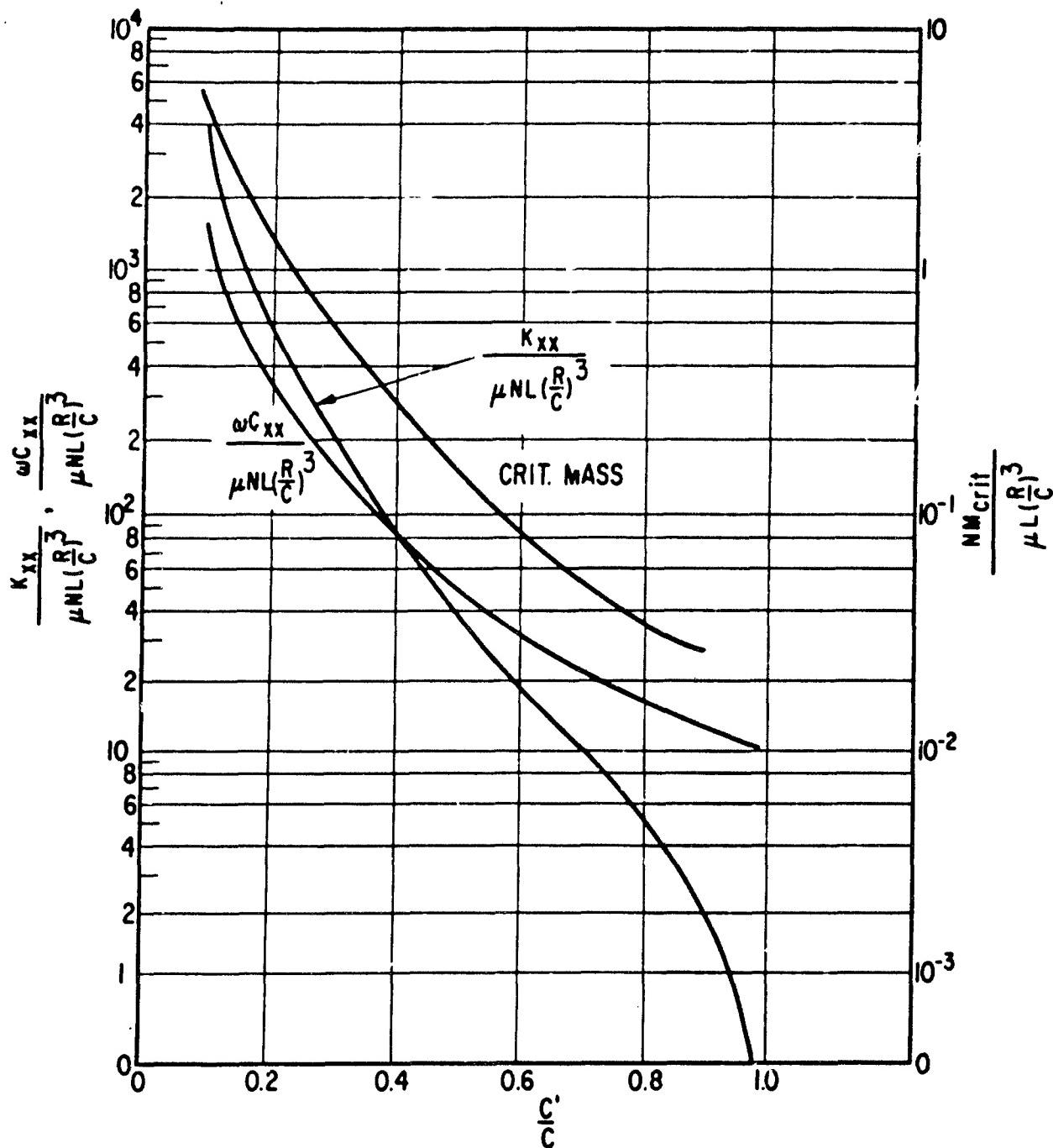


Figure B-55 The 4 Shoe Tilting Pad Bearing, $L/D = .75$, Laminar Film Vertical Rotor, Effect of Preload

b. Liquid Lubricant, Turbulent Film

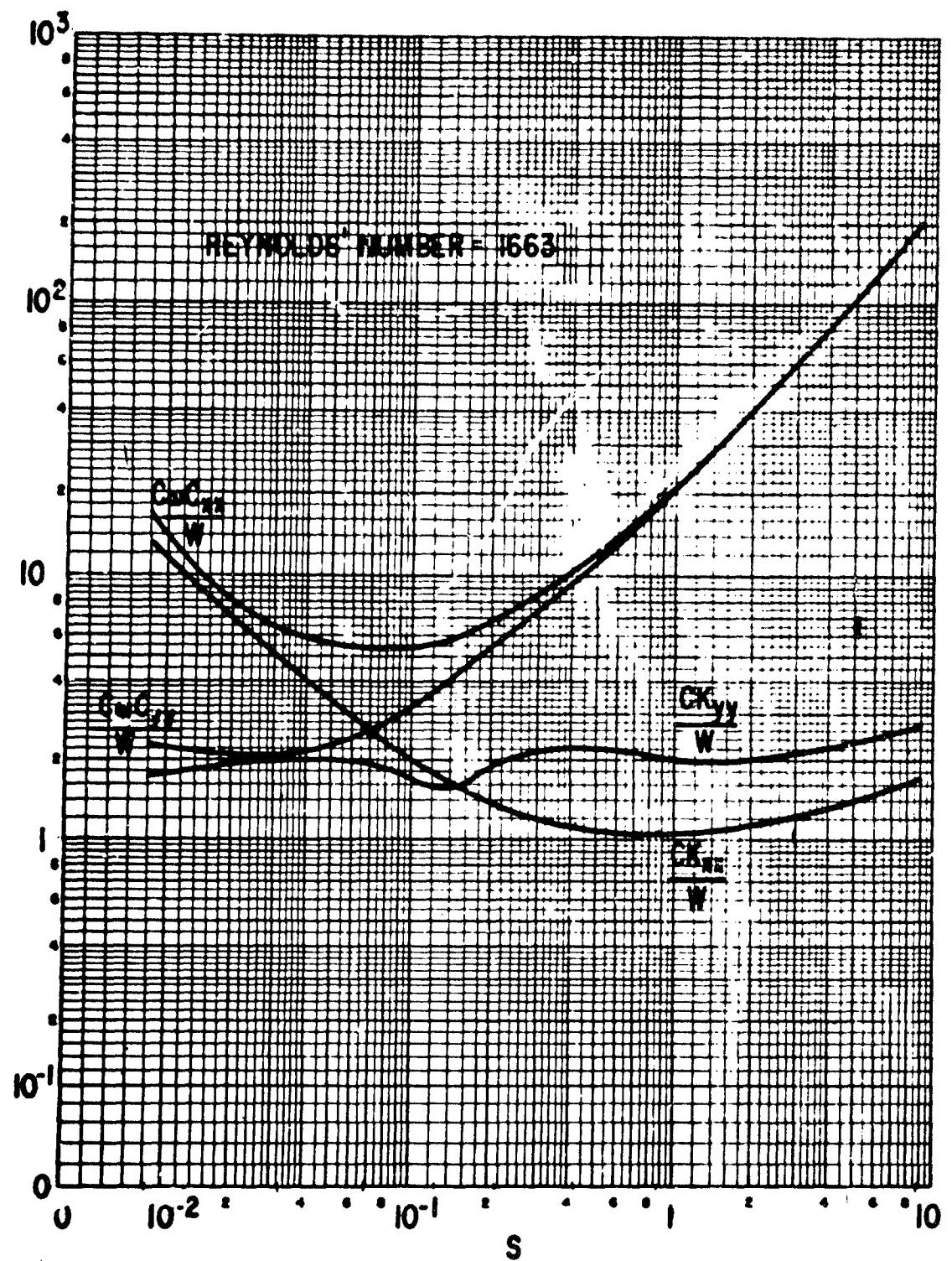


Figure B-56 The Plain Cylindrical Bearing, Turbulent Film Dimensionless Dynamic Coefficients

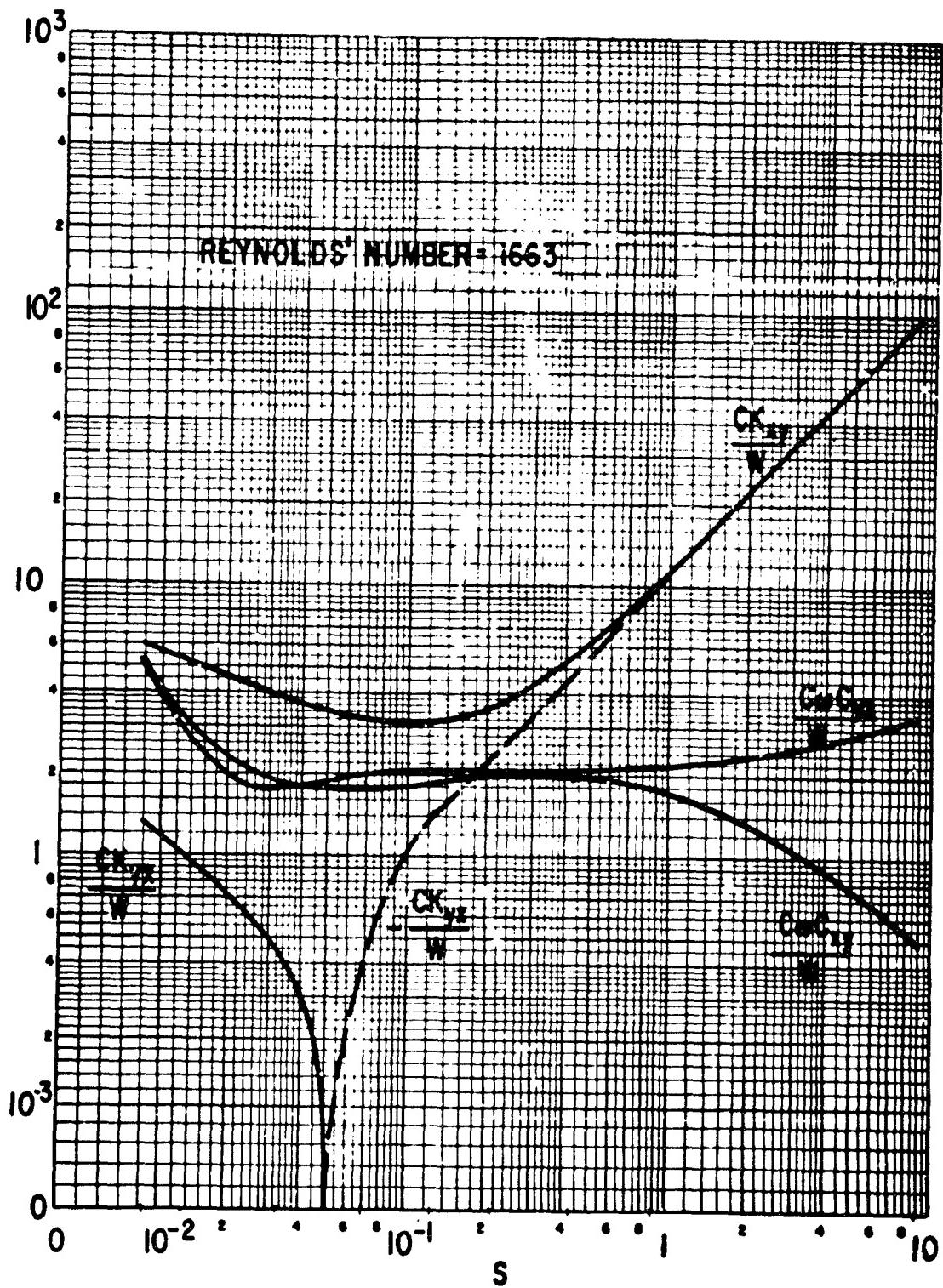


Figure B-57 The Plain Cylindrical Bearing, Turbulent Film Dimensionless Dynamic Coefficients

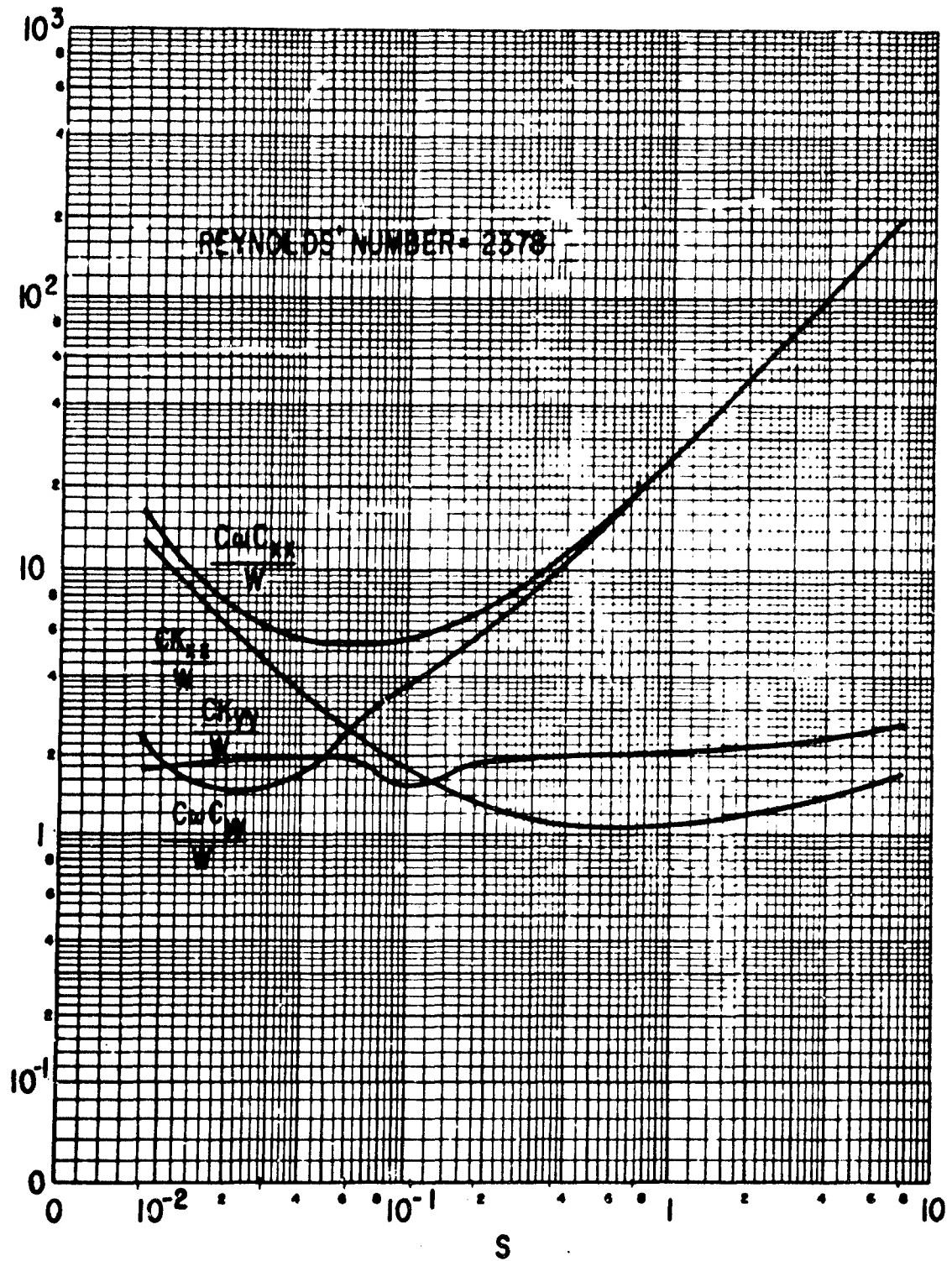


Figure B-58 The Plain Cylindrical Bearing, Turbulent Film Dimensionless Dynamic Coefficients

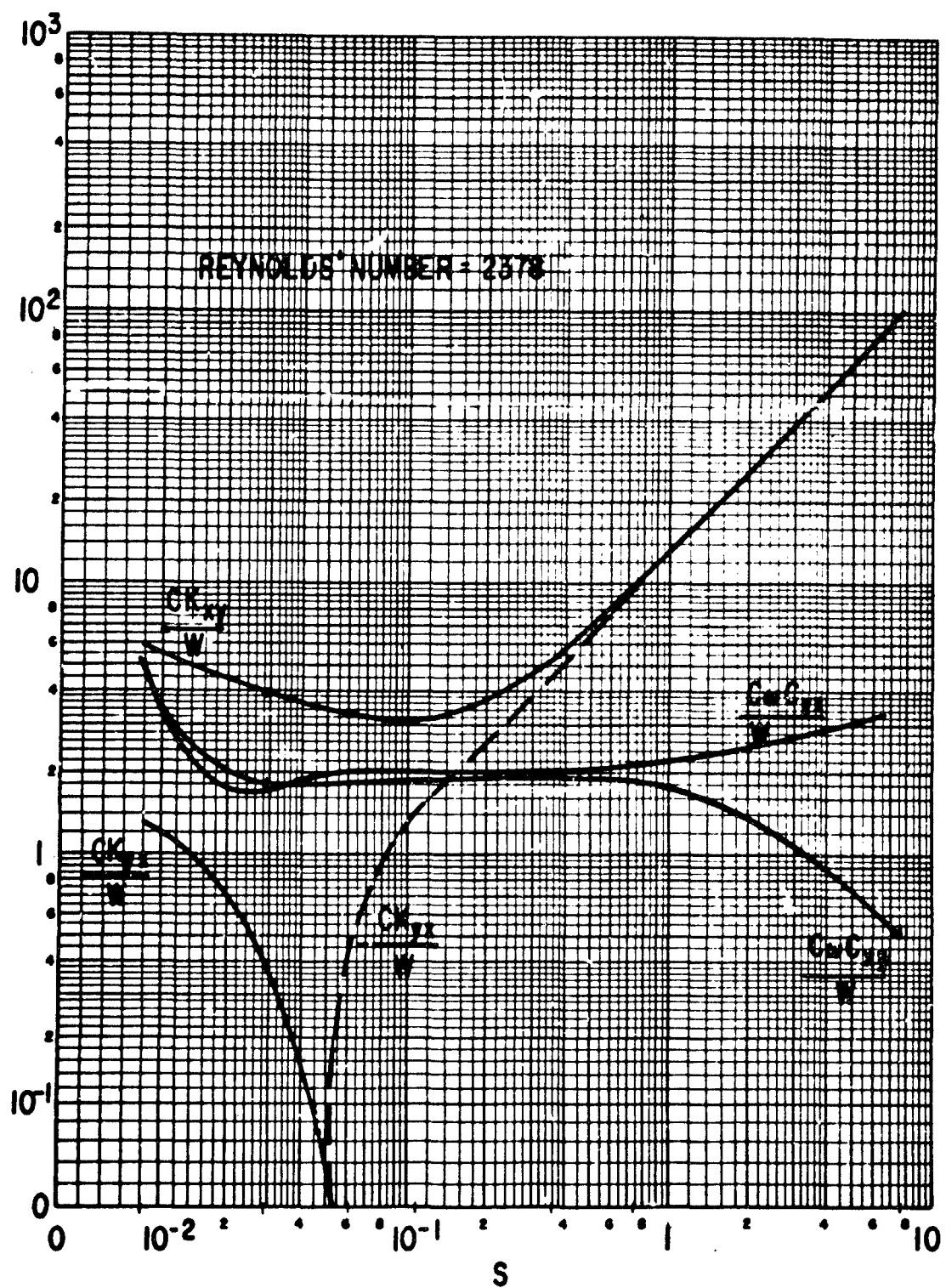


Figure B-59 The Plain Cylindrical Bearing, Turbulent Film Dimensionless Dynamic Coefficients

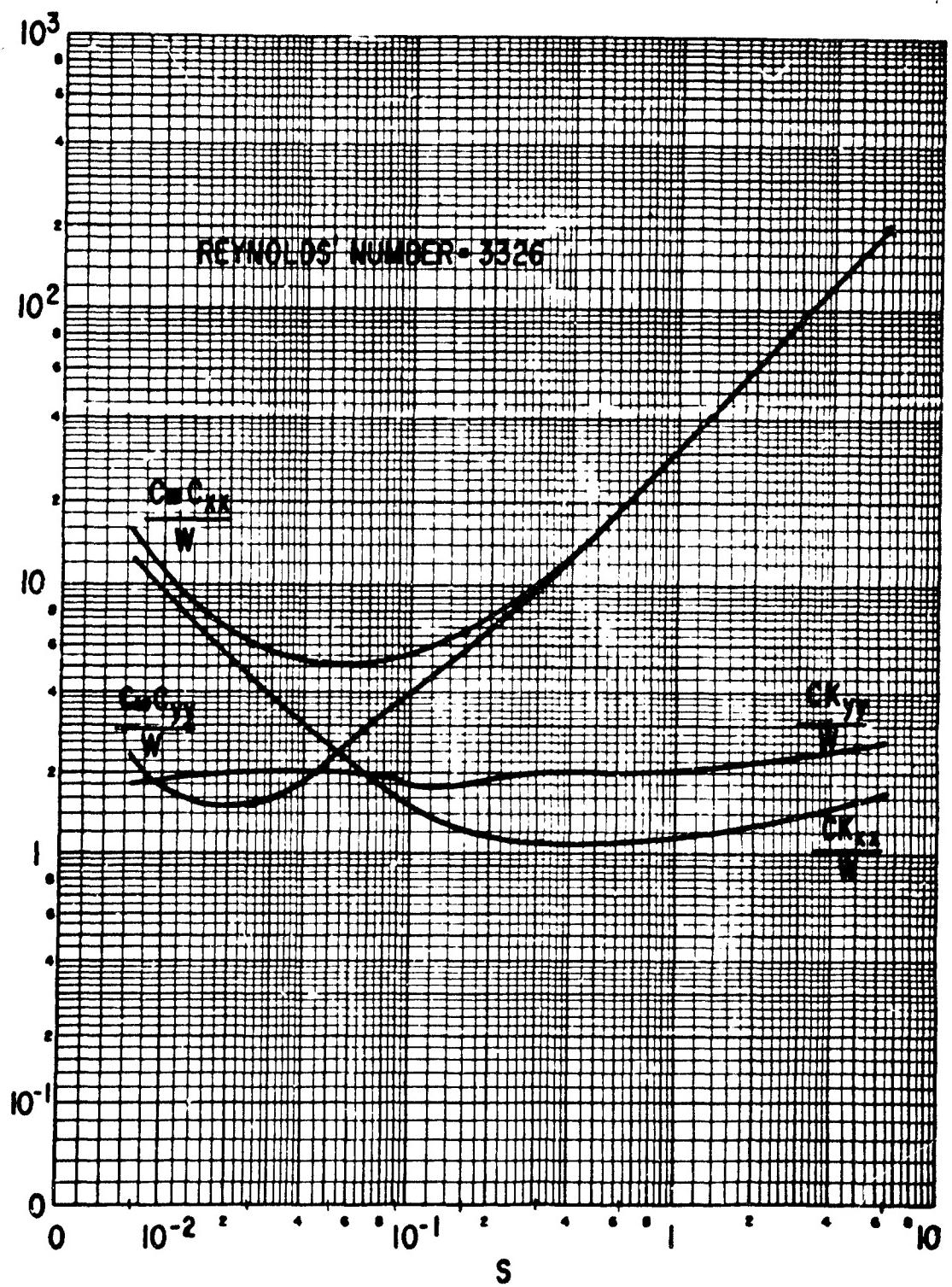


Figure B-60 The Plain Cylindrical Bearing, Turbulent Film Dimensionless Dynamic Coefficients

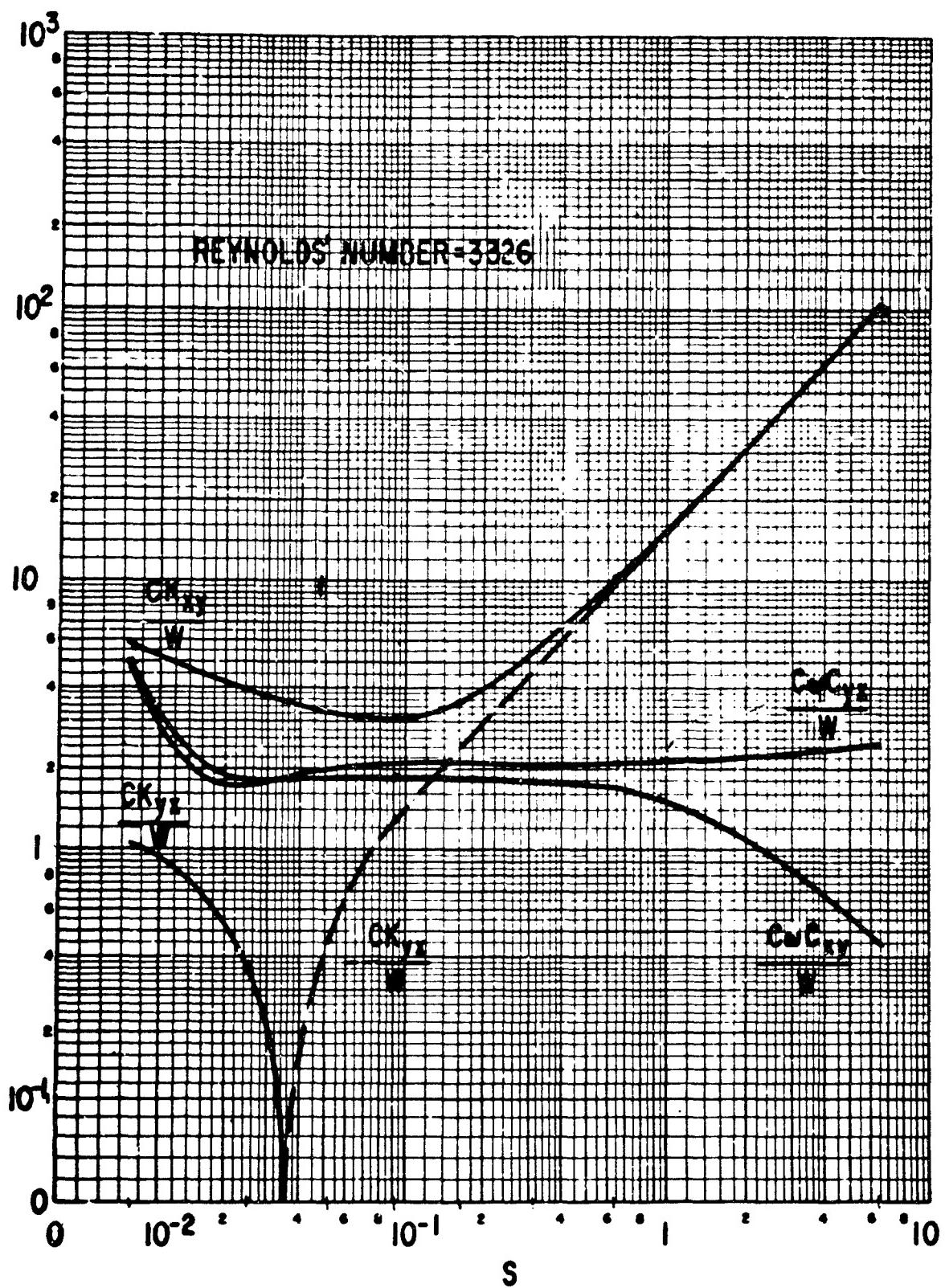


Figure B-61 The Plain Cylindrical Bearing, Turbulent Film Dimensionless Dynamic Coefficients

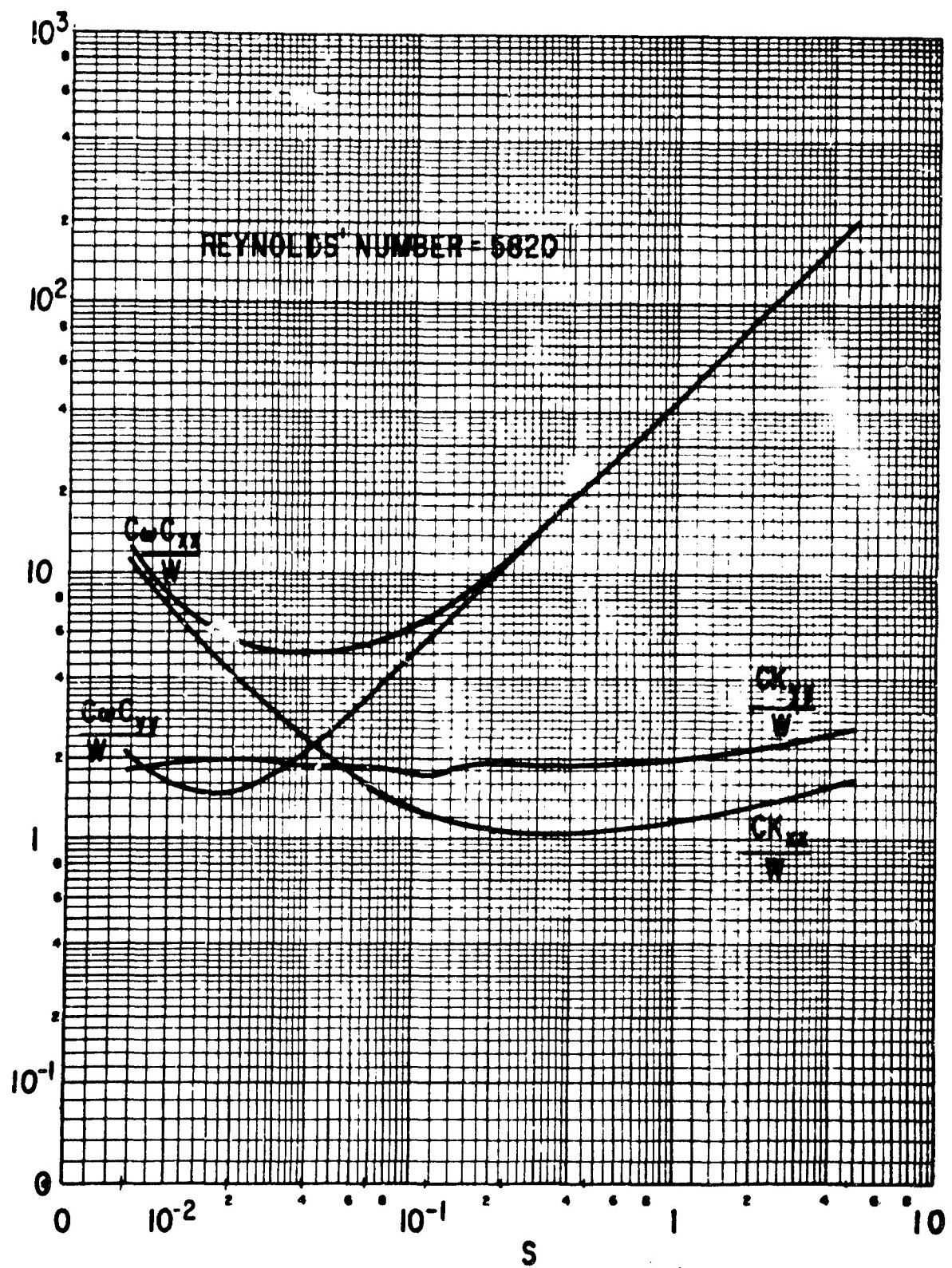


Figure B-62 The Plain Cylindrical Bearing, Turbulent Film Dimensionless Dynamic Coefficients

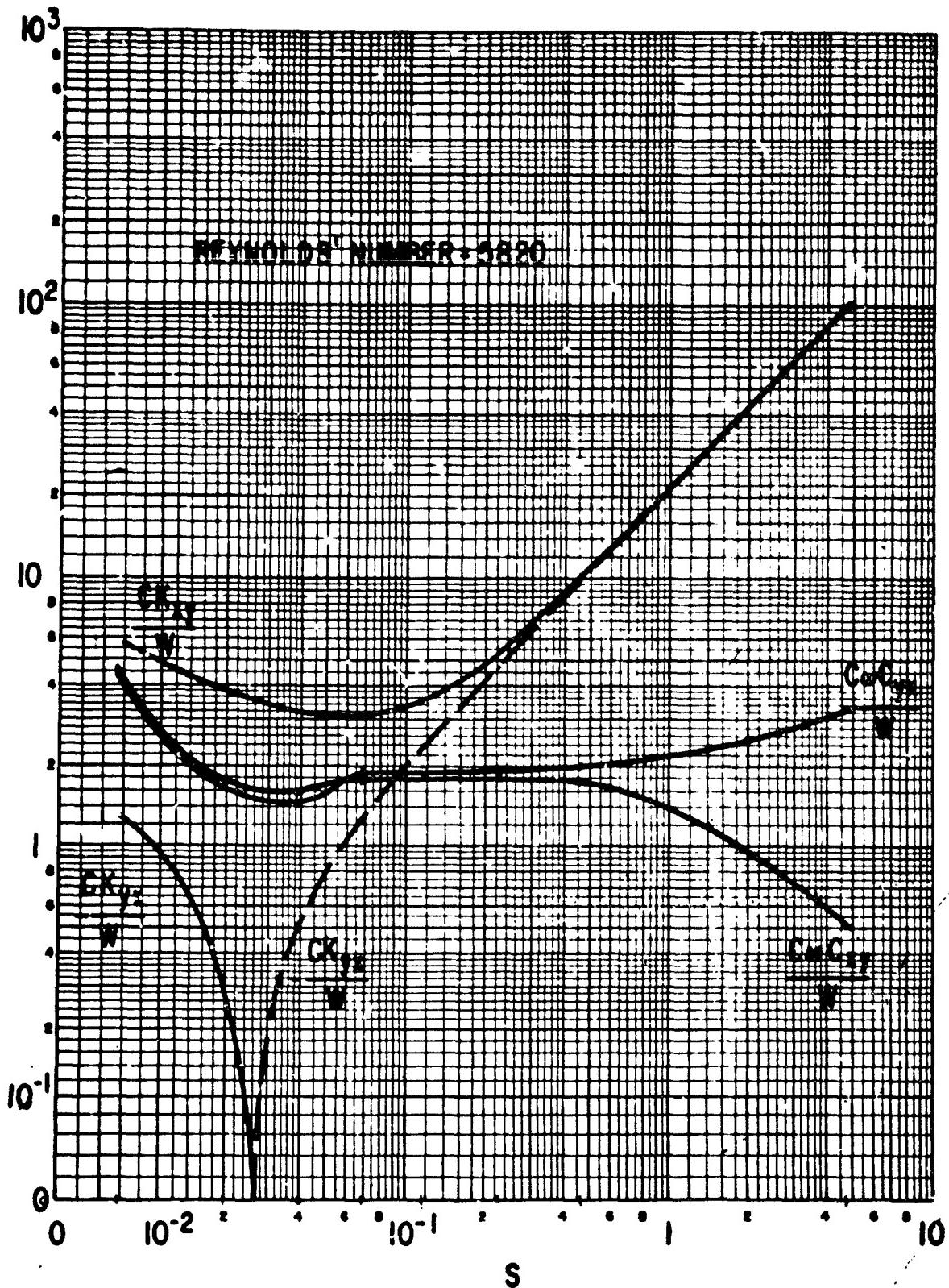


Figure B-63 The Plain Cylindrical Bearing, Turbulent Film Dimensionless Dynamic Coefficients

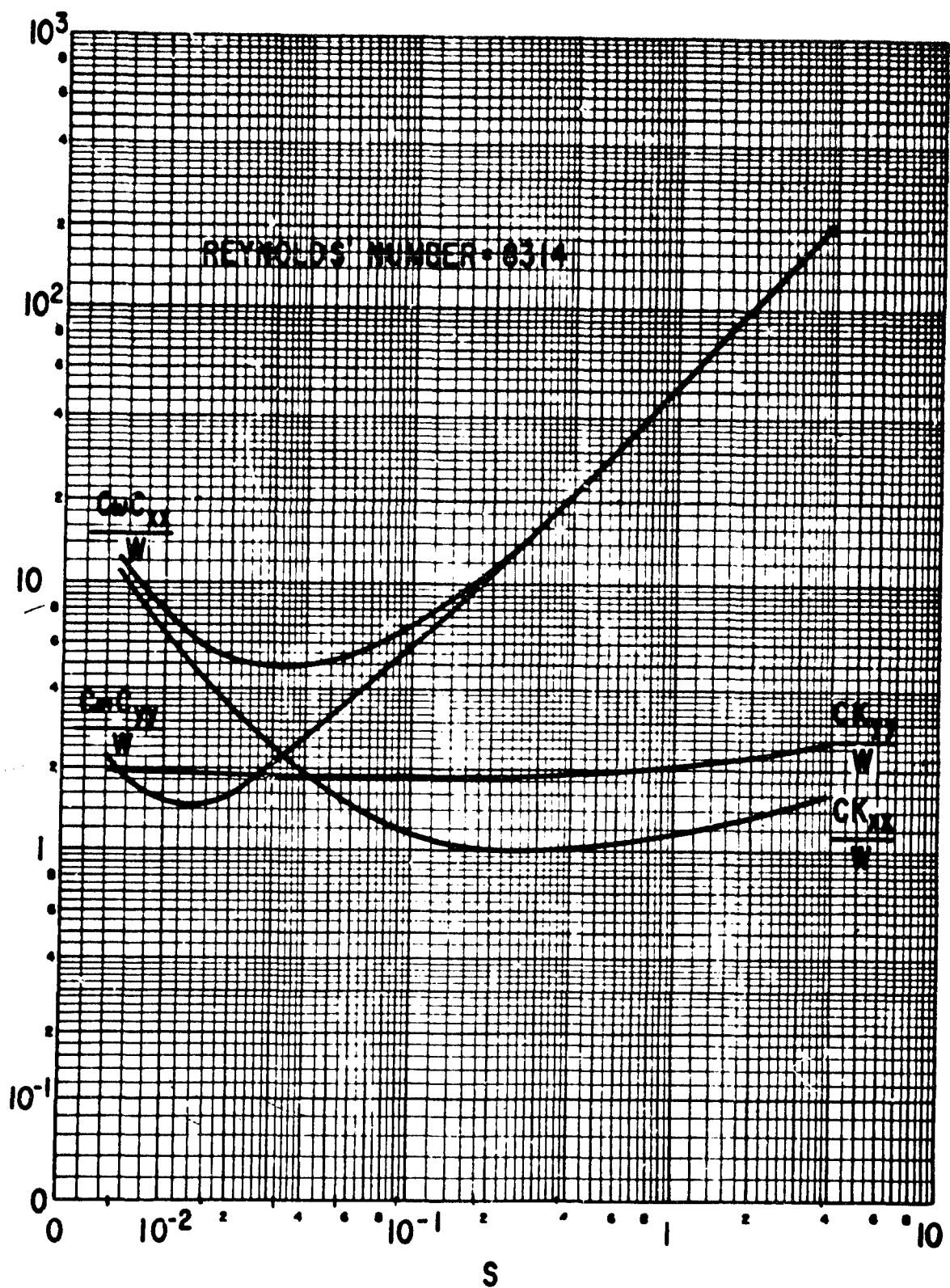


Figure B-64 The Plain Cylindrical Bearing, Turbulent Film Dimensionless Dynamic Coefficients

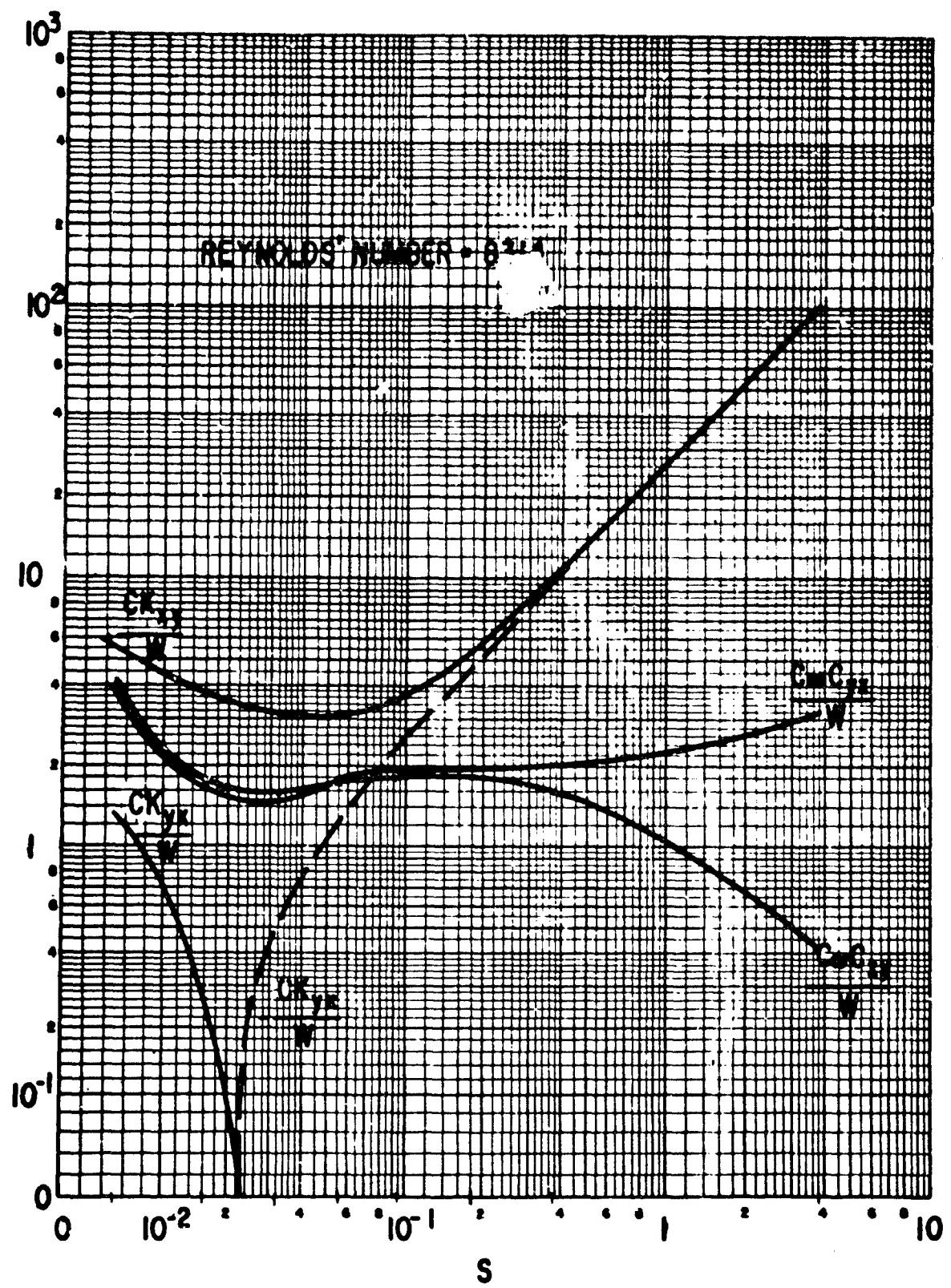


Figure B-65 The Plain Cylindrical Bearing, Turbulent Film Dimensionless Dynamic Coefficients

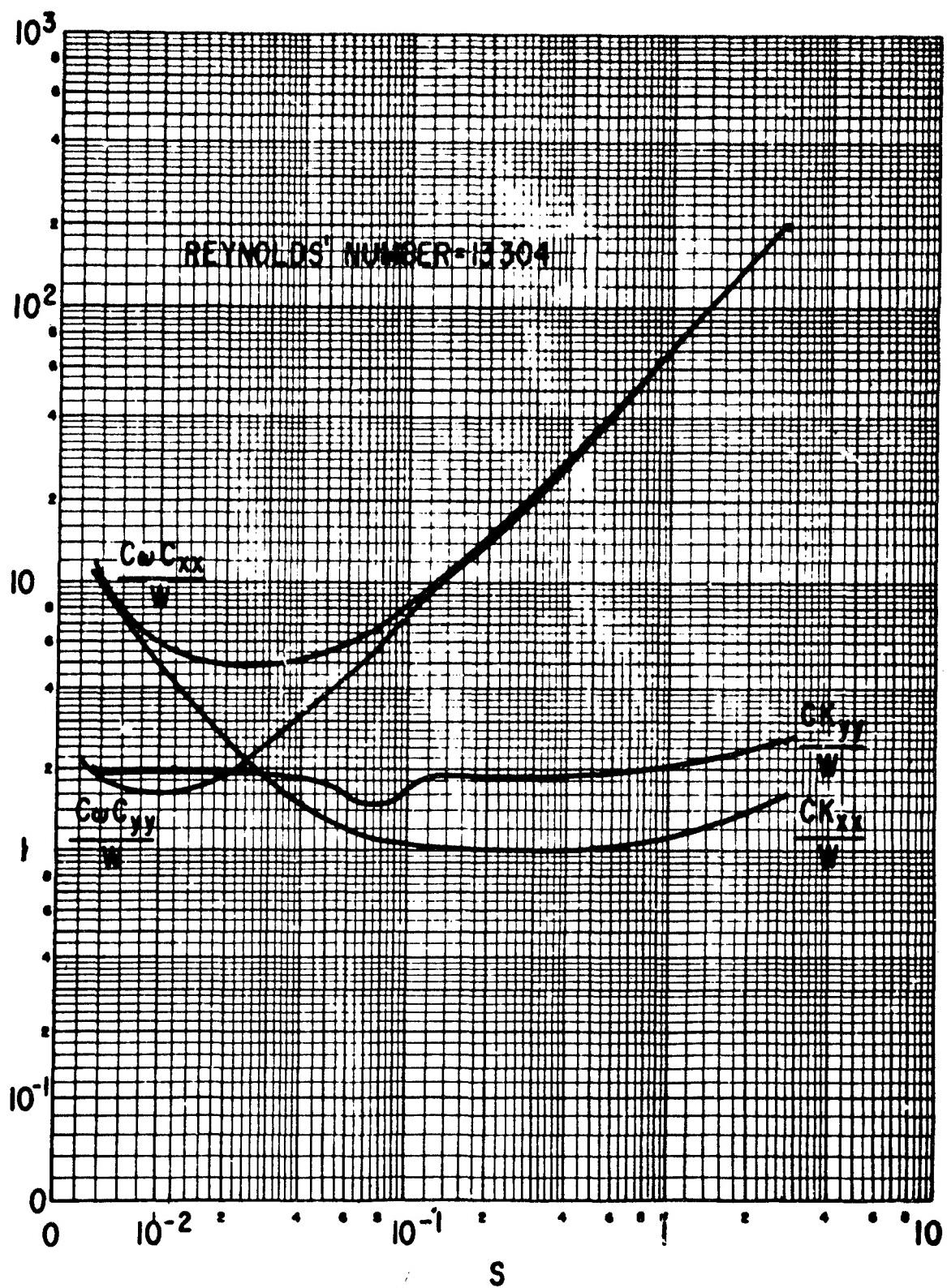


Figure B-66 The Plain Cylindrical Bearing, Turbulent Film Dimensionless Dynamic Coefficients

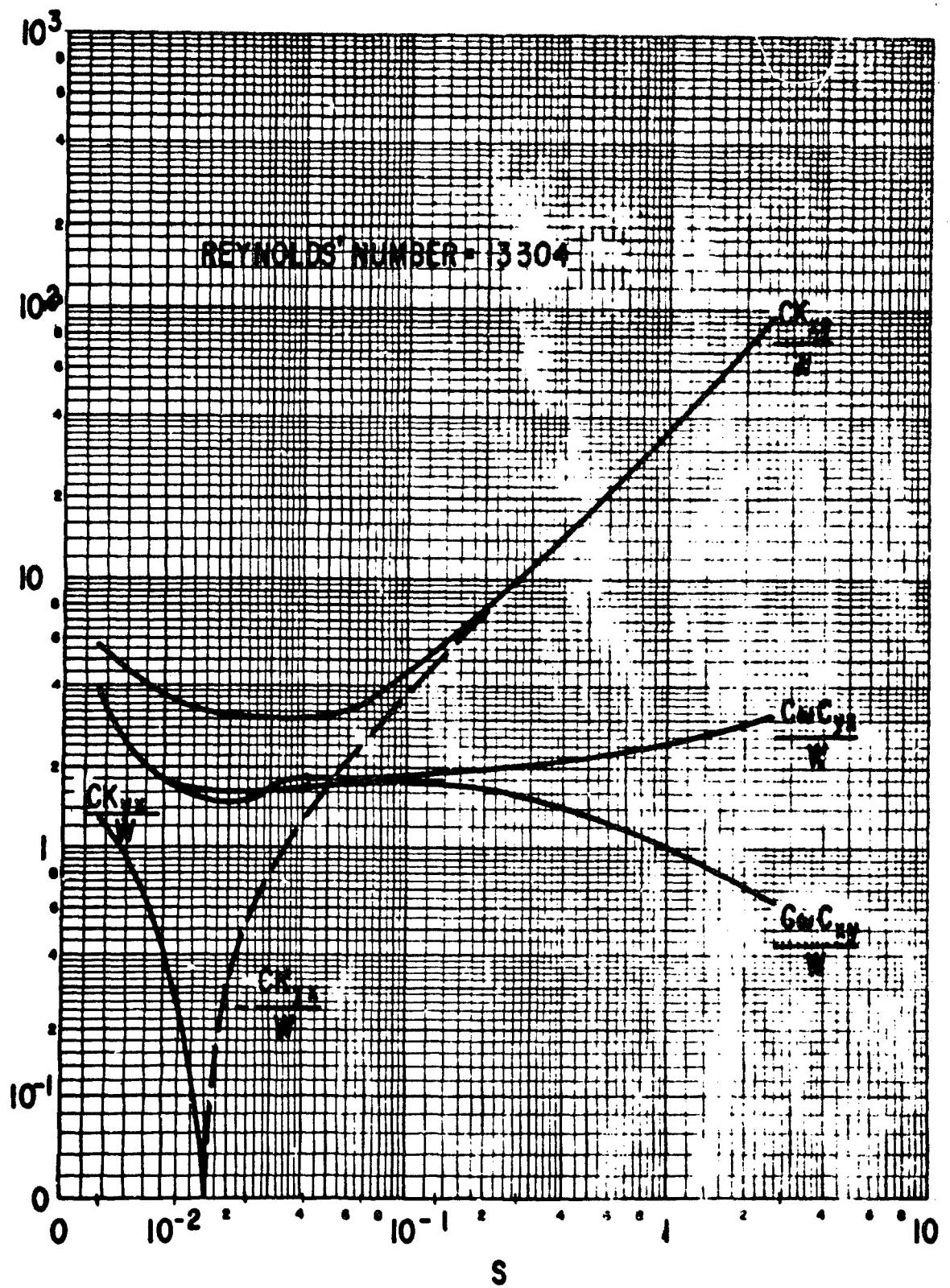


Figure B-67 The Plain Cylindrical Bearing, Turbulent Film Dimensionless Dynamic Coefficients

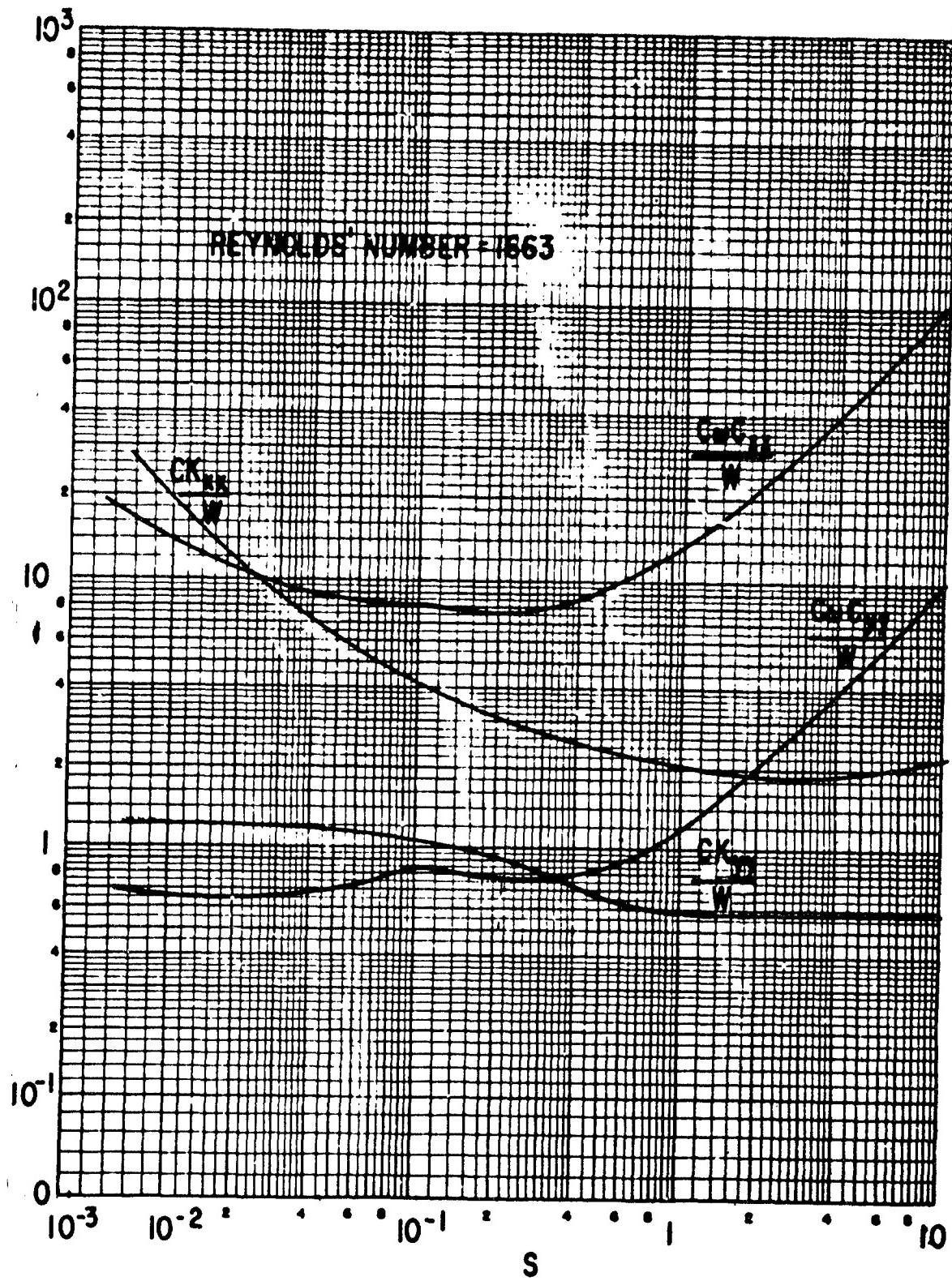


Figure B-68 The 100 Degree Partial Bearing, Centrally Loaded, Turbulent Film Dimensionless Dynamic Coefficients

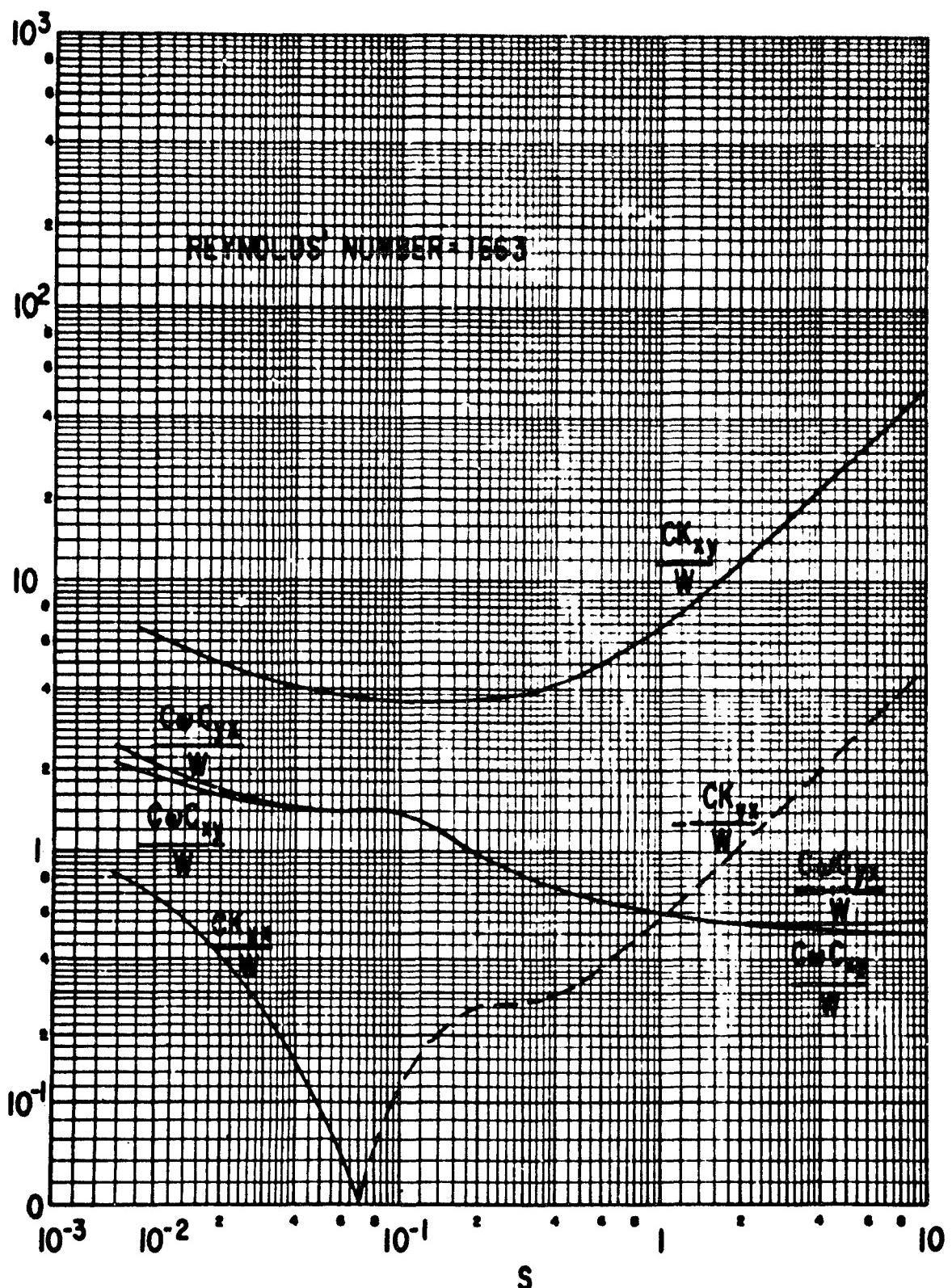


Figure B-69 The 100 Degree Partial Bearing, Centrally Loaded, Turbulent Film Dimensionless Dynamic Coefficients

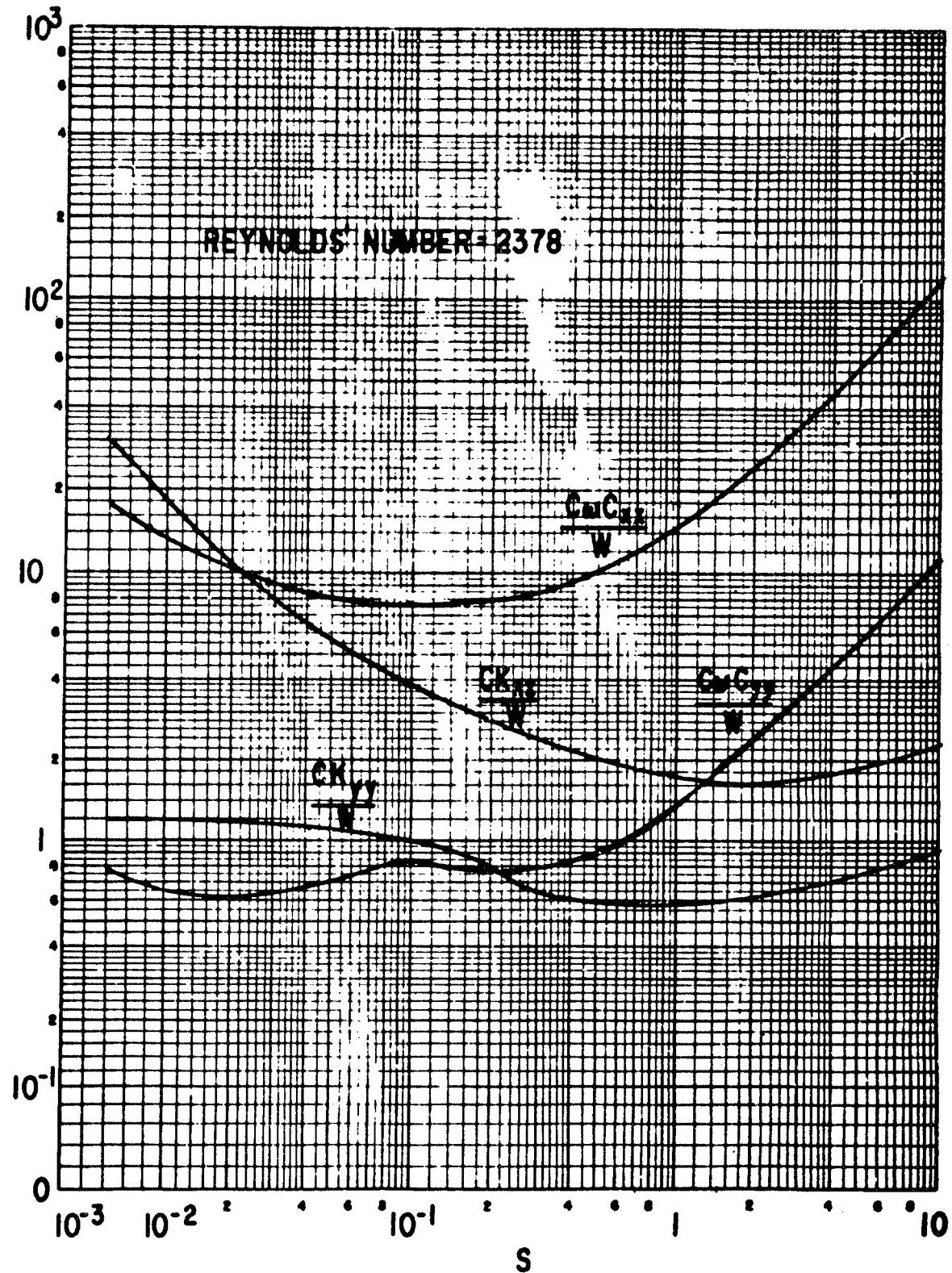


Figure B-70 The 100 Degree Partial Bearing, Centrally Loaded, Turbulent Film Dimensionless Dynamic Coefficients

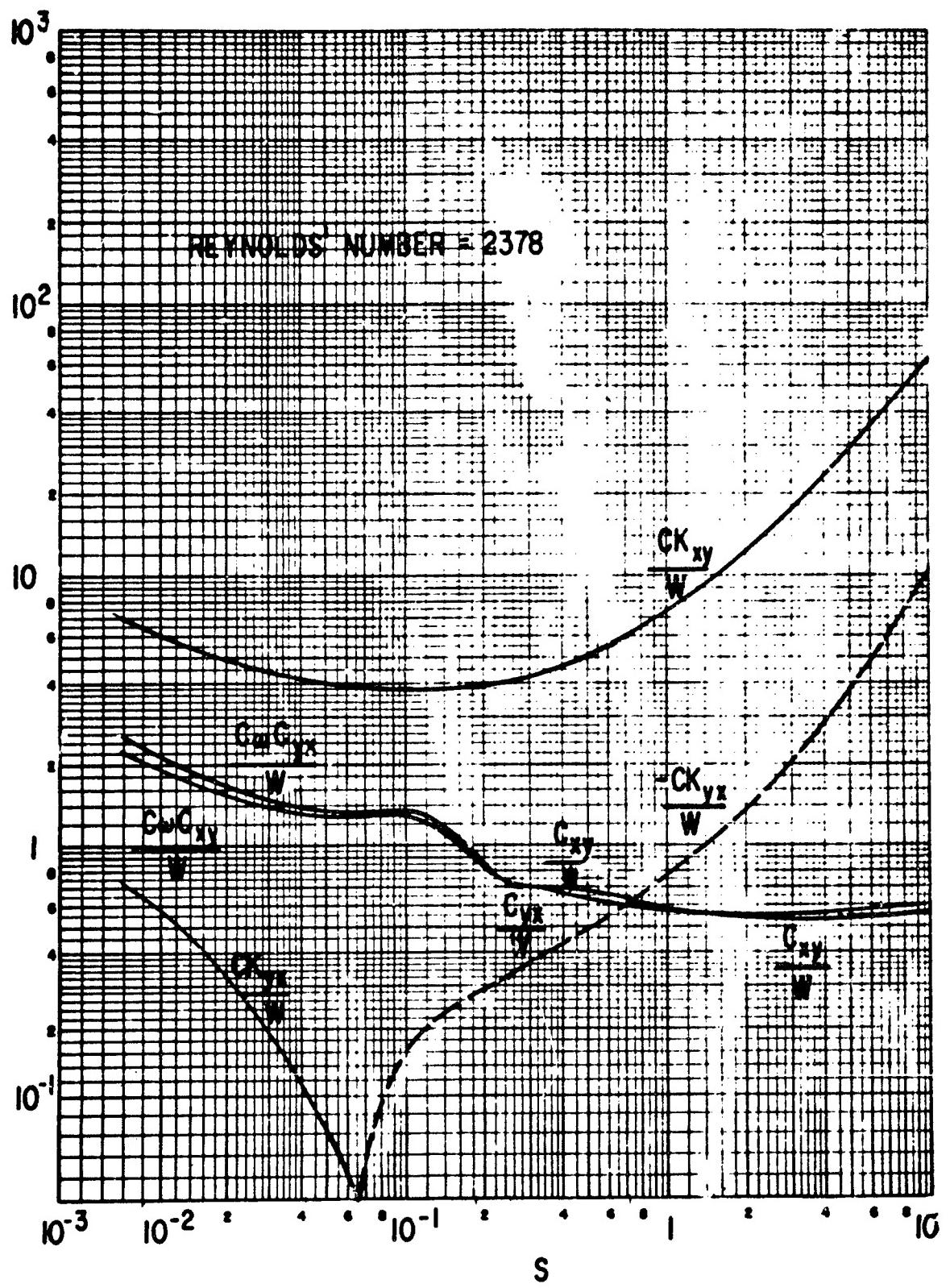


Figure B-71 The 100 Degree Partial Bearing, Centrally Loaded, Turbulent Film Dimensionless Dynamic Coefficients

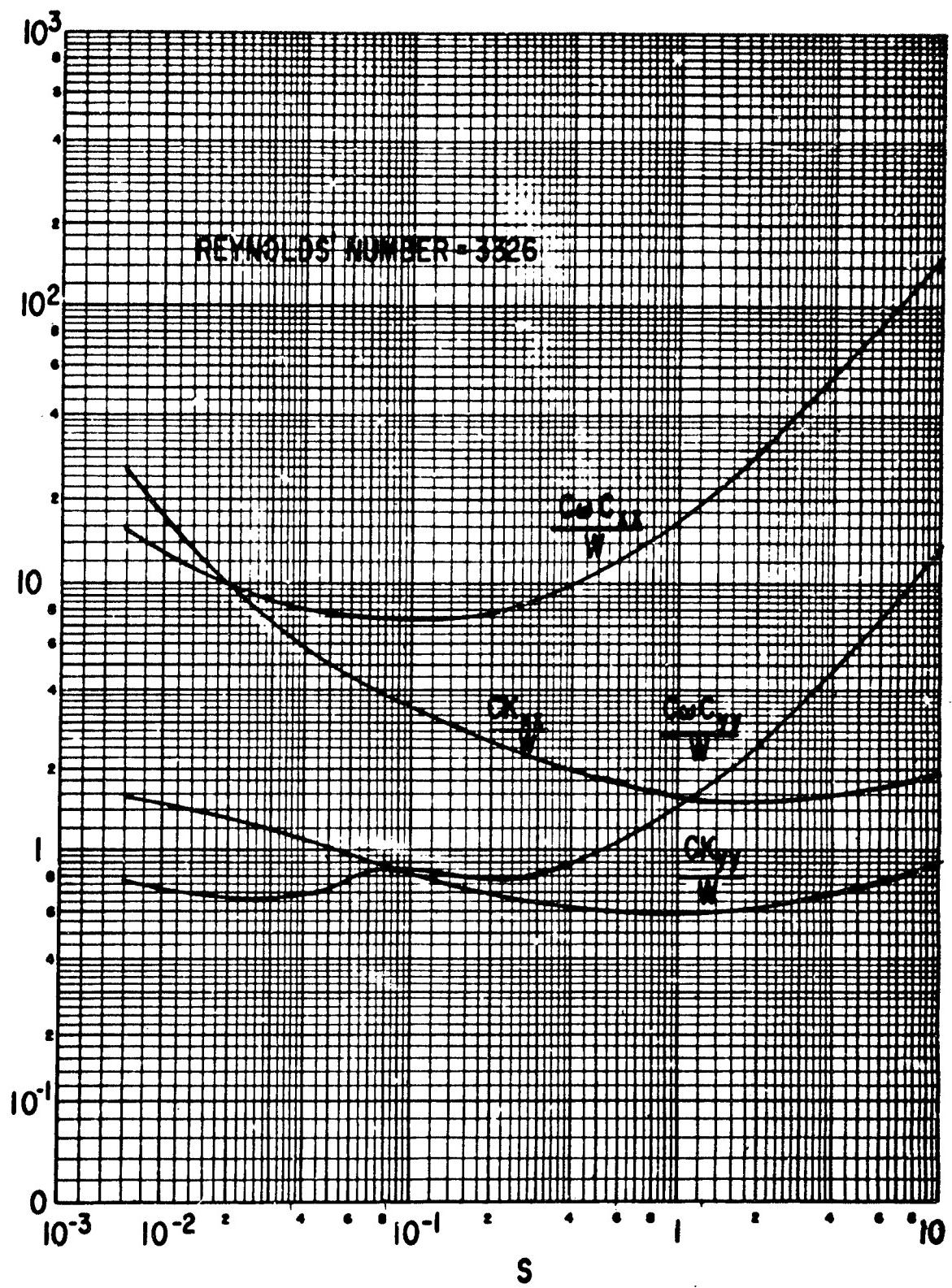


Figure B-72 The 100 Degree Partial Bearing, Centrally Loaded, Turbulent Film Dimensionless Dynamic Coefficients

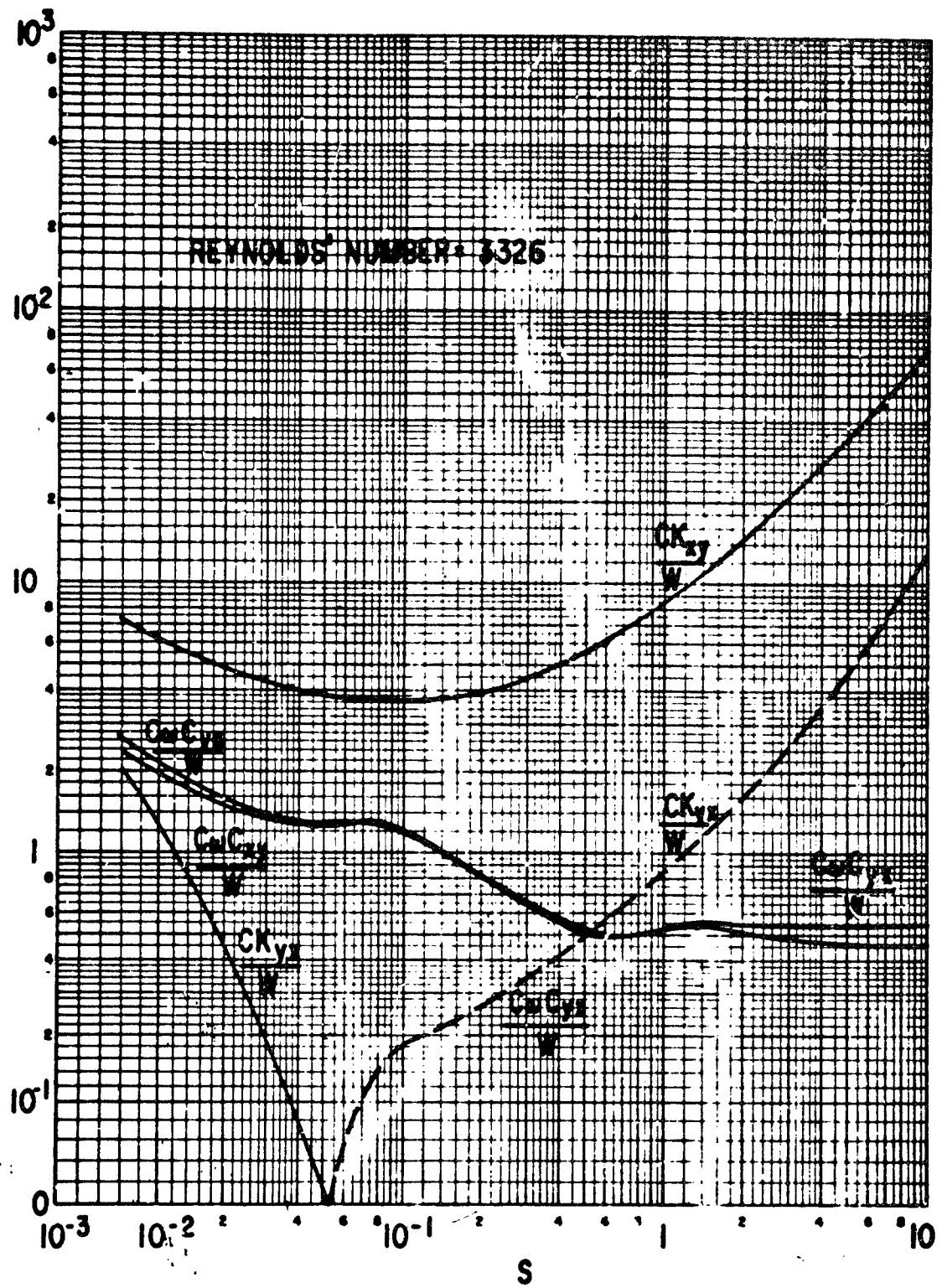


Figure B-73 The 100 Degree Partial Bearing, Centrally Loaded, Turbulent Film Dimensionless Dynamic Coefficients

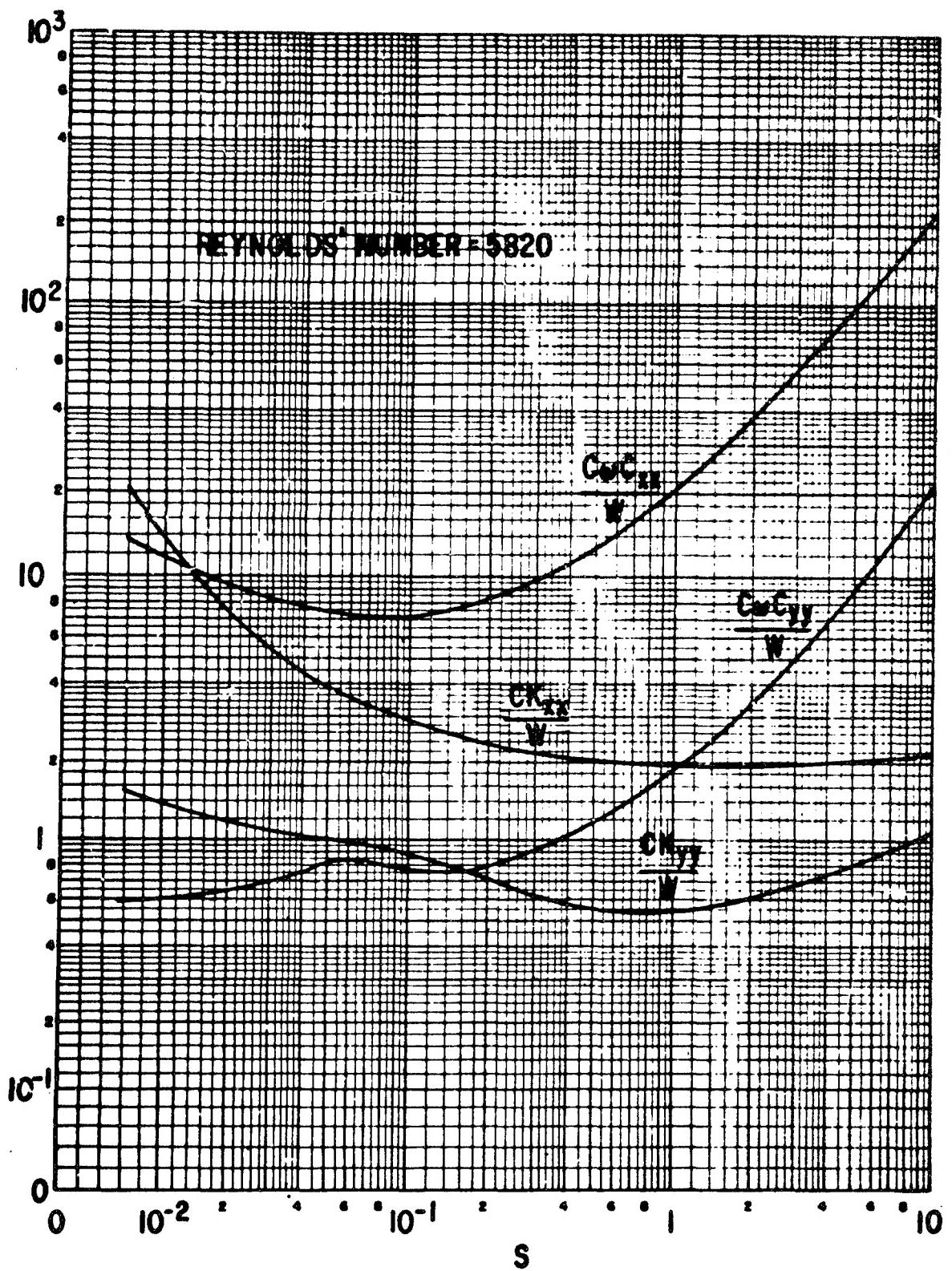


Figure B-74 The 100 Degree Partial Bearing, Centrally Loaded, Turbulent Film Dimensionless Dynamic Coefficients

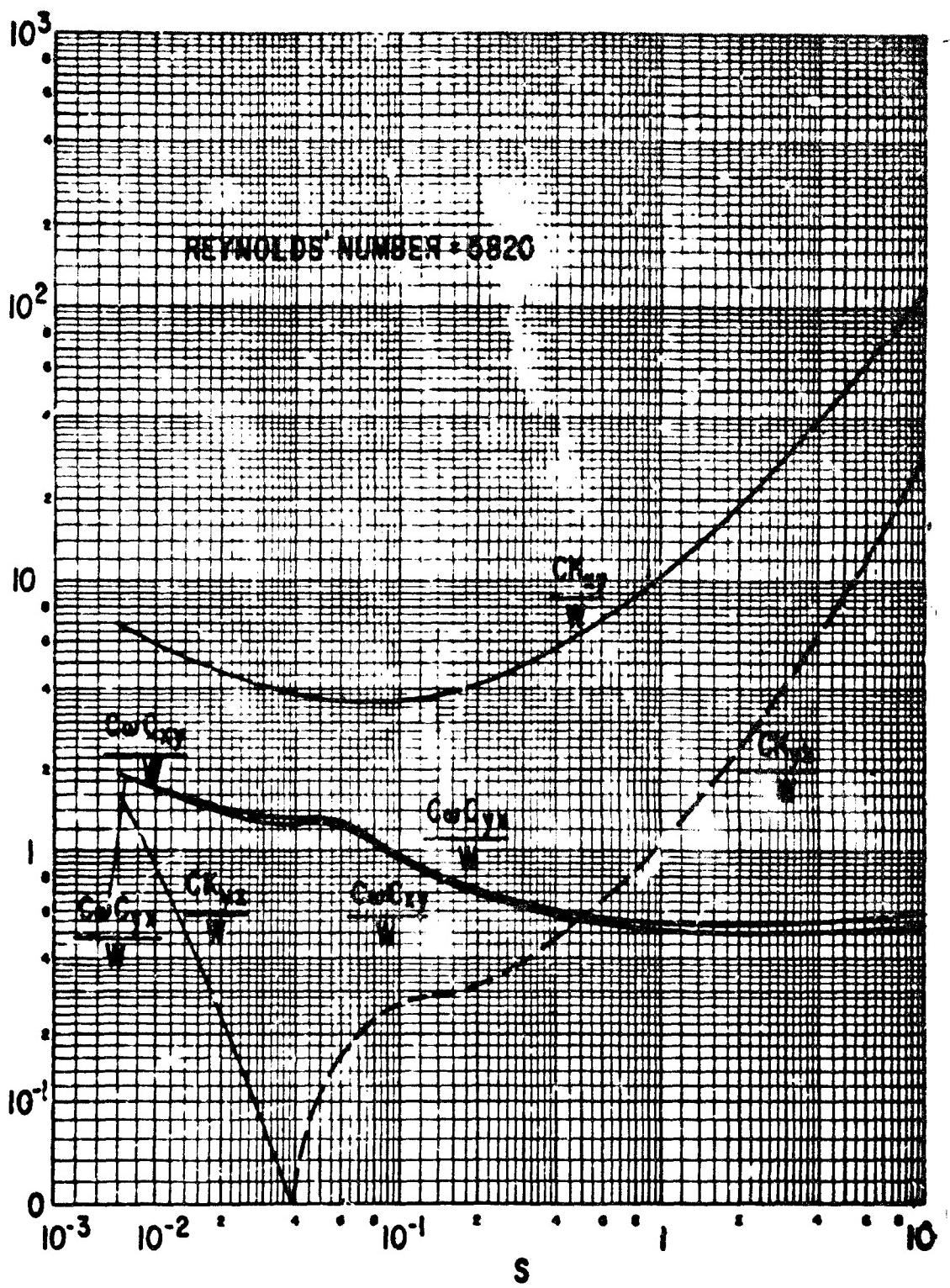


Figure B-75 The 100 Degree Partial Bearing, Centrally Loaded, Turbulent Film Dimensionless Dynamic Coefficients

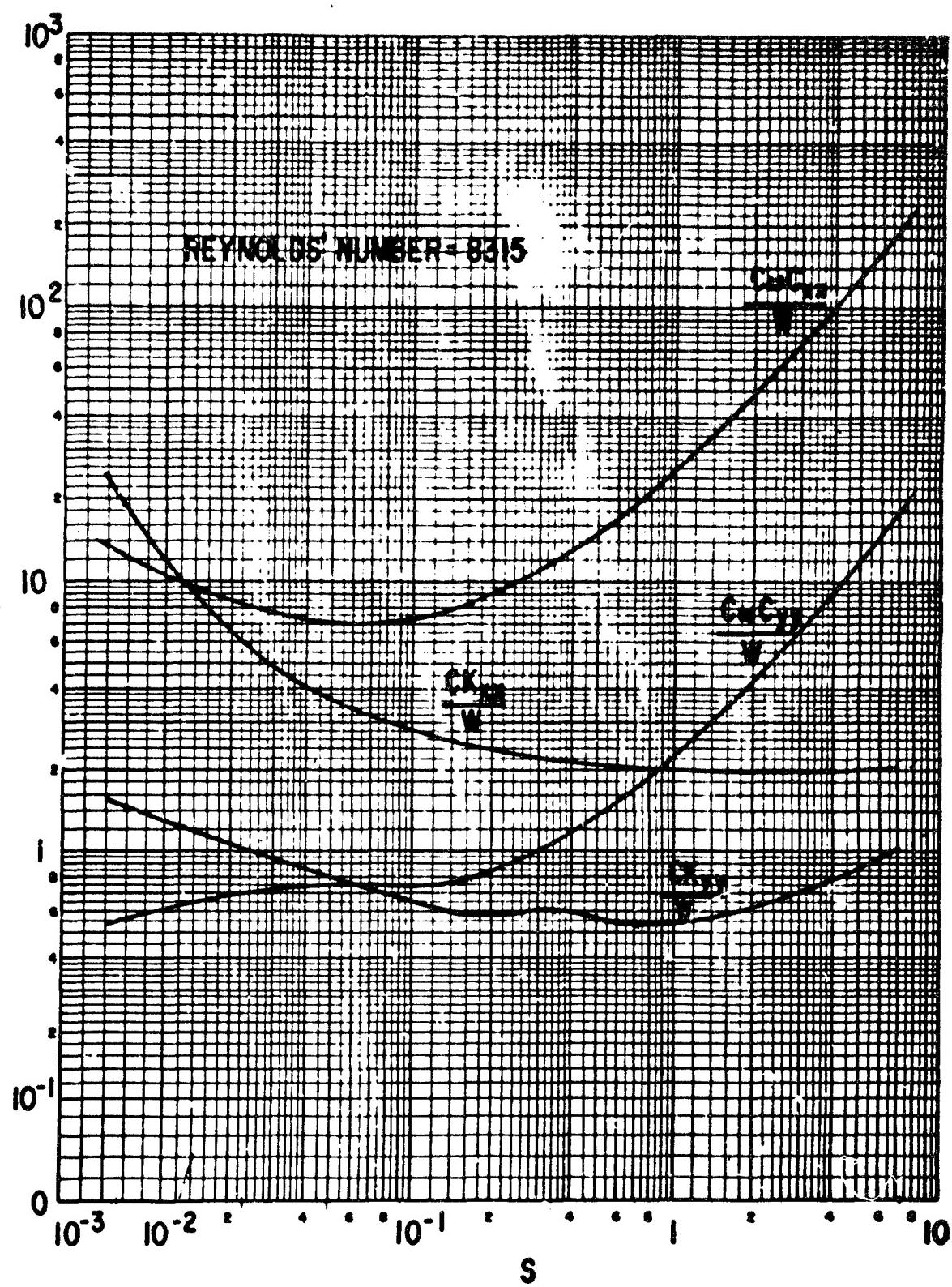


Figure B-76 The 100 Degree Partial Bearing, Centrally Loaded, Turbulent Film Dimensionless Dynamic Coefficients

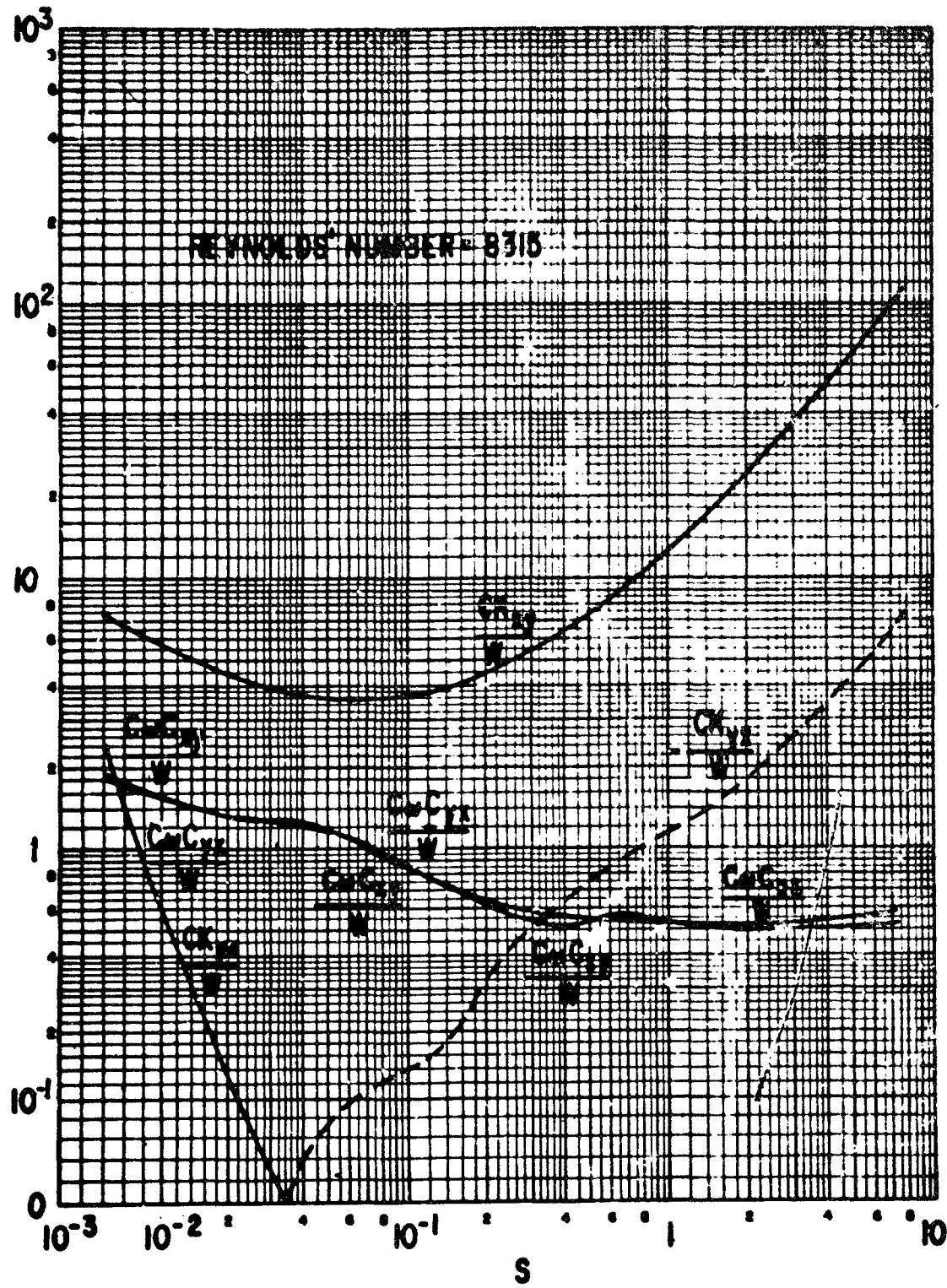


Figure B-77 The 100 Degree Partial Bearing, Centrally Loaded, Turbulent Film Dimensionless Dynamic Coefficients

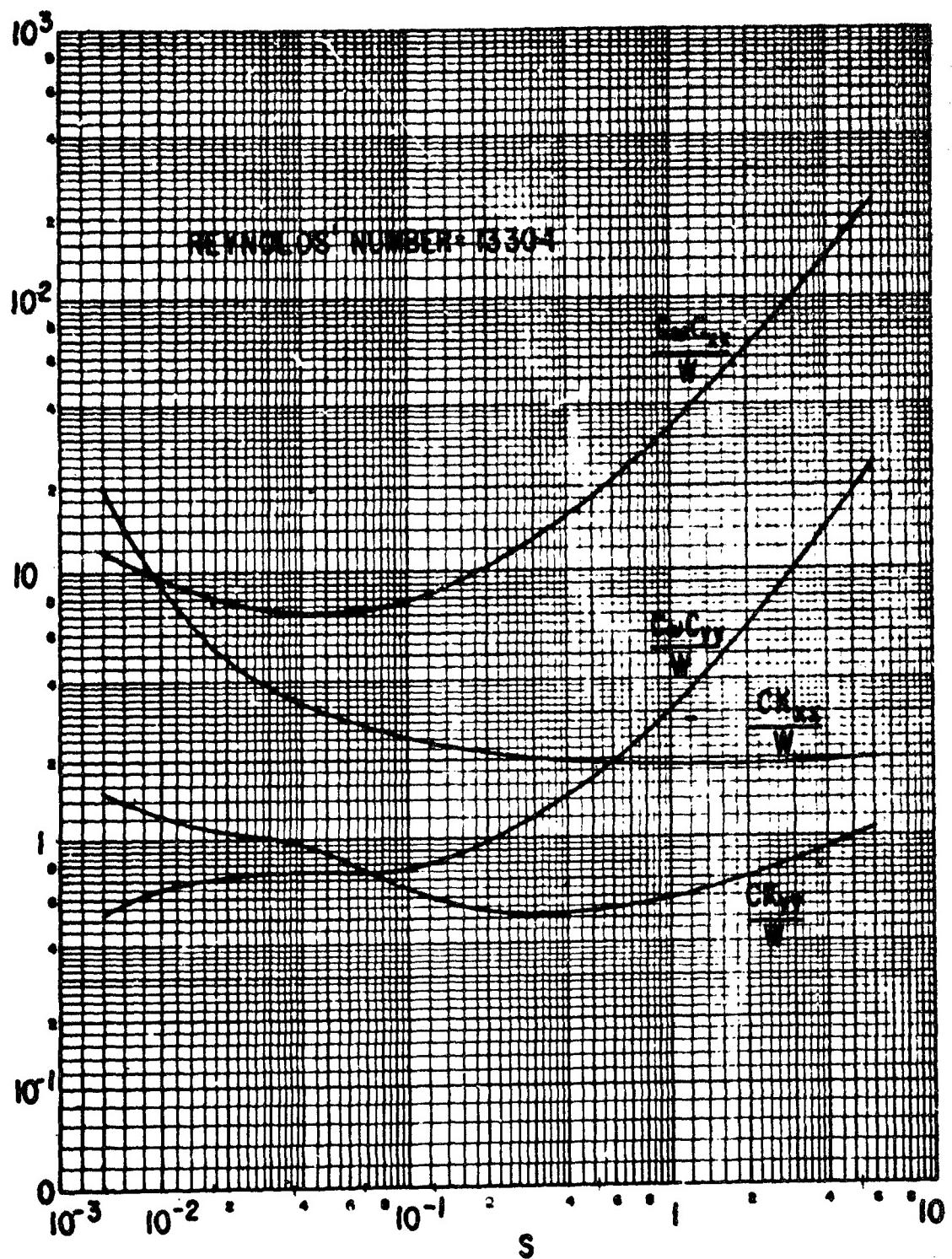


Figure B-78 The 100 Degree Partial Bearing, Centrally Loaded, Turbulent Film Dimensionless Dynamic Coefficients

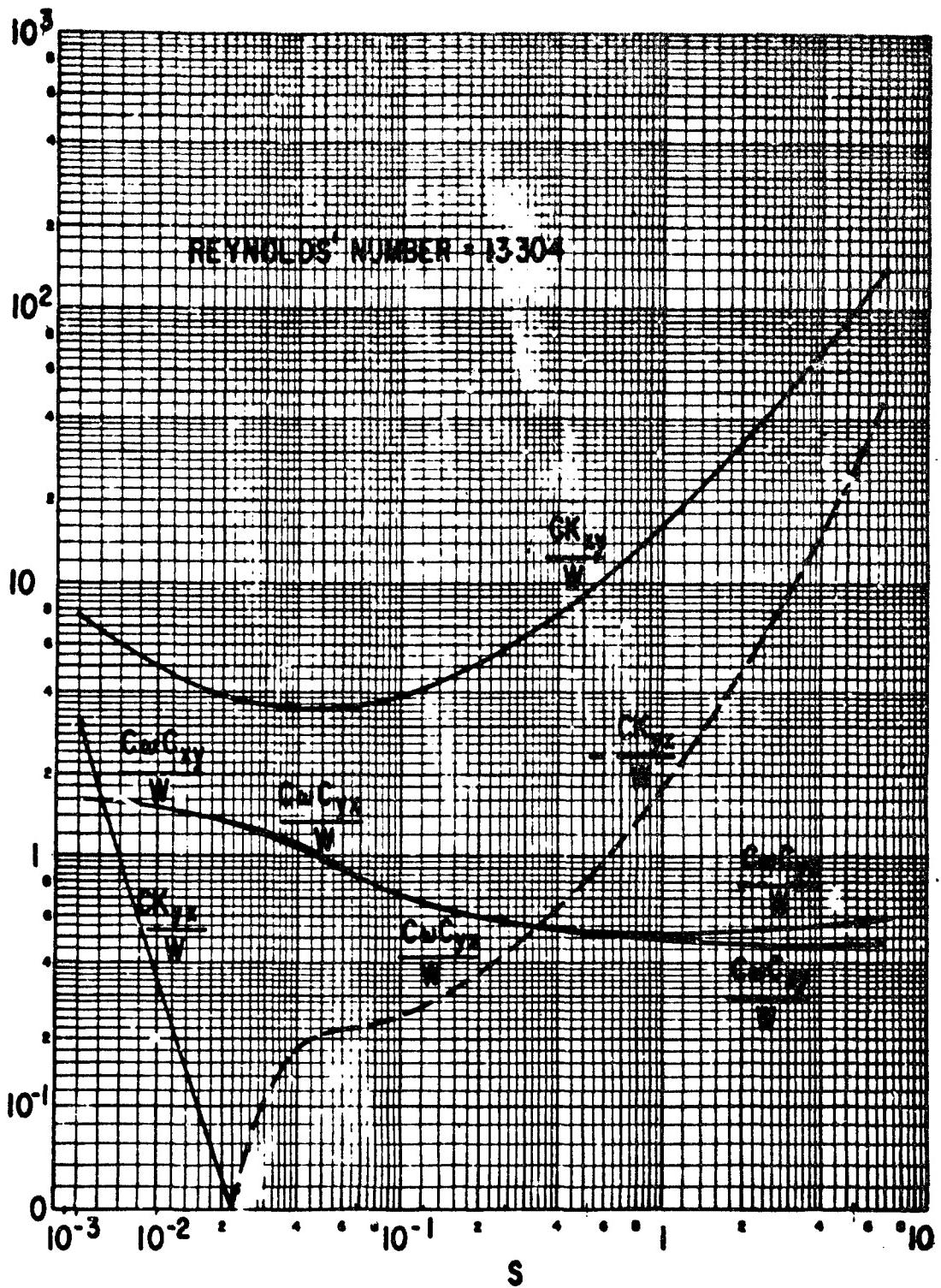


Figure B-79 The 100 Degree Partial Bearing, Centrally Loaded, Turbulent Film Dimensionless Dynamic Coefficients

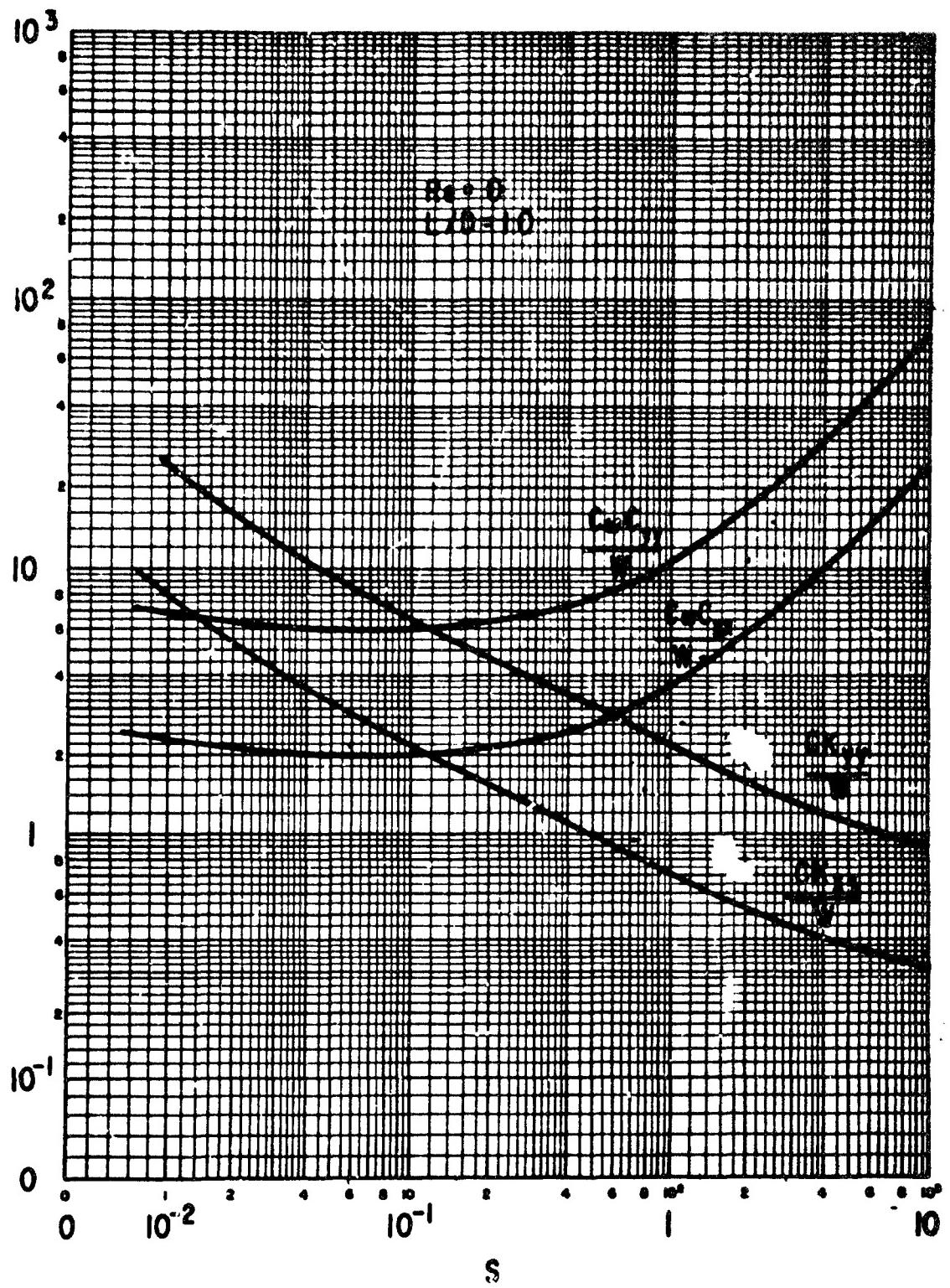


Figure B-80 The 4 Shoe Tilting Pad Bearing, Turbulent Film
Load between Pads
 $C'/C = 1$, No Pad Inertia

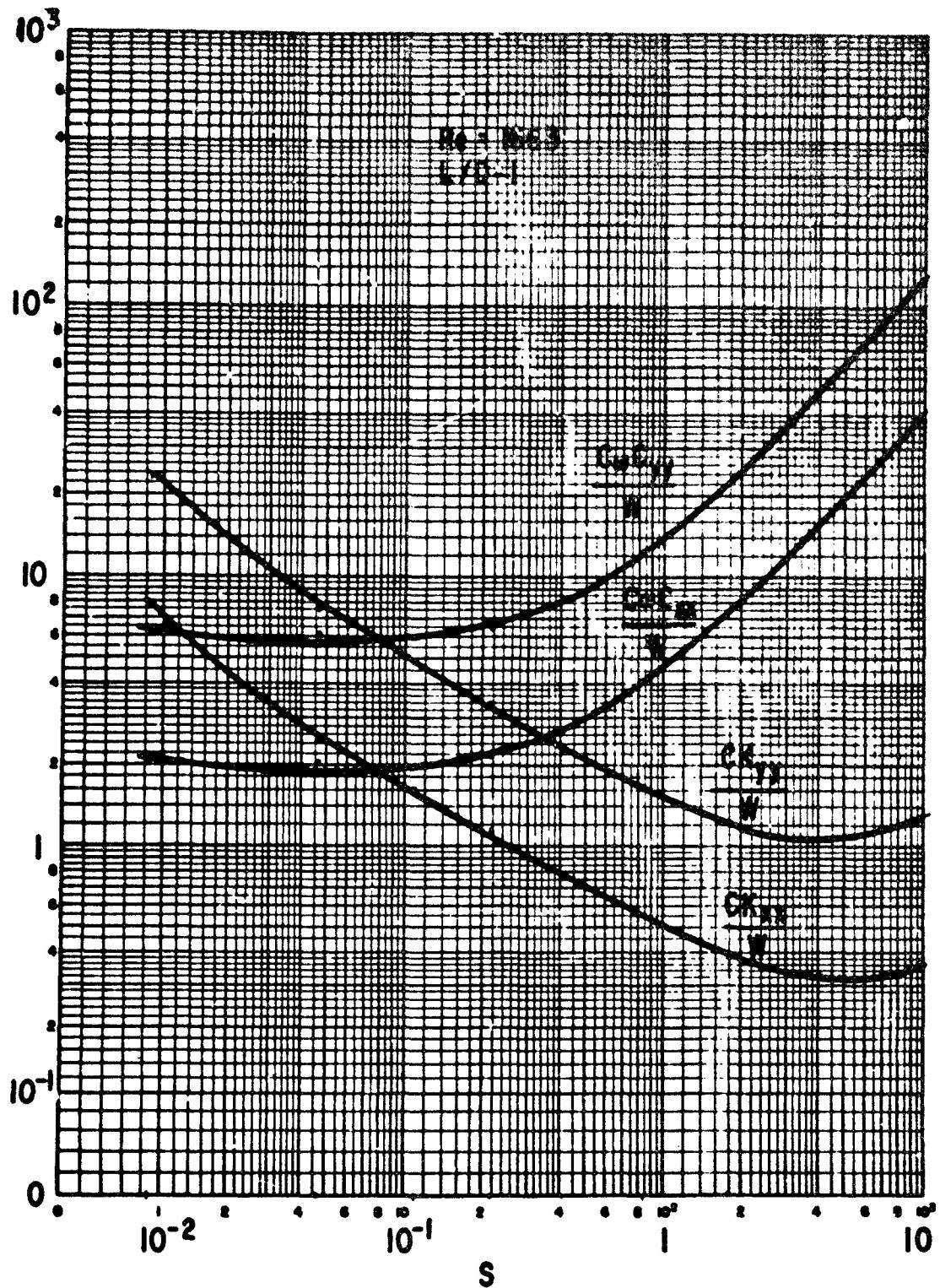


Figure 3-81 The 4 Shoe Tilting Pad Bearing, Turbulent Film
Load between Pads
 $C'/C = 1$, No Pad Inertia

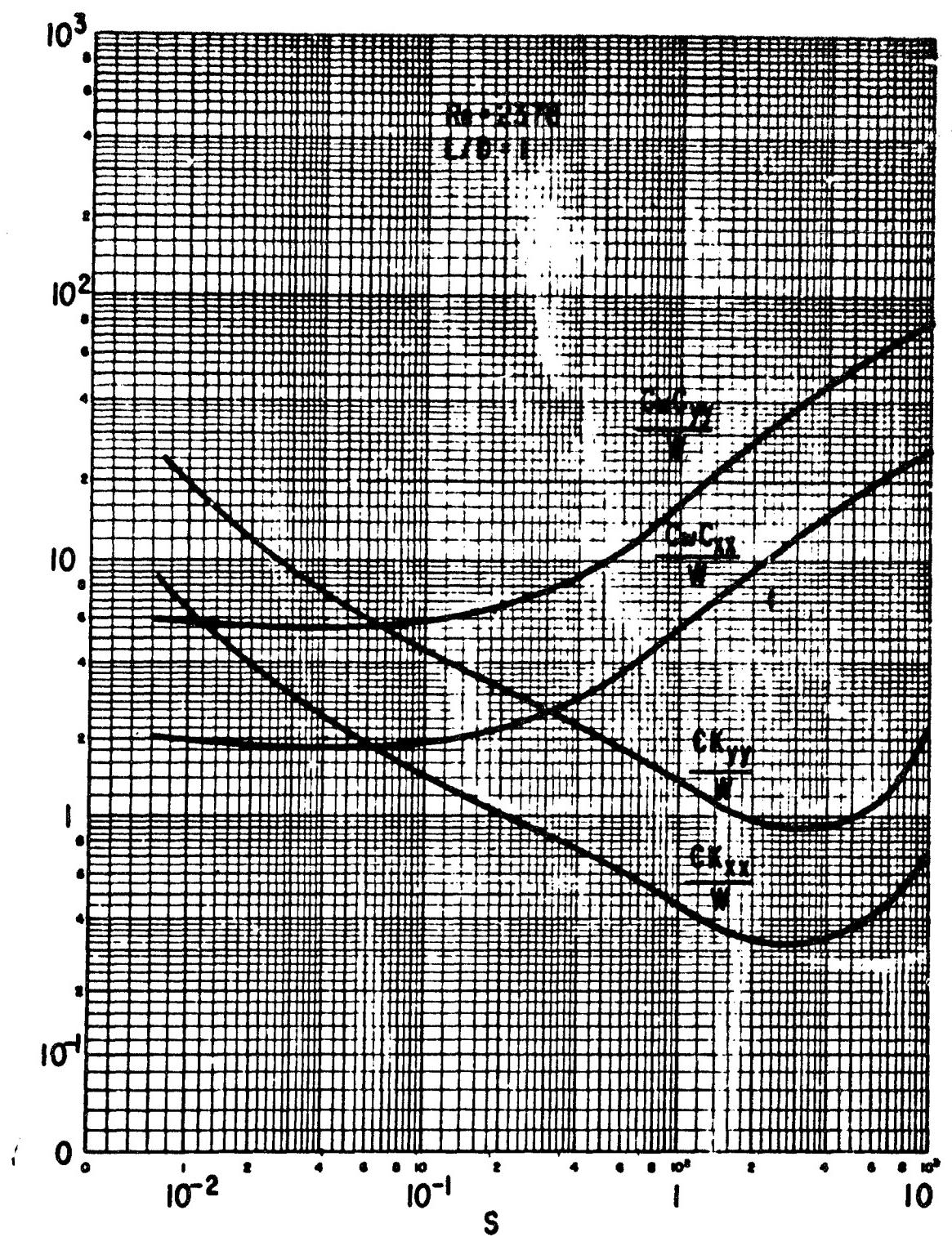


Figure B-82 The 4 Shoe Tilting Pad Bearing, Turbulent Film
Load between Pads
 $C'/C = 1$, No Pad Inertia

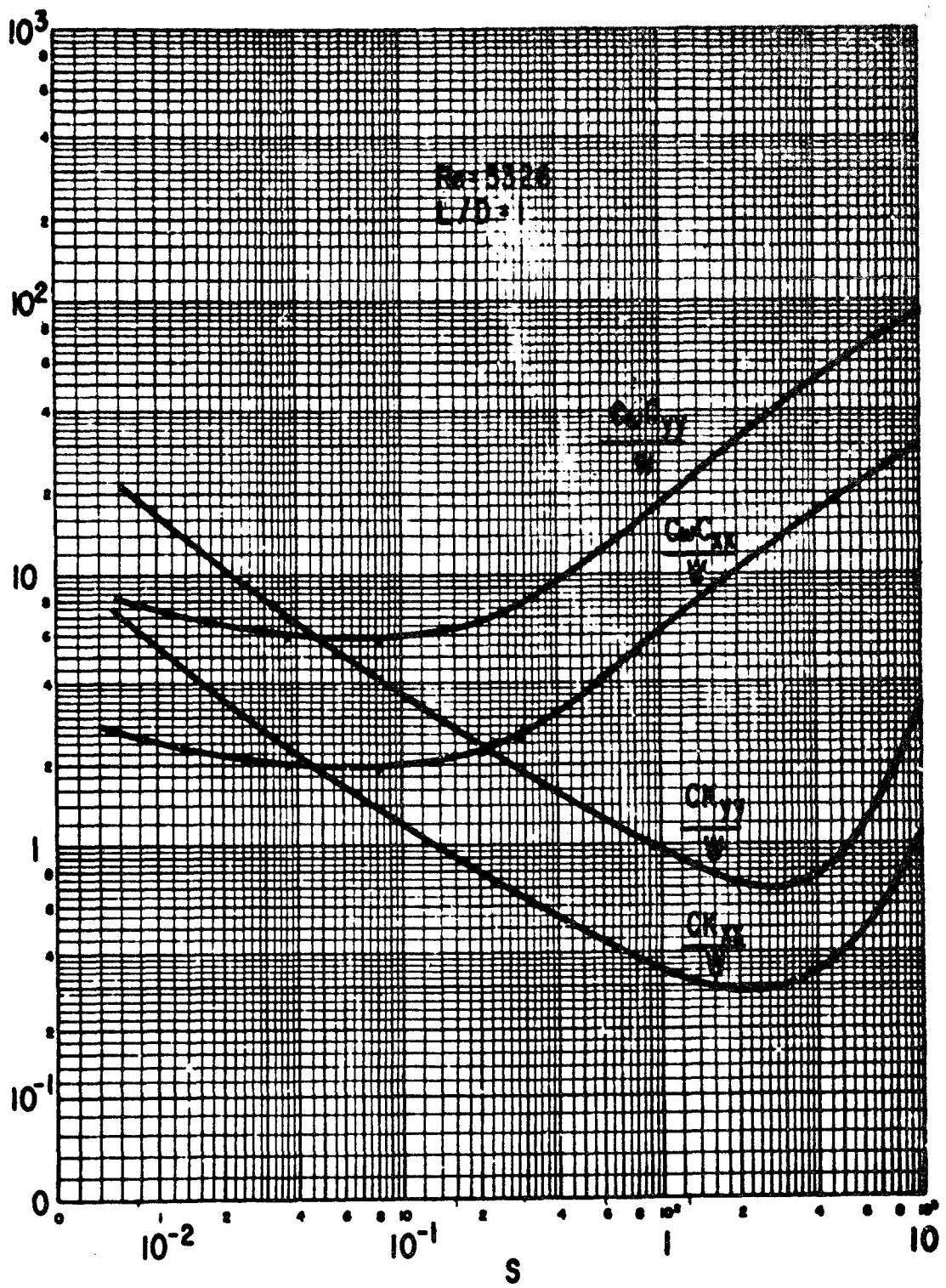


Figure B-83 The 4 Shoe Tilting Pad Bearing, Turbulent Film
Load between Pads
 $C'/C = 1$, No Pad Inertia

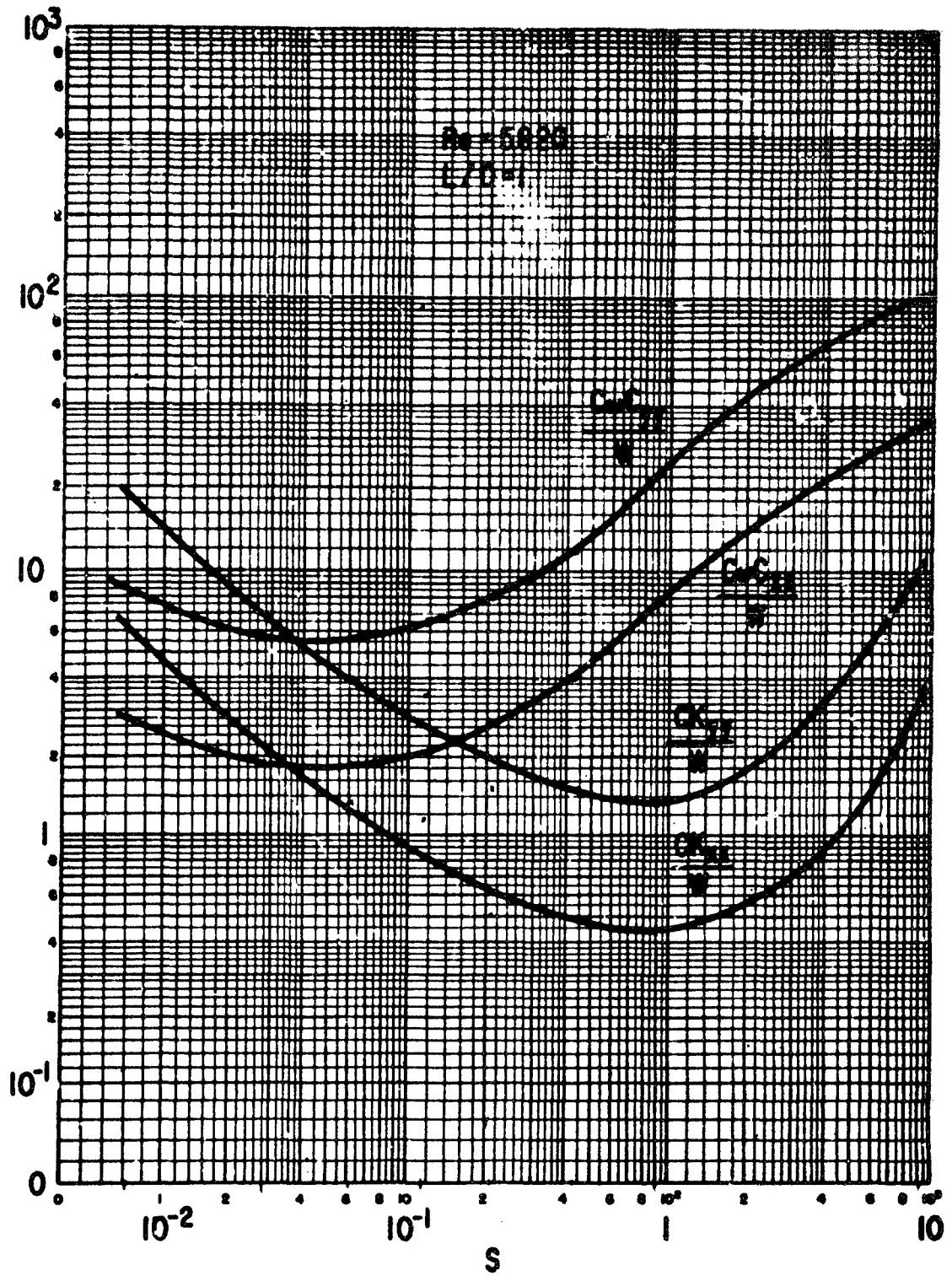


Figure B-84 The 4 Shoe Tilting Pad Bearing, Turbulent Film
Load between Pads
 $C'/C = 1$, No Pad Inertia

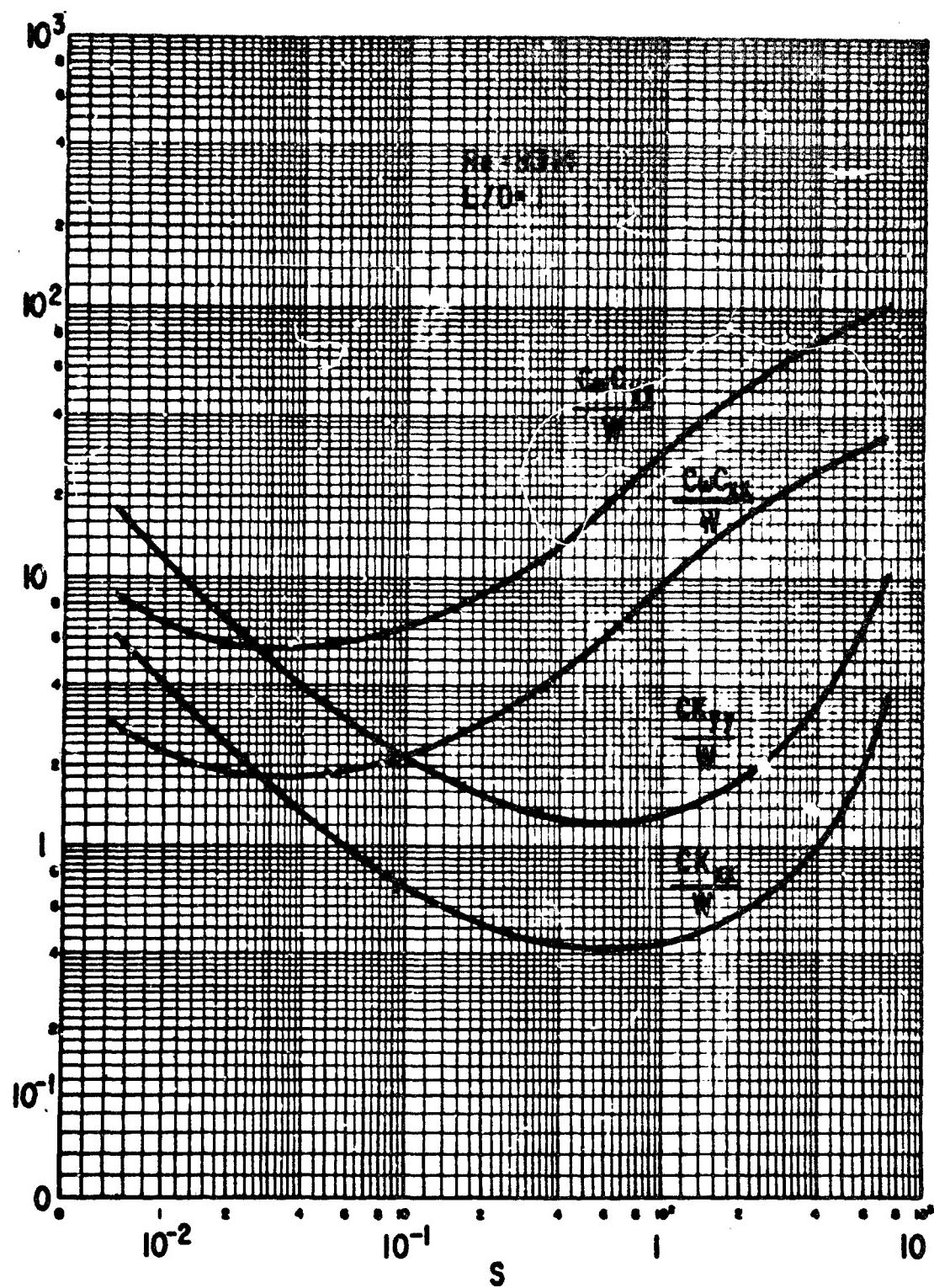


Figure B-85 The 4 Shoe Tilting Pad Bearing, Turbulent Film
Load between Pads
 $C'/C = 1$, No Pad Inertia

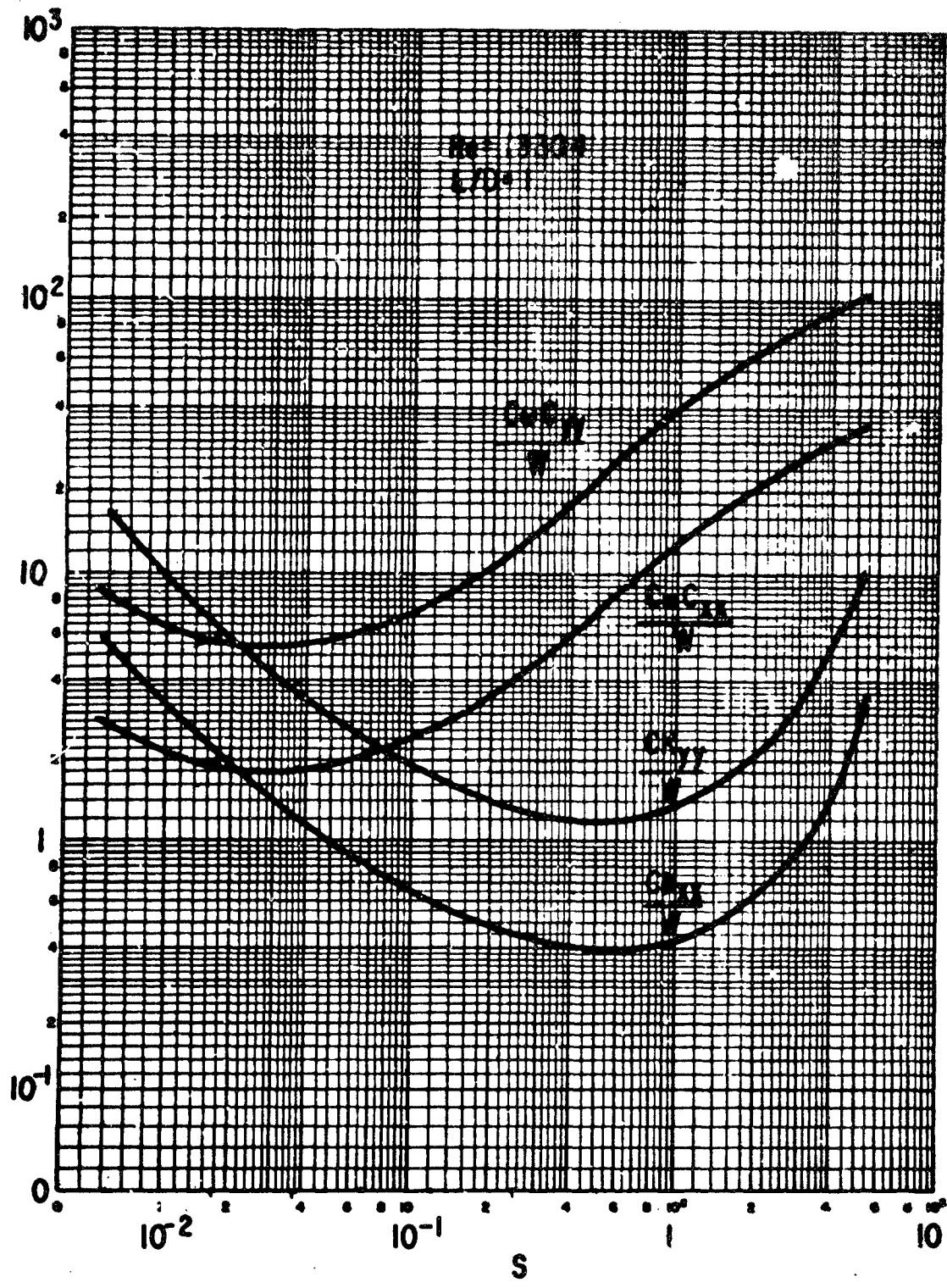


Figure B-86 The 4 Shoe Tilting Pad Bearing, Turbulent Film
Load between Pads
 $C'/C = 1$, No Pad Inertia

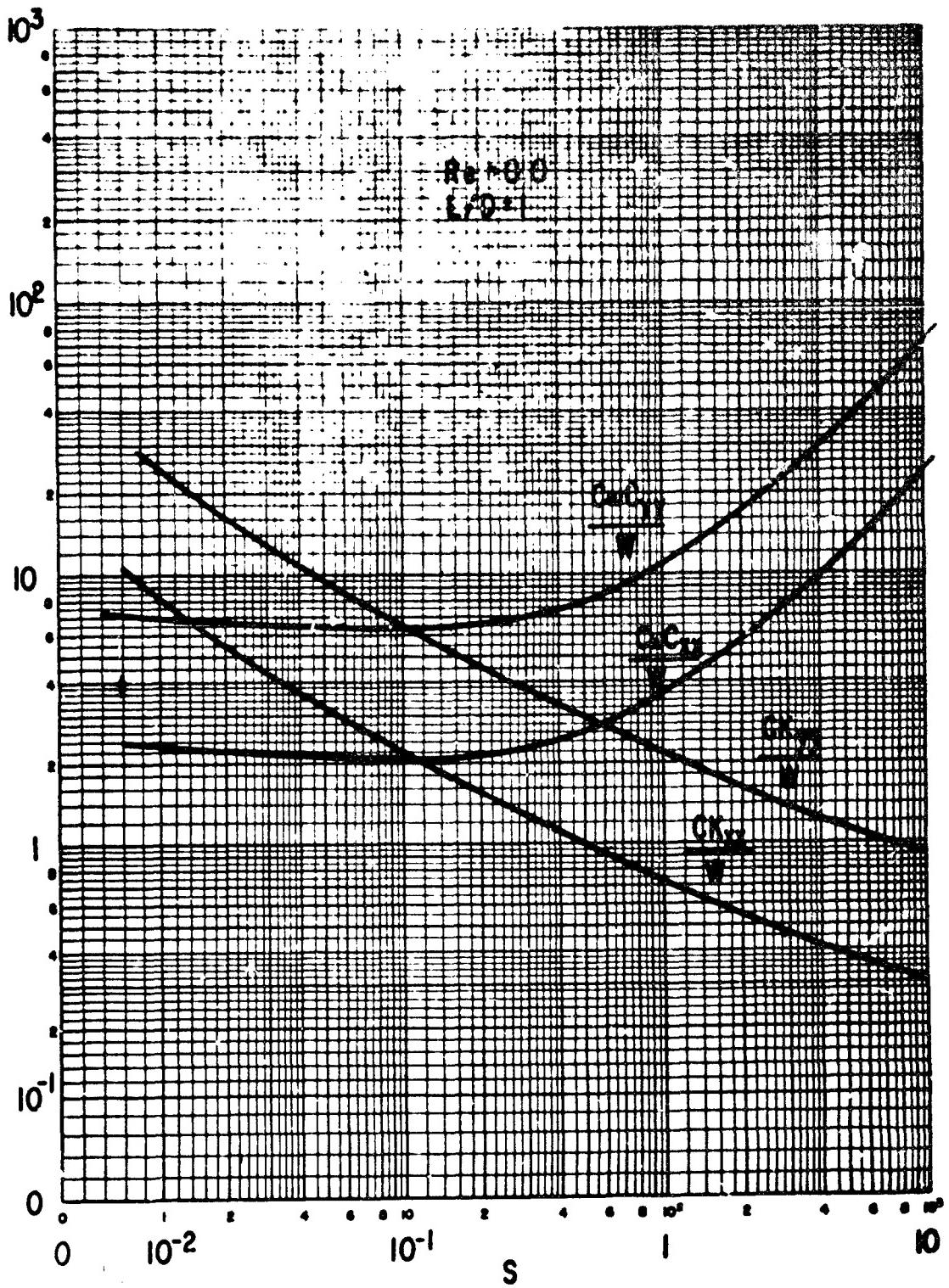


Figure B-87 The 3 Shoe Tilting Pad Bearing, Turbulent Film
Load between Pads
 $C'/C = 1$, No Pad Inertia

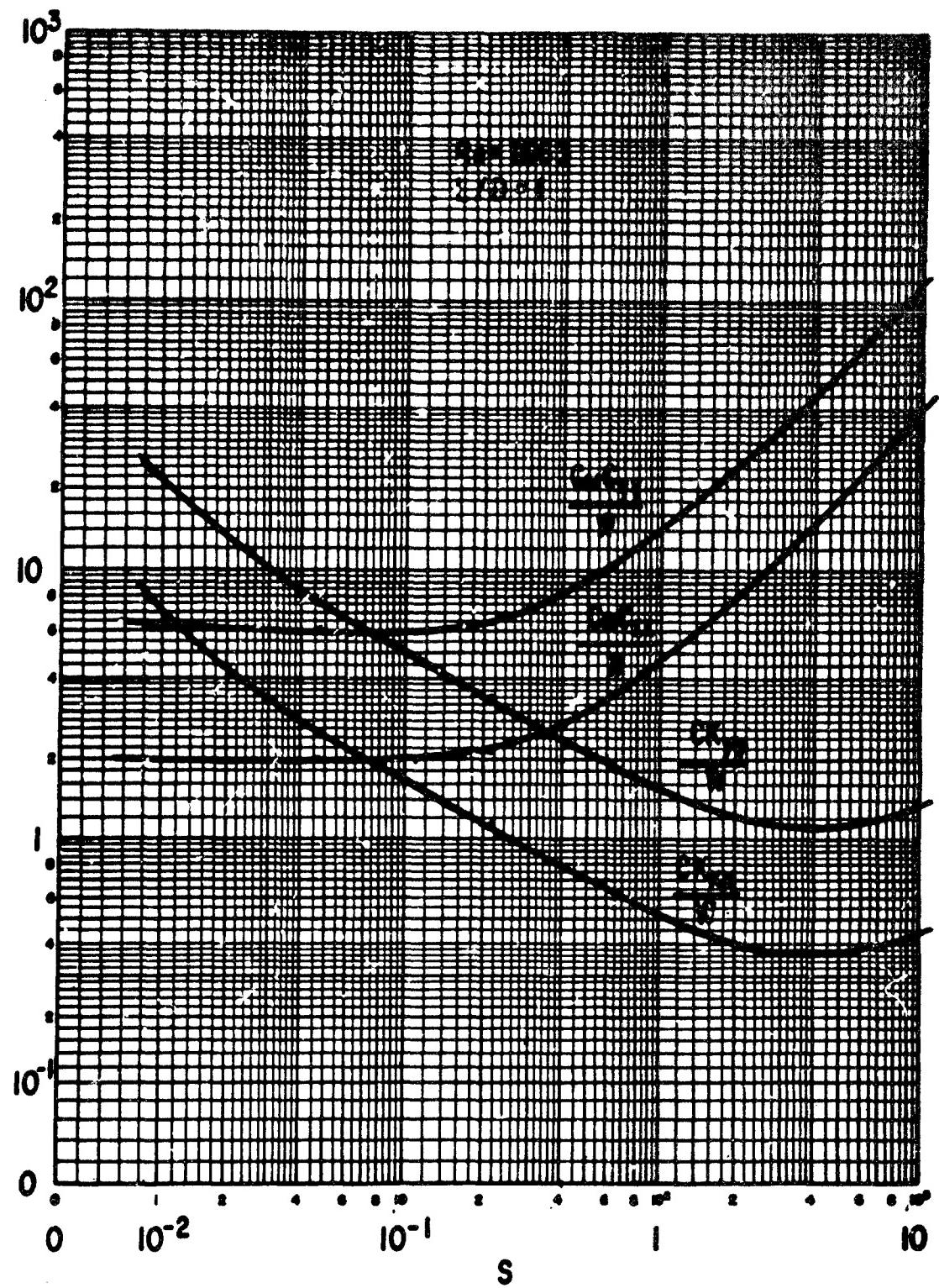


Figure B-88 The 3 Shoe Tilting Pad Bearing, Turbulent Film
Load between Pads
 $C'/C = 1$, No Pad Inertia

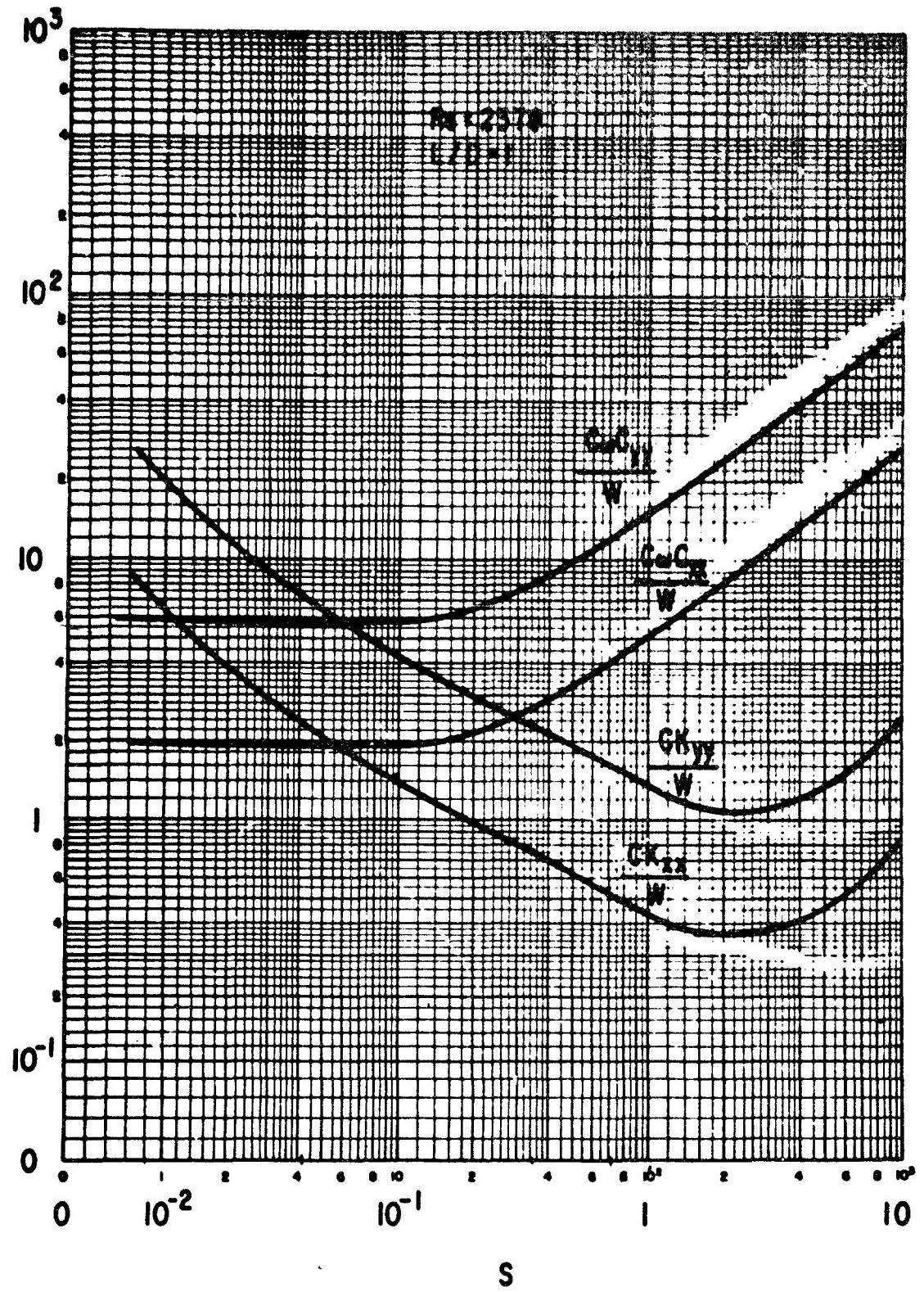


Figure B-89 The 3 Shoe Tilting Pad Bearing, Turbulent Film
Load between Pads
 $C'/C = 1$, No Pad Inertia

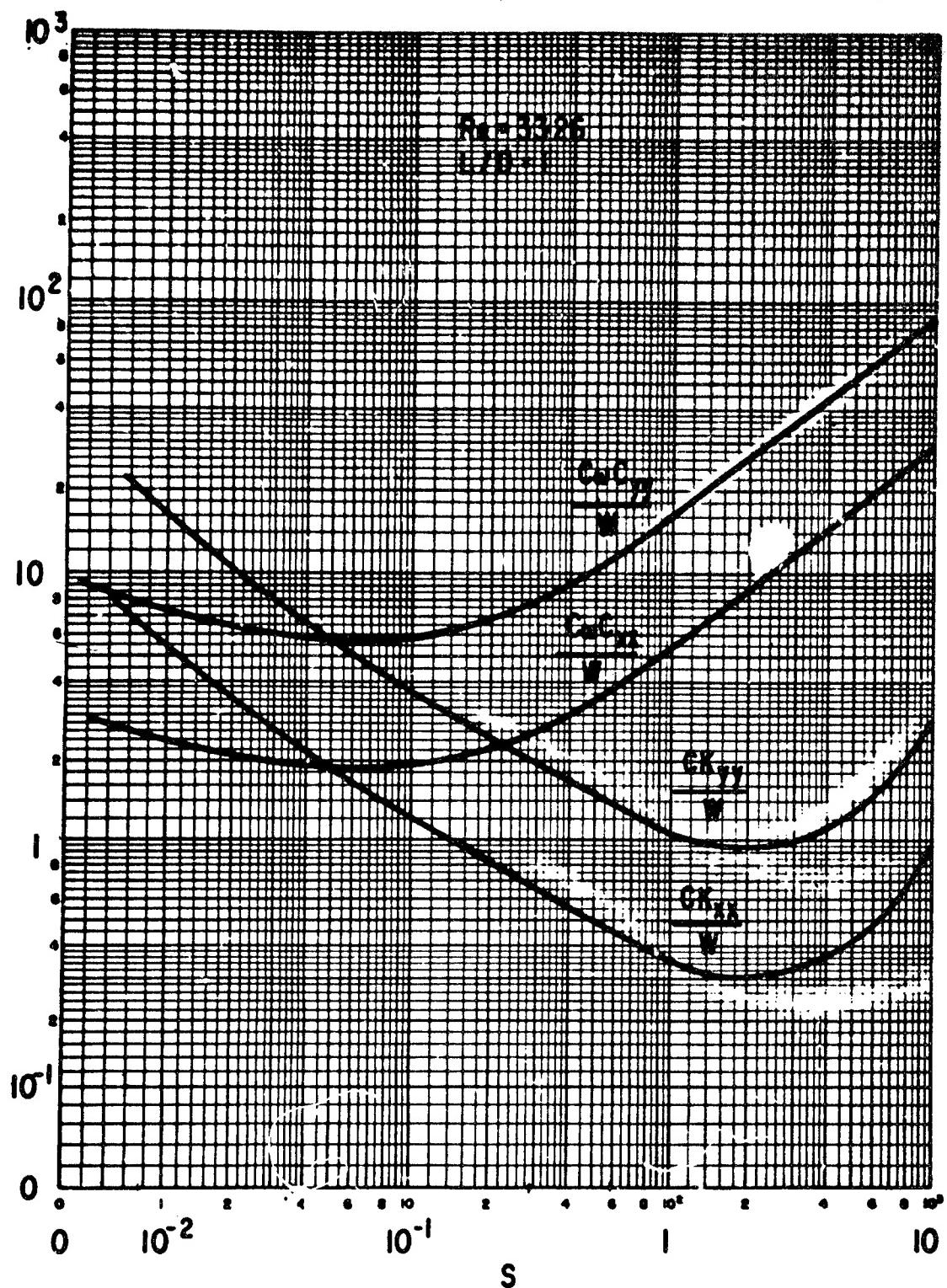


Figure B-90 The 3 Shoe Tilting Pad Bearing, Turbulent Film
 Load between Pads
 $C'/C = 1$, No Pad Inertia

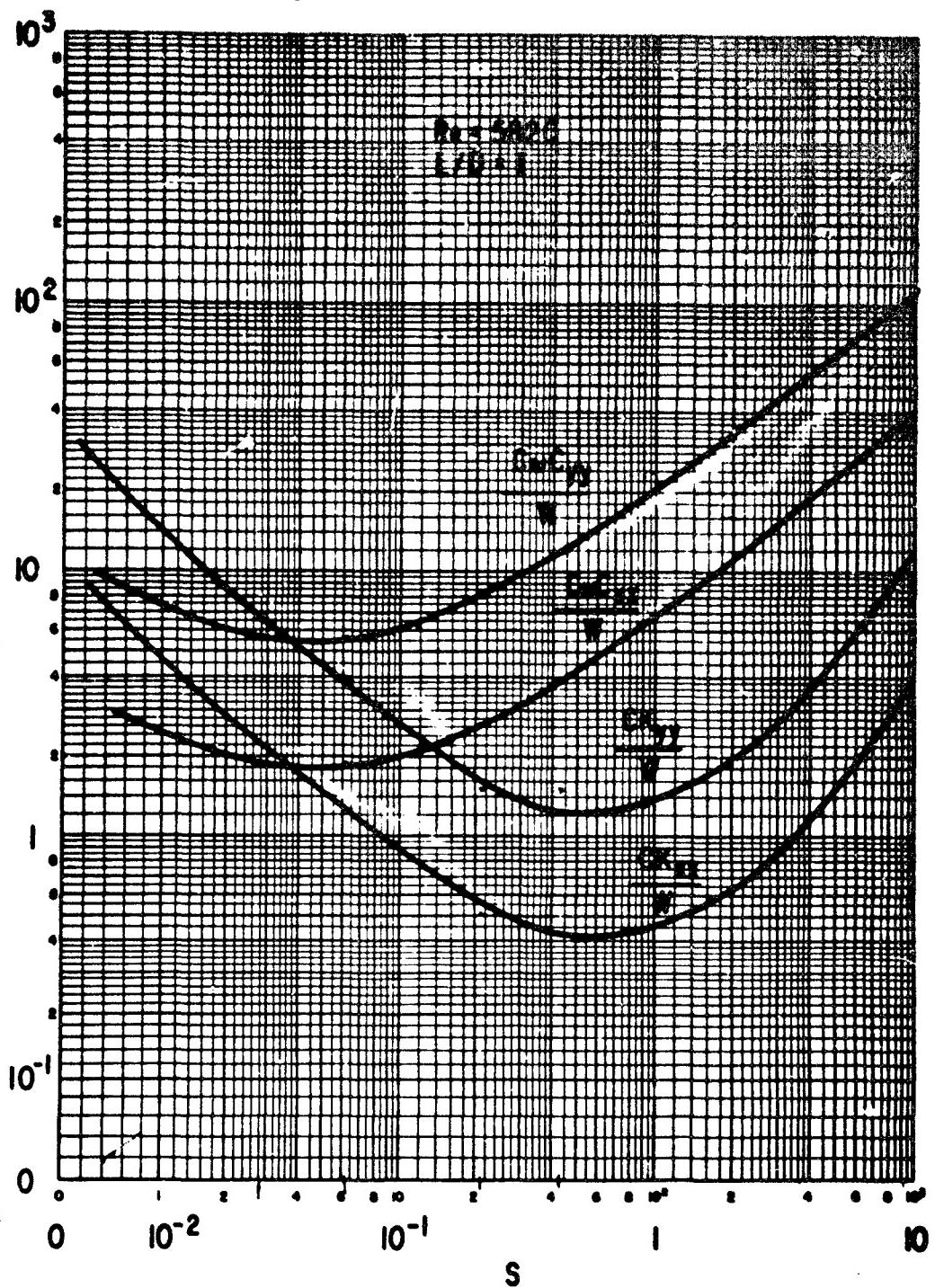


Figure B-91 The 3 Shoe Tilting Pad Bearing, Turbulent Film
Load between Pads
 $C'/C = 1$, No Pad Inertia

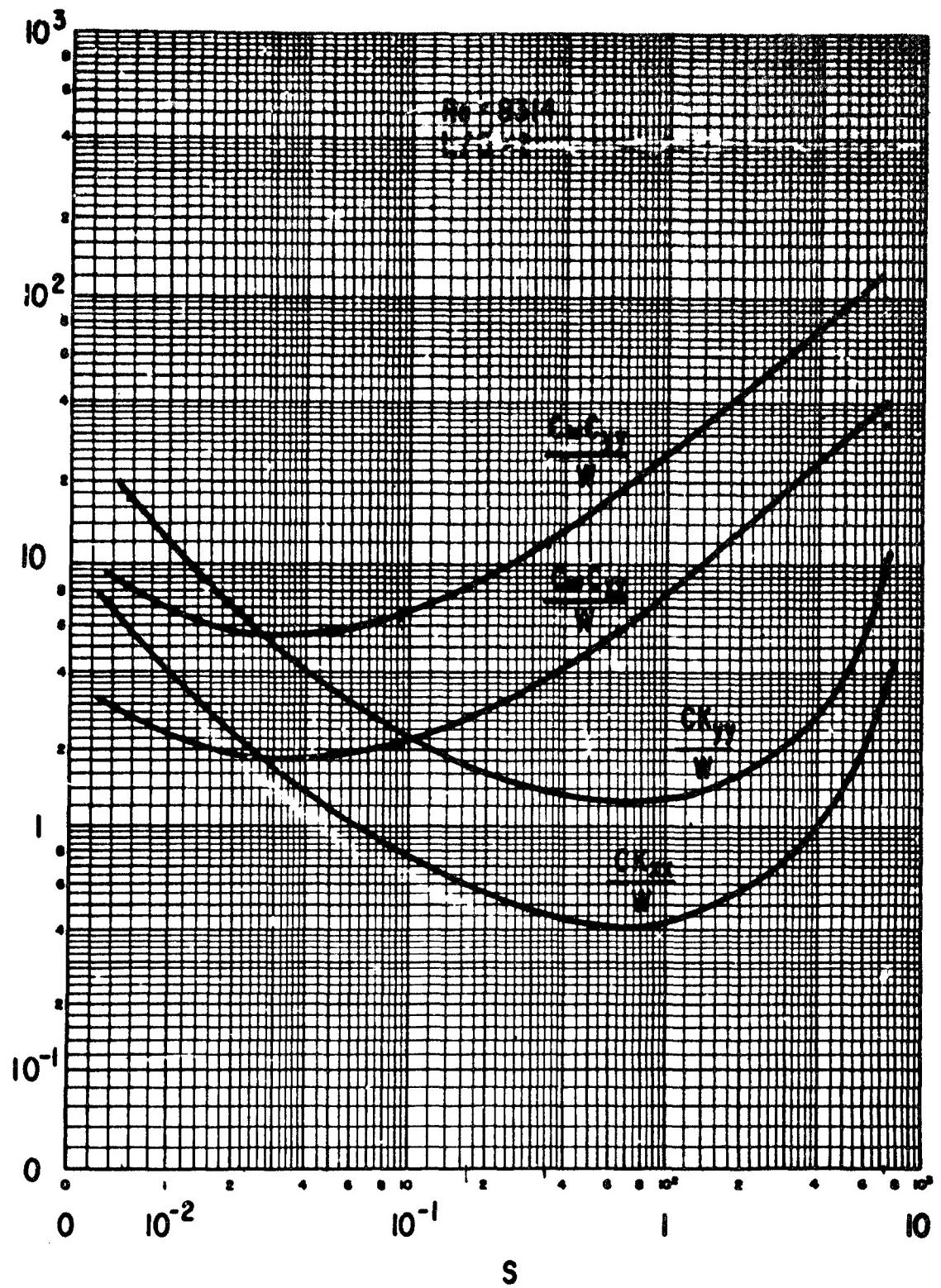


Figure B-92 The 3 Shoe Tilting Pad Bearing, Turbulent Film
Load between Pads
 $C'/C = .1$, No Pad Inertia

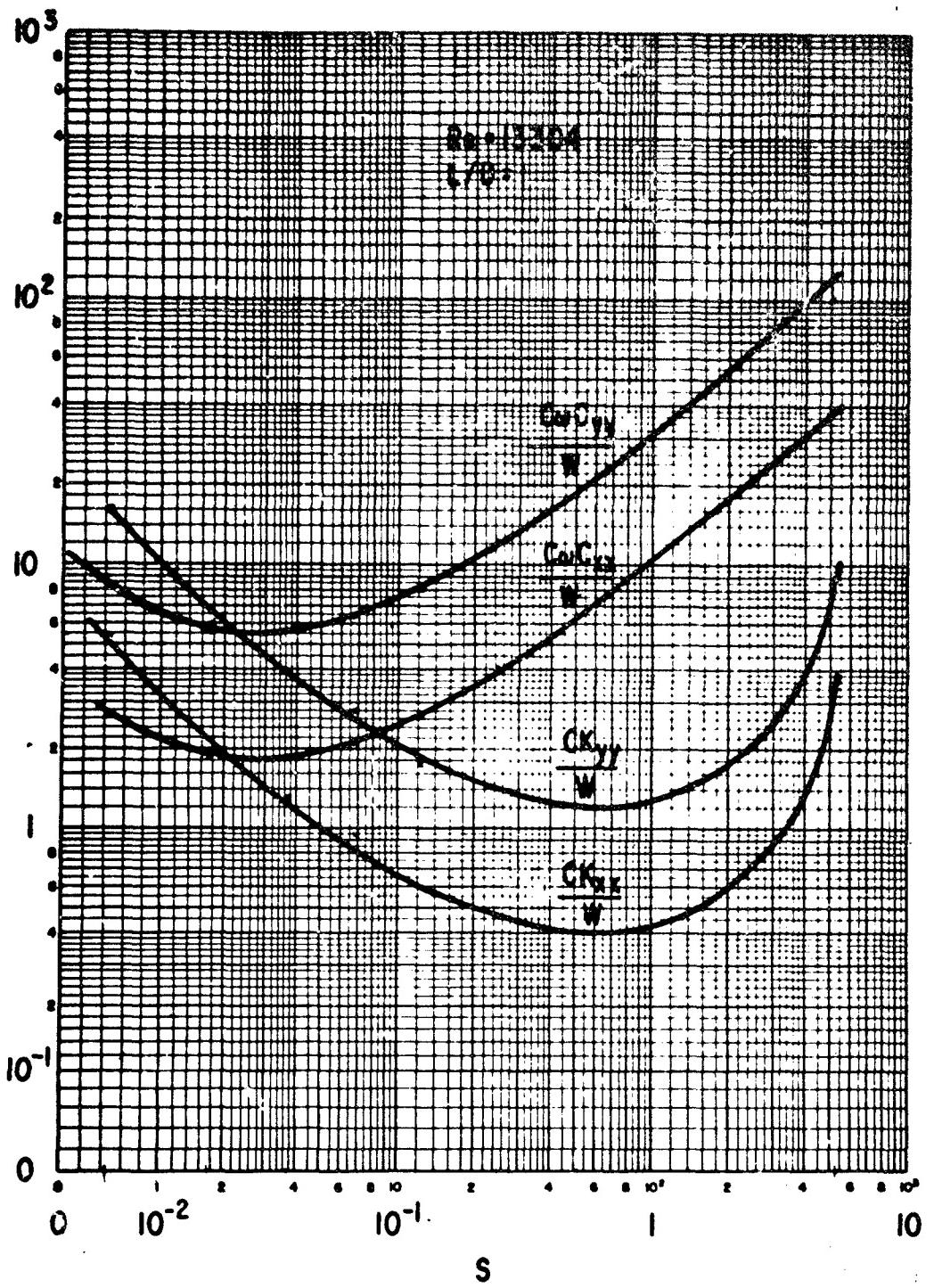


Figure B-93 The 3 Shoe Tilting Pad Bearing, Turbulent Film
 Load between Pads
 $C'/C = 1$, No Pad Inertia

c. Gas Lubricant, Hydrodynamic Bearing

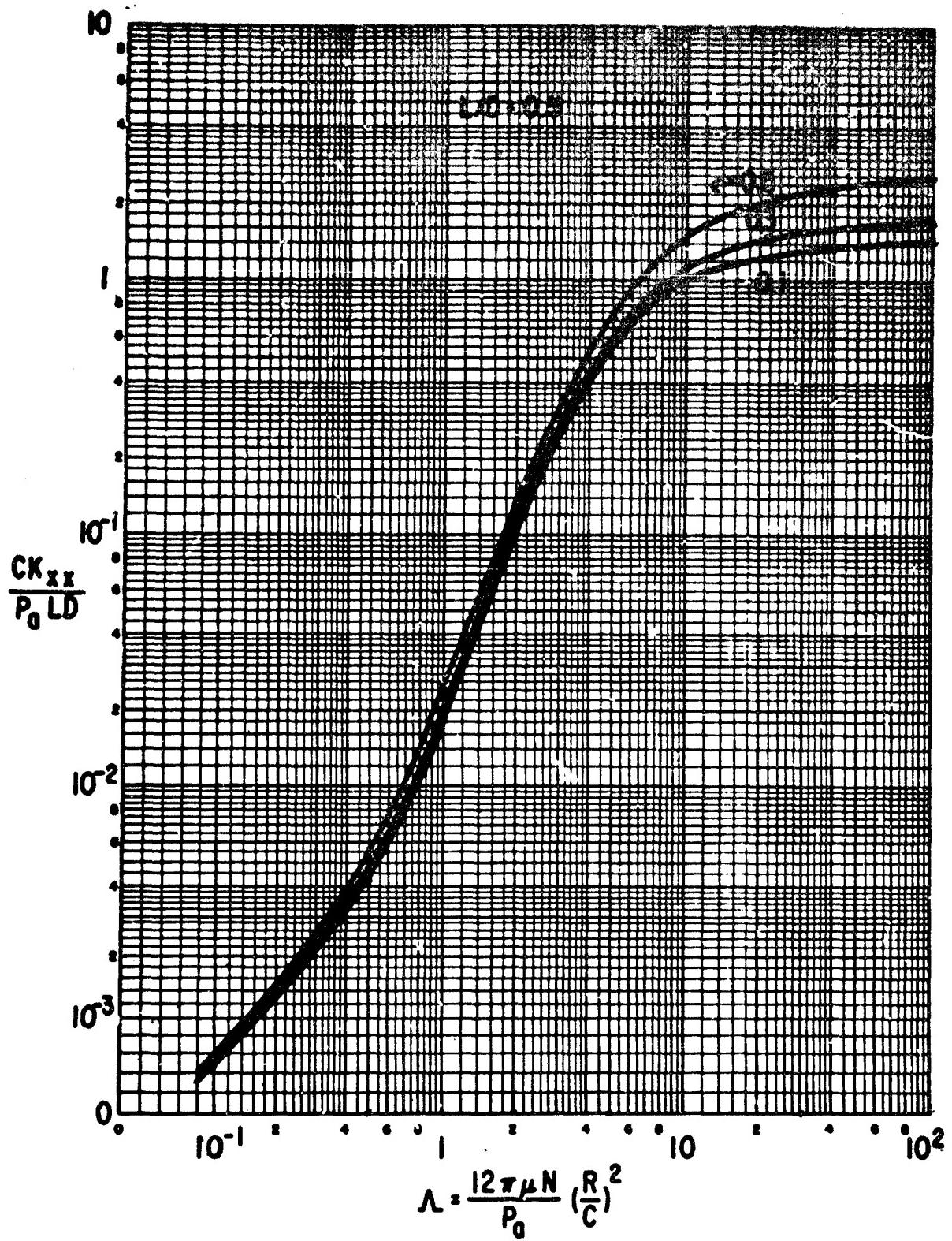


Figure B-94 The Plain Cylindrical Bearing, Gas Lubricated Dimensionless Dynamic Coefficients

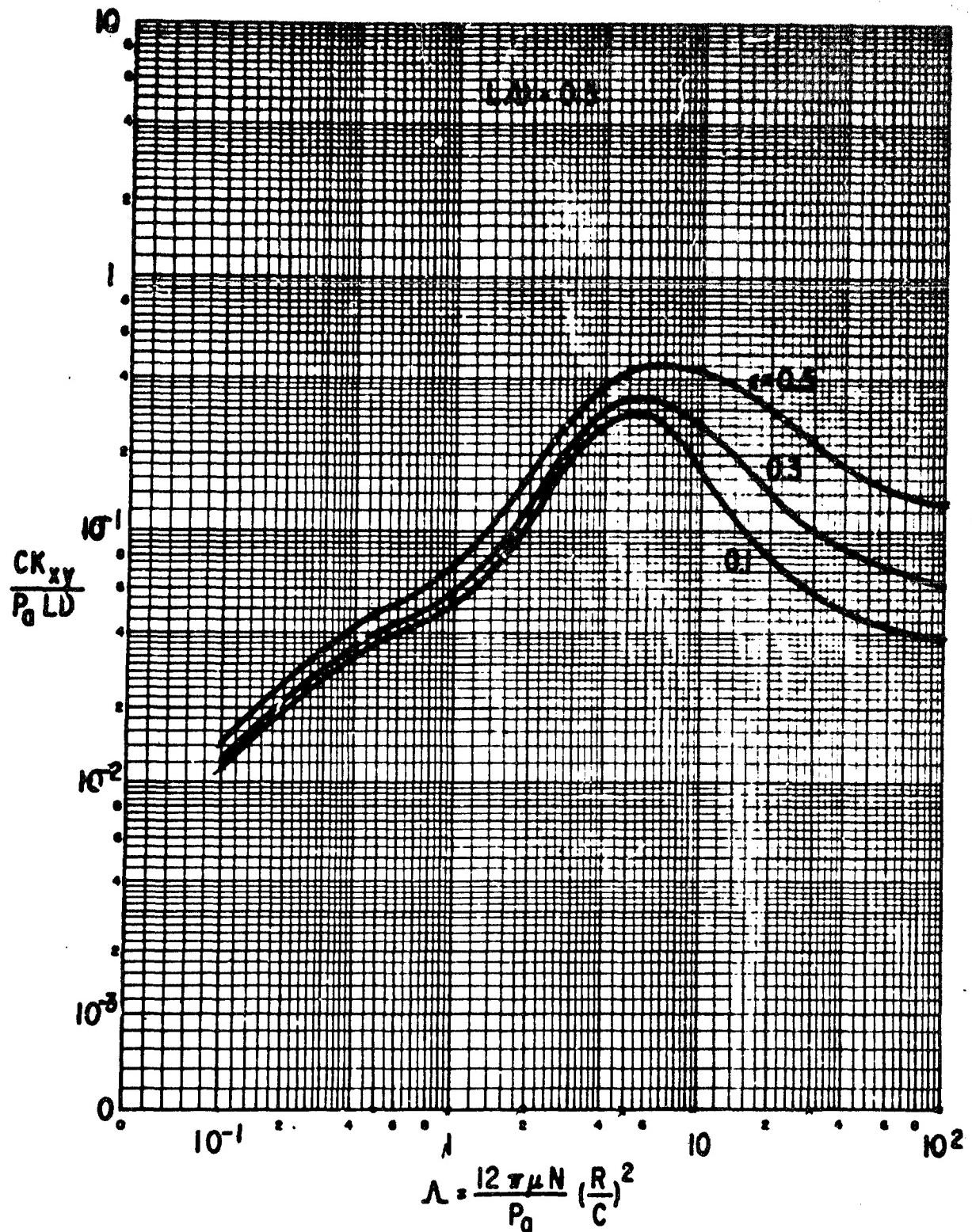


Figure B-95 The Plain Cylindrical Bearing, Gas Lubricated Dimensionless Dynamic Coefficients

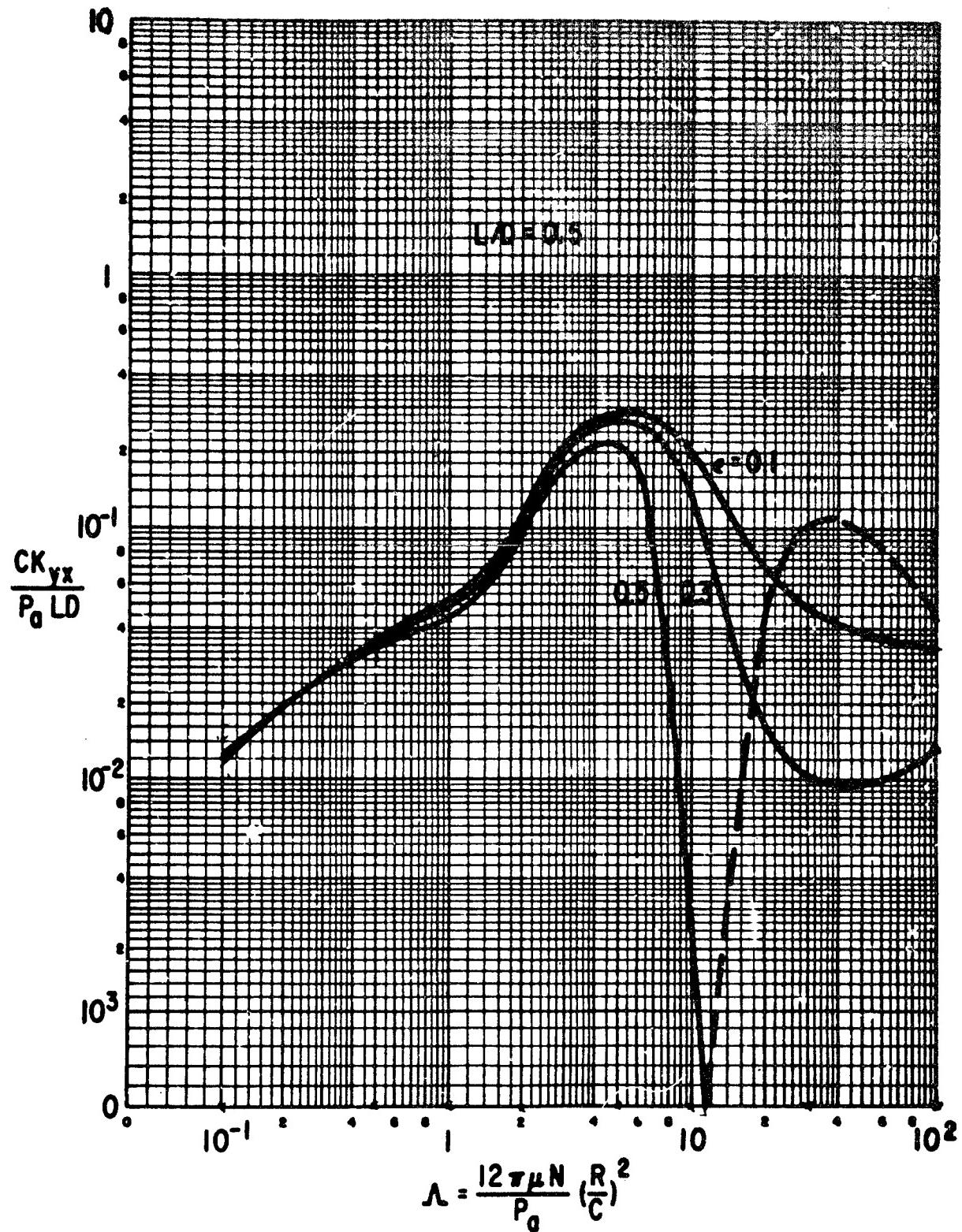


Figure B-96 The Plain Cylindrical Bearing, Gas Lubricated Dimensionless Dynamic Coefficients

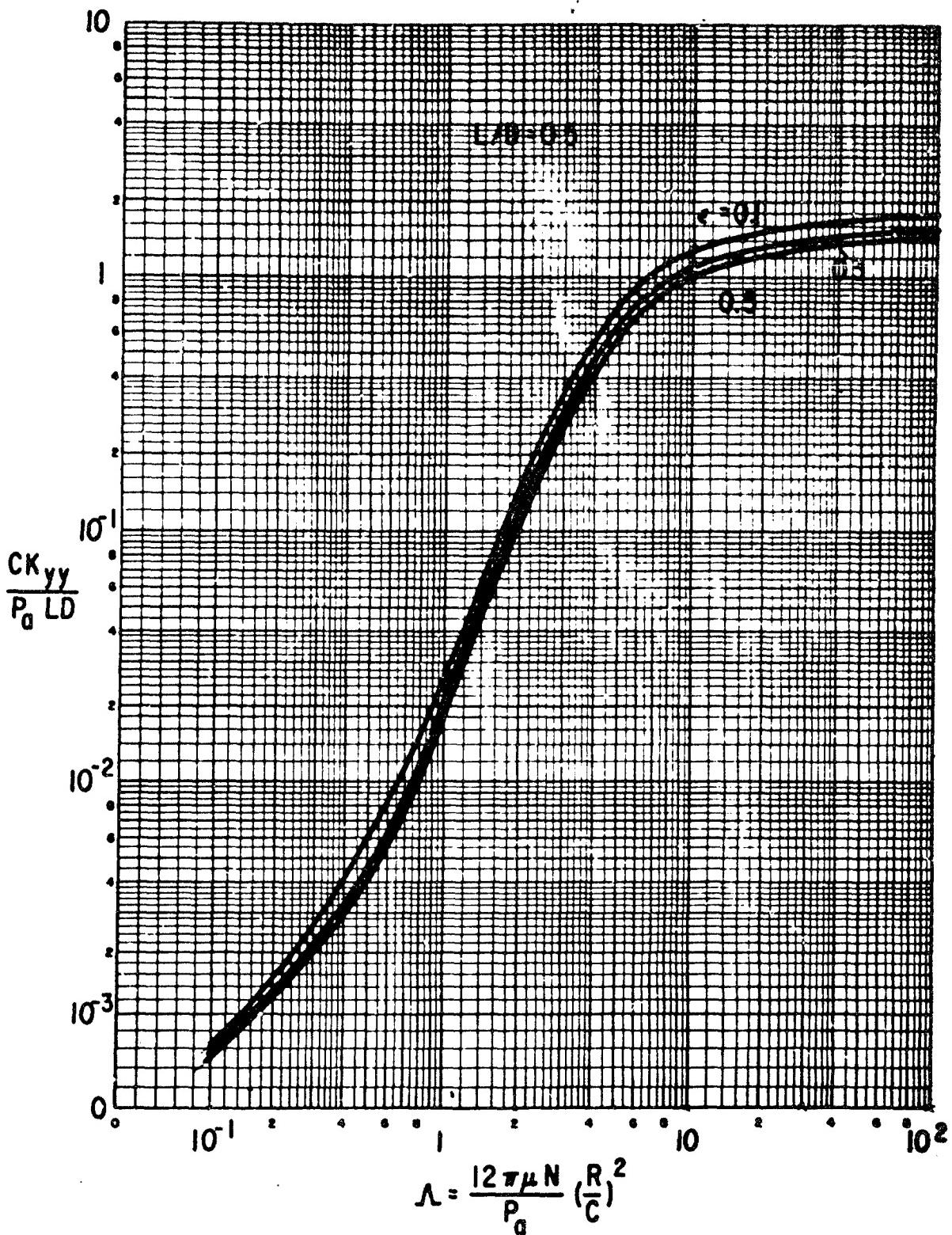


Figure B-97 The Plain Cylindrical Bearing, Gas Lubricated Dimensionless Dynamic Coefficients

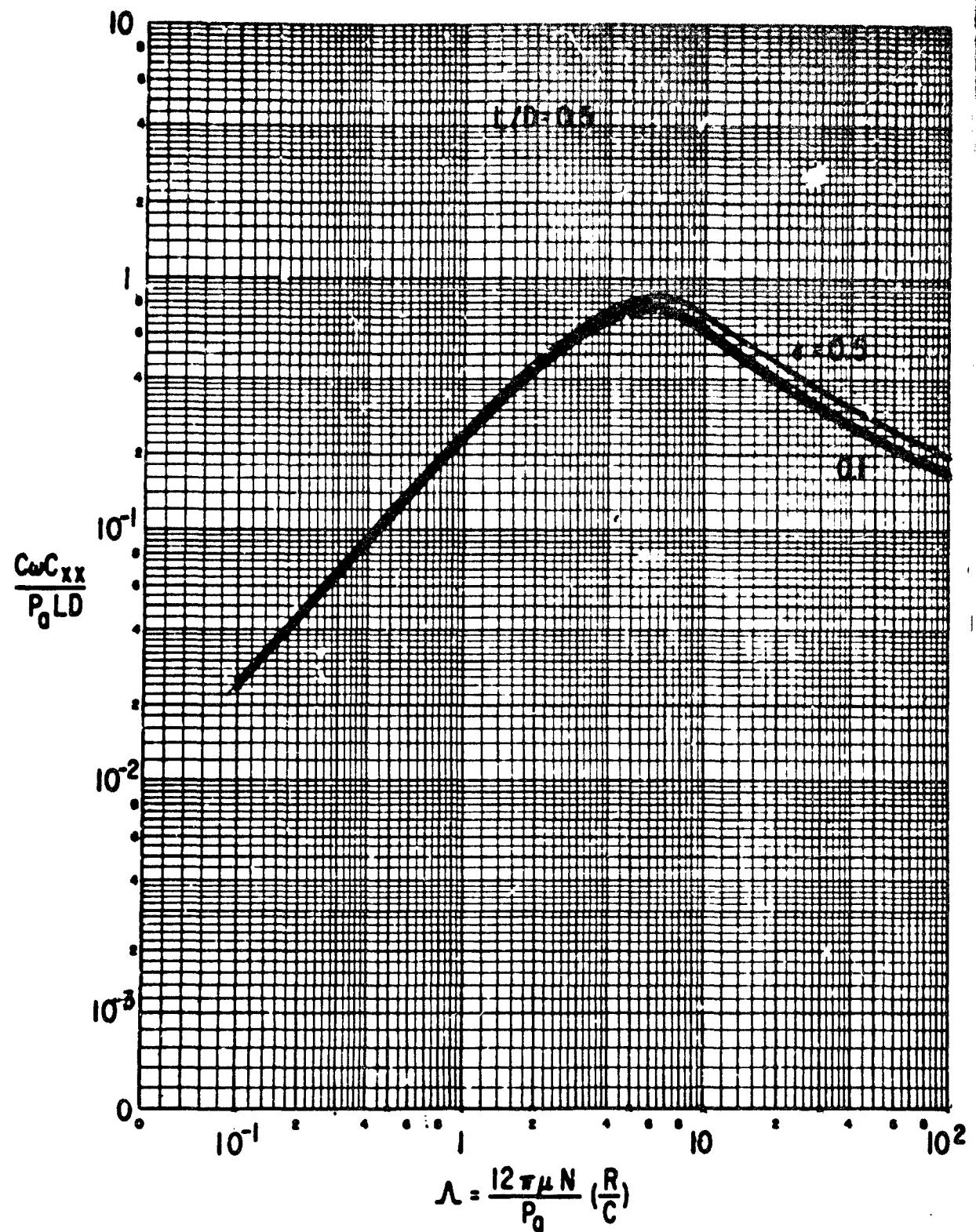


Figure B-98 The Plain Cylindrical Bearing, Gas Lubricated Dimensionless Dynamic Coefficients

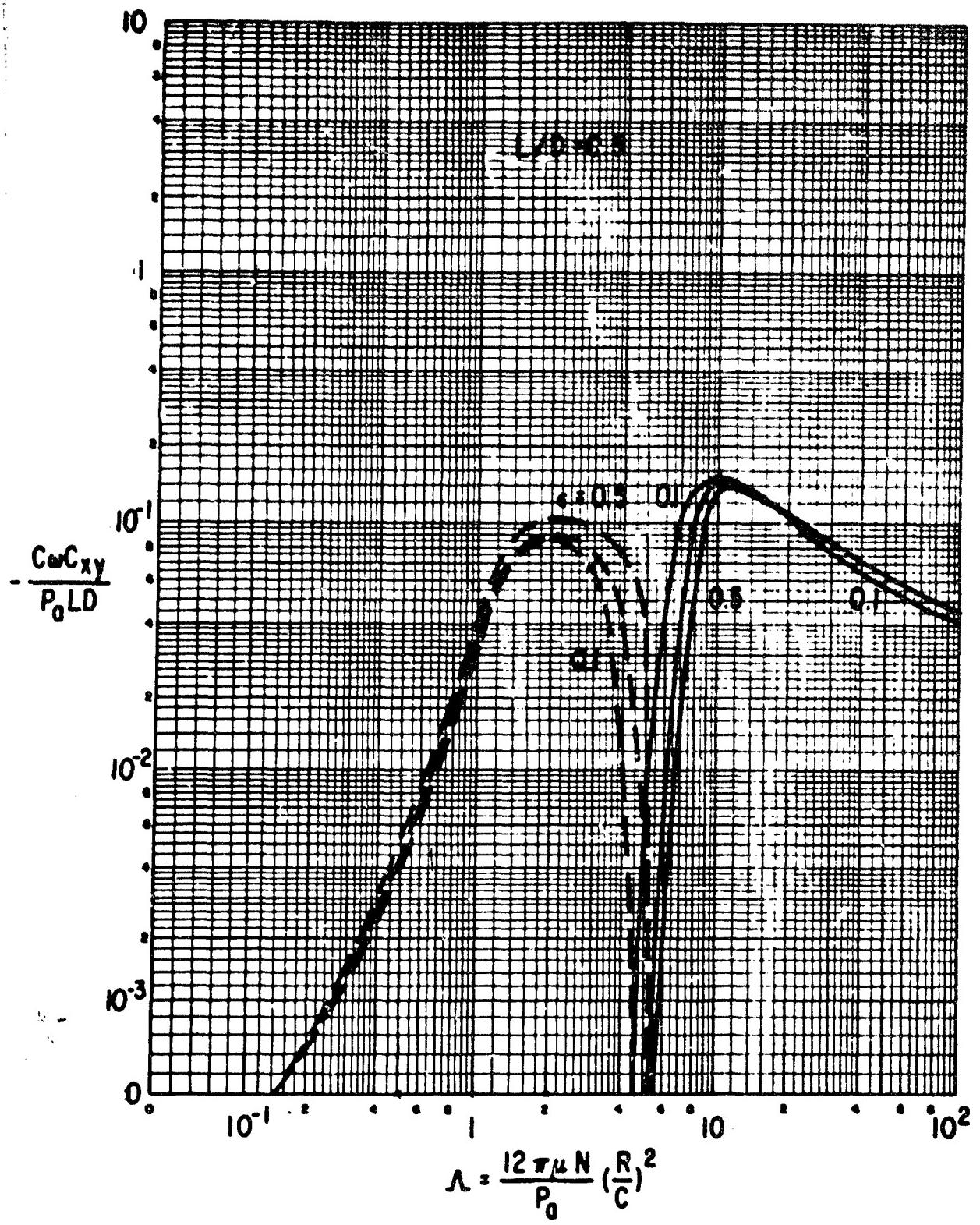


Figure B-99 The Plain Cylindrical Bearing, Gas Lubricated Dimensionless Dynamic Coefficients

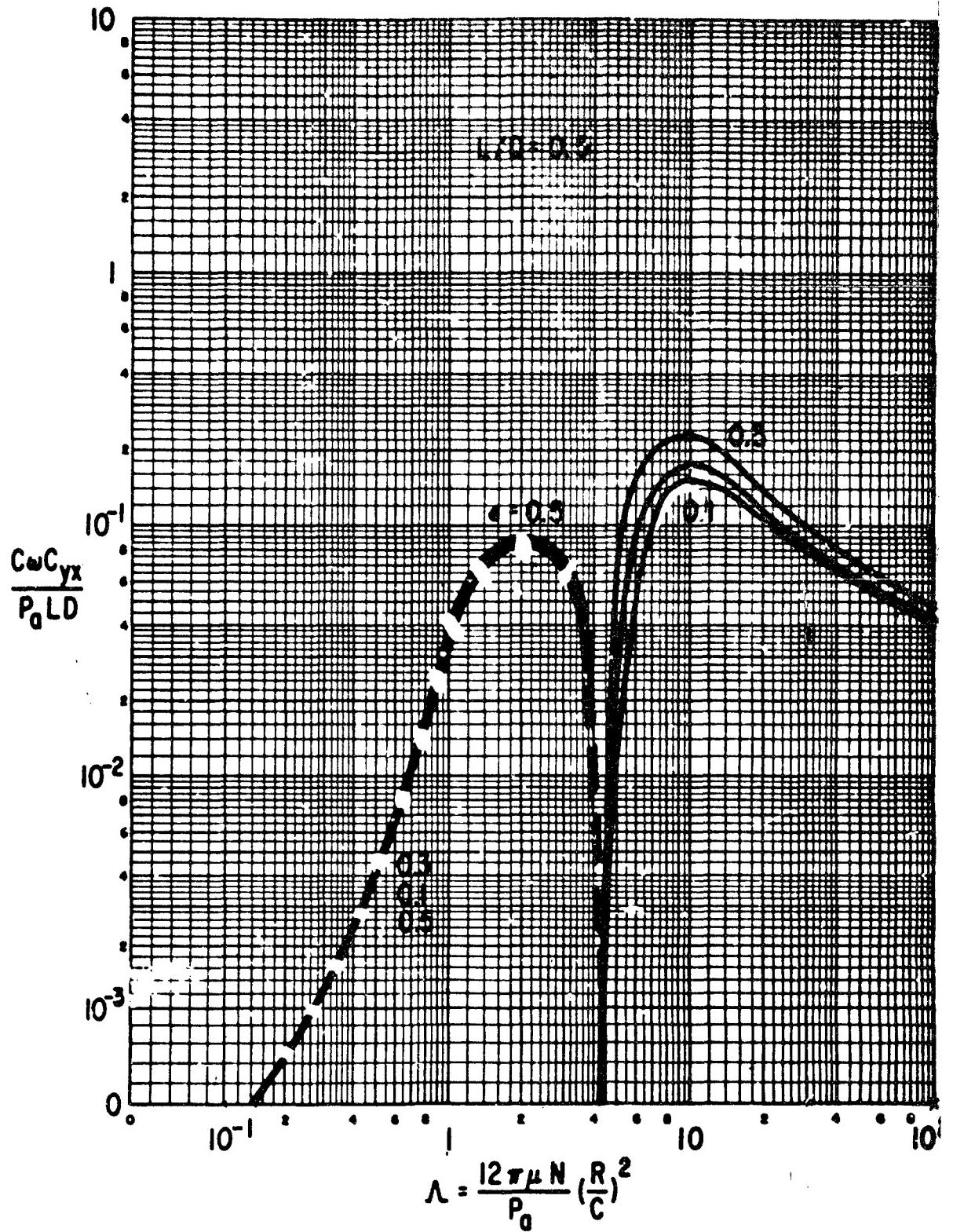


Figure B-100 The Plain Cylindrical Bearing, Gas Lubricated Dimensionless Dynamic Coefficients

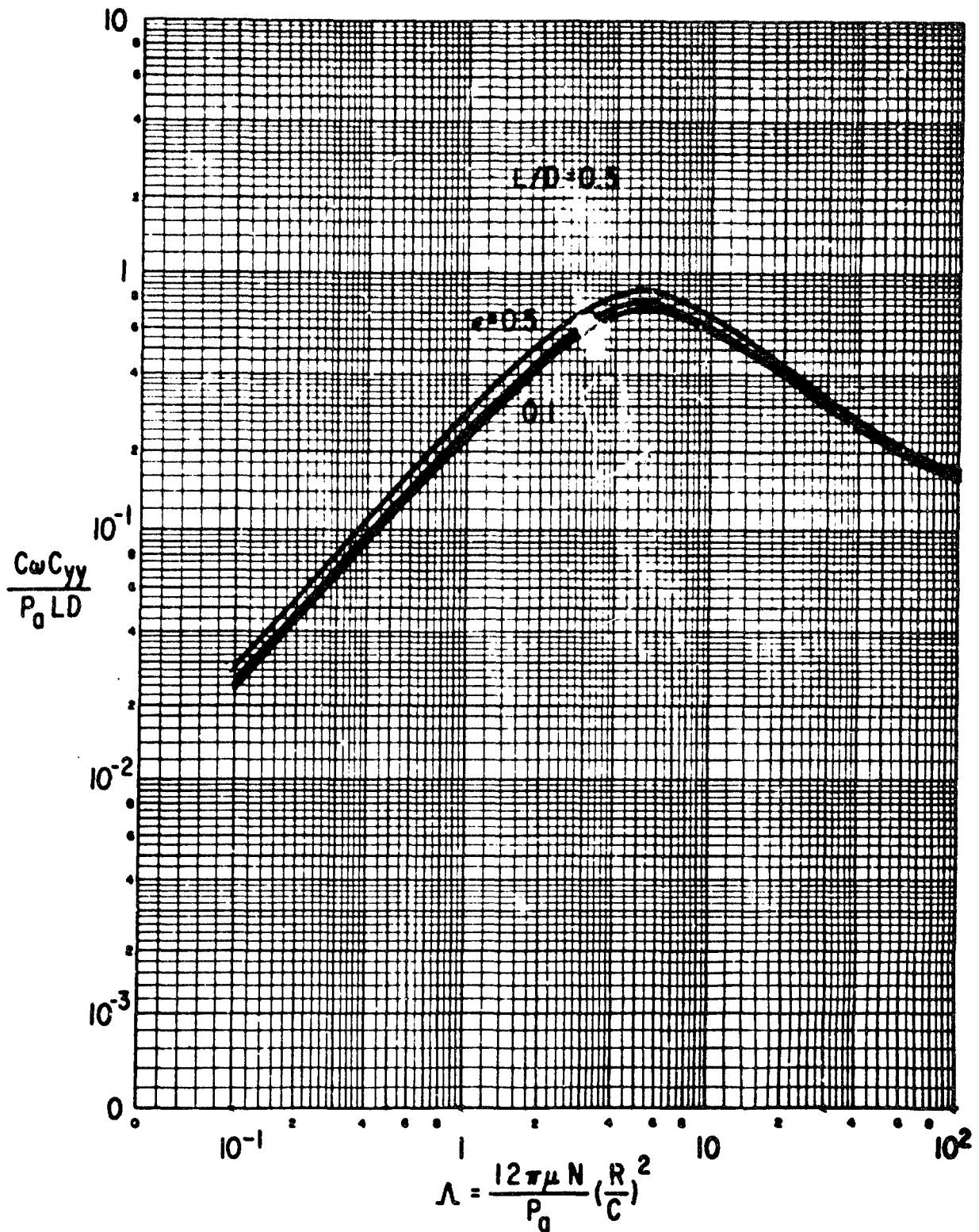


Figure E-101 The Plain Cylindrical Bearing, Gas Lubricated Dimensionless Dynamic Coefficients

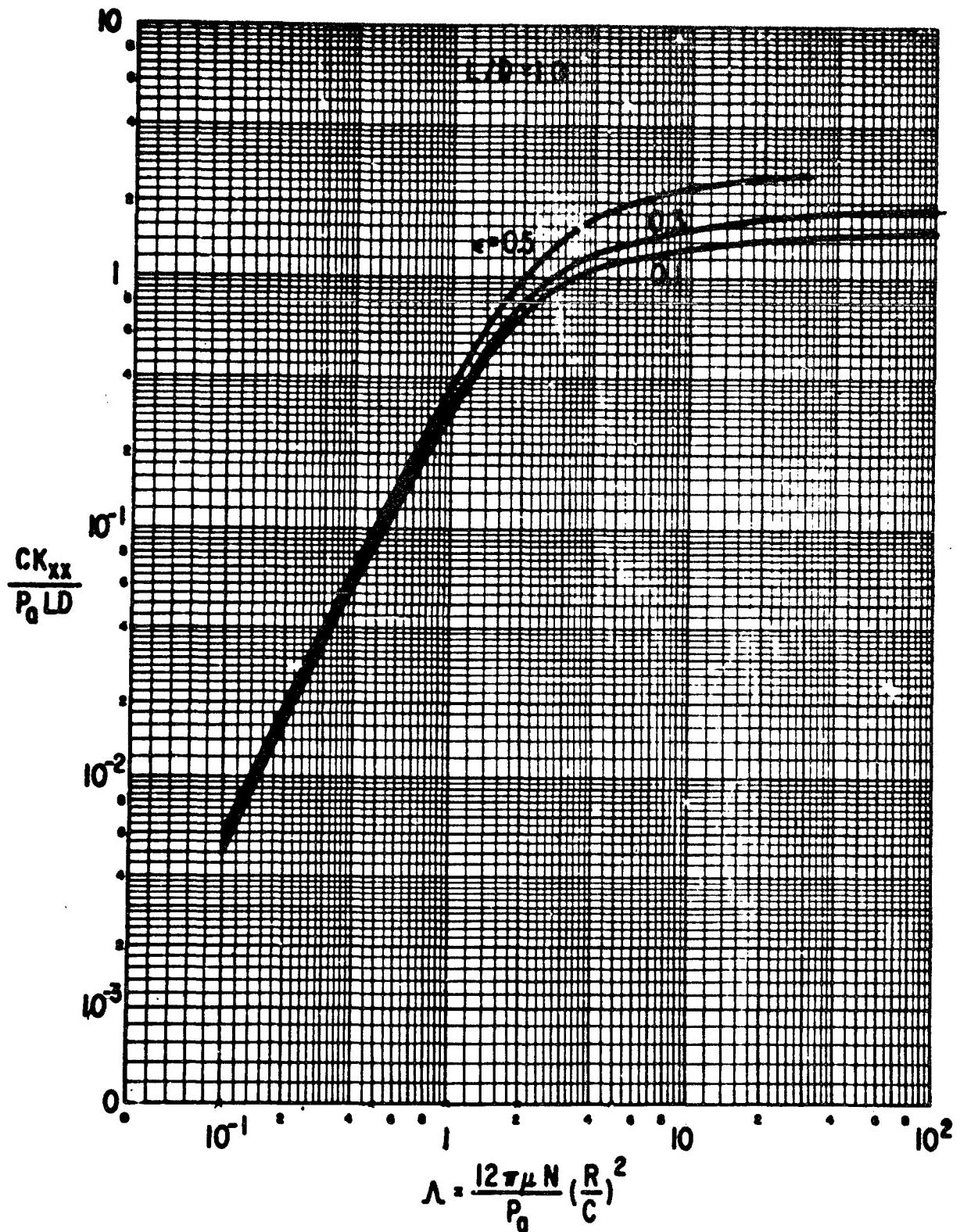


Figure B-102 The Plain Cylindrical Bearing, Gas Lubricated Dimensionless Dynamic Coefficients

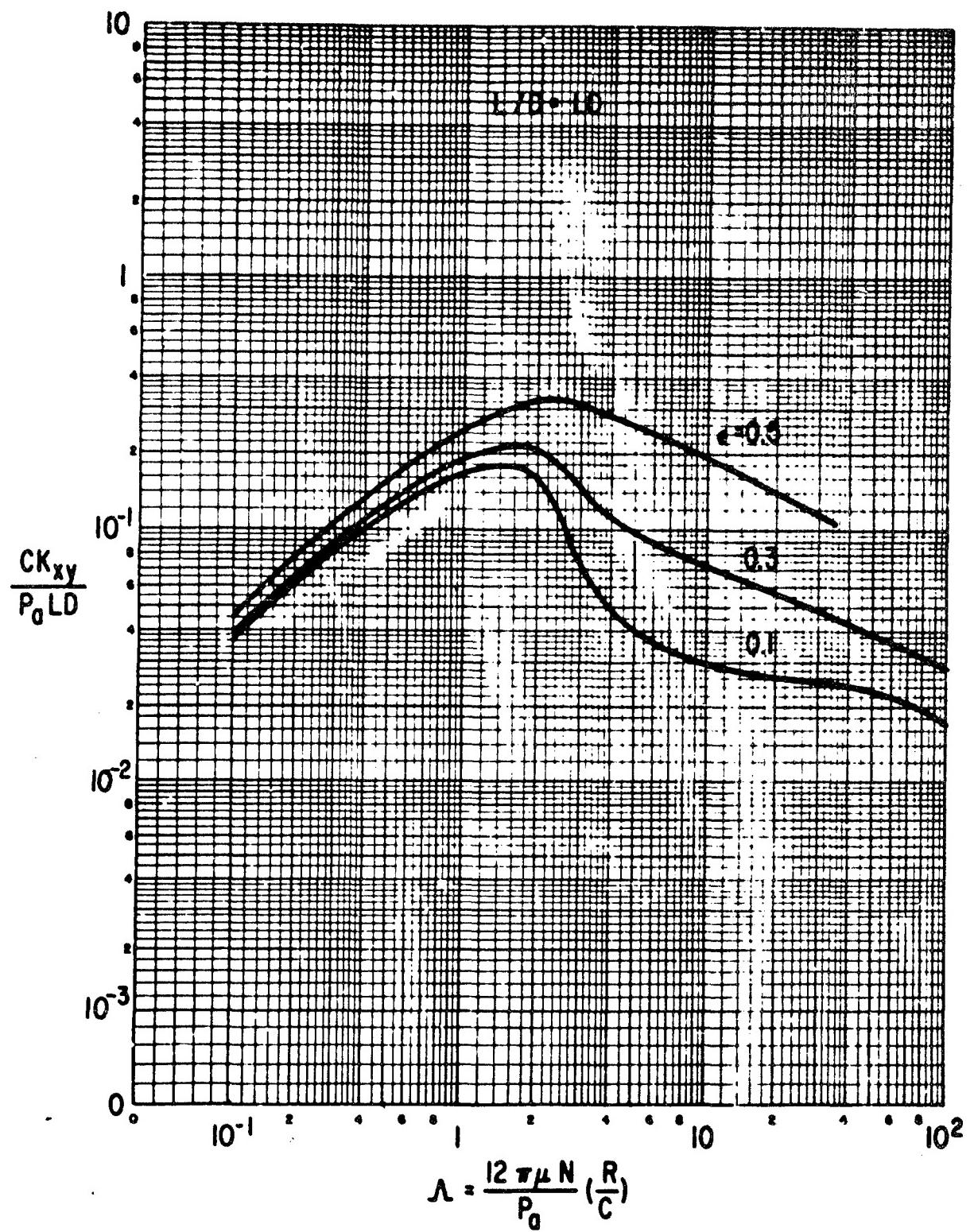


Figure B-103 The Plain Cylindrical Bearing, Gas Lubricated
Dimensionless Dynamic Coefficients

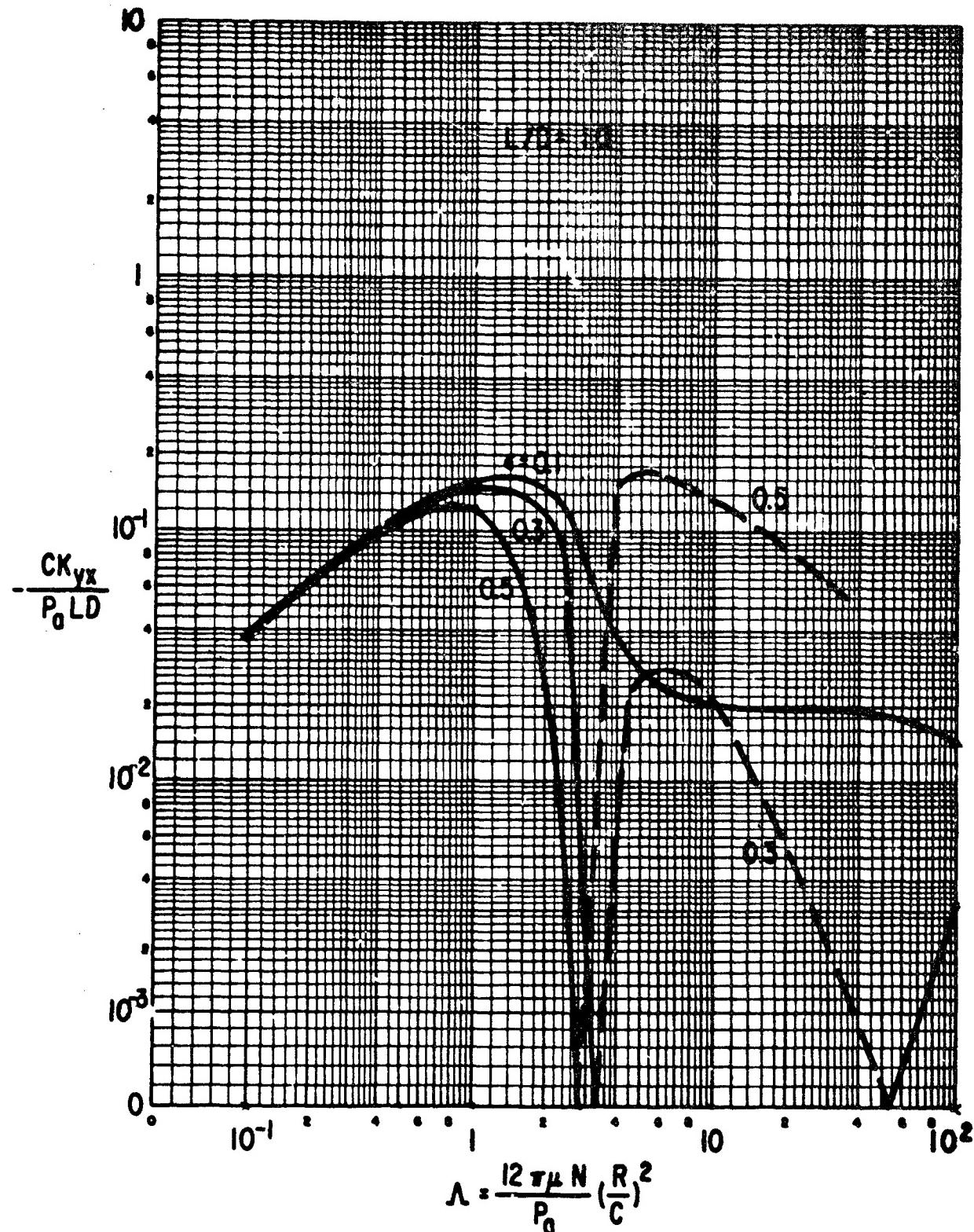


Figure B-104 The Plain Cylindrical Bearing, Gas Lubricated Dimensionless Dynamic Coefficients

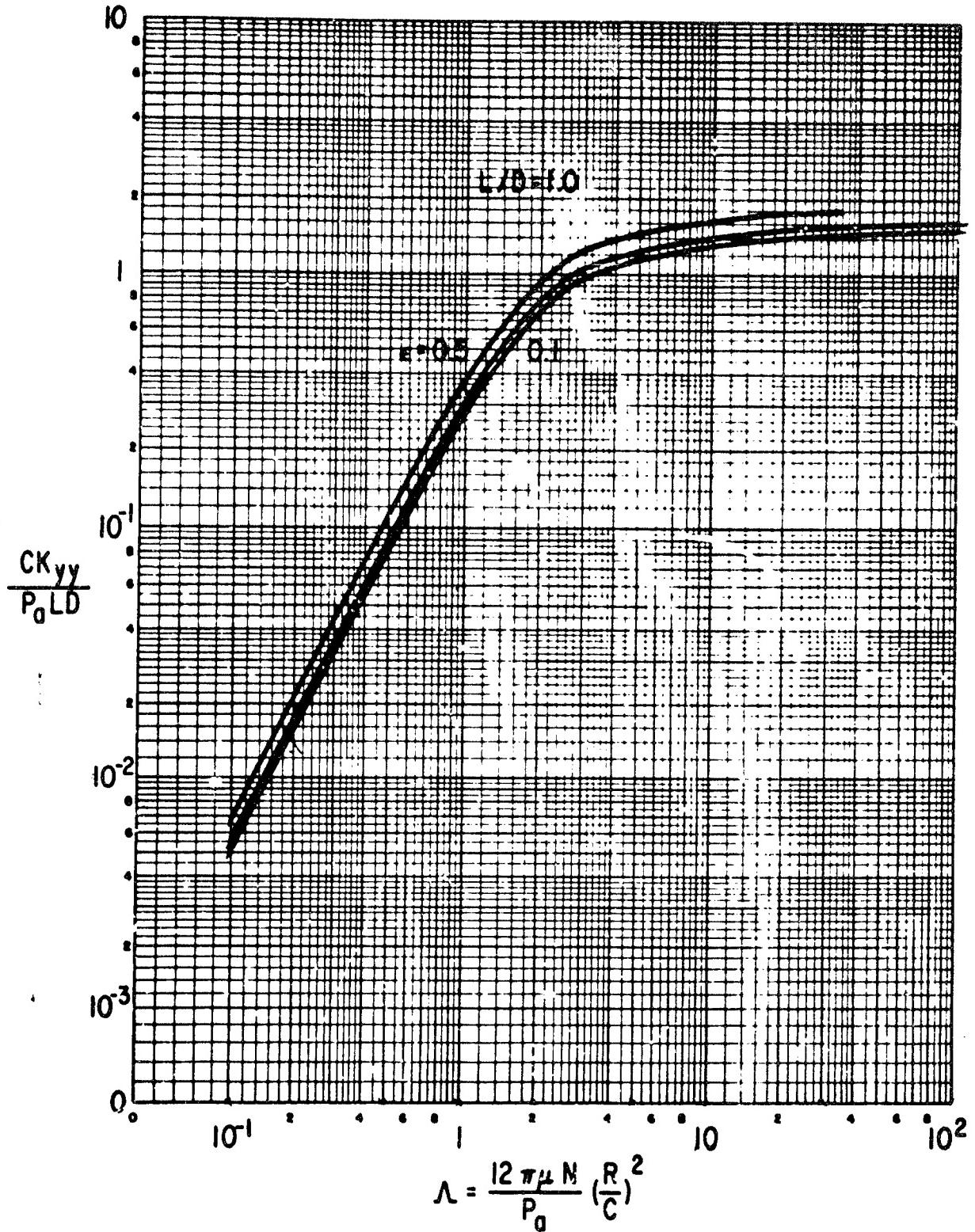


Figure B-105 The Plain Cylindrical Bearing, Gas Lubricated Dimensionless Dynamic Coefficients

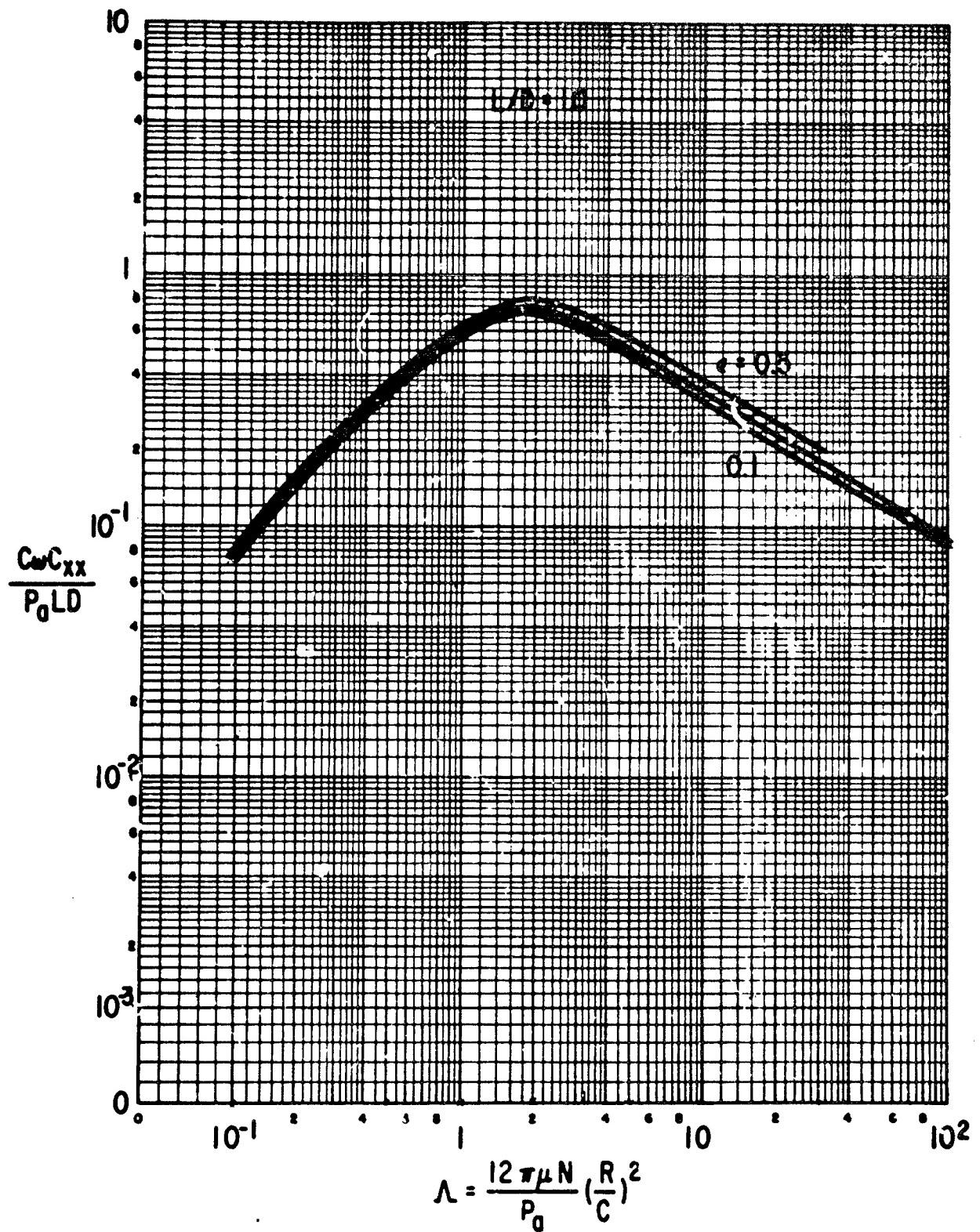


Figure B-106 The Plain Cylindrical Bearing, Gas Lubricated Dimensionless Dynamic Coefficients

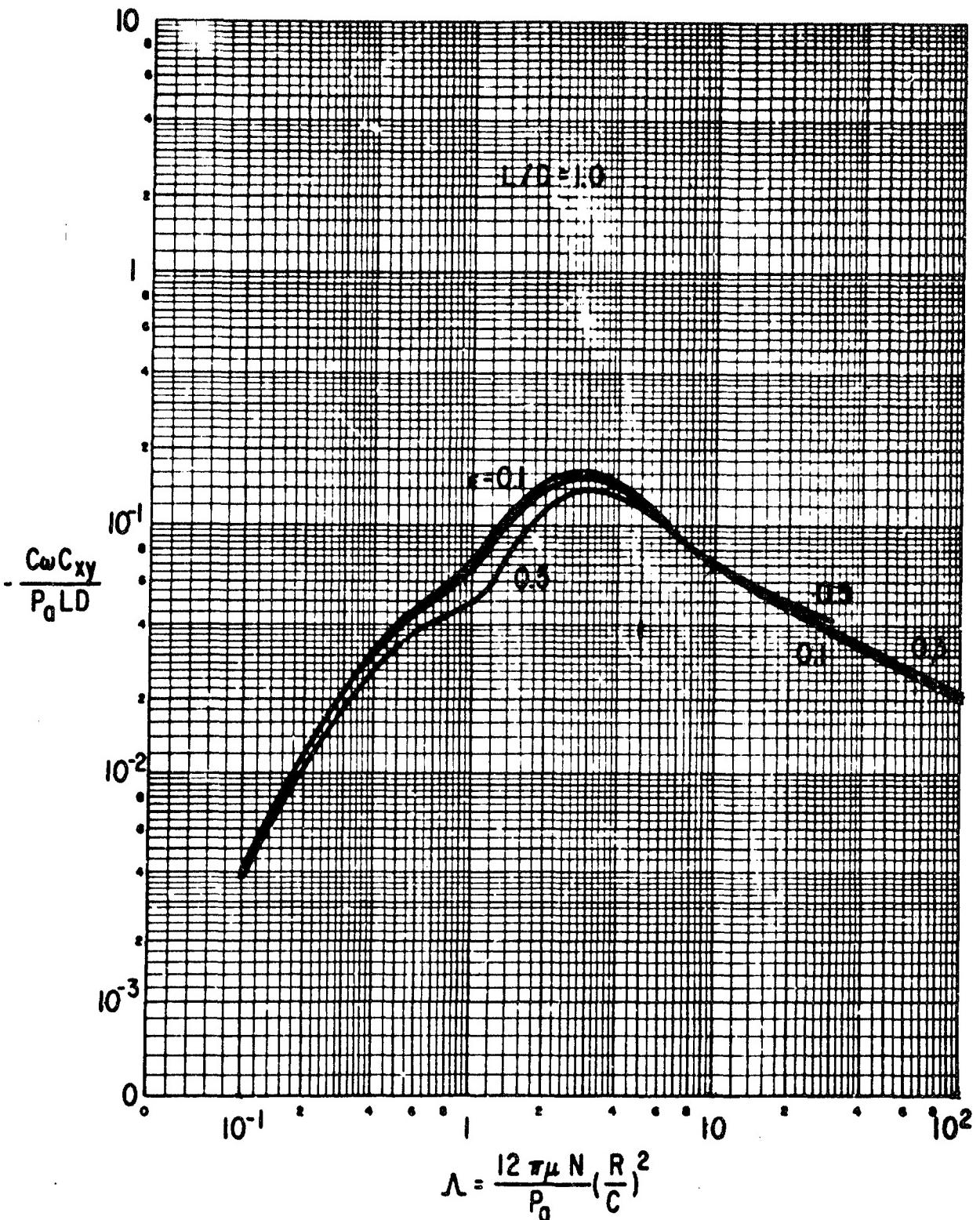


Figure B-107 The Plain Cylindrical Bearing, Gas Lubricated Dimensionless Dynamic Coefficients

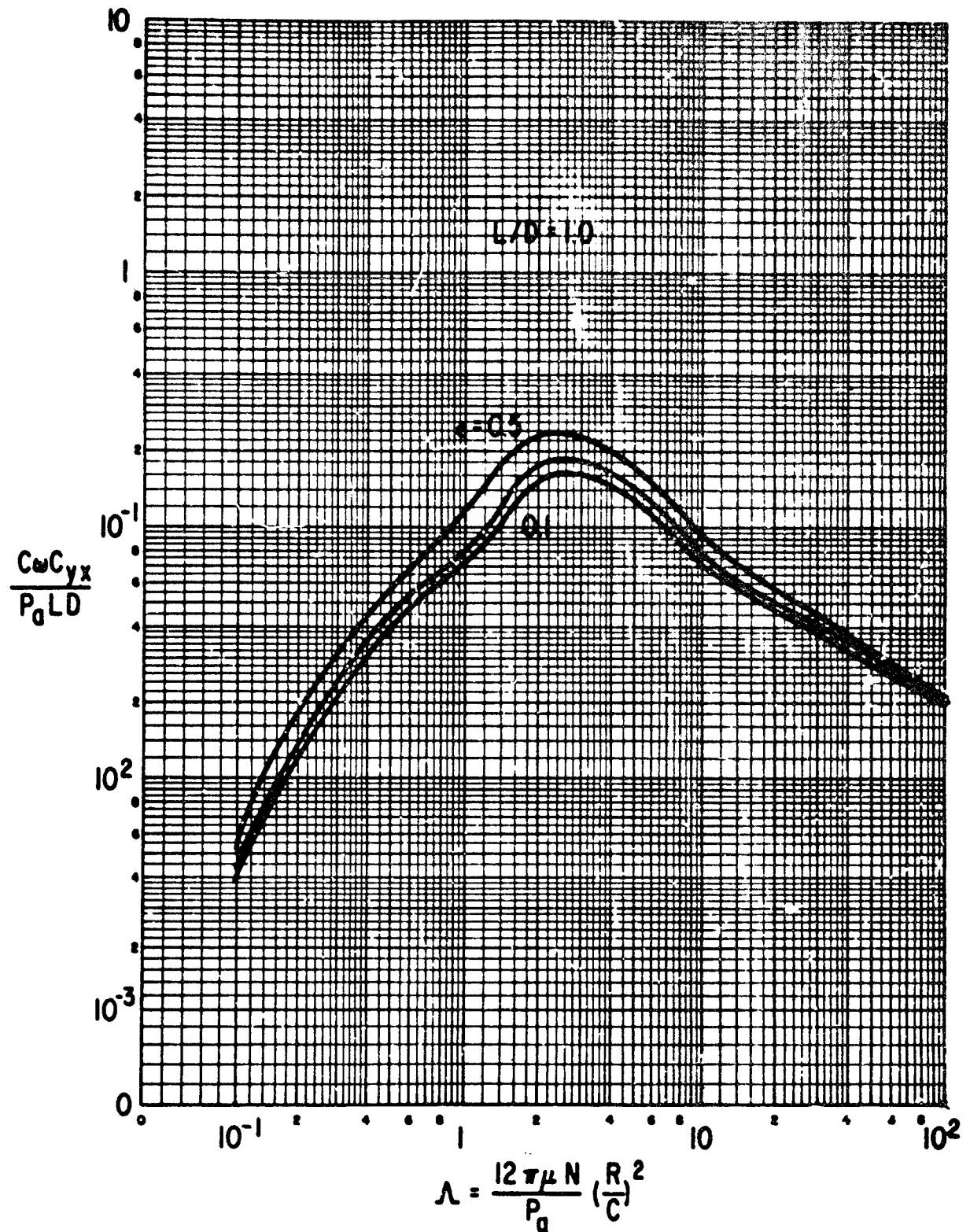


Figure B-108 The Plain Cylindrical Bearing, Gas Lubricated Dimensionless Dynamic Coefficients

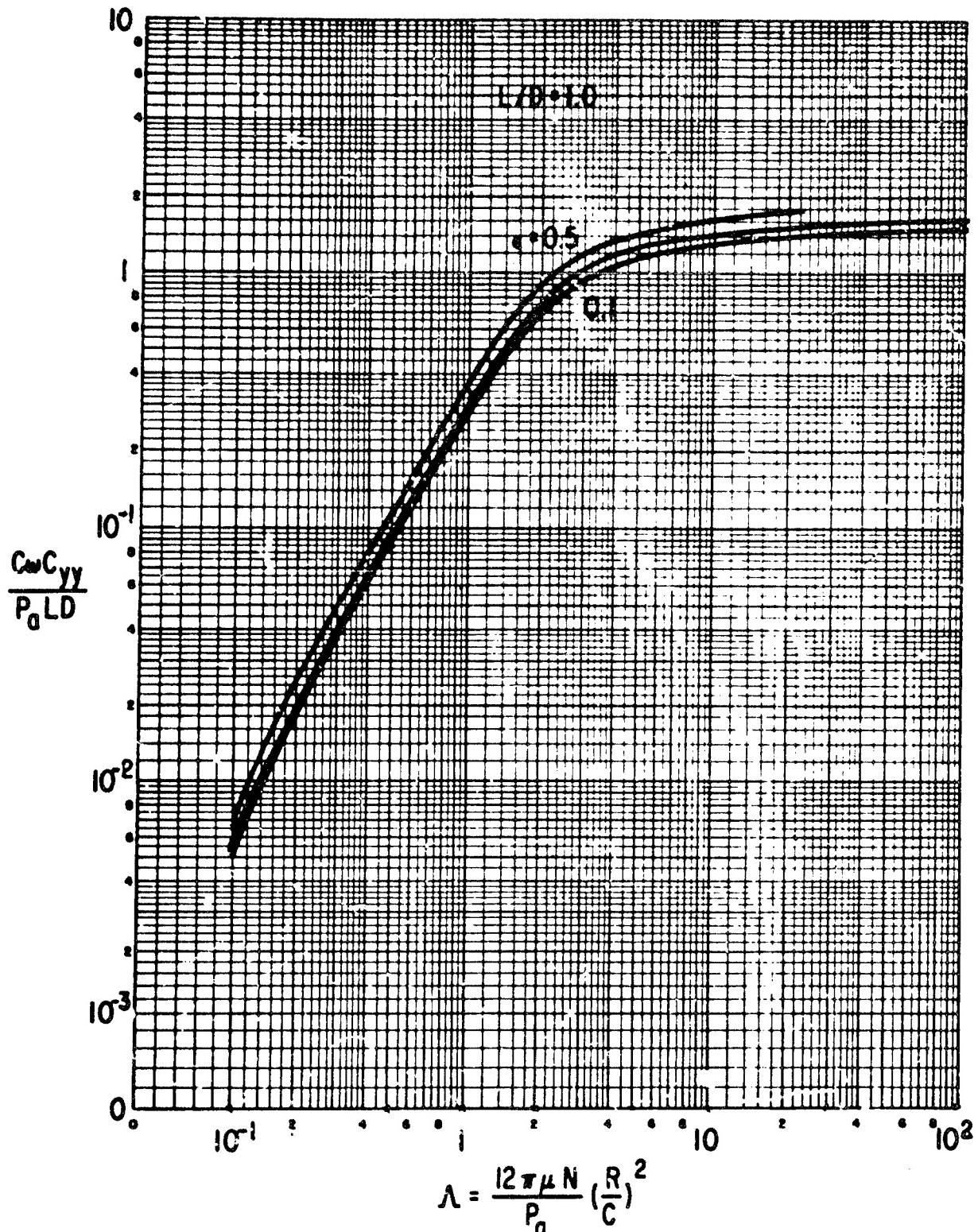


Figure B-109 The Plain Cylindrical Bearing, Gas Lubricated Dimensionless Dynamic Coefficients

d. Gas Lubricant, Hydrostatic Bearing

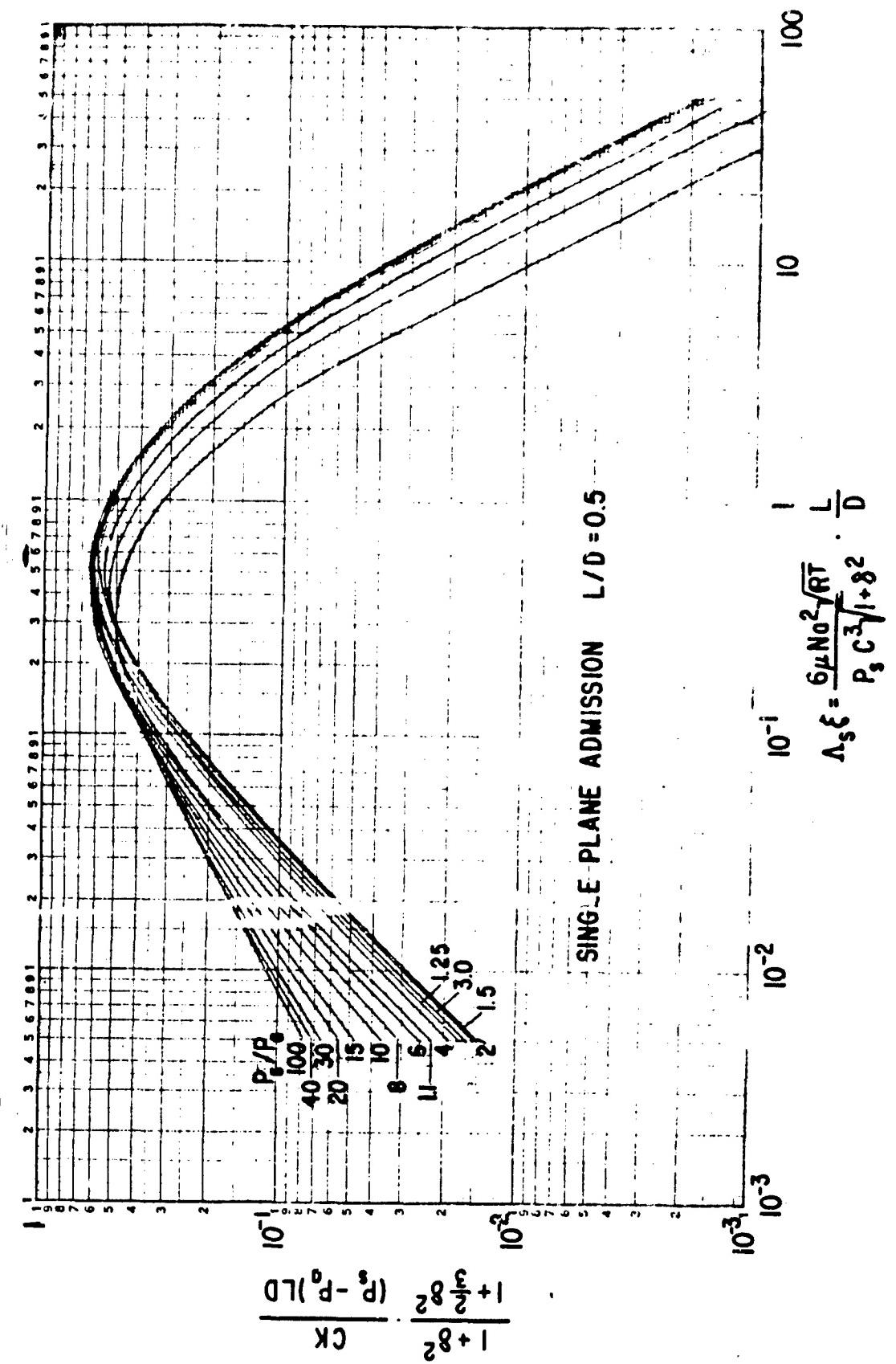
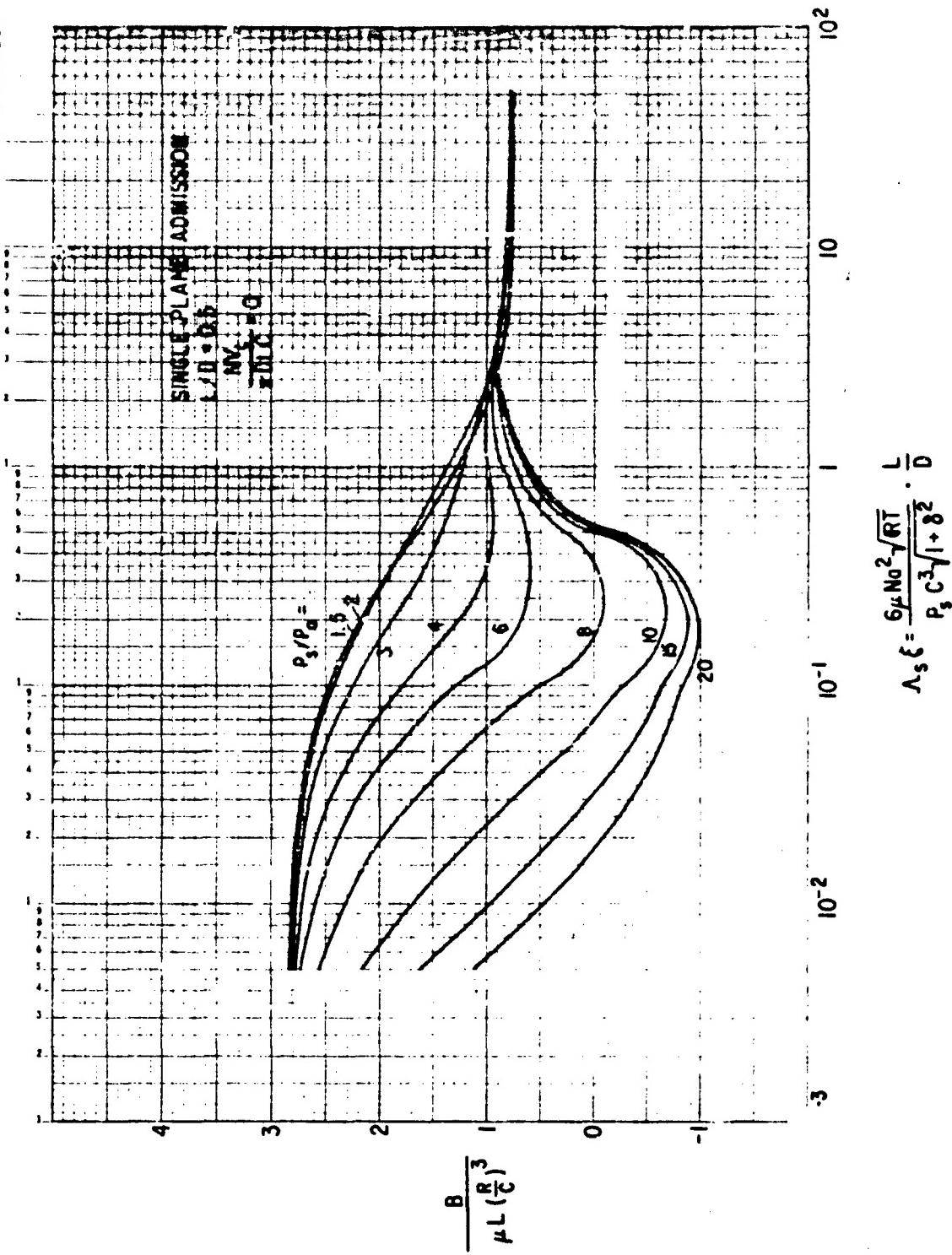


Figure B-110 The Hydrostatic Gas Bearing, $\frac{L}{D} = .5$, Single Plane Admission Dimensionless Stiffness

Figure 8-111. D- hydrostatic Gas Bearing L - S. Single Plane Admission



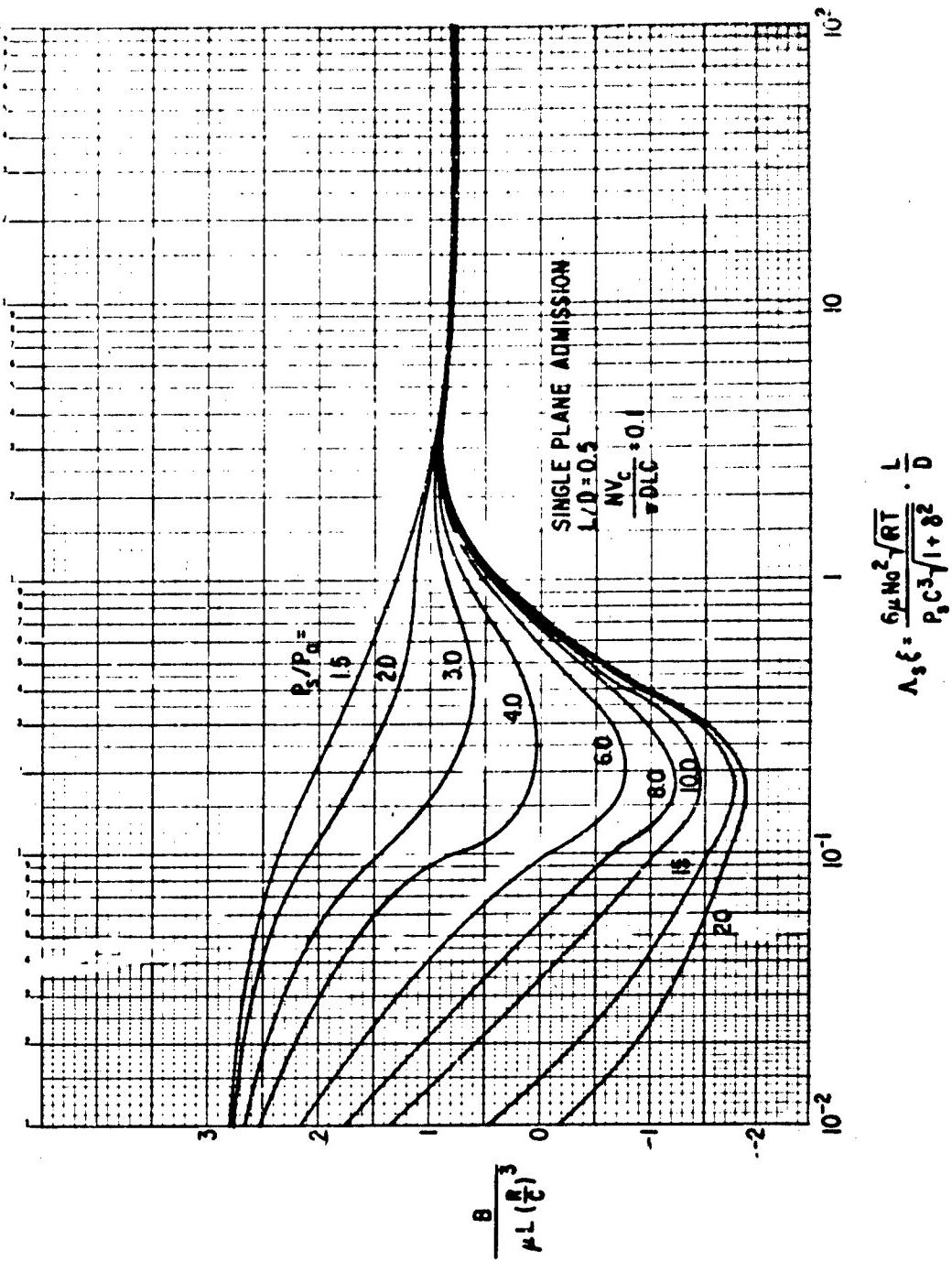
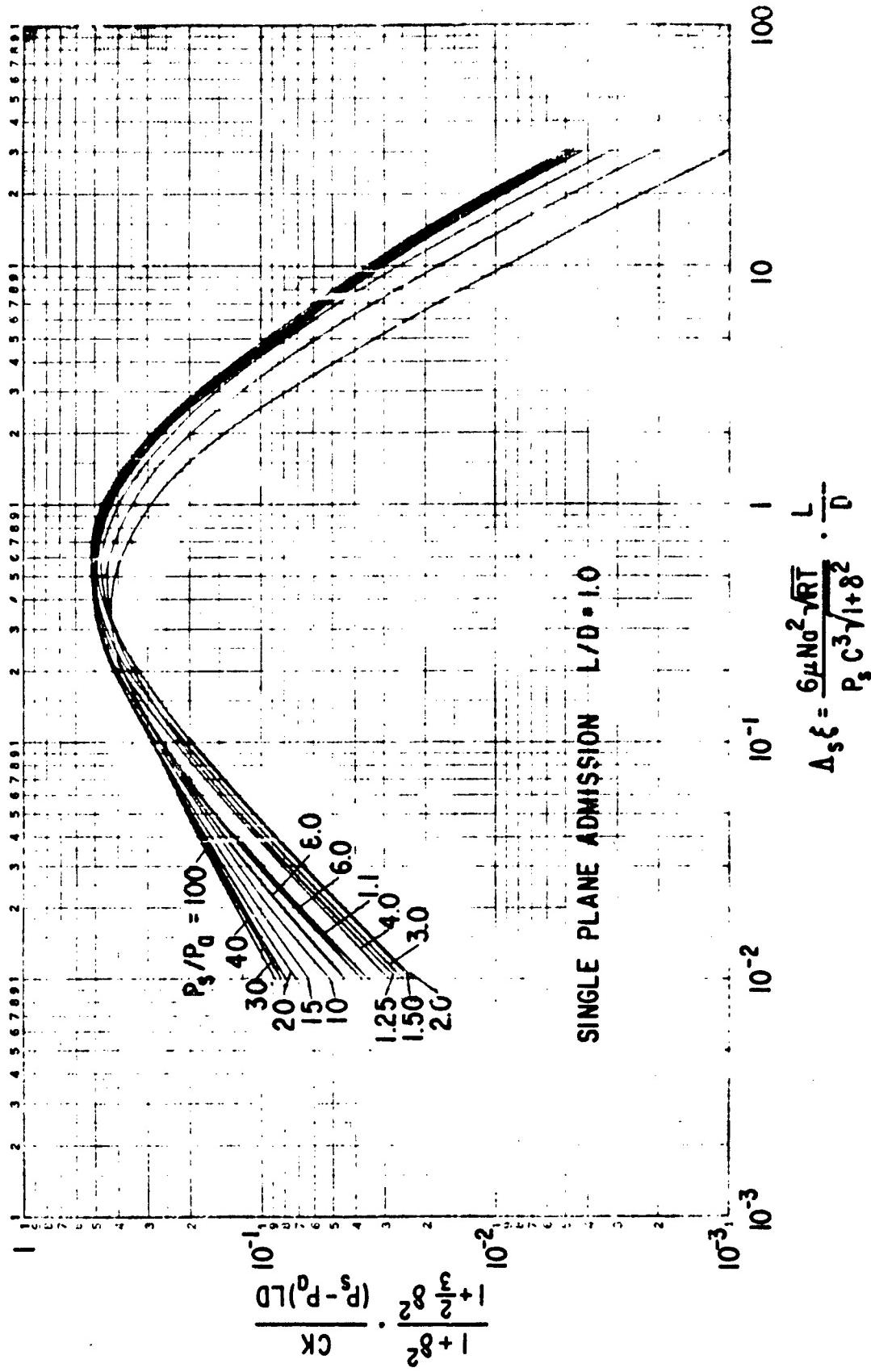


Figure B-112 The Hydrostatic Gas Bearing, $\frac{B}{D} = .5$, Single Plane Admission Dimensionless Damping

Figure B-113 The Hydrostatic Gas Bearing, $\frac{L}{D} = 1$, Single Plane Admission Dimensionless Stiffness



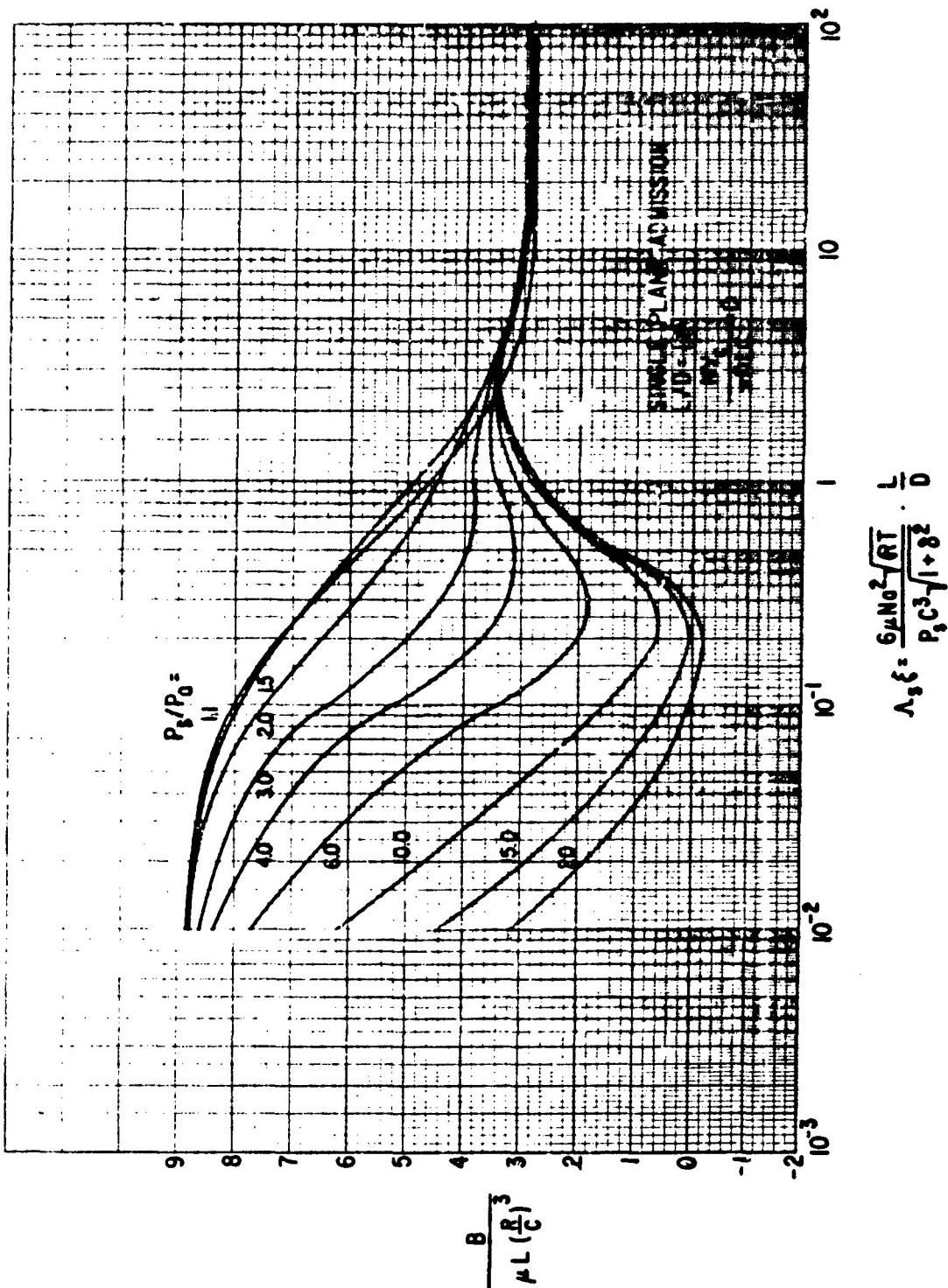
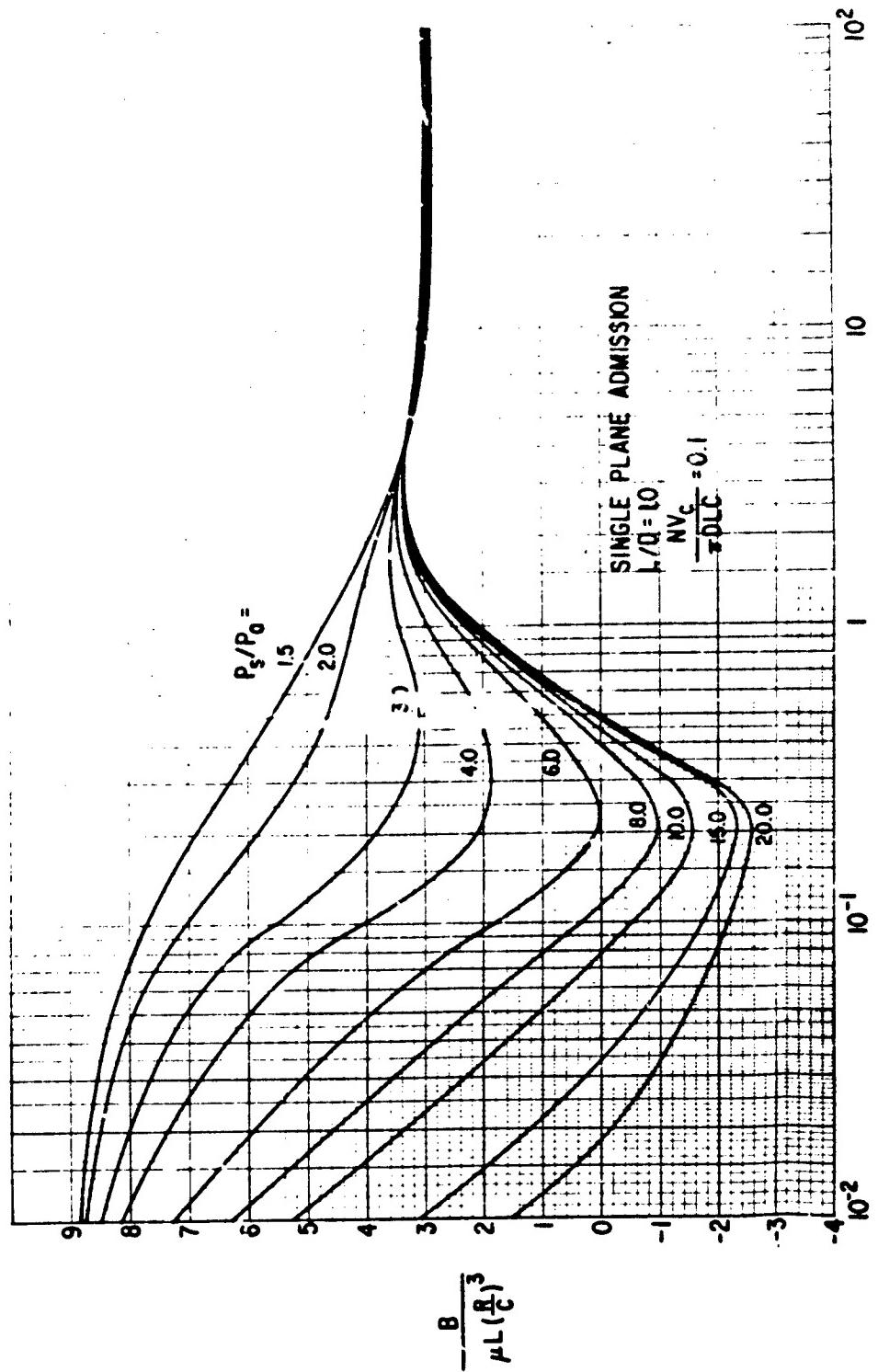


Figure B-114 The Hydrostatic Gas Bearing, $\frac{L}{D} = 1$, Single Plane Admission Dimensionless Damping

$$\Lambda_s \xi = \frac{6\mu N_0^2 \sqrt{RT}}{P_s C^3 \sqrt{1+8^2}} \cdot \frac{L}{D}$$

Figure B-115 The Hydrostatic Gas Bearing, $\frac{L}{D} = 1$, Single Plane Admission Dimensionless Damping



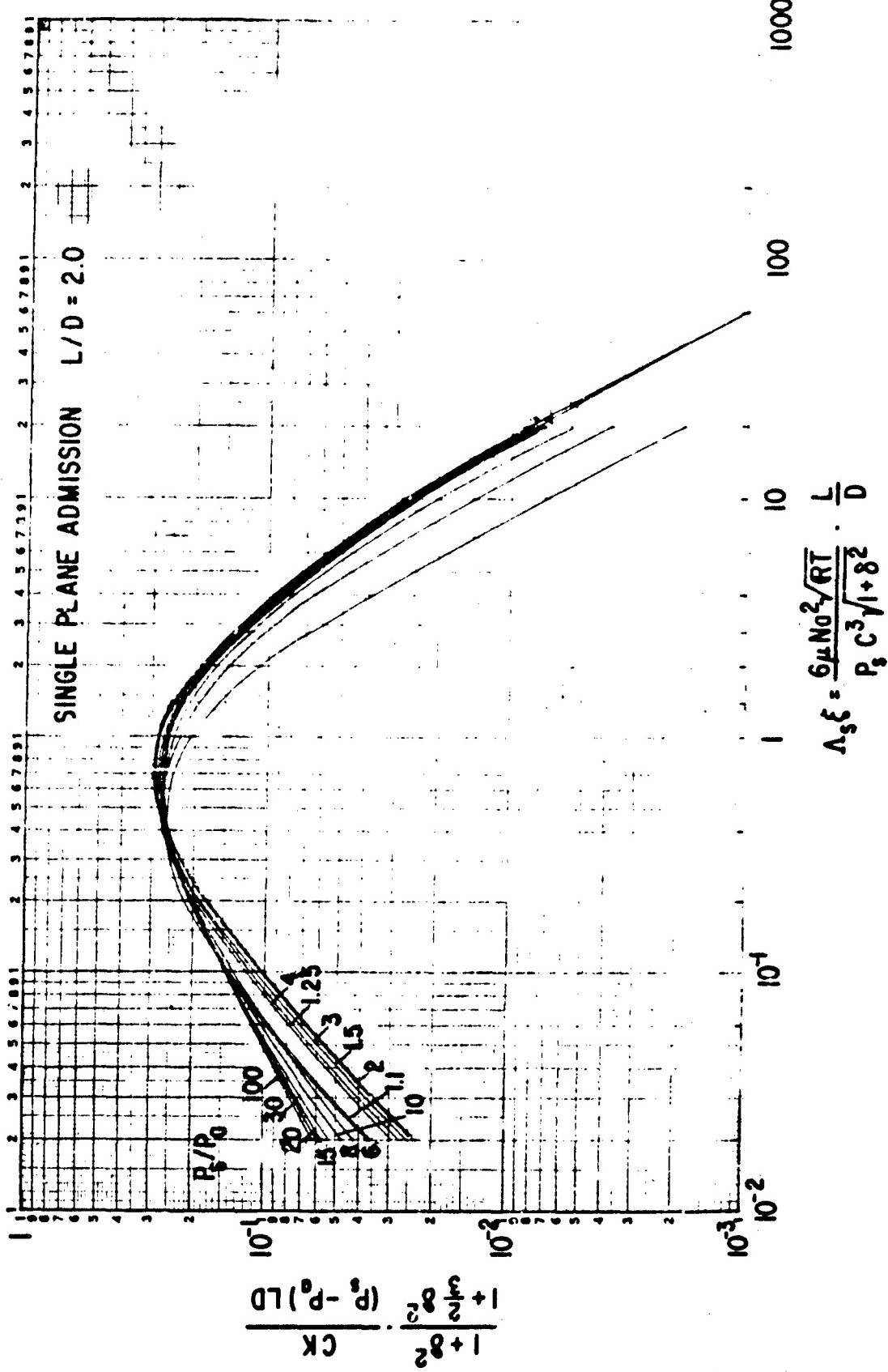


Figure B-116 The Hydrostatic Gas Bearing, $\frac{L}{D} = 2$, Single Plane Admission Dimensionless Stiffness

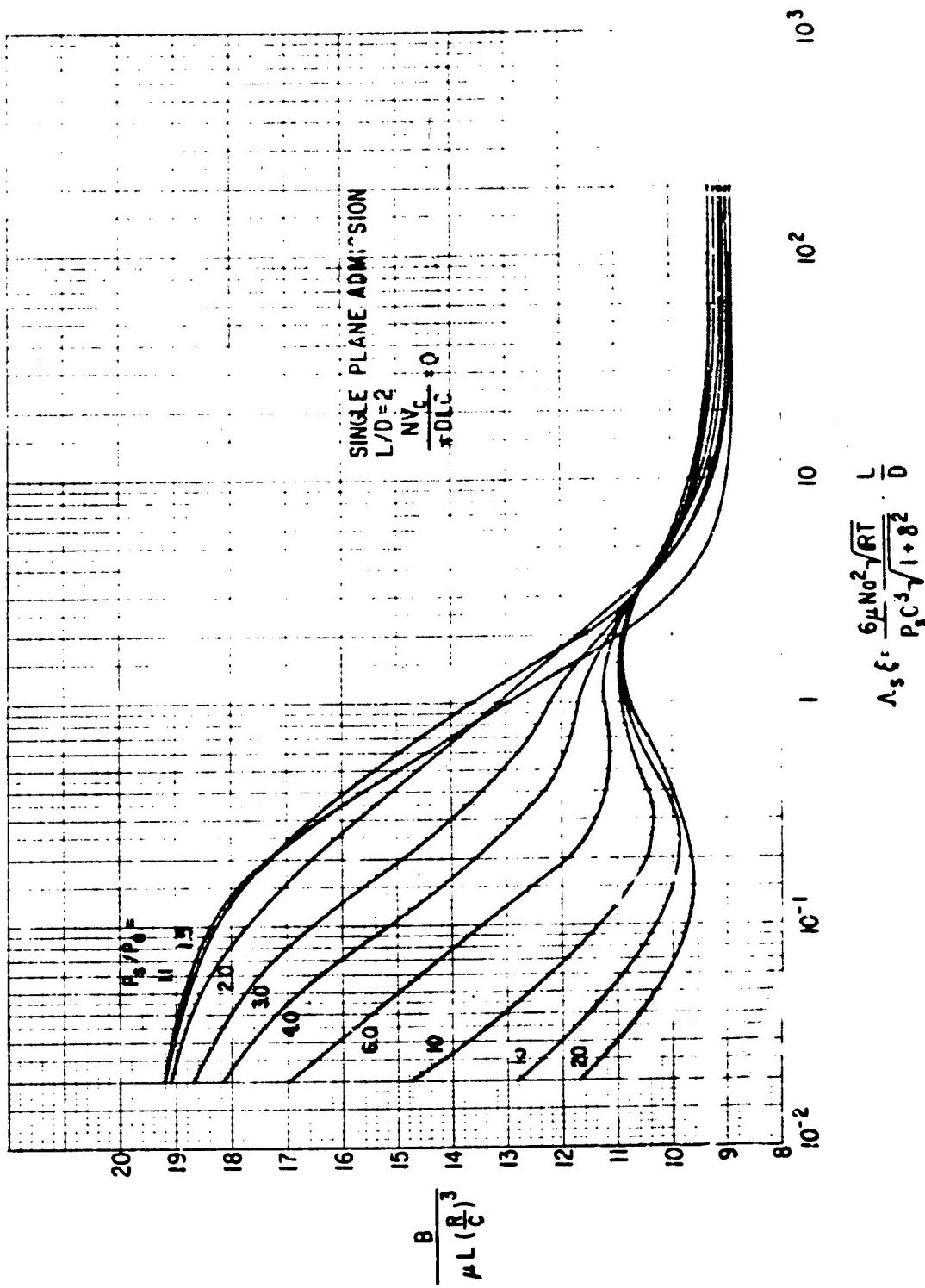


Figure B-117 The Hydrostatic Gas Bearing, $\frac{L}{D} = 2$, Single Plane Admission Dimensionless Mapping

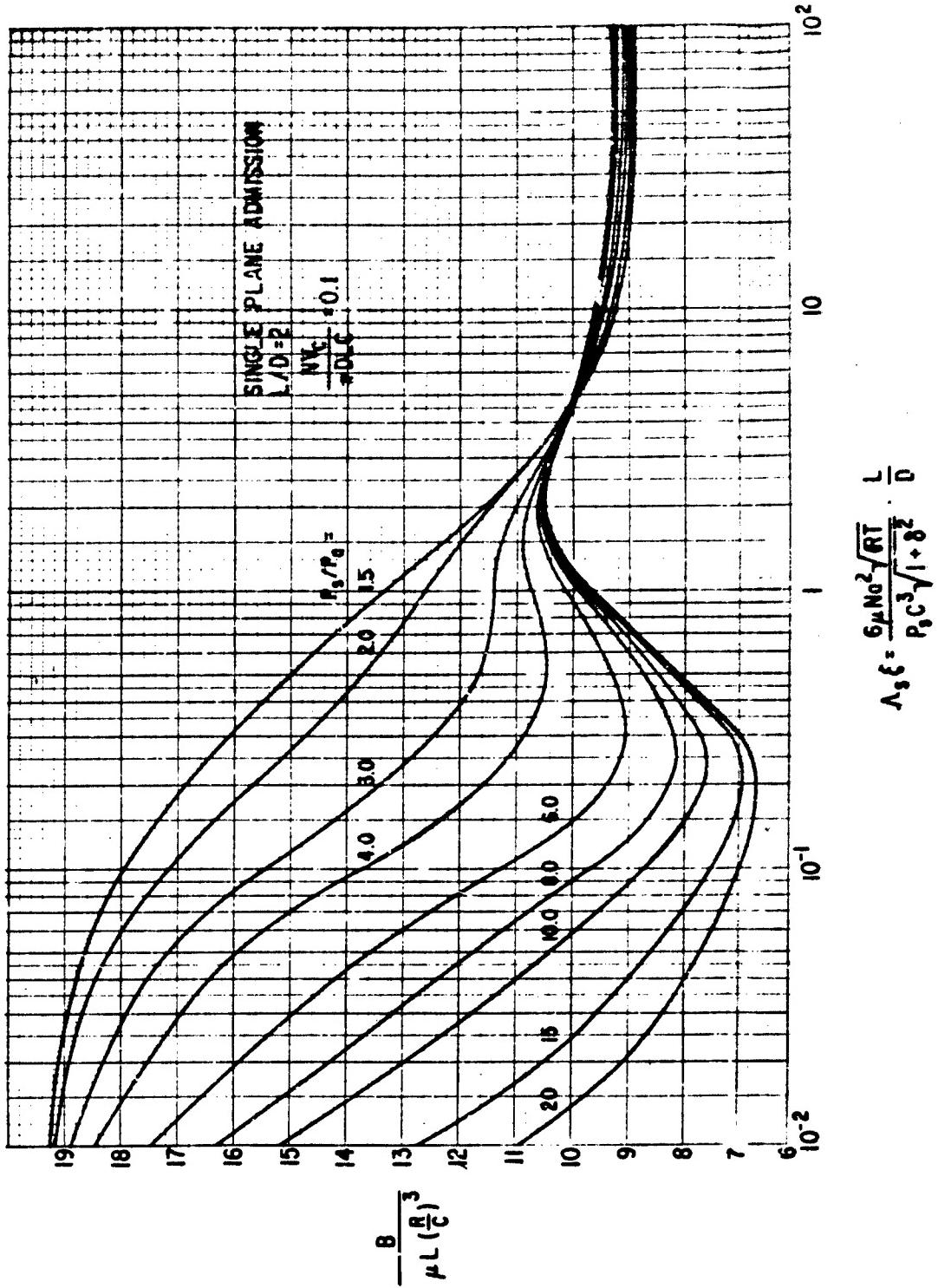
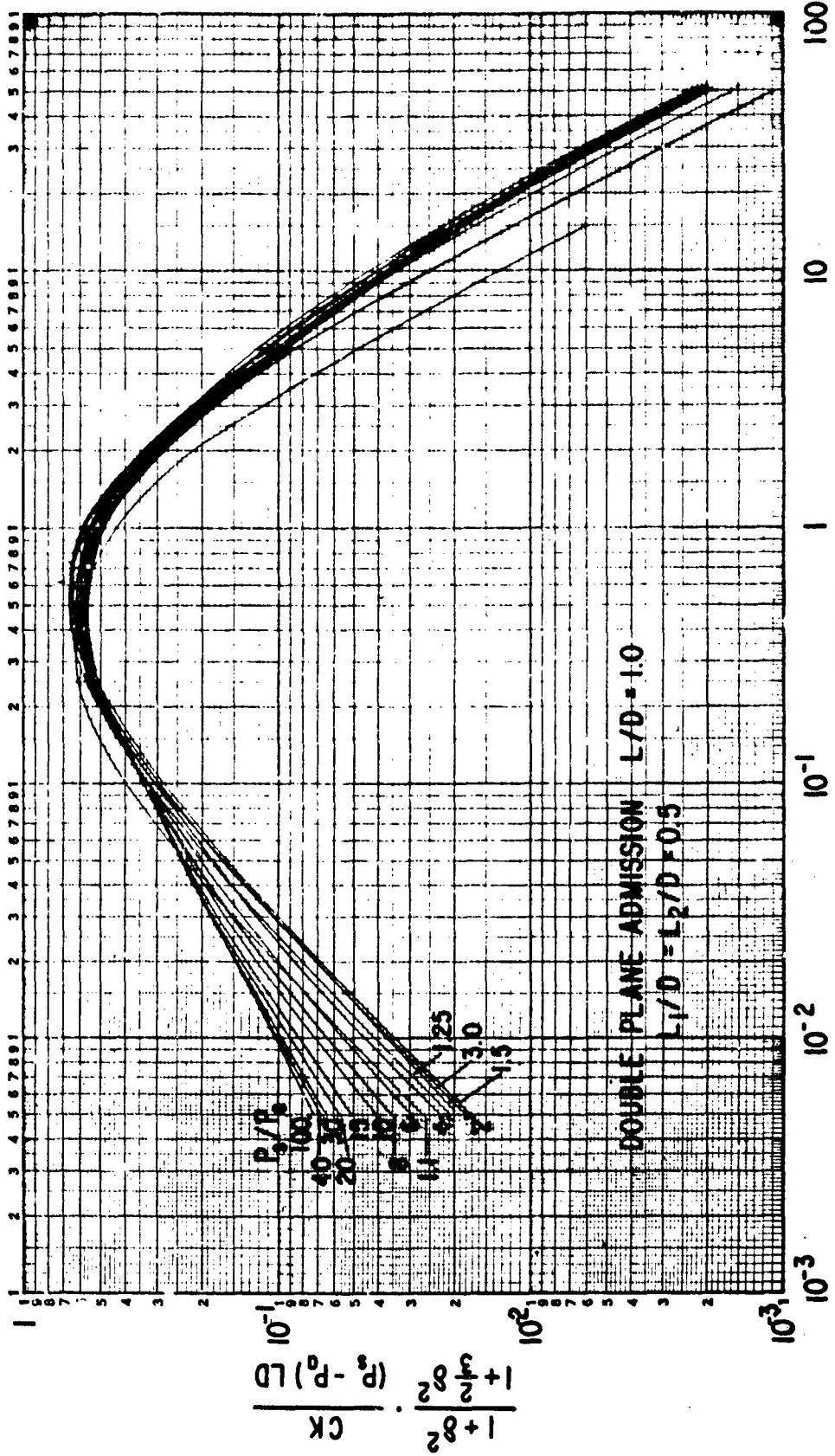


Figure B-118 The Hydrostatic Gas Bearing, $\frac{L}{D} = 2$, Single Plane Admission Dimensionless Damping

$$\Delta_s \xi = \frac{6\mu N_0^2 \sqrt{RT}}{P_s C^3 l^{1.82}} \cdot \frac{l^2}{D}$$



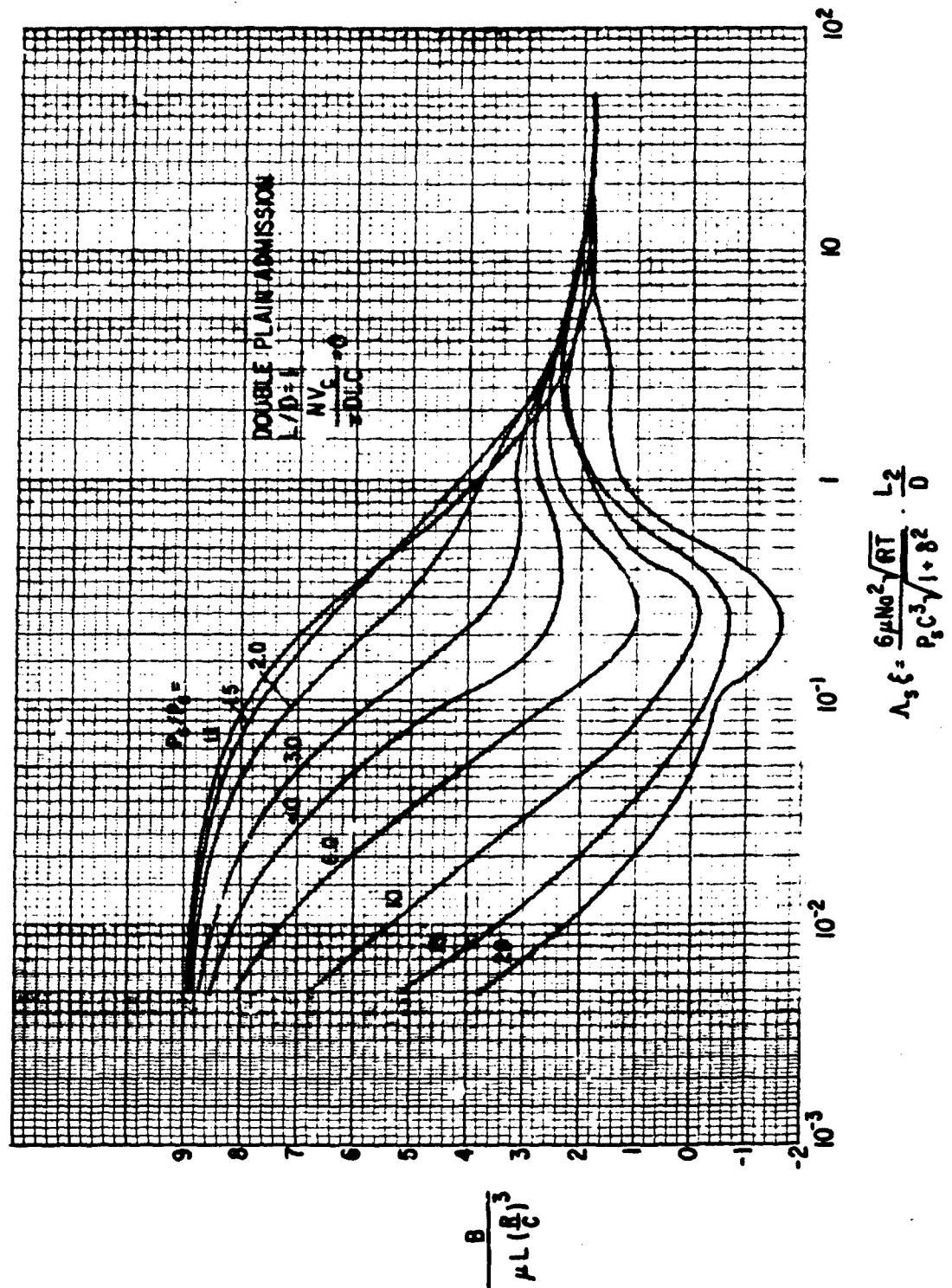
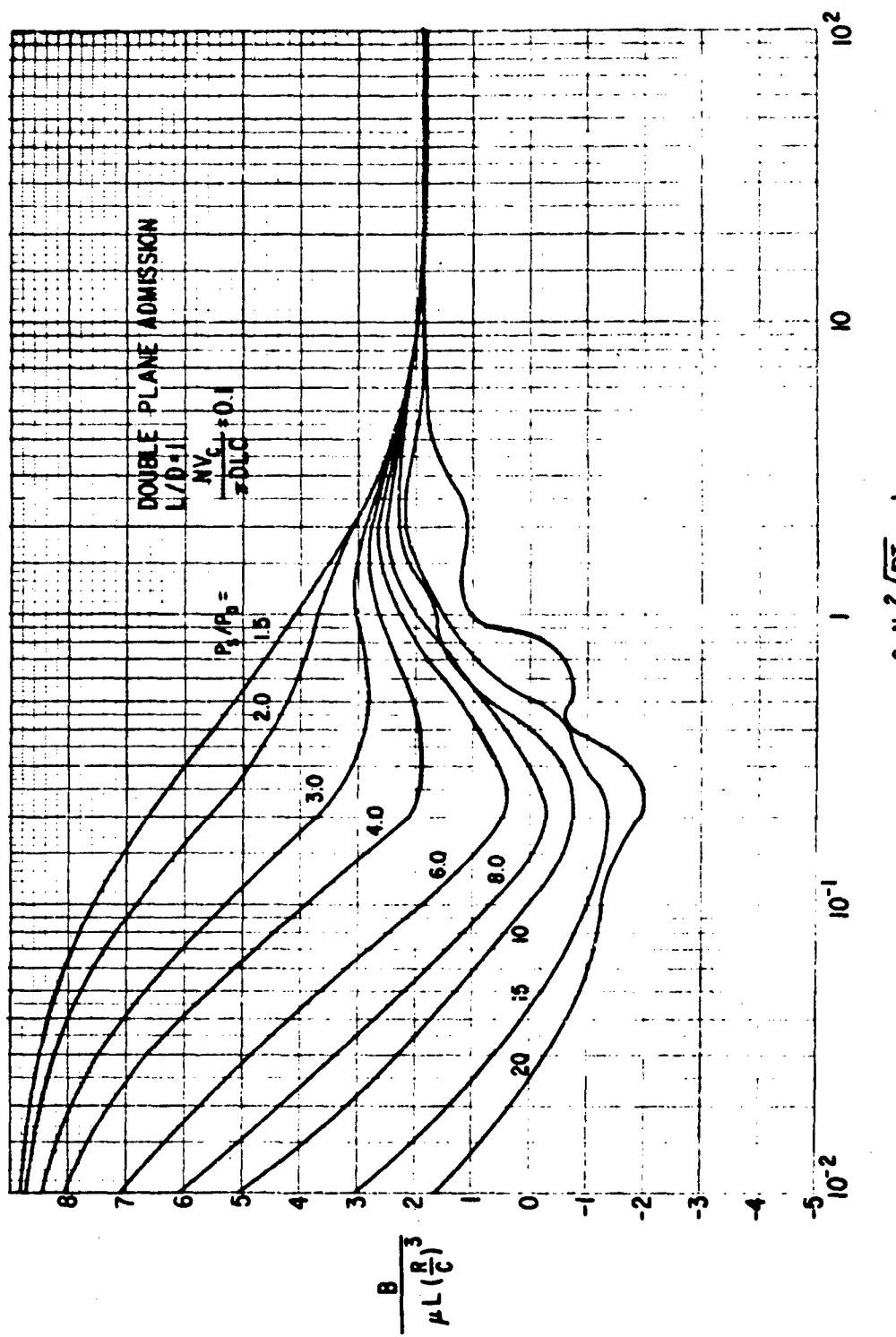


Figure E-120 The Hydrostatic Gas Bearing, $\frac{L}{D} = 1$, Double Plane Admission Dimensionless Damping

$$\Lambda, \xi = \frac{6\pi N_0^2 \sqrt{RT}}{P_0 C_p^3 / (1 + g^2)} \cdot \frac{L^2}{D}$$



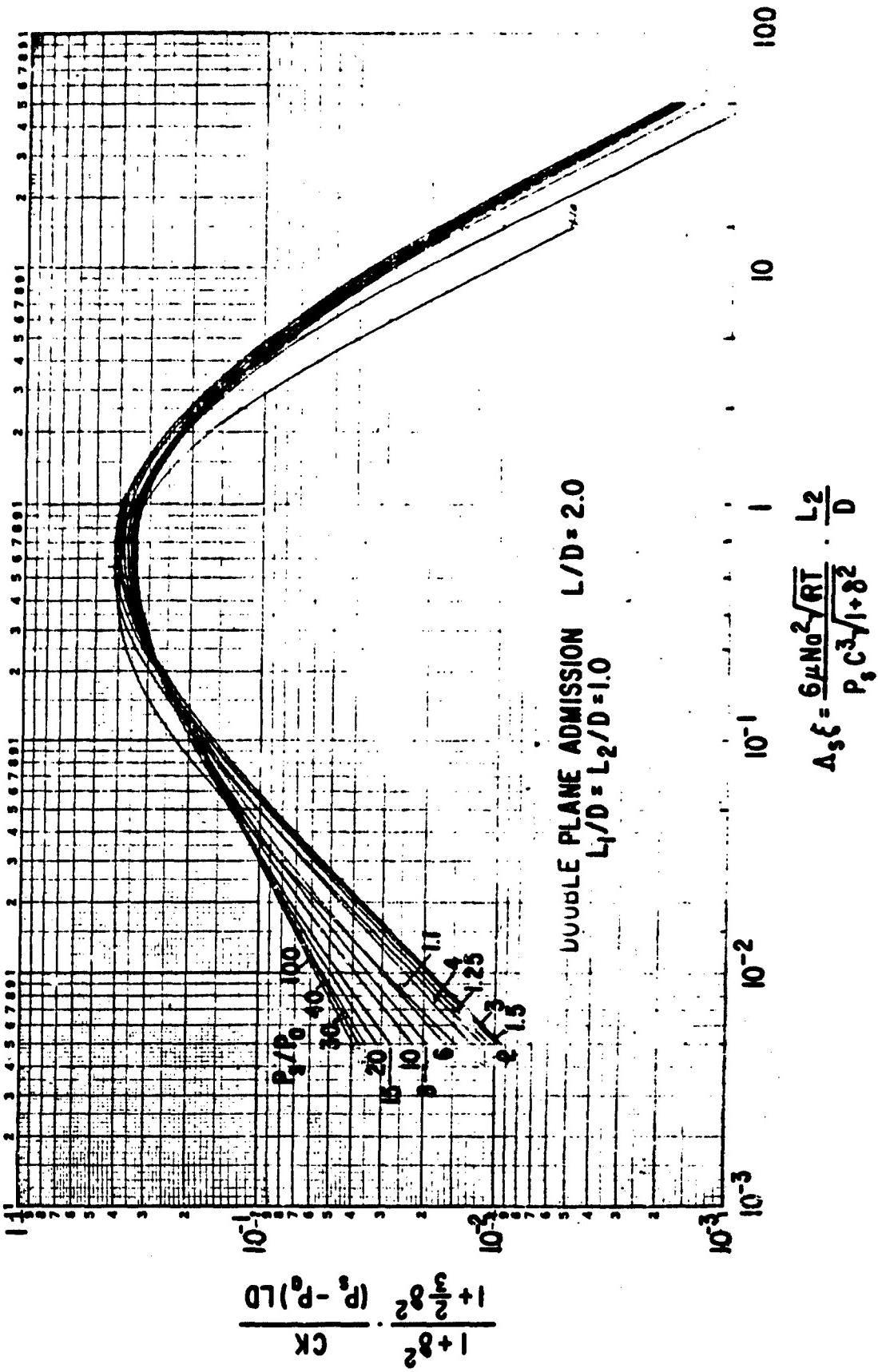
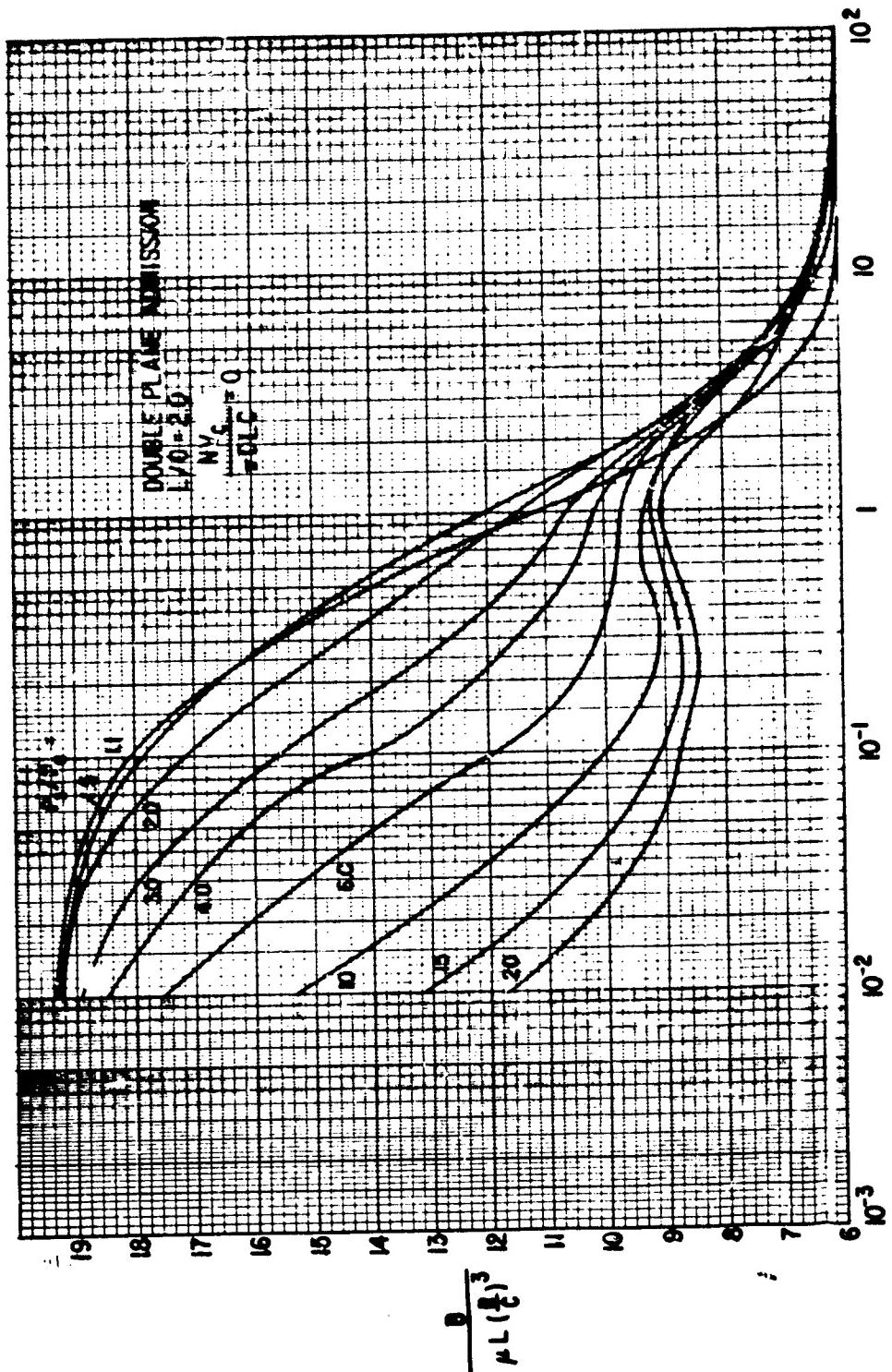
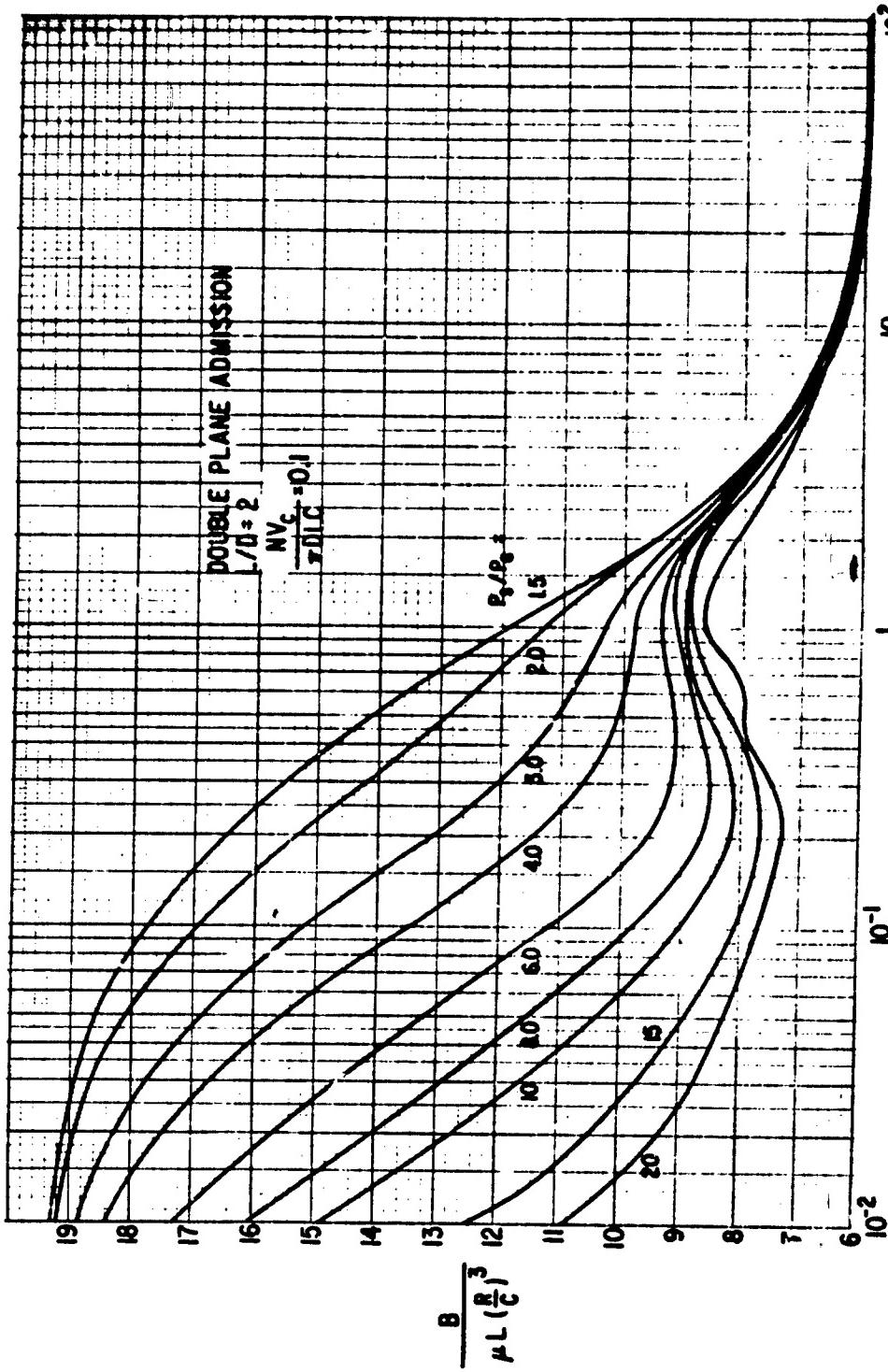


Figure B-122 The Hydrostatic Gas Bearing, $\frac{L}{D} = 2$, Double Plane Admission Dimensionless Stiffness

$$A_s \xi = \frac{6\mu N_0^2 \sqrt{RT}}{P C^3 / (1 + \delta^2)} \cdot \frac{L_2}{D}$$





$$\lambda_s \xi = \frac{6\mu N_a^2 \sqrt{R T}}{P_s C^3 \sqrt{1 + \delta^2}} \cdot \frac{L^2}{D}$$

Figures B-124 The Hydrostatic Gas Bearing, $\frac{B}{D} = 2$, Double Plane Admission
Dimensions in millimeters

THE STABILITY OF A ROTOR-BEARING SYSTEMDiscussion

A rotor supported in fluid film bearings is susceptible to an instability known as fractional frequency whirl ("oil whip"). The instability mechanism derives from the hydrodynamic action in the bearing film where, at a certain disturbance frequency value, the film loses its damping ability. This instability frequency is an inherent property of the film and depends on the operating conditions of the bearing. It is normally expressed by its ratio with respect to the rotational speed. Thus, if the frequency is denoted as ν radians/sec and the angular rotor speed is ω radians/sec the frequency ratio is ν/ω which is dimensionless. The value of the ratio is a function of the eccentricity ratio ϵ (hence, also of the Sommerfeld Number S). For high eccentricity ratios most liquid lubricated bearings are stable such that $\frac{\nu}{\omega}$ is zero or non-existent for approximately $\epsilon > .8$. As ϵ decreases $\frac{\nu}{\omega}$ increases rapidly and levels off with a value of .5 for all $\epsilon < .6$ to .7. Hence, hydrodynamic instability is also called fractional frequency whirl or "half-frequency whirl".

For disturbance frequencies less than the instability value the effective fluid film damping is negative becoming positive for frequencies higher than the instability frequency. If the rotor-bearing system is disturbed away from its equilibrium, it will seek to whirl with its lowest resonant frequency. When the resonant frequency is higher than the bearings inherent instability frequency the disturbance will die out and the system is stable. On the other hand, if the resonant frequency is less than the instability frequency the negative film damping will cause the initial disturbance to grow and the system is unstable. Therefore, the threshold between stability and instability is determined by the requirement that the instability frequency equals the system resonant frequency.

The resonant frequency of the rotor-bearing system depends on the flexibility of the rotor, the stiffness of the bearings and the mass of the rotor. Thus, to define the threshold of instability by means of general design charts requires that both the rotor and bearing parameters are included. In the present design charts, the rotor is assumed to be rigid so that the rotor mass is the only rotor

parameter. The additional effect of rotor flexibility and support flexibility can be estimated by calculations as demonstrated later.

Use of the Design Charts

The design data for the instability threshold are given in Figs. C-1 to C-17 covering a wide selection of bearing types.

a. Liquid Lubricant, Laminar Film

Figs. C-1 to C-7 apply to bearing types with an incompressible lubricant and a laminar film. As a function of the Sommerfeld number S (defined on page 27) the curves give the dimensionless critical rotor mass:

$$\text{Dimensionless Critical Rotor Mass} = \frac{\sqrt{CMW}}{\mu DL \left(\frac{R}{C} \right)^2}$$

where:

- D - Journal diameter, inch
- R - $\frac{1}{2} D$, Journal radius, inch
- L - Bearing length, inch
- C - Radial clearance, inch
- μ - Lubricant viscosity, lbs.sec/in^2
- W - Bearing load, lbs.
- M - Rotor mass per bearing, $\text{lbs.sec}^2/\text{in}$

The rotor mass per bearing may be computed as:

$$M = \left[1 - \frac{(\text{Distance from bearing to CG of rotor})}{(\text{Rotor span between bearings})} \right] \cdot (\text{Total rotor mass}, \frac{\text{lbs.sec}^2}{\text{in}})$$

Thus, if the rotor is horizontal and gravity is the only radial load, then:

$$M = \frac{W}{g} \quad (\text{horizontal rotor, gravity load})$$

where:

$$g = 386 \text{ in/sec}^2$$

The procedure for determining the threshold speed is then: calculate the dimensionless rotor mass according to the equation given above. Enter the appropriate design chart and read off the corresponding value of the Sommerfeld

number. The speed corresponding to this Sommerfeld number is the threshold speed, i.e. the rotor speed at onset of instability. If the operating speed is higher than the threshold speed the design must be revised.

The charts assume the rotor and the pedestals to be rigid. However, the threshold speed with a flexible rotor and flexible pedestals can be calculated on the basis of the given design charts. Let the stiffness of the bearing support be $K_s \frac{\text{lbs}}{\text{in}}$ and the stiffness of the rotor $K_r \frac{\text{lbs}}{\text{in}}$. The latter stiffness can be taken as the lateral stiffness of the rotor by itself when a force is applied at the CG. Make the two stiffness values dimensionless:

$$\bar{K}_r = \frac{CK_r}{W} \quad \bar{K}_s = \frac{CK_s}{W}$$

and introduce the parameter:

$$k = \frac{\bar{K}_r \cdot \bar{K}_s}{\bar{K}_r + \bar{K}_s}$$

Note, that if the rotor is rigid:

$$k = \bar{K}_s \quad (\text{rigid rotor, flexible pedestal})$$

whereas for a flexible rotor but rigid pedestals:

$$k = \bar{K}_r \quad (\text{flexible rotor, rigid pedestals})$$

Next, choose a value S of the Sommerfeld number and find the corresponding value of the dimensionless rotor mass from the design charts. Denote this value as \bar{M}_o . Define a dimensionless effective bearing stiffness by:

$$K_B = (\pi S \bar{M}_o)^2$$

Then the dimensionless critical rotor mass for the flexible rotor and the flexible pedestal, corresponding to the selected Sommerfeld number value, becomes:

$$\left[\frac{\sqrt{CMW}}{\mu DL \left(\frac{R}{C} \right)^2} \right]_{\substack{\text{flex. rotor} \\ \text{flex. pedest.}}} = \bar{M}_o \sqrt{\frac{k}{k+K_B}}$$

Repeating the procedure for several values of the Sommerfeld number defines a new curve for the dimensionless critical rotor mass. Entering this curve with the originally calculated value of the dimensionless rotor mass determines the Sommerfeld number and, hence, the rotor speed at the threshold of instability.

No instability design charts are given for the tilting pad bearing. All the design data for the dynamic coefficients of the tilting pad bearing assume that the pivoted shoes have no mass inertia and under that condition the tilting pad bearing is inherently stable. In practice, of course, the shoes will have some inertia but as long as the phase angle between the shoe motion and the journal motion is less than 90 degrees the bearing will be stable. The condition under which the phase angle becomes equal to 90 degrees can be determined from Figs. B-37 to B-48. Here the dimensionless critical shoe inertia, labeled "Critical Mass" on the curves, is plotted against the Sommerfeld number. It is expressed by:

$$\text{Dimensionless Critical Shoe Inertia} = \frac{CWM_{\text{crit}}}{[\mu DL(\frac{R}{C})^2]^2}$$

where:

$$M_{\text{crit}} = I/R^2, \text{ lbs.sec}^2/\text{in}$$

I - Mass moment of inertia of a shoe around a longitudinal axis passing through the pivot, lbs.in.sec²

R - Journal radius, inch

The other symbols are defined on Page 27.

Hence, in checking the stability of the tilting pad bearing calculate the dimensionless shoe inertia, enter the design charts and read off the corresponding value of the Sommerfeld number. This value should be greater than the operating Sommerfeld number.

b. Liquid Lubricant, Turbulent Film

Figs. C-8 to C-14 apply to the plain cylindrical and the 100 degree partial bearing with an incompressible lubricant and a turbulent film. The curves give the dimensionless critical rotor mass as a function of the Sommerfeld number S for a wide range of Reynolds numbers. The procedure for using the

charts is completely analogous to the procedure described above for the laminar film bearings with the exception that the dependency of the Reynolds number on the rotor speed must be included. The Reynolds number is defined by:

$$Re = \frac{\pi N D C}{\mu}$$

(for symbols, see Page 27). N is the speed in RPS and is also a factor in the Sommerfeld number:

$$S = \frac{\mu N D L}{W} \left(\frac{R}{C}\right)^2$$

Hence, in using Figs. C-8 to C-14 compute first the dimensionless rotor mass (see Page 202), enter one of the charts and read off the corresponding Sommerfeld number. Based on this value calculate the rotor speed and the Reynolds number. If the obtained value of the Reynolds number differs significantly from the Reynolds number for which the chart is valid repeat the procedure until both the Sommerfeld number and the Reynolds number yield the same rotor speed. The resulting value of the rotor speed is the speed on the threshold of instability.

c. Gas Lubricant, Hydrodynamic Bearing

For the gas lubricated bearing the design parameters are:

$$\text{Compressibility number: } \Lambda = \frac{12\pi\mu N}{P_a} \left(\frac{R}{C}\right)^2$$

$$\text{Dimensionless bearing load: } \frac{W}{P_a L D}$$

$$\text{Dimensionless critical rotor mass} = -\frac{M_p}{\mu^4 L \left(\frac{R}{C}\right)^5}$$

where:

N - Rotor speed, RPS

P_a - Ambient pressure, psia

and the other symbols are defined on Page 27. The rotor mass per bearing, M , is determined as outlined on Page 202.

Figs. C-15 to C-17 apply to the stability of the plain cylindrical gas bearing for three values of the length-to-diameter ratio. The rotor and the bearing pedestals are assumed to be rigid. To use the charts compute the dimensionless bearing load and the dimensionless rotor mass, enter the appropriate figure and read off the value of the compressibility number Λ . From this value calculate N which is then the rotor speed at the threshold of instability. The rotor-bearing should not be designed to operate beyond the threshold speed.

If the rotor and the bearing pedestals are flexible the threshold speed is lowered. Let the pedestal stiffness be $K_s \frac{\text{lbs}}{\text{in}}$ and the rotor stiffness $K_r \frac{\text{lbs}}{\text{in}}$ as discussed on Page 203. Make the two values dimensionless:

$$\bar{K}_r = \frac{CK_r}{P_a LD} \quad \bar{K}_s = \frac{CK_s}{P_a LD}$$

and compute the dimensionless, combined rotor-support stiffness:

$$k = \frac{\bar{K}_r \bar{K}_s}{\bar{K}_r + \bar{K}_s}$$

For the given dimensionless bearing load choose a value of Λ and read off the corresponding value of the dimensionless critical rotor mass from the design chart. Call this value \bar{M}_o . Define a dimensionless effective bearing stiffness as:

$$K_B = \frac{\Lambda^2}{288} \bar{M}_o$$

Then the dimensionless critical rotor mass for the flexible rotor with the flexible pedestal can be calculated from:

$$\left[\frac{MP_a}{\mu^2 L \left(\frac{R}{C} \right)^5} \right]_{\text{flex. rotor}} = \frac{k}{k + K_B} \cdot \bar{M}_o$$

flex. pedestal.

By repeating the procedure for several Λ -values a new design curve is obtained. Entering this curve with the originally calculated value for the dimensionless rotor mass determines the value of the compressibility number and, hence, the

rotor speed at the threshold of instability.

If the desired operating speed is above the calculated threshold speed, it is necessary either to revise the design, or if this is insufficient, to go to another bearing type such as the tilting pad bearing or the hydrostatic gas bearing. The latter bearing type is considered below. For the tilting pad bearing no design data are available for studying its stability. However, as long as the mass inertia of the shoes is small the tilting pad bearing is inherently stable. An estimate of the critical value for the shoe mass inertia can be obtained from the design curves for an incompressible lubricant given in Figs. B-37 to B-48 when the proper bearing dimensions and gas lubricant properties are used.

d. Gas Lubricant, Hydrostatic Bearing

When the speed of a rotor supported in hydrostatic gas bearings becomes sufficiently high the hydrodynamic lubrication action in the bearings starts to be significant. A hydrostatic bearing operating under these conditions is called the hybrid gas bearing. Due to the hydrodynamic action the hybrid bearing is susceptible to fractional frequency whirl ("hybrid instability"). Only limited design data are available on hybrid instability (see Ref.19) and because of their incompleteness they are not included in the present report. However, it is possible to give a simple rule for obtaining an approximate estimate of the threshold speed, namely:

$$\text{Threshold Speed} = (1.6 \text{ to } 2) \cdot (\text{1st Critical Speed with purely Hydrostatic Bearing})$$

In calculating the 1st critical speed the hydrostatic bearing stiffness obtained from Figs. B-110 to B-124 should be used. Since the rotor for a gas bearing application is almost always rigid the critical speed may be computed from the equations given on Page 235.

Besides hybrid instability the hydrostatic bearing may experience another form of instability called pneumatic hammer. This instability is in most cases independent of the rotor speed and is, therefore, basically associated with the design of the bearing. It derives its energy from the supply pressure and is analogous to the action in pneumatic tools. A design of a hydrostatic gas bearing can be checked for pneumatic hammer by means of the design charts for the

dimensionless damping, Figs. B-111 to B-124. Whenever the damping is negative the bearing is unstable. Hence, to use the charts for the purpose of checking stability calculate the restrictor coefficient A_s , the supply pressure ratio P_s/P_a (see Page 69) and enter the design charts to determine if the damping is negative. If this is the case the design must be modified or the bearing may be made inherently compensated (i.e. the feeder holes are not provided with orifice restrictors).

DESIGN CHARTS FOR
HYDRODYNAMIC INSTABILITY

a. Liquid Lubricant, Laminar Film

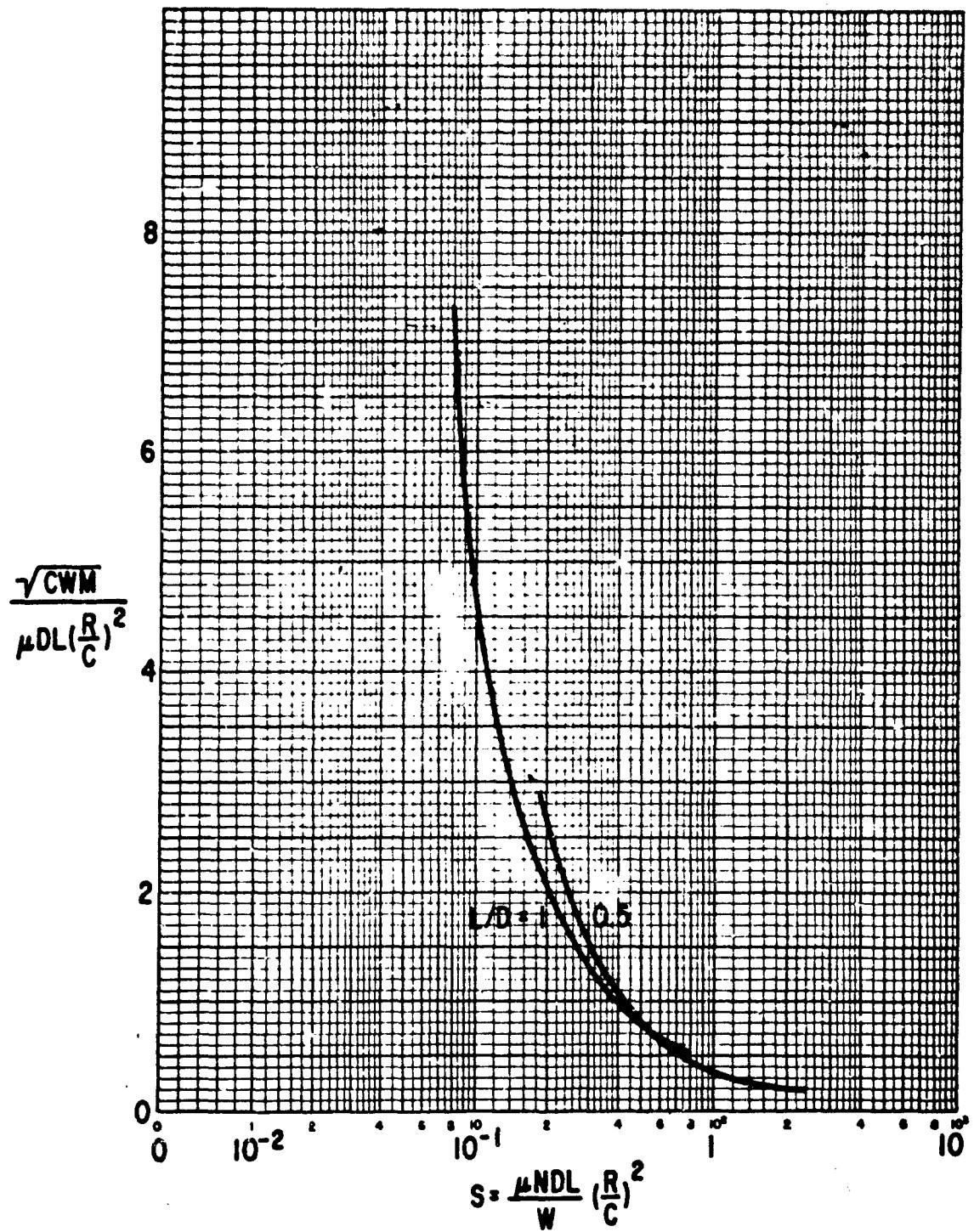


Figure C-1 The Plain Cylindrical Bearing, Laminar Film Critical Motor Mass at Onset of Instability
211

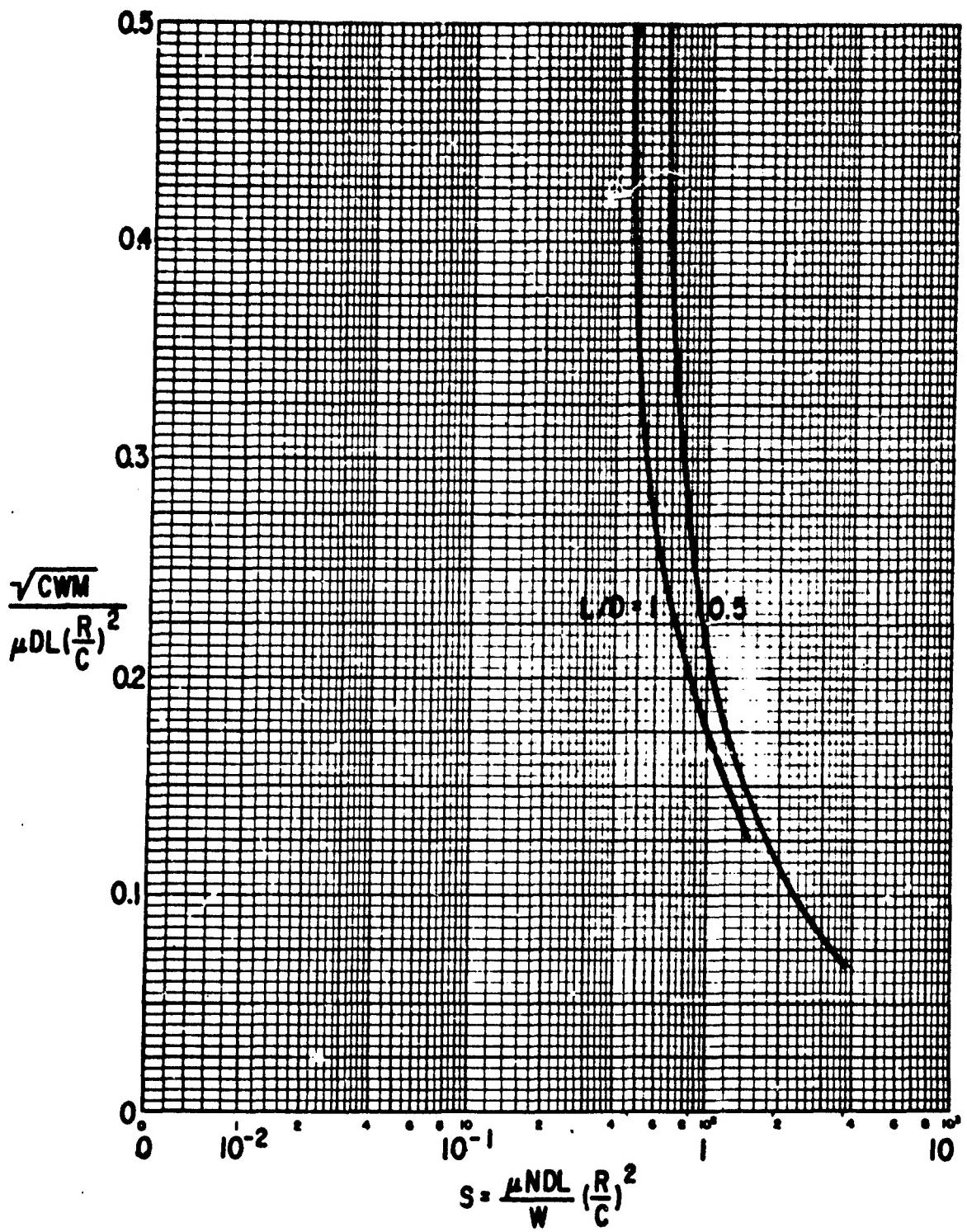


Figure C-2 The 4-Axial Groove Bearing, Laminar Film
 Critical Rotor Mass at Onset of Instability
 212

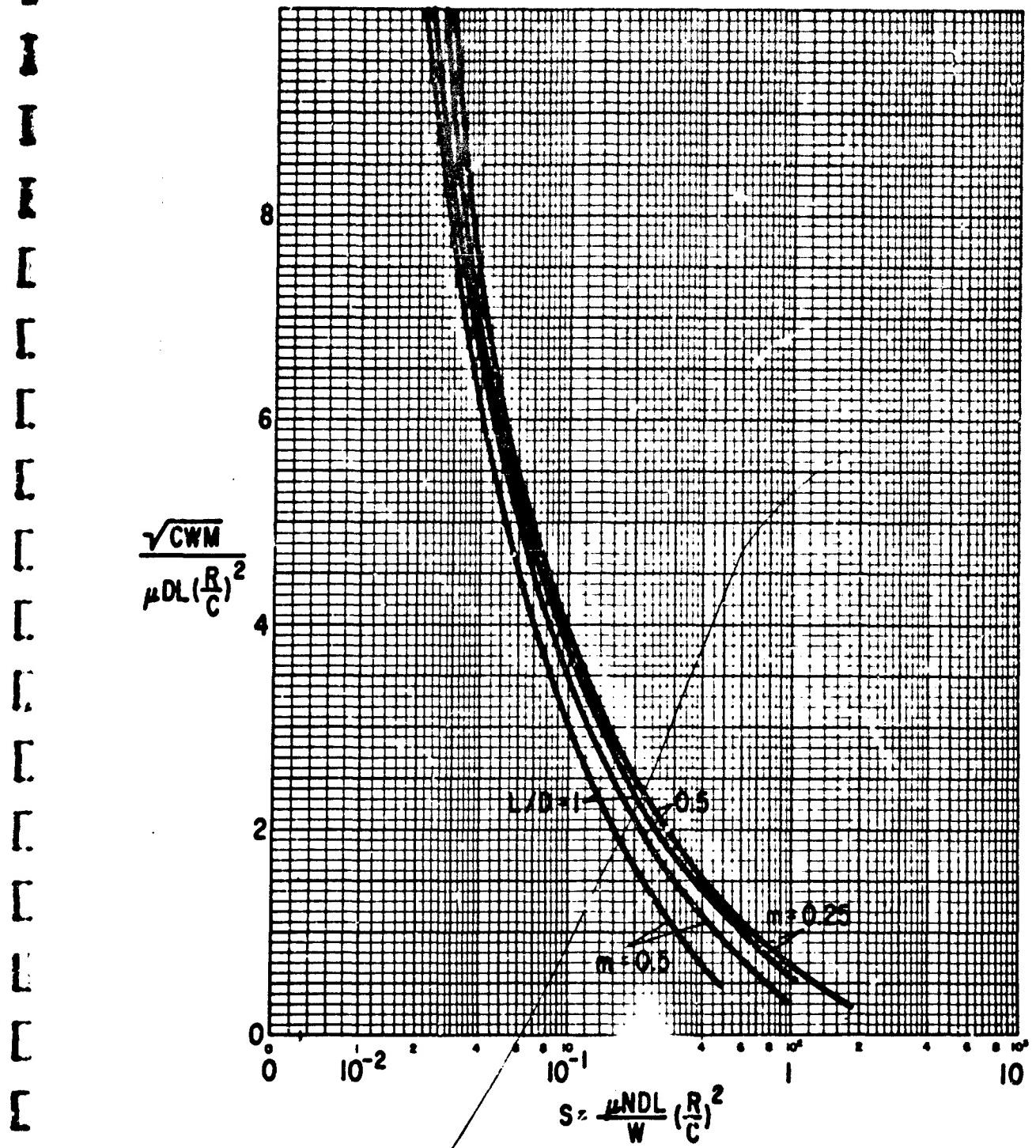


Figure C-3 The Elliptical Bearing, Laminar Film Critical Rotor Mass at Onset of Instability
213

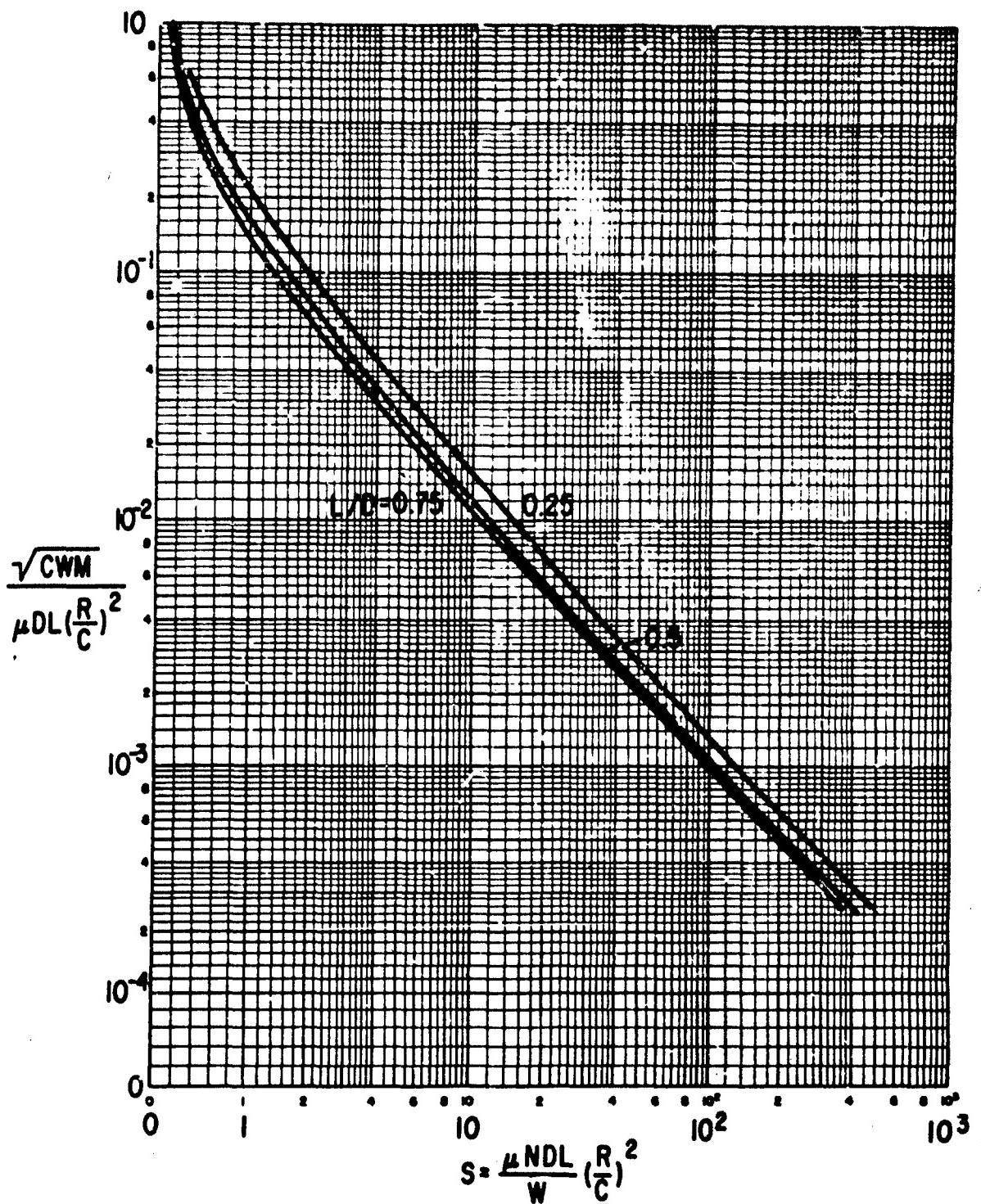


Figure C-4 The 50 Degree Partial Bearing, Centrally Loaded, Laminar Film Critical Rotor Mass at Onset of Instability

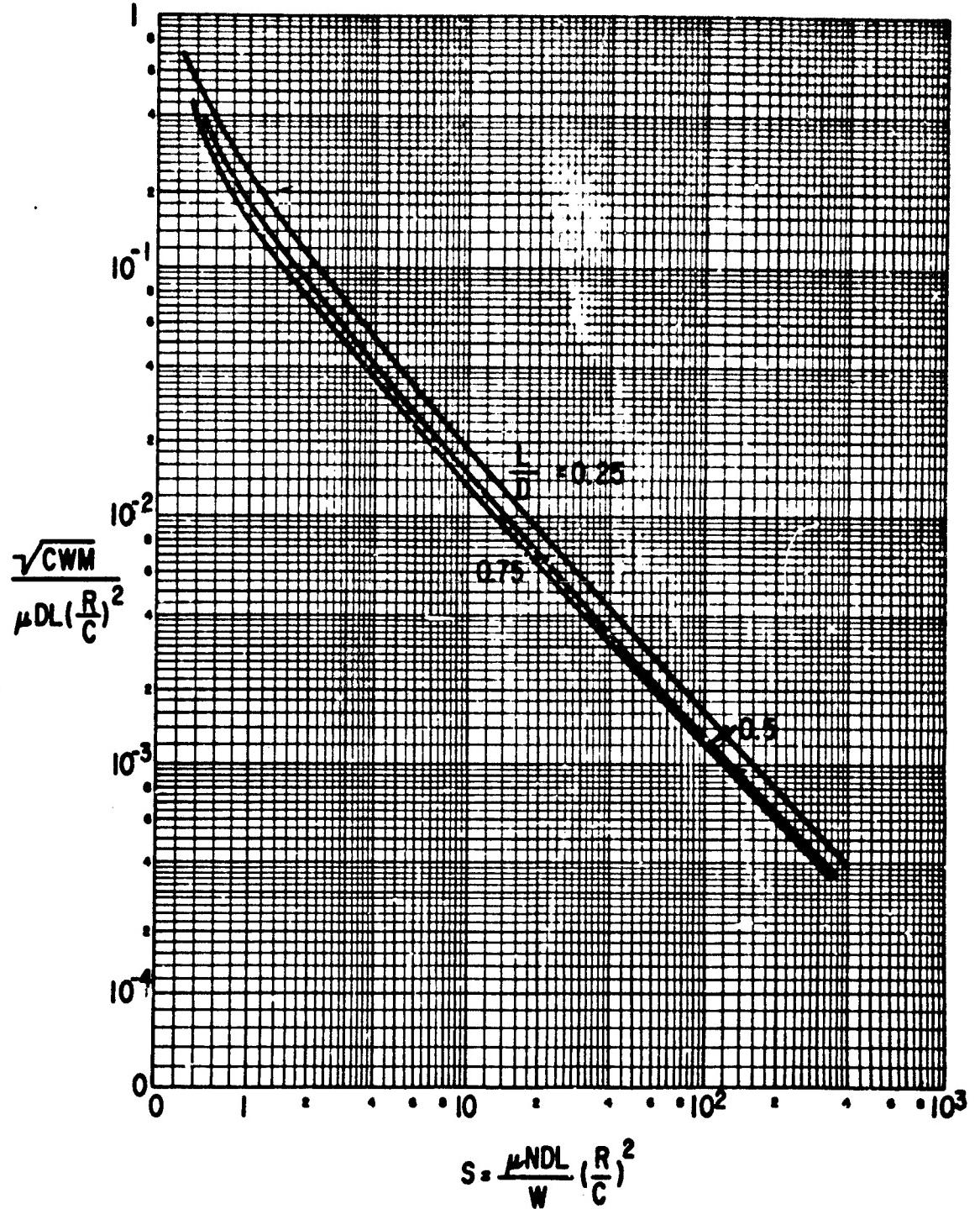


Figure C-5 The 60 Degree Partial Bearing, Centrally Loaded, Laminar Film Critical Rotor Mass at Onset of Instability

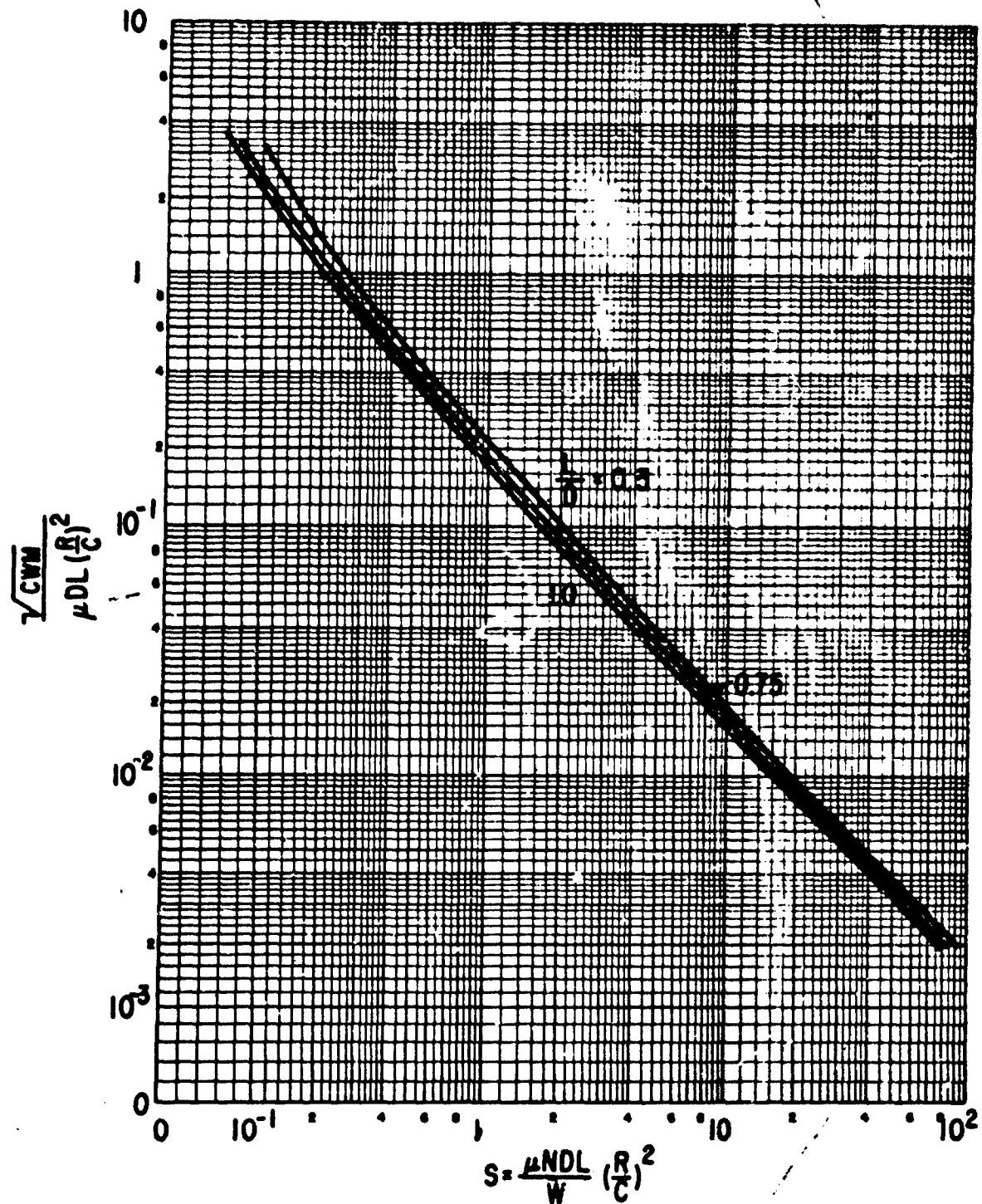


Figure C-6 The 80 Degree Partial Bearing, Centrally Loaded, Laminar Film Critical Rotor Mass at Onset of Instability

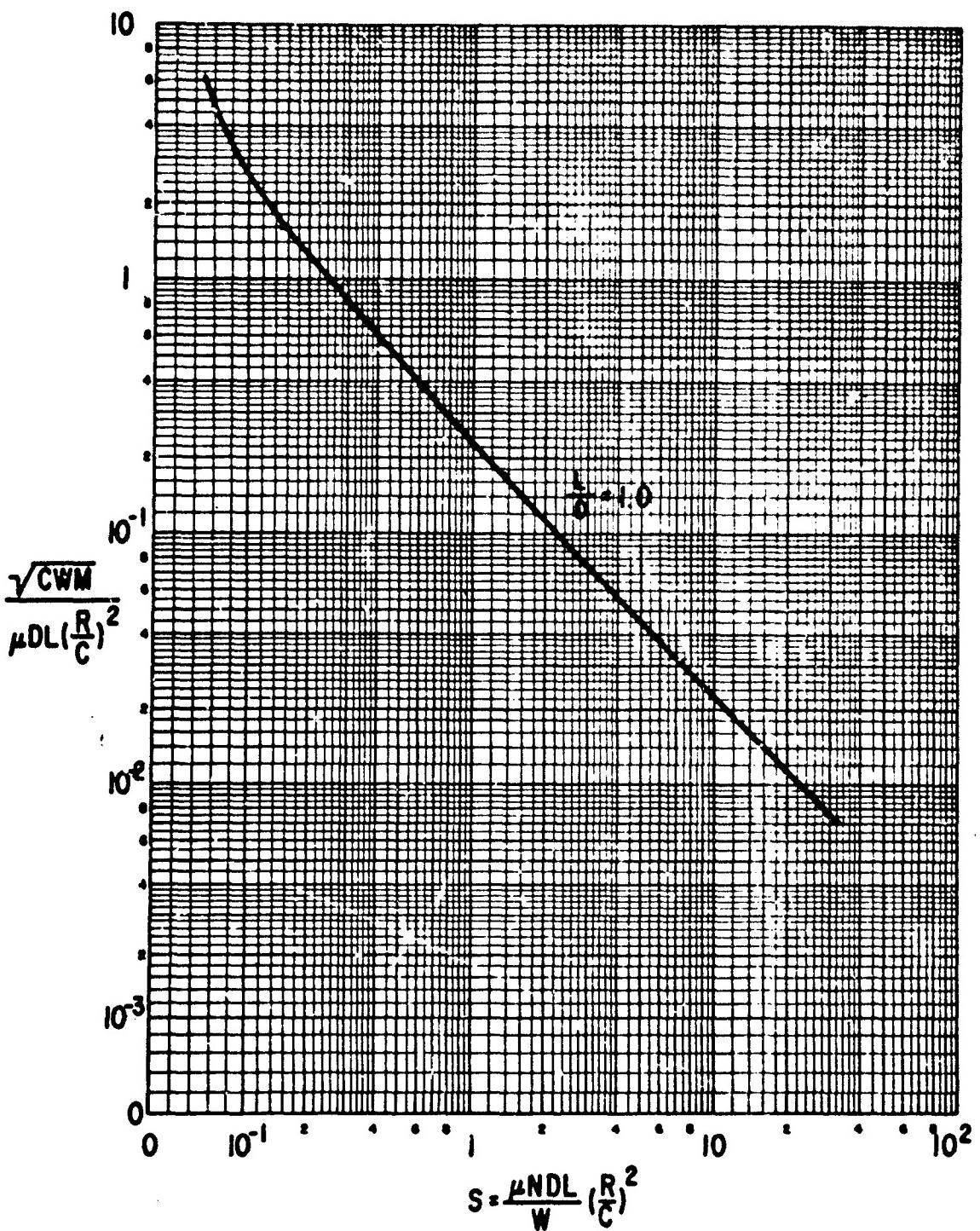


Figure C-7 The 100 Degree Partial Bearing, Centrally Loaded, Laminar Film Critical Rotor Mass at Onset of Instability

b. Liquid Lubricant, Turbulent Film

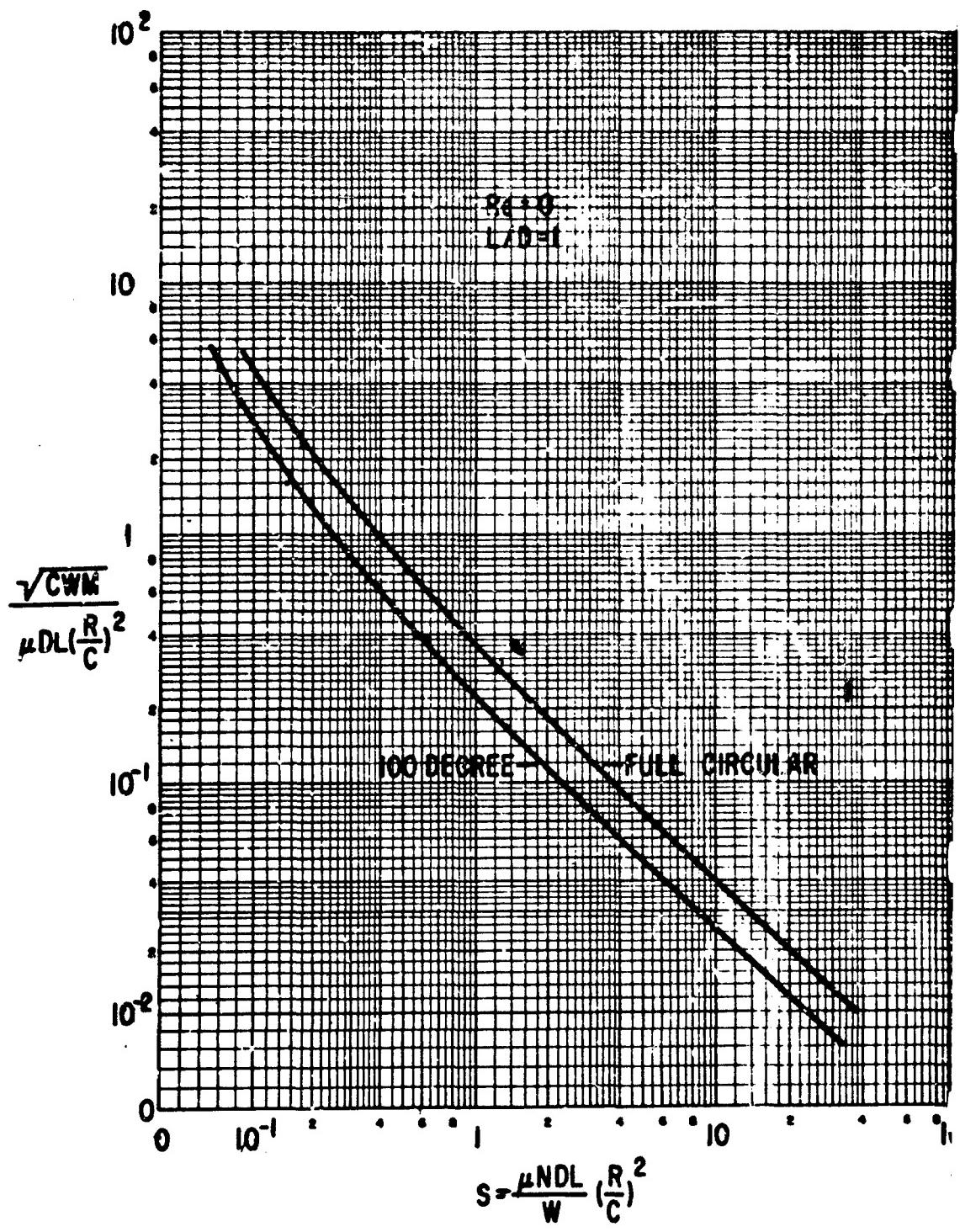


Figure C-8 The Plain Cylindrical and the 100 Degree Partial Bearing,
 Turbulent Film
 Critical Rotor Mass at Onset of Instability
 219

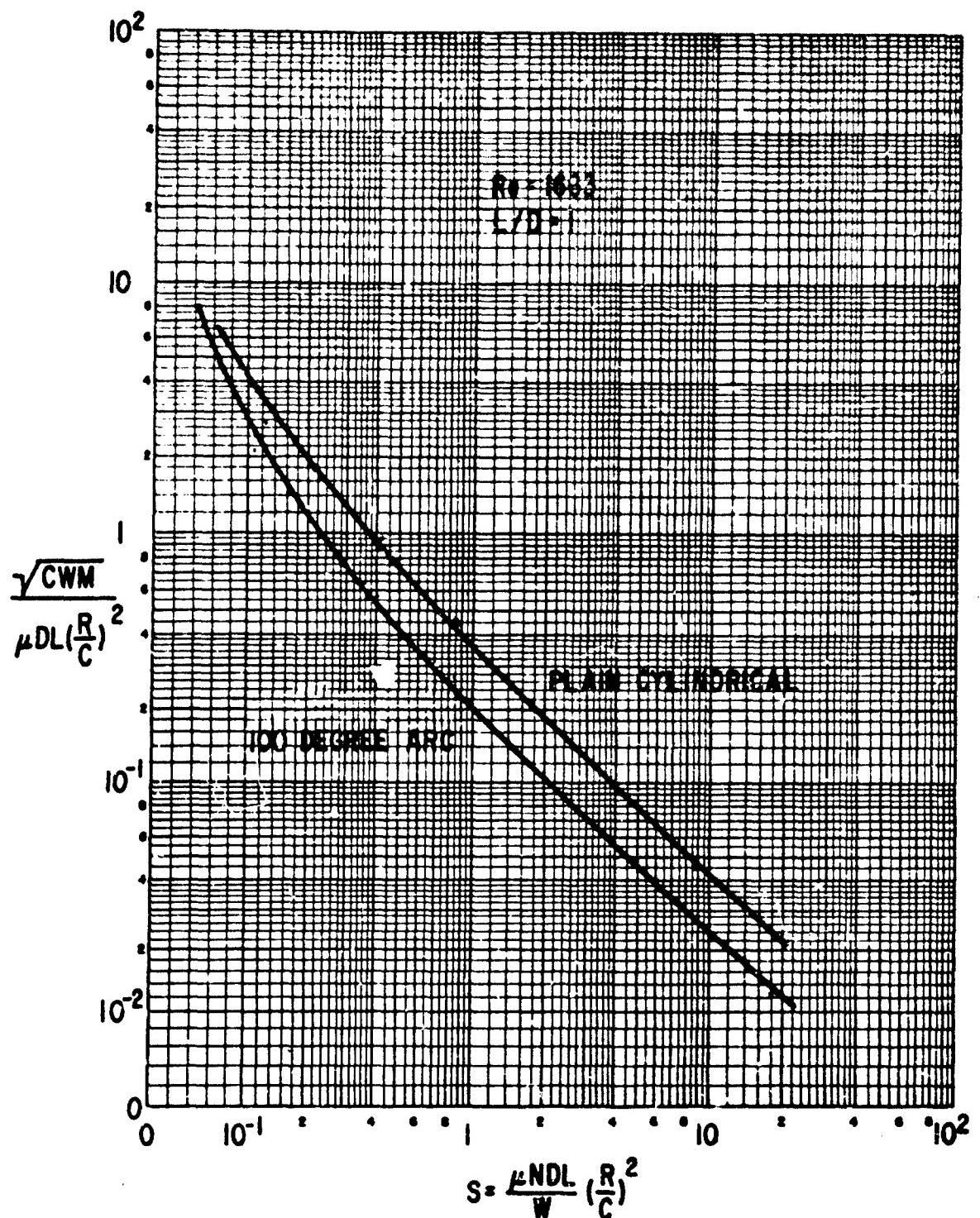


Figure C-9 The Plain Cylindrical and the 100 Degree Partial Bearing,
Turbulent Film
Critical Rotor Mass at Onset of Instability

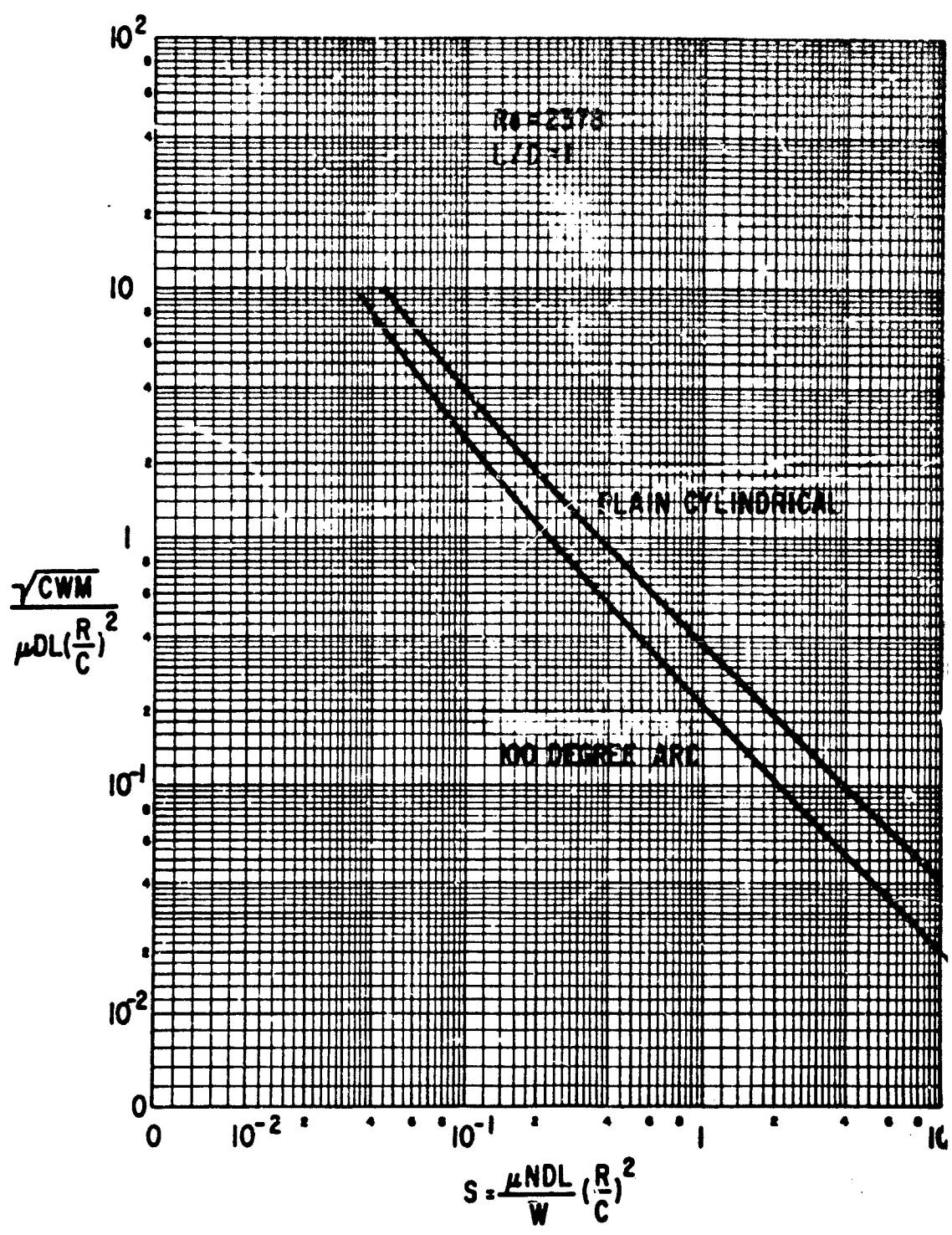


Figure C-10 The Plain Cylindrical and the 100 Degree Partial Bearing,
Turbulent Film
Critical Motor Mass at Onset of Instability

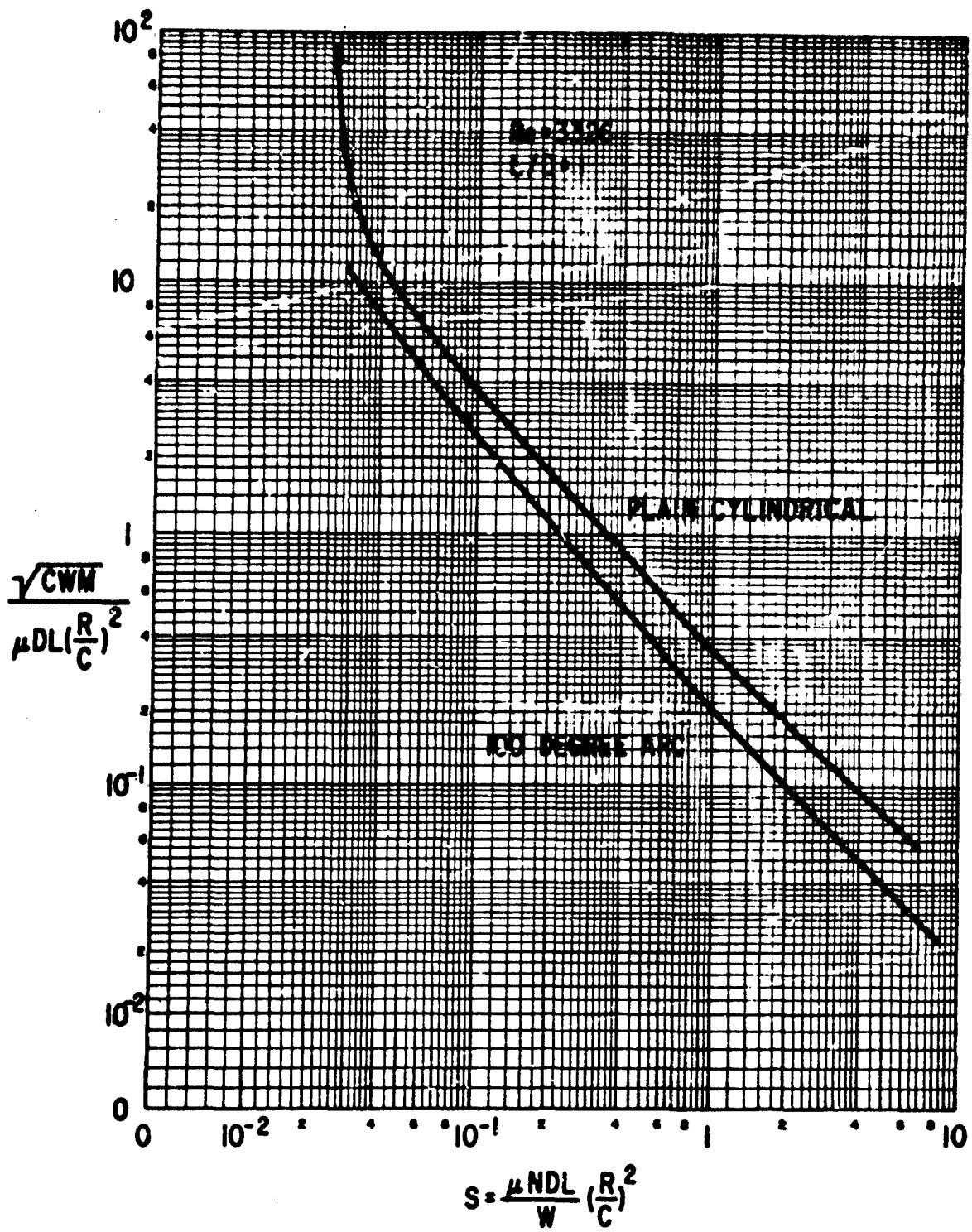


Figure C-11 The Plain Cylindrical and the 100 Degree Partial Bearing,
 Turbulent Film
 Critical Rotor Mass at Onset of Instability
 222

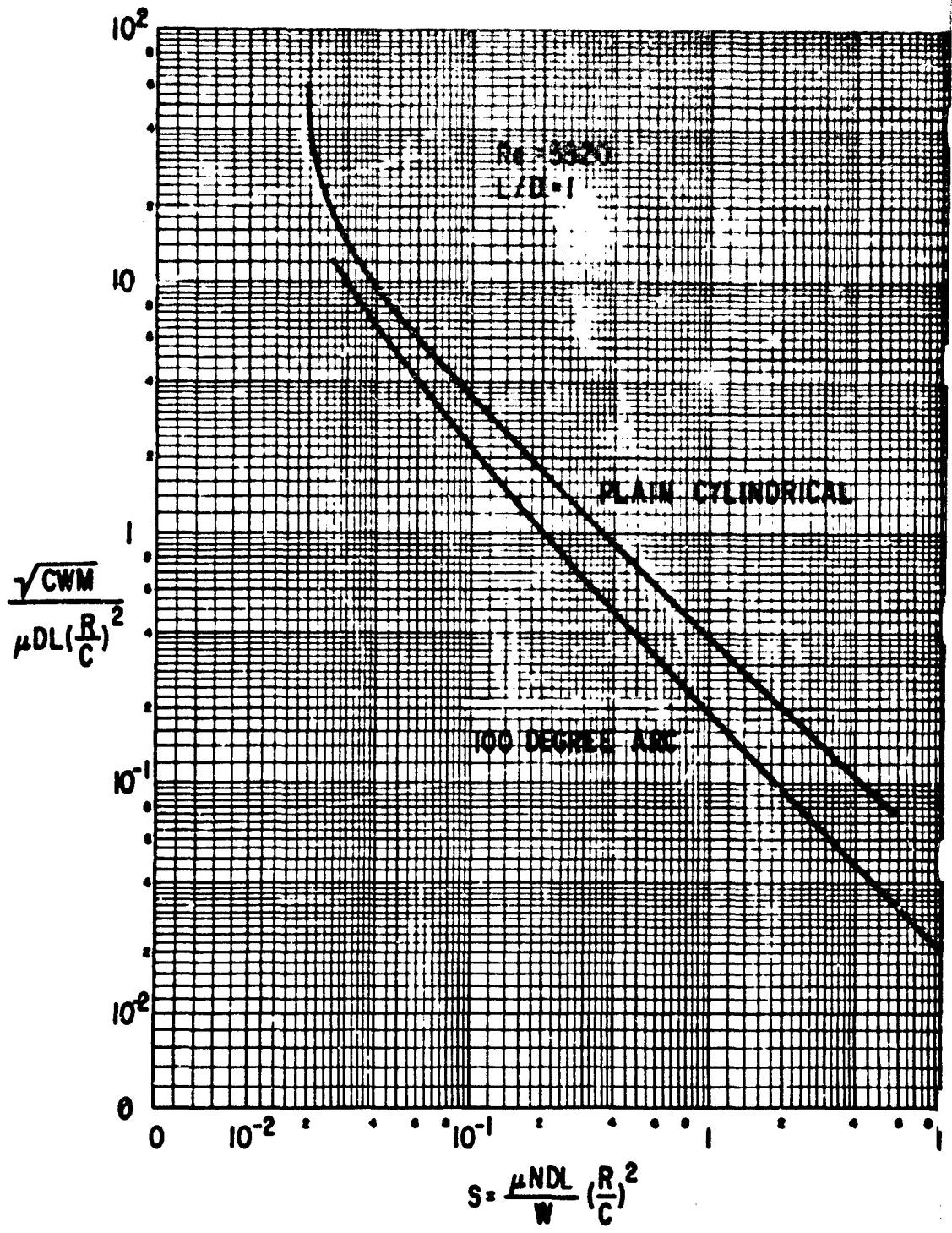


Figure C-12 The Plain Cylindrical and the 100 Degree Partial Bearing,
Turbulent Film
Critical Rotor Mass at Onset of Instability
223

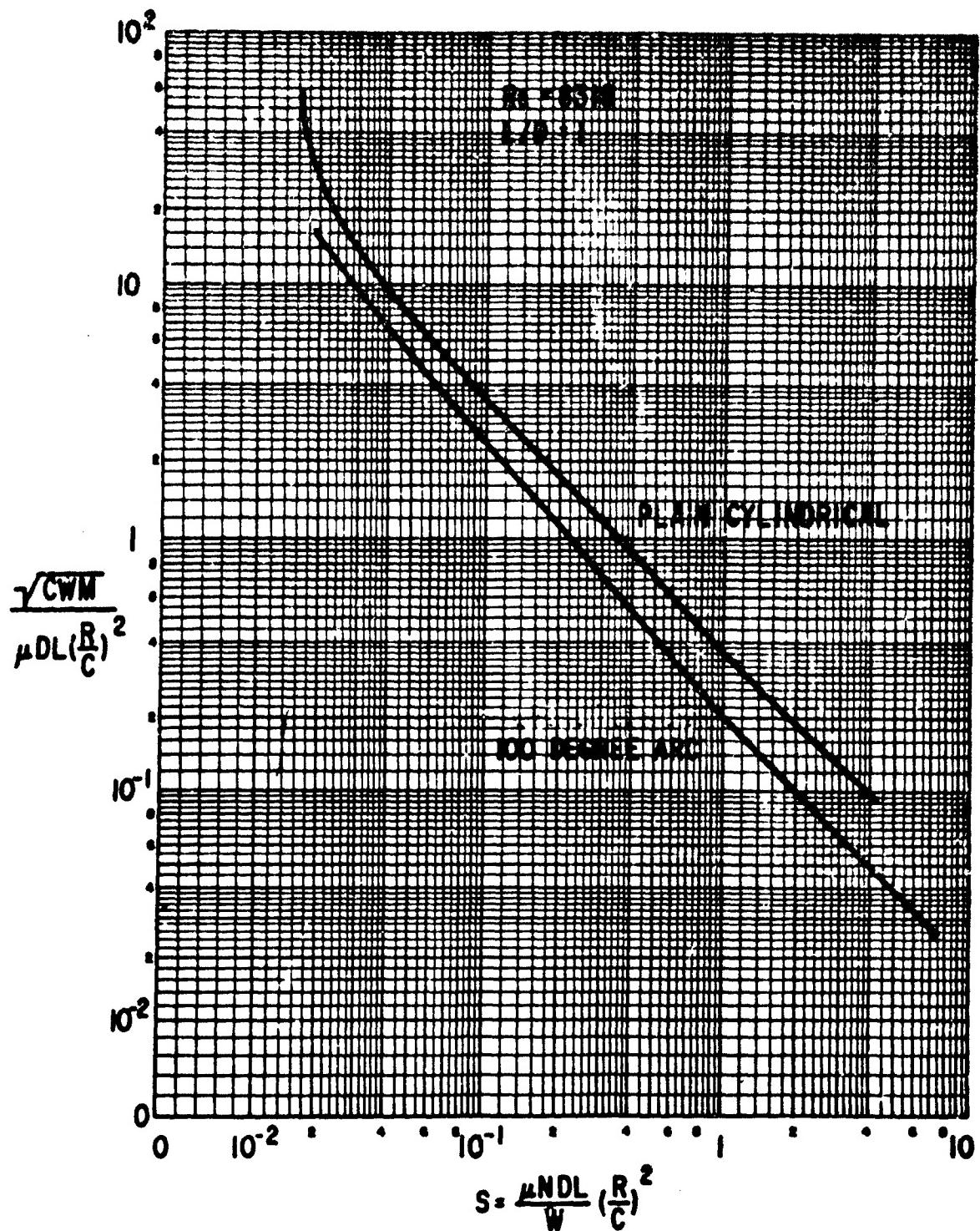


Figure C-13 The Plain Cylindrical and the 100 Degree Partial Bearing,
Turbulent Film
Critical Rotor Mass at Onset of Instability

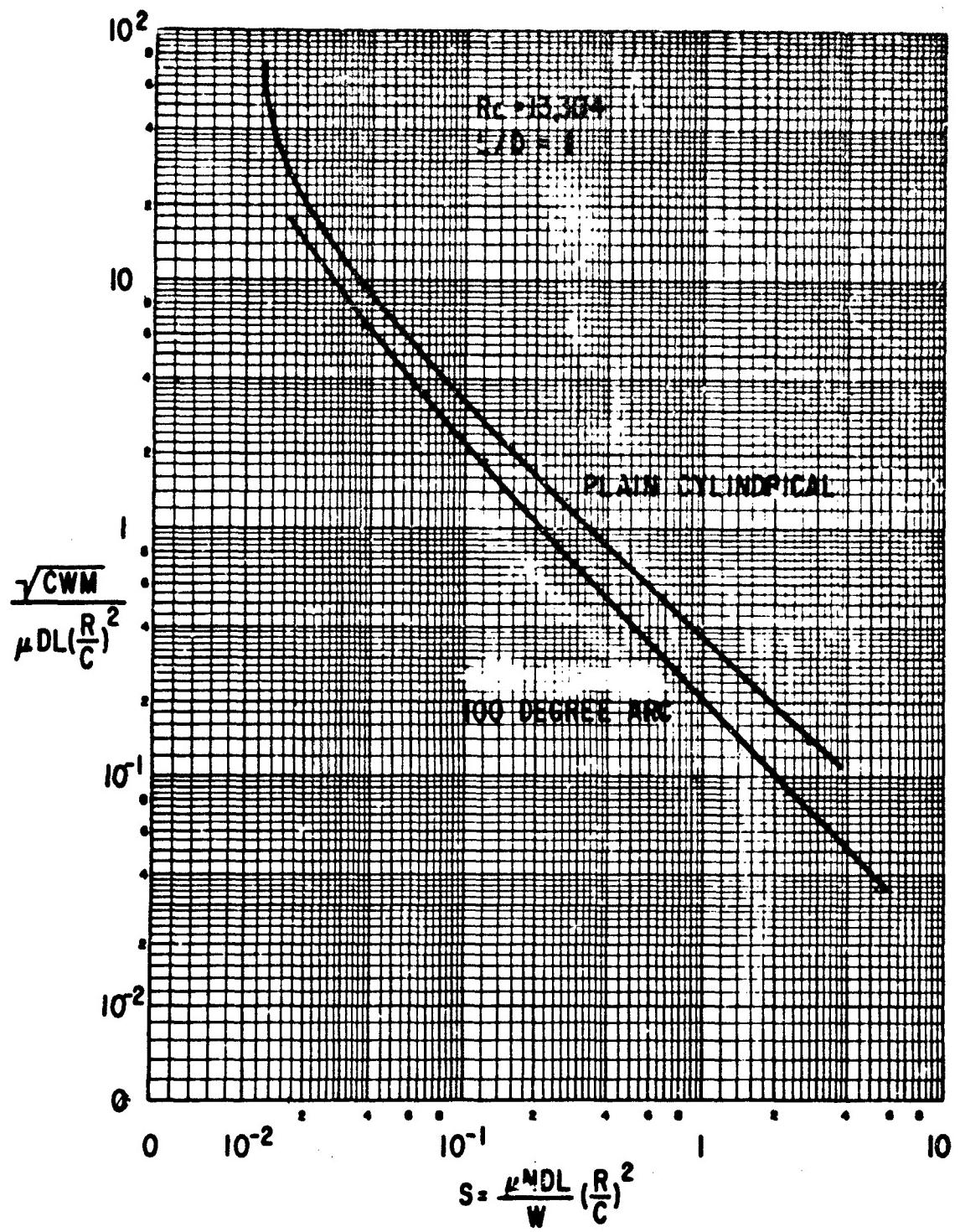
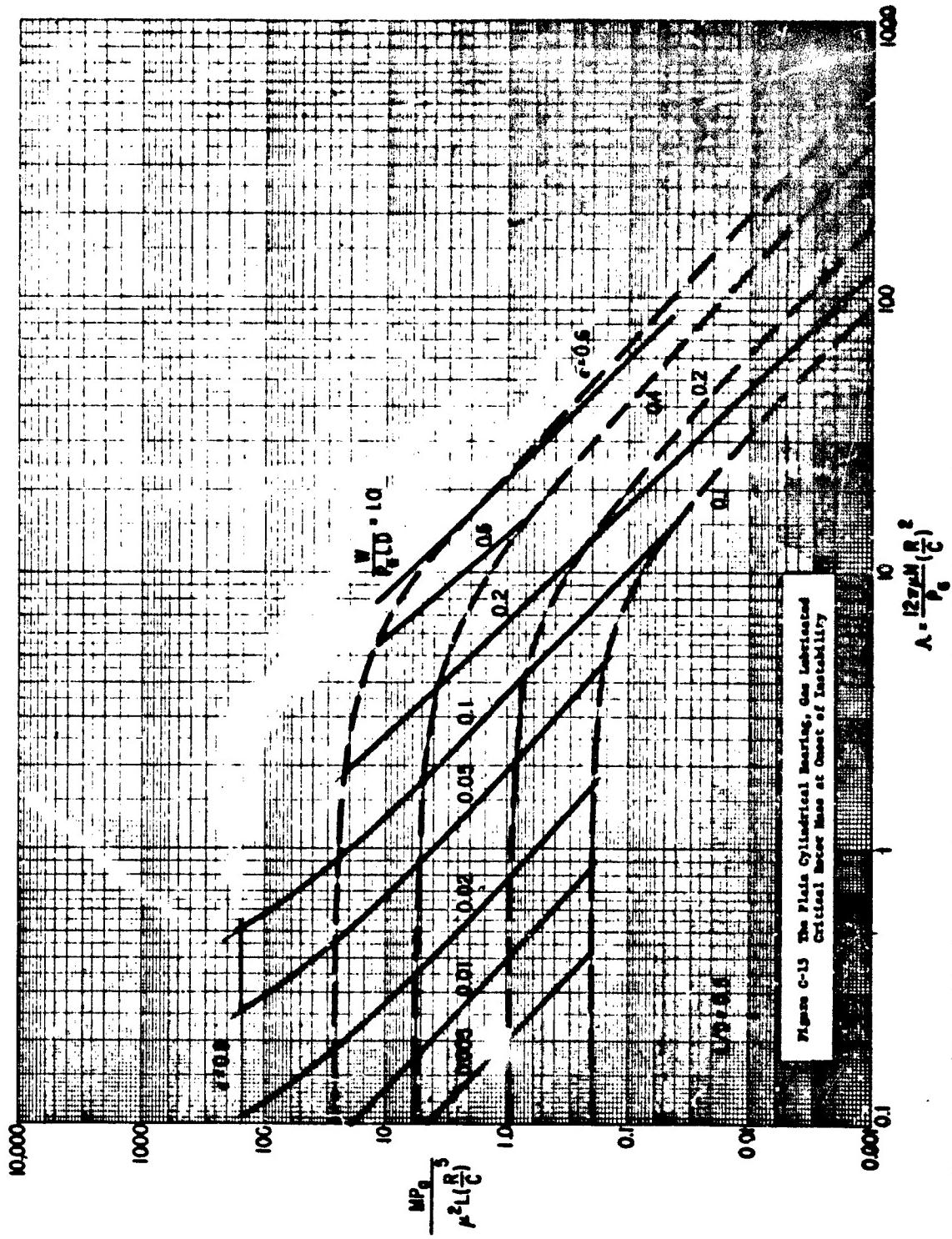
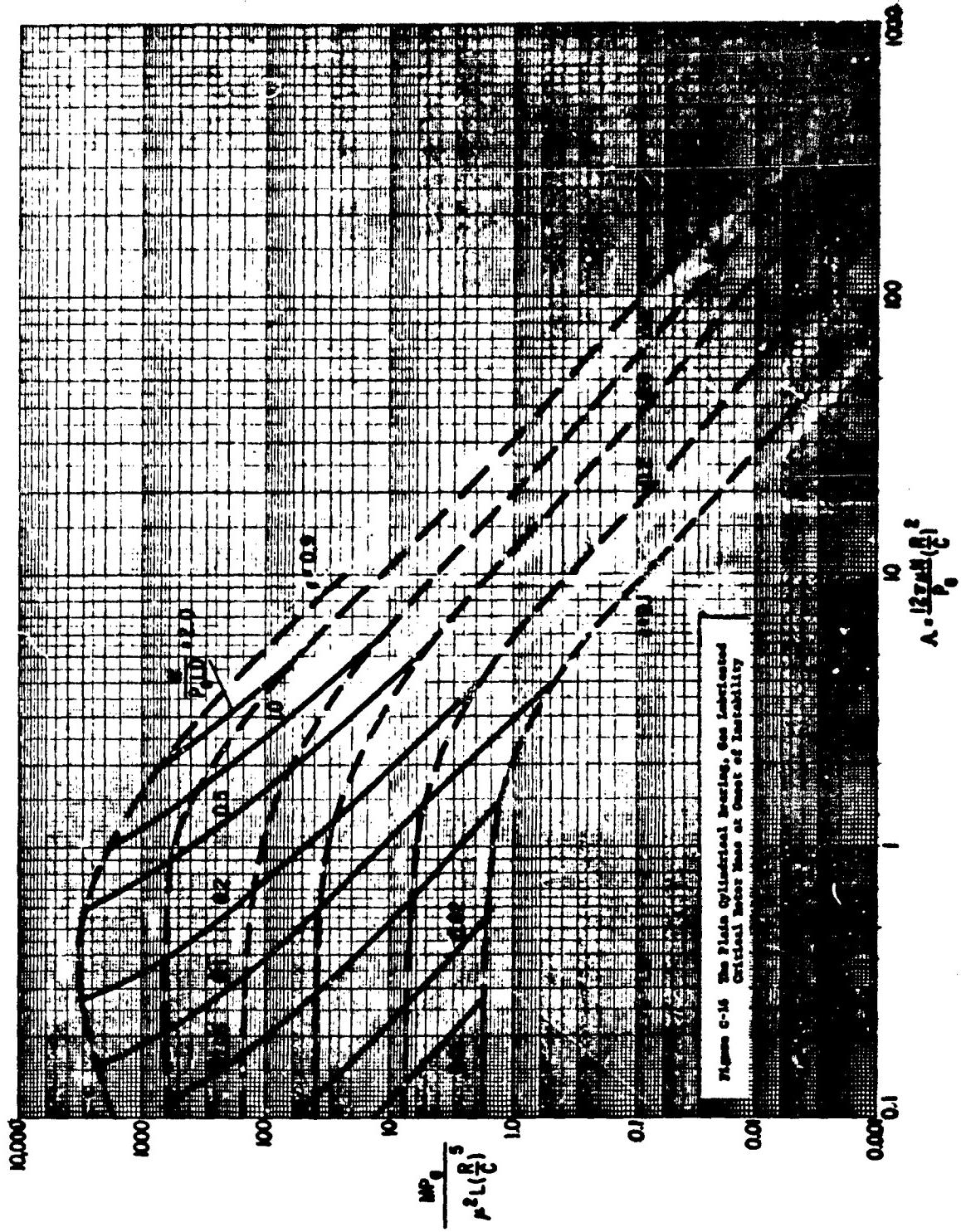
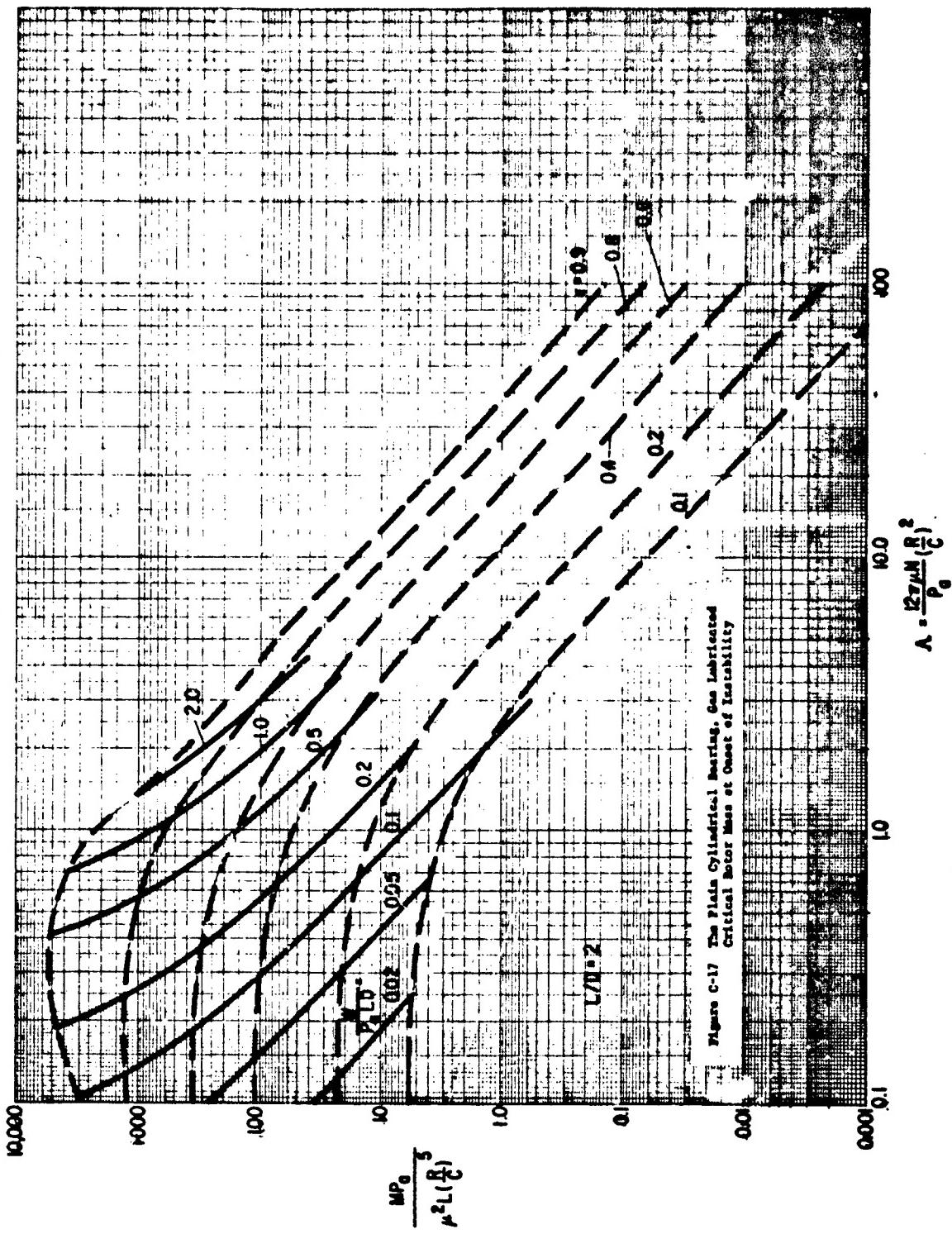


Figure C-14 The Plain Cylindrical and the 100 Degree Partial Bearing,
Turbulent Film
Critical Rotor Mass at Onset of Instability

c. Gas Lubricant, Hydrodynamic Bearings







THE CRITICAL SPEEDS AND RESPONSE OF A ROTOR-BEARING SYSTEMDiscussion

The rotor-bearing system is a dynamic system which possesses both inertia, flexibility and damping. The rotor itself is an elastic beam of variable cross-section and with a variable mass distribution. The fluid film bearings are represented by a set of 8 linear coefficients: spring and damping coefficients, and the pedestals may also be flexible and have inertia. In this way the overall system may be represented as shown in Fig. 12. A more detailed representation of the bearing coefficients is shown in Fig. 13.

The very complex system made up of the rotor, its bearings and its supporting structure possesses a large number of resonant frequencies. If any of these resonances are excited in the operating speed range large amplitudes may build up and prevent further operation of the machine. This is clearly illustrated in Fig. 2 where the amplitude of the journal in the bearings becomes very large upon encountering a resonance in the pedestal structure at approximately 24,000 RPM. Not only is this amplitude too large from a safety point of view but the resonant condition also makes it much more difficult to balance the unit.

Even though, as illustrated by the above example, other resonances may be important the most pronounced resonances are in general the critical speeds of the rotor-bearing system. They are excited by the unbalance in the rotor and the amplitude is only limited by the amount of damping present in the bearings. It is, however, evident that if the bearings have too much damping they will behave as if they were rigid and, thus, would be unable to dissipate any energy from the rotor motion. Consequently, the rotor amplitude would be very large.

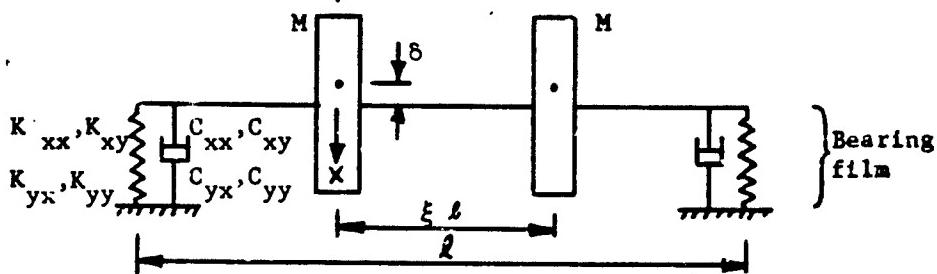
To calculate the critical speeds and the unbalance amplitude response for an arbitrary rotor configuration supported in fluid film bearings with 8 dynamic coefficients requires a computer program. In such a program the rotor itself is approximated by a number of discrete masses connected by flexible, weightless shaft sections, see Fig. 12. The shaft sections have the same stiffness as in the actual rotor and the actual mass distribution is approximated by the discrete masses. The idealized rotor can be brought to represent the actual one with

as close an accuracy as desired by choosing a large number of mass stations. The values of the bearing coefficients to be used in the calculations can be obtained from the design charts given in this report, see Fig. B-1 to B-124.

Although accurate calculations require a computer program it is still desirable to have information available from which the critical speed and the unbalance response can be estimated. Such information is especially valuable when comparing different bearing types and their influence on the performance of the rotor-bearing system. The design charts in Figs. D-1 to D-40 have been prepared for this purpose.

Use of the Design Charts

The design charts are based on a simple rotor model, namely a rotor consisting of two heavy discs on a flexible shaft and supported in two similar fluid film bearings. The rotor is symmetric about its midspan and the unbalance is introduced by letting the two masses be eccentric by a distance δ inch:



The chosen rotor model can also be used to represent a rotor with a single central mass. Hence, the results are equally valid for both rotor configurations.

The rotor stiffness is expressed by means of influence coefficients. Thus, α_{11} is the rotor deflection at the location of the first disc due to a force of 1 lb at the same location. Similarly, α_{12} is the deflection at disc no. 1 caused by 1 lbs force at the location of disc no. 2. Due to the imposed symmetry of the rotor the influence coefficient α_{22} at disc no. 2 equals α_{11} . Introduce the definitions:

$$\begin{aligned} \alpha &= \begin{cases} \alpha_{11} + \alpha_{12} & (\text{1st critical speed}) \\ \alpha_{11} - \alpha_{12} & (\text{2nd critical speed}) \end{cases} \\ &= \begin{cases} 1 & (\text{1st critical speed}) \\ \xi, \text{ see Fig. above} & (\text{2nd critical Speed}) \end{cases} \end{aligned}$$

The dimensionless design parameters used in the charts are:

$$\text{Sommerfeld number: } S = \frac{\pi N D L}{W} \left(\frac{R}{C} \right)^2$$

$$\text{Rotor flexibility parameter: } \rho = \frac{W \alpha}{\xi^2 C}$$

$$\text{Speed ratio: } \frac{\omega}{\omega_n}$$

$$\text{Normalized rotor amplitude: } \frac{x}{\delta}$$

where:

D Journal diameter, inch

R = $\frac{1}{2} D$, journal radius, inch

L Bearing length, inch

C Radial clearance, inch

N Rotor speed, RPS

M Mass of one disc lbs.sec²/in

W Bearing reaction, lbs.

x Max. whirl amplitude at location of the discs, inch

δ Eccentricity of CG of the discs, inch

$\omega = 2\pi N$, angular rotor speed, radians/sec

ω_n Critical angular speed of rotor in rigid bearings, radians/sec

The rigid bearing critical speeds can be expressed as:

$$\omega_n = \sqrt{\frac{1}{M\alpha}}$$

which gives both the first and the second critical speed (rigid bearings) dependent on the value used for α . The unbalance induced by giving the discs the eccentricity δ is such that for the first critical speed the discs are displaced in the same direction (static unbalance) and for the second critical speed the displacements are in opposite directions (dynamic unbalance).

To apply the design charts to an actual rotor-bearing system it is necessary to know the values of the rotor flexibility parameter ρ and the rigid bearing critical speeds ω_n . However, an accurate calculation of ω_n , especially for the second

critical speed, is not readily accomplished for an arbitrary rotor geometry with access to a computer program. On the other hand, if a computer program is available anyway the design charts would be of little value in investigating a particular rotor-bearing system. Instead, the purpose of the design charts is to make it possible to compare various bearing types with regard to their influence on the critical speeds and the unbalance response. Hence, for using the design charts it is not necessary to have accurate values for the rotor flexibility parameter and the critical speeds of the rigidly supported rotor. On this basis the results obtained from the charts will give relative values.

To investigate a particular rotor its total mass and mass moment of inertia about a transverse axis through the CG should be computed. Denote the total mass as M and the mass moment of inertia as I . Set:

$$\xi = \sqrt{\frac{I}{Ml^2}}$$

where:

l - Rotor span between bearings, inch

Evaluate the rotor influence coefficients α_{11} and α_{12} with respect to position on either side of the CG, i.e. position 1 at a distance $\frac{1}{2}\xi l$ to the left of the CG and position 2 at the same distance to the right of the CG. In this way α becomes known and together with the values of M and ξ found previously the necessary information is available to compute ρ and ω_n .

Since the fluid film bearings are represented by 8 dynamic coefficients the effective bearing stiffness in the horizontal direction differs from the effective stiffness in the vertical direction. Hence, there will be two relative resonances associated with each critical speed of the rotor-bearing system. At each of t

two resonances the whirl amplitude of the rotor has a relative maximum. The lowest resonance is denoted as "Minor" and the highest resonance is denoted as "Major" on the design charts. Which of the two resonances is actually the most pronounced can be found from the design charts, Figs. D-21 to D-40. However, the speed range between the minor and the major resonances should in general be expected to yield relatively large whirl amplitudes such that in the actual application the system critical speeds will appear as broad amplitude peaks.

The design charts are arranged in two groups: Figs. D-1 to D-20 giving the critical speeds and Figs. D-21 to D-40 giving the corresponding amplitudes. Each chart covers a wide variation in the rotor flexibility parameter ρ and for each value of ρ there are two curves labeled "Minor" and "Major" as explained above. The abscissa for the curves is the Sommerfeld number S defined previously.

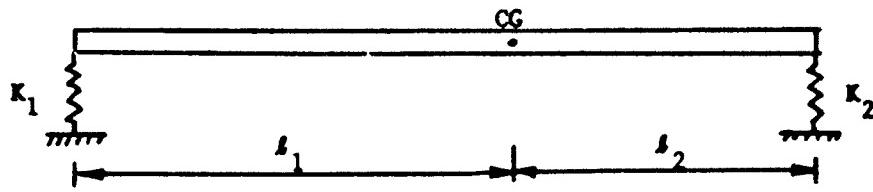
In Figs. D-1 to D-20 the ordinate gives the value of the speed ratio $\frac{\omega}{\omega_n}$ at the minor and major resonances associated with the critical speeds. The charts apply to both the first and the second critical speeds but such that the value of α and, hence, the values of ρ and ω_n are different depending which critical speed is investigated. When ρ and ω_n are computed the critical speed resonances can be determined as the intersections between the appropriate design curves and the function:

$$\frac{\omega}{\omega_n} = \frac{2\pi \cdot W}{\mu DL\omega_n \left(\frac{R}{C}\right)^2} \cdot S$$

The two corresponding values of the Sommerfeld number can be used directly to enter the proper design charts of Figs. D-21 to D-40 and read off the normalized rotor amplitude $\frac{x}{S}$. x is the rotor amplitude as shown in the Fig. on Page 231. Since in an actual application the unbalance is not known (i.e. the magnitude of S is unknown) the ratio $\frac{x}{S}$ should be considered as an amplification factor which indicates the rotors sensitivity to unbalance. When ρ and ω_n correspond to the first critical speed the applied unbalance is a static unbalance whereas for the second critical speed the unbalance is a dynamic unbalance.

When the rotor is very stiff (i.e. $\rho = 0$), which is usually the case in gas bearing machinery, the two first critical speeds (the rigid body modes, see Page 14)

can be calculated from the equation:



$$\omega_n = \sqrt{\frac{1}{2} (\omega_c^2 + \omega_t^2) \mp \sqrt{\frac{1}{4}(\omega_c^2 - \omega_t^2)^2 + \omega_{ct}^4}} \quad \text{radians/sec}$$

where:

$$\omega_t^2 = \frac{K_1 + K_2}{M_t} \quad \text{radians}^2/\text{sec}^2$$

$$\omega_c^2 = \frac{K_1 l_1^2 + K_2 l_2^2}{(I - I_p)} \quad \text{radians}^2/\text{sec}^2$$

$$\omega_{ct}^4 = \frac{(-K_1 l_1 + K_2 l_2)^2}{M_t (I - I_p)} \quad \text{radians}^4/\text{sec}^4$$

and:

K_1, K_2 Bearing stiffness, lbs/in

l_1, l_2 Distances from bearings to CG of rotor, inch

M_t Total mass of rotor, lbs.sec²/in

I Transverse rotor mass moment of inertia around CG, lbs.in.sec²

I_p Polar rotor mass moment of inertia, lbs.in.sec²

(see: Timoshenko: "Vibration Problems in Engineering", D. Van Nostrand Co.N.Y)

When the supporting bearings are hydrostatic gas bearings the bearing stiffnesses K_1 and K_2 can be found directly from Figs. B-110 to B-122. For hydrodynamic gas bearings and hydrodynamic bearings in general the 8 dynamic coefficients can be determined from Figs. B-1 to B-109. The corresponding bearing stiffness to be used with the above equation can either be taken in the approximate form:

$$K \approx \frac{1}{2} (K_{xx} + K_{yy})$$

or, if both the minor and the major resonances are desired:

for the minor resonance: $K \approx K_{yy}$

for the major resonance: $K \approx K_{xx}$

A more exact equation can be expressed as:

$$K = \frac{1}{2} (K_{xx} + K_{yy}) \pm \frac{\frac{1}{4}(K_{xx} - K_{yy})(\omega C_{xx} - \omega C_{yy}) + \frac{1}{2}(K_{xy}\omega C_{yx} + K_{yx}\omega C_{xy})}{A}$$

(minus corresponds to the minor resonance, plus to the major resonance)

where A is the positive, real solution of:

$$\Lambda^4 + \left[\frac{1}{4}(K_{xx} - K_{yy})^2 + K_{xy}K_{yx} - \frac{1}{4}(\omega C_{xx} - \omega C_{yy})^2 - \omega C_{xy}\omega C_{yx} \right] \Lambda^2$$

$$- \left[\frac{1}{4}(K_{xx} - K_{yy})(\omega C_{xx} - \omega C_{yy}) + \frac{1}{2}(K_{xy}\omega C_{yx} + K_{yx}\omega C_{xy}) \right]^2 = 0$$

DESIGN CHARTS FOR
CRITICAL SPEEDS AND RESPONSE OF A MOTOR-BEARING SYSTEM

a. Critical Speeds

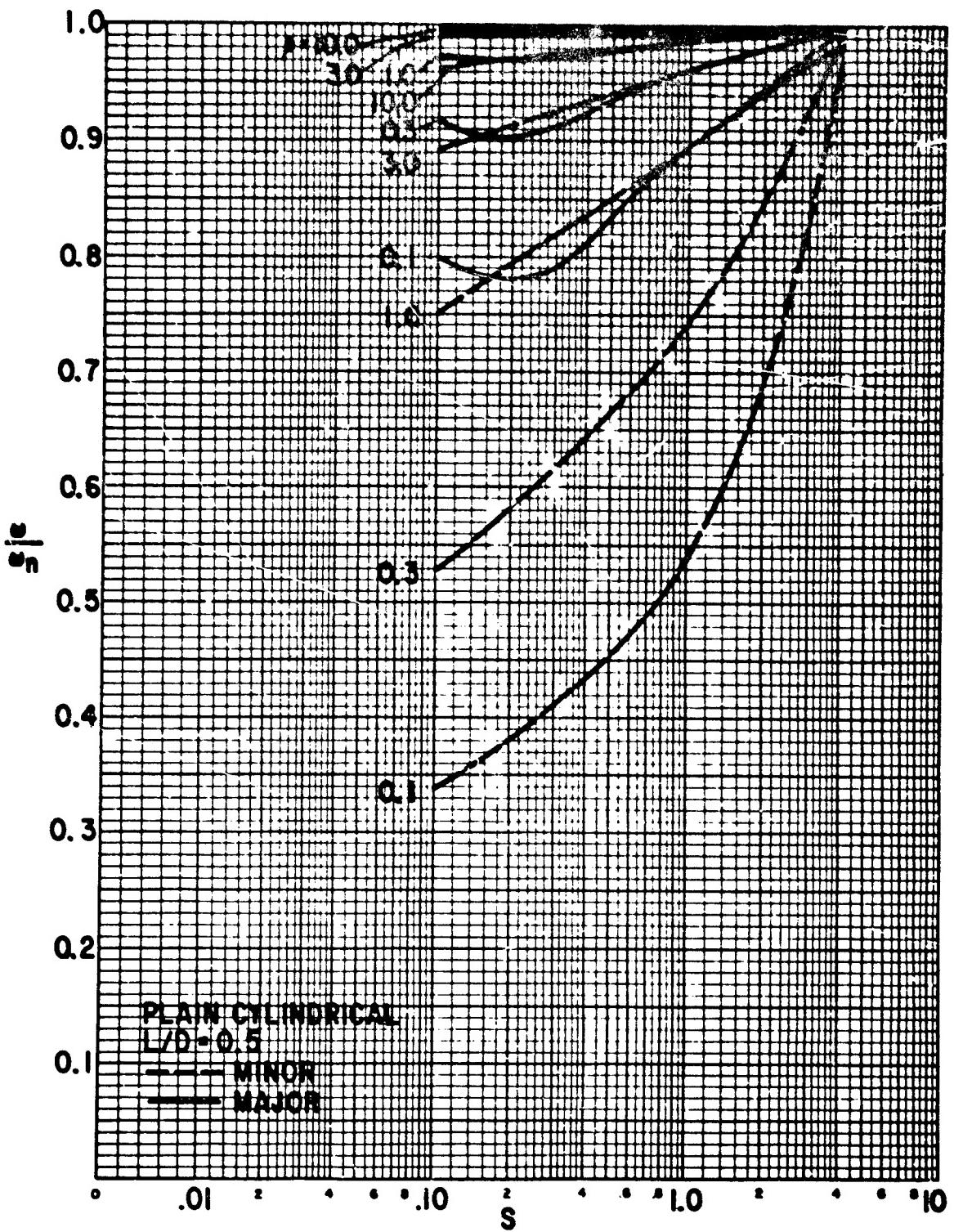


Figure D-1 Critical Speeds of Rotor-Bearing System
Plain Cylindrical Bearings, $L/D = .5$, Laminar Film

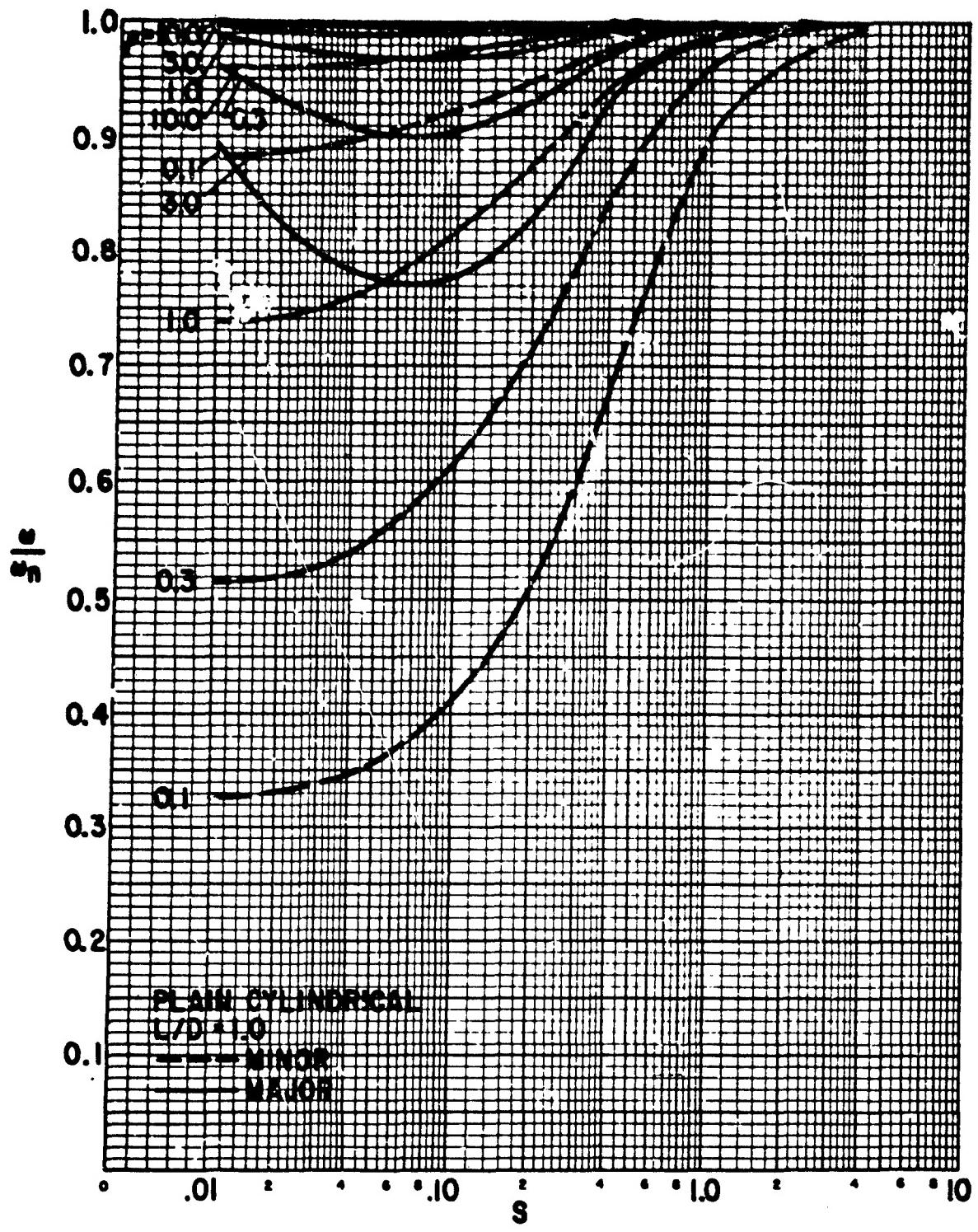


Figure D-2 Critical Speeds of Rotor-Bearing System
Plain Cylindrical Bearings, L/D = 1, Laminar Film

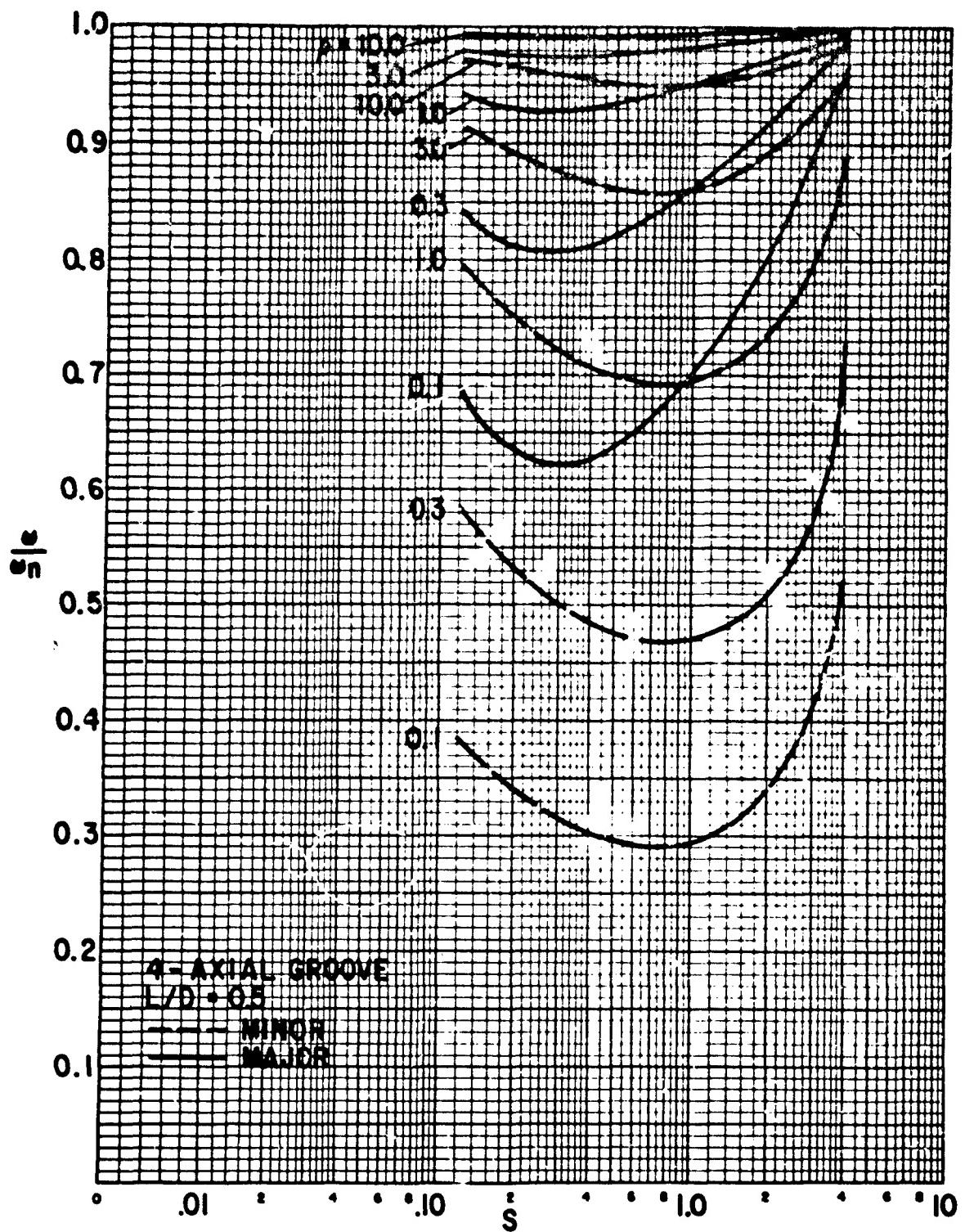


Figure D-3 Critical Speeds of Rotor-Bearing System
 4-Axial Groove Bearings, $L/D = .5$, Laminar Film
 241

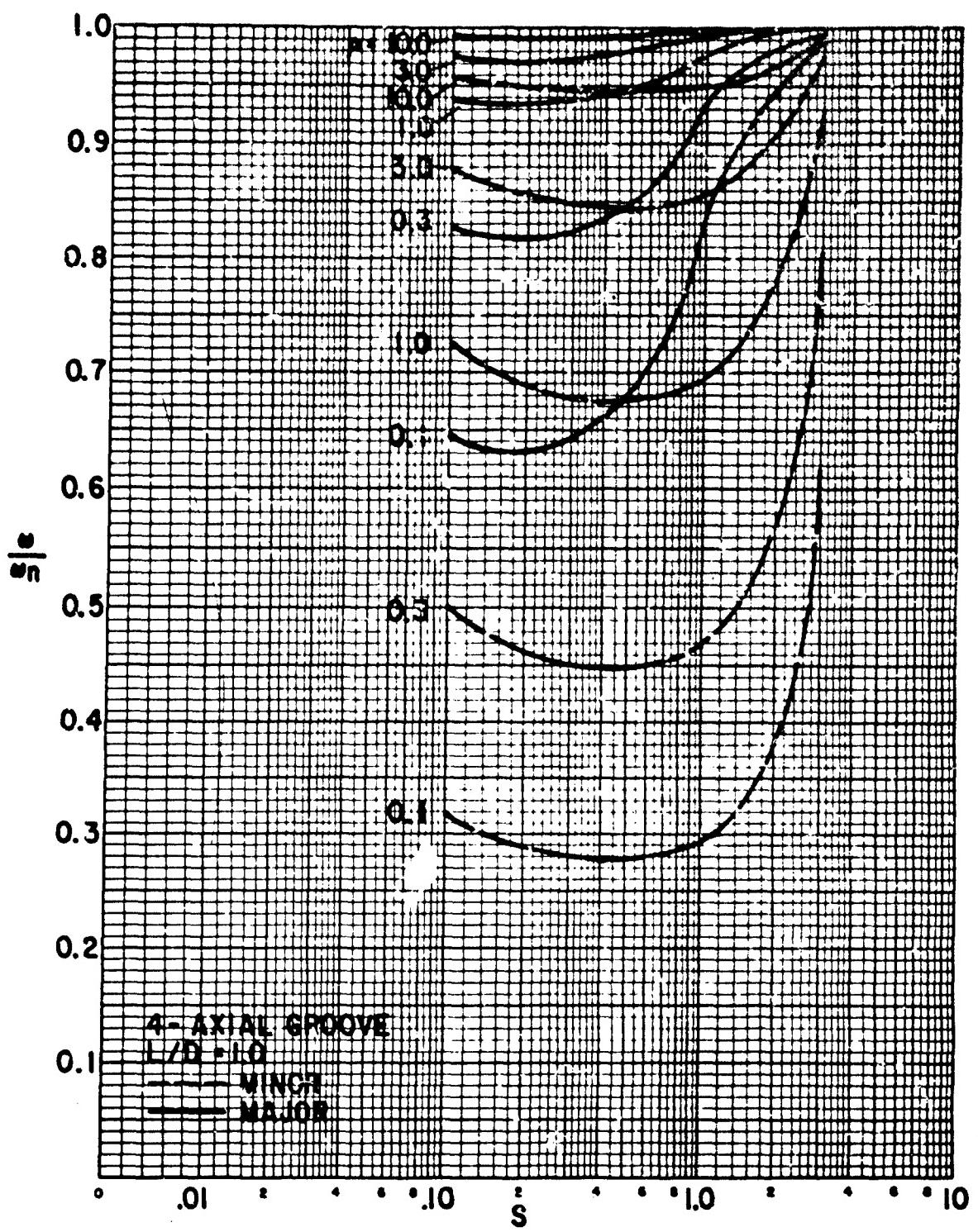


Figure D-4 Critical Speeds of Rotor-Bearing System
4-Axial Groove Bearings, $L/D = 1$, Laminar Film

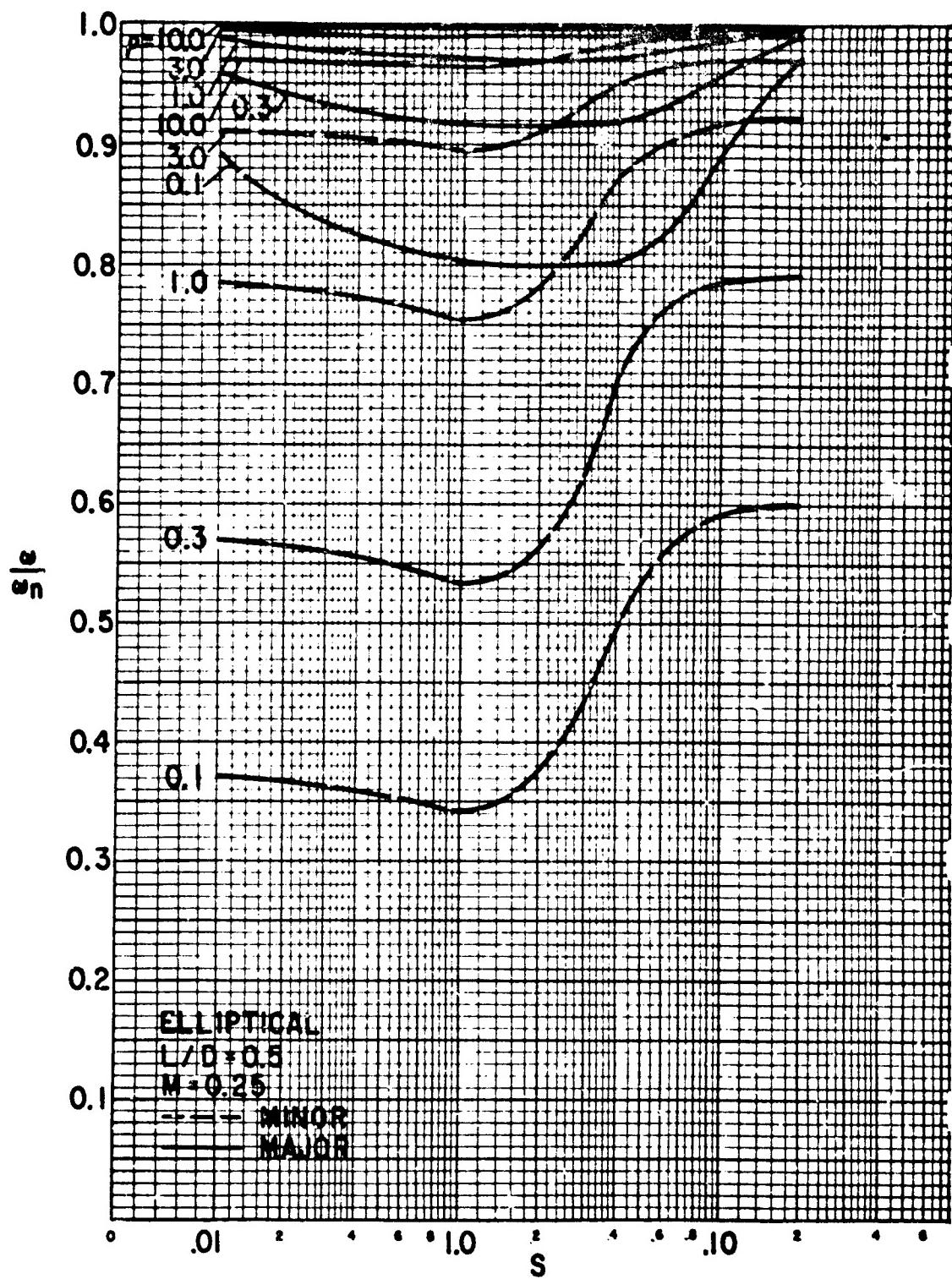


Figure D-5 Critical Speeds of Rotor-Bearing System
 Elliptical Bearings, $L/D = .5$, $m = .25$, Laminar Film
 243

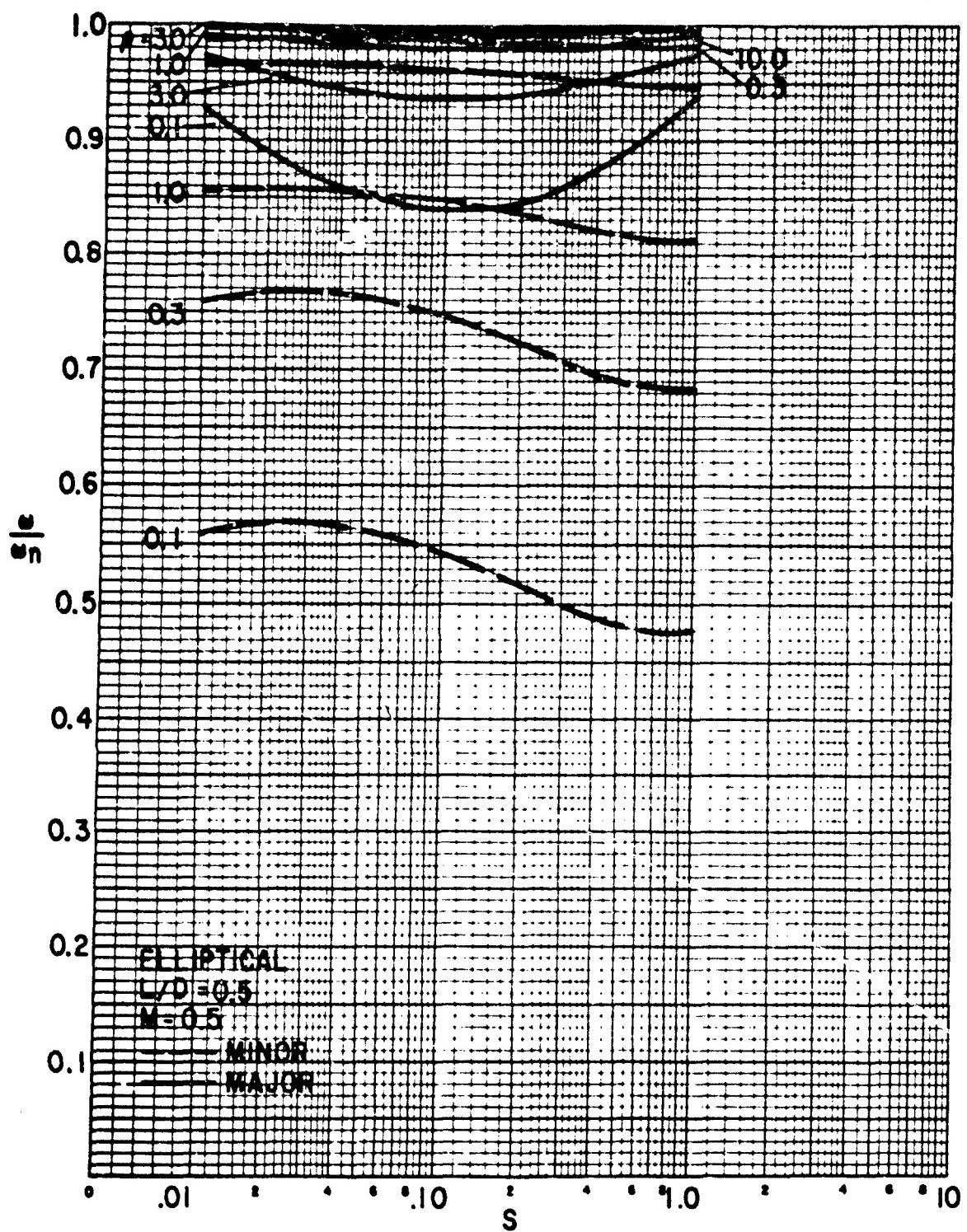


Figure D-6 Critical Speeds of Rotor-Bearing System
 Elliptical Bearings, $L/D = .5$, $m = .5$, Laminar Film

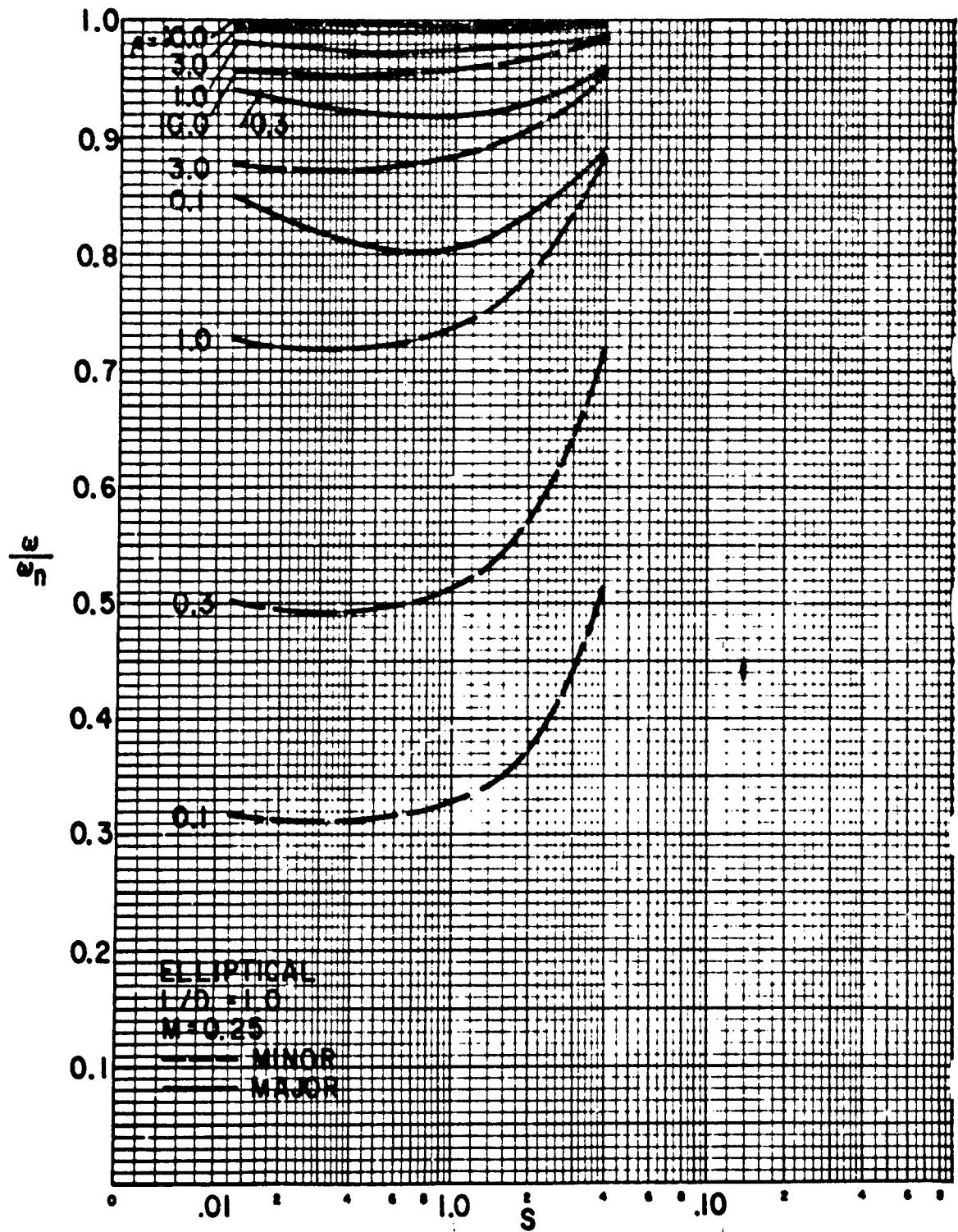


Figure D-7 Critical Speeds of Rotor-Bearing System
Elliptical Bearings, $L/D = 1$, $m = .25$, Laminar Film

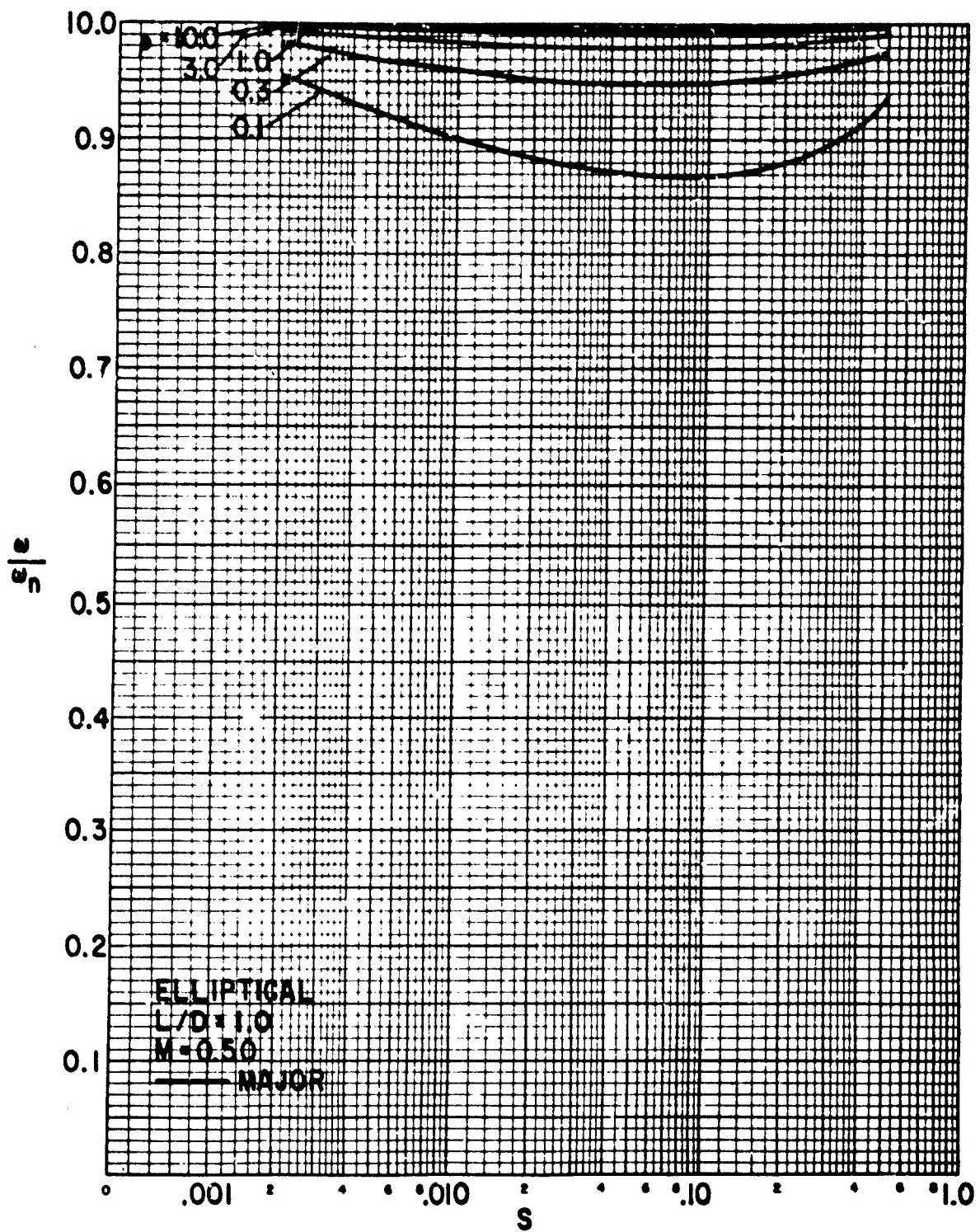


Figure D-8 Critical Speeds of Rotor-Bearing System
 Elliptical Bearings, $L/D = 1$, $m = .5$, Laminar Film

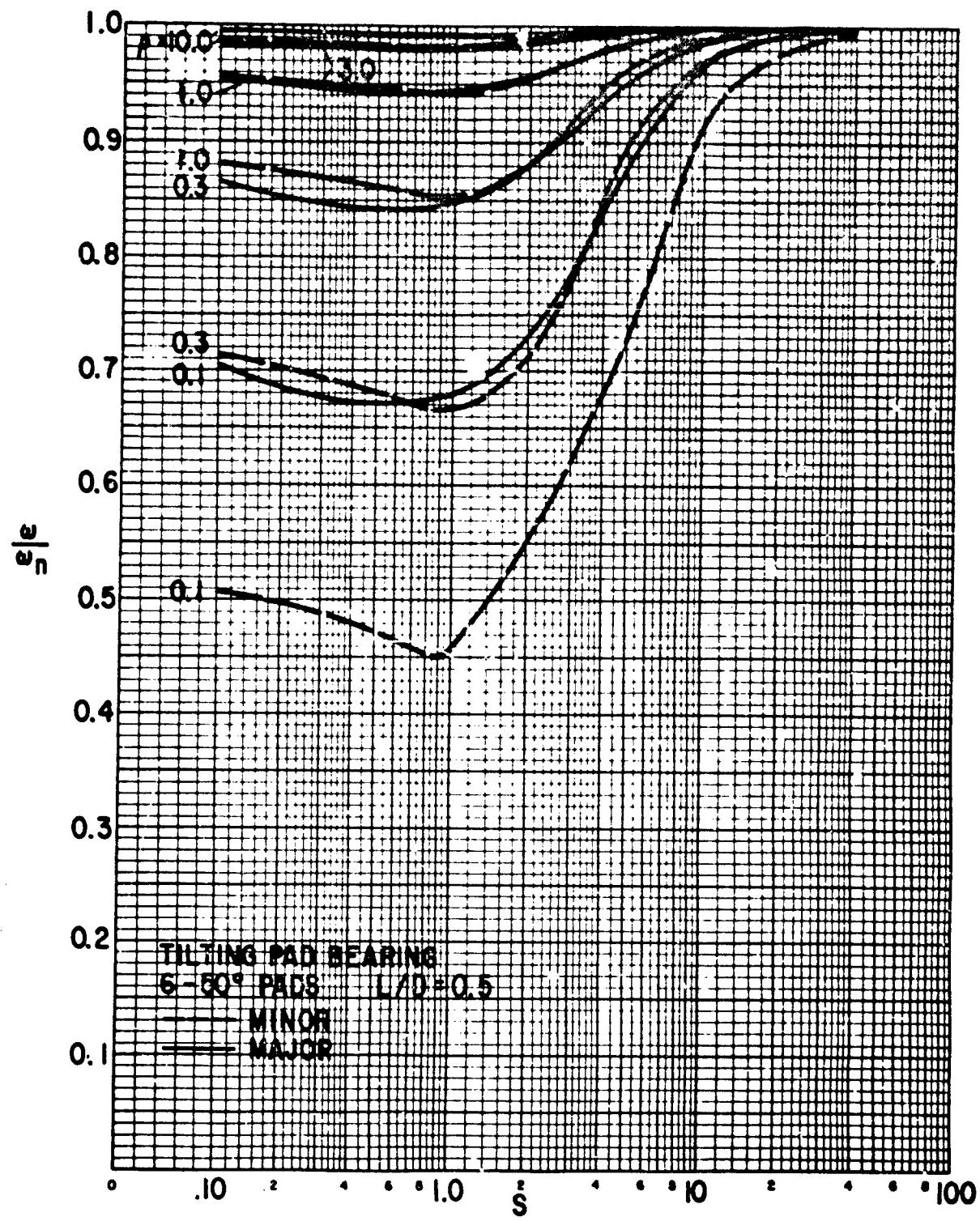


Figure D-9 Critical Speeds of Rotor-Bearing System
 6 Shoe Tilting Pad Bearings, $L/D = .5$, Load between Pads

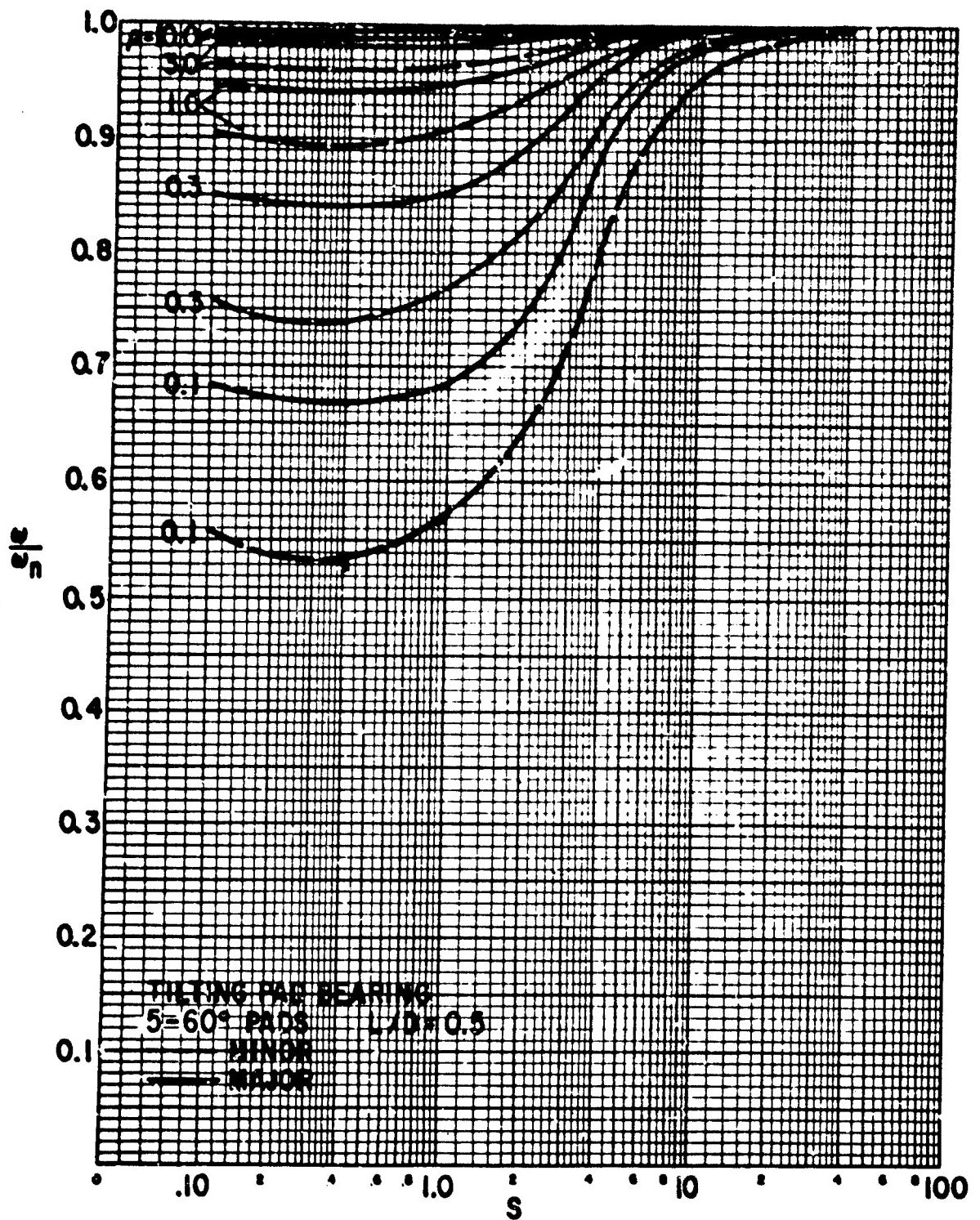


Figure D-10 Critical Speeds of Rotor-Bearing System
 5 Shoe Tilting Pad Bearings, $L/D = .5$, Load between Pads

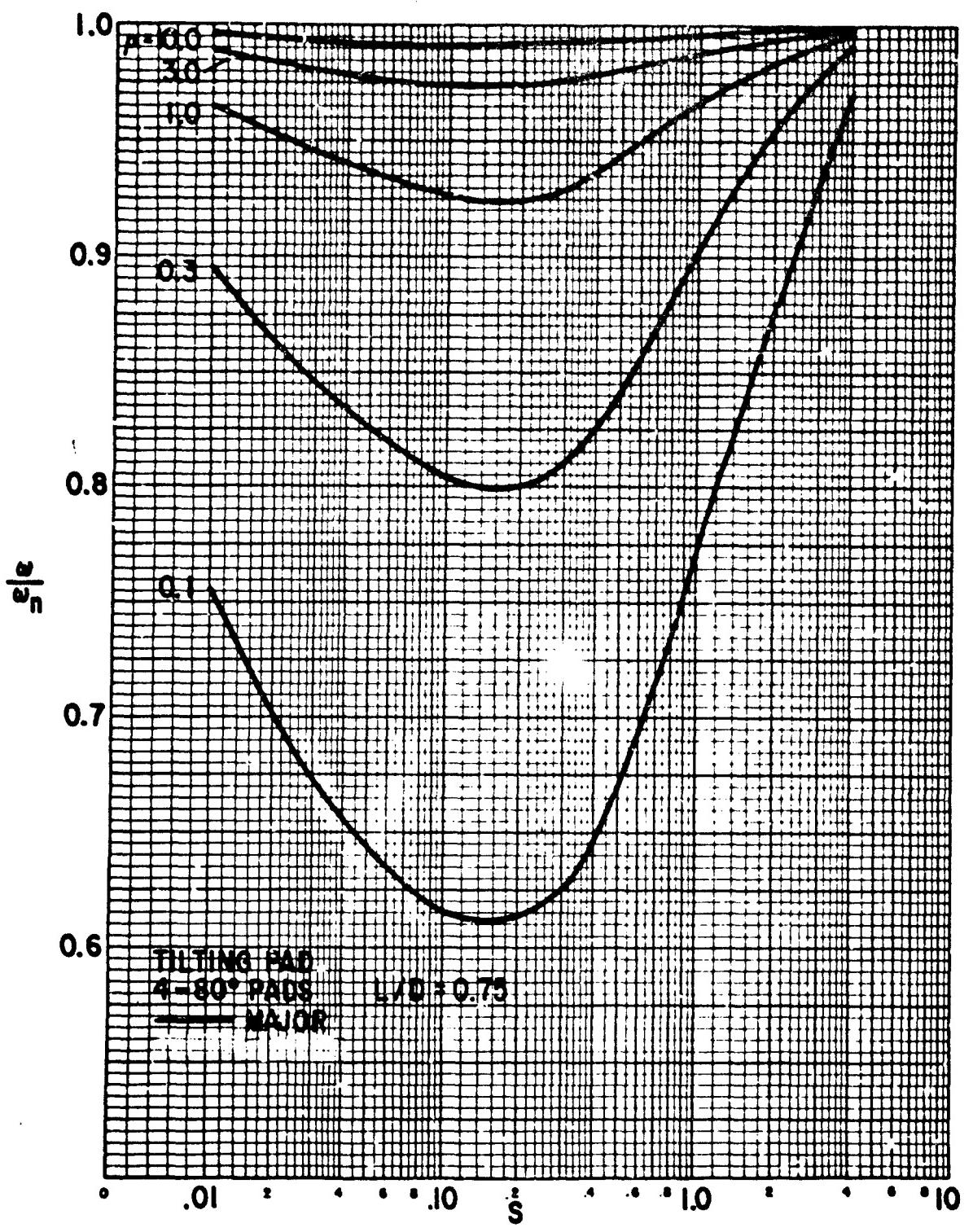


Figure D-11 Critical Speeds of Rotor-Bearing System
 4 Shoe Tilting Pad Bearings, $L/D = .75$, Load between Pads

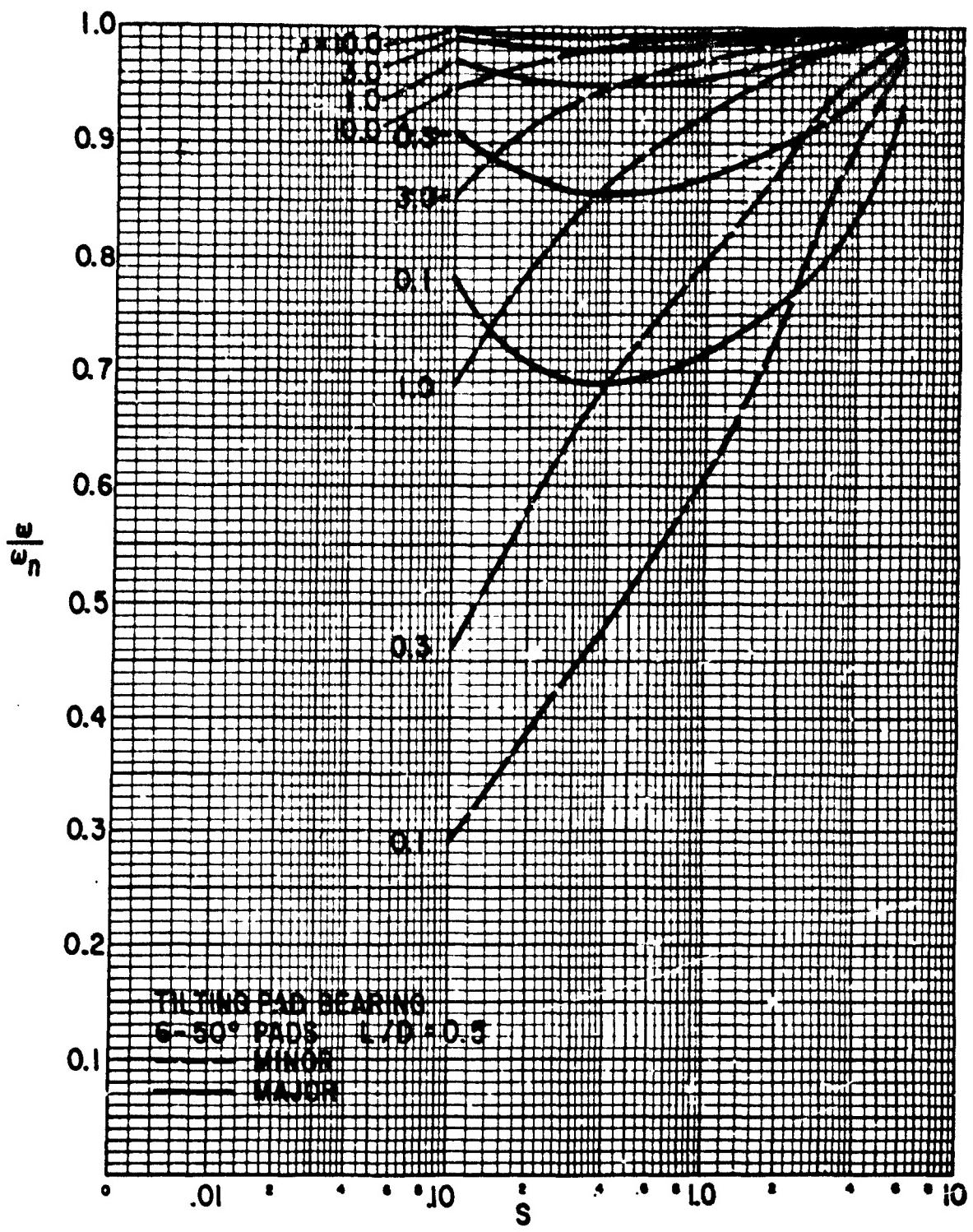


Figure D-12 Critical Speeds of Rotor-Bearing System
6 Shoe Tilting Pad Bearings, $L/D = .5$, Load on Pad

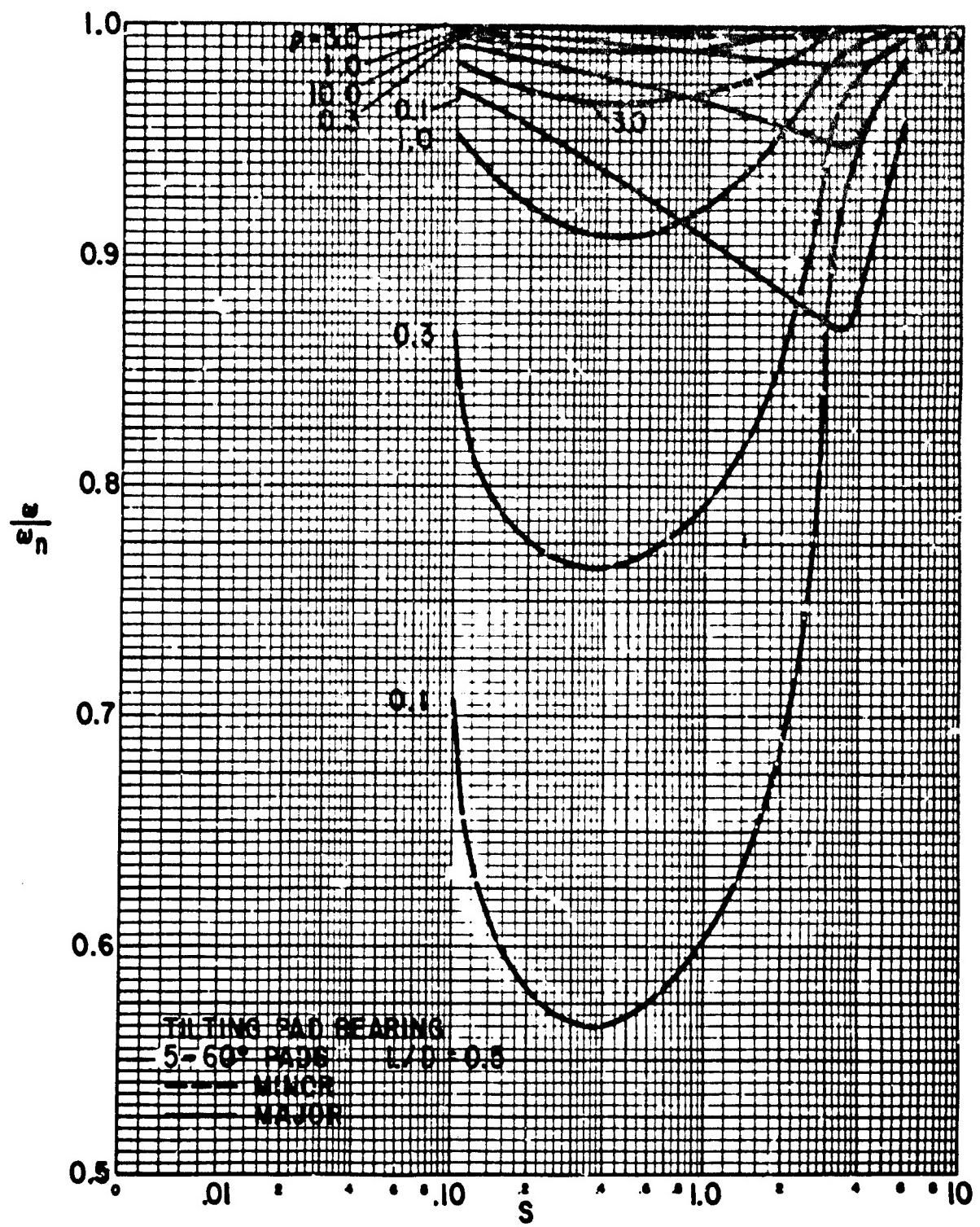


Figure D-13 Critical Speeds of Rotor-Bearing System
5 Shoe Tilting Pad Bearings, $L/D = .5$, Load on Pad

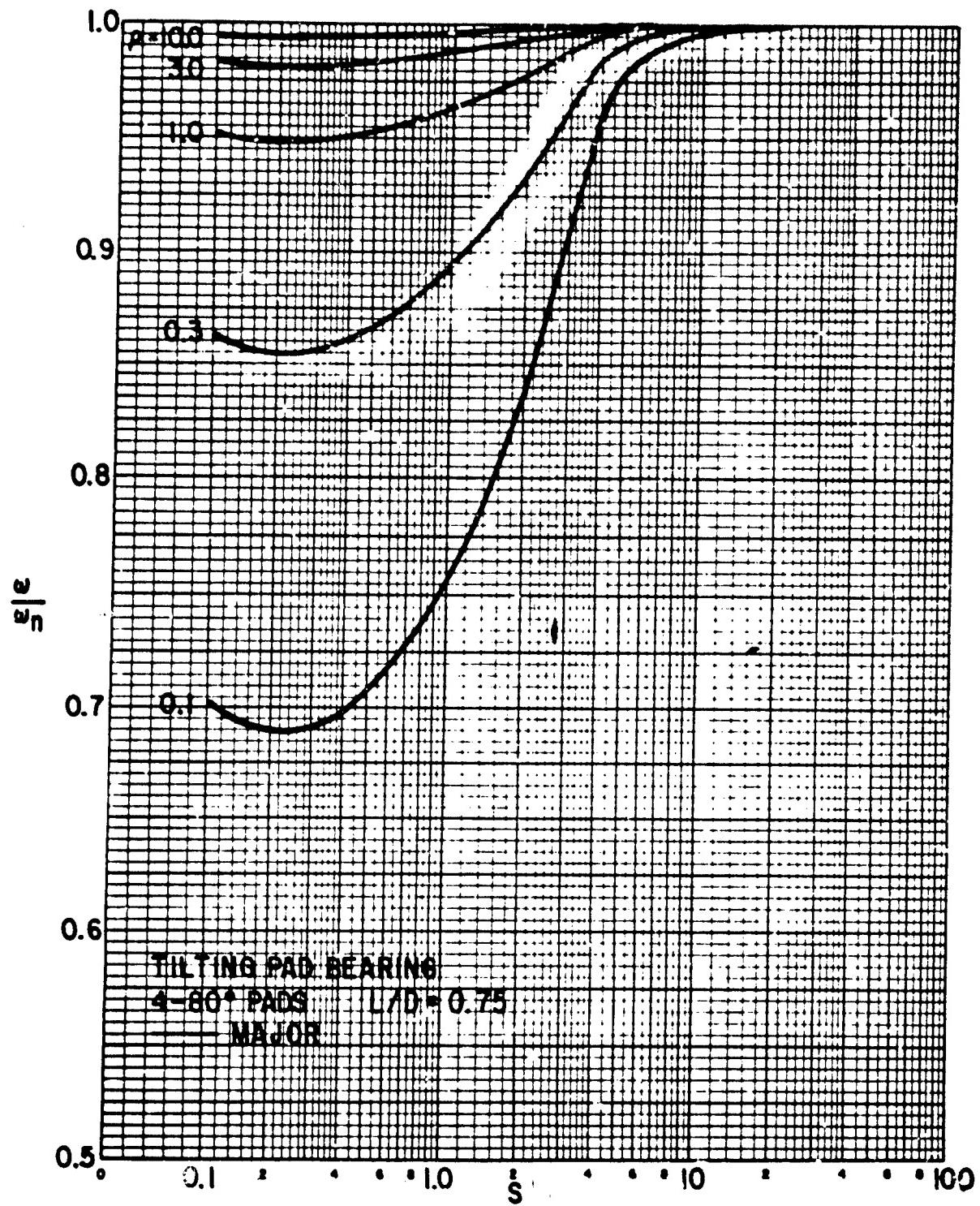


Figure D-14 Critical Speeds of Motor-Bearing System
 4 Shoe Tilting Pad Bearings, $L/D = .75$, Load on Pad

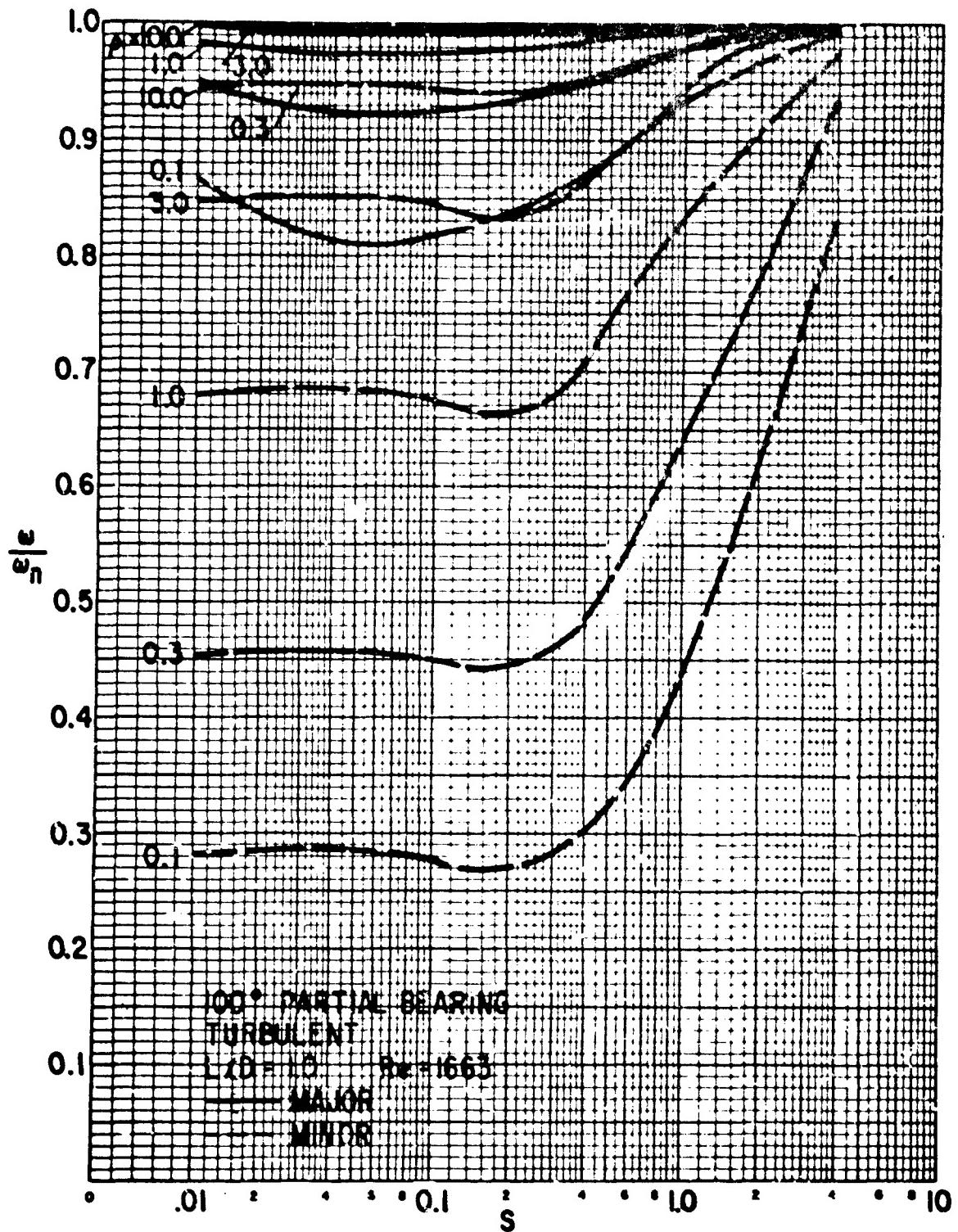


Figure D-15 Critical Speeds of Rotor-Bearing System
100 Degree Partial Bearings, $L/D = 1$, Turbulent Film

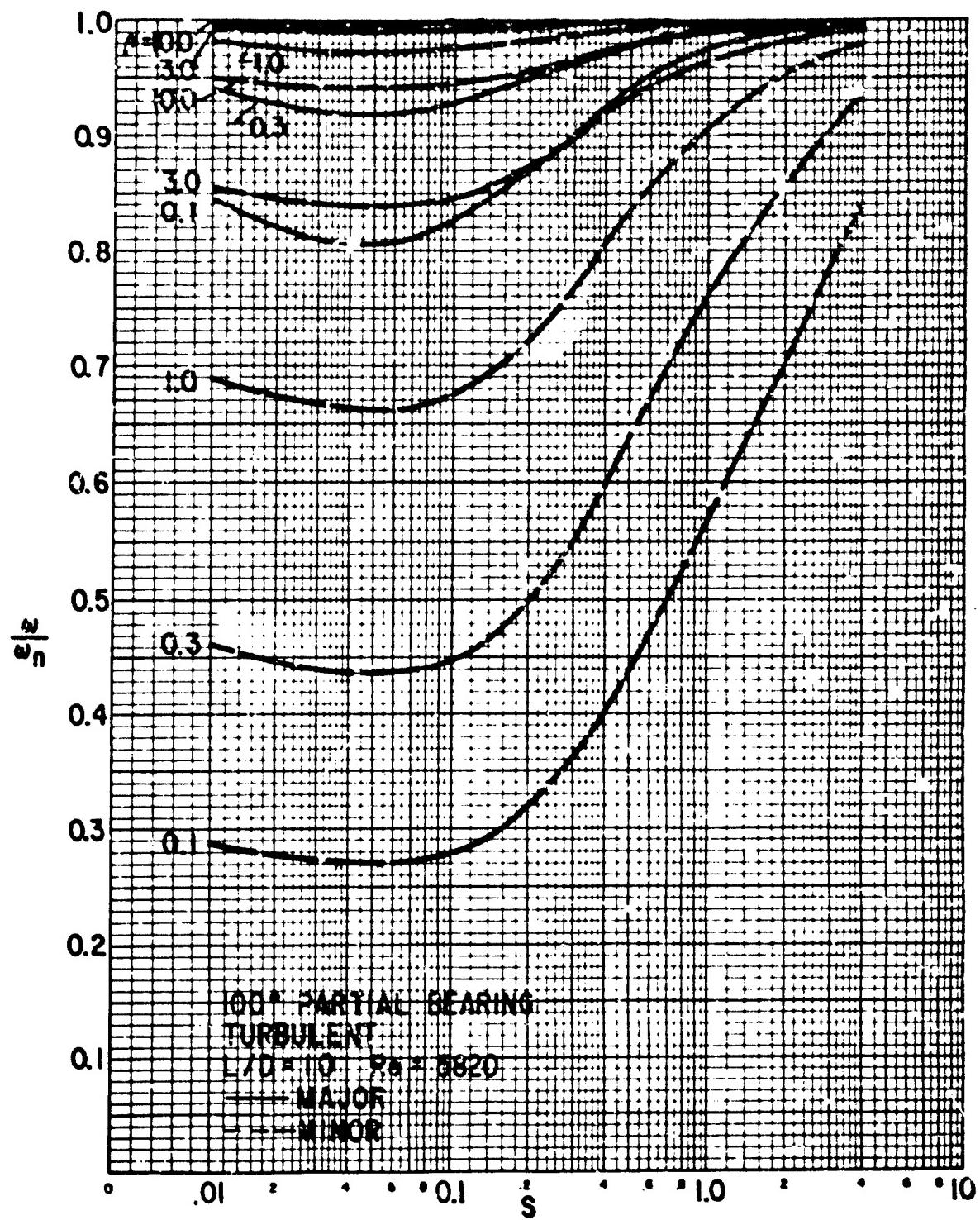


Figure D-16 Critical Speeds of Rotor-Bearing System
 100 Degree Partial Bearings, $L/D=1$, Turbulent Film

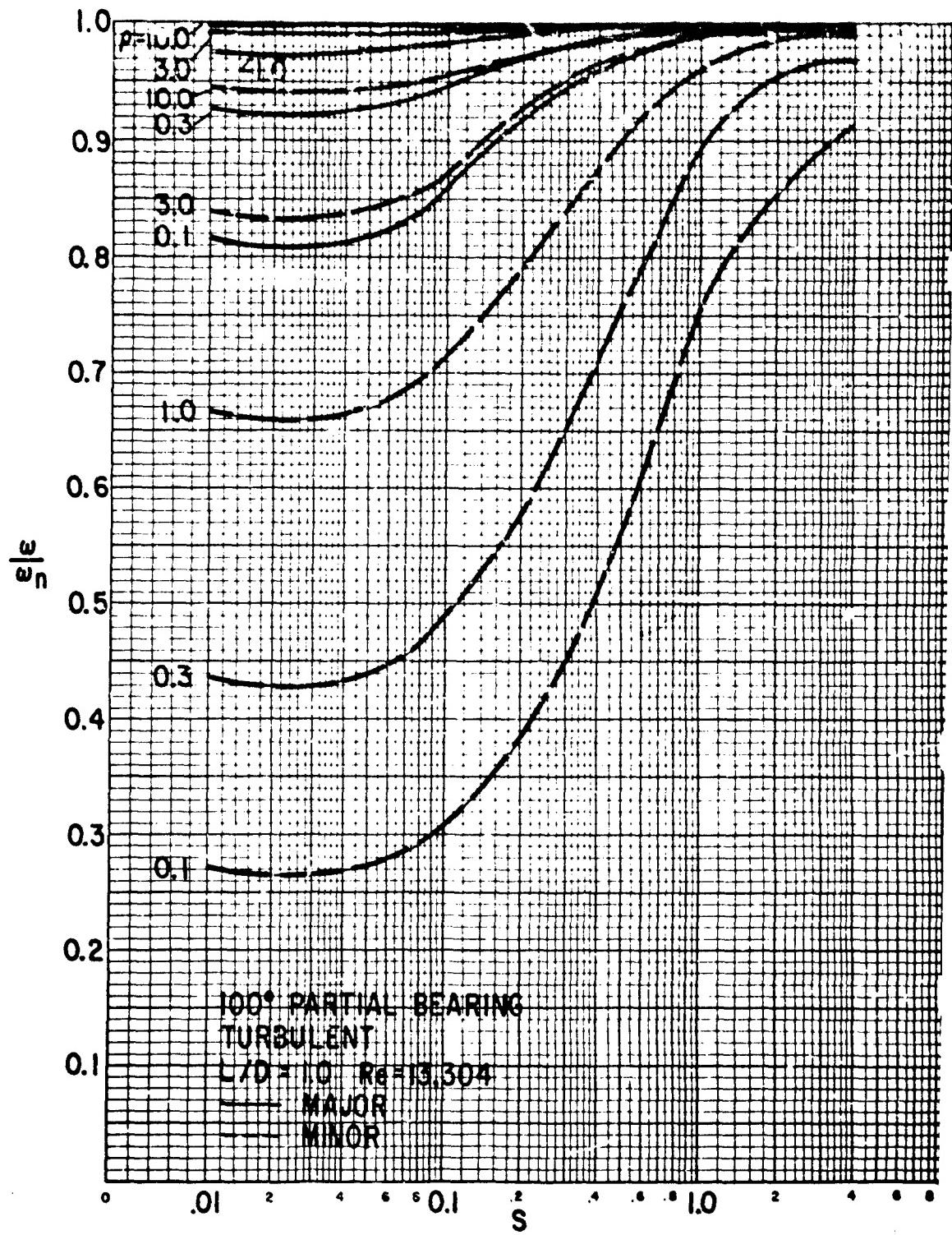


Figure D-17 Critical Speeds of Rotor-Bearing System
 100 Degree Partial Bearings, $L/D=1$, Turbulent Film

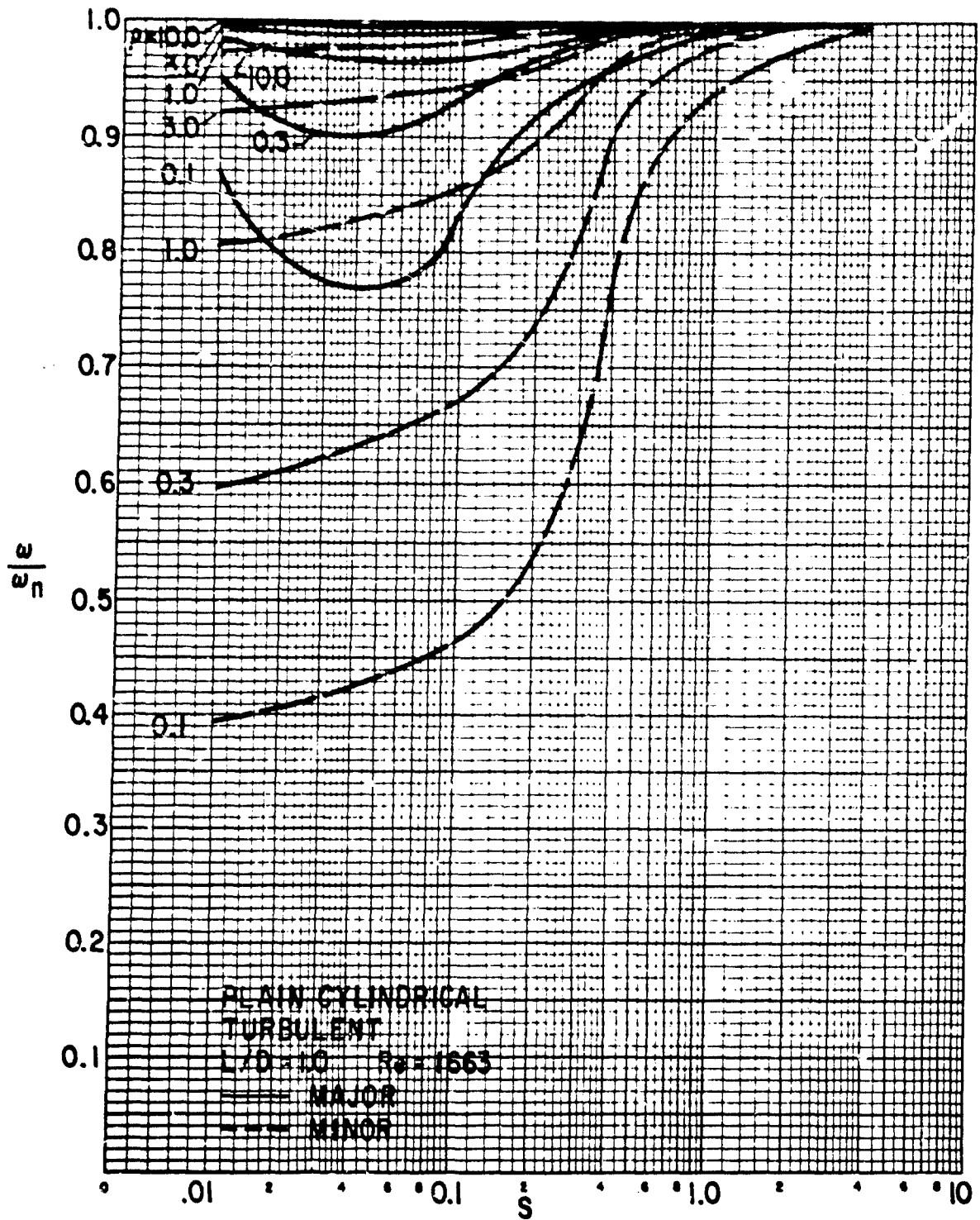


Figure D-18 Critical Speeds of Rotor-Bearing System
 Plain Cylindrical Bearings, $L/D = 1$, Turbulent Film

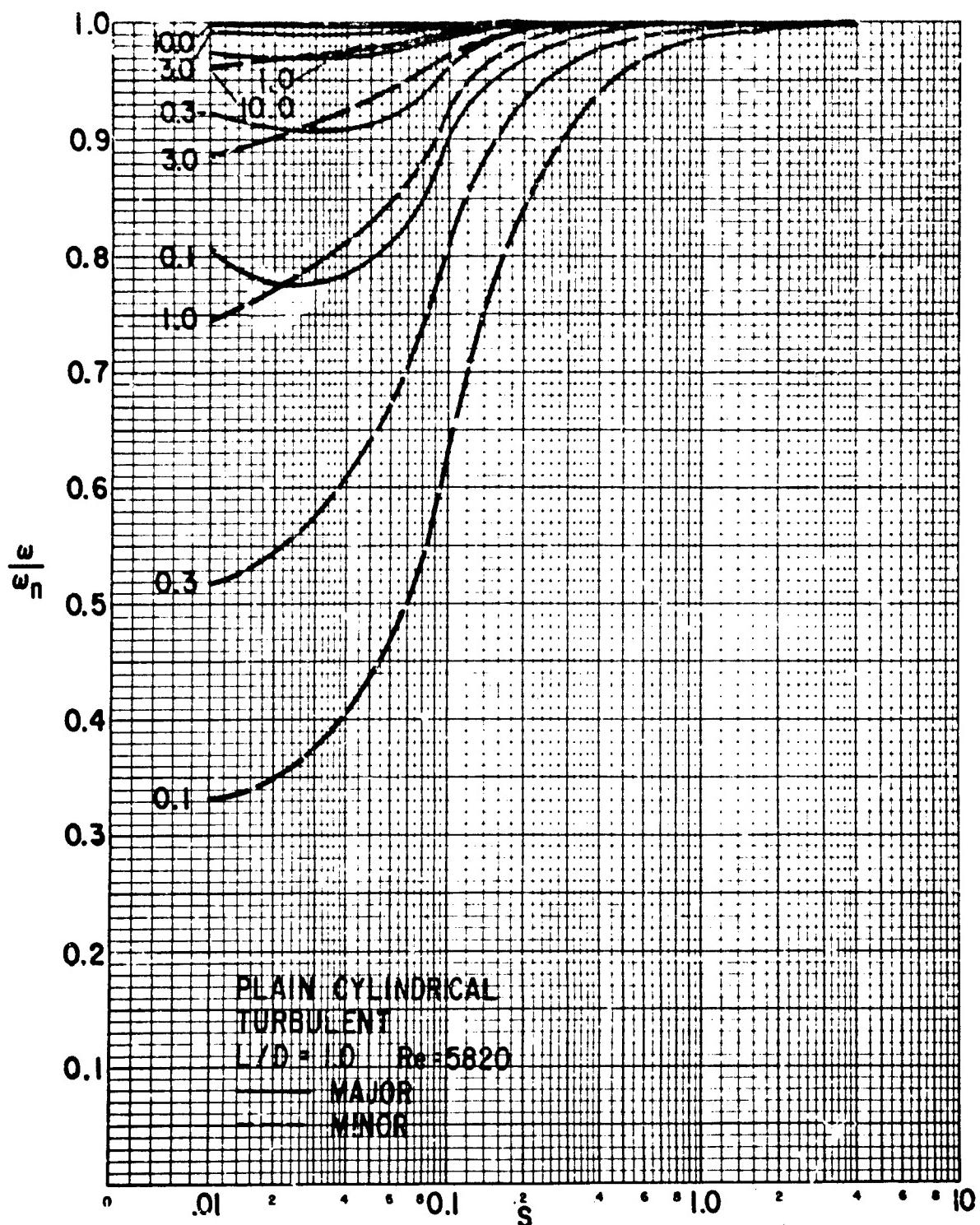


Figure D-19 Critical Speeds of Rotor-Bearing System
 Plain Cylindrical Bearings, $L/D = 1$, Turbulent Film

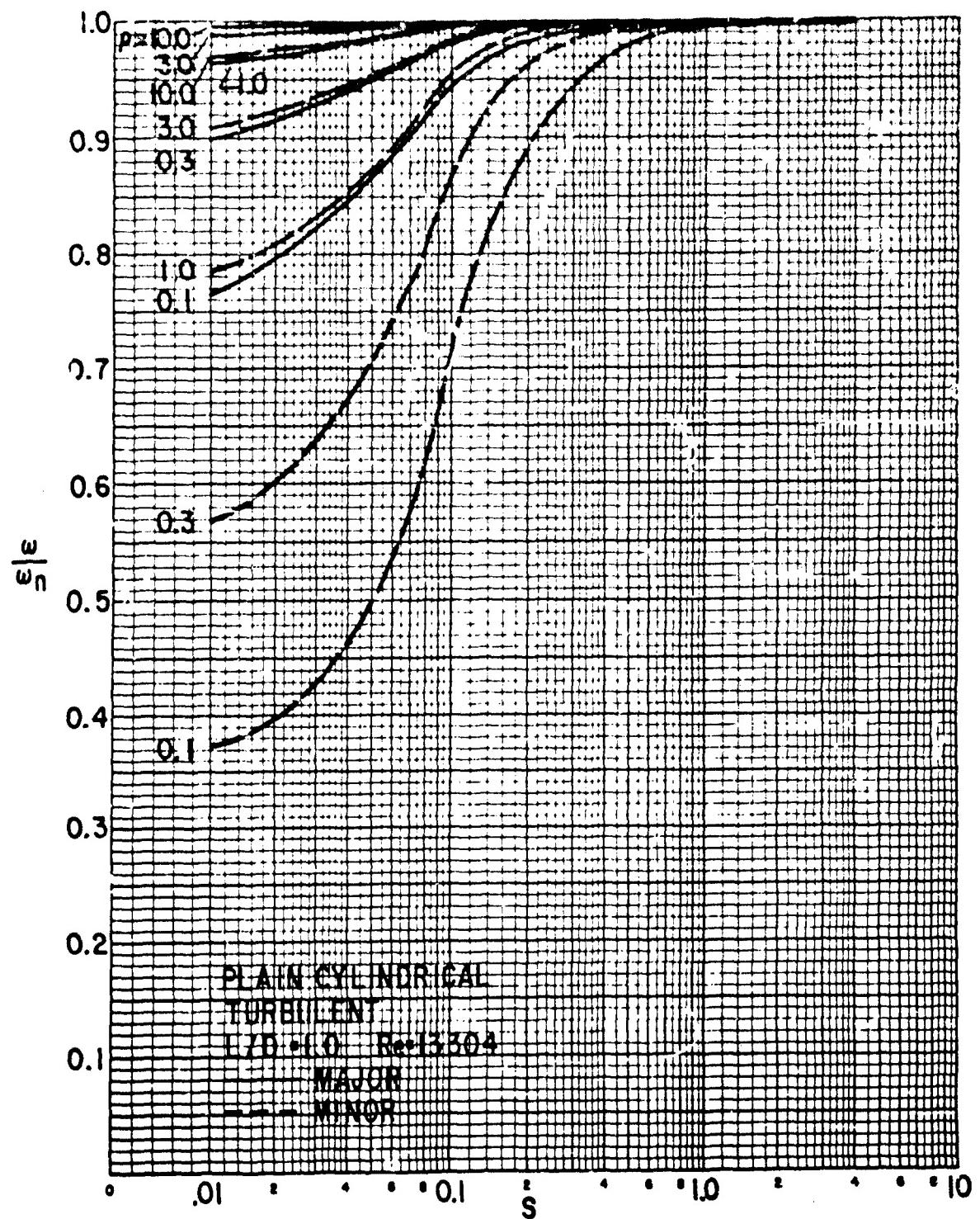


Figure D-20 Critical Speeds of Rotor-Bearing System
Plain Cylindrical Bearings, $L/D = 1$, Turbulent Film

b. Unbalance Response

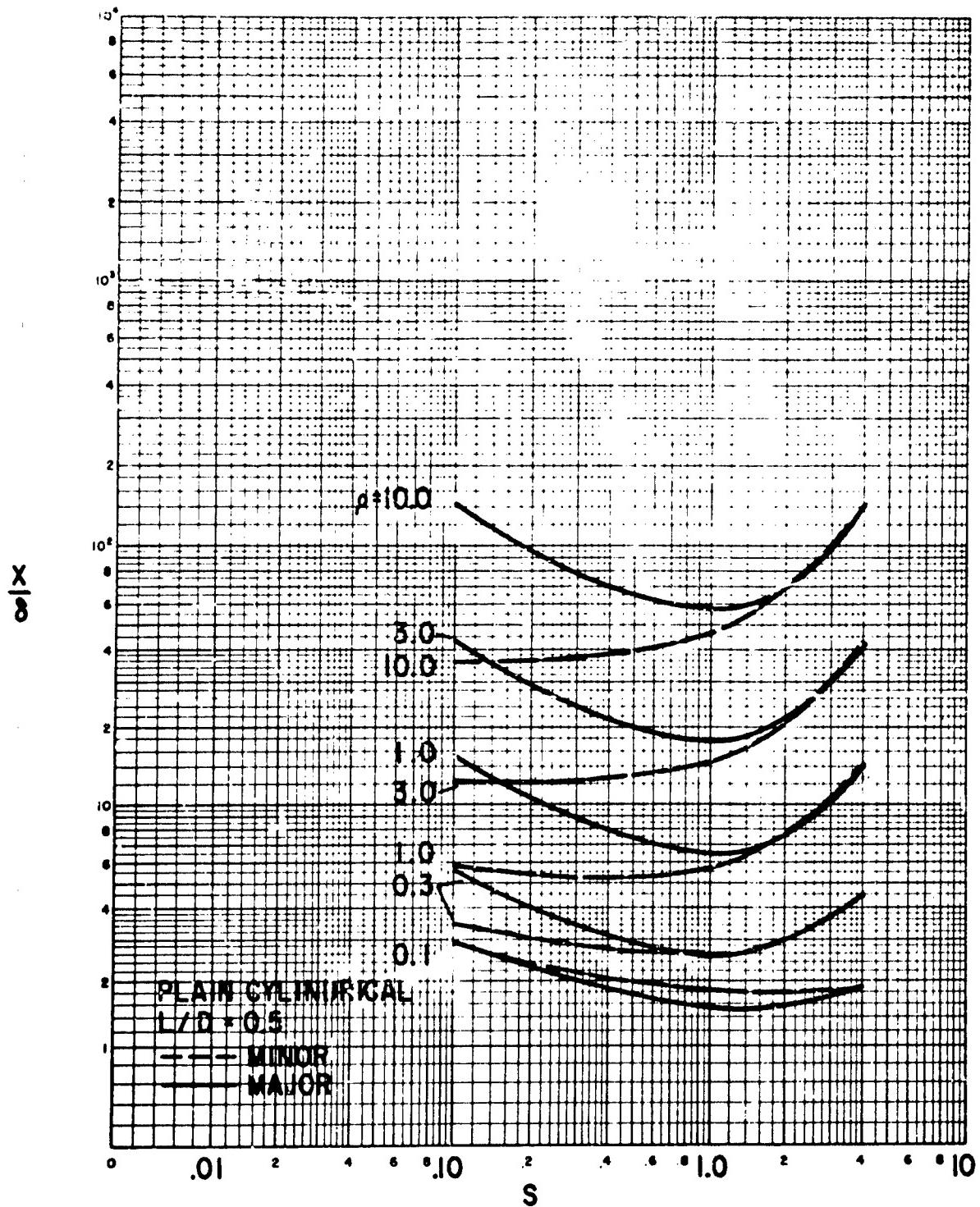


Figure D-21 Dimensionless Rotor Amplitude at the Critical Speed
Plain Cylindrical Bearings, $L/D = .5$, Laminar Film

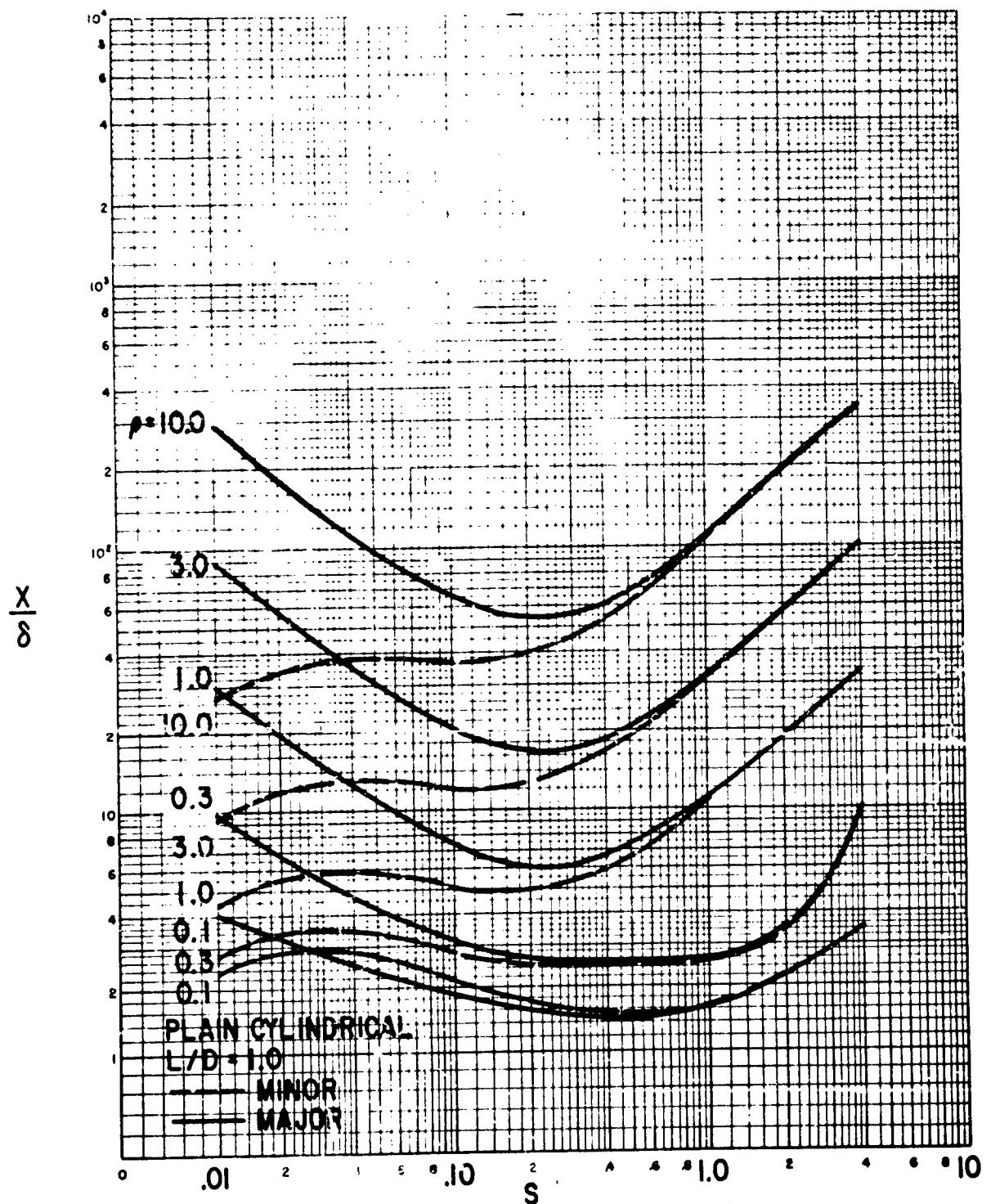


Figure D-22 Dimensionless Rotor Amplitude at the Critical Speed
 Plain Cylindrical Bearings, $L/D = 1$, Laminar Film

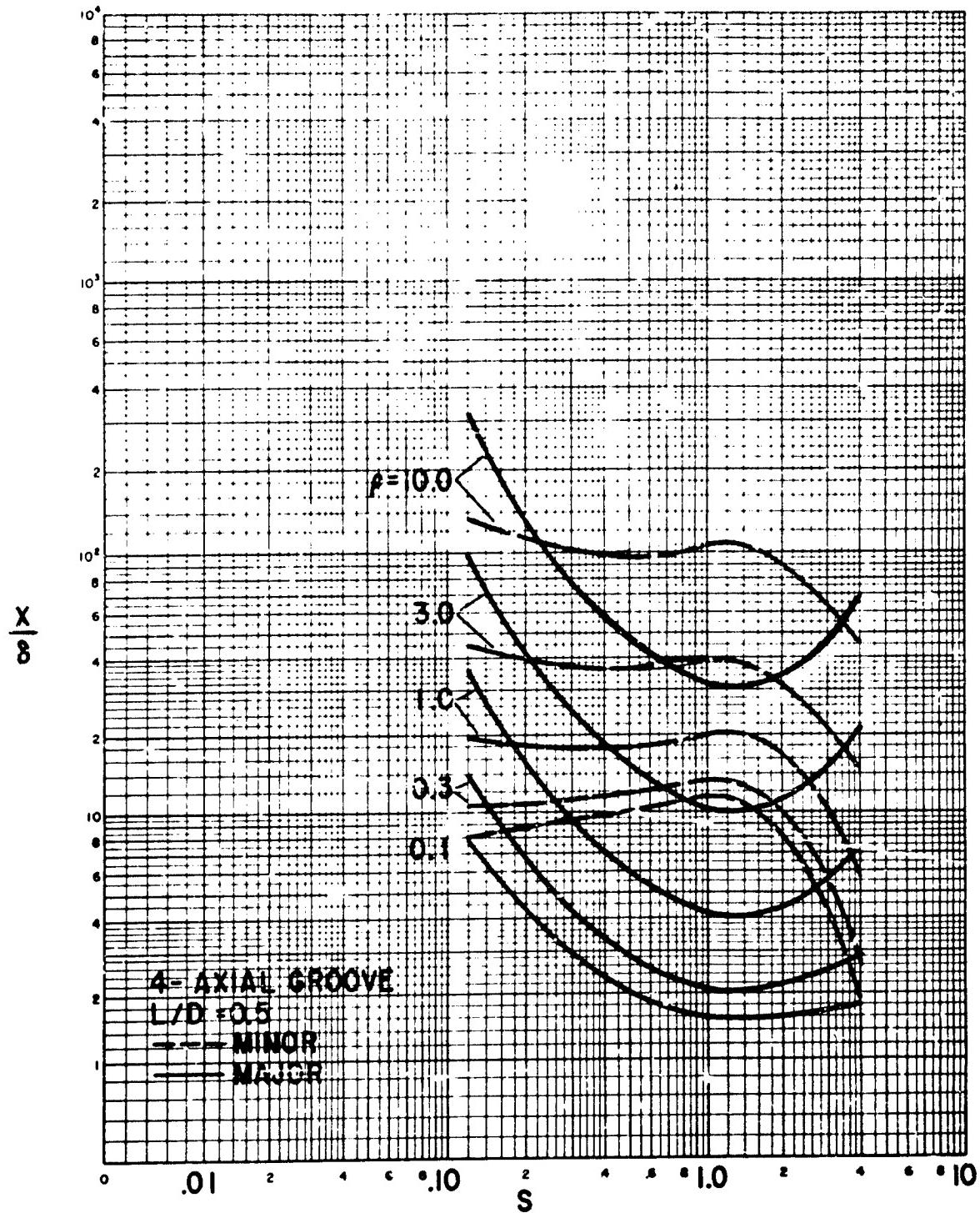


Figure D-23 Dimensionless Rotor Amplitude at the Critical Speed
4-Axial Groove Bearings, $L/D = .5$, Laminar Film

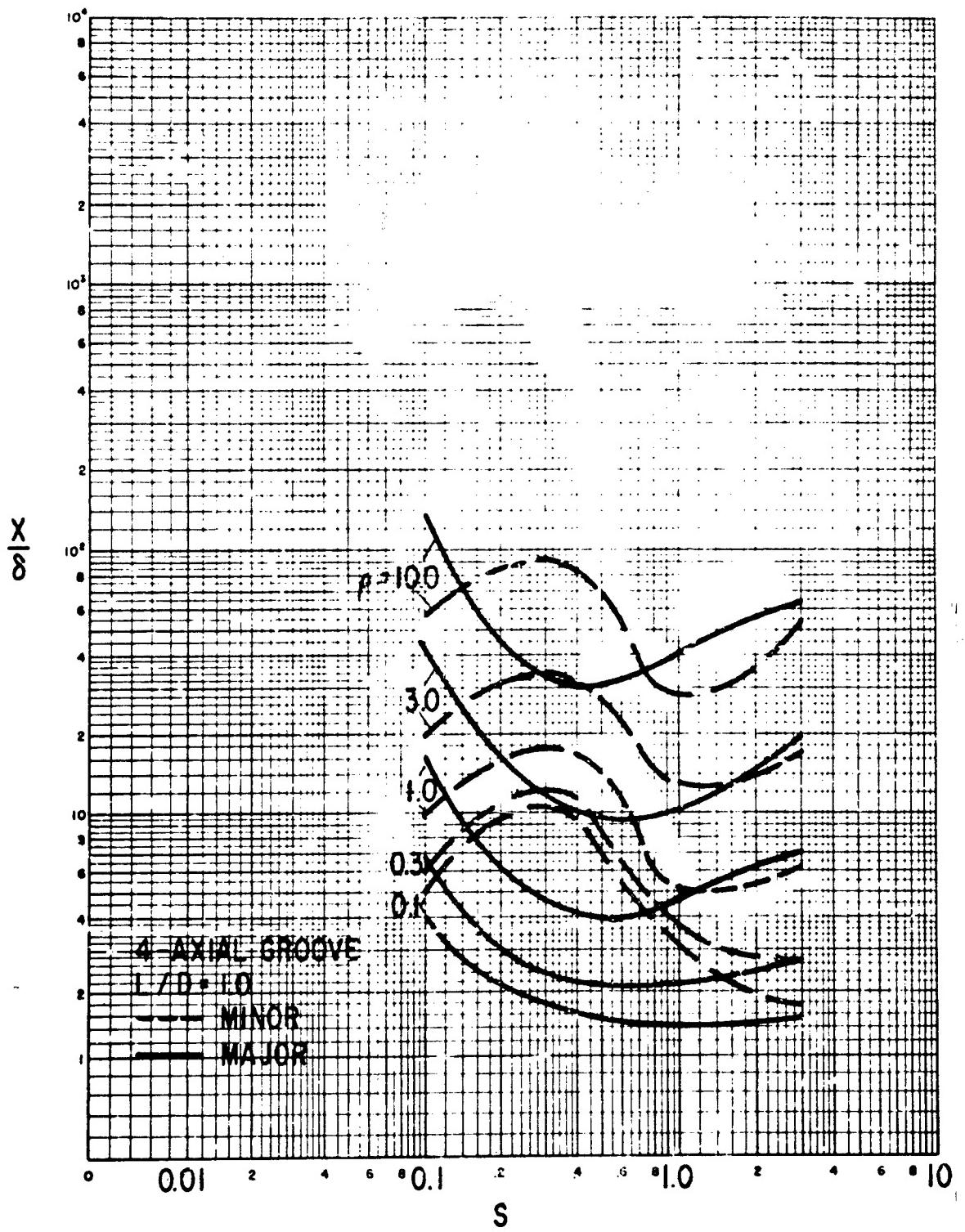


Figure D-24 Dimensionless Rotor Amplitude at the Critical Speed
4-Axial Groove Bearings, $L/D = 1$, Laminar Film

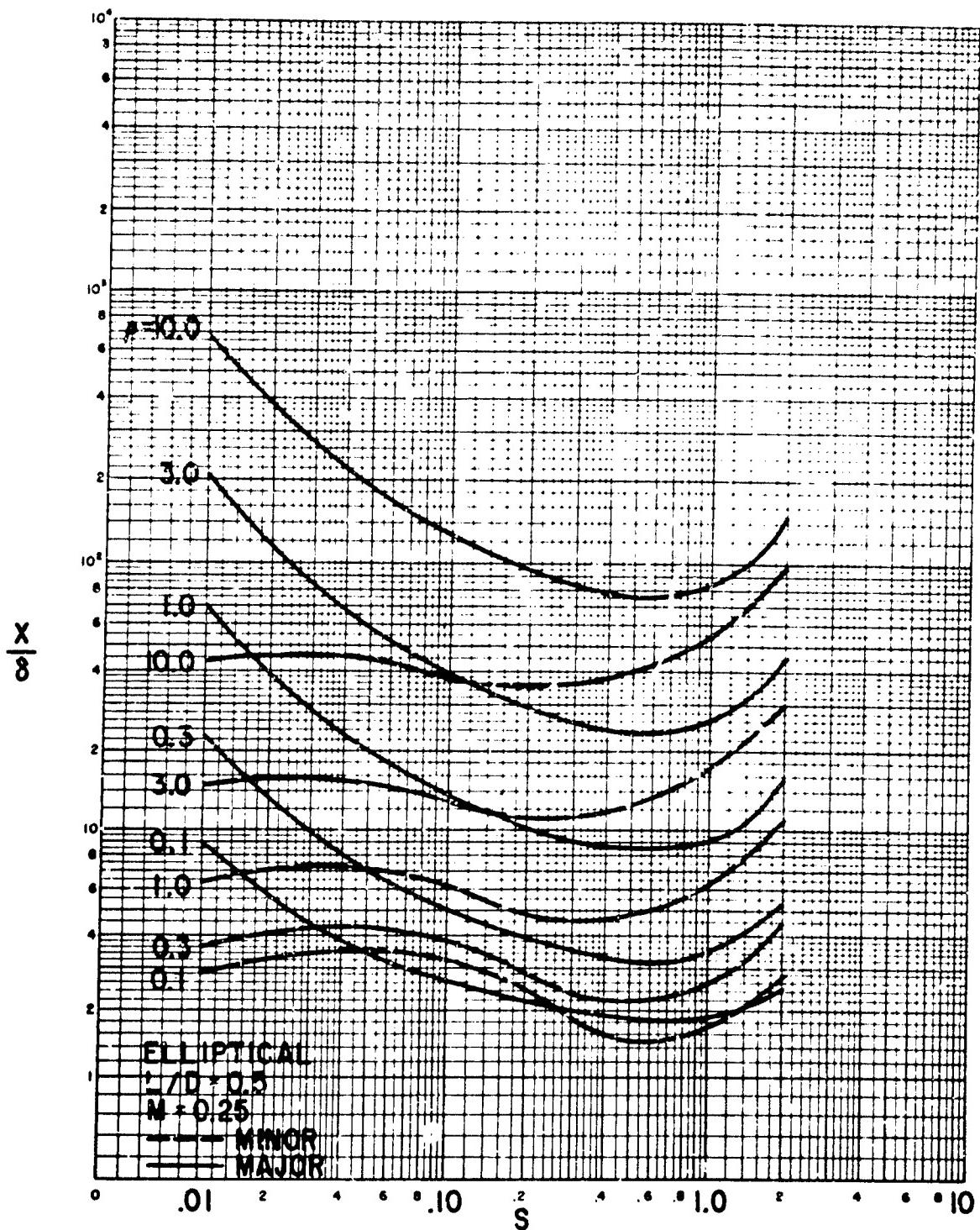


Figure D-25 Dimensionless Rotor Amplitude at the Critical Speed
Elliptical Bearings, $L/D = .5$, $m = .25$, Laminar Film

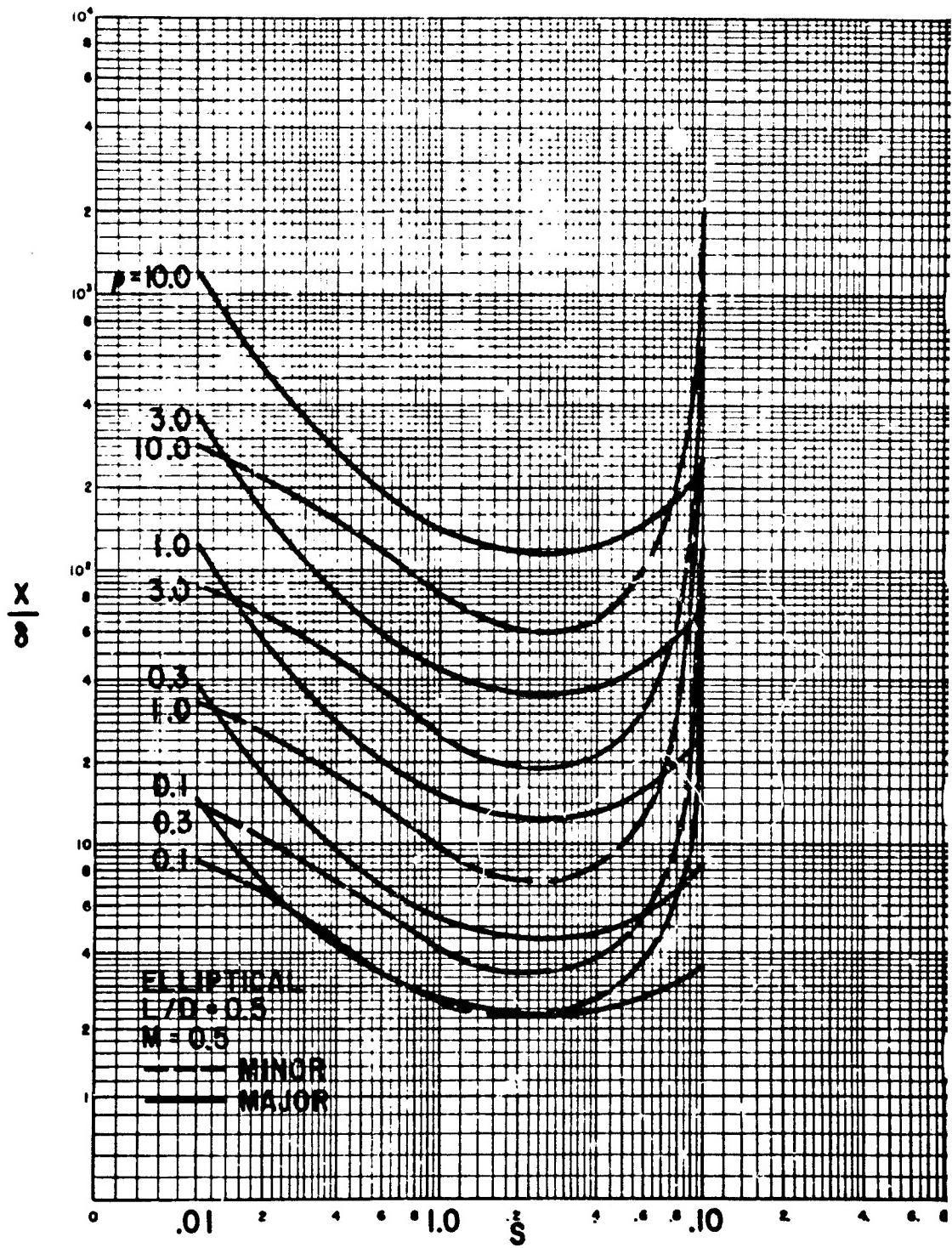


Figure D-26 Dimensionless Rotor Amplitude at the Critical Speed
 Elliptical Bearings, $L/D = .5$, $m = .5$, Laminar Film

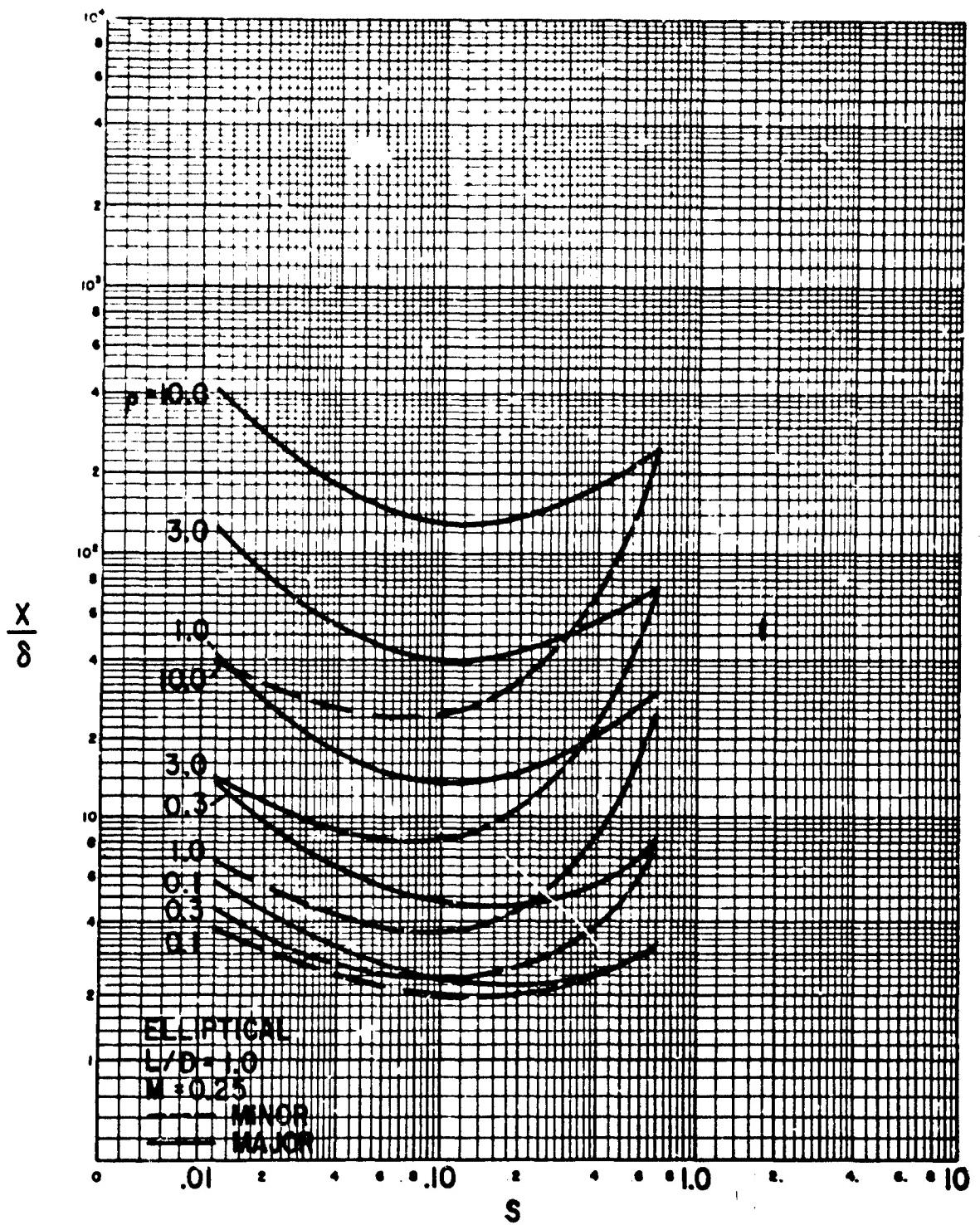


Figure D-27 Dimensionless Rotor Amplitude at the Critical Speed
 Elliptical Bearings, $L/D = 1$, $m = .25$, Laminar Film

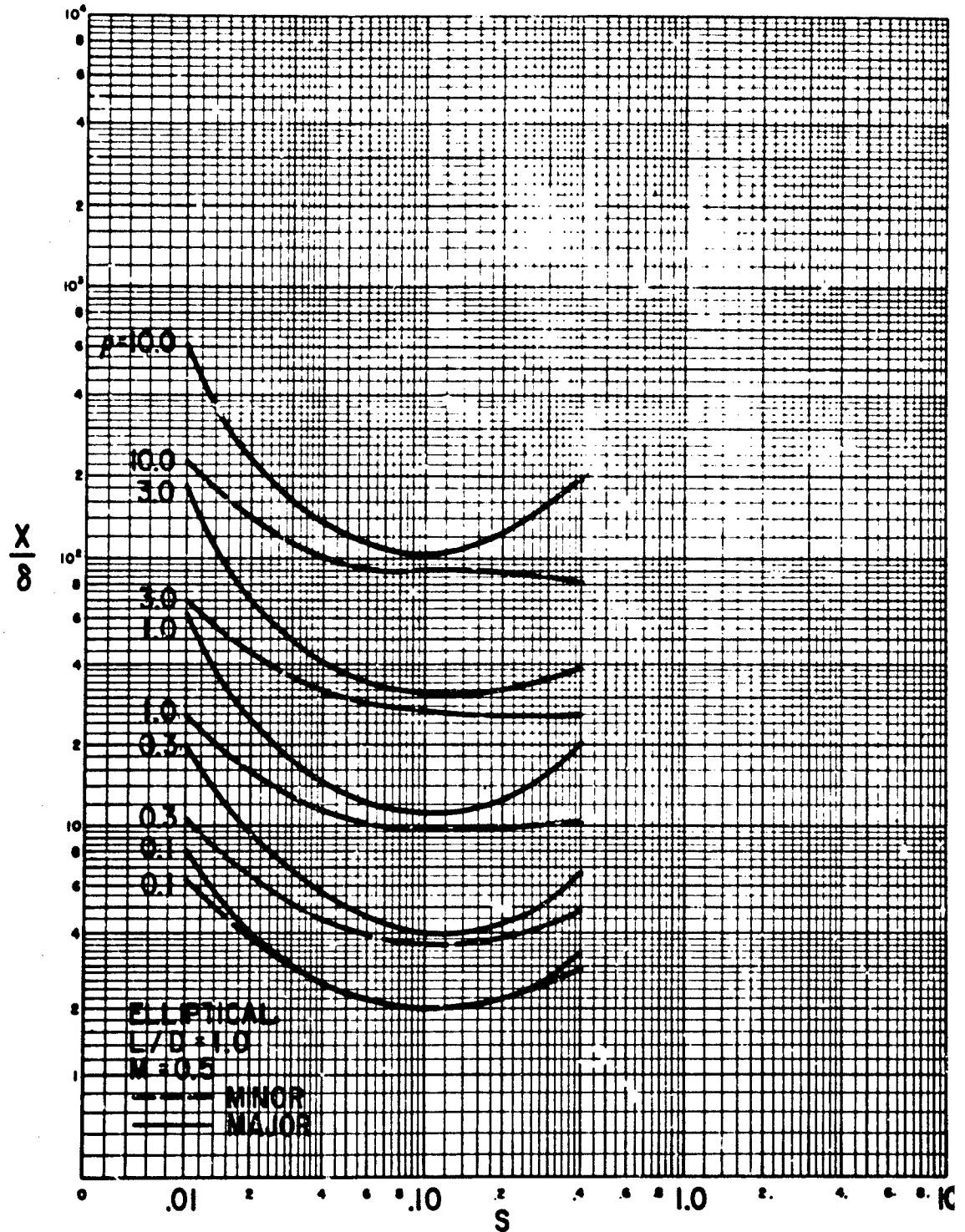


Figure D-28 Dimensionless Rotor Amplitude at the Critical Speed
 Elliptical Bearings, $L/D = 1$, $m = .5$, Laminar Film

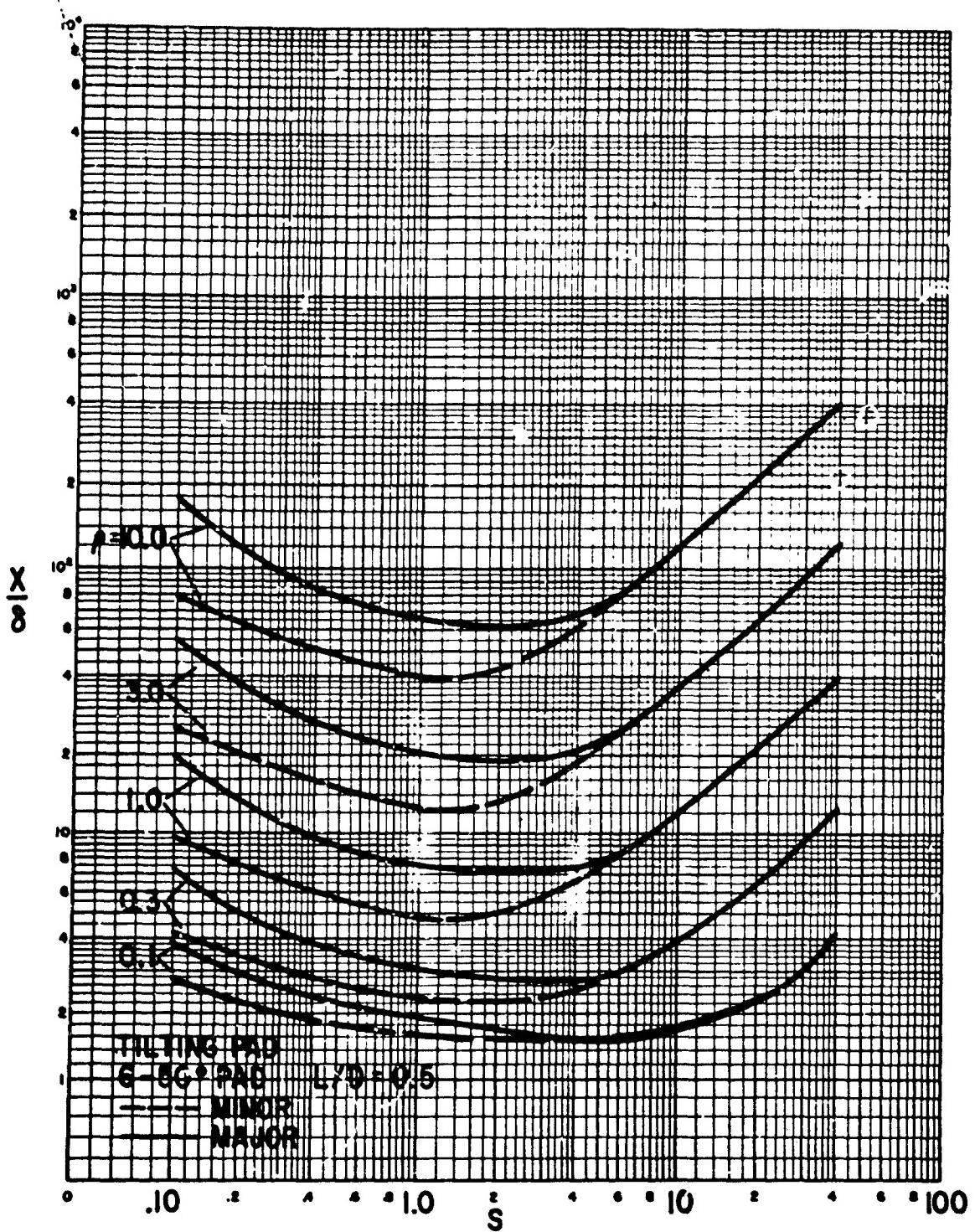


Figure D-29 Dimensionless Rotor Amplitude at the Critical Speed
 6 Shoe Tilting Pad Bearings, $L/D = .5$, Load between Pads

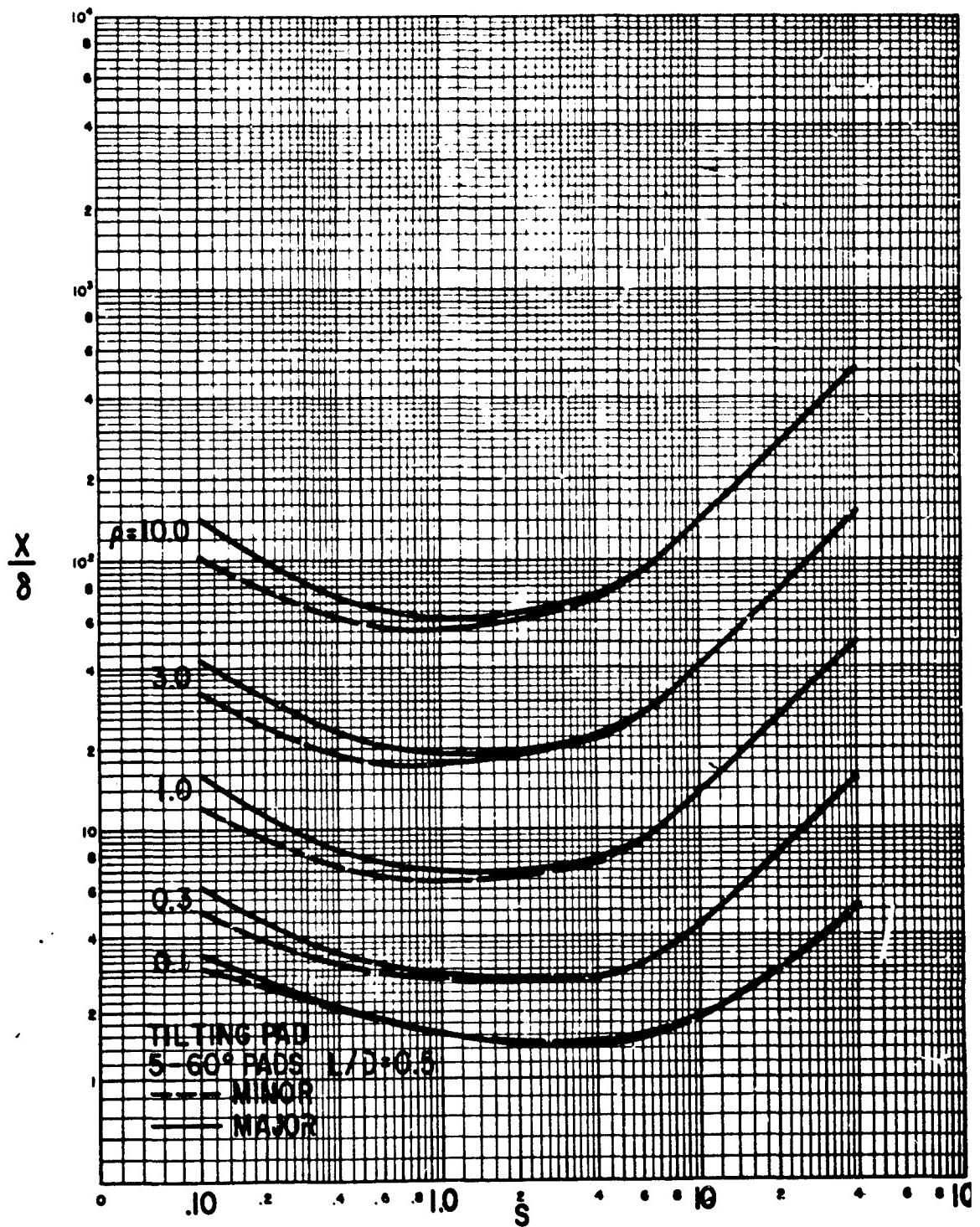


Figure D-30 Dimensionless Rotor Amplitude at the Critical Speed
 5 Shoe Tilting Pad Bearings, $L/D = .5$, Load between Pads

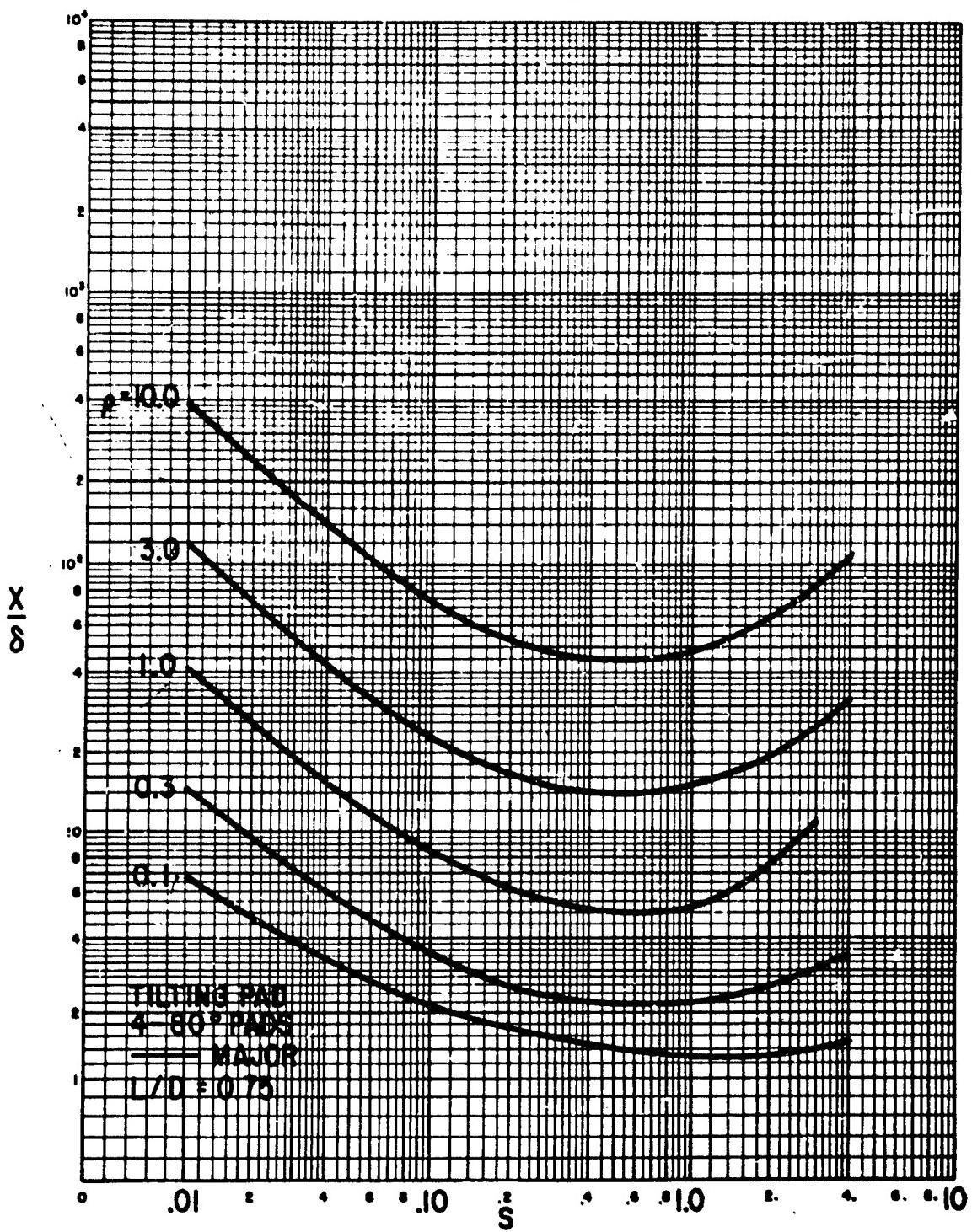


Figure D-31 Dimensionless Rotor Amplitude at the Critical Speed
4 Shoe Tilting Pad Bearings, $L/D = .75$, Load between Pads

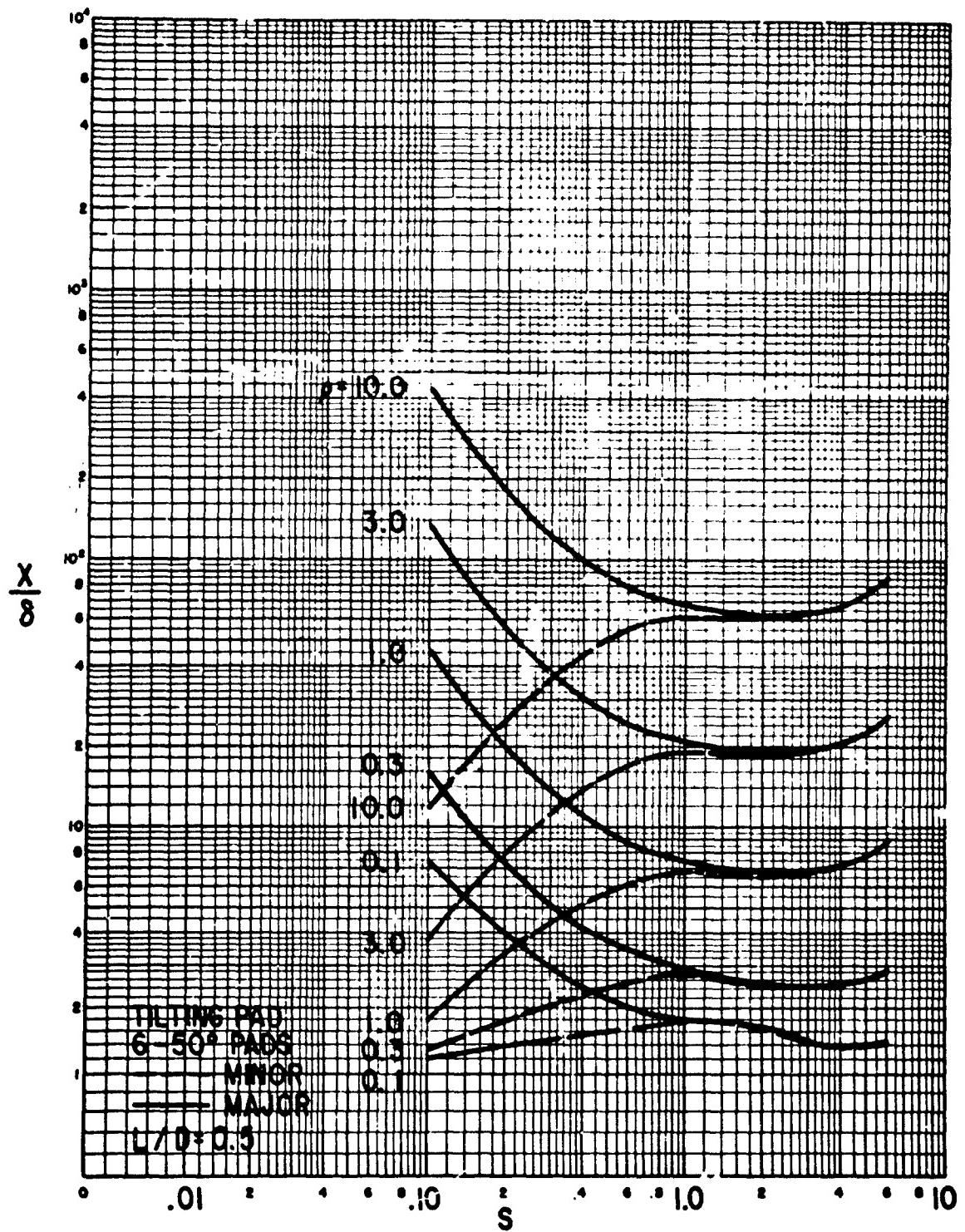


Figure D-32 Dimensionless Rotor Amplitude at the Critical Speed
6 Shoe Tilting Pad Bearings, $L/D = .5$, Load on Pad

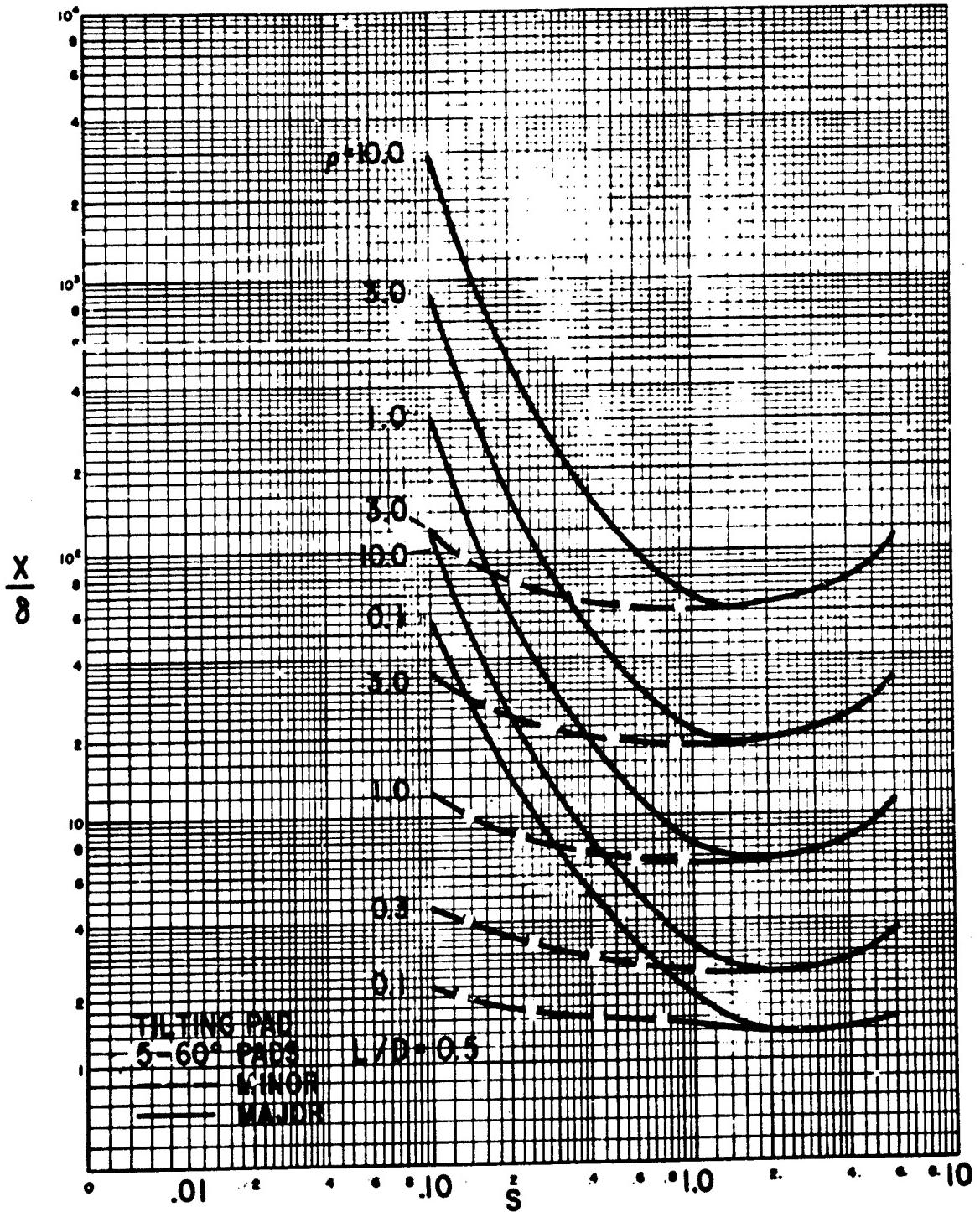


Figure D-33 Dimensionless Rotor Amplitude at the Critical Speed
5 Shoe Tilting Pad Bearings, L/D = .5, Load on Pad

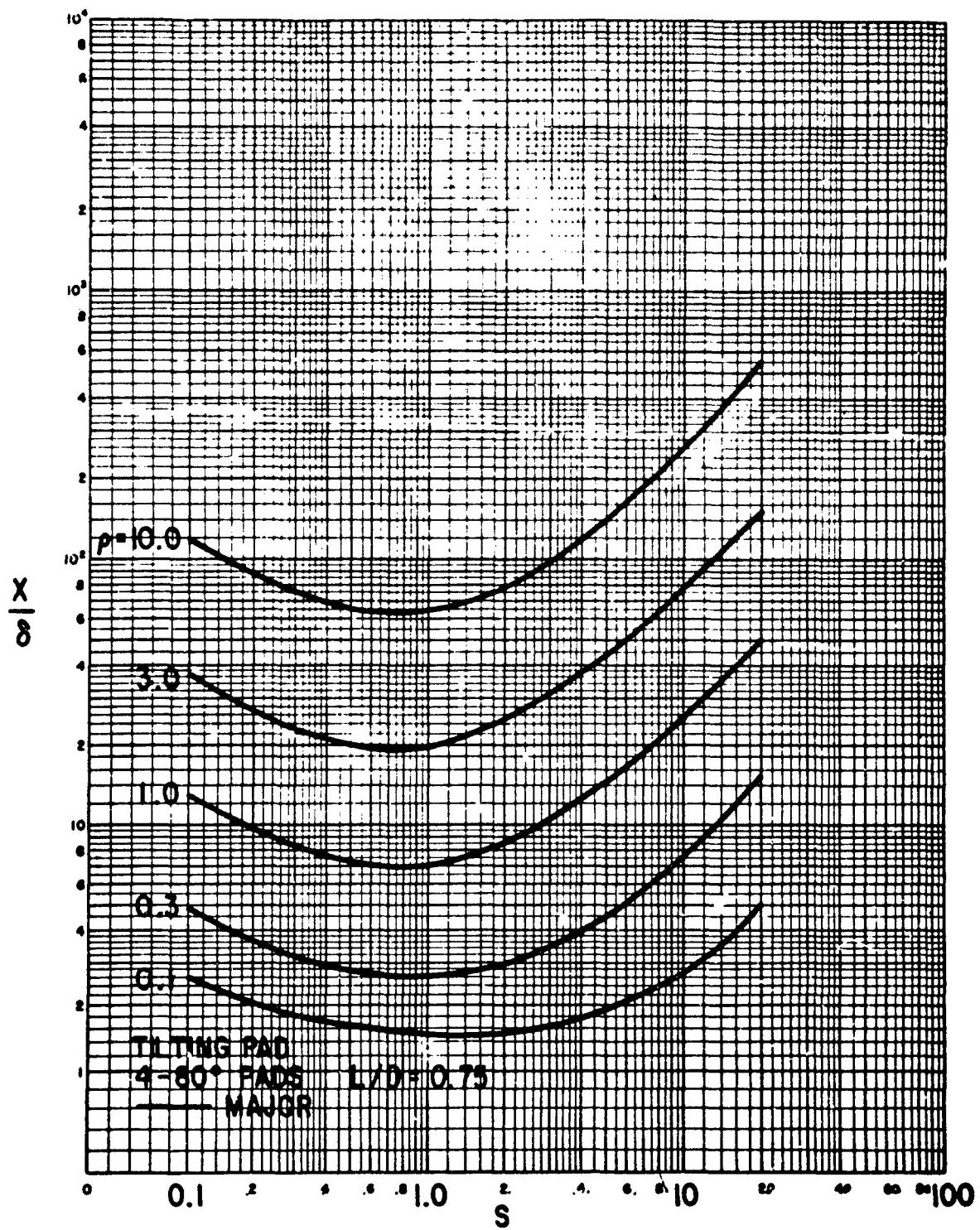


Figure D-34 Dimensionless Rotor Amplitude at the Critical Speed
4 Shoe Tilting Pad Bearings, L/D = .75, Load on Pad

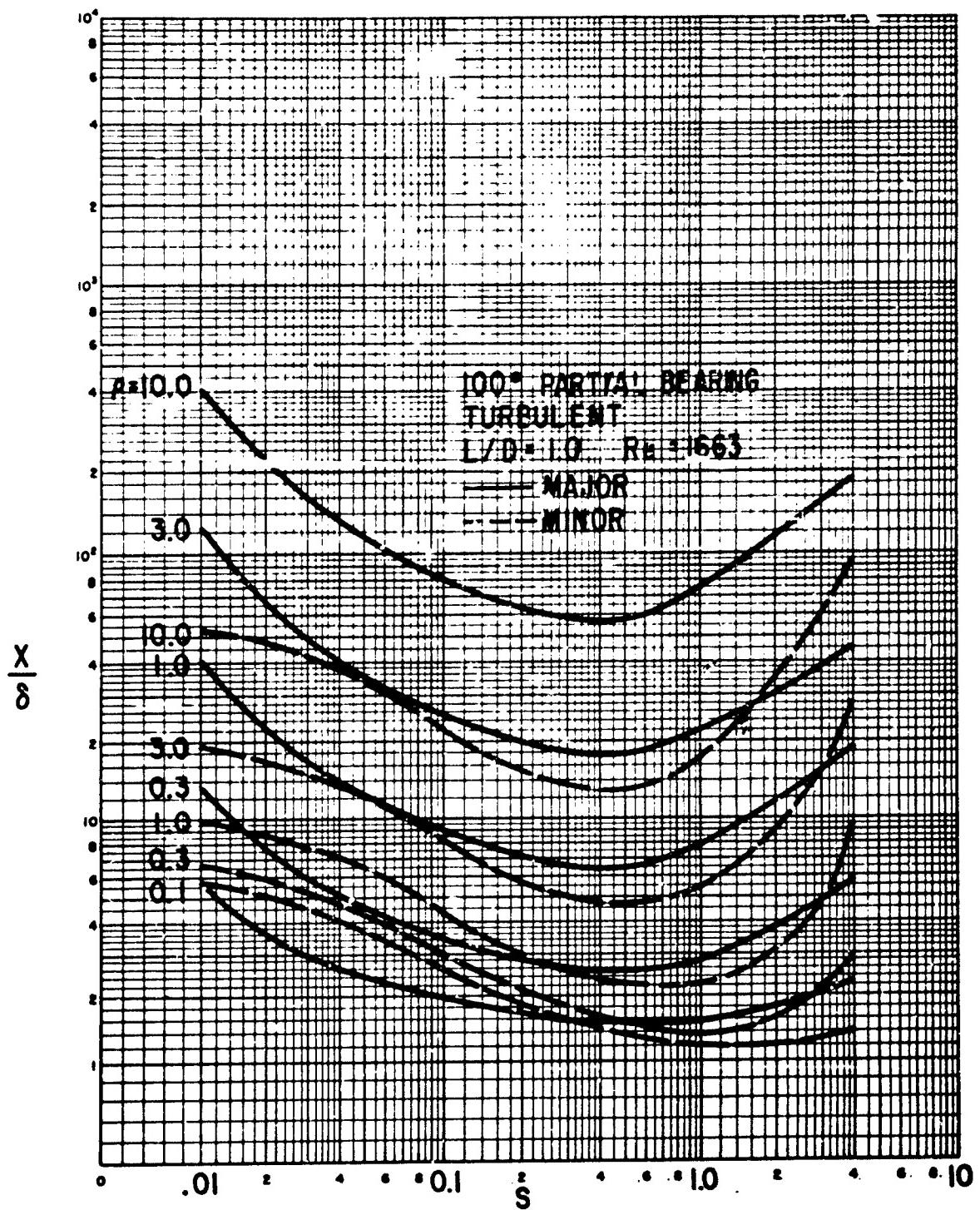


Figure D-35 Dimensionless Rotor Amplitude at the Critical Speed
100 Degree Partial Bearings, $L/D = 1$, Turbulent Film

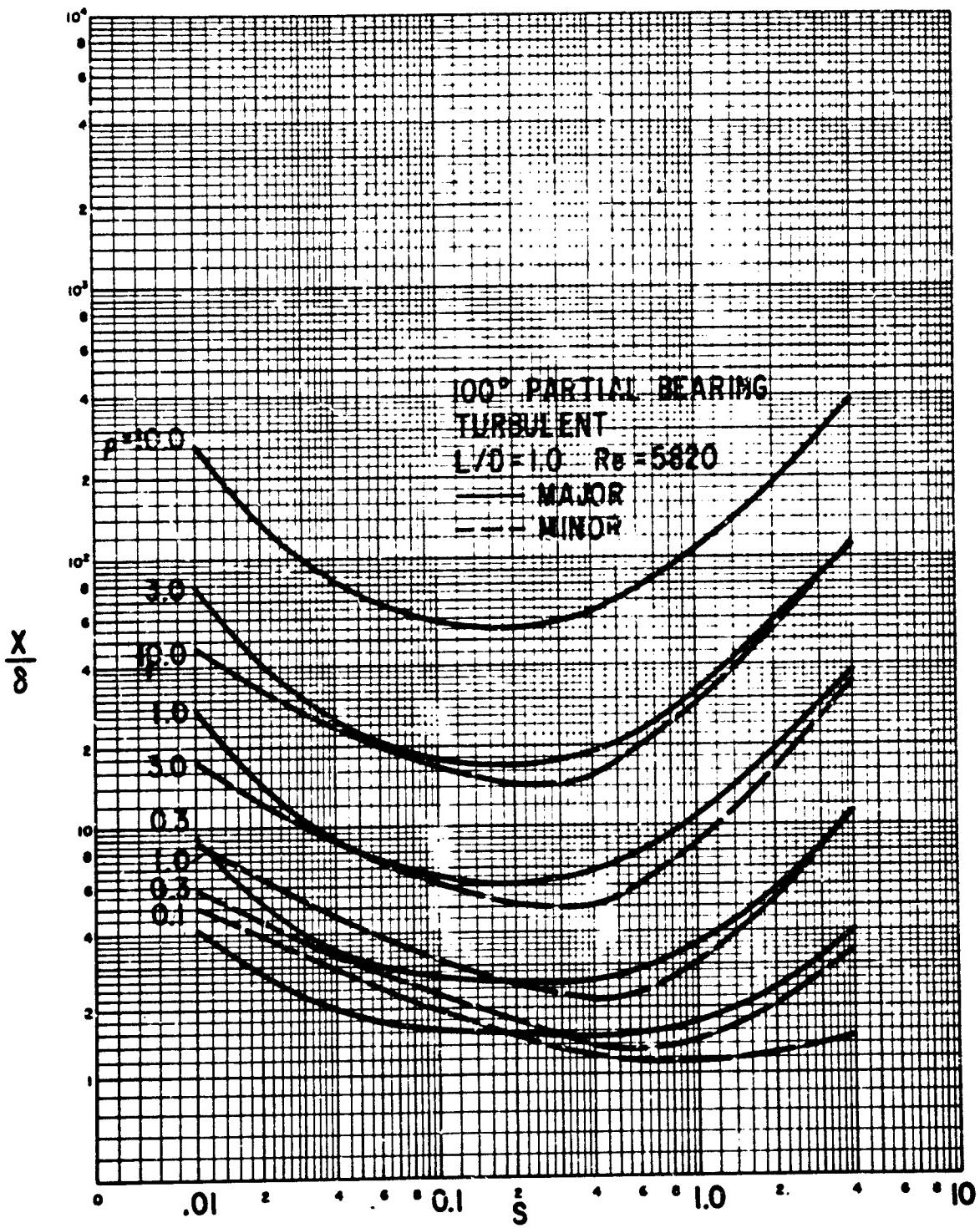


Figure D-36 Dimensionless Rotor Amplitude at the Critical Speed
 100 Degree Partial Bearings, $L/D = 1$, Turbulent Film

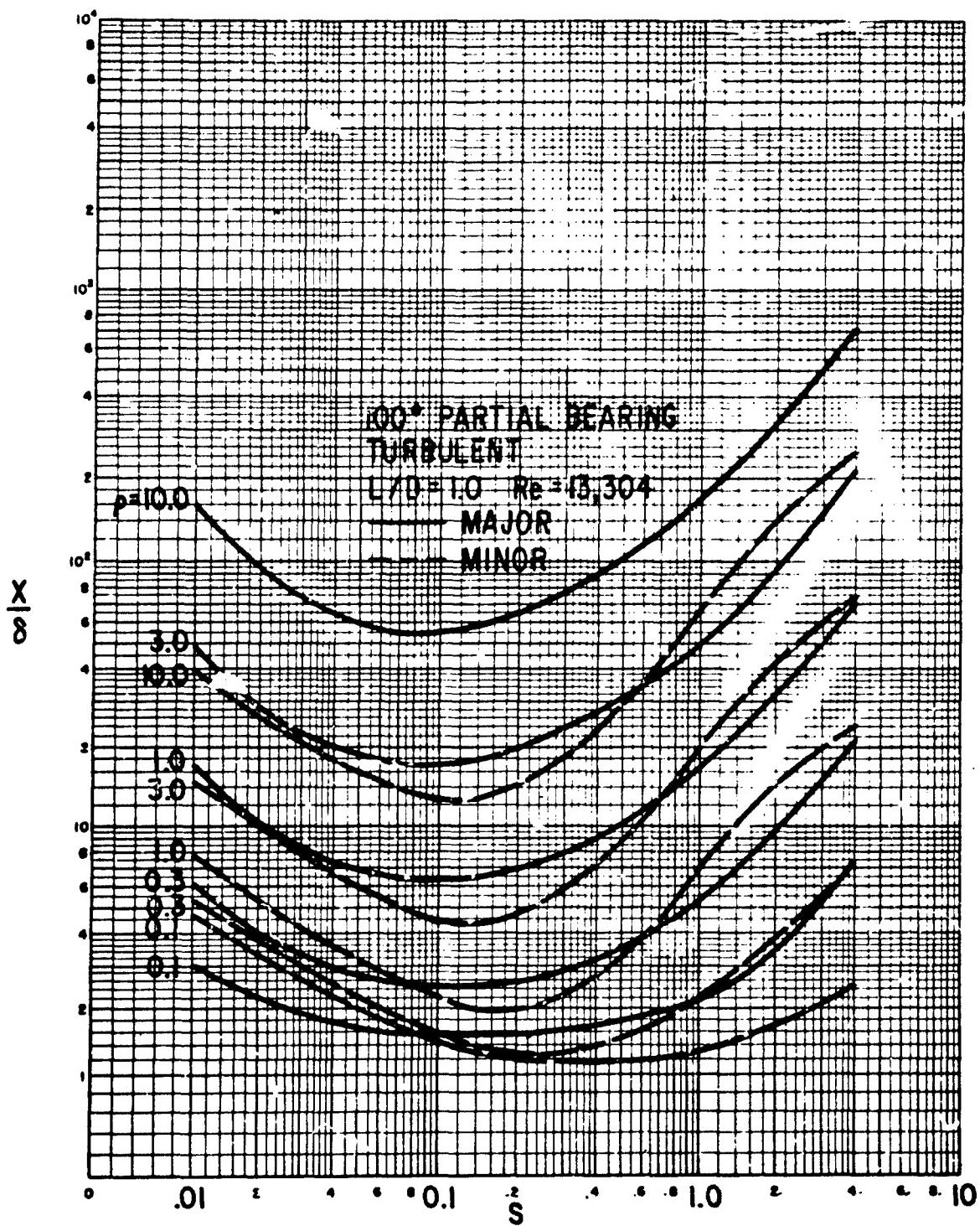


Figure D-37 Dimensionless Rotor Amplitude at the Critical Speed
100 Degree Partial Bearings, $L/D = 1$, Turbulent Film

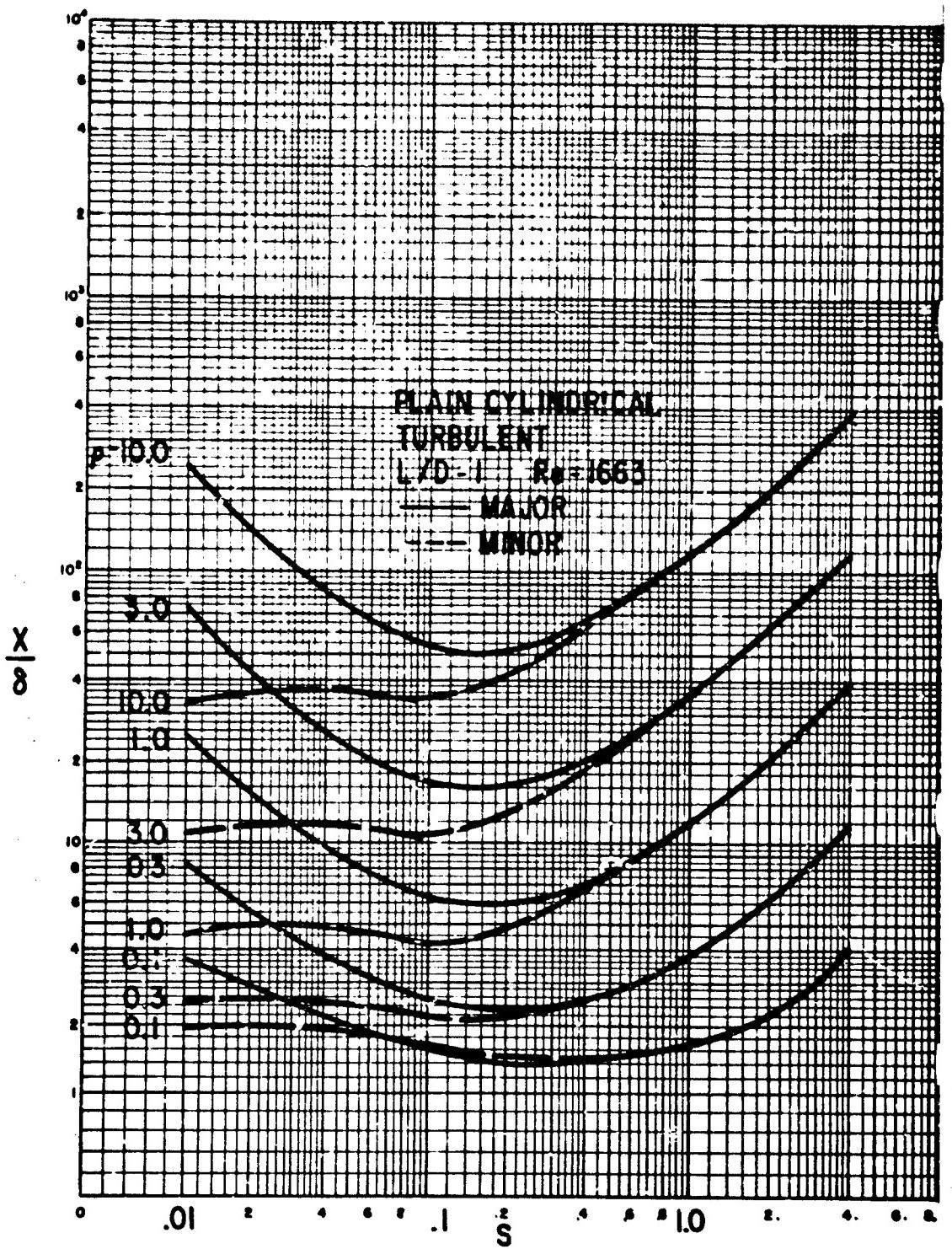


Figure D-38 Dimensionless Rotor Amplitude at the Critical Speed
 Plain Cylindrical Bearings, $L/D = 1$, Turbulent Film

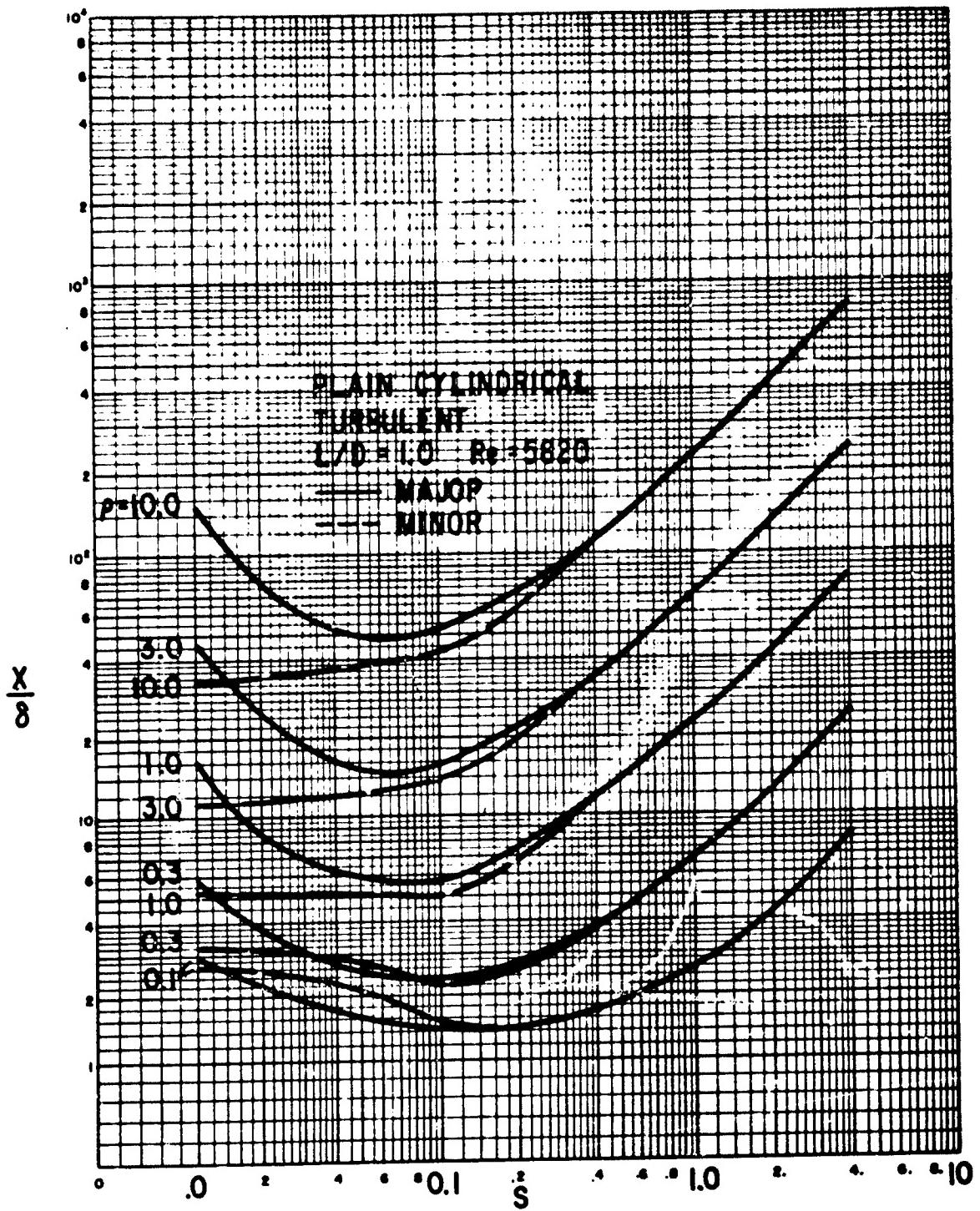


Figure D-39 Dimensionless Rotor Amplitude at the Critical Speed
 Plain Cylindrical Bearings, $L/D = 1$, Turbulent Film

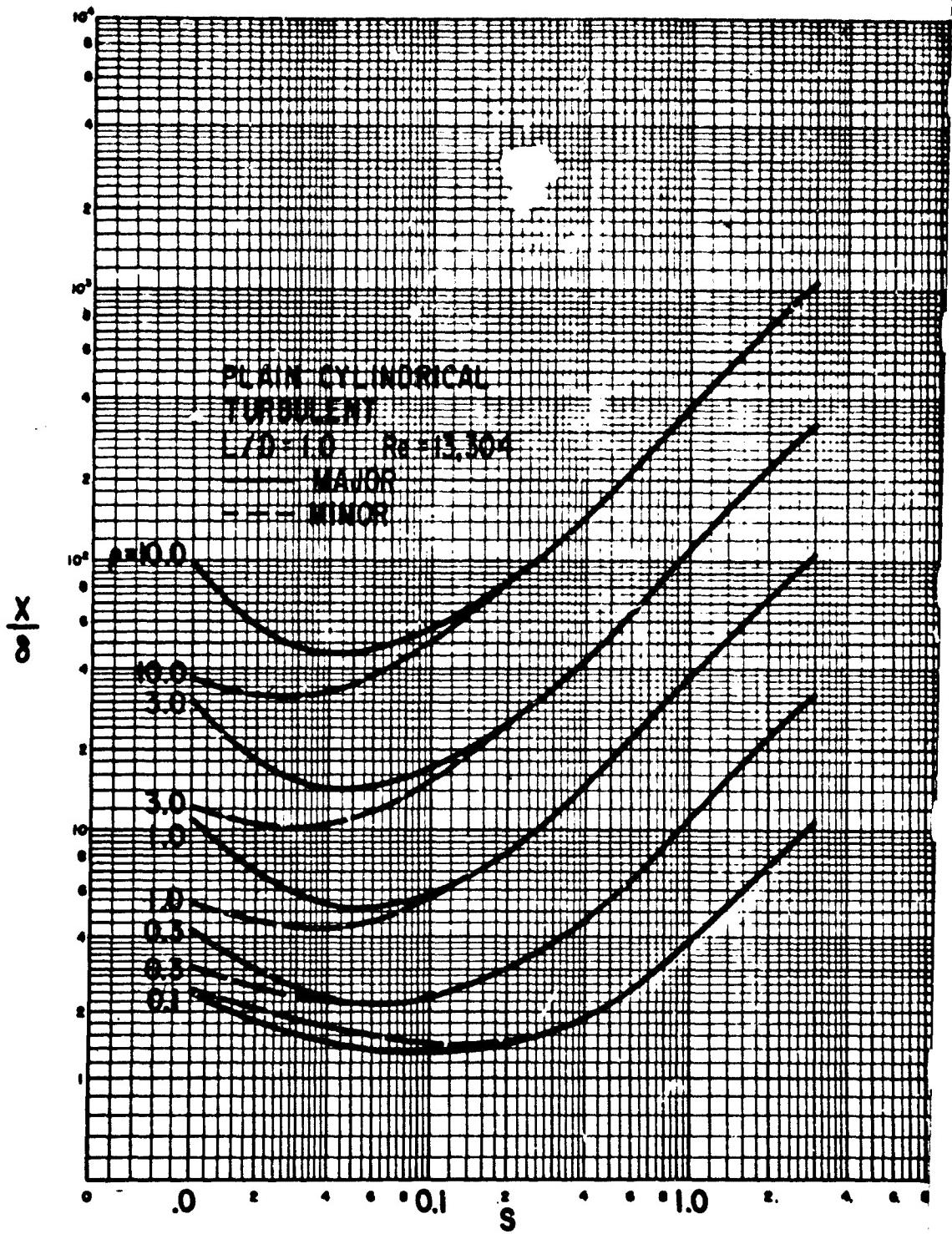


Figure D-40 Dimensionless Rotor Amplitude at the Critical Speed
 Plain Cylindrical Bearings, $L/D = 1$, Turbulent Film

VIII

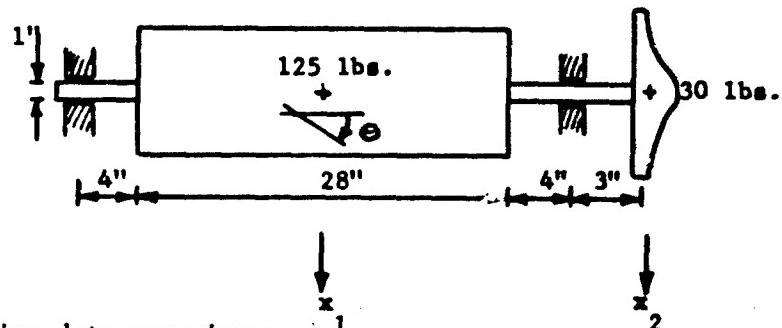
NUMERICAL EXAMPLES

Three numerical examples are given to illustrate the use of the design charts. For this purpose three different rotor-bearing systems have been selected: one configuration where the rotor is flexible and the bearings are oil lubricated, and two configurations with a rigid rotor where the bearings in one case operate with a turbulent film and in the second case the bearings are gas lubricated.

The configurations are chosen to be typical rather than representing any particular application. The calculations are concerned with the dynamics of the systems: the dynamic bearing coefficients, the critical speeds and the stability. The steady-state performance is in general not considered.

a. Flexible Rotor, Laminar Bearing Film

An electrical motor is mounted on a shaft between two bearings. The motor drives a pump wheel which is overhung at one end:



The following data are given:

Total rotor weight:	155 lbs.
Bearing reactions:	60 lbs. and 95 lbs.
Bearing span:	28 inch
Shaft diameter:	1 inch
Youngs modulus for shaft:	$3 \cdot 10^7$ lbs/in ²
Design speed:	5,000 RPM
Journal bearing type:	4-axial groove bearings
Bearing diameter:	D = 1 inch
Bearing length:	L = 0.5 inch

Radial clearance:	$C = 0.001 \text{ inch}$
Oil:	SAE 10 at 120°F
Oil viscosity:	$\mu = 24 \text{ centipoise} = 3.5 \cdot 10^{-6} \text{ lbs.sec/in}^2$
Oil density:	$\rho = 0.0307 \text{ lbs/in}^3 = 7.95 \cdot 10^{-5} \text{ lbs.sec}^2/\text{in}^4$

It is desired to investigate the critical speeds, the unbalance response and the stability of the given rotor-bearing system to determine if the performance of the system is satisfactory with the selected rotor and bearing dimensions.

For analysis purposes the rotor can be considered to consist of two masses: the pump wheel with a weight of 30 lbs. and the motor rotor, weighing 125 lbs. with a transverse mass moment of inertia of $6,940 \text{ lbs.in}^2$ and a polar moment of inertia of 260 lbs.in^2 . The shaft is 1 inch in diameter with dimensions as shown in the figure.

Consider first the stiffness of the rotor. The rotor has three degrees-of-freedom namely the amplitude x_1 of the motor rotor, the amplitude x_2 of the pump wheel and the angular displacement θ of the motor rotor. Let the three quantities be identified by subscript 1, 2 and 3, respectively, and let α denote an influence coefficient such that α_{22} means the shaft deflection at the wheel due to a 1 lb. force at the same position. Similarly, α_{23} means the deflection at the wheel due to a 1 lb.in. moment at the CG of the motor rotor. From standard beam formulas (See: R.J. Roark: "Formulas for Stress and Strain", McGraw-Hill Book Co., New York) the values of the influence coefficients are determined to be:

$$\alpha_{11} = 7.24 \cdot 10^{-6} \frac{\text{in}}{\text{lbs}}, \quad \alpha_{12} = -8.15 \cdot 10^{-6} \frac{\text{in}}{\text{lbs}}, \quad \alpha_{13} = 0 \quad \text{lbs}^{-1}$$

$$\alpha_{22} = 28.05 \cdot 10^{-6} \frac{\text{in}}{\text{lbs}}, \quad \alpha_{23} = -0.771 \cdot 10^{-6} \frac{\text{in}}{\text{lbs}}, \quad \alpha_{33} = 0.0223 \cdot 10^{-6} \frac{\text{radians}}{\text{lbs.in}}$$

The values are based on a Young's modulus of $3 \cdot 10^7 \text{ lbs/in}^2$ and a cross-sectional shaft moment of inertia of 0.0491 in^4 , corresponding to a 1 inch diameter. The three inertias become:

$$\text{mass of motor rotor} = 125/386 = 0.324 \text{ lbs.sec}^2/\text{in}$$

$$\text{mass of pump wheel} = 30/386 = 0.0777 \text{ lbs.sec}^2/\text{in}$$

$$\text{mass moment of inertia of motor rotor} = (6,940-270)/386 = 17.3 \text{ lbs.in.sec}^2$$

The equations of motion become:

$$\ddot{x}_1 = -\alpha_{11} \cdot 0.324 \cdot \ddot{x}_1 - \alpha_{12} \cdot 0.0777 \cdot \ddot{x}_2 - \alpha_{13} \cdot 17.3 \cdot \ddot{\theta}$$

$$\ddot{x}_2 = -\alpha_{12} \cdot 0.324 \cdot \ddot{x}_1 - \alpha_{22} \cdot 0.0777 \cdot \ddot{x}_2 - \alpha_{23} \cdot 17.3 \cdot \ddot{\theta}$$

$$\ddot{\theta} = -\alpha_{13} \cdot 0.324 \cdot \ddot{x}_1 - \alpha_{23} \cdot 0.0777 \cdot \ddot{x}_2 - \alpha_{33} \cdot 17.3 \cdot \ddot{\theta}$$

where \ddot{x}_1 means the x_1 - acceleration, etc. Let the rotor speed be $\omega \frac{\text{radians}}{\text{sec}}$
whereby $\ddot{x}_1 = -\omega^2 x_1$, etc., and substitute the previously derived values for the influence coefficients to get:

$$(2.345 \cdot \omega^2 - 10^6) x_1 - 0.633 \cdot \omega^2 \cdot x_2 = 0$$

$$-2.64 \cdot \omega^2 x_1 + (2.18 \cdot \omega^2 - 10^6) x_2 - 13.33 \cdot \omega^2 \theta = 0$$

$$-0.0599 \cdot \omega^2 x_2 + (0.386 \cdot \omega^2 - 10^6) \theta = 0$$

From the last equation:

$$\theta = \frac{0.0599 \omega^2}{0.386 \cdot \omega^2 - 10^6} x_2$$

in which case the determinant for the $x_1 - x_2$ - equations can be written:

$$\begin{vmatrix} (2.345 - \frac{10^6}{\omega^2}) & -0.633 \\ -2.64 & (2.18 - \frac{10^6}{\omega^2} - \frac{13.33 \cdot 0.0599}{(0.386 - \frac{10^6}{\omega^2})}) \end{vmatrix} = 0$$

By trial and error the two lowest solutions for ω become:

$$1st \text{ rotor resonance: } \omega = 524 \frac{\text{rad}}{\text{sec}} = 5,000 \text{ RPM}$$

$$2nd \text{ rotor resonance: } \omega = 865 \frac{\text{rad}}{\text{sec}} = 8,250 \text{ RPM}$$

These resonances will be lowered due to the effect of the flexibility of the bearing film. To get an estimate of this effect it may be noted that the first of the two rotor resonances basically corresponds to the resonance of the motor rotor on the shaft. Hence, with a mass of $0.324 \text{ lbs.sec}^2/\text{in.}$ the total rotor

stiffness yielding a frequency of 524 radians/sec becomes 86,000 lbs/in. Since the design charts consider the rotor to be symmetric with half the rotor mass assigned to each of the two bearings the rotor stiffness to be used in the charts should be taken as half of the total stiffness value, i.e.:

$$K_r = 43,000 \frac{\text{lbs}}{\text{in}}$$

The effective influence coefficient α (see page 231) becomes:

$$\alpha = \frac{1}{K_r} = 2.325 \cdot 10^{-5} \frac{\text{in}}{\text{lbs}}$$

and the rotor mass per bearing is $0.162 \text{ lbs.sec}^2/\text{in}$.

The bearings are oil lubricated and are of the 4-axial groove type. The journal diameter is: $D = 1$ inch and the bearing length is: $L = 0.5$ in. The radial clearance is: $C = 0.001$ inch and the oil is SAE 10 at 120 F with:

$$\text{Viscosity: } \mu = 24 \text{ centipoise} = 3.5 \cdot 10^{-6} \text{ lbs.sec/in}^2$$

$$\text{Density: } \rho = 0.0307 \text{ lbs/in}^3 = 7.95 \cdot 10^{-5} \text{ lbs.sec}^2/\text{in}^4$$

With a bearing load of: $W = 62.5$ lbs the Sommerfeld number becomes:

$$S = \frac{3.5 \cdot 10^{-6} \cdot N \cdot 1 \cdot 0.5}{62.5} \left(\frac{0.5}{0.001} \right)^2 = 7 \cdot 10^{-3} \cdot N$$

To determine the first critical speed use Fig. D-3. With $\omega_n = 524 \frac{\text{rad}}{\text{sec}}$ the relationship between the Sommerfeld Number and the speed ratio is:

$$S = 0.585 \cdot \frac{\omega}{\omega_n}$$

The rotor flexibility parameter is:

$$\rho = \frac{62.5 \cdot 2.325 \cdot 10^{-5}}{0.001} = 1.45$$

Plot the curve of S versus $\frac{\omega}{\omega_n}$ on Fig. D-3 and determine the intersections with the curves corresponding to the calculated ρ -value:

$$\text{for major resonance: } \frac{\omega}{\omega_n} = 0.98, S = 0.573$$

$$\text{for minor resonance: } \frac{\omega}{\omega_n} = 0.88, S = 0.515$$

The corresponding response is found from Fig. D-23 as:

$$\text{for major resonance: } \frac{x}{\delta} = 7$$

$$\text{for minor resonance: } \frac{x}{\delta} = 23$$

Hence the minor resonance is the most pronounced and the first critical speed of the system becomes (in approximation):

$$1\text{st critical speed} = 5,000 \cdot 0.88 = 4,400 \text{ RPM}$$

The second critical speed is predominantly controlled by the overhung pump wheel and actually the design charts do not apply to this case. However, it is close enough to the first critical speed that the same reduction factor can be used so that:

$$2\text{nd critical speed} = 8,250 \cdot 0.88 = 7,300 \text{ RPM}$$

The above calculations are only approximate and should be checked by more elaborate methods such as a computer program. For this purpose it is necessary to know the dynamic bearing coefficients. From the figure on page 280 the bearing reactions are found to be:

$$\text{for left hand bearing: } W = 60 \text{ lbs. i.e., } \frac{W}{C} = 6 \cdot 10^4 \text{ lbs/in}$$

$$\text{for right hand bearing: } W = 95 \text{ lbs. i.e., } \frac{W}{C} = 9.5 \cdot 10^4 \text{ lbs/in}$$

At 4,400 RPM the Sommerfeld Number becomes:

$$\text{for left hand bearing: } S = 0.535$$

$$\text{for right hand bearing: } S = 0.338$$

Using Figs. B-5 and B-6 the dynamic coefficients can be computed:

for left hand bearing

$$K_{xx} = 2.46 \cdot 10^5 \frac{\text{lbs}}{\text{in}}, K_{xy} = 1.8 \cdot 10^5 \frac{\text{lbs}}{\text{in}}, K_{yx} = 2,400 \frac{\text{lbs}}{\text{in}}, K_{yy} = 5.8 \cdot 10^4 \frac{\text{lbs}}{\text{in}}$$

$$C_{xx} = 430 \frac{\text{lbs.sec}}{\text{in}}, C_{xy} = -195 \frac{\text{lbs.sec}}{\text{in}}, C_{yx} = 4.2 \cdot \frac{\text{lbs.sec}}{\text{in}}, C_{yy} = 10.4 \frac{\text{lbs.sec}}{\text{in}}$$

for right hand bearing

$$K_{xx} = 4.65 \cdot 10^5 \frac{\text{lbs}}{\text{in}}, K_{xy} = 3.09 \cdot 10^5 \frac{\text{lbs}}{\text{in}}, K_{yx} = 16,000 \frac{\text{lbs}}{\text{in}},$$

$$K_{yy} = 1.06 \cdot 10^5 \frac{\text{lbs}}{\text{in}}$$

$$C_{xx} = 595 \frac{\text{lbs.sec}}{\text{in}}, C_{xy} = -340 \frac{\text{lbs.sec}}{\text{in}}, C_{yx} = -5.2 \frac{\text{lbs.sec}}{\text{in}}, C_{yy} = 2.1 \frac{\text{lbs.sec}}{\text{in}}$$

These values can be used directly as input to a computer program for calculating the detailed unbalance response of the rotor-bearing system and to check the stability at the selected speed. If the response or the stability is investigated at other speeds the above procedure can be repeated to obtain the value of the bearing coefficients at the new speed.

The stability of the rotor-bearing system can also be investigated by means of the present design charts. Since it is found above that the lowest resonance (the first critical speed) is basically governed by the motor rotor mass, the mass per bearing is set equal to : $M = 0.162 \frac{\text{lbs.sec}^2}{\text{in}}$ and the rotor stiffness is $K_r = 43,000 \frac{\text{lbs}}{\text{in}}$. The corresponding bearing load is: $W = 62.5 \text{ lbs}$. Compute the dimensionless rotor mass parameter:

$$\frac{\sqrt{CMW}}{\mu DL \left(\frac{R}{C}\right)^2} = \frac{\sqrt{0.001 \cdot 0.162 \cdot 62.5}}{3.5 \cdot 10^{-6} \cdot 1.0 \cdot 5 \cdot (0.5 \cdot 10^3)^2} = 0.23$$

From Fig. C-2 the corresponding Sommerfeld Number is: $S = 0.94$ which yields a speed of: $N = 134 \text{ RPS} = 8,040 \text{ RPM}$. This is the speed at the threshold of instability if the rotor is rigid. However, since the rotor is flexible the actual threshold speed will be lower. Following the procedure outlined on page 203 the reduction due to the rotor flexibility may be computed as given below:

$$k = \frac{CK}{W} = \frac{0.001 \cdot 43,000}{62.5} = 0.688$$

from Fig. C-2:

<u>N, RPS</u>	<u>S</u>	<u>M_o</u>	<u>K_B = [77SM_o]²</u>	<u>M_o . √{k/(k + K_B)}</u>
100	0.7	0.355	0.6085	0.259
117	0.82	0.28	0.521	0.211
134	0.94	0.23	0.461	0.178

The last column gives the modified dimensionless rotor mass parameter as a function of Sommerfeld number. With the above calculated mass parameter of 0.23 the Sommerfeld number at the threshold of instability becomes: $S = 0.78$ which corresponds to a speed of:

$$\text{Speed at threshold of instability} = 111 \text{ RPS} = 6,650 \text{ RPM}$$

Returning to the previously calculated response at the first critical speed: $\frac{x}{\delta} = 23$ an estimate can be made of the level of balance required for the motor rotor. Let the maximum tolerated rotor displacement be: $x = 0.0005$ in. The eccentricity of the motor rotor is δ and may be expressed as:

$$\delta = \frac{\text{Unbalance, lbs.in)}}{(\text{Rotor weight, lbs})} = \frac{\text{Unbalance}}{125}$$

Thus:

$$\text{Max. unbalance} = 125 \cdot \frac{x}{\delta} = 125 \cdot \frac{0.0005}{23} = 0.0027 \text{ lbs.in} = 0.043 \text{ oz.inch}$$

The required balance level of the pump wheel cannot be analyzed by means of the design charts. For this purpose a computer program may be applied. However, the calculations performed above indicate that the maximum unbalance of the pump wheel should not exceed approximately 0.01 oz.in.

Finally, the operating speed of the unit is 5,000 RPM. Computing the corresponding Sommerfeld number the bearing eccentricity ratio can be determined from Fig. A-1 and the friction power loss can be estimated from the equation given on page 24 :

	<u>S</u>	<u>e</u>	<u>Min. Film Thickness, inch</u>	<u>Power Loss, HP</u>
Left hand bearing	0.608	0.555	0.000445	0.069
Right hand bearing	0.384	0.625	0.000375	0.073
Total				0.14 HP

The major conclusion to be derived from the review of the dynamic performance of the unit is that the shaft is too flexible. The operating speed is too close to the first critical speed and the bearings are sufficiently stiff that any modification of them will not contribute to changing the critical speed. The very flexible shaft also makes the rotor quite sensitive to any unbalance. Hence, the design of the rotor must be changed. The most effective way is to increase the shaft diameter if the resulting increase in the power loss is acceptable.

b. Rigid Rotor, Turbulent Bearing Film

A small rigid rotor is supported in two Mercury lubricated bearings. The system has the following data:

Total rotor weight: 10 lbs.

Transverse minus polar mass moment of inertia of rotor: $(I - I_p) = 88.8 \text{ . lbs.in}^2 = 0.23 \text{ lbs.sec}^2 \text{ in.}$

Bearing reactions: 5 lbs. and 5 lbs.

Bearing span: 10 inch

Design speed: 40,000 RPM

Journal bearing diameter: $D = 0.625 \text{ in.}$

Bearing length: $L = 0.625 \text{ in.}$

Radial clearance: $C = 0.0007 \text{ in.}$

Lubricant: Mercury

Lubricant temperature: 400 F

Lubricant viscosity: $\mu = 1.51 \cdot 10^{-7} \text{ lbs.sec/in}^2$

Lubricant density: $\rho = 0.475 \text{ lbs/in}^3 = 1.23 \cdot 10^{-3} \text{ lbs.sec}^2/\text{in}^4$

It is desired to select the bearing type for the application.

The rotor weighs 10 lbs and can be taken as being symmetric such that the load on each bearing is 5 lbs and the rotor mass per bearing becomes:

$$M = \frac{5}{386} = .013 \text{ lbs.sec}^2/\text{in}$$

The journal diameter is: $D = 0.625 \text{ in.}$ and the bearing length is: $L = 0.625 \text{ in.}$ The radial clearance is: $C = 0.0007 \text{ in.}$ which is relatively large but needed to accommodate thermal expansions and to provide adequate cooling. With these dimensions and the known lubricant properties the bearing parameters can be calculated. Denoting the speed as N (in RPS) we get:

$$\text{Sommerfeld number: } S = \frac{1.5 \cdot 10^{-7} \cdot 0.625 \cdot 0.625}{5} \frac{(0.3125)^2}{0.0007} = 2.46 \cdot 10^{-3} \cdot N$$

$$\text{Reynolds number: } Re = \frac{\pi \cdot 1.23 \cdot 10^{-3} \cdot N \cdot 0.625 \cdot 0.0007}{1.51 \cdot 10^{-7}} = 11.2 \cdot N$$

The operating speed is 40,000 RPM. Investigate first if it is possible to use a simple bearing type like a plain cylindrical bearing or a grooved bearing.

For study purposes the latter type can be represented by a 100 degree partial bearing.

It seems evident that the most difficult problem is instability. Hence, calculate the dimensionless rotor mass parameter:

$$\frac{\sqrt{CMW}}{\mu DL \left(\frac{R}{C}\right)^2} = \frac{\sqrt{0.0007 \cdot 0.013 \cdot 5}}{1.51 \cdot 10^{-7} \cdot 0.625 \cdot 0.625 \cdot \frac{0.3125^2}{0.0007}} = 0.547$$

Entering Fig. C-9 with this value and using the curve for a 100 degree partial bearing gives: $S = 0.39$. The corresponding speed becomes:

$$\text{Speed at instability threshold} = \frac{0.39}{0.00246} = 159 \text{ RPS} = 9,500 \text{ RPM}$$

The corresponding Reynolds number is 1770 which is sufficiently close to the value of 1663 for which Fig. C-9 is valid. Thus, a 100 degree partial bearing yields a threshold speed of 9,500 RPM which is far too low for the application.

Next, enter Fig. C-11 with the calculated rotor mass parameters and use the curve for the plain cylindrical bearing to get:

$$S = 0.64, \text{ i.e. } N = \frac{0.64}{0.00246} = 266 \text{ RPS} = 15,600 \text{ RPM}$$

The corresponding Reynolds number becomes 2910 which agrees well with the value of 3326 for which Fig. C-11 is valid. Hence, the threshold speed is 15,600 RPM for a plain cylindrical bearing which is not acceptable.

It can, therefore, be concluded that no "fixed geometry" bearing is likely to ensure stable operation. Among the other possible bearing types (the floating ring bearing, the externally pressurized bearing, etc.) the tilting pad bearing is the one for which most experience is available. It will, therefore, be investigated if the tilting pad bearing is adequate for the present application. To check its stability it is sufficient to check if the pivoted shoes follow the journal motion. For this purpose Fig. B-45 can be employed to get an estimate even if the chart assumes the film to be laminar. For a speed of 40,000 RPM = 667 RPS the Sommerfeld number becomes: $S = 1.64$. The corresponding critical mass is found to be:

$$\frac{CMW_{crit}}{\left[\mu DL \left(\frac{L}{C}\right)^2\right]^2} = 0.85$$

or

$$M_{crit} = 0.367 \text{ lbs.sec}^2/\text{in} = \frac{\text{mass inertia of shoe}}{(0.3125)^2}$$

Hence,

$$\text{Critical mass moment of inertia of shoe} = 0.0359 \text{ lbs.in.sec}^2 = 13.85 \text{ lbs}$$

If the shoe is a 90 degree arc its "curved" length is: $\pi \cdot 0.625/4 = 0.49$ in. With a length of 0.625 inch, a thickness of 0.25 inch and a density of 0.283 lbs/in^3 its mass moment of inertia is approximately:

$$\text{Mass moment of inertia of shoe} = 0.49 \cdot 0.625 \cdot 0.25 \cdot 0.283 \cdot \frac{(0.49)^2}{12} = 0.000435 \text{ lbs.in}^2$$

which is far below the critical value. Hence, the tilting pad bearings will be stable.

The dynamic bearing coefficients can be found from Figs. B-80 to B-86. Once these coefficients are determined the critical speeds may be calculated directly since the tilting pad bearing has no cross-coupling terms. The procedure is illustrated below. It consists of the following steps:

1. assume a rotor speed N , RPS
2. calculate the corresponding Reynolds number and Sommerfeld number
3. enter the appropriate design chart (or interpolate) to find the spring coefficients
4. calculate the corresponding critical speed
5. if the calculated critical speed differs greatly from the assumed speed, repeat the procedure.

The rotor mass per bearing is $0.013 \text{ lbs.sec}^2/\text{in}$, the transverse mass moment of inertia minus the polar mass moment of inertia of the rotor is: $(I-I_p) = 88.8 \text{ lbs.in}^2 = 0.23 \text{ lbs. in.sec}^2$ and the bearing span is: $\delta = 10 \text{ in}$. If the bearing stiffness is called $K \frac{\text{lbs}}{\text{in}}$ the critical speeds become:

$$\text{1st critical speed} = \frac{1}{2\pi} \cdot \sqrt{\frac{K}{0.013}} \text{ RPS}$$

$$\text{2nd critical speed} = \frac{1}{2\pi} \cdot \sqrt{\frac{\frac{1}{2} K \delta^2}{0.23}} = \frac{1}{2\pi} \cdot \sqrt{\frac{K}{0.0046}} \text{ RPS}$$

The bearing reaction is: $W = 5 \text{ lbs.}$ and the radial clearance is: $C = .0007 \text{ in.}$ such that:

$$\frac{W}{C} = 7.14 \cdot 10^3 \frac{\text{lbs}}{\text{in}}$$

Following the outlined procedure the calculations yield:

$$N = 125 \text{ RPS} \quad S = 0.308 \quad Re = 1400$$

$$\text{from Fig. B-81: } K_{xx} = 6,400 \frac{\text{lbs}}{\text{in}}, \quad C_{xx} = 21.8 \frac{\text{lbs.sec}}{\text{in}}$$

$$\text{i.e. 1st critical speed, minor resonance} = \frac{1}{2\pi} \cdot \sqrt{\frac{6,400}{0.013}} = 112 \text{ RPS} = \underline{\underline{6,700 \text{ RPM}}}$$

$$N = 180 \text{ RPS} \quad S = 0.443 \quad Re = 2020$$

$$\text{from Figs. B-81 and B-82: } K_{yy} = 15,350 \frac{\text{lbs}}{\text{in}}, \quad C_{yy} = 55.6 \frac{\text{lbs.sec}}{\text{in}}$$

$$\text{i.e. 1st critical speed, major resonance} = \frac{1}{2\pi} \cdot \sqrt{\frac{15,350}{0.013}} = 173 \text{ RPS} = \underline{\underline{10,400 \text{ RPM}}}$$

$$\text{from Figs. B-81 and B-82: } K_{xx} = 5,200 \frac{\text{lbs}}{\text{in}}, \quad C_{xx} = 18.6 \frac{\text{lbs.sec}}{\text{in}}$$

$$\text{i.e. 2nd critical speed, minor resonance} = \frac{1}{2\pi} \cdot \sqrt{\frac{5,200}{0.0046}} = 169 \text{ RPS} = \underline{\underline{10,200 \text{ RPM}}}$$

$$N = 250 \text{ RPS} \quad S = 0.615 \quad Re = 2800$$

$$\text{from Figs. B-82 and B-83: } K_{yy} = 10,930 \frac{\text{lbs}}{\text{in}}, \quad C_{yy} = 52.7 \frac{\text{lbs.sec}}{\text{in}}$$

$$\text{i.e. 2nd critical speed, major resonance} = \frac{1}{2\pi} \cdot \sqrt{\frac{10,930}{0.0046}} = 245 \text{ RPS} = \underline{\underline{14,700 \text{ RPM}}}$$

It should be noted that the bearing damping is sufficiently high that the system is critically damped at all the calculated resonances. Thus, at the first cri-

speed:

$$\text{Critical damping} = 2 \cdot \sqrt{K \cdot .013} = \begin{cases} 18.2 \frac{\text{lbs.sec}}{\text{in}} & (\text{1st critical, minor}) \\ 28.2 \frac{\text{lbs.sec}}{\text{in}} & (\text{1st critical, major}) \end{cases}$$

Similarly for the second critical speed. Thus, the critical speeds will have influence on the rotor performance. It can, therefore, be concluded that the pad bearing ensures satisfactory performance of the system from the point of view of rotor-bearing dynamics.

c. Rigid Rotor. Hydrostatic Gas Bearings

A rotor has the following data:

weight: 90 lbs.

transverse mass moment of inertia at CG: 7,230 lbs.in²

bearing span = 20.7 in.

distance from bearing #1 to CG = 11.5 in

journal diameter = 2.5 in

max. journal bearing length = 3.75 in.

The operating conditions are:

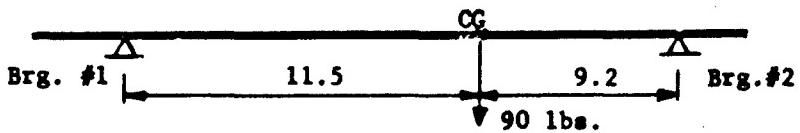
normal operating speed = 32,000 RPM = 533 cps

max. overspeed = 36,000 RPM = 600 cps

max. available supply pressure = 325 psia

gas = air at 120°F

It is desired to select the dimensions of the hydrostatic bearings for this application. The bearing reactions are found to be



for bearing 1: W = 40 lbs.

for bearing 2: W = 50 lbs.

Hence, use W = 50 lbs. for design purposes. Since the rotor is heavy for the required top speed it is necessary to have the bearing as stiff as possible in order to avoid hydrodynamic instability. Therefore, the journal bearings are chosen to have double plane admission. From the approximate relationships:

$$\frac{W}{(P_s - P_a)L D} \approx 0.25$$

get:

$$(P_s - P_a)L = \frac{50}{0.25 \cdot 2.5} = 80$$

With $L = 3.75$ in. it is evident that the required load carrying capacity is easily achieved. Turning to the bearing stiffness it is necessary to have:

$$\text{lowest critical speed} > 0.6 \cdot (\text{max. speed})$$

The lowest critical speed can be estimated by assigning a rotor mass equal to the load of the heaviest loaded bearing, i.e. bearing No. 2. Hence, the required stiffness K may be estimated from,

$$\frac{1}{2\pi} \sqrt{\frac{K}{50/386.07}} > 0.6 \cdot 600 = 360 \text{ cps}$$

$$K > 6.6 \cdot 10^5 \frac{\text{lbs}}{\text{in}}$$

Choose the optimum value of the restrictor ratio:

$$\Lambda_s \xi = 0.7$$

and let the bearing have the maximum allowable length:

$$L = 3.75 \text{ in.}$$

$$\text{i.e. } \frac{L}{D} = \frac{3.75}{2.5} = 1.5$$

$$\text{and } \xi = \frac{L}{D} = 0.75$$

For an estimated operating pressure ratio of: $P_s/P_a = 2$ the dimensionless stiffness is determined by interpolation between Figs. B-119 and B-122:

$$\frac{1 + \xi^2}{1 + \frac{2}{3}\xi^2} \cdot \frac{CK}{(P_s - P_a)L D} = 0.47$$

The journal bearing clearance is selected such that:

$$\frac{C}{R} = 0.6 \cdot 10^{-3}$$

$$\text{i.e. } C = 0.6 \cdot 10^{-3} \cdot 1.25 = 0.75 \cdot 10^{-3} \text{ in.}$$

To get the maximum stiffness the feeder holes should be orifice restricted with as little inherent compensation as practical, i.e. $\delta = 0$. Then the actual stiffness becomes:

$$K = \frac{1}{0.75 \cdot 10} \cdot (P_s - P_a) \cdot 3.75 \cdot 2.5 \cdot 0.47 = 5.88 \cdot 10^3 (P_s - P_a)$$

Therefore

$$P_s - P_a > \frac{6.6 \cdot 10^5}{5.88 \cdot 10^3} = 113 \text{ psi}$$

or:

$$P_s > 113 + 120 = 233 \text{ psia}$$

To allow some margin set the actual operating supply pressure equal to 275 psia. Since the maximum available supply pressure is 325 psia the required stiffness can be obtained with the chosen bearing dimensions.

The lubricant is air at 120°F with the properties:

$$\text{viscosity: } \mu = 2.8 \cdot 10^{-9} \frac{\text{lbs.sec}}{\text{in}^2}$$

$$\text{gas constant: } R = 2.472 \cdot 10^5 \frac{\text{in}^2/\text{sec}^2}{\text{R}}$$

$$\text{i.e. } RT = 2.472 \cdot 10^5 \cdot (460 + 120) = 1.434 \cdot 10^8 \frac{\text{in}^2}{\text{sec}^2}$$

$$\text{or } \sqrt{RT} = 1.198 \cdot 10^4 \frac{\text{in}}{\text{sec}}$$

To select the number of feeding holes N and the orifice radius a for the journal bearing use the definition of the restrictor coefficient Λ_s :

$$\frac{Na^2}{\sqrt{1+8}} = \frac{P_s C^3}{6\mu\sqrt{RT}} \Lambda_s \frac{275 \cdot (0.75 \cdot 10^{-3})^3}{6 \cdot 2.8 \cdot 10^{-9} \cdot 1.198 \cdot 10^4} \cdot \frac{0.7}{0.75} = 5.3823 \cdot 10^{-4}$$

For $N = 16$ and $\delta = 0$, $a = 5.8 \cdot 10^{-3}$ in. Since it is not feasible to have δ exactly equal to zero, set:

$$\text{with } \underline{N = 16} \quad \underline{a = .006 \text{ in}} \quad (\text{i.e. orifice diameter} = 0.012 \text{ in})$$

With a feeder hole diameter $d = 0.125$ in. the inherent compensation factor becomes:

$$\delta = \frac{a^2}{dC} = \frac{(0.006)^2}{0.125 \cdot 0.75 \cdot 10^{-3}} = 0.384$$

Hence,

$$\frac{1 + \frac{2}{3} \delta^2}{1 + \delta^2} = 0.957$$

so that the reduction in stiffness is less than 5 percent. Check the value of the restrictor coefficient:

$$\Delta \xi = \frac{6 \cdot 2.8 \cdot 10^{-9} \cdot 16 \cdot (0.006)^2 \cdot 1.198 \cdot 10^4}{275 \cdot (0.75 \cdot 10^{-3})^3 \sqrt{1 + .384^2}} \cdot 0.75 = 0.70$$

which agrees with the selected value.

Let the distance from the orifice to the bearing surface be 0.050 in. Then with a hole diameter of 0.125 in. the feeder hole volume becomes: $V_c = 0.613 \cdot 10^{-3} \text{ in}^3$ and the feeder hole volume ratio is

$$\frac{NV_c}{\pi DLC} = \frac{16 \cdot .613 \cdot 10^{-3}}{\pi \cdot 2.5 \cdot 3.75 \cdot .75 \cdot 10^{-3}} = .445$$

which is too high by an order of magnitude from the point of view of susceptibility to pneumatic hammer. Instead make the feeder hole diameter:

$$d = 0.035 \text{ in}$$

and provide the feeder hole with a recess with a diameter of .125 inch and a depth of 0.002 inch.

The feeder volume ratio then becomes:

$$\frac{NV_c}{\pi DLC} = 0.0525$$

which is acceptable. Providing the recess also changes the inherent compensation factor which becomes:

$$\delta = 0.536$$

Based on the already obtained value for the dimensionless stiffness, the actual stiffness becomes:

$$K = \frac{1 + \frac{2}{3} \cdot (0.536)^2}{1 + (0.536)^2} \cdot \frac{1}{0.75 \cdot 10^{-3}} \cdot (275 - 120) \cdot 3.75 \cdot 2.5 \cdot 0.47 = 8.43 \cdot 10^5 \frac{\text{lbs}}{\text{in}}$$

Assume a support stiffness of $3 \cdot 10^6 \frac{\text{lbs}}{\text{in}}$ so that the combined stiffness of the gas film and the support becomes:

$$\text{combined stiffness} = 6.58 \cdot 10^5 \frac{\text{lbs}}{\text{in}}$$

To check the critical speeds of the rotor assume the rotor to be rigid. The mass and mass moment of inertia of the rotor are computed from the given data:

$$\text{rotor mass: } M_t = \frac{90}{386.07} = 0.233 \frac{\text{lbs.sec}^2}{\text{in}}$$

$$\text{rotor mass moment of inertia: } (I - I_p) = \frac{(7,230 - 860)}{386.07} = 16.5 \text{ lbs.in.sec}^2$$

Using the equations on Page 235 with $K_1 = K_2 = 6.58 \cdot 10^5 \frac{\text{lbs}}{\text{in}}$ and $s_1 = 11.5 \text{ in}$ and $s_2 = 9.2 \text{ in.}$, we get:

$$\omega_t^2 = \frac{2 \cdot 6.58 \cdot 10^5}{0.233} = 5.65 \cdot 10^6 \frac{\text{rad}^2}{\text{sec}^2}$$

$$\omega_c^2 = \frac{6.58 \cdot 10^5 (11.5^2 + 9.2^2)}{16.5} = 8.65 \cdot 10^6 \frac{\text{rad}^2}{\text{sec}^2}$$

$$\omega_{ct}^4 = \frac{(6.58 \cdot 10^5 (-11.5 + 9.2))^2}{16.5 \cdot 0.233} = 0.596 \cdot 10^{12} \frac{\text{rad}^4}{\text{sec}^4}$$

and the two lowest critical speeds become:

$$\omega_n = 10^3 \cdot \sqrt{\frac{1}{2} (8.65 + 5.65) \pm \sqrt{\frac{1}{4} (8.65 - 5.65)^2 + 0.596}}$$

Hence:

$$\text{Rigid body critical speeds: } \begin{cases} 372 \text{ cps (translatory mode)} \\ 472 \text{ cps (conical mode)} \end{cases}$$

The lowest critical speed (i.e. 372 cps) is higher than the required 60 per cent of the maximum rotor speed. The second critical speed is 13 per cent below the normal operating speed of 533 cps and should, therefore, not seriously interfere with the rotor operation.

To get an idea of the response at the critical speed determine the damping coefficient. The dimensionless value is obtained by interpolation between Figs. B-120, B-121, B-123 and B-124.

$\frac{L}{D}$	$\frac{Nv_c}{KDLc}$	Dimensionless Damping
1	0	4.0
1	0.1	3.7
2	0	12.0
$\frac{2}{1.5}$	$\frac{0.1}{0.05}$	$\frac{11.8}{7.9}$

where the last line is determined by linear interpolation. The actual damping becomes:

$$B = 2.8 \cdot 10^{-9} \cdot 3.75 \left(\frac{1.25}{0.75 \cdot 10^{-3}} \right)^3 \cdot 7.9 = 383 \frac{\text{lbs.sec}}{\text{in}}$$

The lowest critical speed (the translatory mode) is closely determined by

$$\omega_n \approx \sqrt{\frac{K_1 + K_2}{M}} = \sqrt{\omega_t^2} \frac{\text{radians}}{\text{sec}}$$

(i.e. $\omega_t^2 = 5.65 \cdot 10^6 \frac{\text{rad}^2}{\text{sec}^2}$ or $\sqrt{\omega_t^2} = 385 \text{ cps}$ which is very close to the calculated 372 cps for the translatory mode). Hence, this mode can be considered as the resonance of a mass $0.233 \frac{\text{lbs.sec}^2}{\text{in.}}$ supported by a spring of: $2 \cdot 6.58 \cdot 10^5 = 1.316 \cdot 10^6 \frac{\text{lbs}}{\text{in.}}$. The critical damping is defined as:

$$B_{\text{critical}} = 2 \cdot \sqrt{1.316 \cdot 10^6 \cdot 0.233} = 1106 \frac{\text{lbs.sec}}{\text{in}}$$

Thus, the log-decrement δ is approximately:

$$\bar{\delta} = \frac{2\pi B}{B_{\text{critical}}} = 2.17$$

and the magnification factor (the Q-factor) is closely given by:

$$\text{Q-factor} = \frac{\pi}{\delta} = 1.45$$

Note: the Q-factor gives the ratio between the amplitude at resonance and the amplitude if there was no resonance, i.e. it measures the amplification due to the resonance such that a Q-factor of 1 means no amplification. Thus, the rotor is rather heavily damped.

The operating eccentricity ratio can be calculated from:

$$\epsilon = \frac{W}{CK} = 0.079$$

Finally, a summary of the bearing dimensions and the most important of the design data shall be given:

Bearing Data

Diameter: $D = 2.5$ in.

Length: $L = 3.75$ in.

Length between admission planes: $L_1 = 1.875$ in.

Radial clearance: $C = 0.00075$ in.

Number of admission planes: 2

Number of feeder holes: $N = 16$ (8 holes per admission plane)

Orifice diameter: $2a = 0.012$ in.

Feeder hole diameter: $d = 0.035$ in.

Recess diameter: $= 0.125$ in

Recess depth: $= 0.002$ in.

Length of feeder hole: $\epsilon' = 0.050$ in.

Supply pressure: $P_s = 275$ psia

Radial stiffness: $K = 840,000$ lbs/in.

Operating eccentricity ratio: $\epsilon = 0.079$

Critical speeds of rotor: 372 cps = $22,300$ RPM (translatory mode)

472 cps = $28,300$ RPM (conical mode)

REFERENCES

1. N.F. Rieger, "Rotor-Bearing Dynamics Design Technology. Part 1: "State-of-the-Art" Technical Report prepared for Air Force Aero Propulsion Laboratory, Wright Patterson Air Force Base, under Contract AF33(615)-1895.
2. P. Lewis and S.B. Malanoski, "Rotor-Bearing Dynamics Design Technology. Part 4: Ball Bearing Design Data" Technical Report prepared for Air Force Aero Propulsion Laboratory, Wright Patterson Air Force Base, under Contract AF33(615)-1895.
3. O. Pinkus and B. Sternlicht, "Theory of Hydrodynamic Lubrication", McGraw-Hill Book Company, Inc. New York.
4. D.F. Wilcock and E.R. Booser, "Bearing Design and Application", McGraw-Hill Book Company, Inc. New York.
5. J.W. Lund and B. Sternlicht, "Rotor-Bearing Dynamics with Emphasis on Attenuation", JOURNAL OF BASIC ENGINEERING, TRANS.ASME, Series D, vcl. 84, 1962.
6. F.K. Orcutt and E.B. Arwas, "Analysis of Turbulent Lubrication, Volume 1" MTI 64TR19, Technical Report prepared for NASA, Lewis Research Center, under Contract No. NAS w-771.
7. F.K. Orcutt, C.W.Ng, J.H. Vohr and E.B. Arwas, "First Quarterly Report, Lubrication Analysis in Turbulent Regime", NASA CR-54195, Technical Report prepared for NASA, Lewis Research Center, under Contract No. NAS w-1021.
8. J.W. Lund, "Spring and Damping Coefficients for the Tilting-Pad Journal Bearing", TRANS. ASLE, Vol. 7, Nov. 4, Oct. 1964.
9. J.W. Lund, "The Hydrostatic Gas Journal Bearing with Journal Rotation and Vibration", JOURNAL OF BASIC ENGINEERING, TRANS.ASME, Series D, vol.86, 1964.
10. A.C. Hagg and G.O. Sankey, "Elastic and Damping Properties of Oil-Film Journal Bearings for Application to Unbalance Vibration Calculation", JOURNAL OF APPLIED MECHANICS, Vol. 25, 1958.
11. A.C. Hagg and G.O. Sankey, "Some Dynamic Properties of Oil-Film Journal Bearings with Reference to the Unbalance Vibration of Rotors", JOURNAL OF APPLIED MECHANICS, vol. 23, 1956.
12. B. Sternlicht, "Elastic and Damping Properties of Cylindrical Journal Bearings", TRANS. ASME, Series D. vol. 81, 1959.

13. P.C. Warner, "Static and Dynamic Properties of Partial Journal Bearings", JOURNAL OF BASIC ENGINEERING, TRANS. ASME, Series D, Vol. 85, 1963.
14. B. Sternlicht, H. Poritsky and E.B. Arwas, "Dynamic Stability Aspects of Cylindrical Journal Bearings using Compressible and Incompressible Fluids", Proceedings of the First International Symposium on Gas Lubricated Bearings, ONR/ACR-49, October 1959.
15. P.C. Warner and R.J. Thoman, "The Effect of the 150-Degree Partial Bearing on Rotor-Unbalance Vibration", JOURNAL OF BASIC ENGINEERING, TRANS. ASME, Series D, Vol. 86, 1964.
16. J. W. Lund, "The Stability of an Elastic Rotor in Journal Bearings with Flexible, Damped Supports", Accepted for publication in JOURNAL OF APPLIED MECHANICS, 1965.
17. H.S. Cheng and C.H.T. Pan, "Stability Analysis of Gas-Lubricated, Self-Acting, Plain Cylindrical Journal Bearings of Finite Length, Using Galerkin's Method", JOURNAL OF BASIC ENGINEERING, TRANS. ASME, Series D, vol. 87, 1965.
18. C.W. Ng, "Linearized PH Stability Theory for Finite Length, Self-Acting, Gas-Lubricated Plain Journal Bearings", ASME Paper No. 64 LUB-28, presented at ASME-ASLE International Conference, Washington, D.C., Oct. 1964.
19. J.W. Lund, "A Theoretical Analysis of Whirl Instability and Pneumatic Hammer for a Rigid Rotor in Pressurized Gas Journal Bearings", Submitted for publication to JOURNAL OF BASIC ENGINEERING, 1965.
20. S. Timoshenko, "Vibration Problems in Engineering", D. Von Nostrand Company, Inc., New York.
21. S. Timoshenko, "Strength of Materials, Part II: Advanced Theory and Problems", D. Van Nostrand Company, Inc., New York.

UNCLASSIFIED
Security Classification

DOCUMENT CONTROL DATA - R&D

(Security classification of title, body of abstract and indexing annotation must be entered when the overall report is classified)

1. ORIGINATING ACTIVITY (Corporate author) Mechanical Technology Incorporated 968 Albany-Shaker Road Latham, New York 12110	2a. REPORT SECURITY CLASSIFICATION UNCLASSIFIED
	2b. GROUP N/A

3. REPORT TITLE

Rotor-Bearing Dynamics Design Technology, Part III: Design Handbook
for Fluid Film Type Bearings

4. DESCRIPTIVE NOTES (Type of report and inclusive dates)

Final Report for period 1 April 1964 - 1 April 1965

5. AUTHOR(S) (Last name, first name, initial)

Lund, Jorgen W., Arwas, Elie B., Cheng, H.S., Ng, C.W., Pan, Coda H.T., and Sternlicht, B.

6. REPORT DATE

April 1965

7a. TOTAL NO. OF PAGES

280

7b. NO. OF REPS

21

8a. CONTRACT OR GRANT NO.

AF33(615)-1895

8b. ORIGINATOR'S REPORT NUMBER(S)

MTI-65TR14

8c. PROJECT NO.	3044
8d. Task No.	304402
8e. OTHER REPORT NO(S) (Any other numbers that may be assigned this report)	
AFAPL-TR-65-45, Part III	

10. AVAILABILITY/LIMITATION NOTICES Qualified requesters may obtain copies of this report from DDC. Foreign announcement and dissemination of this report by DDC is not authorized. Release to foreign nationals is not authorized. DDC release to the clearing house for Federal Scientific and Technical Information (formerly OTS) is not authorized.

11. SUPPLEMENTARY NOTES

12. SPONSORING MILITARY ACTIVITY

USAF

RTD

Air Force Aero Propulsion Laboratory
Wright-Patterson AFB, Ohio 45433

13. ABSTRACT

This design handbook presents data and methods for use in analyzing the dynamical performance of a rotor supported in fluid film type bearings. The data are given in form of design charts covering :

1. The dynamic bearing coefficients
2. The onset of hydrodynamic instability
3. The critical speeds and the unbalance response of a simple rotor-bearing system.

The design charts are in dimensionless form and cover a wide range of bearing geometries and operating conditions.

Several different types of fluid film bearings are considered together with various forms of lubrication.

Incompressible Lubricant

<u>Laminar</u>	Plain Cylindrical Bearing 4-Axial Groove Bearing Elliptical Bearing Partial Bearings Tilting Pad Bearing
----------------	--

Compressible Lubricant

<u>Self-acting Bearings</u>	Plain Cylindrical Bearing
-----------------------------	---------------------------

<u>Turbulent</u>	Plain Cylindrical Bearing Partial Bearing Tilting Pad Bearing
------------------	---

<u>Externally Pressurized</u>	Plain Cylindrical Bearing Single Plane Admission Plain Cylindrical Bearing Double Plane Admission
-------------------------------	--

DD FORM 1 JAN 64 1473

UNCLASSIFIED

Security Classification

UNCLASSIFIED

Security Classification

1. KEY WORDS	LINK A		LINK B		LINK C	
	ROLE	WT	ROLE	WT	ROLE	WT
Bearings Lubrication Fluid Film Hydrodynamic Hydrostatic Rotor-Bearing Dynamics Stability Critical Speed Laminar Film Turbulent Film						

INSTRUCTIONS

1. ORIGINATING ACTIVITY: Enter the name and address of the contractor, subcontractor, grantee, Department of Defense activity or other organization (corporate author) issuing the report.

2a. REPORT SECURITY CLASSIFICATION: Enter the overall security classification of the report. Indicate whether "Restricted Data" is included. Marking is to be in accordance with appropriate security regulations.

2b. GROUP: Automatic downgrading is specified in DoD Directive 5200.10 and Armed Forces Industrial Manual. Enter the group number. Also, when applicable, show that optional markings have been used for Group 3 and Group 4 as authorized.

3. REPORT TITLE: Enter the complete report title in all capital letters. Titles in all cases should be unclassified. If a meaningful title cannot be selected without classification, show title classification in all capitals in parenthesis immediately following the title.

4. DESCRIPTIVE NOTES: If appropriate, enter the type of report, e.g., interim, progress, summary, annual, or final. Give the inclusive dates when a specific reporting period is covered.

5. AUTHOR(S): Enter the name(s) of author(s) as shown on or in the report. Enter last name, first name, middle initial. If military, show rank and branch of service. The name of the principal author is an absolute minimum requirement.

6. REPORT DATE: Enter the date of the report as day, month, year, or month, year. If more than one date appears on the report, use date of publication.

7a. TOTAL NUMBER OF PAGES: The total page count should follow normal pagination procedures, i.e., enter the number of pages containing information.

7b. NUMBER OF REFERENCES: Enter the total number of references cited in the report.

8a. CONTRACT OR GRANT NUMBER: If appropriate, enter the applicable number of the contract or grant under which the report was written.

8b, 8c, & 8d. PROJECT NUMBER: Enter the appropriate military department identification, such as project number, subproject number, system numbers, task number, etc.

9a. ORIGINATOR'S REPORT NUMBER(S): Enter the official report number by which the document will be identified and controlled by the originating activity. This number must be unique to this report.

9b. OTHER REPORT NUMBER(S): If the report has been assigned any other report numbers either by the originator or by the sponsor, also enter this number(s).

10. AVAILABILITY/LIMITATION NOTICE: Enter any limitations on further dissemination of the report, other than those imposed by security classification, using standard statements such as:

(1) "Qualified requesters may obtain copies of this report from DDC."

(2) "Foreign announcement and dissemination of this report by DDC is not authorized."

(3) "U. S. Government agencies may obtain copies of this report directly from DDC. Other qualified DDC users shall request through _____."

(4) "U. S. military agencies may obtain copies of this report directly from DDC. Other qualified users shall request through _____."

(5) "All distribution of this report is controlled. Qualified DDC users shall request through _____."

If the report has been furnished to the Office of Technical Services, Department of Commerce, for sale to the public, indicate this fact and enter the price, if known.

11. SUPPLEMENTARY NOTES: Use for additional explanatory notes.

12. SPONSORING MILITARY ACTIVITY: Enter the name of the departmental project office or laboratory sponsoring (paying for) the research and development. Include address.

13. ABSTRACT: Enter an abstract giving a brief and factual summary of the document indicative of the report, even though it may also appear elsewhere in the body of the technical report. If additional space is required, a continuation sheet shall be attached.

It is highly desirable that the abstract of classified reports be unclassified. Each paragraph of the abstract shall end with an indication of the military security classification of the information in the paragraph, represented as (TS), (S), (C), or (U).

There is no limitation on the length of the abstract. However, the suggested length is from 150 to 225 words.

14. KEY WORDS: Key words are technically meaningful terms or short phrases that characterize a report and may be used as index entries for cataloging the report. Key words must be selected so that no security classification is required. Identifiers, such as equipment model designation, trade name, military project code name, geographic location, may be used as key words but will be followed by an indication of technical context. The assignment of links, rules, and weights is optional.

UNCLASSIFIED

Security Classification